DAMAGE IDENTIFICATION IN ENGINEERING STRUCTURES FROM CHANGES IN MEASURED DYNAMIC RESPONSE

by

Victor Mark Richards

A submission presented in fulfilment of the requirements of the
University of Glamorgan/Prifysgol Morgannwg for the degree of
Doctor of Philosophy

PhD

July 2000

Collaborating establishments: The Building Research Establishment Ltd.
Ove Arup and Partners Research and Development.

Funding provided by: The University of Glamorgan.

CERTIFICATE OF RESEARCH

This is to certify that, apart from where specific reference to other publications is made, the work presented in this thesis is the result of the investigations undertaken by the candidate.

.....
V. M. Richards
(Candidate)

.....
(Date)

.....
Dr R. Delpak
(Director of studies)

.....
Dr B. R. Ellis
(Supervisor)

.....
Professor R. Wiltshire
(Supervisor)

.....
I. Feltham
(Supervisor)

.....
(Date)

DECLARATION

This is to certify that neither this thesis, nor any part of it, has been presented in candidature for any degree at any other academic institution.

.....

V. M. Richards

(Candidate)

DEDICATION

To my mother, father and sisters

ACKNOWLEDGEMENTS

Any research project is only possible due to the contributions and considerable effort afforded to the progression and development of the study aims by dedicated individuals. This project is no exception. The candidate would like to express his appreciation to all those who contributed throughout the course of the studies that have lead to this thesis, without which the compilation of this work would certainly not have been as enlightening as was experienced.

Before offering thanks to individual contributors to this work, it is clear that without the support of the Directorate and Management of University of Glamorgan, who provided, without exception, all the financing required for the undertaking of this project, this work would not have been possible.

In circumstances where insight and oversight are required to drive ideas forward, there are always individuals who can reflect on experience to provide considered judgement and advice on the best course of action needed to achieve the required aims. Within the framework of this project, Dr R. Delpak has certainly fulfilled the idealism of such an individual, to whom the candidate expresses sincere gratitude for his guidance throughout this study.

There is also another distinct kind of person whose influence on the development of an individual's knowledge infuses admiration and aspiration towards a particular desired educational maturity. The candidate considered Dr Brian Ellis to be one such person, and it is appropriate here to praise the considerable contribution that he, and the Management at BRE, have made with the provisions of the dynamic test measuring equipment that was used in this project. Additionally, gratitude is expressed to Dr Ellis for his contributions in solving many of the technical issues raised by the candidate from time to time.

Special thanks are also due to Dr David Moore of BRE who secured for the candidate unlimited access to the Large Building Test Facility at the Cardington structural laboratories.

The candidate would also like to profoundly thank the contributions of Professor Ron Wiltshire and Mr Ian Feltham for their significant help during those parts of the study that required knowledge of a specialist nature, which would have otherwise been outside the attainable scope of the project.

Finally, the candidate considers himself fortunate to have received the ever-present security that is a loving family, which is forever appreciated even though not always expressed. And to Gabriele, without whom the metaphorical scales of professional and personal life would not balance as perfectly as they do when we are together.

ABSTRACT

Identifying the structural characteristics of buildings, and the structural components, using measured dynamic response could provide engineers with an early warning system of the occurrence of damage. The key to such an approach is to understand how the processes of damage, which may be caused as a result of a single specific event or as part of natural deterioration, influences the dynamic response properties. By understanding how the processes involved in damage affect the latter, engineers can make use of this information, which could provide a basis for remedial action.

This research project was initiated to study where damage identification, using measured dynamic characteristics, could be of particular advantage over more commonly adopted visual based methods. To achieve a thorough investigation into the beneficial aspects of this non-invasive and non-destructive process, a comprehensive study has been compiled and presented in this thesis, which aims to provide detailed information of those circumstances when the technique is most appropriate. The research examines how natural frequencies, mode shapes and damping characteristics are affected by damage, and provides detailed results of investigations carried out to determine the sensitivity of these properties to deliberately induced structural defects. The study focuses on a full-scale eight-storey steel-framed building, which was constructed for the purposes of research in structural engineering.

To commence the work, a study is presented that compares natural frequencies representative of the whole-frame behaviour of the building during specific stages of construction, to similar characteristics determined from calculations. This comparison reveals that calculations prepared using a detailed analytical model of the structure do not represent the information found from measurement, which is thought to be a general observation that would be encountered in other similar studies. A method is presented that allowed calibration of the prepared numerical model against the measured values, which is vital if changes in the structure, as a result of damage, are to be interpreted from natural frequency measurements collected over time.

Similar comparisons were carried out on one of the floors within the above-mentioned building. In this case, a more refined numerical model of the structure was prepared and was used to calibrate calculated natural frequencies of the floor against those measured directly from the structure before and after damage. To achieve the calibration, the methodology formulated from studies on the whole-frame was utilised, with additional rigour being introduced into the procedure to allow the imposed damage to be quantified in further detail.

A detailed laboratory investigation was carried out, which examined the changes that occurred to the natural frequency, damping and mode shapes of localised slab panels. These panels were prepared to represent localised sub-elements of the aforementioned floor slab, and were tested under both static and dynamic load conditions to allow imposed damage and dynamic characteristic changes to be identified and compared. The former of these loading conditions was considered to provide a controlled means of introducing damage, which was quantified by recording strain and displacement data during the procedures associated with the test. To interpret the damage caused by

this process, a number of numerical models are presented, which model the characteristics thought to be attributed to the defects due to the static loads. Comparing this information to that obtained from the dynamic load tests reveals the sensitivity of the dynamic characteristics and how they are influenced by the development of the progressive damage.

Finally, due to certain characteristics that were observed from the measurements recorded during the dynamic load testing above, a number of mathematical models are presented, which show how the adjusted dynamic behaviour of the damaged structure can be calculated. This last phase of the research provides additional detail of the way the dynamic response of the panels changes after damage had occurred, which has been considered to offer an additional means of recognising the onset of structural damage.

LIST OF CONTENTS

LIST OF FIGURES

LIST OF TABLES

LIST OF SYMBOLS

[C]	A matrix containing damping terms.
$[K]$	A matrix containing structural stiffness terms (before damage).
$[\delta K]$	A matrix containing the change in structural stiffness terms after damage.
$[\bar{K}]$	Structural stiffness matrix compiled in the GRIND computer program (chapter 4).
$[M]$	A matrix containing structural mass terms.
$[\bar{M}]$	Structural mass matrix compiled in the GRIND computer program (chapter 4).
$[\bar{S}]$	A matrix comprising components of the structural stiffness and mass matrix for solution of the eigen-problem using Cholesky's method (chapter 4).
$[\Omega]^2$	A matrix containing measured natural frequencies of an undamaged structure.
$[\delta\Omega]^2$	A matrix containing the value of the change of measured natural frequencies obtained from a structure after damage.
$[k_{ij}]$	Stiffness matrix representing the structural properties of an element between nodes labelled i and j (where i and j are integer values) (chapter 4).
$\{\Delta\}$	Eigen-vector calculated using Cholesky's method (Chapter 4).
$\{\delta\}$	Vector of displacement and rotation terms (chapter 4 and 5).
$\{\phi\}$	(i) eigen-vector, or (ii) a vector containing mode shape information.
Ω	Definition of measured natural frequency corresponding to 'error-based' damage identification methods (chapter 2).
θ	Whole-frame torsion mode (chapter 4).
Γ	Calculated whole-frame modal mass (chapters 4 and 5).
Π_{norm}	Normalised post-cracking bending moment (chapter 8).
$\Psi_{a,c}$	Ratios relating to the change in whole-frame modal stiffness between two modes of vibration (chapters 4 and 5).

$\Im$	Ratio of Π_{norm} to χ_{norm}.
$\Re$	Calculated whole-frame modal stiffness (chapters 4 and 5).
α	(i) Error term (chaper 2), (ii) contact ratio between the framing elements of a steel-framed building and a block-work infill wall (chapters 4 and 5).
α_m	Value of α corresponding to the measured natural frequency f_m (chapter 5).
β	A quantify used to calculate the Frequency Variation Profile (FVP) used in conjunction with the calibration process (chapters 5 and 6).
β_d	Calculated value of β corresponding to the measured natural frequency of the damaged floor slab (chapter 6).
β_m	Calculated value of β corresponding to the measured natural frequency f_m (chapter 5).
$\beta_{m,\alpha}$	Modified β_m value to take account of the added parameter α (chapter 5).
χ	Curvature.
χ_{norm}	Normalised post-cracking curvature values.
δ	Displacement (Chapter 4).
ε	(i) General term for strain (chapter 8), (ii) perturbation term (chapter 9).
ε_c	Compressive strain in concrete.
ε_{cr}	Tensile strain in concrete corresponding to f_{cr}.
ε_{ct}	Tensile strain in concrete corresponding to f_{ct}.
ε_o	Compressive strain in concrete corresponding to f_c'.
ϕ	Mode shape.
γ	A function used to adjust the characteristics of a linear visco-elastic Frequency Response Function (chapter 9).
φ	(i) Rotation (chapter 4), (ii) phase angle (chapter 9).
ϖ^2	Eigen-values calculated using Cholesky's method (chapter 4).
ω	Definition of calculated natural frequency corresponding to 'error-based' damage identification methods (chapter 2).
ω_f	Forcing frequency.
ω_n	Natural frequency of the n^{th} mode (n = 1 unless otherwise noted).
λ	Variation of α (chapter 5).

μ	(i) Modular ratio between steel and block-work (chapter 5), (ii) component in Duffing's equation (chapter 9).
μ_v	Variance error.
ρ	Degree of joint fixity (chapters 5 and 6).
ρ_d	Degree of fixity corresponding to the damaged floor slab (chapter 6).
τ_{bond}	Bond stress at the interface of steel and concrete (chapter 8).
$\tau_{initial}$	The initial value of τ_{bond} at the point at which concrete cracking commences.
υ	Poisson's ratio.
ξ	(i) An adjustment parameter used in conjunction with the calibration of measured and calculated frequencies (chapter 5), (ii) an adjustment parameter used in the calculation of tensile stress (chapter 8).
ζ	Viscous damping coefficient.
ζ_{mod}	Modified damping coefficient.
B_n	Bias error.
C	Torsion constant (chapter 6).
$D_{x,y,z}$	Displacement terms in the finite element formulation (chapter 5).
E	Young's modulus.
E_c	Young's modulus for concrete.
E_r	Maximum error term (chapter 2).
E_s	Young's modulus for steel.
F_{bond}	Calculated bond force between the interface of steel and concrete (chapter 8).
F_o	Uni-axial dynamic force magnitude calculated relative to time.
F_w	Calculated dynamic force produced by the eccentric mass excitation device when excited at a forcing frequency of ω_f.
H	(i) Building height (chapter 4), (ii) Height of block-work (chapter 5).
I	Bending inertia.
L	Length of block-work infill wall.
L_{shear}	Shear span (chapter 8).
R	Radius of curvature.
R^2	Correlation value.
$R_{x,y,z}$	Rotation terms in the finite element formulation (chapter 5).

S	Spring stiffness for use with the substitute frame method (chapter 5).
S1, S2	Concrete / steel panel references.
X	Displacement amplitude.
X_{max}	Peak steady-state amplitude at the natural frequency.
a, b and n	Constants (chapter 9).
f	Calculated fundamental frequency (chapter 4).
f_β	Calculated natural frequency corresponding to the value of β (chapters 5 and 6).
f_c	Concrete compressive stress (N/mm^2).
f_c'	Peak concrete strength ((N/mm^2).
f_{cr}	Concrete tensile strength (N/mm^2).
f_{ct}	Concrete tensile stress (N/mm^2)
f_d	Measured natural frequency obtained from the damaged floor slab (chapter 6).
f_{GRIND}	Natural frequency calculated using the GRIND program (chapters 5 and 6).
f_m	(i) Measured whole-frame natural frequency (chapter 4 and 5), (ii) measured natural frequency obtained from the undamaged floor slab (chapter 6).
f_o	Calculated fundamental natural frequency of a floor slab (chapter 6).
$f(t)$	Dynamic force with respect to time t.
$f_{x,y}$	Calculated fundamental natural frequency of a floor slab with orthotropic structural characteristics (chapter 6).
$f_{1,2,3,4}$	Calculated natural frequencies corresponding to extreme fixity conditions (chapters 5 and 6).
$f_{cu(air)}$	Concrete cube strength determined from samples cured in air.
$f_{cu(28day)}$	Concrete cube strength determined from samples cured in water at 20°C for 28 days.
$g(x)$	A trial function used to adjust the linear differential equation of the motion to match measured characteristics.
$i, j, m, n,$ q, p, r	As subscripts only: Integer values.

k_n	Modal stiffness of mode n (where n is an integer values, which can be taken as 1 unless otherwise noted) (chapter 4).
m_n	Modal mass of mode n (where n is an integer values, which can be taken as 1 unless otherwise noted) (chapter 4).
m	Modal mass (when not used as a subscript integer).
m_w	Mass on dynamic excitation device.
r	Distance from centre of rotation to centre of mass (m_w) – used in conjunction with the eccentric mass excitation device.
$x(t)$	Displacement with respect to time t.
$\dot{x}(t)$	Velocity with respect to time t.
$\ddot{x}(t)$	Acceleration with respect to time t.
x_p	Perturbed displacement solution.
x_u	Unperturbed displacement solution.
$\lvert x \rvert$	Absolute value of x, where x is a real value.

LIST OF ACRONYMS AND ABBREVIATIONS

BRE	Building Research Establishment Ltd
BSWTC	British Steel Welsh Technology Centre
COMAC	Co-ordinate Modal Assurance Criteria
DOF	Degree-Of-Freedom (also as 'dof')
EW	East West
FE	Finite Element
FFT	Fast Fourier Transform
FRF	Frequency Response Function
FVP	Frequency Variation Profile
GRIND	GRINter frame Dynamic analysis
GSA	General Structural Analysis
HPB	Half Power Bandwidth
ICL	Imperial College London
MAC	Modal Assurance Criteria
M-C	Moment - Curvature
NS	North South
PMF	Precision Metal Forming Ltd
RC	Reinforced Concrete
SODE	Second Order Differential Equation
TF	Transfer Function
mdof	Multi degree-of-freedom
sdof	Single degree-of-freedom

CHAPTER 1

Damage Identification in Engineering Structures from Changes in Measured Dynamic Response - Introduction

1.1 Foreword

In the years since this research project commenced the candidate has witnessed, albeit through the eyes of the media, a number of devastating and catastrophic structural failures that have been caused as a result of strong motion earthquakes. Some of the most recent and destructive of these, which will surely remain in the minds of the global community for many years to come, are:

- 15th June 1999, Tehuacán in México: claiming the lives of fourteen people and injuring 200.
- 17th August 1999, Izmit in Turkey: leading to the deaths of 15,000 persons and leaving over 300,000 homeless.
- 7th September 1999, Athens in Greece: resulting in 143 lives lost and causing injury to 86.
- 21st September 1999, Chi-Chi in Taiwan: claiming the lives of more than 2000 people, injuring many thousands and leaving over 100,000 homeless.

The loss of human life caused by these devastating events are often the result of structural failure induced by the earthquake, which in many cases has been related to poor workmanship and unseen defects [Earthquake Engineering Research Institute (2000)]. These factors are a reminder of how engineers and scientists have a responsibility of ensuring that the most appropriate and up-to-date knowledge of structural behaviour is disseminated and applied to the developments of new buildings and bridges in earthquake affected areas.

Not withstanding the importance of new development in these situations, there is also a need to ensure that on-going defects, which could be caused by earthquakes, are recognised. Indeed, a larger emphasis is always placed on preservation of infrastructure after such events, which is often assessed on a visual basis to compile comprehensive reports that are used to identify re-development cost.

1.2 The Present Research

The above discussion has identified one situation where defects in buildings and problems relating to substandard construction practices could have an influence on the integrity of a structure and its overall performance. However, methods of identifying defects and structural weaknesses that occur, either as part of natural deterioration or as a result of short-term specific events such as earthquakes, usually rely on visual inspection, which can be time-consuming and in some cases inaccurate. The latter point being particularly true for instances when defects occur within the fabric of structural members.

This research project was initiated due to the necessity of offering engineers a more reliable and time efficient means of identifying if such defects exist in a structure. The aim of the work is to establish whether measurements of vibration can be used to yield information concerning the condition of a structure, as a whole and on an individual member basis. The identification method is intended to be completely non-destructive. To identify the damage, the main assumption is that the affected parts will have an influence on stiffness characteristics, which in turn will change the dynamic behaviour of the structure in question. This is possible due to the relationships that exist between the stiffness, mass and natural frequency, and the method of damage identification performed in this way seeks to correlate physical alterations to changes that may be observed in measured dynamic response information.

An example of studies that have adopted this approach was reported by Adams *et al* (1975), these authors being among the first to consider its use. As such the method itself is not new, and since the aforementioned study, other authors have considered the approach applying its principles mainly within mechanical engineering disciplines. However, although there is now a considerable volume of supportive published research material available on this subject, its applicability to the field of civil and structural engineering remains relatively unexplored.

To investigate its application to the latter, this study will focus on the dynamic characteristics of an eight-story steel-framed building considering its whole-frame and

sub-element behaviour before and after deliberate structural damage. The above building was constructed within the Large Building Test Facility (LBTF), Cardington, UK, which is a laboratory environment used especially for the testing of buildings, and is managed by the Building Research Establishment Ltd (BRE). The facility houses a number of multi-storey structures that have been made from a variety of construction materials, each building being used for a wide range of research projects.

Principally, the current research will consider the following:

(i) Use measurements of structural vibration to determine the natural frequency, damping and mode shape characteristics of the building and certain parts of its elements. This will be conducted in three stages, treating the building at different levels of structural complexity.

(ii) Using (i) above, establish if structural defects can be identified from changes in the aforementioned characteristics, after situations of damage, and provide evidence to support (or otherwise) its effectiveness.

(iii) Identify the dynamic characteristics that are sensitive to the changes that occur to structural components as a result of damage.

With this information, conclusions will be drawn regarding the applicability of the method with the aim of promoting its use as a non-destructive approach to damage assessment and the on-going performance monitoring of building structures.

1.3 Synopses of the Studies Ahead

Chapter 2 introduces the philosophy of using dynamic characteristics to identify damage and gives a review of work that has been published over the past three decades on research carried out in this area. Although prepared to identify the main contributors to the subject area, the chapter also reflects on the methodologies that have emerged and identifies the assumptions and approach that are carried forward throughout the subsequent chapters of this thesis. The chapter draws attention to a number of numerical methods that have been proposed to identify damage, but also

comments on the practicality of these methods, which aim to correlate 'perfect' mathematical solutions with the 'in-perfect' behaviour of real structures.

Chapter 3 outlines the methods that have been adopted by other authors to determine the dynamic characteristics of structures from measurements of vibration response. Highlighting the most frequently adopted vibration measurement techniques, which includes a discussion of the methods used to induce vibration motion, this chapter describes the procedures that were used to determine the required information for the studies presented in subsequent chapters. To complete the chapter, a list of equipment used together with a specification is included, which outlines a standardised test set-up adopted for all vibration measurement work in this study.

An important aspect of damage identification, which is based on an interpretation of vibration response, is the need to be able to relate observed dynamic characteristics to the actual physical properties of the structure. Chapter 4 commences the main work by presenting the results of studies carried out on two numerical models, which were prepared to simulate the whole-frame dynamic behaviour of the 'as-built' eight-storey building. By comparing calculated and measured natural frequencies, the chapter shows that differences can arise, which are not necessarily easy to justify. This identified the first problem, i.e. the problem of diagnosing reasons for the discrepancies regularly found to exist between measured and calculated dynamic characteristics of large structures – even when damage is known not to be present.

To overcome the problems identified in chapter 4, a calibration methodology is presented in chapter 5, which allows the cause of such discrepancies to be identified. Using a computer model and a calibration procedure compiled by the candidate, the chapter shows how certain aspects of the structural behaviour of the building can be examined to identify their more probable characteristics. A calibrated model of the structure is then presented that reflects the properties of the building using natural frequencies and mode shapes obtained from measurements. The chapter finally concludes with a discussion on the practicality of using the proposed method to identify damage from whole-frame dynamic characteristics.

In chapter 6 the study is continued by applying the formulated calibration methodology for identification of damage in one of the steel and concrete composite floor within the eight-storey building. Using response measurements taken from the floor, the chapter describes the calibration procedures used to obtain accurate calculated natural frequencies and mode shapes relating to the pre and post-damage condition of a given floor. Then, by comparing the results obtained from the calibrated models, conclusions are drawn regarding the extent of the damage, which is identified using a scalar quantity produced from the calibration procedure.

Chapter 7 examines in detail the influence of damage on the dynamic characteristics of local representative panels of the floor slab studied in chapter 6. The study, which focuses on the results of static and dynamic tests obtained from a comprehensive laboratory programme carried out at the University of Glamorgan, shows that the dynamic characteristics, natural frequency and damping, can be used to identify the on-set of damage in structural elements. Considerable emphasis has also been placed on the amplitude dependency of the aforementioned characteristics and how the latter relates to the amount of imposed damage. To obtain this information, a combination of impact and steady-state load situations were used, from which transient response, decay-of-vibration and frequency response functions were determined. Static loads were applied to the panels to induce controlled damage. The extent of degradation was ultimately assessed using information drawn from moment-curvature relationships that were prepared using measured strain and displacement data. With this information, a comparison between the static load and dynamic load data was compiled, from which conclusions were drawn regarding the effectiveness of the damage identification proposals.

Chapter 8 presents a study that was undertaken to confirm the mechanisms responsible for the induced 'damage' observed from strain and displacement data. This work was undertaken to strengthen the assumption proposed in chapter 7 that the panel damage was the result of concrete cracking. Using a number of numerical studies, the chapter shows how a range of constitutive material models were used to provide an accurate representation of the panel through applied load conditions. To achieve the latter, a computer program was prepared by the candidate, which allowed additional behaviour

characteristics to be studied relating to the steel-concrete interaction. The result was a model that was found to predict the static load behaviour of the panels, from which the existence of the induced damage was confirmed.

Chapter 9 proposes a mathematical model that matches the non-linear frequency response characteristics of the damaged panels found from measurements. The study offers a method that could be used as an additional means of identifying the on-set of damage, which is found to indicate the progressive nature of the defects induced applying the static load.

Chapter 10 contains the conclusions drawn from the study, and offers recommendations for future work.

Finally, appendices have been included that contain:

Appendix A: The rationale of modal testing and the methods adopted to determine the natural frequency and damping of all the structural parts considered in this thesis.

Appendix B: Data relating to the construction of the eight-storey steel-framed building, which identifies the structural members and geometry of the building in its 'as-built' condition.

Appendix C: Data from the laboratory tests conducted as the University of Glamorgan, which supports the information given in chapter 7.

Appendix D: Contains a list of the published papers and other activities prepared by the candidate and the research team.

CHAPTER 2

Damage Identification in Engineering Structures from Changes in Measured Dynamic Response – A Review of Literature

2.1 Introduction

"Damage (a) detection, (b) identification and, (c) location. (i) Non-destructive evaluation, and, (ii) system identification".

The above are some of the key words used to describe a non-invasive technique for the identification of changes that may exist in a structural system, due to damage or degradation, from studies carried out on measured dynamic characteristics. In general terms, the method is based on the assumption that if these characteristics show patterns of change over time, physical alterations – possibly linked to damage – could be the cause.

The approach is logical and is based on the knowledge that the dynamic characteristics of a structure – natural frequency(ies) and mode shape(s) – depend on properties of stiffness, mass and system geometry. Should any of these properties alter, the dynamic characteristics would also indicate some change. And, as the aforementioned characteristics can be determined from measurements of the vibration response of a structure [see Ewins (1984), McConnell (1996)], it should be possible to identify damage, which may have altered the properties of the structure, providing an inexpensive and convenient damage identification tool.

This chapter provides a review by discussing a number of reports that have been published to investigate and promote the application of this damage detection approach. From the reviewed literature, two categories of research have emerged, which can be classified under the following headings:

(i) Methods based on combined studies of measured vibration response signals and analytical models of structures: Within this category, the usual approach is to form a numerical model of the structure – usually with the Finite Element (FE)

method – the dynamic analysis solution of which is compared to characteristics determined from vibration measurements. To identify (and sometimes locate) damage, a representative set of defect scenarios are considered analytically until a match with the characteristics from measurements is obtained. The scenario that gives analytical results to match the measurements is then chosen as being the most probable cause of damage. Alternatively, instead of considering a representative set of possible damage sites manually, methods has been proposed that aim to automatically 're-generate' analytical models using measured vibration information. The latter aiming to produce a 'best-fit' numerical representation of the damaged structure, from which the defects can be identified qualitatively.

(ii) Methods based on continual appraisal of vibration response measurements: Unlike the previous category, the methods that fall into this grouping generally aim to identify damage from comparisons made between measurement taken either (a) from a large number of similar structures, or (b) measurements of a single structure over frequent intervals of time. Both these approaches aim to identify damage from differences between successive measurements, thereby defining damage quantitatively.

2.2 Damage Identification using Numerical Models of Structural Behaviour

Damage identification using numerical models of structural behaviour have developed over a period of approximately three decades. A common theme throughout these methods is the reliance on FE analysis where it is assumed that a structure can be represented in numerical form using, for example, theories based on the 'stiffness matrix' approach [Ghali and Neville (1989)]. The differences between variants of the methods stem from the methodology used to determine a numerical representation of the structural damage.

2.2.1 Methods based on 'error minimisation' or 'maximisation' principles

2.2.1.1 Method by Cawley and Adams

Adams *et al* (1975) and Cawley and Adams (1979) considered the damage identification problem as one involving small change to the natural frequencies of a structure. Adopting the stiffness matrix approach (neglecting damping), these authors modified the eigen-value problem [Meirovitch (1986)], to give,

$$\{([K]+[\delta K])-([\Omega]^2+[\delta\Omega]^2)([M]+[\delta M])\}(\{\phi\}+\{\delta\phi\})=0 \qquad (2.1)$$

where $[K]$ and $[M]$ are the stiffness and mass matrices of the structure in question respectively, and the inclusion of δ denotes small change (perturbations) to the matrices in the presence of damage. $[\Omega]^2$ and $\{\phi\}$ are the eigen-values in matrix form and the eigen-vector respectively. Manipulating eqn.(2.1), and assuming the mass properties of a structure are not altered, Cawley and Adams (1979) proposed that the amount by which the natural frequency of a structure changed (as a result of damage) could be determined using,

$$\{\phi\}^T[\delta K]\{\phi\}-[\delta\Omega]^2\{\phi\}^T[M]\{\phi\}=0 \qquad (2.2a)$$

where

$$[\delta\Omega]^2=\frac{\{\phi\}^T[\delta K]\{\phi\}}{\{\phi\}^T[M]\{\phi\}} \qquad (2.2b)$$

and normal matrix operations apply. Using these expressions, the above authors found that changes observed to the natural frequency $[\delta\Omega]^2$ of a structure from measurements could by used directly to calculate stiffness change $[\delta K]$. The calculated stiffness change could then be compared to analytically based scenarios of damage to identify the most probable cause and location. However, the authors were quick to point out that eqn.(2.2b) has many solutions that depend on the number of natural frequencies, which even if successfully measured, could lead to erroneous damage identification when limited information was available.

In an attempt to reduce possible errors, the aforementioned authors discovered a relationship between damage extent (and location) and the natural frequency of any two-vibration modes. The above authors also noticed that localised stiffness changes in a structure influenced individual natural frequencies is a unique way, which could be evaluated numerically from a ratio between two vibration modes. The method still relied on the numerical analysis of possible damage scenarios, but an 'error location technique' was derived to identify the 'maximum error' between the calculated and measured frequency changes in the vibration modes being considered. This approach was called a 'sensitivity' method and was based on a parameter that examined the 'sensitivity' of vibration modes (i.e. mode susceptibility to change under certain damage conditions) given by,

$$e_{rij} = \left[\frac{\left\{ \frac{s_{ri}}{s_{rj}} \right\}}{\left\{ \frac{\delta\Omega_i}{\delta\Omega_j} \right\}} \right] - 1, \text{ when } \left\{ \frac{s_{ri}}{s_{rj}} \right\} \geq \left\{ \frac{\delta\Omega_i}{\delta\Omega_j} \right\} \tag{2.3a}$$

and

$$e_{rij} = \left[\frac{\left\{ \frac{\delta\Omega_i}{\delta\Omega_j} \right\}}{\left\{ \frac{s_{ri}}{s_{rj}} \right\}} \right] - 1, \text{ when } \left\{ \frac{s_{ri}}{s_{rj}} \right\} < \left\{ \frac{\delta\Omega_i}{\delta\Omega_j} \right\} \tag{2.3b}$$

where s_{ri} and s_{rj} are the sensitivity of mode i and j respectively to changes (damage) at location r; $(\delta\Omega_i)$ and $(\delta\Omega_j)$ are the change in the i^{th} and j^{th} natural frequencies obtained from measurements. The most probable damage was then defined when the total error, E_r, was at a maximum, which was calculated using,

$$E_r = \frac{100 e_{\min}}{e_r}, \text{ where } \quad e_r = \sum e_{rij} \tag{2.4}$$

and $e_{\min}$ is the minimum e_{rij} value. Since these proposals, a number of other authors have suggested methods that rely on similar basic principles. Hearn and Testa (1991), for example, proposed a method for the detection of damage in frame structures

reducing the reliance on the overall structure by representing the stiffness problem [eqn.(2.2a)] in terms of individual member matrices. Applying the method to truss and frame type structures, the authors found that the computational demand was significantly less than the original Cawley and Adams (1979) method proving that eqn.(2.2a) could be written as,

$$[\delta\Omega]_i^2 = \frac{\{\phi_N\}_i^T [\delta k_N] \{\phi_N\}_i}{\{\phi_N\}_i^T [M] \{\phi_N\}_i} \tag{2.5}$$

where $\{\phi_N\}_i$ and $[\delta k_N]$ relate to the i^{th} mode shape and stiffness change respectively of the N^{th} member. Adopting the philosophy that damage is unique to the ratio of change in two mode frequencies, and presenting $[\delta k_N]$ as a scalar quantity $\alpha_N [k_N]$ that was eventually eliminated, then gave,

$$\frac{[\delta\Omega]_i^2}{[\delta\Omega]_j^2} = \frac{\left[\dfrac{\{\phi_N\}_i^T [k_N] \{\phi_N\}_i}{\{\phi_N\}_i^T [M] \{\phi_N\}_i}\right]}{\left[\dfrac{\{\phi_N\}_j [k_N] \{\phi_N\}_j}{\{\phi_N\}_j^T [M] \{\phi_N\}_j}\right]} \tag{2.6}$$

Messina *et al* (1996) also chose to modify the original Cawley and Adams (1979) method by introducing, what the authors termed, a 'Damage Location Assurance Criterion (DLAC)' written as

$$|DLAC(s)| = \frac{\{\delta\Omega\}^T \{\delta\omega\}_s^2}{[\{\delta\Omega\}^T \{\delta\Omega\}][\{\delta\omega\}_s^T \{\delta\omega\}_s]} \tag{2.7}$$

where $\{\delta\Omega\}$ is a vector of measured natural frequencies, and $\{\delta\omega\}_s$ is the same modal frequencies predicted by analysis assuming damage at location s.

2.2.1.2 Methods by Friswell et al

Friswell *et al* (1994) later supported by Penny *et al* (1993) and Salawu (1997) questioned the sensitivity approach proposed by Cawley and Adams (1979) stating that it '...lacked predictive quality'. These authors proposed that a more accurate prediction of possible damage could be gained if the error were calculated using a linear function having the form,

$$\log_e\left(\frac{\Omega_i}{\Omega_j}\right) = \log_e(\alpha) + \beta_1 \log_e\left(\frac{\omega_{p_i}}{\omega_{p_j}}\right) + \varepsilon \tag{2.8}$$

where $\frac{\Omega_i}{\Omega_j}$ is a ratio of the measured frequencies (before and after damage being i and j respectively) and $\frac{\omega_{p_i}}{\omega_{p_j}}$ is a ratio of the calculated frequencies (predicted with an analytical model before and after damage) incorporating assumed scenarios of damage located at position p within the structure. ε was denoted as being an 'error quantity' whose properties were related to the 'variance and covariance' of the measured frequency values. To signify an exact prediction of damage, the calculated parameters of α, β_1 and ε would be determined as unity, deviations from which suggesting that further modification to the assumed damage extent / location would be required.

Friswell *et al* (1996) later considered damage detection as a process involving 'natural selection' or 'generic processes'. Using a 'penalty function' approach, this report explored the possibility of identifying errors between calculated and measured modal properties of individual modes, as opposed to the 'modal pairing' outline above. The aim of the damage location process was the calculation of an error function, given by

$$J = W_\omega J_\omega + W_\phi J_\phi + W_s \delta_s \tag{2.9}$$

where W_ω, W_ϕ and W_s are 'weighting factors' and J_ω and J_ϕ were 'frequency and mode shape error functions' defined by,

$$J_{\omega} = \sum_{i=1}^{n} \left(\frac{\Omega_i^{\,2} - \omega_i^{\,2}}{\Omega_i^{\,2} + \omega_i^{\,2}} \right)^2 \tag{2.10}$$

$$J_{\phi} = \sum_{i=1}^{n} \left(\{\phi\}_{mi} - \{\phi\}_{ci} \right)^T \left(\{\phi\}_{mi} - \{\phi\}_{ci} \right) \tag{2.11}$$

where n = 1, 2, 3, ..., number of modes used in the calculations. In these equations, Ω_i and ω_i are the calculated and measured natural frequencies of mode i, while $\{\phi\}_{mi}$ and $\{\phi\}_{ci}$ are the corresponding measured and calculated normalised mode shape respectively. δ_s in eqn.(2.9) was used merely as a switch to limit the growth of the overall expression (i.e. a dirac delta function) in the event that more than one damage site was present in the structure. The aim was then to minimise eqn.(2.9) providing a best-fit between the measured and calculated data. This was achieved using a 'generic algorithm', which was discussed in detail by Friswell *et al* (1995) and is similar in principle to other minimisation techniques such as the root-mean-squared approach.

Cases and Aparicio (1994) also proposed a simpler version of this technique maintaining similar minimisation principles between calculated and measured properties determined using,

$$J = \sum_{i=1}^{n} [\Omega_i - \omega_i]^2 + \sum_{l=1}^{m} \sum_{i=1}^{n} [\{\phi\}_{mi}(l) - \{\phi\}_{ci}(l)] \tag{2.12}$$

where Ω_i and $\{\phi\}_{mi}(l)$ are measured natural frequency and mode shape respectively, and the corresponding calculated properties are ω_i and $\{\phi\}_{ci}(l)$. In eqn.(2.12) r is as noted above, while l refers to localised parts of the structure, which may comprise a number of sub-elements (i.e. m elements). Damage was then identified from numerical models of assumed damage, following a similar approach to the method of the previously cited reports.

2.2.1.3 Method by Zimmerman et al

Zimmerman and Kaouk (1992), and Zimmerman *et al* (1995a & b) followed closely the proposals of Cawley and Adams (1979), but instead of relying on the modal pairing philosophy, these authors showed that,

$$d_i \equiv ([K]-\omega_i{}^2[M])\{\phi\}_i = ([\delta K]-\omega_i{}^2[M])\{\phi\}_i \equiv [Z]_i\{\phi\}_i \qquad (2.13)$$

where ω_i and $\{\phi\}_i$ are the measured i^{th} natural frequency and corresponding mode shapes respectively, taken from the damaged structure, and d_i was termed the 'damage vector'. The advantage of this approach over modal pairing was that the damage could be located using the matrices of the undamaged structure without modification, i.e. the original $[K]$ and $[M]$ matrices prepared for the undamaged structure. To locate the damage an 'error maximisation technique' was used, given by

$$d_i{}^j = \| z_i{}^j \| . \| \phi_i \| \cos(\alpha_i{}^j) \qquad (2.14)$$

where $d_i{}^j$ is the j^{th} component of the damage vector d_i, with $\| z_i{}^j \|$ and $\| \phi_i \|$ being the row norms of $[Z]_i$ and $\{\phi\}_i$ respectively. $\alpha_i{}^j$ is a rotation angle between $\| z_i{}^j \|$ and $\|\phi_i\|$, which deviates from 90° if the d_i vector contains error, which in turn is used to signify damage.

2.2.3 Methods based on 'correlation' principles

2.2.3.1 The 'MAC' and 'COMAC' approach

The identification of damage from measured mode shapes using the Modal Assurance Criterion (MAC) and the Co-ordinate Modal Assurance Criterion (COMAC), or variations thereof, have been proposed by a number of authors. The methods stem originally from the usual practice of correlating calculated mode shapes (obtained from FE analysis for example) and measurements, which aimed to validate the accuracy of analytical models. In simple terms, the MAC and COMAC are indices

that allow the correlation of two mode shapes to be determined using a numerical quantity as the indicator. These data can relate to single (MAC) or multiple (COMAC) modes of vibration, which were proposed by Allemang and Brown (1983) and Lieven and Ewins (1988)] respectively as,

$$\left|MAC(\{\phi\}_u,\{\phi\}_d)\right| = \frac{\left|\{\phi\}_u{}^T\{\phi\}_d\right|^2}{(\{\phi\}_u{}^T\{\phi\}_u)(\{\phi\}_d{}^T\{\phi\}_d)} \tag{2.15}$$

$$\left|COMAC(\{\phi\}_u,\{\phi\}_d)\right| = \frac{\sum_{i=1}^{n}\left[\{\phi\}_{u_i}\{\phi\}_{d_i}\right]^2}{\sum_{i=1}^{n}\{\phi\}_{u_i}{}^2\sum_{i=1}^{n}\{\phi\}_{d_i}{}^2} \tag{2.16}$$

where $\{\phi\}_u$ and $\{\phi\}_d$ are vectors containing the mode shape corresponding to the undamaged and damaged structure respectively. It is seen from these expressions that the MAC and COMAC can be used to indicate the change between mode shapes measured from a structure suspected of being damaged. The results is an index ranging from a value of unity (for a perfect fit – representing no change and thus no damage) to a value less than one if damage is present. Therefore, in theory, the amount of the deviation from unity will signify the severity of damage.

2.2.3.2 Modified 'MAC' methods

Variations to the original MAC and COMAC coefficients have been proposed by Meneghetti and Maggiore (1995) where a Local Modal Stiffness Sensitivity (LMSS) expression was formulated to relate ratio changes in measured natural frequencies of a damaged structure to those obtained when no damage was present. Shi *et al* (1998) used similar principles to quantify damage in framed structures from changes in modal strain energy. A single expression termed the 'Modal Strain Energy Change Ratio (MSECR)' was proposed and used to provide an indication of the deviation of the strain energy in a structure before and after damage.

Pandey *et al* (1991) considered a theory termed the 'curvature mode shape' technique, which was devised to offer an alternative to the MAC. The method was based on the assumption that structural damage could be detected from curvature increases at the location of the defect. The method was shown to be more sensitive to damage compared to an assessment made using mode shape changes from the MAC ratios. However, the proposals depended on the acquisition of curvature information from a vibrating structure, which may in practice be difficult to achieve.

Samman and Biswas (1994a) also proposed an adjustment to the basic MAC and COMAC equations where measured response signatures of acceleration or velocity were used instead of mode shape information. These adjusted formulations were termed 'Signature Assurance Criterion (SAC)' and 'Cross Signature Assurance Criterion (CSAC)' and were based on a similar ratio quantity as portrayed by the MAC and COMAC.

2.2.4 Methods based on 'stiffness matrix adjustment'

The methods that are based on 'stiffness matrix adjustment' differ from the previous approaches in that the aim is usually to calculate the properties of a damaged structure directly from vibration response measurement. The philosophy is to numerically 're-generate' the characteristics of a structure using principles similar to the FE method involving matrix-based analysis. The difference between this and the previous methods is that the numerical quantities within the structure matrices are allowed to 'search' for a solution that best suits the measured values. By releasing the numerical quantities of the matrix elements from the strict formulation of the FE method, and allowing a solution to be obtained for the stiffness matrix using measured vibration data, damage is determined relative to 'adjusted' stiffness properties.

The essence of the matrix adjustment approach was demonstrated by Agbabian *et al* (1991) where time-domain velocity response data was used to re-generate the stiffness matrices of a framed structure. The method invoked conventional principles of structural dynamics [as Meirovitch (1986) for example] to describe the motion of a structure during vibration using a multi-degree-of-freedom (mdof) model given by,

$$[C]\dot{x}(t)+[K]x(t)=f(t)-[M]\ddot{x}(t) \tag{2.17}$$

where $[C]$ and $[K]$ are damping and stiffness matrices respectively, and $f(t)$ represents the forcing function applied to the structure to induce excitation. $x(t)$ is displacement with respect to time, and the dot notation indicates differentiation with respect to time. To calculate the structural damage, eqn.(2.17) was considered in a form given by the above authors as,

$$[R]\{\alpha\}=\{b\} \tag{2.18}$$

where $[R]$ is a matrix, the elements of which define the response of the structure with time, and $\{b\}$ and $\{\alpha\}$ are vectors containing vibration response measurements and the unknown structural stiffness values respectively. Based on eqn.(2.18), a solution was obtained using Gaussian distribution [see Press *et al* (1992)] and probability density functions [see Weltner *et al* (1986)], which aimed ultimately to estimate the most probable damage sites utilising a given volume of response measurements in $\{b\}$. The method was demonstrated on a system comprising 6 dof's where '...600 separate non-overlapping response signals...' were required to successfully re-generate the stiffness matrix of the damaged structure. However, the response measurements themselves were calculated from a theoretical model of the structure using the FE method, which makes it difficult to interpret the true accuracy of the method suggested from the example used for the demonstration.

The previous example highlights the main problem associated with matrix updating in that a large amount of data is often needed before a reliable assessment of damage is achieved. To reduce the reliance on this laborious process, updating algorithms have evolved that aim to recognise the most probable damaged locations in the structure by introducing additional algorithms into the solution process. With these additional features in place, the usual approach is to concentrate on localised parts of the system matrices using an FE model of the original (un-damaged) structure as a commencing point. Gudmundson (1982), Salane and Baldwin (1990), Friswell and Penny (1992), Zhang *et al* (1994), Stubbs *et al* (1995) and Crema *et al* (1995) have all reported on

such an approach (offering slightly different methodologies) that aim to increase accuracy and reduce the amount of response data needed to identify the damage.

Other approaches include Ahmadian *et al* (1996) where sub-structuring procedures were used to concentrate the adjustment on localised parts of the stiffness matrix. And Friswell *et al* (1997) proposed a rigorous 'mathematical approach' to this philosophy using a 'parameter subset selection technique'.

2.2.5 Methods based on numerical modelling of the damage

A number of approaches have emerged that aim to evaluate the influence of incorporating a model of the damage into the behavioural predictions determined from conventional analysis (FE being one example). The philosophy within this group of damage identification methods is to replicate the vibration behaviour of the damage in a numerical way and examine its influence on the overall structure. By varying the extent and location of the damage, calculated and measured response information is compared to determine the most likely solution. The basic approach is therefore similar to previously cited methods, but the difference stems from the manner in which the damage itself is modelled.

2.2.5.1 Methods based on modify FE analysis

Hu and Liang (1993) adjusted the conventional FE formulation of a prismatic beam element [see Zienkiewicz (1977)], by simulating damage (in this case cracks) as infinitesimal springs. The method was used to compare measured and predicted natural frequencies and their corresponding mode shapes, which were compared with measured properties in an attempt to locate damage. The authors claimed success in the method, showing that frequency and mode shape change, which occurred after situations of inflicted damage (deliberate saw cuts) could be detected.

Krawczuk (1992) had earlier proposed a 'cracked Timoshenko beam element', which could be used for vibration analysis. Introducing flexibility terms into the formulation, a 'Timoshenko beam' was used to model non-propagating cracks positioned at the

mid-point of the member. Natural frequencies and mode shapes were calculated to correspond to various crack depths to demonstrate the amount by which these characteristics would change. Chondros and Dimarogonas (1998) considered a similar refinement to this method proposing a modified '...Euler-Bernoulli beam formulation...' as the basis that would allow single and double-edge cracks to be incorporated. Calculations of vibration response prepared for short aluminium bars of varying lengths containing deliberate saw cuts gave predicted behaviour that was said to compare well with measurements. Ruotolo *et al* (1996) also derived a model for the analysis of cracked (damaged) cantilever beams, which could predict harmonic vibration taking account of the '...opening and closing...' of the damage during vibration. The formulation was based on an Euler-beam FE, which had two dofs at each node allowing transverse displacement and out-of-plane rotation to be calculated. Mannan and Richardson (1990) and Brandon and Mathias (1995) have also conducted similar studies of this type.

It should be noted, however, that in all the aforementioned cases, the test structures used to trial the methods were basic (short steel rods and cantilevers for example) with its application to larger elements not being reported.

2.2.5.2 Method based on constitutive material models of damage

Studies have also focused on the dynamic behaviour of damaged structural materials. These formulations are usually termed 'dynamic damage constitutive models', which aim to relate the degradation of material strength with their influence on the vibration characteristics in the structure. Qingbin *et al* (1996) proposed such a method where 'damage variables', obtained from stress-strain relationships of concrete in uni-axial tension, were used to predict the level of excitation at which damage would occur in concrete beams. Oller *et al* (1996) proposed a similar method, but concentrated on constitutive models on fibre reinforced composite materials offering several relationships to obtain the elasto-plastic behaviour of the material. Again, the method aimed to predict the onset of damage under low frequency uni-axial load.

Hu and Liang (1993), later improved by Peng and Fang (1997), formulated constitutive models for the analysis of elasto-plastic materials where material characteristics were included in the predictive model. The latter author, focusing on uni-axial cyclic load, proposed a '...thermo-mechanically consistent continuum damage model...'. The formulation used '...deviatoric and volumetric...' stress-strain relationships to predict the strength degradation of concrete subjected to amplitude varying low frequency load.

2.2.6 An example to demonstrate the application of selected damage identification methods cited above

2.2.6.1 A hypothetical problem

A cantilever of constant stiffness, mass and elastic modulus of unit length, L, is shown in Figure 2.1 together with its finite element model counterpart. The cantilever model comprises 10 uniform elements connected by 11 nodes. To restrict the size of the problem the nodal degrees-of-freedom (dof's) have been limited to translation and rotation out-of-plane to the cantilever length. The result is a structure with 20 dof's with lumped masses assigned to each node, while all dof's are restrained at the support node to simulate a fully fixed case. Therefore, each node has 2 dof's numbered sequentially starting at node 1 nearest to the support. The task is to locate the presence of damage within the length of the cantilever.

2.2.6.2 Solution using the Cawley and Adams (1979) proposals

Damage was simulated by imposing a 10% reduction in flexural rigidity (EI) at element number 6 (see Figure 2.1) resulting in a change to the rotational stiffness in the cantilever model at nodes 6 and 7. Assuming that the mass properties of the structure are unaffected by these alterations, the natural frequency change of the first eight modes was calculated. Equations (2.3a & b) and (2.4) gave the results shown graphically in Figure 2.2. In Figure 2.2, it is should be noted that damage is identified as being coincident with the point were maximum calculated error – 'E_r' is found. Thus, an error value $E_r = 100(\%)$ is a perfect identification of the damage location, the

latter being relative to the element layout and numbering system adopted for the numerical model. In addition, the likelihood of identifying the location of the damage increases as more modes of vibration are considered, which allows the relationship between a greater number of 'mode pairs' to be treated. The terminology 'mode pair' is a reflection on that used in the publications that have considered this approach, i.e. Cawley and Adams (1979) for example, and relates to calculations performed using any two mode shape data sets. [See eqns.(2.3a), (2.3b) and (2.4) for the relevance of the mode pairing approach].

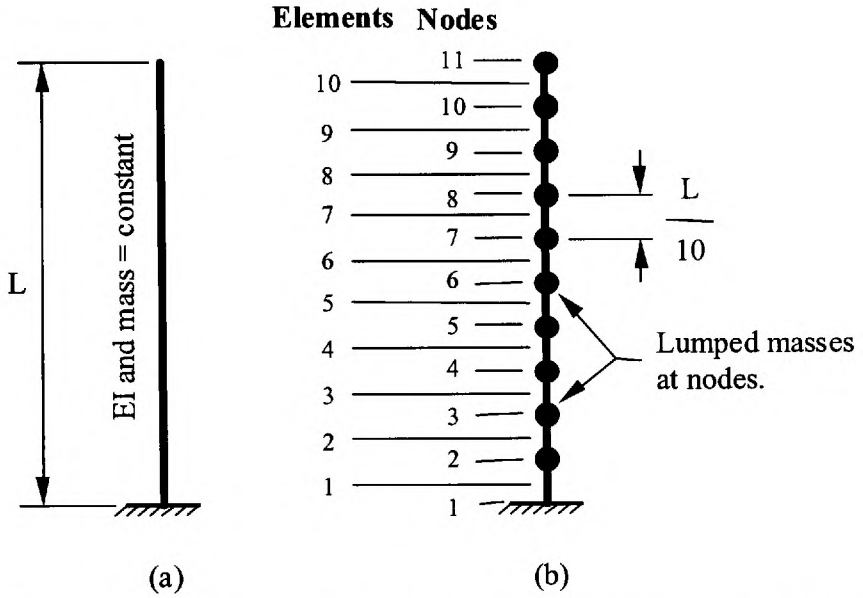

Figure 2.1 – Diagrammatic illustration of (a) a cantilever structure and (b) its FE model.

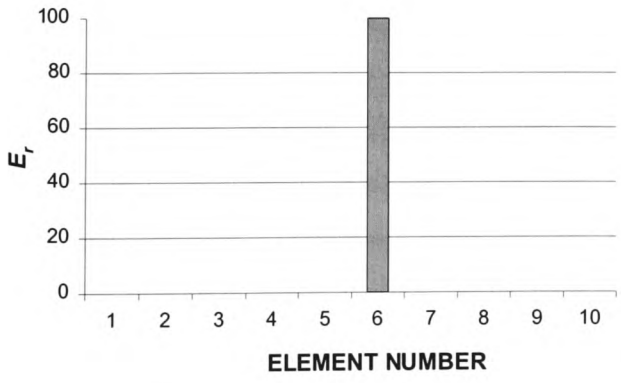

Figure 2.2 – The location of damage in a cantilever structure assuming an exact simulation of the defect has been found (8 mode pairs considered).

It is seen from Figure 2.2 that the method has successfully predicted the location of the damage by correctly identifying the maximum error, E_r, as being at element number 6. This was found from calculations prepared using eight 'mode pairs' (i.e. the pairing of mode 1 with modes 2 to 9 inclusive), the mode shape results of which being determined assuming that damage was a 10% stiffness reduction at element number 6.

Figures 2.3(a) and (b) illustrate the calculated error E_r for the same problem assuming that the damage extent was not correctly specified in the analysis. To calculate E_r in this case, it was assuming that the damage could be represented as a 5 and 15% reduction in stiffness at element number 6 (i.e. different from the actual damage), the results of which being indicated in Figures 2.3(a) and (b) respectively. In both cases, element 6 is highlighted as the damaged member, which is a correct identification. But, the figures also show that marginal damage could be present in all other elements. This can still be regarded as a successful detection of the damage, as the error E_r associated with element number 6 dominates. However, if the amount of mode pairs considered in the calculation of E_r is reduced, (i.e. reducing the amount of available data on the damaged structure) a misleading representation of the damage emerges. An example of the latter is given by Figure 2.4 where the calculated values of E_r based on one mode pair (i.e. mode 1 and mode 2) are illustrated.

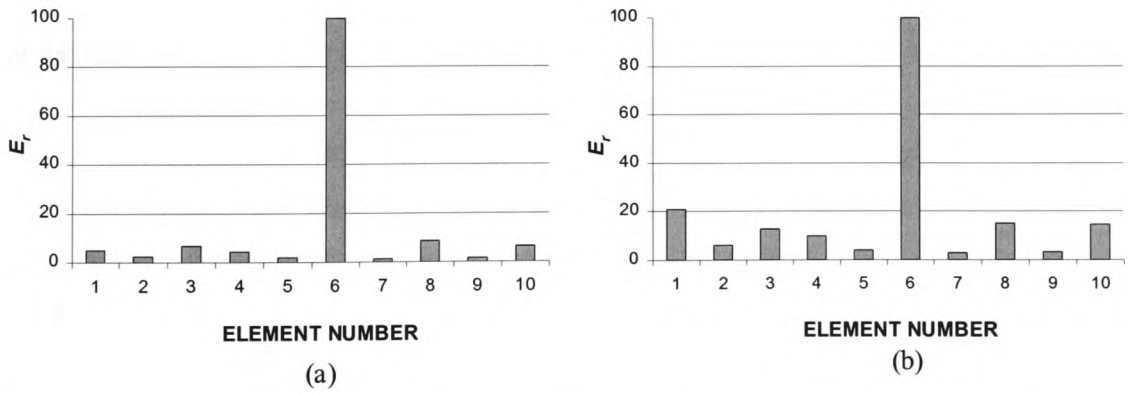

Figure 2.3 – Damage location within the cantilever with (a) 5% stiffness reduction and (b) 15% stiffness reduction at element number 6 to representing damage (8 mode pairs considered).

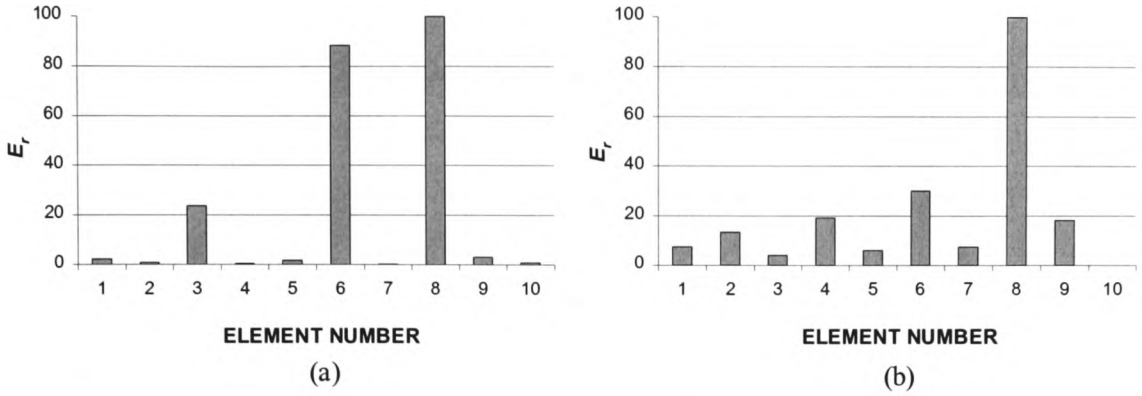

Figure 2.4 – Damage location within the cantilever with (a) 5% stiffness reduction and (b) 15% stiffness reduction at element number 6 to representing damage (one mode pairs considered).

2.2.6.3 Solution using the approach of Zimmerman et al

Using the example set out above, the solution to eqn.(2.14) with correct interpretation of the damage (i.e. 10% stiffness reduction) gave the results illustrated graphically by Figure 2.5. However, introducing a similar misrepresentation of the damage as considered in the previous example [i.e. assuming a 5% stiffness reduction - see Figures (2.3(a) only] the error, α, presented by Figure 2.6 illustrates that the location of the damage is no longer clearly defined.

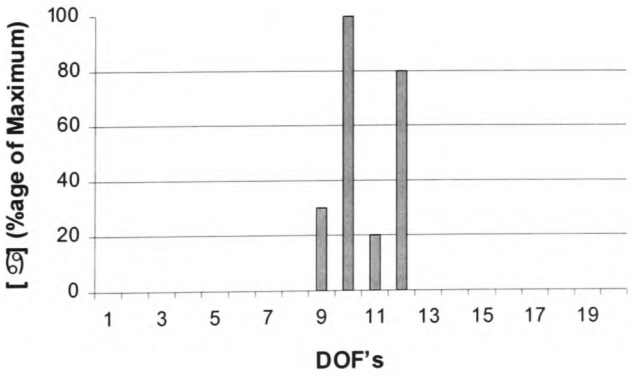

Figure 2.5 – Damage detection assuming perfectly captured modal properties from the damaged cantilever (Based on 1st mode results).

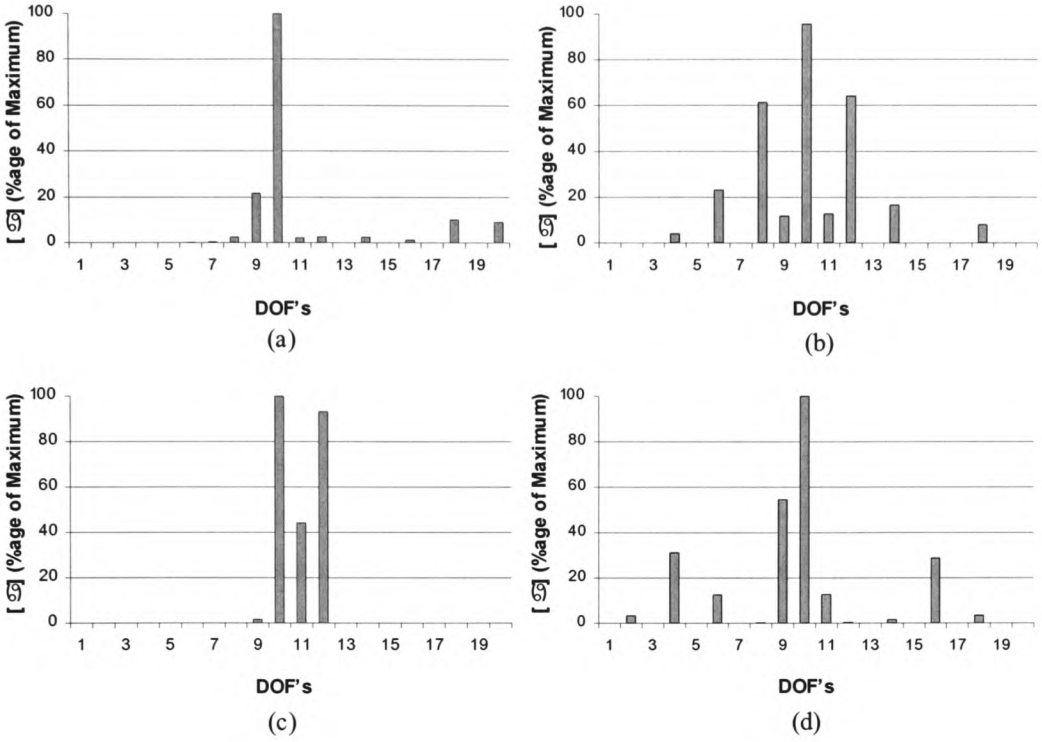

Figure 2.6 – Damage detection assuming 5% stiffness reduction in the mode shape measurements, using data from (a) 1st mode, (b) 2nd mode, (c) 3rd mode, and (d) 4th mode.

2.2.6.4 Discussion

These simple examples highlight a number of problems that are associated with damage identification carried out using mode shape data that could be collected from simple structures. To simulate the possible inaccuracies that could be incorporated into the analytical assessment of damage using the above-considered methods, a simple exercise based on the incorrect assignment of stiffness at the damage site was treated. Based on these examples, the following comments can be made.

(i) The correct location and identification of defects is dependent on the accuracy of the measured data used for numerical processing. This applies to both natural frequency and mode shape information, where it may be difficult in practice to collect such information without incorporating some form of error.

(ii) The accuracy of the method increases proportionally to the amount of data available. Therefore, to ensure that the error in the identification process is reduced as much as possible, data from as many locations throughout the structure, representing as many modes of vibration as is possible, should be obtained. In practice this also may be difficult to achieve due to limitations imposed by the means used to collect vibration measurements. The rotational degrees-of-freedom at discrete locations within a structure being one such example.

(iii) If errors are encountered or exaggerated as a result of the problems listed above, an incorrect assessment of damage could be made.

2.3 Damage Identification using Changes in the Dynamic Characteristics Alone

The main principle of all aforementioned methods is to use measured vibration data to identify defects after known occurrences of damage and to compare the results to a numerical model. However, alternative methods, which were identified earlier as either (a) continual monitoring of dynamic characteristics throughout the life of the structure or (b) comparing the results of a large number of similar structures, are becoming more popular. Both (a) and (b) above are not normally concerned with the justification of damage (or its location) found by a computationally based analytical model, which is fundamental to the methods cited in previous sections in this chapter. Generally, the procedure considered for these identification methods is to study carefully the manner in which the dynamic characteristics change (or are seen to vary) and how they can be related to the type of processes that are assumed to cause the damage. By treating the problem as one that is not wholly dependable on the results produced from an analytical solution (e.g. the FE method), the approach is often to identify damage from characteristic trends observed in measured vibration data on many similar structures. Therefore, by building up a library of how these characteristics are affected by particular cases of damage (e.g. the onset of possible failure from excessive static pre-load), the ultimate aim is to use the observations to detect defects in other similar structures.

2.3.1 Methods based on a comparison of many structures

A good example where repeated measurements were used to identify defects from a large number of similar structures was reported by Ellis (1998) where ambient vibration measurements of pinnacles at the Palace of Westminster, London, were examined. The above report discussed the findings obtained from natural frequency results of 534 stone pinnacles of various size groupings (comprising a number of similar structures in each) located around the roof perimeter of the aforementioned structure. The approach was to locate the pinnacles that may have been affected by damage (e.g. material deterioration). The aim was achieved by compiling measured natural frequency readings in order to identify those pinnacles that did not conform to the trends observed from all others. Using this approach, the author showed that from the total number of pinnacles tested, 5 structures were identified as showing frequencies that did not conform to the majority, which rationalised the number of members considered for closer inspection. Mehrabi and Corley (2000) also reported on studies of a similar nature where the approach was chosen as a method used to monitor cables of suspension bridges.

2.3.2 Methods aimed at developing a library of performance indicators

Researchers at the University of Nottingham [Owen *et al* (1996), Das *et al* (1997) and Eccles *et al* (1997, 1999)] have contributed significantly to this form of damage identification, which aims to build a library of performance indicators for use with bridge monitoring. The aforementioned authors have studied carefully the dynamic characteristics of reinforced concrete beams and have examined these properties during phases of deliberately imposed damage. To introduce the damage, the authors chose to use progressive static loading, applied in a variety of ways, which allowed the influence of incremental stiffness changes on the natural frequency and mode shapes to be examined. The significant conclusions drawn by the authors from these studies were (a) the measured natural frequencies of similar beams subject to identical static load conditions changed in a repeatable manner, and (b) these changes were found to correspond to observations of definite structural damage. With regard to the latter point it was found that applied static load levels, which induced initial cracking of the

concrete beams, coincided with a notable change to the natural frequencies. However, the authors make it clear that mode shape measurements did not provide results of sufficient sensitivity to highlight similar characteristic changes.

Salane *et al* (1987) also gave a discussion of this approach, which studied the transient and steady state vibration behaviour of a three-span bridge subjected to various levels of induced damage. The study focused on the decay-of-vibration characteristics of the bridge as well as its response to various frequencies of force excitation (i.e. the Frequency Response Function or 'FRF'), from which both were seen to change depending on the level of damage imposed.

Garstka *et al* (1993) and Sedeghi *et al* (1993) proposed a method, which assigned 'damage indicators' to cyclical reinforced concrete cylinders. These authors considered the possibility of assessing the rate and extent of progressive damage inflicted on structures subjected to earthquake type loads (i.e. non-periodic vibration). They found that the '...energy absorbent characteristics...' (damping) of the members changed as the amount of damage was increased. Using several similar studies, the authors established a repeatable trend, from which a set of indices was defined relative to applied load intensity. These indices were proposed as a means of damage detection for use on other similar structures.

2.4 A Sample of Published Reports showing the Application of Damage Identification Methods to Structures of Varying Scale

2.4.1 Studies carried out on small-scale (model) structures

Sanders *et al* (1989) reported on a study to detect damage in model cantilever members made from fibre reinforced composite materials. The study aimed to investigate (a) how damage affected the internal elastic constants of the material, and (b) how these changes influenced the stiffness of the overall structure. The authors used an 'error-based' procedure to detect cracking and inter-laminar de-lamination in composite fibre reinforced cantilever members measuring 760mm long, 10mm deep

and 25mm wide. A modified FE formulation was used to determine the natural frequencies of the cantilever using 40 beam elements. Using the aforementioned analysis, the authors reported the successful detection of deliberately introduced discrete damage, which was performed by comparing results from the proposed formulation with data from a standard FE model. However, due to the latter point, it is questionable if the presented conclusion would be repeated should the study be carried out on a real (more complex) structure.

Ismail *et al* (1990) examined the affect of saw cut damage inflicted on aluminium bars. The former authors considered bars of dimensions 10mm deep, by 65mm wide each having a length of 460mm supported at one end by a clamp to simulate a cantilever structure, while the latter chose 300mm length members. In both cases, damage was inflicted at various locations along the bars, which was later considered analytically using 'spring-loaded hinges' in a FE model. Comparing natural frequency measurements to the FE calculations, the authors found discrepancies even before damage was inflicted, which were assumed to be the result of inaccuracies between the modelled clamp support and its actual properties. The authors also found damage detection difficult as changes made to the model in an attempt to locate the damage produced equally plausible changes in the calculated frequencies found when refinements were made to the simulated clamp support.

Mazurek and Dewolf (1990) report on a study that used measured natural frequencies obtained from a model two-span bridge that had been deliberately damaged. The bridge measured 100mm wide having two spans of approximately 2.25m each, which were continuous over the central support. The cross section was fabricated from steel plates and angles, while vehicle loading on the bridge was simulated using two steel weights mounted on rollers. Two scenarios of damage were considered, the first being failure of the central support (i.e. its removal), while the second aimed to simulate a crack in the steel deck at a pre-determined location, which was to reduce the bridge bending stiffness by 81%. Unsurprisingly, the response of the structure was seen to change dramatically when the bridge was subjected to the first damage case, which was acknowledged by the authors as being the anticipated result. The second case changed the measured frequencies by 11.4%, 4.3% and 3.4% for modes 1, 2 and 3

respectively. From these results, the authors proposed that natural frequency measurements offered great potential for the detection of damage in bridge structures. But due to the small-scale of the tests, and owing to the simplicity of the laboratory model, the authors could only propose the method as 'feasible' with no guarantee of success at full scale.

Liu (1995) used a matrix adjustment procedure to re-calculate the stiffness and mass matrices of a damaged cantilever truss using a FE model as the analytical basis. The author used '...perturbation theory and the 'Monte Carlo' method to establish the number of modes needed to minimise the coefficient of variance...', which would signify the correct damage case. The aim of the study was to identify the amount of measured data required to accurately locate damage in truss like structures. Applying the method to a structure with 17 dof's, the author suggests both mode shapes and natural frequency values for a minimum of 5 modes would be necessary to confidently predict the member properties of the considered structure (thus indicating damaged extent and location). However, the author concluded that this would only be possible if the data were retrieved with no incorporated errors, which was accepted as being highly unlikely.

Meinhold *et al* (1996) investigated damage inflicted on reinforced concrete plates by correlating results from FE analysis with measured values. Incremental static load was used to inflict damage on the plates in stages up to their ultimate capacity, between which vibration data was collected to determine the natural frequencies. Comparing measured frequency results to FE calculations, the authors were able to correlate a number of the lower mode frequencies of the structures by incorporating the known location of damage into the analytical model. However, the authors did not present detail of the correlation making it difficult to assess the actual success gained from the study.

Samman and Biswas (1994b) used vibration measurements obtained from both full-size and laboratory-scale bridges. Using a modified MAC, termed the SAC method, the authors found that mode shapes measured from the model before and after deliberately inflicted damage indicated that changes could be identified. The method

used to cause the damage to the laboratory model, which measured 2.5m by 1.2m on plan, comprising saw cuts in its steel beam flanges. SAC values ranging from 1 to 0.96 were obtained when saw cut depths from zero (no damage) to 51mm were imposed. The authors concluded that the observed SAC value change was reasonable evidence to support the method as an indicator of damage.

A similar study was considered by Wolff and Richardson (1989) and by Almapalli *et al* (1997) where the MAC and COMAC ratios were used in their original form to detect damage in large-scale laboratory models. The main conclusion drawn from these studies was that the aforementioned coefficients were found to change in a manner that corresponded to the severity of imposed damage. However, in all the above cases that involve the use of standard or modified MAC methods, no account of repeatability was discussed where the results from only one laboratory structure were used to form the conclusions.

2.4.2 Studies carried out on large-scale (civil / structural engineering) structures

Maguire and Severn (1987) considered three full-sized civil engineering structures comparing the measured frequencies to the results gained from FE analysis. The report discussed a number of facets for vibration testing, which included its possible use as a damage identification tool reporting that the instrumented hammer test (described in chapter 3) could offer a convenient means of obtaining natural frequency readings. The authors noted that changes were observed in the natural frequencies of a beam when its tendons were exposed for inspection by removing localised areas of concrete. The reduction of the natural frequencies, based on a comparison of before and after concrete removal, was noted as being approximately 1.5%. However, no comment was made regarding the extent of change that occurred to the stiffness of the beam in order to induce the observed natural frequency alteration. Wood *et al* (1991) also conducted a similar study, choosing to consider both reinforced and post-tensioned concrete beams. The conclusions of this work also indicated that the natural frequencies of the members changed after damage, but the change in the values (based on 7 vibration modes) was at most 0.6%.

Jauregui and Farrar (1996) conducted hypothetical studies on a full-sized three-span bridge. The authors used a series of 'error-based' algorithms to successfully locate the most probable locations of various damage cases, which were analytically simulated using FE model by introducing small changes to its section and geometrical properties. However, due to the hypothetical nature of the study it is difficult to assess if the level of damage imposed analytically would be detected from tests conducted on the real structure.

Farrar and Cone (1995) and Salawu (1997b) used vibration measurements from full-scale bridges to detect damage. To test the method, deliberate damage was inflicted on the structure, which ranged from support bearing replacement to the introduction of saw cuts to simulate cracking. The former of these cases produced changes to the vibration behaviour of the bridge, which corresponded to analytical predictions. The study also incorporated the stiffness adjustment of the replaced bearings at the supports. The latter point, however, highlighted discrepancies between the measured behaviour and analytical prediction when the inflicted damage was simulated within the bridge using the same analytical model. A similar outcome was reported by Mayers (1995) where a numerical 'damage indicator' was used to quantify deliberate structural changes (saw cuts) made to a three-span full-scale bridge. Although this author claimed that the damage could be accurately quantified (and located), pre-studies carried out before the introduction of the structural changes also suggested that damage had been inflicted.

2.5 Discussion and the Way Forward

2.5.1 Main points to note from the review

The aforementioned authors claim that damage could be identified (and sometimes located) in a structure using dynamic characteristics as an indicator. The justification given to prove the validity of the cited methods are based on principles that are in accordance with the rules governing the assumptions of each approach, therefore making it difficult to criticise their formulation directly. However, each of the

proposed methods have been prepared to make the detection of damage in real structures a convenient and reliable process, and it is here that varied opinions appear to have emerged. Some of these opinions are supportive (usually those proposing the method) but others identify problems that highlight the weakness of the method by, for example, attempting to match ideal (or exact) theories to structures that may not reflect such mathematical perfection. The main points to be noted from the review can be expressed as follows.

When using 'Error-based' or 'matrix adjustment' techniques:

(i) Care should be taken to ensure that measurement error (i.e. non-structural related vibrations or 'noise') is avoided. Friswell *et al* (1997), Alampalli *et al* (1997) and Samman and Biswas (1994a) realised this problem stating that should error be present in the measured response data, then it is highly likely that incorrect damage will be identified using these techniques. Other authors such as Agbabian *et al* (1991), Zimmerman and Kaouk (1992), Messina *et al* (1996), and Shi *et al* (1998) imply a similar awareness finding that noise could significantly influence the identification process, as damage and its locations is directly associating with the measured data being used.

(ii) It is important to collect as much vibration data as is possible from the physical structure, which should be conducted on as many modes of vibration as can be obtained. Although a number of authors have attempted to determine the 'optimum' amount of data that would be required to make an accurate identification of damage, it is clear that the actual requirements are far from universally applicable. In general, the greater the volume of available data (i.e. natural frequencies and associated mode shapes) the greater are the chances that the existence of damage will be identified.

(iii) If (i) and (ii) are satisfied with a high degree of confidence, it is important to ensure that the computer model used to interpret the damage is a true reflection of the structural changes. Although the reports included in this chapter have concluded successful outcomes to the problem of damage identification / location, little evidence was found of authors demonstrating the applicability of the chosen numerical solution, and how it may relate to actual structural conditions. One possible way of achieving this could be to ensure that the

numerical solution that represents the undamaged structure are calibrated against the measured vibration from the 'pristine' structure, which would provide a 'benchmark' for subsequent measurements.

The above points are based on the discussions presented in the reports that have been cited in this chapter, which as such do not reflect on the studies that are presented in subsequent chapters of this thesis. However, even at this stage there are a number of items that are unclear. The most prominent of these being how successfully the vibration behaviour of larger structures (e.g. buildings, bridges etc.) can be measured and modelled. Additionally, the sensitivity of the dynamic characteristics to damage within these structures is not definitive, and a large gap exists between the approaches considered for small-scale and larger structures. One way of closing this gap could, therefore, be to establish clear definitions of where dynamic characteristics could be used to detect particular categories of damage in structures of a certain type and size. This is the approach that has recently started to develop, which was identified above as the methods that are based on continual monitoring that aim to establish definite trends in structures of a particular type. The advantages of this approach over that of other methods are:

(i) Damage identification is not dependent on a computer simulation of the assumed damage.
(ii) The identification of damage location is not generally the aim, but the recognition of how particular characteristics are influenced by its presence are the objective.
(iii) A library of damage and the way it affects the dynamic behaviour of similar structures can be established.

2.5.2 The way forward

The way forward adopted in this thesis will be to make use of a number of the salient points that have been recognised from all the above methods. The aim will therefore mainly be to:

(i) Establish if damage can be identified from changes in the dynamic characteristics of various structures determined from measured vibration-response data. These studies will concentrate on the structure and parts thereof, as identified in chapter 1.

(ii) Use numerical models of the structure in question, which will consider the various sub-structure levels in as much detail as necessary, to compare the measured dynamic characteristics with calculated solutions. This will then allow conclusions to be drawn regarding the sensitivity of various sub-structural levels to damage.

(iii) Depending on the level of structural complexity being studied, a range of dynamic characteristics will be considered in order to identify if repeatable trends can be recognised from the dynamic characteristics corresponding to various levels of damage.

CHAPTER 3

The Methodology for Dynamic Testing and the Approach used to Determine the Dynamic Characteristics of Structures from Measured Response Signals

3.1 Introduction

It has been discussed in chapter 2 that the detection of damage in engineering structures using vibration measurements depends almost exclusively on the two main factors. (i) The quality of vibration data obtained, and (ii) how this data can be related to the overall characteristics of the structure under test. The latter factor is usually assessed by forming a numerical model of the structure, which is often used to correlate with the observations obtained from the measurements. With regard to the former, to recognise if damage has influenced the dynamic characteristics of a structure, it is clear that the vibration data collected should be of a quality that will allow a consistent set of results to be achieved. This is an important aspect of damage detection performed in this manner, as the usual philosophy is to interpret the resulting changes to the dynamic characteristics as being indicative of structural damage. To ensure that consistent data and subsequent dynamic information are determined from the structures considered in this thesis, vibration test methods and the methodologies used to determine the dynamic characteristics should first be established and standardised.

This chapter is presented in three parts, which can be categorised as follows:

(i) A review of published literature that outlines a number of reported methods used by other authors to measure the vibration response and interpret the dynamic characteristics of engineering structures.

(ii) A description of the equipment used to measure the vibration response of the structures considered in this thesis, which will also include a specification of the instrumentation adopted.

(iii) A discussion of the methodologies used to determine the dynamic characteristics from the vibration response measurements.

3.2 Determining the Dynamic Characteristics of Engineering Structures – A Review of Published Literature

Without intending to give an exhaustive and in-depth review of all available vibration testing and analysis techniques, a cursory overview of the more prominent methods that have been used in the fields of civil and structural engineering is given as follows.

3.2.1 Methods used to induce vibration of engineering structures

To study the vibration response of a structure, a number of methods have been put forward that excite the structure in a manner that will allow vibration response data to be recorded with the aim of collecting good quality and consistent dynamic characteristics.

3.2.1.1 Impact induced vibration using an instrumented hammer

To retrieve dynamic characteristics from a structure it is common to use an approach that initiates excitation by means of an initial input energy source, usually in the form of an impact load. By recording the response of the structure (the output) that is induced by this initial force (the input), a correlation between the input and the output responses can be made to provide information about the way the structure absorbs and disperses energy. Correlating input and output characteristics in this manner allows the transfer of the input force through the structure to be established, thus providing information on the system behaviour. This correlation is then used to interpret the dynamic characteristics of the structure, which is commonly termed Transfer Function (TF).

The application of the hammer test to obtain a measure of the dynamic characteristics of a structure has been documented in many texts on the subject, Ewins (1986) and McConnell (1996) being two examples, which cover aspects such as digital signal processing and signal analysis. Maguire and Severn (1987) gave a good overview of a number of the main issues for the method and described in detail the processes involved in capturing and analysing signals obtained from the hammer test.

Reynolds *et al* (1998) and Pavic *et al* (1994, 1996) reported on a study where the natural frequencies of a reinforced concrete slab were determined from tests performed using a 5.4kg instrumented hammer. The slab, which measured 15m square having a thickness of 250mm, was made from high strength concrete and was supported by four columns located symmetrically near its corners. Initially, the study aimed to measure the frequencies of the structure in as many of its natural modes as possible and to identify how these values changed during the phased construction of a false floor system. The authors identified a total of nine modes of vibration at three construction phases, these being (1) bare concrete floor, (2) floor panelling loosely connected, and (3) floor panelling securely fixed in position. From these tests, the authors found that a reasonable measure of the slab natural frequencies could be obtained and they also showed how the values change as surface treatments were added. However, the observed frequency change was small (within ± 2%), and as the authors did not give detail regarding the accuracy of the measurement, it is difficult to assess the true value of the findings. Nevertheless, the authors suggest that the approach can be used to determine the natural frequencies of floor slabs successfully, later demonstrating its application to large concrete floors in buildings [Pavic *et al* (1997)].

3.2.1.2 Impact vibration induced by human activity

The study of human induced vibration and the effects of human-structure interaction are subjects that are continually evolving. A large volume of published work on these issues is already available and the continual interest that is presented by such reports demonstrates that human activity, and its effect on structural components, is a specialist subject in itself.

It is not intended here to give a review of the literature that is currently available on these subjects, as it is sufficient to say that these reports are vast and vary in both quality and approach. For the most part, current research interest appears to be concentrating on the study of human induced vibrations on slender concrete floor structures, some examples of which have been reported by Caverson and Williams (1994), Williams and Waldron (1994), Anderson and Nayfeh (1996), Plum and Svensson (1993), Ellis *et al* (1996) and Ellis and Ji (1996). However, without dealing specifically with the detail of these reports there is one type of human induced

vibration that has been used to provide an initial force purely to extract natural frequency and damping information. This type of loading has been referred to in literature as the 'heel-drop' test and has become commonplace in the testing of full-scale structures, such as floor slabs, due to its simplicity and effectiveness.

Wyatt (1989) and Osborne and Ellis (1990) have described the 'heel-drop' test procedure as being performed by a single person standing at the location on the structure where the impact load is to be applied. Then, raising the body onto the balls of the feet followed by an immediate dropping of the body weight onto the heels generates a dynamic force, which is greater in magnitude than the force caused by the body at rest. A measure of the amount of force is generally not recorded, as the aim is simply to generate input energy so that vibration of the structure is induced.

In general terms, a measurement of ambient vibration produced in this manner yields limited information if the magnitude of the force that was responsible for the vibration is not known in detail. However, if the only information required from the structure is an estimate of its natural frequency, then ambient vibration response information (e.g. the response caused by impact) is all that is required [Ellis (1995)]. Under this condition, the heel-drop test has been an effective means of initiating vibration and has been used to determine the response of building floors by authors such as Osborne and Ellis (1990), Caverson *et al* (1994), Ellis *et al* (1993), and Plum and Svensson (1993).

3.2.1.3 Forced vibration by electro-dynamic shaker

For the study of larger structures (for example – full-scale buildings or 'whole-structures') the heel-drop approach becomes less practical as the level of input energy required to induce vibration would need to be relatively large. To overcome this problem, researchers have used mechanical exciters, which can impart large force magnitudes on a scale commensurate with the vibration of whole-structures. These methods can also offer an accurate means of imparting dynamic force that is in-tune with the natural oscillatory behaviour of the structure under test, i.e. sinusoidal motion. Pavic *et al* (1997) and Reynolds *et al* (1998) describe the use of such a device, which comprised of a portable self contained excitation unit, which housed a vibrating 45kg mass that could be used to induce a dynamic force along a single axis. When set in

motion, this mass provided a controllable dynamic force, the speed of which could be varied to any desired frequency within a certain range. The excitation force produced by the device was used to induce both sinusoidal and burst type (or 'chirp') loading situations (primarily on concrete floors), which were generated via a 'digital function ensemble device' prepared on a designated micro computer linked to the excitation unit. This system has been adopted for research at the Centre for Cement and Concrete (CCC) at the University of Sheffield and has been reported in several publications by this institution over the past decade, examples being Pavic *et al* (1994, 1996), Waldron *et al* (1996), Pavic (1997).

Williams and Tsang (1988) also used a similar device (with a comparable level of excitation mass) to determine the forced vibration response of a five-storey fire station drill tower, reporting that sufficient force could be generated to allow an examination of the first five of its vibration modes.

3.2.1.4 Forced vibration using an eccentric-mass excitation device

An alternative to a force that depends a mass vibration along a single axis, is a range of mechanical devices that are based on two contra-rotating masses have been developed by the Building Research Establishment (BRE), UK. One of the first descriptions of this system was reported in a paper by Jeary and Ellis (1981), and later by Littler (1988). These were used to provide a source of excitation for a range of structures of varying sizes. The devices were reported to vary in size. Examples of their use have been used include the vibration of glass panels, concrete floor slabs, and large structures such as dams and tall buildings. With this system, BRE have been studying the vibration performance of structures for a period now exceeding two decades. During this time a large amount of experience and knowledge has been acquired, which has been expressed and reflected in publications world-wide.

The device itself operates on the principle that the two masses (which rotate in opposite senses) produce centrifugal forces that are relative to the speed at which they are rotated. As these weights rotate in opposite directions, the resultant affect is a sinusoidal excitation force that peaks when the weights coincide and are nullified when they are at opposite ends of their oscillatory cycle. The flexibility of the

individual devices are evident from their specifications, which stipulate that a variety of forcing magnitudes can be applied to any given structure using a range of weight sizes, which can be added to the rotation parts of the device. Combining this with the accuracy to which the speed of rotation can be controlled (0.005 Hz), the device offers a convenient means of vibrating structures at any frequency within a certain range. To calculate the magnitude of dynamic force, that is imparted to a structure by the oscillating masses, a simple relationship. This multiplies the mass of the rotating parts with the respective acceleration of motion, the magnitude of which is calculated using,

$$F_w = F_o \sin(\omega_f t) \tag{3.1a}$$

where

$$F_o = m_w r \omega_f{}^2 \tag{3.1b}$$

and F_w is the force generated when the mass of m_w (sum of two weights) is spun at a speed of ω_f (in radians / second) at radius r from the centre of rotation with time t. Depending on the size of structure being tested, and thus the level of input energy required, the force can be varied by adjusting m_w.

3.2.2 Determining the dynamic characteristics of a structure from periodic, non-random vibration response measurements

Throughout all publications considered by this review, the assumption that is normally adopted considers the dynamic response of a structure as 'an adding together' of individual well-separated vibration motions. A further assumption normally considered is that these individual motions are sinusoidal in nature, the frequency of which are dependent on the stiffness, mass and damping properties of the structure under test. Although not always found to be the case, this assumption is important, as it is the basis on which 'modal analysis' (which is the term often used for studies that determine the dynamic characteristics of structures) is based. The rationale and basic principles of modal analysis are included in Appendix A, based on which the following information can be determined if a record of the vibration response of a structure is known.

3.2.2.1 Determination of the natural frequency of a structure using FFT methods

A convenient way to determine natural frequencies of a structure from measured vibration response signals is to use a Fast Fourier Transform (FFT) algorithm. A basic description of the FFT is also given in Appendix A, which in its simplest possible terms is a means of expressing a time dependent response signal (induced by some form of input force) in terms of its frequency domain counterpart. To accomplish this transformation, the FFT uses principles of Fourier series [Jean Baptise Joseph Fourier (1768 – 1830)] which in essence, provided a means of identifying sinusoidal components of a periodic signal – i.e. the Fourier components [Cooley and Tukey (1967)]. These components portray the frequency content – or 'spectral density' – of original recorded vibration response, which is normally called the 'autospectrum' (singular) or 'autospectra' (plural) of the measured data. And, as the motions of the individual vibration modes of a structure are assumed to be sinusoidal in nature, the FFT approach allows natural frequencies to be identified from the Fourier components that comprise the measured vibration response.

3.2.2.2 Natural frequency and damping from decay-of-vibration signals

If the rationale of modal testing is correct it should be possible, under curtain conditions, to obtain measured signals from a structure, which contain components that are dominated - if not solely governed - by a single mode of vibration. i.e. a single component of sinusoidal motion. In this condition the structural response can be regarded as one that can be compared to a linear single-degree-of-freedom (sdof) system provided that the response is periodic and non-random. Appendix A gives the mathematical background to such a system where vibration energy is dissipated in the form of a viscous (velocity dependant) function – termed a 'visco-elastic' model. If a structure exhibits similar behavioural trends to the visco-elastic model, it should be possible to determine its dynamic characteristics from a correlation of measured and calculated response vibration signals.

This is the approach reported in numerous papers by researchers at BRE where the mathematical solution for a free oscillator (see Appendix A) has been used to determine damping and natural frequencies of structures from measured decay-of-

vibration signals using a curve fitting approach. Osborne and Ellis (1990), Ellis (1994), and Ellis and Ji (1996) are examples where this approach has been shown to be very successful, where damping and natural frequencies were determined for various types of floor construction.

3.2.2.3 Natural frequency and damping from forced steady-state vibrations

The dynamic characteristics of a structure have also been determined from vibration response signals initiated using steady-state forcing devices, such as the electro-dynamic shaker (identified earlier). Adopting a similar approach as described above (i.e. the correlation of measured and calculated data) damping and natural frequency can be determined.

Imperial College London (ICL) have prepared a number of computer programs to determine these characteristics in this way and have been developed as a commercially available package for use with devices such as that mentioned above. This suite of software (called ICATS) was written by researchers at ICL under the directorship of Professor D. J. Ewins [the basis of which are discussed in Ewins (1986)].

BRE, on the other hand, [discussed by Jeary and Ellis (1981, 1983)] have developed software for use with their eccentric mass excitation equipment (described earlier). To determine the damping and natural frequency of a structure under test using this software, the steady-state vibration response [i.e. vibration amplitude against frequency – or Frequency Response Function (FRF)] is first recorded and later compared to the mathematical solution of a visco-elastic model. The results obtained from the completed test aim to provide damping results as a percentage of critical viscous damping (critical being 100%), and natural frequencies, which are both achieved from the correlation process.

3.2.3 Determining the dynamic characteristics of a structure from stationary random vibration response measurements

Random vibration is another source from which researchers have attempted to determine the dynamic characteristics of large structures. Examples were structural

vibrations may be regarded as random are situations such as wind induced motion of a tall building, or the vibration of a bridge subject to non-periodic traffic loads. If the amplitude of motion under these conditions is small then it is likely that the response characteristics will be linear and the vibration can be regarded as a linear random process [Cao *et al* (1997)].

Due to the increasing interest in the measurement and determination of dynamic characteristics of large structures, over recent years a number of reports have been published that are based on the use of random response records. Littler and Ellis (1992) for example reported on a detailed study of a building at Hume Point (London Borough of Newham) using wind induced response data. Mazurek and DeWolf (1990) also reported on the use of random data to determine the damping and natural frequencies of a model road bridge. The tests were performed on a model scale to calibrate the results obtained from measurements taken from a full-scale bridge.

Jeary and Ellis (1983) pointed out that considerable care must be taken when interpreting the results from measurements obtained in this way as large errors can occur if the data itself in not correctly validated. However, these authors state that validation of the data is not always carried out and this can lead to misuse of random data. To clarify a number of instances where these errors could occur, a discussion has been included here to outline a number of aspects that should be considered when using this type of response data.

3.2.3.1 Establishing stationarity

As discussed by Jeary and Ellis (1981, 1983), Ellis and Littler (1988), Littler and Ellis (1990, 1992), Jeary (1992) and Cao *et al* (1995, 1997), the most important requirement of random data, if it is to be used to extract statistical information, is the need to ensure that the response data is "stationary" and that it possess characteristics that are representative of the structural response at any particular instance of time. Jeary (1992) described this as '... occurring when statistical quantities measured from a data set are invariant with the passage of time.'

For the purposes of this discussion it is not intended to give detail of the means by which "stationarity" can be evaluated. This theory is explained in numerous texts such as the one by Newland (1993). It is therefore sufficient here to recognise that a stationary process, or a stationary signal, is that which contains statistical characteristics that reflect those of other similar processes, or signals. In this situation the more data obtained, and thus the more signals used to identify, say, the vibration response of a structure, the more likely it will be that stationarity could be identified from an average of collected data. Interpreted strictly in terms of the response of a structure to wind, for example, it can be deduced that a signal is only stationary if an ensemble average of many recorded signals show that these averages are independent of the passage of time, i.e. they contain repeatable statistical characteristics. Taking this one step further, if a signal that forms the ensemble average is found to completely represent the average as a whole, then the signal is said to be ergodic.

To define an ensemble average of random vibration signals as being perfectly stationary requires either an infinite number of finite length signals or a signal of infinite length. This is obviously not practical in real terms and it is only possible to express the quality of stationarity relative to a level usually defined as a 'level of confidence', which is based on the amount of data available to produce the ensemble average signal. Alternatively, if a limited amount of random data is available, it is possible to partition a single vibration signal into individual signals of similar length and ensemble the information to check for the presence of random trends. This method is referred to as the 'trend test' and was used by Cao *et al* (1997) to establish confidence levels in single random vibration signals of known stationary data taken from the Hume Point structure previously studied by Littler and Ellis (1992).

It is clear that the confidence level of stationarity is relative to the amount of vibration data collected from a structure, but it is also dependent on the assurance that the data collected relates to similar conditions of applied loading. Good examples where these aspects have been taken into account are given by a collection of reports that have been prepared on the Hume Point structures already identified in the previous discussion. These reports, written by Littler and Ellis (1988, 1990 & 1992) and Cao *et al* (1997), make comprehensive use of data collected from a 23 storey building. Initially, the authors point out that a total of five ensemble average signals were

prepared using vibration signal taken from various wind speeds. The five ensemble averages therefore represented information that related to conditions when the wind direction was within certain radius segments of the building. These ensemble averages contained a minimum of fifty mutually exclusive records, each containing 16384 data points, which represented 1024 seconds of vibration response. Based on this length of signal, each record was said to have a variance error of 14.1% and a bias error at the 'Half-Power Band width- (HPB)' point of 0.15%, both errors referring to the spectral content of the signals when analysed using FFT procedures. This data was also said to be stationary with the individual signals being taken from a larger sample comprising over 2250 hours of data, which offered a good representation of the structural response. The data was then used to extract the natural frequencies of the structure and damping ratios of each of the identified modes taking into account the accuracy available from the amount, length and sample size presented by the collected vibration response records.

The above discussion pointed out that bias and variance errors were defined as being dependent on the quality of the spectral content of the signal. To provide more detail as to the meaning and significance of these errors, a discussion on each has been included below.

3.2.3.2 'Bias' error

To assign a value of natural frequency or damping to a structure a clear definition of the peak structural response must be achieved. The FFT will provide the basis for this definition, but at response frequencies, where the amplitude is found to change rapidly, there is a distinct relationship between the response data requirement and the accuracy of the obtained results. This relationship is most critical at amplitudes close to, and coincident with, the resonance frequencies of a system as it is these parts that will most influence the interpretation of natural frequency and damping estimates of random signals.

This relationship is best known as the 'bias' error and represents the percentage deviation of the FRF from that of a response, which has perfectly captured the system characteristics.

Bendat and Piersol (1980) showed one method of gauging this error where a Taylor series expansion was used to compare continuous data and discrete data points of a single FFT resonance amplitude peak. This expression was given as,

$$\mu_b = \frac{1}{3}\left(\frac{B_e}{B_n}\right)^2 \tag{3.2}$$

where μ_b is the bias error, B_e is the resolution of the captured response signal and B_n is the HPB of the a single resonance peak obtained from the signal using an FFT approach. The HPB is the width, in frequency units, of a spectral peak coincident with $\frac{1}{\sqrt{2}}$ times the maximum amplitude of a single resonance peak about the resonance frequency. For lightly damped, visco-elastic systems this value was given in mathematical terms by Dimarogonas (1996) as,

$$B_n = 2\zeta\omega_n \tag{3.3}$$

where ζ and ω_n are the viscous damping ratio (expressed as a percentage of critical damping in decimal form) and natural frequency respectively of the n^{th} mode. Therefore, a reduced bias error will in effect signify a greater accuracy in the estimation of damping properties reflected by the spectral content of a measured response signal.

3.2.3.3 Variance error

The variance error is a statistical quantity that indicates the deviation of a single vibration signal from the mean of many signals. In terms of vibration analysis, this can be interpreted as the correlation of a vibration response signal relative to the mean of many other similar signals and is expressed by summing the square of the deviation from the mean value. This error can be gauged from the square root of the reciprocal of the number of vibration signals averaged together, [McConnell (1996)], i.e.

$$\mu_v = \frac{1}{\sqrt{N_r}} \tag{3.4}$$

where μ_v is the variance error and N_r is the number of signals averaged to give the mean. Therefore, a mean signal compiled from 100 signals should ensure a variance error of no more than $\pm 10\%$.

3.2.4 Other methods of determining dynamic characteristics from random data

The above discussion has concentrated primarily on the use of random data to extract dynamic characteristics assuming (1) stationarity, and (2) sufficiency of data available to make statistically accurate estimations. If these conditions are not satisfied then the information obtained from the random data cannot be guaranteed.

In an attempt to remove the dependence on data volume and to provide a method that does not relate accuracy to the information, which can be extracted from spectral analysis techniques (such as the FFT), other methods of analysing response data have been examined.

3.2.4.1 From non-stationary data

Jeary (1992), for example, proposed a method to obtain non-linear damping characteristics from non-stationary data using a technique call the 'random decrement' approach. The method itself was based on proposals originally offered by Cole (1968), which used a Laplace operator to simulate structural response as a non-linear viscous sdof model of several superimposed sinusoidal waves. The essence of the resulting equations used to extract the damping characteristics resemble a Fourier series, which was matched to the measured response via a least-squares fitting exercise. Data used to check the validity of the models were taken from vibration tests conducted on two full-scale building structures (the National Westminster Tower in London and a tower block at the University of Leicester). The author praised the method overall, but expressed frustration over the fact that many other response signals obtained from different structures, besides those identified above, could not be represented using the derived expressions. This was due primarily to a lack of

comparison with the fundamental assumptions considered in the method formulation, i.e. decay of vibration not exhibiting exponential decay type behaviour.

3.2.4.2 Alternative spectral analysis techniques for use with stationary data

As an alternative to the FFT, which has a limited spectral resolution that depends on the amount of vibration data present in a response signal, other techniques such as the Auto-Regression (AR) and Auto-Regression Moving Average (ARMA) techniques, and the Maximum Entropy Method (MEM) have been considered.

Snæbjörnsson *et al* (1996) for example used the AR and ARMA techniques to establish dynamic characteristics from single random vibration signals of 130 seconds in length. These signals were captured from a multi-storey building in Mexico and represented the motion of the structure in high wind. Each signal contained 26,000 data points, obtained using a capture rate of 200Hz, but no comment or evidence was shown of these signals being checked for stationarity. Cao *et al* (1997) on the other hand, used the AR method and the MEM technique to compare their accuracy with other more conventional methods using data that was known to be stationary. In their study, the authors describe that the AR method aims to represent the vibration response with an expression of the form,

$$x_t = \alpha_1 x_{t-1} + \alpha_2 x_{t-2} + \ldots + \alpha_m x_{t-m} + a_t \tag{3.5}$$

where a_t is white noise with zero mean variance, while α_j (j = 1, 2, ..., m) and the order of m are to be determined from a concept known as the maximum entropy of AR. The aim of the study was therefore to consider a range of AR models representing various values of m to find its optimum order. Invoking principles that were termed 'Final Prediction Error' (PFE), which depended on the amount of data points comprising a measured response signal, the authors showed that for the Hume Point structure (identified earlier) accurate FRFs could be identified from single signals containing 2048 data points using eqn.(3.5) with an order m of 27. However, this was found to be specific to the Hume Point structure only with other structures probably requiring a different order depending on the signal quality obtained. Other observations were also discussed, which related to signals containing larger data

samples and the identification of minimum data sample size. However, the main conclusions drawn from the study was that dynamic characteristics obtained using this method were not as accurate as those determined with FFT-based analyses. This is primarily due to the signals being stationary with a high degree of confidence, which was a conclusion drawn from a previous study that had used a much larger quantity of data samples to confirm stationarity.

3.3 The Test Equipment and Methodologies used to Determine the Dynamic Characteristics of the Structures in the Present Work

3.3.1 Introduction

The above review of literature provides an indication of the type of test and the methods most often reported to determine the dynamic characteristics of natural frequency and damping of structures. For the purposes of the present study, where the aim is to establish the use of this information to detect damage in structures of varying size, it was decided to use well proven test equipment and methods in order to record structural vibration. This is to ensure that the subsequent dynamic characteristics, determined from the measured response signals, are interpreted with the knowledge that all data was collected with the same recording specification. Although the use of different testing methods may not have an influence on the results finally achieved, it is the candidate's opinion that standardisation of the test methodologies is important so that the possibility of discrepancies within data sets (due to instrumentation variations) are eliminated.

3.3.2 The test equipment

To satisfy the above, it was decided to use a single test-equipment set-up throughout the present studies. This set-up comprises the necessary instrumentation to (i) record free vibration response (e.g. induced by impact load) and (ii) measure the response of the structures to forced vibration events (using the eccentric-mass method). The equipment to be used had been developed by BRE, aspects of which have already been discussed in the literature review above. Figure 3.1 gives a schematic illustration of

this equipment, which indicates ① the excitation device, ② the signal acquisition and conditioning equipment, and ③ the data storage and signal viewing facilities (any modifications to this set-up will be identified in the appropriate parts of subsequent chapters).

3.3.3 Instrumentation and equipment specifications

A specification of the equipment outlined in Figure 3.1 is included below for completeness.

3.3.3.1 Velocity transducers (geophones)

The velocity transducers (or geophones) to be used are manufactured by 'Geosource Exploration Products Division' and are of type 'SM-4' as defined in trade literature prepared by the manufacturer. The voltage output of the transducers is 28.8 volts/m/second, which allows vibration velocity to be determined from a linear multiplication of this value, and represents motion along a single axis of the instrument. In terms of its physical size, the geophone measures 25.4mm in diameter with a height of 32mm, and is connected to an aluminium 'tripod like' base. This allows the transducer to be positioned vertically on the surface of the test structure with vibration being measured along the vertical axis of the geophone. Combined with an advantage of small (an overall weight of 132 grams excluding cables), the geophone is easy to move and convenient to install at any location in a structure (restricted only by its dimensions).

3.3.3.2 Acceleration transducers

The accelerometers to be used in the present work have an output of 2.5 volts/g (where g is acceleration due to gravity) with a range of ±2g. The sizes of the transducers are approximately 50mm in length and 25mm in width, and measure acceleration along the axis of the longest dimension. To locate each transducer, a 100mm steel cube is used that incorporates 'tripod like' steel feet, which ensures that the accelerometer rest securely on the surface of the structure under test. The accelerometers have no limitations with regard to the axis in which vibration motion can be measured, i.e.

either vertical or horizontal, depending on the orientation to which the instrument is placed on the test structure.

3.3.3.3 Variable-frequency filter

The frequency filter to be used is manufactured by 'Kemo Limited' and has a trade name of VBF/8. This hardware has high pass and low pass filtering options and is also fitted with variable gain AC/DC input coupling. The frequency filtering ability encompasses a wide range from 0.01Hz to 100kHz with a peak filter resolution of 0.01Hz between 0.1Hz and 10Hz. A signal amplification facility is also available with this device, which can be used to magnify the voltage from transducers (up to a maximum of 16 channels) by up to ten times. Standard mains supply (110 or 240 volts) is used to power the filter, which has overall dimensions of approximately 300mm high × 500mm wide × 300mm deep.

3.3.3.4 Analogue to digital converter

To convert the signal from the velocity and acceleration transducers, the output signal from which a voltage pulse is comprised, an Analogue to Digital Converter (ADC) needs to be used. The ADC that will be used in the present work is manufactured by 'Cambridge Electronic Design Ltd' and has a trade name of 'CED 1401*plus*'. This unit can accommodate up to 16 analogue input (range ± I0 volts) and 8 digital output channels and has an on-board microprocessor (32-bit running at a clock-speed of 20MHz) for fast ADC. To power this hardware a standard mains supply can be used, while its overall dimensions are approximately 400mm wide × 90mm high × 400mm deep.

3.3.3.5 Stepper drive and variable speed drive motor

Depending on the size of the structure to be tested, BRE have a range of excitation devices (based on the eccentric mass principles), which in turn have a range of drive motors of varying capacity for use with the above devices. Although a range of these exciters will be used in the present study, detail regarding the smallest device is described (i.e. used in connection with tests performed on the floor slab panels –

chapter 7). The specification given here is therefore typical of the equipment comprising the full range of mechanical exciters developed at BRE.

The stepper drive is manufactured by 'Parker Ltd' and has a trade name of 'CD35' and is to be used in conjunction with a variable speed motor to drive the eccentric mass excitation devices. With a resolution of 200 steps per 1 Hz, this stepper drive will allow forced-vibration frequencies with an accuracy of 0.005Hz to be applied to the structures. Linked to the variable speed motor, which will in turn be connected to the eccentric mass device via a steel drive shaft, the combination of drive motor and stepper unit will be used to induce sinusoidal steady-state motion.

3.3.3.6 The mechanical eccentric mass device

A range of the mechanical exciters has been made by BRE, each of which relies essentially on the same principles. These principles, which describe how the dynamic excitation-force is generated, have been presented in section 3.2.1.4 and thus will not be repeated here.

3.3.3.7 The portable computer and data storage

The portable computer, as incorporated in the equipment set-up of Figure 3.1, is the main storage and analysis device, recording the digital output produced from the ADC. Having a 486 DX 33MHz microprocessor, the computer is fitted with data acquisition hardware that allows digital information to be stored on a hard disk for processing. The data stored by the computer is not continuous, but will be composed of discrete data points, the number of which is governed by parameters chosen by the operator. For the most part, the number of data points stored on the computer will be relative to the time period over which signals from the transducers are required. In addition, a 'rate of data capture' is specified that designated the time interval at which the computer stores vibration response data. Therefore, an example of the amount of data that will be collected could be:

- total time for data capture = 8 seconds
- rate of data capture = 1000 Hz

for which the computer would store 8000 data points, each representing the response of the structure under test at time intervals of 0.001 seconds.

3.3.4 Methodologies to be used to determine the dynamic characteristics from the measured vibration response signals

The methodologies for the determination of structural dynamic characteristics from measured vibration signals will be based on a suite of computer programs prepared by BRE. To give a cursory overview of the functions of these programs, the following narrative identifies the dynamic characteristics that will be determined in the present work.

3.3.4.1 Determining the natural frequency with an Fast Fourier Transform (FFT) method

The basis principles on which the FFT technique is based have been described in section 3.2.2.1.

3.3.4.2 Determining the natural frequency and damping from measured decay-of-vibration response signals

Publication prepared by BRE (cited in section 3.2.2.2) have shown that the visco-elastic model can simulate accurately the behaviour of tall buildings, concrete floors and concrete panels. Relying on this experience, all damping properties determined in this work assume that the vibration behaviour of the structures complies with the rationale of model testing (Appendix A) and that the damping properties of the natural modes are viscous (visco-elastic model).

To measure the decay-of-vibration of the structure under test, the study will consider two approaches:

(i) Inducing a condition of steady state vibration with the eccentric mass device can generate a decay-of-vibration signal. The approach involves three basic steps (a) vibrate the structure at its natural frequency, (b) switch off the excitation source

(i.e. by switching of the drive motor), and (c) record the ensuing decay response of the structure commencing at the point when (b) is performed.

(ii) The vibration caused by impact loads is also a condition where single mode vibration may occur. Therefore, to add to the information that is obtained from (i) above, the decay-of-vibration that occurs subsequent to an impact load event will also be considered. (This method is applicable only to the studies that will be conducted on the composite slab panels).

Then, to calculate the damping and natural frequency for the measured decay-of-vibration signals, eqn.(A.13) will be used (as presented in Appendix A). A designated computer program (prepared by BRE) will be implemented to obtain the dynamic behaviour, which are characterised from a correlation of the aforementioned equation and the recorded vibration data.

3.3.4.3 Determining natural frequency and damping from Frequency Response Functions (FRFs)

The natural frequency and damping will also be determined using frequency response information, i.e. the displacement behaviour of the structure relative to a range of vibration frequencies that include the natural frequency of the structure under test. The name given to this test will be termed the 'frequency sweep' and will make use of the eccentric mass device to generate the required vibration forces.

The procedure to be followed when carrying out this test is defined by the operations performed by a 'task-specific' computer program (by BRE) that records and analyses all response data. The basic procedure and the task performed during the test can be itemised with the following points:

(i) Operator – To commence the tests, vibrate the structure at a pre-determined frequency until a steady-state motion is achieved and record the vibration response (either acceleration or velocity).

(ii) Computer – Integrate the recorded signal, which is captured by the computer over a set 4 seconds period, and calculate the peak displacement from an average of 5 response signals.

(iii) Operator – Increase the excitation frequency taking care to ensure that the interval of its change is sufficiently small to allow a detailed FRF to be obtained. If the chosen interval is too large, especially close to the natural frequency, the peak amplitude at resonance may not be captured accurately.

Items (i) to (iii) are repeated until a full FRF is obtained, which for a single mode of a viscously damped structures should contain a dominant resonant peak. Finally, to determine the natural frequency and damping, the computer program correlates the stored peak displacement data with the steady-state solution to the visco-elastic model [eqn.(A.8) – Appendix A] until a best-fit is obtained. The latter is fulfilled using a least-squares procedure, and is displayed visually on the computer screen allowing the correlation to be assessed for accuracy by the operator.

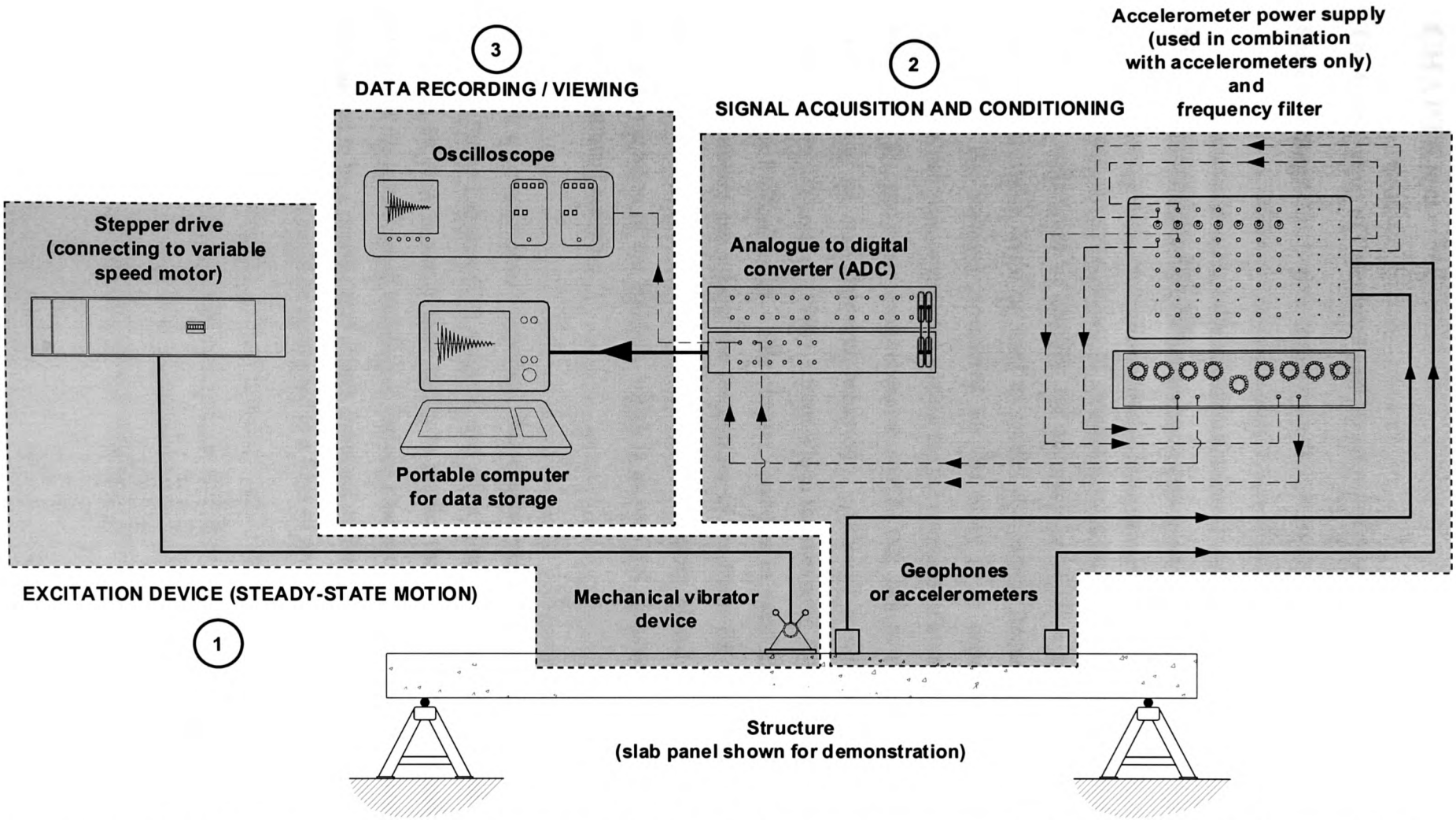

Figure 3.1 – Schematic diagram showing the equipment used to obtain vibration response measurements from the structures in the present work.

CHAPTER 4

The Comparison of Calculated and Measured Natural Frequencies of a Full-Scale Building

4.1 Introduction and Aim

To commence the examination of structural complexity versus damage detection a study was undertaken to identify the accuracy to which a number of traditional analytical methods could be used to predict the natural frequencies of a full-scale building. The building considered for the study is an eight-storey steel-framed structure, which was constructed wholly for the purposes of building research and has been used for numerous comprehensive studies that aim to contribute to a better understanding of real structural behaviour. Although a similar study has been published by Ellis and Ji (1996) – from which the measured data of the steel framed building has been obtained – this chapter considers in detail the accuracy to which analytical models can predict the frequencies of the frame for use with the damage detection methodologies. More emphasis is therefore placed on the whole-frame stiffness variation of the building, which is an area not discussed in the work of the aforementioned authors.

To enable a comprehensive appraisal, this chapter examines two analytical methods, (i) a full Finite Element (FE) analysis, and (ii) a simplified condensed frame model. This will be done to verify their ability to predict the natural frequencies and mode shapes of the steel-framed building at various phases of its construction. If damage is considered to be a process that affects structural stiffness then, for the purposes of this study, construction could be contrasted to a form of reverse damage.

4.2 Comparing Analytically Predicted and Measured Dynamic Characteristics

To give an overview of other similar studies, this section discusses a number of reports that have been prepared from work carried out to examine the dynamic performance of tall buildings. The discussion considers reports that were compiled to compare measured and calculated characteristics, but also deals with publications that have dealt with theoretical models proposed to offer convenient estimates of real structural behaviour.

4.2.1 Simple empirical formulae

Ellis (1980) demonstrated the difficulties encountered when attempting to calculate natural frequencies of full-scale structures with a study that sought to compare the measured and calculated values of 17 buildings. The main conclusion to emerge from this report was that predictions based on principles from classical vibration analysis were found to provide unreliable results. Consequently, this prompted the author to identify an empirical 'best-fit' relationship that could be used to predict the fundamental natural frequency of other similar buildings. This was achieved using measured frequencies from 163 buildings based on publications prepared by various authors. Using this formula, the author noted that a more reliable prediction could be achieved, which offered an approximate estimate of the whole-frame fundamental-sway natural frequency, which can be applied to other similar tall buildings. The relationship proposed is simple and convenient to use, as follows,

$$f = \frac{46}{H} \tag{4.1}$$

where f and H are the fundamental natural frequency in Hz and height of the building in metres respectively, having an 88% correlation with the measured data from the 163 buildings. Jeary and Ellis (1983) later proposed additional similar predictors to calculate higher whole-frame sway and torsion modes given by,

$$f = \frac{58}{H} \tag{4.2}$$

$$f = \frac{72}{H} \tag{4.3}$$

respectively. However, the authors point out that the formulae are only quick fit solutions where mode shape characteristics are neglected.

4.2.2 Frame analysis by continuum element modelling

To obtain a model that could provide natural frequency and mode shape information Chajes *et al* (1993, 1996) used strain energy principles to formulate a continuum model that included bending, shear and axial degrees-of-freedom (dofs). The authors described the continuum as a series of 'cells' formulated to condense the characteristics of a building into individual single representative elements. The elements comprised nine dofs, which aimed to capture the stiffness and mass of successive storeys of a building frame. A comparative study with measured dynamic characteristics of a building was then made relating to the fundamental whole-frame sway frequencies of a 47-storey building. The measured frequencies were obtained from power spectral density functions of acceleration-time history recordings using FFT analysis. The authors reported good agreement between the calculated and measured results showing tolerances of within ± 10%.

Takabatake (1996) offered an alternative to this approach suggesting that the column layout of a tall building frame could be visualised as a collection of concentric 'tubes'. The formulation was again referred to as a continuum model where each storey of the building was represented by single elements each comprising bending, shear and torsion characteristics. The above author showed that a good natural frequency correlation with results obtained from other analytical methods could be achieved. However, apart from comparisons with other numerical analysis, the author did not offer any indication of its accuracy in relation to measured characteristics.

Luz *et al* (1981, 1989, 1990, 1991), Hefei and Luz (1986) and Hampe and Schwarz (1994) developed a continuum model with horizontal displacement and torsion

capabilities. The philosophy adopted by these authors was to prepare a formulation that 'mapped' the characteristics of a structure onto a single continuum element. The difference between this approach and the previously discussed continuum models was that the entire structure was represented by a single element avoiding discrete floor by floor properties. The formulated equation of motion was solved using a 'Ritz procedure' allowing frequencies and mode shapes to be calculated. Comparative studies between calculated and measured natural frequencies were also carried out by Luz (1992) using a 12-storey concrete framed building at the University of Stuttgart together with a 35 metre high church tower and a 45m long steel girder bridge. In all cases the author claimed good correlation, which was achieved after calibration with structure variables such as material properties and support conditions. However, no specific data regarding this calibration process was given making it difficult to identify the main causes of the original discrepancies.

4.2.3 Frame analysis by sub-structure modelling

Sub-structuring has its roots in classical theories of the FE method. The basic principle of sub-structuring, which is formulated from original theories of FE, is to reduce the size and numerical content of a large problem to one that can be solved with significantly smaller computational effort. To achieve this, a process of nodal condensation is undertaken that reduces the total number of structural dofs of an original problem, yet at the same time retaining all the characteristics as if the condensed dofs still remained. The condensed dofs are usually termed the 'slaves', while the remaining dofs, called the 'masters', are modified to include the properties of the slave dofs. The result is a computationally efficient solution that can be used to obtain accurate calculations of the behaviour of framed structures that encapsulate the characteristics offered by the FE formulation.

Sub-structuring has been covered in many texts on the subject of FE analysis, an example being Zienkiewicz (1977), and as such will not be treated in any great detail here. However, proposals to increase the efficiency of the method was given by Leung and Cheung (1980, 1981) where a method called the 'second-level finite element' analysis was proposed. As these authors point out, the original sub-

structuring procedures require a significant amount of matrix inversion calculations, which can place a significant demand on computational effort even when fast computer processing is involved. Their proposal, therefore, was to remove the dependency on such inverse operations and to use a technique that introduced a transformation approach that effectively reduced an original problem size by a system of association. This method was applied to solve natural frequencies of large frames, which gave results that matched the solution given by its full FE model counterpart, yet required no matrix inverse operations normally required with the sub-structuring approach. However, no comparison with measured frequency values was given.

4.2.4 Frame analysis using the 'Grinter substitute frame'

Roberts and Wood (1981a & b) reported on a method called the 'Grinter substitute frame', which was used to predict the whole-frame behaviour of tall building subjected to static load conditions. The method itself has been published in numerous reports, such as Wood (1974a, b & c) and Wood and Roberts (1975), where it was used to predict the non-time dependant sway deflection of steel framed buildings subjected to wind loading. Roberts and Wood (1981a) and Williams *et al* (1983) then considered its use to calculate the natural frequencies of similar framed structures. It is with this regard that the popularity and appeal of this method has grown, and was shown by Howson (1979, 1985) and Howson and Williams (1985) to offer quick results by computer when compared to more laborious processing of a full frame analysis. However, these latter reports did not offer any indication of comparative studies with measured results, concentrating primarily on its formulation for computer programming.

4.2.5 Frame analysis by full FE analysis

All the analytical methods identified above aim to reduce the computational effort and time required calculating the natural frequencies of a building. However, given the available power of modern day computers and the speed at which these machines can provide solutions to even the largest of problems, practitioners usually turn to the FE method, in its original form, to obtain results. The results of such analyses are

regularly used to indicate the expected natural frequencies of structures, yet there is often no evidence to suggest that the predicted results are representative of the real behaviour. Wise *et al* (1996), for example, calculated natural frequencies of a multi-storey framed structure in Germany quoting calculated whole-frame sway motion values to three decimal places. However, no comparison was made to the real behaviour, casting question over the accuracy of such predictions.

Ellis and Ji (1996) undertook a study to compare measured and calculated natural frequencies of the eight-storey steel-framed structure also considered in this chapter, simulating every element within the frame of the building using a FE model. To ensure a rigorous assessment of the predictive accuracy of the model, various construction phases were considered. Focussing on the lower natural frequencies of the fundamental sway and torsion vibration modes, measurements of natural frequency were recorded for five-construction phases, with mode shape data being captured at each phase.

The FE model used for comparison with the measurements varied in complexity depending on the construction phase being considered, which for the final phase was the completed building comprising:

- 1374 three-dimensional thick beam elements,
- 128 three-dimensional bar elements,
- 318 three-dimensional thin shell elements,
- 126 space membrane elements.

The final model was therefore defined geometrically by 764 node points, forming the connectivity points for the FE elements, having an overall total of more than 4,500 dofs. The mass of the structure was also modelled to match the observed distribution of weight throughout the building, which simulated sandbags that had been positioned on each floor to represent the service load of the building when in use.

Using measured frequencies obtained from records of ambient and forced vibration response, a comparison with the calculations showed that on average the FE analysis miscalculated the natural frequencies by up to ±20%.

4.2.6 Discussion on review

The review has given a cursory overview of numerical methods that can be used to calculate the natural frequencies of multi-storey framed buildings. These methods are computationally efficient, which is a facet that is expressed by the authors of the methods included in the above discussions. However, no matter how rigorous the analytical assumptions, real proof of accuracy can only be gauged if the measured response of the structure is available.

4.3 Construction Data of the Eight-Storey Steel-Framed Building

To understand the problems that can be encountered when attempting to calculate the natural frequencies of full-scale buildings for use with the damage detection methodology, a study was undertaken that compared the results obtained from two analytical methods to measurements taken from a full-scale building. The building used for the study is a structure located at the Building Research Establishment's Cardington laboratories.

4.3.1 The building construction

The building itself has an overall size of 21m (North – South [NS]) by 45m (East – West [EW]) on plan with an overall height of 33.5m measured from the surface of the laboratory floor to the finished level of the upper-most floor. Comprising a total of eight-storeys, the construction of the building is dominated by steel framing with in-situ concrete floors placed at each of the floor levels. The foundation of the building is a reinforced concrete slab structure that has an overall thickness of approximately 1m, which also forms the strong floor to the laboratory, and was especially constructed to support large structures for testing.

The precise construction details of the building have been given by Bravery (1993). However, important aspects relating to the building, which will have an influence on

the analytical assumptions, are outlined below. Other important information is included in Appendix B.

4.3.1.1 Stability

The building frame was designed as a 'no-sway' structure with a braced lift-shaft and two braced stair-cases located within the building. The location of these braced regions gives the building its global stability, which was designed to resist horizontal loads that may be applied to the structure as a result of wind or construction forces.

4.3.1.2 Beams and columns

The frame of the building comprises structural beams and columns made from structural steel universal sections of type and size stipulated by BS4: Part 1 (1993). These elements form the main load bearing members of the building and were designed assuming continuous columns and simply supported beams. To produce continuity of the columns throughout the entire height of the building, substantial connections were incorporated at the splice positions, while beam to column connections are simple 'cleat' type plates designed primarily to transfer shear only.

The layout of the building follows a convenient grid pattern that is formed primarily by the location of the column members. These columns, which are of 'H' cross-section type, have their stronger axis of bending orientated to coincide with the EW axis of the building offering greater stiffness to motion than in the NS direction. Main load bearing beams then span between these columns to form a grid coincident with the principal axes of the columns.

4.3.1.3 The floor construction

The concrete floor system, which in the scheme of the overall construction was placed after the completion of the building frame, is of a type produced from profiled steel deck units with an in-situ concrete layer. The usual approach to its placing is to first fix the steel profiles to the beams of the frame and later add the concrete layer to

provide a continuous floor element. Before concreting, steel stud pins are positioned at regular intervals over the length of each beam so that when the floor is complete the steel profile, in-situ concrete and steel beams are all physically connected. This system is often referred to as 'composite construction' where the final floor can be regarded as a single element that combines the properties of both the steel beams and the hardened concrete floor. A wire mesh was placed within the top surface of the concrete, which helps distribute lateral loads as well as control crack development of the concrete during its hydration process.

4.3.1.4 The in-fill panel walls

To enclose the space formed by each floor, block work panel walls were installed around the perimeter of the building. On the east and west faces of the building, these panel walls completely enclosed the space between the floors and columns of each storey. On the north and south elevations these walls were also constructed at each floor level, yet their height was shorter at 900mm.

4.3.2 The construction phases

To facilitate a rigorous assessment of the natural frequencies of the building, this study considered the measured results of four separate construction phases, which relate to similar phases described by Ellis and Ji (1996).

Construction phase 1:

Phase 1 represented a point when the entire steel frame comprising steel beams, columns and bracing was complete and the steel deck units that form the support for concrete placing were in position. At this stage, the steel deck units, which were produced by Precision Metal Forming (PMF) and are 0.9mm in thickness, were fastened to the beams of the frame by welding. These welds are common to this floor system and are usually incorporated as part of the steel shear stud assembly, which are used to provide the composite action of the completed floor. In this condition, the stiffness of the building as a whole is dependent on the properties of the columns and

the bracing configuration. Therefore, with the stiffer axis of the columns being in the EW axis of the frame, the NS direction will offer greater resistance to sway motion.

Construction phase 2:

At phase 2, the construction of all floors had been complete with each comprising of steel deck units, steel shear studs, reinforcing mesh and a lightweight concrete layer. The overall thickness of each finished floor was 130mm having a profiled cross-section with orthotropic stiffness properties. The out-of-plane bending stiffness of the orthotropic floor has its larger stiffness about the EW axis of the building, which in terms of the whole frame properties of the building will offer greater stiffness to motion in the NS direction.

Construction phase 3:

At phase 3, the perimeter block-work walls had been installed at each storey on the north, south, east and west faces of the building. This arrangement added further stiffness to the building along the EW and NS axes, further increasing the sway motion resistance of the overall frame in these directions.

Construction phase 4:

At the fourth and final phase the building was complete, with sandbag weights added to simulate the effect of service load on the building as if it were in use. Uniformly distributed over the area of the seven floors, the weight of the sandbags were 1100kg, with each occupying a space on plan of approximately 1.5m square. In total, 208 such sandbags were positioned on floors 1, 2, 3, 4, 6, and 7, while 169 bags were installed on floor 8. Floor 5 was left empty.

4.4 Dynamic Characteristics of the Steel-Framed Building from Measured Response and 'As-constructed' Information

The measured frequency results given by Ellis and Ji (1996) focus on the sway and torsion modes of the whole-frame and were obtained from a combination of forced and ambient response records.

4.4.1 The natural frequencies from ambient vibration response measurements

To measure the natural frequencies of the building, Ellis and Ji (1996) used the signal conditioning and data storage equipment as outlined in chapter 3. A laser interferometer provided a convenient means to capture the velocity response of the structure caused by air movements in the laboratory. Using a capture rate of 200Hz, a series of signals were recorded and stored that represented 409.6 seconds of structural vibration. Based on this combination of capture rate and record length the autospectra of the measured signals, which was obtained from a fast Fourier transform of the signals (resolution of 0.002Hz), it was possible to quote natural frequencies to two decimal places.

Table 4.1 shows the results, where the abbreviations used relate to the sway modes of the building along its EW and NS axes, while the rotation mode of the structure is referenced by the symbol θ. The number shown along side each of these references, for both sway motion and torsion, represent the mode order corresponding to the natural frequency values.

4.4.2 Natural frequency and damping from forced vibration tests at construction phase 4

The forced vibration tests were used to generate structural response records of the steel-framed building for use with frequency sweep and decay-of-vibration investigations (see chapter 3). To vibrate the building in the desired modes a total of four exciters were used, which were positioned on the top floor of structure. Recordings of acceleration then formed the basis of the signals used to identify the natural frequencies and damping characteristics, as well as their amplitude dependence. Tables 4.2 and 4.3 present the information acquired, which is all the available information obtained from these tests.

Table 4.1 – Measured natural frequencies for the steel framed building [from Ellis and Ji (1996)].

Construction Phase	EW1	NS1	θ1	EW2	NS2
1	1.31	1.55	1.67	-	-
2	0.69	0.83	0.89	2.10	2.44
3	0.75	1.31	1.64	2.13	3.81
4	0.66	0.93	1.22	1.9	2.63

Table 4.2 – Natural frequencies and damping characteristics of the building at construction phase 4 obtained from forced vibration tests [from Ellis and Ji (1996)].

Mode	EW1	NS1	θ1	EW2
Natural frequency (Hz)	0.617	0.804	0.959	1.835
Viscous damping (expressed as a % of critical)	2.25	2.46	3.28	2.79

An illustration of the assumed building motion, corresponding to each of these measurements, is shown in Figure 4.1.

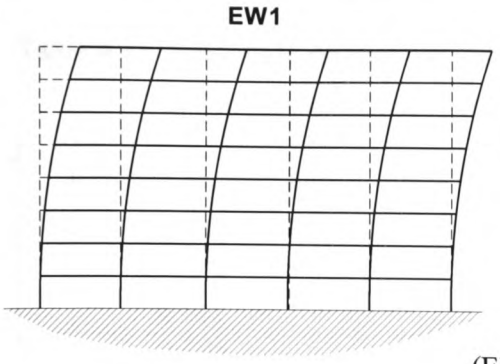

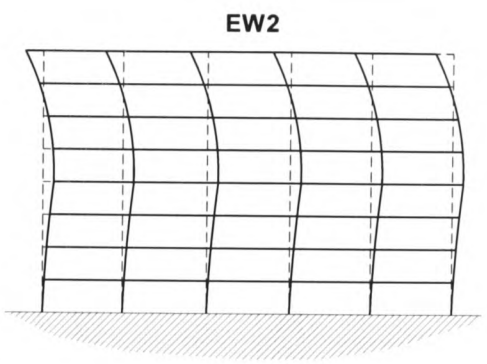

East - West Mode 1
Stage Frequency (Hz)

1	1.31
2	0.69
3	0.75
4	0.66

(Elevation on building looking North. Broken line represents the basic geometry of the structure).

East - West Mode 2
Stage Frequency (Hz)

1	-
2	2.10
3	2.13
4	1.90

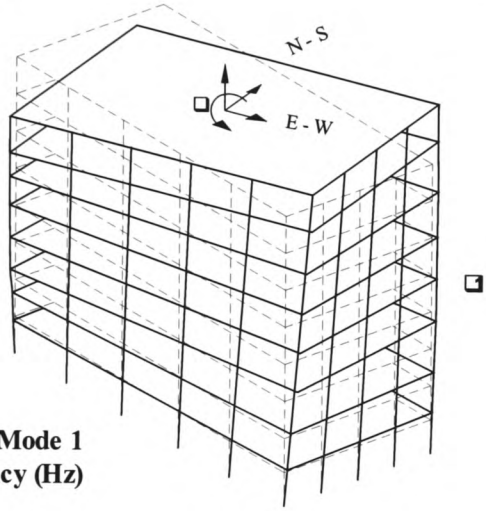

Rotational Mode
Stage Frequency (Hz)

1	1.67
2	0.89
3	1.64
4	1.22

North - South Mode 1
Stage Frequency (Hz)

1	1.55
2	0.83
3	1.64
4	0.93

Rotational Mode Shape

North - South Mode 2
Stage Frequency (Hz)

1	-
2	2.44
3	3.81
4	2.63

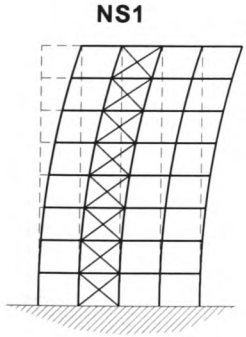

Cross-members represent part of the structural stability elements in the form of pin-ended diagonal bracing.

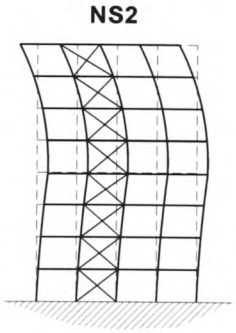

North - South Mode 1

North - South Mode 2

Figure 4.1 – Idealised mode shapes of the eight-storey steel-frames building corresponding to the values shown in Table 4.1

Table 4.3 – Amplitude dependence of natural frequency and damping of the building at construction phase 4 from decay of vibration signals (EW1 only)

Relative amplitude	Natural frequency (Hz)	Viscous damping (expressed as a % of critical)
1.000	0.611	2.87
0.366	0.636	1.81
0.181	0.645	1.28
0.106	0.647	1.02
0.062	0.656	0.85

4.4.3 Measured mode shapes of the building at construction phase 4

Mode shapes of the structure at construction phase 4 were recorded using the forced vibration equipment. The procedure adopted to achieve this information involved the use of two accelerometers, one to record the response at various locations throughout the structure, which was then related to a reference signal measured from a second accelerometer maintained at a constant location. The results from these tests are shown schematically by Figure 4.2, which offers the most convenient means of presenting such information.

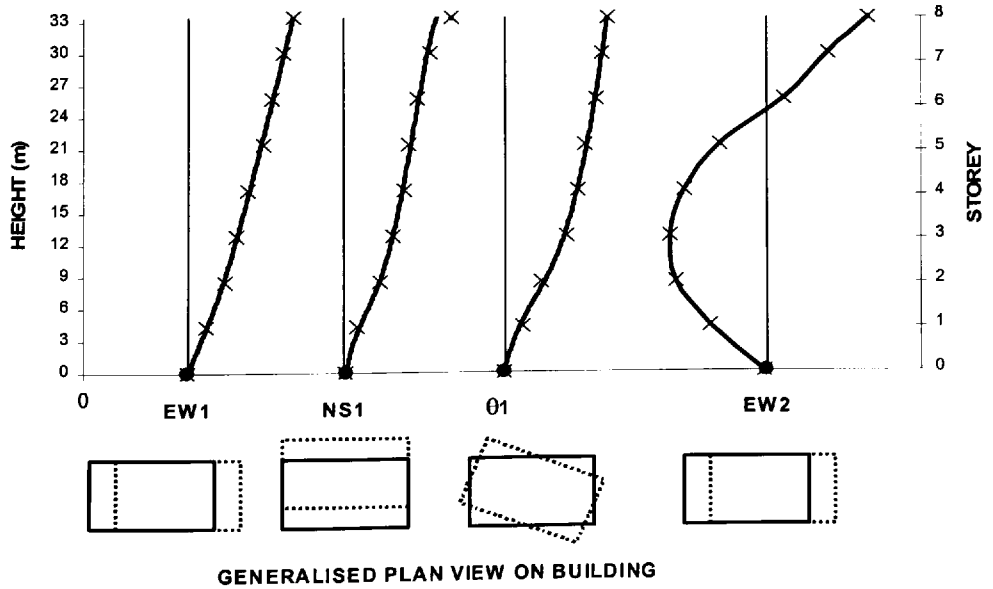

Figure 4.2 – Mode shapes of the steel-framed building at construction phase 4

4.4.4 The calculated mass of the building

Table 4.4, which is based on information given by Bravery (1993) present the calculated weight of the building at each storey. These storey mass calculations carried out using material weights for lightweight concrete, steel and masonry of 1.9 tonne/m^3, 7.85 tonne/m^3 and 1.9 tonne/m^3 respectively.

Table 4.4 – Calculated weight of the building at each construction phase using the frame construction details as given by Bravery (1993)

Storey Level	**Construction phase 1**	**Construction phase 2**	**Construction phase 3**	**Construction phase 4**
1	45.7	290	331.7	560.6
2	47.9	292.2	333.9	562.8
3	40.8	285.1	326.8	555.7
4	40.8	285.1	326.8	555.7
5	36.2	280.5	322.2	322.2
6	33.8	278.1	319.8	548.7
7	33.8	278.1	319.8	548.7
8	45.2	289.5	331.2	517.2
Total weights				
Steelwork	230 tonne	230 tonne	230 tonne	230 tonne
Floor construction	94 tonne	2048 tonne	2048 tonne	2048 tonne
Masonry	-	-	335 tonne	335 tonne
Sandbags	-	-	-	1559 tonne
Building weight	324 tonne	2278 tonne	2613 tonne	4172 tonne

(All weights are quoted in tonnes and storey level 8 represents the upper most floor of the building).

4.4.5 Calculated whole frame modal stiffness change at each construction phase

The measured frequencies and calculated masses provide sufficient information to allow the stiffness variation of the structure to be identified for each of the construction phases. To do this, a simple expression will be introduced that describes the relationship between the stiffness, mass and the natural frequency, which is given by,

$$\omega_n = \sqrt{\frac{K_n}{m_n}} \tag{4.4}$$

where ω_n is the natural frequency, K_n is the modal stiffness and m_n is the modal mass of the structure corresponding to mode n (n = 1, 2, 3, ...). To implement the above expression here, assumptions regarding the interpretation of these terms must first be introduced. Assuming that K_n and m_n relate directly to the modal stiffness and modal mass of the frame as a whole respectively, it should be possible to gain a quantitative estimate of their change based on the information that is available. Therefore, if the total mass of the building at each construction phase was indicative of its modal mass, i.e. the ratio of change of mass at each phase has a similar ratio change as the modal mass, the ratio of stiffness change can be calculated. The expression used for this calculation is a simple manipulation of eqn.(4.4) and can be written as,

$$\Psi = \frac{K_i}{K_j} = \frac{\omega_i{}^2 m_i}{\omega_j{}^2 m_j} \tag{4.5}$$

where Ψ is the ratio change of modal stiffness, and thus overall stiffness, in relation to the measured frequency "ω" and the calculated total mass of the building "m" from construction phase i to j. Therefore, if the mass of the building can be calculated from its constituent parts and their properties at each construction phase, the modal mass and modal stiffness ratio changes can be found (assuming that "ω" is available). This information is presented in Table 4.5, which gives the relative whole-frame stiffness for each construction phase.

Table 4.5 – Whole building stiffness change at each construction phase from measured natural frequencies and calculated mass properties

Mode	Phase	Successive change					Change relative to phase 1				
		i	j	$\frac{m_i}{m_j}$	$\frac{\omega_i^2}{\omega_j^2}$	Ψ_a	i	j	$\frac{m_i}{m_j}$	$\frac{\omega_i^2}{\omega_j^2}$	Ψ_c
EW1	1	1	1	1	1	1	1	1	1	1	1
	2	2	1	7.031	0.277	1.947	2	1	7.031	0.277	1.947
	3	3	2	1.147	1.181	1.355	3	1	8.065	0.328	2.645
	4	4	3	1.597	0.774	1.236	4	1	12.88	0.253	3.258
NS1	1	1	1	1	1	1	1	1	1	1	1
	2	2	1	7.031	0.287	2.018	2	1	7.031	0.287	2.018
	3	3	2	1.147	2.491	2.857	3	1	8.065	0.714	5.758
	4	4	3	1.597	0.504	0.804	4	1	12.88	0.360	4.637
θ1	1	1	1	1	1	1	1	1	1	1	1
	2	2	1	7.031	0.284	1.996	2	1	7.031	0.284	1.996
	3	3	2	1.147	3.396	3.895	3	1	8.065	0.964	7.775
	4	4	3	1.597	0.553	0.883	4	1	12.88	0.533	6.865
Mode	**Phase**	**Successive change**					**Change relative to phase 2**				
EW2	1	-	-	-	-	-	-	-	-	-	-
	2	2	2	1	1	1	2	2	1	1	1
	3	3	2	1.147	1.029	1.180	3	2	1.147	1.029	1.180
	4	4	3	1.597	0.796	1.271	4	2	1.832	0.819	1.5
NS2	1	-	-	-	-	-	-	-	-	-	-
	2	2	2	1	1	1	2	2	1	1	1
	3	3	2	1.147	2.438	2.796	3	2	1.147	2.438	2.796
	4	4	3	1.597	0.477	0.762	4	2	1.832	1.162	2.129

("-" Indicates that measured frequencies was not available for calculation).

General observations:

(i) Construction phase 1 to 2: The completion of the composite floor slab throughout the building at phase 2 effectively increased the stiffness of the whole-frame in each axis by an approximately equal amount. In percentage terms this increase is approximately 90 – 100%, calculated relative to the properties of the frame at phase 1, and is consistent for the EW1, NS1 and θ1 modes.

(ii) Construction phase 2 to 3: Installation of the block-work walls around the perimeter of each floor has a marked affect on the NS and EW sway, and the torsion behaviour of the frame. This observation reinforces the argument that in-fill block-work walls offer additional stiffness to a building, which is confirmed

by the work of Smith (1963). The effect is more pronounced for the NS sway and the torsion behaviour, where the panel walls installed on the east and west elevations of the building effectively enclose the space between the beams and columns of the frame. The result was an increase to the whole-frame stiffness between construction phase 2 and 3 in the NS direction by approximately 180-190% ($\Psi_a \approx 2.8$), which is reflected in the calculations of both NS1 and NS2. Similarly, the torsion stiffness changes significantly between these phases, but the increase is larger at almost 290% ($\Psi_a \approx 3.9$). The whole frame stiffness in the EW direction also changes but is much smaller at approximately 20 to 35% ($\Psi_a \approx 1.2$, $\Psi_a \approx 1.35$ respectively), which is consistent for both the EW1 and EW2 calculations. These changes clearly demonstrate the different stiffening effects of the block-work walls on the north and south elevations of the building.

(iii) Construction phase 3 to 4: The addition of the sandbag loading is the only difference between construction phase 3 and 4. However, the calculations presented in Table 4.4 suggest that the added mass effectively increased the EW sway stiffness by approximately 20 – 25% ($\Psi_a \approx 1.24$) while reducing the NS and torsion stiffness by 20% and 12% ($\Psi_a \approx 0.8$, $\Psi_a \approx 0.88$) respectively. This is an interesting observation as the calculations appear to advocate that the substantial building weight increase has the effect of 'shifting' stiffness from one axis to the other, i.e. the total increase in EW stiffness is proportional to the reduction in the NS and θ modes.

4.5 The Analytical Models

Two analytical models were used to calculate the natural frequencies of the steel-framed building for comparison with the measured information. Categorised as (1) full FE analysis, and (2) the Grinter substitute frame method, this section gives detail relating to the assumptions taken into account during the preparation of both models.

4.5.1 The full FE analysis

The main assumption inherent in all FE analytical work is that an adequate representation of a structure can be achieved from a collection of mathematical functions, which are formulated to embody the main characteristics and behaviour of elements comprising the structure when subjected to load. Most modern applications of this technique are carried out using computer programs that have been written to offer the user a comprehensive library of such functions that can be assembled to reflect the geometry, properties and fundamental features of the structure being modelled. The eight-storey steel-framed building was modelled in this way using a computer program produced by Oasys, which is a subsidiary company of consulting engineers Ove Arup and Partners. The product name of the program used, which is a commercially available program, is GSA and is an acronym for 'General Structural Analysis'. With this program a total of four models were prepared, each incorporating a range of finite elements to simulate the building at the various construction phases identified previously.

Construction phase 1:
To form the geometry of the frame, which would also allow the incorporation of additional features present in other construction phases, a total of 764 nodes were identified. This number of nodes matched those of the model prepared by Ellis and Ji (1996), which represents the main joint positions of the structural parts of the building. Beam, column and bracing members were then introduced to these nodes using classical three-dimensional beam type elements. With regard to the boundary conditions assumed for these members, all beam and bracing members were modelled assuming 'pin' type connections at their ends, while the columns were assumed to be continuous over their entire length.

To model the properties of the steel decking units at each floor of the building, orthotropic shell elements were introduced to represent the slab grid. The section properties assigned to these shell elements simulated the characteristics of the profiled steel deck units with the stiffer axis being orientated in the north-south direction of the building.

Construction phase 2:

To represent construction phase 2, the model was adjusted to include the properties of the concrete slab. This was achieved in a similar way as explained above, where the properties of the shell elements were assigned values appropriate to the orthotropic nature of the complete slab system. The completed model then comprised beam, column and bracing, as defined for phase 1, with the slab being modelled as a continuous series of shell elements covering the entire area of each floor. To ensure that the slab model reflected the substantial in-plane stiffness of each floor, isotropic membrane elements was added to the model and assigned a thickness coincident with the average dimensions of the concrete deck. The mass properties of these elements were then nullified so as not to duplicate the weight of the concrete floor already incorporated in the shell properties.

Construction phase 3:

The masonry panels installed around the perimeter of the building, for construction phase 3, were modelled using isotropic membrane elements. On the east and west faces of the frame, the connectivity of these elements were assigned relative to the beam / column joints of the frame, which in turn is a representation assuming a 'perfect' interaction of the frame and the panel block-work at these locations.

Construction phase 4:

Finally, to represent phase 4, the mass of the sandbags was incorporated assuming a uniformly distributed mass, which was assigned relative to the number installed on each floor.

4.5.1.1 Tabulated properties of the FE models

The properties of the completed FE models are presented in Table 4.6. To aid the interpretation of these properties it should be noted that the model was geometrically set out assuming that the east-west axis of the building being orientated along the x-axis of the model, with the north-south and vertical axes coinciding with the y and z axes respectively. This referencing system can be referred to as the 'global co-ordinate system'

Table 4.6 – Details of the finite elements (global co-ordinate system)

Model No.	**Member**	**Element type**	**Number of nodes**	**Characteristics included in the FE models at the element nodes**					
				R*x*	**R*y***	**R*z***	**D*x***	**D*y***	**D*z***
1	Columns	3D Beam	2	yes	yes	yes	yes	yes	yes
	Beams (EW)	3D Beam	2	yes	no	yes	yes	yes	yes
	Beams (NS)	3D Beam	2	no	yes	yes	yes	yes	yes
	Bracing	Bar	2	no	no	no	yes	yes	yes
	Deck	Shell	4	yes	yes	no	no	no	no
2 (in addition to 1)	Slab	Shell	4	yes	yes	no	no	no	no
		Membrane	4	no	no	no	yes	yes	yes
3 (in addition to 2)	Block work panels	Membrane	4	no	no	no	yes	yes	yes
4	No additional elements								
All	Column bases	-	-	no	no	no	yes	yes	yes

Abbreviations:
R*x*, R*y* and R*z* are rotational degree-of-freedom characteristics,
D*x*, D*y* and D*z* are displacement degree-of-freedom characteristics.

4.5.2 The Grinter substitute frame

The FE method offers a comprehensive solution to this particular problem, but its drawback is that data preparation is substantial. If only natural frequencies are required, this task can very quickly become excessively onerous. In such cases a feasible alternative is to use an 'approximate' whole-frame technique, which can offer solutions to a reasonable degree of accuracy when compared to results gained using more complex analysis such as the FE method. Roberts and Wood (1981a & b) and Williams *et al* (1983) reported on the Grinter substitute frame, which is one such approximate method as introduced in the review of literature discussed earlier in this chapter. Despite the attention given by these authors to the calculation of natural frequencies of plane frame structures, the candidate is not aware of any previous application to three-dimensional frames, although the extension is straightforward.

4.5.2.1 Fundamental assumptions relating to the eight-storey steel-framed building

It is assumed, in the first instance, that the frame motion during sway vibration is uniform in a direction parallel to the EW or NS axis of the building. The other primary assumptions are:

(i) The axial deformation of column members is ignored, as the vertical displacement of the frame during whole-frame sway motion is considered negligible in relation to any horizontal movement.

(ii) Rotations at the beam and column connections throughout each storey are assumed to be approximately equal, which is applicable to any level of the frame. i.e. as sway of the frame occurs, the displacements and rotations at the joints of individual floors are numerically identical.

(iii) Each beam within the building frame has a column member at both of its ends.

(iv) The motion of the building, corresponding to the calculated natural frequencies, is dominated primarily by whole-frame sway behaviour and possible coupling effect between sway and torsion modes is weak.

(v) The beams to column joints of the frame are assumed to be rigid. For vibration analysis this approach is justified as Wyatt (1989) reports that "... structural continuity under dynamic motion has the effect that column stiffness commonly contributes significant end restraint, even when the beam connections are of a form that would normally be regarded as permitting rotation."

(vi) The in-plane stiffness of each floor is large relative to its out-of-plane stiffness and no relative movement between columns will occur. During sway motion it is therefore assumed that the displacement of each column will be numerically similar.

(vii) The mass of the building at each storey level can be represented as a lumped mass at a single location. This allows a convenient representation of structural mass and is ideal for calculations that aim to identify whole-frame sway characteristics only.

4.5.2.2 Condensing the three-dimensional frame into a plane frame form

The first step is to condense the three-dimensional frame into a model that is sufficiently simple to facilitate manipulation, but is capable of yielding accurate results. Initially, any columns or beams that lie off-grid are 'relocated' to the nearest on-grid location. Next, the regular three-dimensional frame is condensed into an equivalent two-dimensional frame lying parallel to the EW (or NS) axis depending on the sway mode being considered. Therefore, the plane frame column stiffness at a typical storey level can be calculated from:

$$\sum(\text{Stiffness of column } Ai_1 + \text{Stiffness of column } Ai_2 + \ldots + \text{Stiffness of column } Ai_n) \tag{4.4}$$

where A and n relate to the grid line referencing system, and i is the storey level at which the column section properties are being calculated. In a similar fashion, the beam stiffness is obtained from,

$$\sum(\text{Bending stiffness of beam } Ai_1\text{-}Bi_1 + \text{Bending stiffness of beam } Ai_2\text{-}Bi_2 + \ldots \ldots + \text{Bending stiffness of beam } Ai_n\text{-}Bi_n) \tag{4.5}$$

where A-B relates to a beam bounded by two columns. The composite nature of the floor slab is included in the bending stiffness calculations at the appropriate construction phases. Beams and in-fill walls that are perpendicular to the axis being considered are included as structural mass only, i.e. the contribution of the member lying in the orthogonal sway direction, to the one being considered, are deemed to add weight only.

On completion of this procedure, i.e. for all beam and column members at each level of the structure, the equivalent plane frame elevation is obtained, which can be visualised as a two-dimensional structure comprising the section properties of all

parallel frames. Figure 4.3 illustrates the basic philosophy of this procedure in a diagrammatic way.

4.5.2.3 Condensing the plane frame into a Grinter substitute frame

The next step is to perform a similar condensation procedure on the equivalent plane frame. Therefore, the stiffness of the Grinter frame column at a typical storey level, say level *i*, can be taken as the sum of the column stiffness at storey level *i* of the plane frame. In a similar manner the Grinter beam stiffness are calculated from the sum of the beam stiffness at the corresponding storey level. The length of beam and column members in the compiled Grinter frame will remain consistent with their dimensions in the original building frame. Where these dimensions vary, especially where the beam members are concerned, the dominant dimension can be used. The final frame achieved after the condensation process is given by Figure 4.4.

4.5.2.4 Calculating the natural frequencies and mode shapes of the Grinter substitute frame

To calculate the natural frequencies and mode shapes of the Grinter substitute frame the candidate compiled a computer program called GRIND (GRINter frame Dynamic analysis) using the FORTRAN 77 language. The program was written assuming that each storey of the compiled Grinter frame could be represented using classical theories of FE analysis by Zienkiewicz (1977). Using this approach, which implemented matrix type operations, the required natural frequencies and mode shapes could be achieved from the eigen-value problem corresponding to the whole-frame element arrangement. The main sequence of calculations performed by the program can be summarised to the following points:

(i) Compile the element stiffness matrices of each storey using the following element formulation,

$$[K_i]\{\delta_i\} = \begin{bmatrix} \frac{12EI_c}{L_c^3} & \frac{6EI_c}{L_c^2} & -\frac{12EI_c}{L_c^3} & \frac{6EI_c}{L_c^2} & 0 \\ \frac{6EI_c}{L_c^2} & \frac{4EI_c}{L_c} & -\frac{6EI_c}{L_c^2} & \frac{2EI_c}{L_c} & 0 \\ -\frac{12EI_c}{L_c^3} & -\frac{6EI_c}{L_c^2} & \frac{12EI_c}{L_c^3} & -\frac{6EI_c}{L_c^2} & 0 \\ \frac{6EI_c}{L_c^2} & \frac{2EI_c}{L_c} & -\frac{6EI_c}{L_c^2} & \frac{4EI_c}{L_c}+\frac{4EI_b}{L_b} & \frac{2EI_b}{L_b} \\ 0 & 0 & 0 & \frac{2EI_b}{L_b} & \frac{4EI_b}{L_b} \end{bmatrix} \begin{Bmatrix} \delta_{x1} \\ \varphi_{z1} \\ \delta_{x2} \\ \varphi_{z2} \\ \varphi_{z3} \end{Bmatrix} \quad (4.6)$$

where $\delta_{x1,2}$ and $\varphi_{z1,2}$ are the in-plane displacements and rotations respectively of the column member, while φ_{z3} is the in-plane rotation of the beam. $[K_i]$ and $\{\delta_i\}$ are therefore the stiffness matrix and displacement vector respectively for storey level i. The material Young's modulus E, bending inertia values for the column and beam, I_c and I_b respectively, and the element length (L_c and L_b) appropriate to the members of the frame being assigned accordingly.

(ii) Compile the structure matrix comprising a summation of the individual storey elements of the frame using a numerical referencing system to represent the nodes of the model. The storey element matrix of eqn.(4.6) is defined using the following abbreviations,

$$[K_i] = \begin{bmatrix} [k_{11}]_i & [k_{12}]_i & \\ [k_{21}]_i & [k_{22}]_i & \\ & & [k_{33}]_i \end{bmatrix} \quad (4.7)$$

where i is the storey level, the final structure matrix will have the form given by,

$$[\bar{K}]=\begin{bmatrix} [k_{11}]_1 & [k_{12}]_1 & 0 & 0 & 0 & \cdots & \cdots & \cdots \\ [k_{21}]_1 & [k_{22}]_1+[k_{11}]_2 & 0 & [k_{12}]_2 & 0 & \cdots & \cdots & \cdots \\ 0 & 0 & [k_{33}]_1 & 0 & 0 & \cdots & \cdots & \cdots \\ 0 & [k_{21}]_2 & 0 & [k_{22}]_2+[k_{11}]_3 & 0 & \cdots & \cdots & \cdots \\ 0 & 0 & 0 & 0 & [k_{33}]_2 & \cdots & \cdots & \cdots \\ \vdots & \vdots & \vdots & \vdots & \vdots & \ddots & & \\ \vdots & \vdots & \vdots & \vdots & \vdots & & \ddots & \\ & & & & \vdots & & & \ddots \end{bmatrix} \quad (4.7)$$

where $[\bar{K}]$ indicates that the matrix is in terms of the whole structure.

(iii) Assign the boundary conditions, which depend mainly on the chosen base node condition. To impose these conditions the approach adopted was based on the removal of the rows and columns of the structure stiffness matrix appropriate to the restrained dofs.

(iv) Compile the structure mass matrix, which is comprised of a simple lumping of the storey weights in a matrix format in the usual way, i.e. the structure mass matrix will be a diagonal matrix with values coincident with the column displacement terms of the storey element matrix in (ii) above.

(v) Form the generalised eigen-value problem and convert it to a standard form given by,

$$[\bar{M}]\{\delta\}=\varpi^2[\bar{K}]\{\delta\} \quad (4.8a)$$

$$[\bar{S}]\{\Delta\}=\varpi^2\{\Delta\} \quad (4.8b)$$

Cholesky's method is used as described by Griffiths and Smith (1991), where ϖ^2 and $\{\Delta\}$ are respectively the eigen-value in radians per second and its associated eigen-vector corresponding to the matrix $[\bar{S}]$.

(vi) Calculate all eigen-values and eigen-vectors of the standard problem in (v) using a Jacobi algorithm as discussed by Press *et al* (1992).

(vii) Recover the eigen-vectors relating to the structure matrices $[\bar{K}]$ and $[\bar{M}]$ from the Cholesky routine and normalise the results for convenience.

A flow chart, which represents this sequence in the computer program, is given in Figure 4.5.

4.6 The Results of the Analysis

4.6.1 Natural frequencies calculated using the full FE frame analysis

A large amount of information concerning the natural frequencies of the building can be obtained from the FE analysis, which can include local vibration modes as well as the global behaviour of the structure. However, this can be a disadvantage when the analysis aims to concentrate only on the sway and torsion modes of the building. This problem stems mainly from the computation process of the FE program used, which will identify all modes of vibration relative to their frequencies in numerical order. Therefore, to focus the analysis on a limited number of the modes, Table 4.6 shows the natural frequencies calculated by the GSA program limiting the analysis to the first six modes of the frame for each construction phase.

The main reason for restricting the number of modes was primarily due to the amount of time required by the computer to solve the natural frequencies of the frame. On average, each computer run required 15 hours of processing time, which excluding additional runs needed to correct accidental errors present in the input data, meant a full working week of pure processing time to gain all construction phase results. Although this did not present a problem for the candidate, the computer required to process the calculations was a 'Sun – Sparks' machine with approximately 128Mb of random access memory, which was located at a consulting engineers office outside of university control. Analysis was therefore limited due to the demands on the computer to solve problems other than that described in this chapter.

Table 4.7 – Natural frequency values obtained from the full FE analysis

Mode order		1	2	3	4	5	6
Phase 1	**Frequency**	1.66	1.83	2.09	2.53	3.03	3.84
	Mode	EW θ	θ1	NS θ	L1	θ2	L2
Phase 2	**Frequency**	0.83	1.04	1.30	1.81	2.04	2.16
	Mode	EW θ	NS θ	θ1	L1	B1	B2
Phase 3	**Frequency**	1.06	1.99	2.04	2.17	2.54	2.75
	Mode	EW1	NS1	B1	B2	θ1	B3
Phase 4	**Frequency**	0.90	1.80	2.04	2.14	2.54	2.75
	Mode	EW1	NS1	B1	θ1	B2	B3

(All frequency values are in Hz, i.e. cycles per second)
Abbreviations:

L	Local modes (e.g. beam vibration)	θ	Whole frame torsion vibration
EW	East-west whole frame vibration	NS	North-south whole frame vibration
B	Local vibration in frame bracing		

Combinations:

EW θ	EW and θ modes combined	NS θ	NS and θ modes combined
EW1	Fundamental EW mode	NS1	Fundamental NS mode

L1, L2 etc – Fundamental, second etc of local modes
B1, B2 etc – Fundamental, second etc of frame bracing modes.

4.6.2 Natural frequencies and mode shapes from the GRIND computer program

The calculated natural frequencies and their associated mode shapes obtained from the GRIND computer program are shown in Table 4.8. The table contains values assuming the base of the frame to be either fixed of pinned, which describes whether rotation is restrained or permitted respectively, and concentrates on the fundamental whole-frame sway values of EW1, EW2, NS1 and NS2 only.

4.6.3 Calculated whole-frame stiffness change from the analytical results

Using the calculated frequencies from both the full FE frame and GRIND it is possible to calculate the whole-frame stiffness change following the methodology used to evaluate similar information from the measured frequencies. However, as the calculations provide significantly more information to that available from the measured properties, two approaches were considered.

4.6.3.1 Whole frame stiffness change using the frequency results from the full FE analysis

Due to uncertainties regarding the precise and correct mode characteristics reflected by the analytical results from the full FE calculations, the whole frame stiffness change for this model was obtained in a similar fashion as described previously for the measured frequencies.

4.6.3.2 Whole frame stiffness change using the results from GRIND

The Grinter substitute frame assumes pure whole frame sway modes, which is convenient for a direct calculation of the modal mass and modal stiffness of the building frame. Therefore, instead of using the ratios of mass change identified earlier, the modal mass was calculated directly using,

$$\Gamma = \sum_{i=1}^{8} m_i \phi_i^{\,2} \tag{4.9}$$

where Γ is the calculated whole-frame modal mass after Thomson (1993) using m_i and ϕ_i as the storey mass (Table 4.4) and normalised mode shape amplitude (Table 4.8) respectively at storey i of the Grinter frame. Modal stiffness can then be calculated from,

$$\Re = \varpi^2 \Gamma \tag{4.10}$$

where $\Re$ is the whole-frame modal stiffness, and ϖ is the natural frequency in units of radians per second appropriate to the sway mode being considered. The whole-frame stiffness change can then be achieved from a simple ratio of construction phases following a similar procedure as identified earlier.

The modal mass and modal stiffness calculated for each construction phase using eqns.(4.9) and (4.10) are presented by Table 4.10.

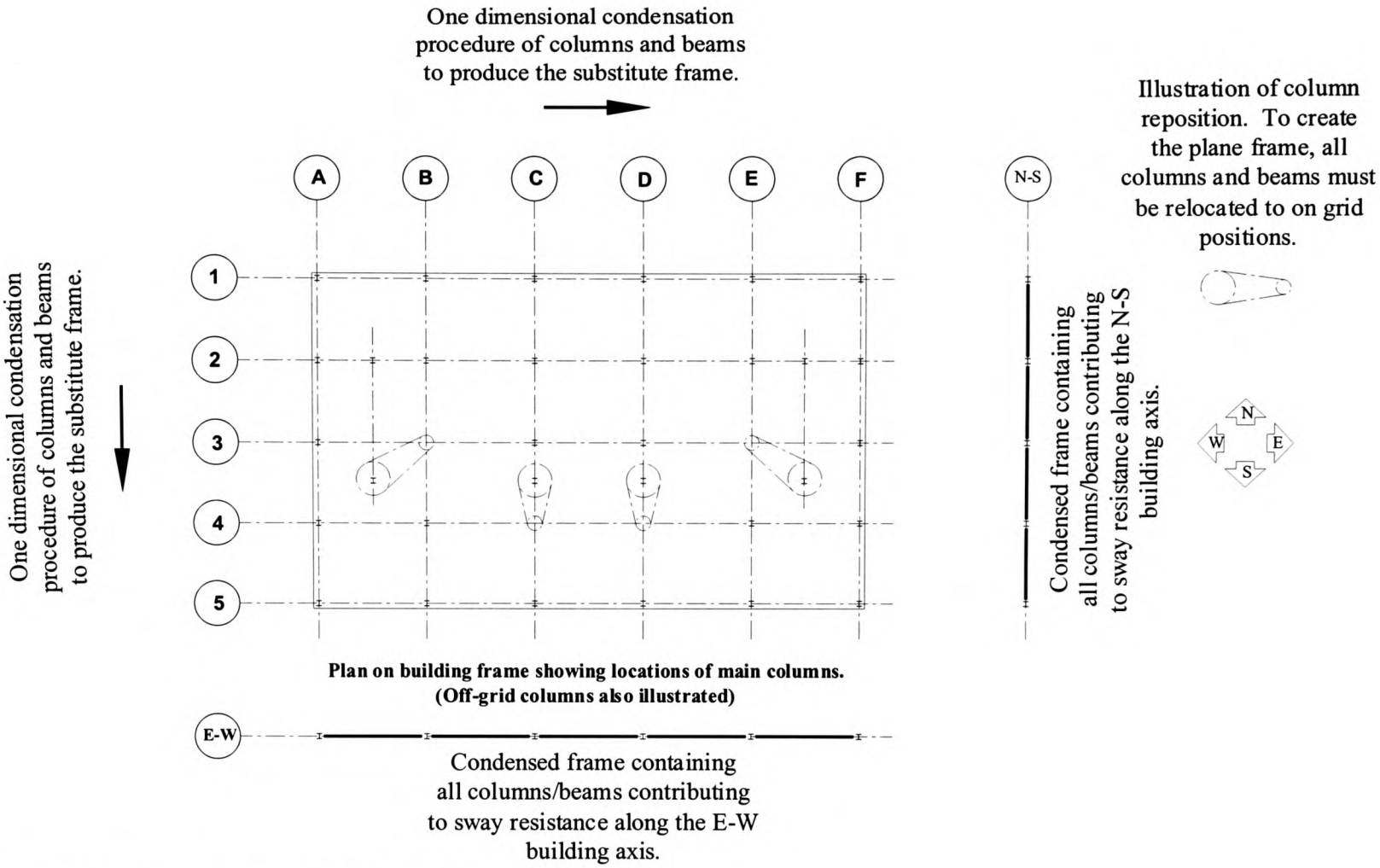

Figure 4.3 – Condensing the three-dimensional frame into a plane frame form

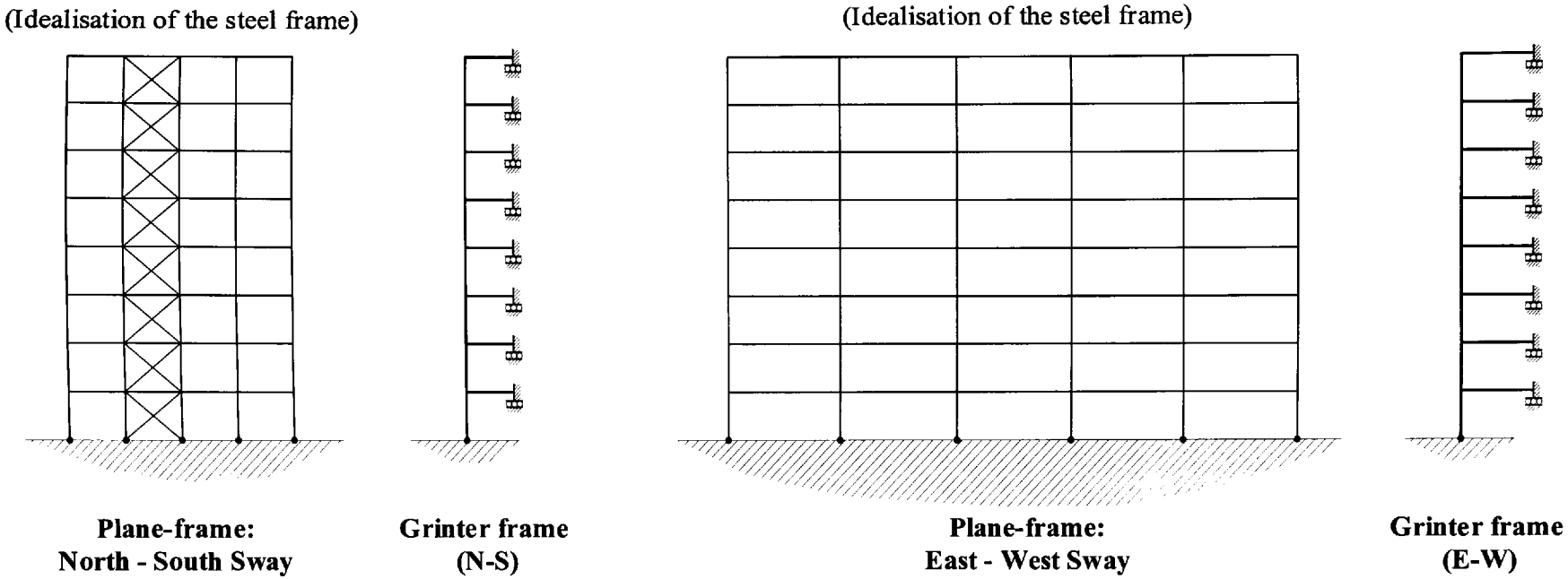

1. Plane frame stiffness obtained by summing all beam and column section properties along grid-lines A to F (or 1 - 5) as outlined in Figure 4.3.
2. Plane frame is further condensed to represent the Grinter frame. Although bracing elements are illustrated, they are initially ignored. Foundations can be assumed to be fixed or pin-ended.

Figure 4.4 – Condensing the plane-frame to the Grinter substitute frame

Table 4.8 – Calculated natural frequencies and mode shapes from the GRIND computer program

Pinned Base Scenario Results																
Mode	**EW1 – Phase:**				**EW2 – Phase:**				**NS1 – Phase:**				**NS2 – Phase:**			
	1	**2**	**3**	**4**	**1**	**2**	**3**	**4**	**1**	**2**	**3**	**4**	**1**	**2**	**3**	**4**
Freq (Hz)	1.01	0.47	0.45	0.36	5.15	2.2	2.09	1.65	1.57	0.66	0.62	0.49	11.81	3.35	3.15	2.49
Floor	Mode shape presented in a normalised numerical format (ϕ)															
1	0.152	0.188	0.188	0.181	-0.374	-0.402	-0.378	-0.399	0.142	0.153	0.155	0.156	-0.552	-0.361	-0.360	-0.380
2	0.292	0.353	0.353	0.351	-0.644	-0.687	-0.644	-0.678	0.274	0.293	0.299	0.299	-0.918	-0.678	-0.638	-0.660
3	0.427	0.503	0.503	0.488	-0.774	-0.819	-0.764	-0.801	0.405	0.429	0.437	0.436	-1.0	-0.759	-0.759	-0.796
4	0.557	0.639	0.638	0.624	-0.743	-0.774	-0.716	-0.745	0.533	0.560	0.569	0.568	-0.761	-0.719	-0.718	-0.749
5	0.679	0.757	0.757	0.744	-0.509	-0.514	-0.463	-0.479	0.659	0.685	0.692	0.692	-0.264	-0.492	-0.492	-0.510
6	0.794	0.855	0.855	0.846	-0.086	-0.067	-0.033	-0.039	0.779	0.8	0.805	0.805	0.321	-0.081	-0.081	-0.090
7	0.9	0.935	0.935	0.929	0.441	0.467	0.482	0.480	0.892	0.904	0.907	0.907	0.699	0.446	0.446	0.443
8	1.0	1.0	1.0	1.0	1.0	1.0	1.0	1.0	1.0	1.0	1.0	1.0	0.930	1.0	1.0	1.0
Fixed Base Scenario Results																
Mode	**EW1 – Phase:**				**EW2 – Phase:**				**NS1 – Phase:**				**NS2 – Phase:**			
	1	**2**	**3**	**4**	**1**	**2**	**3**	**4**	**1**	**2**	**3**	**4**	**1**	**2**	**3**	**4**
Freq (Hz)	1.69	0.71	0.69	0.55	6.89	2.84	2.68	2.16	3.23	1.08	1.02	0.81	16.11	4.45	4.18	3.37
Floor	Mode shape presented in a normalised numerical format (ϕ)															
1	0.032	0.047	0.047	0.045	-0.170	-0.170	-0.162	-0.178	0.028	0.032	0.032	0.034	-0.242	-0.151	-0.151	-0.165
2	0.112	0.154	0.154	0.148	-0.502	-0.497	-0.473	-0.516	0.098	0.109	0.112	0.117	-0.679	-0.451	-0.449	-0.489
3	0.226	0.296	0.296	0.286	-0.813	-0.796	-0.756	-0.817	0.203	0.224	0.228	0.234	-1.0	-0.739	-0.738	-0.797
4	0.383	0.454	0.454	0.440	-0.976	-0.937	-0.887	-0.949	0.338	0.366	0.370	0.374	-0.992	-0.884	-0.883	-0.943
5	0.517	0.614	0.614	0.599	-0.852	-0.789	-0.740	-0.787	0.493	0.523	0.527	0.530	-0.597	-0.783	-0.782	-0.829
6	0.68	0.762	0.762	0.750	-0.407	-0.331	-0.296	-0.326	0.660	0.687	0.690	0.693	0.045	-0.375	-0.374	-0.407
7	0.842	0.891	0.891	0.884	0.254	0.312	0.329	-0.314	0.832	0.848	0.849	0.851	0.529	0.272	0.272	0.255
8	1.0	1.0	1.0	1.0	1.0	1.0	1.0	1.0	1.0	1.0	1.0	1.0	0.878	1.0	1.0	1.0

("Freq" = calculated natural frequency; and the floor numbers represent the storey levels with 8 being the top of the building).

Table 4.9 – The natural frequency and whole-frame stiffness change: comparison between measured and the full FE analysis results

Mode	Construction phase	Measured frequency (f_m)	fnll FE frame frequency	Ellis and Ji (1996)	Measured Ψ_c (Table 4.5)	full FE frame Ψ_c	Ellis and Ji (1996) Ψ_c
EW1	1	1.31	1.66	1.60	1	1	1
	2	0.69	0.83	0.75	1.947	1.758	1.545
	3	0.75	1.06	0.89	2.645	3.289	2.495
	4	0.66	0.90	0.7	3.258	3.786	2.465
NS1	1	1.55	2.09	1.67	1	1	1
	2	0.83	1.04	0.77	2.018	1.741	1.495
	3	1.31	1.99	1.95	5.758	7.311	10.996
	4	0.93	1.80	1.55	4.637	9.554	11.095
θ1	1	1.67	1.83	1.91	1	1	1
	2	0.89	1.3	0.89	1.996	3.001	1.527
	3	1.64	2.54	2.78	7.775	13.178	17.085
	4	1.22	2.14	2.22	6.865	14.938	17.40

(Frequencies are in Hz, and all stiffness ratios are accumulative and are therefore relative to construction phase 1).

Table 4.10 – The natural frequency and whole-frame stiffness change: comparison between measured results and calculation from GRIND

Mode	Construction phase (i)	Pinned base scenario results			Fixed base scenario results			Measured results (from Table 4.4)			Pinned base	Fixed base
		Freq (Hz)	Γ	$\Re$	Freq (Hz)	Γ	$\Re$	Freq (Hz)	$\frac{m_i}{m_1}$	Ψ_c	$\Psi_c = \frac{\Re_i}{\Re_1}$	$\Psi_c = \frac{\Re_i}{\Re_1}$
EW1	1	1.01	135.9	5473	1.69	103.2	11636	1.31	1	1	1	1
	2	0.47	1173	10228	0.71	922.3	18355	0.69	7.031	1.947	1.88	1.58
	3	0.45	1280	10228	0.69	976.6	18355	0.75	8.065	2.645		
	4	0.36	1999	10228	0.55	1537	18355	0.66	12.88	3.258		
NS1	1	1.57	131.2	12757	3.23	98.9	40734	1.55	1	1	1	1
	2	0.66	1008	17327	1.08	779.6	35899	0.83	7.031	2.018	1.38	0.88
	3	0.62	1142	17327	1.02	874.0	35899	1.31	8.065	5.758		
	4	0.49	1828	17327	0.81	1386	35899	0.93	12.88	4.637		
Mode	**(i)**	**Freq (Hz)**	Γ	$\Re$	**Freq (Hz)**	Γ	$\Re$	**Freq (Hz)**	$\frac{m_i}{m_1}$	Ψ_c	$\Psi_c = \frac{\Re_i}{\Re_1}$	$\Psi_c = \frac{\Re_i}{\Re_1}$
EW2	2	2.2	974.2	186155	2.84	1081	344252	2.10	1	1	1	1
	3	2.09	1079	181655	2.68	1214	344252	2.13	1.147	1.180		
	4	1.65	1732	186155	2.16	1869	344252	1.9	1.832	1.5		
NS2	2	3.35	941.4	417088	4.45	1068	835281	2.44	1	1	1	1
	3	3.15	1065	417088	4.18	1211	835281	3.81	1.147	2.796		
	4	2.49	1704	417088	3.37	1863	835281	2.63	1.832	2.129		

(Γ is quoted in tonne units, while $\Re$ is given in terms of kN/m).

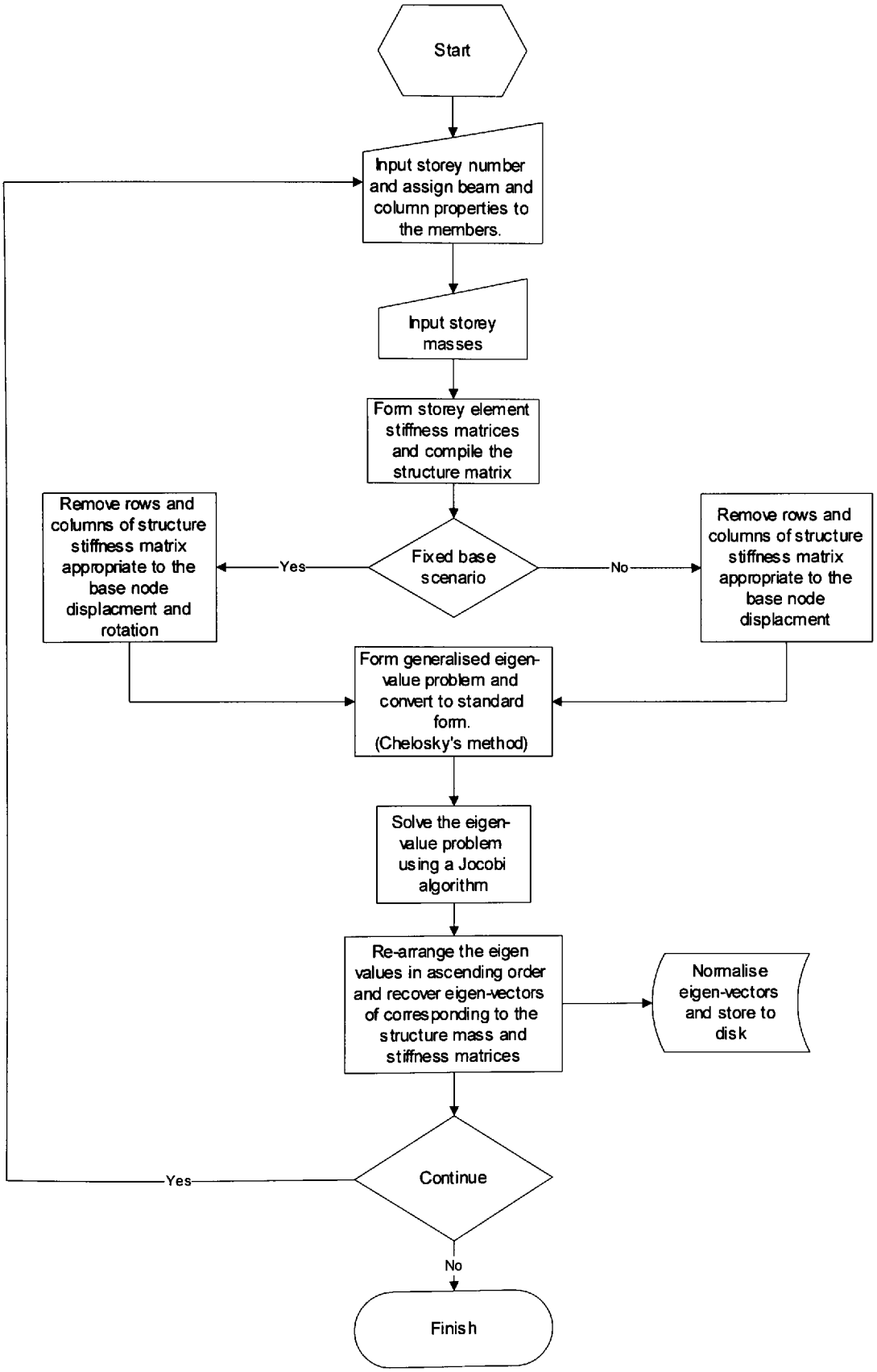

Figure 4.5 – Flow chart of the computer program GRIND

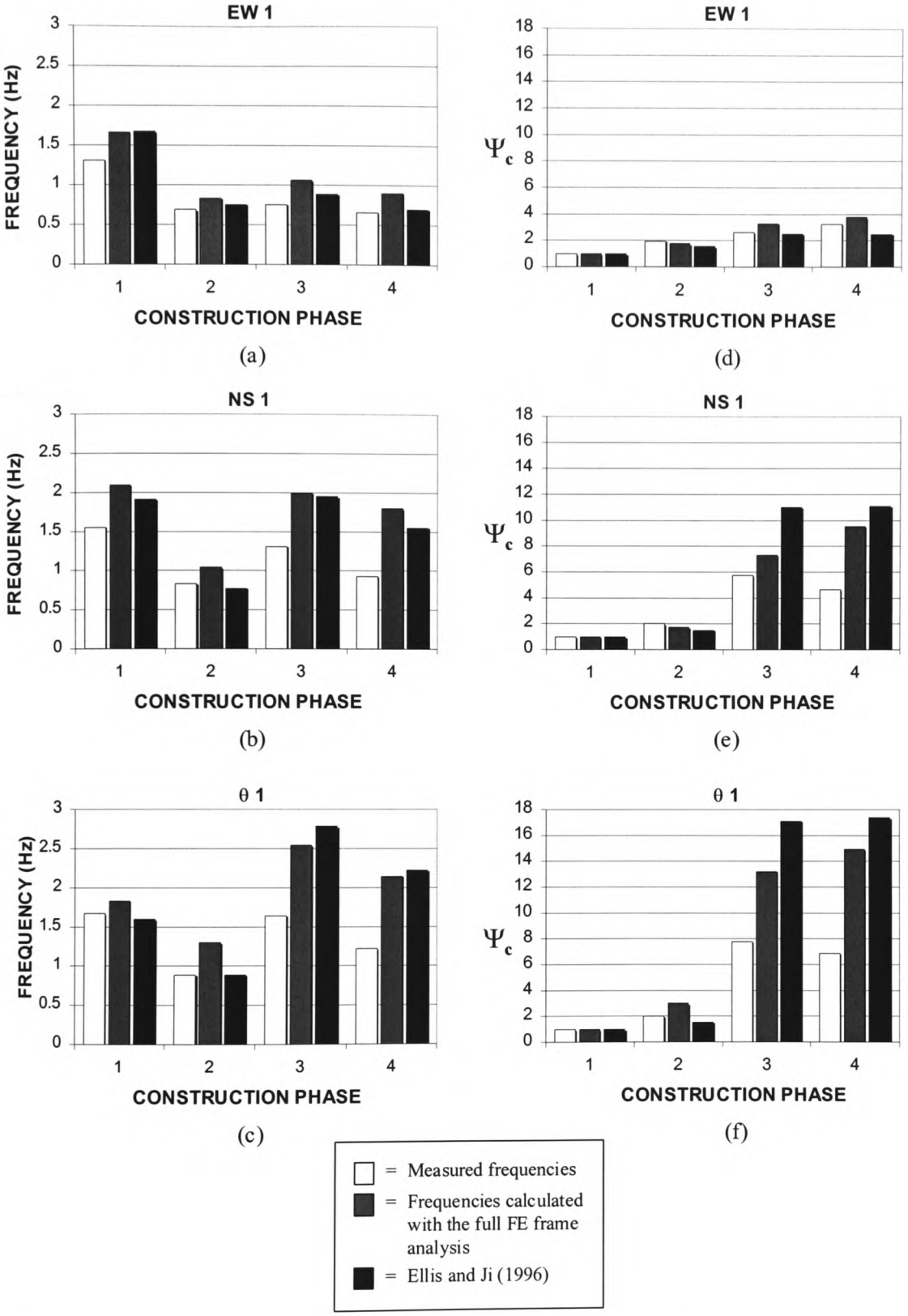

Figure 4.6 – Comparisons between measured and calculated results for the steel-framed building from full FE frame models: (a)+(d) EW 1, (b)+(e) NS 1, (c)+(f) θ1

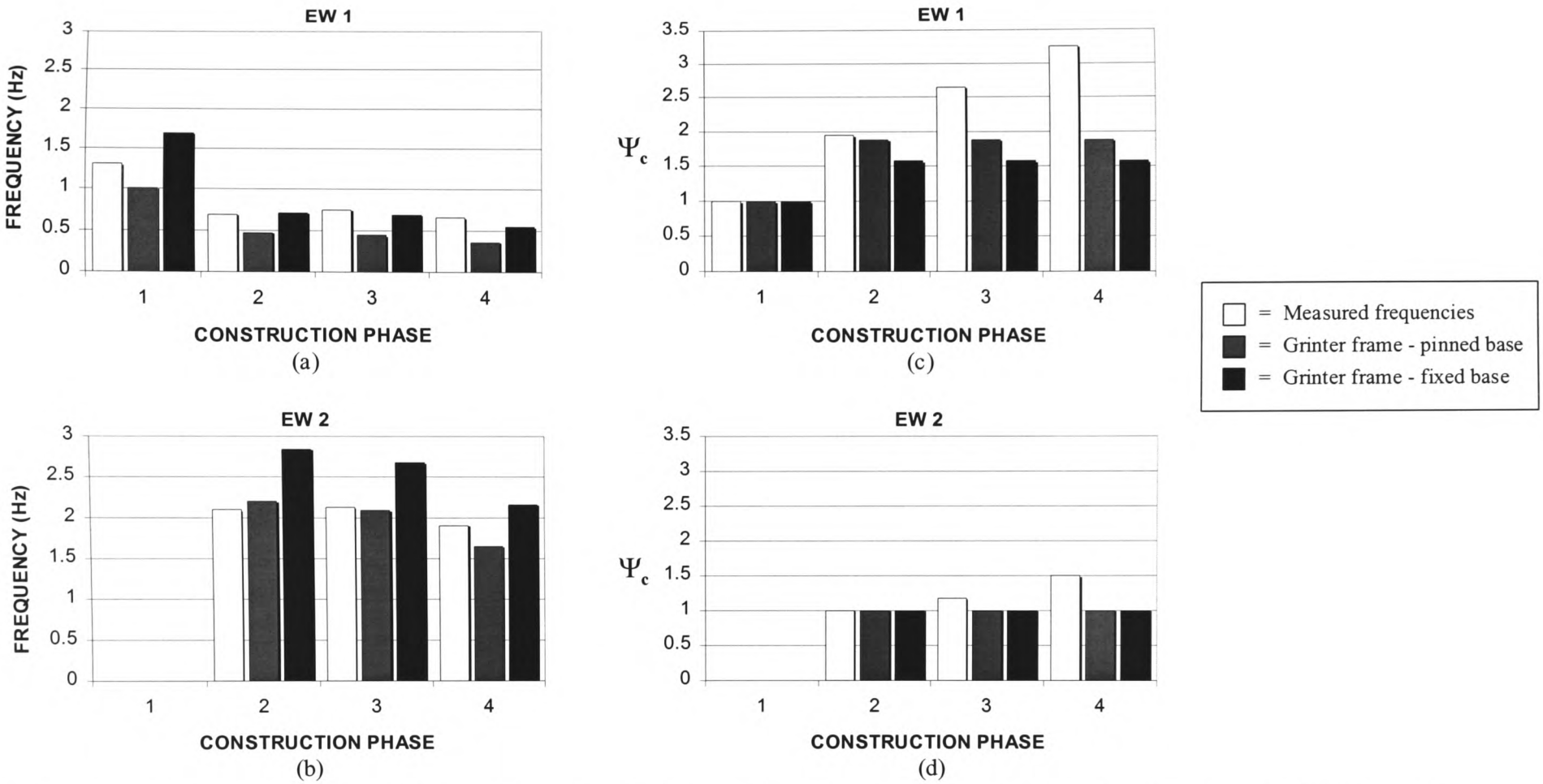

Figure 4.7 – The comparison of natural frequency and whole frame stiffness change from measured results with values obtained from the Grinter substitute frame model: (a)+(c) EW 1, (b)+(d) EW 2

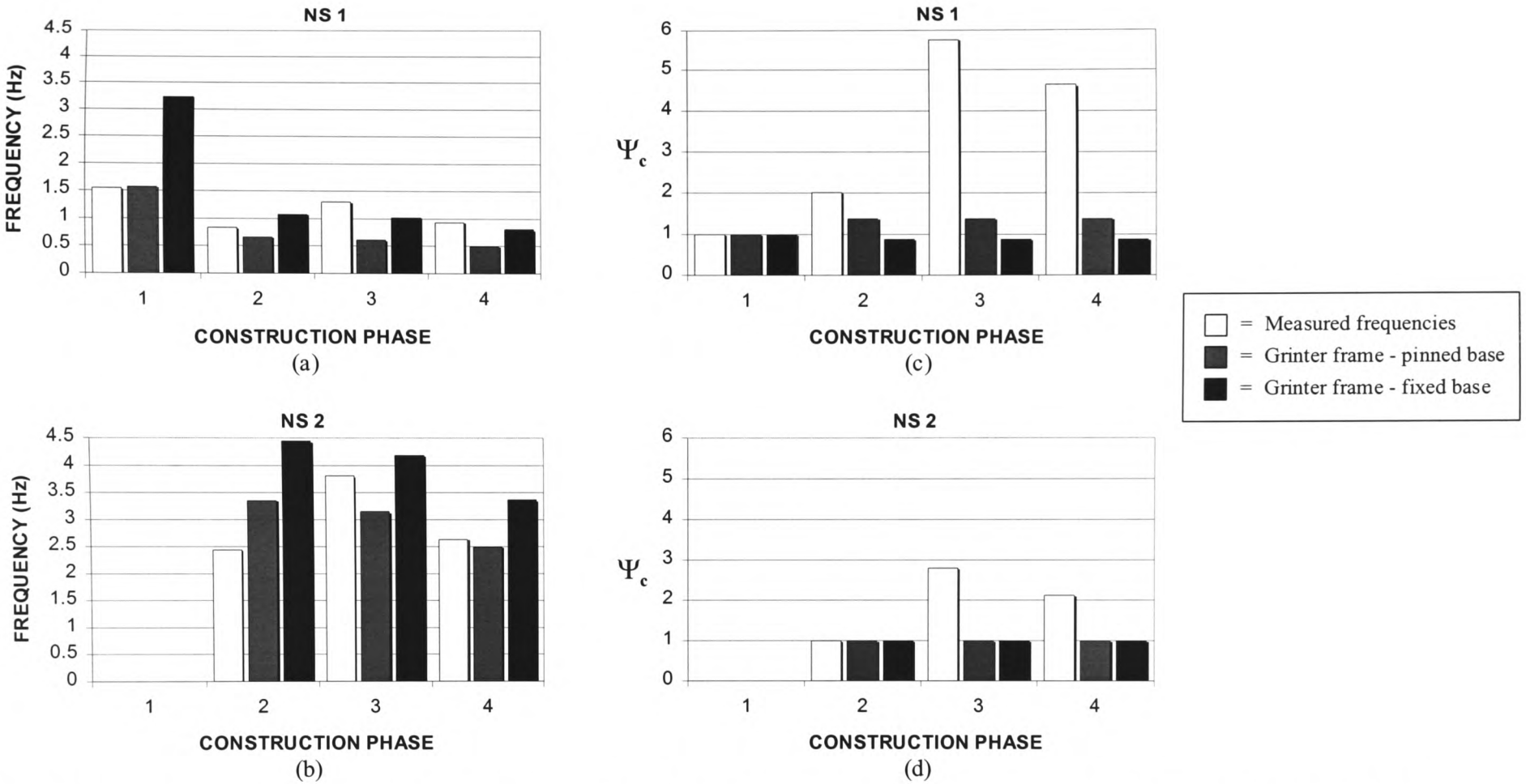

Figure 4.8 – The comparison of natural frequency and whole frame stiffness change from measured results with values obtained from the Grinter substitute frame model: (a)+(c) NS 1, (b)+(d) NS 2

4.7 Comparison and Discussion of Measured and Calculated Results

4.7.1 The full FE frame model

Comparisons of the calculated and measured frequencies for the full FE model are shown in Table 4.9 and have been taken from the values given in Table 4.1 and Table 4.7, which contain the measured and calculated data respectively. The comparison is based on the calculated sway and torsion vibration modes that resemble most the characteristics observed from the measured behaviour. Therefore, although the full frame FE results suggest a number of coupled modes, the most dominant characteristic was assumed to represent the corresponding measured behaviour, e.g. EW θ, which is a coupled east-west sway - torsion mode, was taken as EW as this motion dominated in the calculated behaviour. This rationalisation was also used to interpret the information presented by Ellis and Ji (1996), which gave the results of a similar analytical exercise, providing an additional set of results for comparison with the measured characteristics.

It is to be expected that differences between the calculated and measured natural frequencies will arise as a result of numerical modelling. This is not entirely surprising as the numerical models only offers a representation of the frame, which is based on assumed behaviour patterns. However, what is more important is to establish if the models represent the overall characteristics of the building at the various construction phases, i.e. the whole-frame stiffness of the building about the three principal NS, EW and θ axes. Table 4.9 also gives a comparison of whole-frame stiffness change obtained from the measured properties and calculated results, which for completeness are also shown by the graphs in Figures 4.6(a) to (f).

Observations:

EW 1:

The calculated results of the frame at each of the construction phases agree reasonably well with the measured frequencies. Although there are some discrepancies between the two result sets, the full FE frame model and the values given by Ellis and Ji (1996) reflect the relative change of the whole-frame stiffness with similar proportions seen from the measured frequencies.

NS1 and θ1:

The full FE frame model, and the results of Ellis and Ji (1996), have again provided calculated frequencies that agree with the measurements, but for the NS sway and the torsion modes the comparison is reasonable only for construction phase 1 and 2. At these phases, the frame comprised (i) the steel frame with steel deck in place, and (ii) the steel frame with composite floors complete. The calculated whole-frame stiffness change for these phases compare well with the corresponding measured properties. Comparisons at construction phase 3 and 4, however, highlight significant differences for both the natural frequency values and whole-frame stiffness change. At these phases the calculated whole-frame stiffness change overestimate the measured values by approximately 70 - 120% for the NS1 sway mode ($\Psi_{c(FE)} / \Psi_{c(measured)} \approx 1.7$ & 2.2, phase 3 and 4 respectively) and between 110 - 140% for the θ1 torsion mode ($\Psi_{c(FE)} / \Psi_{c(measured)} \approx 2.1$ & 2.4, phases 3 and 4 respectively). The calculated values appear to portray the stiffening effect of the block-work walls to a much higher degree than their actual influence.

There are a number of reasons that could explain these differences, but the most likely can be attributed to the idealised nature of the modelled block-work panel. In the frame model, the walls were assumed to behave like membrane elements where in-plane forces are transmitted through the elements to the connecting nodes at their boundary. These nodes were chosen to coincide with the nodes that formed the geometry of the frame, which resulted in a model assuming complete interaction between the walls and the frame. In reality this type of behaviour is unlikely and a more accurate solution may have been achieved if the walls had been modelled using the proposals by Smith (1963). In this model, the author assumes that the wall behaves like a diagonal 'spring', which connects between the nodes of the frame in a similar fashion to a diagonal bracing member. By varying the stiffness of this 'spring', it should be possible to examine the effect of non-perfect wall / frame interaction.

In addition to the whole-frame stiffness overestimation, the model has also failed to indicate the relative reduction of stiffness from construction phase 3 to 4, which was seen in the measured results. During these phases the calculated properties suggest

that the frame stiffness remains approximately constant, which would be an expected outcome bearing in mind that no additional stiffening parts were added to the frame at phase 4.

4.7.2 The Grinter substitute frame using GRIND

Table 4.10 gives comparisons of the measured and calculated properties using the results from the Grinter substitute frame, which are also illustrated in the form of a graph by Figure 4.7 and Figure 4.8.

The structural properties of the Grinter substitute frame were prepared following the procedures outlined previously, and as such focussed on the characteristics of the framing members with no regard to the extra stiffening of block-walls. The result was a series of models that enabled calculations of natural frequency, mode shapes, modal mass and modal stiffness for the sway modes neglected the possibility of torsion or coupled vibration. For each of the construction phases, the fixed and pinned base models have provided an indication of how fixity affects the natural frequencies of the frame.

Observations:

EW1 and EW2:

The calculated natural frequencies have provided a reasonable comparison with the measured results for each of the construction phase. From a calculations stand-point the agreement between calculated and measured results are closest using a pinned base for construction phase 1, with best results being obtained with the fixed scenario for phase 4. These observations suggest that as the mass of the building increases the assumed fixity at the base of the frame changes from a pinned case to the fixed type, which appears to have a transition depending on the mass of the building.

NS1 and NS2:

A similar observation with regard to the change of base fixity can also be seen from a comparison of results for the NS modes corresponding to construction phases 1 and 2. However, as with the full FE frame model, the natural frequencies of construction phase 3 and 4 have not been predicted accurately. Although the stiffening affect of the

block-work walls at construction phases 3 and 4 has been neglected, the EW frequencies have been captured reasonably well. NS sway values, on the other hand, show differences, which is likely to be the result of the block-work wall stiffening effects being ignored.

4.8 Concluding Discussion

The conclusions drawn from the studies described in this chapter are summarised by the following discussion.

4.8.1 The full frame FE model

The full frame FE analysis, which considered a model comprising every member of the building frame, gave calculated natural frequencies that agreed reasonably well for sway motion of the steel-framed building in the EW direction at all construction phases. However, when used to interpret sway in the NS and torsion motion modes, substantial differences between measured and calculated frequencies were seen. These discrepancies were due to the inaccurate assumptions considered to model the stiffening influence of the block-work walls located around the perimeter of the building, which overestimated the stiffness of the building frame when installed.

The whole frame stiffness change between the construction phases was also reasonably predicted for the EW sway direction, but similar to the natural frequency calculations, the NS and θ properties were significantly overestimated.

4.8.2 The results from GRIND using the Grinter substitute frame

Calculations of natural frequency using the Grinter substitute frame in its unaltered form has given results that agree reasonably well when compared to the measured frequencies in both the EW and NS modes. From the comparisons it appears reasonable to suggest that the measured natural frequencies corresponding to the calculated modes will fall somewhere within the range of the upper and lower bounds

offered by the pinned or fixed base scenarios considered. However, dealing more importantly with the whole-frame stiffness variation throughout the construction phases, it is clear that the Grinter frame significantly underestimates the properties of the building, especially at phases 3 and 4. These discrepancies are clearly due to the lack of additional stiffness, not included in the Grinter frame, to take account of the stiffening effects of the block-work walls constructed around the perimeter of the building.

4.8.3 Calibration of the analytical models

The main aim of this chapter was to examine if a numerical model of a complete building could be used in conjunction with the damage identification philosophy. Although the full frame FE model has provided frequency results that are an-order-of-magnitude similar to the measured results, it is evident from the whole-frame stiffness comparisons that calibration of the models will be required. At this point one must reflect on the practicalities of proceeding with such a calibration as, remembering that the full frame FE model contains approximately 4,500 dofs, the calibration variables will be enormous. This is further complicated by the possibility that many combinations of different calibration variables will give the same natural frequency solution.

To reduce the number of possible variables, a refined methodology for calibration will be necessary, which will consider the variables on a global scale. If the properties of the structural parts within the frame are similar, it is reasonable from an analytical standpoint to assume that the behaviour of these parts will also be similar. The Grinter substitute frame can now be seen to offer such a rationalised approach, which from the results presented in this chapter appears to hold the potential for such a calibration process. Therefore, to obtain a model that will provide an accurate prediction of the measured natural frequencies, a methodology to calibrate the condensed frame was sought. This methodology is considered in chapter 5.

CHAPTER 5

A Calibration Methodology for the Calculation of Natural Frequency and Mode Shapes using the Grinter Substitute Frame Analysis

5.1 Introduction

The previous chapter has shown that the behaviour of a building can be condensed into a model using the Grinter substitute frame, which enables natural frequencies to be calculated quickly and conveniently. However, the results achieved from the Grinter frame, in its standard form, do not provide sufficiently accurate predictions for use in damage identification.

Reports published by Wood (1974a, b & c) and Roberts and Wood (1981a & b) have proposed a method that examines the static and dynamic behaviour of multi-storey plane-frame structures with varying stiffness characteristics. However, to-date no evidence of a calibration methodology has been defined that allows measured frequencies to be used to determine possible frame variable(s). This chapter proposes a methodology, which is appropriate for use with GRIND (the computer program discussed in chapter 4).

5.2 Calibration Variables Identified by Published Reports

This section gives an introduction to the type of behaviour that tends usually to form the basis of discrepancies between analytical and observed structural frequencies.

5.2.1 The effects of soil-structure interaction

Ellis (1986) reported on the effects of soil-structure interaction between soil and the structural foundations of buildings and discussed methods of how its effects on the natural frequencies, mode shapes and damping of a building could be identified. The above author studied four buildings, one of which was used to give a comprehensive

assessment of the effect of soil-structure interaction. In the discussion the author described that the rigidity of the base of a building has a dependency on the stiffness of the founding soil. To examine its affects on the overall structure, the author conducted forced vibration tests, using the BRE equipment identified in chapter 3, on a 49m high concrete silo tower measuring mode shape, natural frequency and damping characteristics. Particular attention was paid to the motion at the base of the structure. The detailed information obtained from the tower together with results of the remaining three buildings, not comprehensively described in the report, enabled an estimate of the base stiffness for each building to be obtained. The aim of the study was to quantify the elastic modulus of the soils on which the buildings were founded. However, the author pointed out that this quantity depends on the oscillation amplitude of the building during motion, which in turn changes the strain amplitude in the soil at the foundation. This affect was said to have a significant influence on the properties of the soil, and thus on the behaviour of the building. Due to the small sample of buildings considered by the report, the author suggested that it would be unwise to extrapolate too much from the results, but concluded that base stiffness properties can have a significant influence on the calculation of natural frequency and energy dissipation characteristics of a building.

5.2.2 Rotational restraint at joints

It is now well established that jointed structures have properties that are more complex than those assumed for conventional 'free' or 'fixed' connections [Owens and Cheal (1989)]. The complexity is further exaggerated when dealing with vibration behaviour, where the amplitude of motion at the joints is small in comparison with similar effects associated with applied static load. Nader and Astaneh (1996), for example, studied the dynamic behaviour of single storey steel frames focusing on the structural rigidity of three connection types commonly used in conventional steel construction. The connection types considered ranged from simple plate fixings to robust steel plating, which from a design perspective represented those connection types normally assumed to be 'pinned' and 'fixed' respectively. The study demonstrated that the rotational stiffness inherent in a simple plated connection, subjected to oscillatory motion, was not significantly different from those of more

rigid arrangements. Aoki (1996) also discussed this conclusion where the dynamic characteristics of welded and non-welded joints were compared. From this study the author found that the lower mode natural frequencies of simple framed structures, subjected to impact loads, changed only marginally from one joint type to the other. However, higher modes of vibration were affected to a greater degree. These studies highlight the possible influence of joint fixity on the dynamic performance of plane-frame type structures, and as such cannot be ignored when calibrating a numerical model.

5.2.3 Contribution of block-work wall in-fill panels

The influence of non-structural components, such as in-fill panels and façade elements, are often neglected when it comes to the provisions of strength and stiffness in a building. However, studies have shown that these non-structural components can influence the behaviour of buildings by interacting with the framing members. Smith (1963) studied this effect by considering simple steel frames in-filled with block-work wall panels, focusing on their behaviour during in-plane static loading. Considering various heights to width ratios, the author found that the wall increased the stiffness of the frames. The author then proceeded to produce 'design chart' type data that related increased stiffness to the geometry of the frame. Throughout the extensive discussions, which also considered a variety of loading arrangements, the author suggested that the stiffness of such structures is analytically similar to an idealised diagonal spring. The study focussed mainly on the sway deflection of single-storey in-filled frames, but the author proposed that a similar behaviour could be assumed for multi-storey structures.

Chrysostomou (1991) extended this study to consider dynamic loading. The aim of this work was to establish the added strength and stiffness mobilised by the interaction of block-work and steel frames. The author then assessed the reserve strength of such structures when exposed to earthquake type loading producing analytical models that could predict the vibration response of these frames subjected to dynamic loads. Apart from the numerical models, which were the main aim of the work, an interesting

conclusion was drawn from the study, which indicated that the original proposal of a diagonal strut to simulate the added stiffness of in-filled panel remained accurate.

5.3 Discussion Relating to the Calibration of the Grinter Substitute Frame

The advantage of modelling a building frame using a method based on an ensemble of its properties is that the characteristics of the constituent structural parts can be examined on a 'global average' basis. To obtain a model that can provide a better indication of the building frequencies, the global average influence of base fixity, block-work walls and beam / column rotational restraint (identified as possible variable by the above mentioned published reports) will be considered.

The aim of the methodology is to obtain a model that will not only provide accurate natural frequencies but also offer a solution that represents the way the boundary conditions of the frame change as a result of added mass and whole-frame stiffness. These boundary conditions are outlined in the following discussions.

5.3.1 The influence of rotational restraint at the foundation of the frame

The pinned and fixed base scenario frequencies discussed in chapter 4 represent lower and upper bound solutions respectively for the whole frame. These support conditions are extreme cases, but are unlikely to be achieved when considered in the context of real structural behaviour. Ellis (1986) for example showed that the soil-structure interaction at the foundations of buildings varies considerably, which was said to influence the dynamic characteristics of whole frame vibration response. Although it is difficult to suggest that any variation to the stiffness at the base of the steel-framed building, considered here, could be assigned to soil-structure interaction processes, it is feasible that similar effects are present. As outlined in chapter 4, the steel-framed building was constructed on a large strong floor, the stiffness of which could be sufficiently large as to reduce the whole-frame rotation at the foundation to a minimum. Therefore, any rotation that occurs at the base of the building is more

likely to be proportional to the properties at the connection, between the columns and the foundation, in a global average form.

Placed in the context of the results calculated using the GRIND program, these properties are not entirely clear. To fully investigate the extent to which the frequencies of the steel-frame change in the range between the extreme cases presented by either the fixed of pinned base node conditions, a relationship between rotational restraint and calculated natural frequencies will be determined.

5.3.2 The influence of rotational restraint at beam to column connection

It is reasonable to assume that at low vibration amplitudes the connection between a column and a beam offers significant rotational restraint no matter whether the connection was design to be pinned or fixed. This was the conclusion of studies by Nader and Astaneh (1991) and Aoki (1996) and is also mentioned by Wyatt (1989). However, it is not entirely clear from these reports how the characteristics of such joints change should the overall mass of the structure vary. It is feasible to suggest that the vibration amplitude of a structure, at its natural frequency, will increase as the mass of the structure increases, i.e. the vibration amplitude of a structure with constant stiffness considered at stages when the mass properties vary.

Consider for a moment this condition applied to a simply supported beam. Leaving aside the natural frequency changes that would inevitably occur, it would be expected that added mass would increase the amplitude of both mid span displacement and support rotation. Add to this a support restraint system typical to the bolted connections used for the steel-framed buildings, (i.e. one that is not entirely pinned nor fixed), it would be expected that the energy dissipation, and thus rotational restraint characteristics at the joint, would also vary. This was the finding of Plumier and Schleich (1993) where forced sinusoidal vibration at various amplitudes was used to examine the energy dissipation of beam to column connections. Concentrating on parts of the report that considered the form of construction adopted for the steel-framed building, the authors found that the energy absorption at the joints increased as vibration amplitude increased. This phenomena offers an explanation to the

observations by Ellis and Ji (1996) where damping was found to increase and natural frequency decrease when the whole-frame amplitude of the steel-framed building correspondingly increased (see Table 4.3, chapter 4). Reports by Ellis *et al* (1994, 1995 and 1996) also show that amplitude dependence of the dynamic characteristics was observed in other multi-storey buildings.

Leaving aside the amplitude dependence of the dynamic characteristics, the effect of varying joint restraint at the beam to column connections of the building was considered as one of the calibration variables. Again, the aim was to treat the restraint on a global average scale, thereby concentrating the properties at the connections throughout each floor as one overall effect.

5.3.3 The stiffening influence of block-work panel walls

To model the stiffening affect of the block-work walls located on the east and west elevations of the building, the proposals by Smith (1963) were adopted. In this report, the author defined the block-work as a diagonal spring, which is based on the philosophy that in-plane forces are transmitted through the wall, to its corners, with similar efficiency as a diagonal bracing member. The stiffness of this spring was said to depend predominantly on the construction tolerances of the wall itself, as this can be influenced by the degree of contact between the frame of the structure and the wall corners. Based on a single block-work panel, installed within a frame bounded by beams and columns, the stiffness of the idealised spring was defined by Wood (1974a) in a form appropriate for use with the Grinter substitute frame as,

$$S = \frac{2\dfrac{H}{L}}{\left(1+\dfrac{H^2}{L^2}\right)^2}\frac{E_s}{\mu}\alpha t = kN/mm \qquad (5.1)$$

Equation (5.1) can be used as spring stiffness at each storey to simulate the idealised diagonal bracing [Smith (1963)], which has been resolved to give horizontal resistance properties. In addition, H and L are the frame height and width respectively, measured

between neighbouring columns and storey beams, while E_s is the Young's modulus of the steel frame, μ is the steel / block-work modular ratio and t is the thickness of the wall. α is a parameter that represents the degree of contact between the wall and the frame and is expressed as a ratio of the frame dimensions. A ratio of "1" would thus suggest complete contact between the frame and wall. However, the 'contact ratio' is calculated taking account of the deformed profile of a frame during sway deflection, with values by Wood (1974a) typically ranging from 0.002 to 0.3 for motion in the fundamental vibration mode.

5.3.4 Modifying the GRIND program to take account of calibration

In its original form, the GRIND program took account of the fixed or pinned base scenarios using a simple elimination of the rows and columns of the stiffness matrix associated with the dofs being removed. To allow calibration, however, a more general approach was considered where nodal properties could be adjusted depending on the level of joint fixity required. To model variations to the base and beam to column connection joints, the computer program was modified so that a value of rotational restraint could be assigned with a value chosen by the user. The GRIND program then applied the assigned numerical level of restraint to the diagonal elements of the structure stiffness matrix appropriate to the dof being adjusted.

Before each analytical calculation could proceed, restraint values were required comprising horizontal-spring and rotational stiffness at the storey levels and base location. To rationalise the number of variables, common restraint properties were assigned at each storey level, while the base was treated separately.

5.4 The Calibration Parameters for the Grinter Substitute Frame

5.4.1 Calculated natural frequencies corresponding to varying joint fixity conditions

During the rotational restraint on a scale of "0" to "1", which defines pinned to fixed conditions respectively, a consistent relationship was found to exist between extent of fixity and calculated frequency for all construction phases. To illustrate the relationship, Figure 5.1 shows the change of natural frequency of the Grinter frame corresponding to various joint fixity conditions. An interesting facet of the results is that identical natural frequencies were calculated for conditions when the beam to column connections were assumed fixed, with varying base fixity, as those obtained for a fixed base with varying beam to column fixity. This trend was also repeated for the condition when the base was pinned, with beam to column connection fixity varying, and base varying / beam to column pinned.

5.4.1.1 Mathematical formulation of natural frequency for varying conditions of joint fixity

Having established that the trends are consistent for all construction phases, a mathematical formulation was developed by the candidate to allow the natural frequency variation to be obtained relative to any fixity condition. On inspection of the results in the graph of Figure 5.1, similar characteristics to that of a hyperbolic tangent function are seen. Comparing the results of Figure 5.1 with this function illustrates the similarity, which is shown by Figures 5.2(a) and (b). However, the calculated rate of change of natural frequency gained from the Grinter frame indicated a logarithmic variation with respect to the degree of joint fixity. To replicate the logarithmic nature on a scale similar to the results of Figure 5.1, the original hyperbolic tangent function can be adjusted and normalised using,

$$y = \frac{\tanh\left(\tanh^{-1}(\xi) - \dfrac{\log_{10}(10^4\rho)\tanh^{-1}(\xi)}{2}\right)}{-\xi} \qquad (5.2)$$

where y ranges from -1 to +1, while ρ is the degree of fixity at the joint on a logarithmic scale ($0.0001 < \rho < 1$) as shown in Figure 5.2. The fit of eqn.(5.2) is dependent on ξ, which allows adjustments to be made to the hyperbolic tangent profile to suit the results gained from the GRIND program. Finally, to ensure that eqn.(5.2) can be used to calculate the natural frequency of the frame relative to any combination of joint fixity, an adjustment is made to give,

$$\beta = \frac{1}{2n}\left[\left\{\frac{\tanh\left(\tanh^{-1}(\xi) - \frac{\log_{10}(10^4\rho)\tanh^{-1}(\xi)}{2}\right)}{-\xi}\right\} + n\right], (n = 1, 2) \quad (5.3)$$

This equation is universally applicable to all construction phases and is representative of the type of information given by Figure 5.1. Introducing a number of abbreviations to represent the calculated frequencies for the extreme fixity conditions as,

f_1 = fully restrained beam / column connection and fully restrained base

f_2 = fully restrained beam / column connection and pinned base

f_3 = pinned beam / column connection with pinned base

eqn.(5.3) is used to calculated the frequency corresponding to the assigned value of ρ using,

$$f_\beta = f_3 + \beta(f_2 - f_3), \text{ for } (0 < \beta < 1) \text{ i.e. } n = 1 \quad (5.4a)$$

$$f_\beta = f_2 + (\beta - 1)(f_1 - f_2), \text{ for } (1 < \beta < 2) \text{ i.e. } n = 2 \quad (5.4b)$$

where f_β indicates that the frequency is relative to the calculated β value. From a series of comparisons between eqns.(5.4a & b) and the calculated frequencies from the Grinter frame, values of ξ in the range 0.95 to 0.99 were found to give best results.

5.4.1.2 Graphical interpretation of formulation for assessment of joint fixity

The upper and lower bound results that are shown in Figure 5.1 illustrate that a wide variety of base and beam to column connection restraint combinations will provide identical natural frequency results. To identify every combination, appropriate to the frequencies between the upper and lower bounds, would require a significant number of individual frequency-variation-profiles. However, to make the interpretation easier this information can be presented in a graphical form where every possible combination of base and beam to column restraint is considered. This information is shown by Figure 5.3, which was derived by the candidate and satisfies the relationship of eqns.(5.4a & b) for all construction phases.

The diagonal lines that cross the graph of Figure 5.3 represents the combinations of joint fixity that will provide the required calculated natural frequencies. Therefore, using this graphical method, it is possible to identify the combinations appropriate to the measured natural frequency, f_m, using

$$\beta_m = \left(\frac{f_m - f_2}{f_2 - f_3}\right) + 1, \text{ when } (f_3 < f_m < f_2) \tag{5.5a}$$

$$\beta_m = \left(\frac{f_m - f_1}{f_1 - f_2}\right) + 2, \text{ when } (f_2 < f_m < f_1) \tag{5.5b}$$

Therefore, β_m is a numerical ratio ($0 < \beta_m < 2$) that defines the measured frequency f_m, relative to f_1 and f_2 or f_2 and f_3. However, from calculations using the GRIND program it was found that,

$$(f_1 - f_2) = (f_2 - f_3) \tag{5.6}$$

making it possible to calculate any β_m value assuming eqn.(5.5b) only. To give an example, eqn.(5.5b) is used to calculate the fixity combinations appropriate to the measured frequency value of f_m = 2.1Hz, which relates to the measured EW2 mode of construction phase 2 of the steel-framed building. The calculated frequencies for this mode, as given by Table 4.10 in chapter 4, were f_1 = 2.84Hz and f_2 = 2.2Hz, which

gives β_m of 0.84. Therefore, using Figure 5.3, and remembering that the diagonal lines of the graph indicate all possible combinations, two possible conditions are,

- Possible condition 1: base node restraint = 0.008, beam to column restraint = 1
- Possible condition 2: Base node restraint = 1, beam to column restraint = 0.008

5.4.2 Calibration of the block-work panel walls

The effect of including additional spring stiffness in the Grinter frame, which represents the installation of the block-work panels, is to increase the natural frequency of the extreme fixity conditions f_1, f_2 and f_3. To calculate the spring stiffness appropriate to the size of walls within the steel-framed building, eqn.(5.1) was considered using the following data:

- Block-work wall thickness = 140mm
- Compressive strength of blocks = 7 N/mm^2
- H = 4.135m
- Modular ratio = 40
- L = 6.0m and 9.0m
- E_s = 205 kN/mm^2

To obtain the value that would be representative of the number of panel installed on the steel-framed building, a simple multiplication of the calculated stiffness relative to the number of walls at each storey level was adopted.

5.4.2.1 Calculated natural frequencies corresponding to varying spring stiffness

The natural frequencies calculated with additional spring stiffness at each floor level are shown in the form of a graph by Figure 5.4(a). The results shown relate to the EW1 and EW2 frequencies of construction phase 3 and are representative of the variation observed for NS and EW modes of construction phase 3 and 4. The information given by Figure 5.4(a) illustrates the calculated frequency appropriate to various contact ratios, α.

Figure 5.4(b) shows Figure 5.4(a) in a more universally applicable form, where the change of frequency relative to α has been normalised, giving a more meaningful illustration of the rate of frequency change.

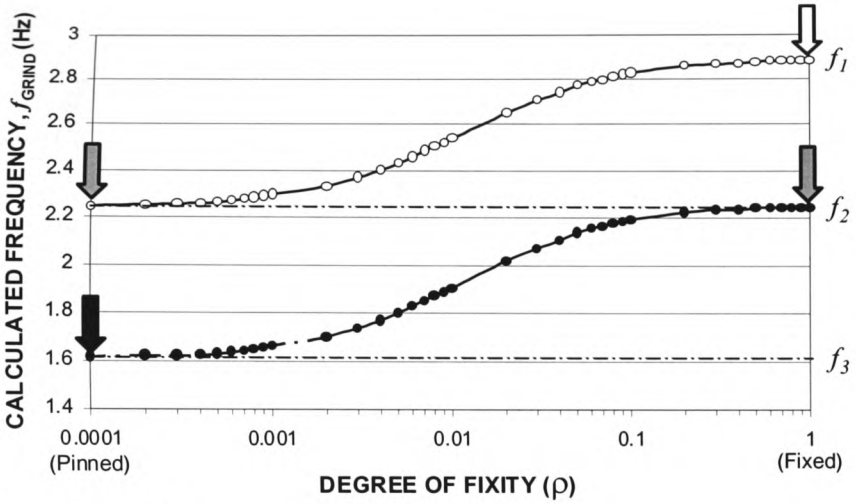

Key:

= Beam to column restraint fixed, base restraint varied (and beam to column restraint varied, base fixed)

= Beam to column pinned, base restraint varied (and beam to column restraint varied, base pinned)

= Frequency corresponding to fixed base, fixed beam to column connection (f_1).

= Frequency corresponding to fixed base, pinned beam to column connection (and pinned base, fixed beam to column connection) (f_2).

= Frequency corresponding to pinned base, pinned beam to column connection (f_3).

f_{GRIND} = Frequency calculated using the GRIND program

Figure 5.1 – Calculated natural frequency of the Grinter substitute frame corresponding to various joint restraint conditions

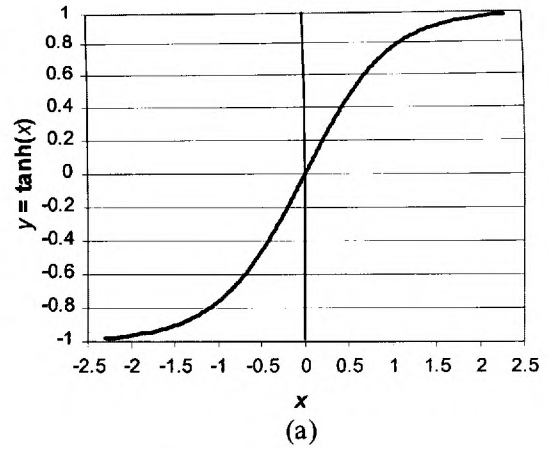

(a)

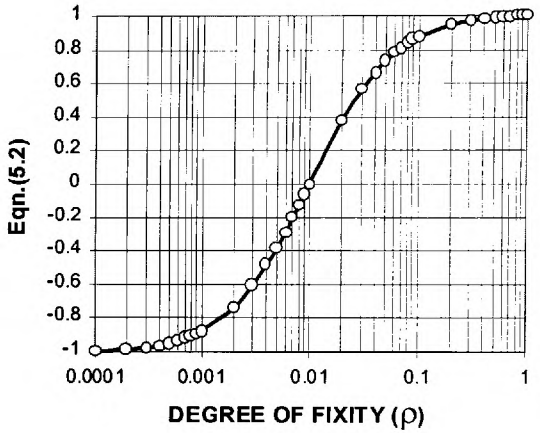

(b)

Figure 5.2 – Comparison of the hyperbolic tangent function between (a) normal scale (b) logarithmic scale

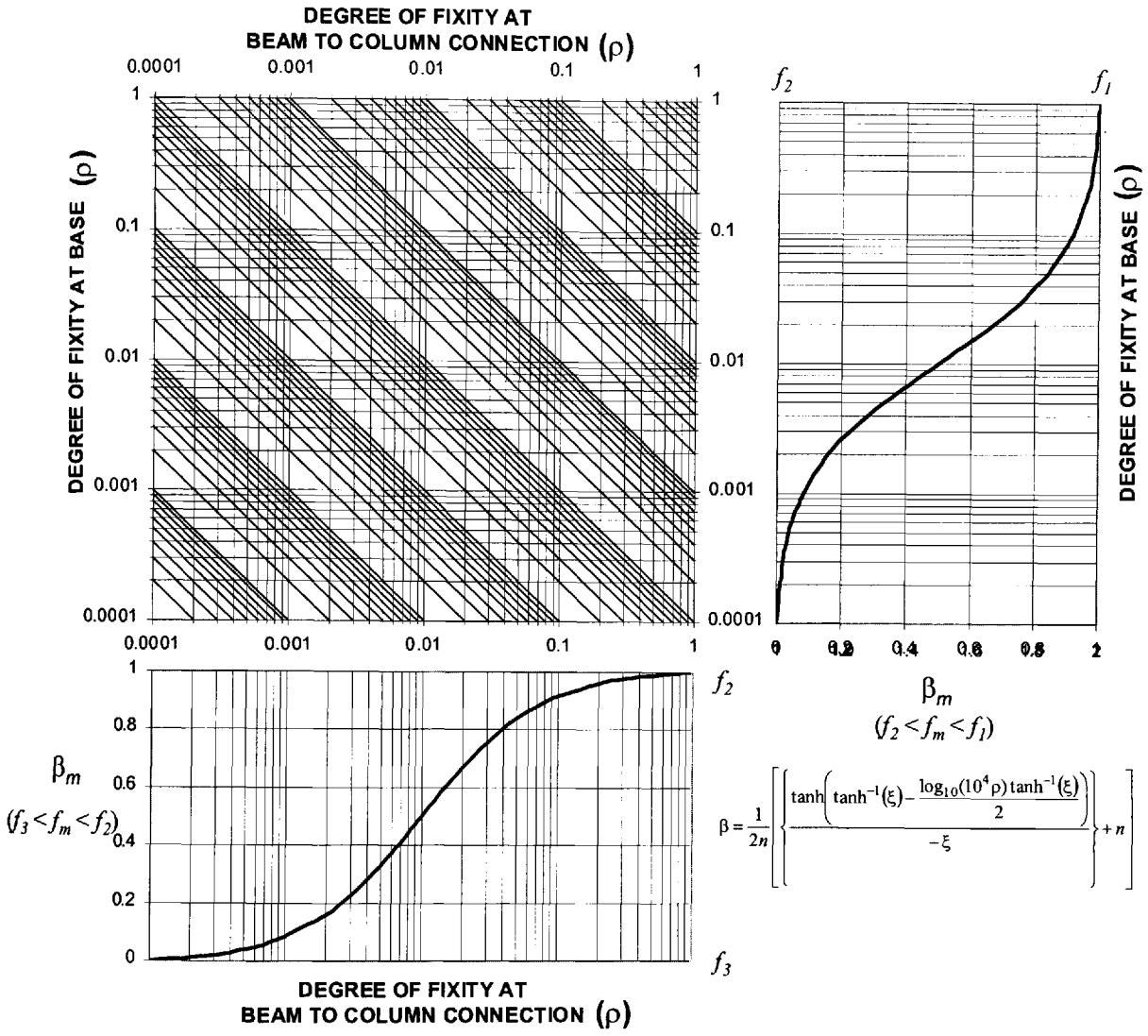

Figure 5.3 – Base and beam to column connection restraint combinations appropriate to the calculated β_m value for the construction phase being considered

5.4.2.2 Mathematical formulation of natural frequency for varying contact ratio, α

The normalised frequency change shown by the graph of Figure 5.4(b), approximates to an expression of the form,

$$\lambda_{1,2} = \alpha^{i} \tag{5.7}$$

where i is a real value that 'tunes' λ ($0 < \lambda < 1$) to the required variation. For best results i was found to be 0.9 and 0.67 for the EW1 (and NS1) and EW2 (and NS2) respectively. The relationship of eqn.(5.7), based on these values, is also included in Figure 5.4(b) from which the natural frequency corresponding to any value of α ($0 < \alpha < 1$) can be calculated using,

$$f_{1,\alpha} = f_1 + \alpha^{i}\left(f_{1,(\alpha_i=1)} - f_1\right) \tag{5.8a}$$

$$f_{2,\alpha} = f_2 + \alpha^{i}\left(f_{2,(\alpha_i=1)} - f_2\right) \tag{5.8b}$$

$$f_{3,\alpha} = (2f_2 - f_1) + \alpha^{i}\left(f_{3,(\alpha_i=1)} - (2f_2 - f_1)\right) \tag{5.8c}$$

Therefore, the only information required to formulate the frequency variation relationship are f_1, f_2 and f_3 when $\alpha = 1$.

5.4.2.3 Calculating the modified β_m value

The consequence of including added spring stiffness to represent block-work walls is to adjust β_m to a modified value. To achieve this it is first necessary to calculate values of α corresponding to the measured frequency, f_m, assuming the extreme conditions given by the frequencies f_1, f_2 and f_3. These values are calculated from eqns.(5.8a) to (5.8c) in the following way,

$$\alpha_{m1} = \sqrt[i]{\frac{f_m - f_1}{f_{1,(\alpha=1)} - f_1}} \tag{5.9a}$$

$$\alpha_{m2} = \sqrt[i]{\frac{f_m - f_2}{f_{2,(\alpha=1)} - f_2}} \tag{5.9b}$$

$$\alpha_{m3} = \sqrt[i]{\frac{f_m - (2f_2 - f_1)}{f_{3,(\alpha=1)} - (2f_2 - f_1)}} \tag{5.9c}$$

where $\alpha_{m1,\,2,\,3}$ indicate α values that correspond to the measured frequency f_m. If f_m is greater than f_1, the modified β_m values can then be obtained from,

$$\beta_{m,\alpha} = \left(\frac{f_m - f_{1,\alpha}}{f_{1,\alpha} - f_{2,\alpha}}\right) + 2, \text{ for } (\alpha_{m1} < \alpha < \alpha_{m2}) \tag{5.10a}$$

$$\beta_{m,\alpha} = \left(\frac{f_m - f_{2,\alpha}}{f_{2,\alpha} - f_{3,\alpha}}\right) + 1, \text{ for } (\alpha_{m2} < \alpha < \alpha_{m3}) \tag{5.10b}$$

where $\beta_{m,\alpha}$ indicates dependence on the contact ratio, α. Finally, eqns.(5.10a) and (5.10b) are subject to the following exceptions,

$$\text{if } f_m < f_1, \text{ then } (0 < \alpha < \alpha_{m2}), (\alpha_{m2} < \alpha < \alpha_{m3}) \tag{5.11a}$$

$$\text{and if } f_m < f_2, \text{ then } (0 < \alpha < \alpha_{m3}) \tag{5.11b}$$

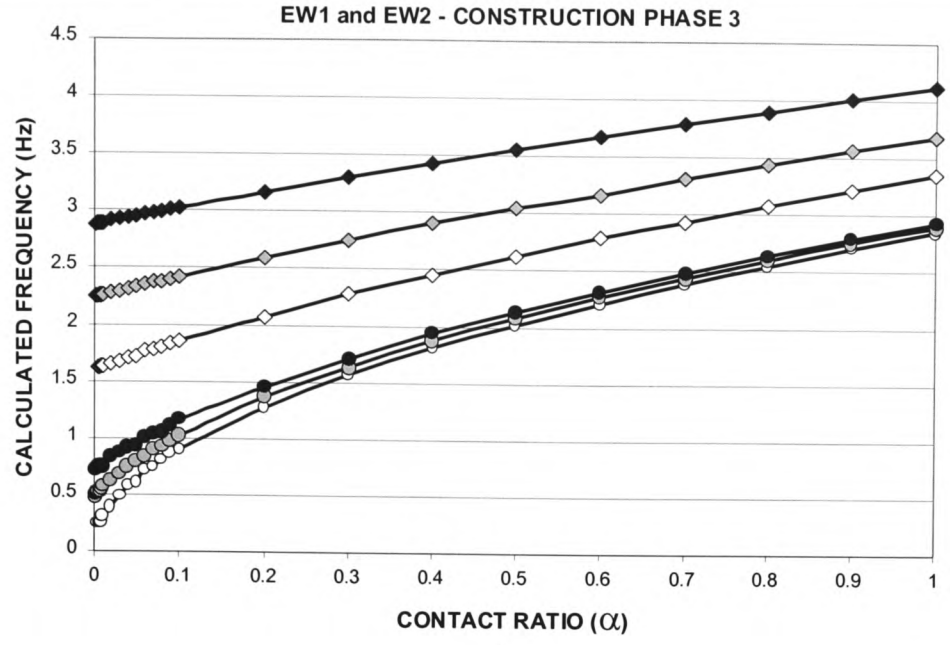

(a)

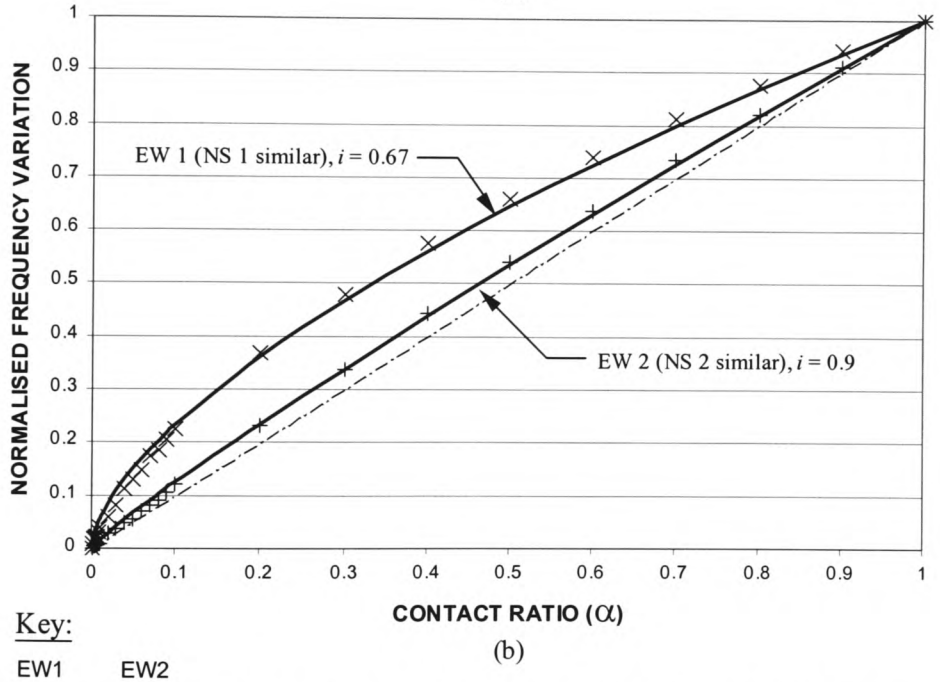

(b)

Key:

EW1 EW2

= Beam to column restraint pinned, base restraint pinned.

= Beam to column restraint fixed, base restraint pinned.

= Beam to column restraint fixed, base restraint fixed.

\+ = Calculated rate of frequency change - EW2 (NS2 similar).

× = Calculated rate of frequency change - EW1 (NS1 similar).

—— = α^i

Figure 5.4 – (a) calculated frequency corresponding to α, (b) normalised rate of frequency change calculated for varying α, (construction phase 3 shown).

5.4.2.4 Variation of $\beta_{m,\alpha}$ for various α values

The inclusion of the block-work walls is applicable only to construction phase 3 and 4. Calculated data for these phases are given by Table 5.1, which was used to construct the $\beta_{m,\alpha}$ variations shown in Figure 5.5(a) and (b).

Table 5.1 – Calculated variables used to define the $\beta_{m,\alpha}$ variation

Variables	Construction phase 3				Construction phase 4			
	NS1	NS2	EW1	EW2	NS1	NS2	EW1	EW2
f_1 (Hz)	1.02	4.18	0.69	2.68	0.81	3.37	0.55	2.16
f_2 (Hz)	0.62	3.15	0.45	2.09	0.49	2.49	0.36	1.65
$(2f_2 - f_1)$ (Hz)	0.22	2.12	0.21	1.5	0.17	1.61	0.17	1.14
f_m (Hz)	1.31	3.81	0.75	2.13	0.93	2.63	0.66	1.90
$f_{1,(\alpha=1)}$ (Hz)	2.93	4.81	2.87	3.84	2.33	3.89	2.28	3.09
$f_{2,(\alpha=1)}$ (Hz)	2.83	4.01	2.82	3.45	2.26	3.18	2.25	2.72
$f_{3,(\alpha=1)}$ (Hz)	2.80	3.73	2.79	3.17	2.23	2.95	2.22	2.51
λ	$\alpha^{0.67}$	$\alpha^{0.9}$	$\alpha^{0.67}$	$\alpha^{0.9}$	$\alpha^{0.67}$	$\alpha^{0.9}$	$\alpha^{0.67}$	$\alpha^{0.9}$
α_{m1}	0.060	0	0.005	0	0.022	0	0.016	0
α_{m2}	0.176	0.745	0.045	0.019	0.125	0.169	0.064	0.198
α_{m3}	0.276	(>1)	0.097	0.339	0.226	0.738	0.118	0.52

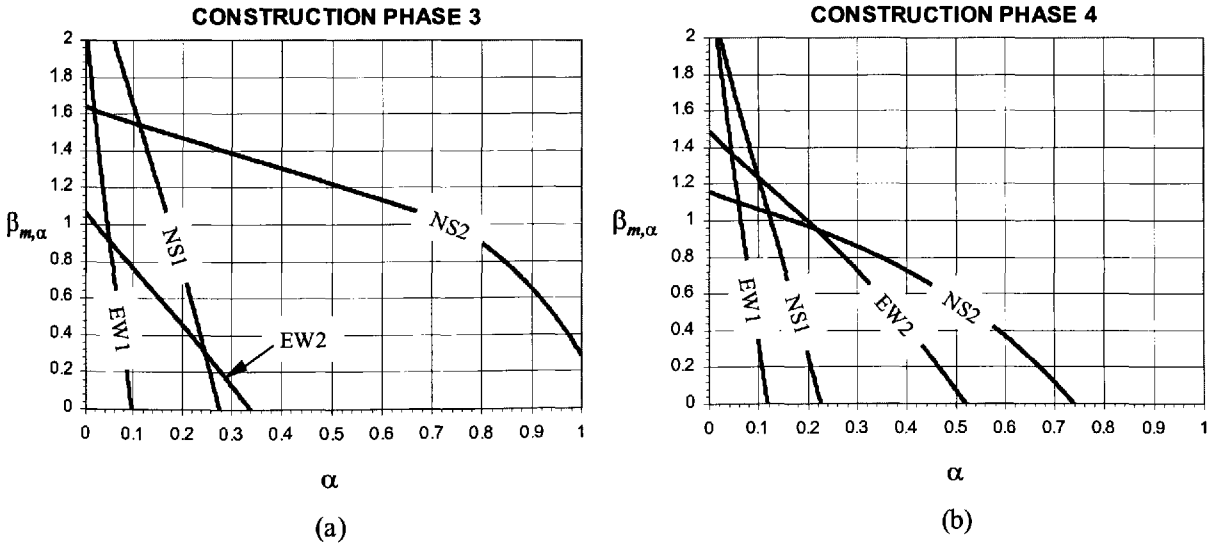

Figure 5.5 – Modified β_m for (a) construction phase 3, and (b) construction phase 4

5.5 Calibration Results Associated with each Construction Phase

The previous section has identified the calibration parameters of the frame, each being considered as influencing the behaviour of the Grinter substitute frame on a global average basis. Using this information the parameters associated with the measured natural frequencies of the steel-framed building can now be identified.

5.5.1 The approach adopted to calibrate the steel-framed building

The formulated criterion enables a large number of possible calibration parameters to be identified. However, it is clear that many possible solutions exist, as the calibration parameters have been developed to encompass a wide range of possible influences. To rationalise the calibration, a methodology was considered that followed predetermined assumptions relating to the behaviour of the building at all construction phases. These assumptions were:

(i) The calculated β_m value at construction phase 1 and 2 give an accurate reflection of the frame properties at these phases indicating the influence of added structural mass and stiffness on the whole-frame properties.

(ii) At construction phase 3 it was assumed that the added mass of the block-work panel walls would not cause a significant change to β_m and its associated $\beta_{m,\alpha}$ value would therefore remain unchanged. This assumption allowed the contact ratio, α, to be identified.

(iii) The α value chosen to satisfy condition (ii) was assumed to represent its magnitude for construction phase 4, enabling the $\beta_{m,\alpha}$ for this phase to be found.

The rationalisation procedure for (i) to (iii) above was considered to be applicable to each mode of vibration, i.e. EW1, EW2, NS1 and NS2, and were thus treated individually to assess the parameters for each of the vibration modes.

5.5.2 Results of calibration

Table 5.2 contains the calibration parameters based on the sequence presented above, which gives two sets of results that represent conditions when:

(*) the beam to column connection rotational restraint of the Grinter frame is maximised, so as to provide a minimised base node restraint value;

(**) the beam to column connection rotational restraint is minimised, so that a maximised base node restraint value can be achieved.

Table 5.2 – Calibration parameters to provide calculated natural frequencies with the Grinter substitute frame, which correspond with the measured frequencies

Construction phase		f_m	α	β_m, $\beta_{m,\alpha}$	**Base ρ**		**Beam/column ρ**	
					min *	**max ****	**max ***	**min ****
EW1	1	1.31	-	1.44	0.008	1	1	0.008
	2	0.69	-	1.92	0.1	1	1	0.1
	3	0.75	0.02	1.92	0.1	1	1	0.1
	4	0.66	0.02	1.68	0.02	1	1	0.02
EW2	1	(no measured frequency value available)						
	2	2.10	-	0.84	0	0.04	0.04	0
	3	2.13	0.22	0.84	0	0.04	0.04	0
	4	1.9	0.22	0.36	0	0.005	0.005	0
NS1	1	1.55	-	0.99	0.001	1	1	0.001
	2	0.83	-	1.4	0.009	1	1	0.009
	3	1.31	0.09	1.4	0.009	1	1	0.009
	4	0.93	0.09	1.7	0.012	1	1	0.012
NS2	1	(no measured frequency value available)						
	2	2.44	-	0.17	0	0.002	0.002	0
	3	3.81	0.68	0.17	0	0.002	0.002	0
	4	2.63	0.68	1.1	0.0015	1	1	0.0015

5.5.3 The whole frame stiffness of the Grinter substitute frame from the calibration results

The whole-frame stiffness of the building associated with the calibration results of Table 5.2 were calculated in a similar manner to the approach identified in section 4.6.3 of chapter 4. To obtain the required information, the modified GRIND program was used to calculate the calibrated mode shapes, which allowed the modal mass, modal stiffness and whole-frame stiffness to be defined. The results from these calculations are presented in Table 5.3 and Table 5.4, which give mode shape and modal property information respectively. The storey mass values for the construction phases has been presented in Table 4.4 of chapter 4.

5.6 Discussion and Comparison of Measured and Calibrated Results

Figure 5.6 and Figure 5.7 presents a comparison between the measured and calculated natural frequencies and their associated whole-frame stiffness variations for the EW and NS modes respectively. With regard to the natural frequencies, the calibration methodology has provided a means of obtaining calculated results that match precisely the measured values. However, the accuracy of the calculated frequencies does not automatically guarantee a true indication of the building characteristics during construction, which is demonstrated by the two result sets considered by the comparison.

Table 5.3 – Calculated natural frequencies and mode shapes incorporating the calibration variables

"*" Beam to column connection rotational restraint of the Grinter frame maximised. base node restraint value minimised																
Mode	**EW1 – Phase:**				**EW2 – Phase:**				**NS1 – Phase:**				**NS2 – Phase:**			
	1	**2**	**3**	**4**	**1**	**2**	**3**	**4**	**1**	**2**	**3**	**4**	**1**	**2**	**3**	**4**
Freq (Hz)	1.31	0.69	0.75	0.66	-	2.10	2.13	1.9	1.55	0.83	1.31	0.93	-	2.44	3.81	2.63
Floor	Normalised vibration amplitude corresponding to the storey levels (ϕ)															
1	0.091	0.036	0.051	0.076	No measured results available	-0.492	-0.345	-0.405	0.144	0.123	0.058	0.114	No measured results available	-0.335	-0.348	-0.399
2	0.203	0.109	0.154	0.190		-0.904	-0.632	-0.687	0.279	0.252	0.155	0.238		-0.606	-0.614	-0.685
3	0.331	0.256	0.289	0.326		-0.980	-0.793	-0.810	0.412	0.388	0.280	0.371		-0.763	-0.754	-0.828
4	0.469	0.427	0.440	0.472		-0.697	-0.782	-0.753	0.541	0.526	0.425	0.508		-0.762	-0.730	-0.781
5	0.609	0.594	0.596	0.620		-0.321	-0.545	-0.484	0.665	0.661	0.578	0.645		-0.578	-0.522	-0.534
6	0.740	0.747	0.745	0.761		0.122	-0.107	-0.040	0.788	0.787	0.730	0.775		-0.182	-0.123	-0.105
7	0.877	0.883	0.881	0.888		0.578	-0.443	0.481	0.894	0.899	0.871	0.893		0.373	0.414	0.438
8	1.0	1.0	1.0	1.0		1.0	1.0	1.0	1.0	1.0	1.0	1.0		1.0	1.0	1.0
"**" Beam to column connection rotational restraint minimised. base node restraint value maximised																
Mode	**EW1 – Phase:**				**EW2 – Phase:**				**NS1 – Phase:**				**NS2 – Phase:**			
	1	**2**	**3**	**4**	**1**	**2**	**3**	**4**	**1**	**2**	**3**	**4**	**1**	**2**	**3**	**4**
Freq (Hz)	1.31	0.69	0.75	0.66	-	2.10	2.13	1.9	1.55	0.83	1.31	0.93	-	2.44	3.81	2.63
Floor	Normalised vibration amplitude corresponding to the storey levels (ϕ)															
1	0.029	0.03	0.040	0.041	No measured results available	-0.259	-0.159	-0.200	0.024	0.033	0.033	0.028	No measured results available	-0.347	-0.339	-0.160
2	0.105	0.098	0.136	0.138		-0.669	-0.468	-0.532	0.088	0.114	0.113	0.099		-0.614	-0.613	-0.488
3	0.214	0.245	0.268	0.271		-1.0	-0.755	-0.838	0.186	0.232	0.230	0.205		-0.752	-0.773	-0.817
4	0.348	0.418	0.418	0.422		-0.986	-0.896	-0.999	0.313	0.376	0.374	0.339		-0.727	-0.773	-1.000
5	0.499	0.587	0.577	0.580		-0.784	-0.762	-0.883	0.463	0.534	0.531	0.493		-0.520	-0.585	-0.928
6	0.664	0.743	0.731	0.734		-0.357	-0.325	-0.449	0.633	0.696	0.694	0.660		-0.121	-0.190	-0.528
7	0.833	0.881	0.873	0.875		0.232	0.306	0.217	0.814	0.853	0.852	0.831		0.415	0.369	0.200
8	1.0	1.0	1.0	1.0		0.902	1.0	1.0	1.0	1.0	1.0	1.0		1.0	1.0	1.0

("Freq" = calculated natural frequency; and the floor numbers represent the storey levels with 8 being the top of the building).

Table 5.4 – The natural frequency and whole frame stiffness change: comparison between measured and calibrated results

Mode	Construction phase (j)	Option reference (*) as defined in Table 5.3			Option reference (**) as defined in Table 5.3			Measured results (chapter 4, Table 4.4)			Ψ_c*	Ψ_c**
		Freq (Hz)	Γ*	$\Re$*	Freq (Hz)	Γ**	$\Re$**	Freq (Hz)	$\frac{m_j}{m_1}$	Ψ_c	$\frac{\Re^*_j}{\Re^*_1}$	$\frac{\Re^{**}_j}{\Re^{**}_1}$
EW1	1	1.31	119.0	8062	1.31	99.9	6768	1.31	1	1	1	1
	2	0.69	844.9	15880	0.69	835.4	15702	0.69	7.031	1.947	1.969	2.32
	3	0.75	970.4	21549	0.75	939.6	20865	0.75	8.065	2.645	2.673	3.083
	4	0.66	1599	27497	0.66	1492	25657	0.66	12.88	3.258	3.411	3.790
NS1	1	1.55	132.8	12596	1.55	94.7	8982	1.55	1	1	1	1
	2	0.83	965.5	26258	0.83	775.5	21091	0.83	7.031	2.018	2.084	2.348
	3	1.31	945.1	64030	1.31	875.5	59315	1.31	8.065	5.758	5.083	6.604
	4	0.93	1678	57295	0.93	1306	44593	0.93	12.88	4.637	4.549	4.965
Mode	**(j)**	**Freq (Hz)**	**Γ***	**$\Re$***	**Freq (Hz)**	**Γ****	**$\Re$****	**Freq (Hz)**	$\frac{m_j}{m_1}$	Ψ_c	$\frac{\Re^*_j}{\Re^*_1}$	$\frac{\Re^{**}_j}{\Re^{**}_1}$
EW2	2	2.10	1151	200389	2.10	1186	206482	2.10	1	1	1	1
	3	2.13	1071	191826	2.13	1112	199170	2.13	1.147	1.180	0.957	0.965
	4	1.9	1758	250545	1.9	2032	289594	1.9	1.832	1.5	1.25	1.402
NS2	2	2.44	884.8	270962	2.44	913.6	214731	2.44	1	1	1	1
	3	3.81	1005	575938	3.81	1051	602299	3.81	1.147	2.796	1.867	2.805
	4	2.63	1793	489611	2.63	2044	558151	2.63	1.832	2.129	1.807	2.599

(Γ is quoted in tonne units, while $\Re$ is given in terms of kN/m. Shaded areas illustrate the best candidate results when compared to the whole frame stiffness gained from the measured properties. (j) indicated in this table is included merely to aid the interpretation of the calculated values shown, i.e. j = 1, 2, 3 or 4).

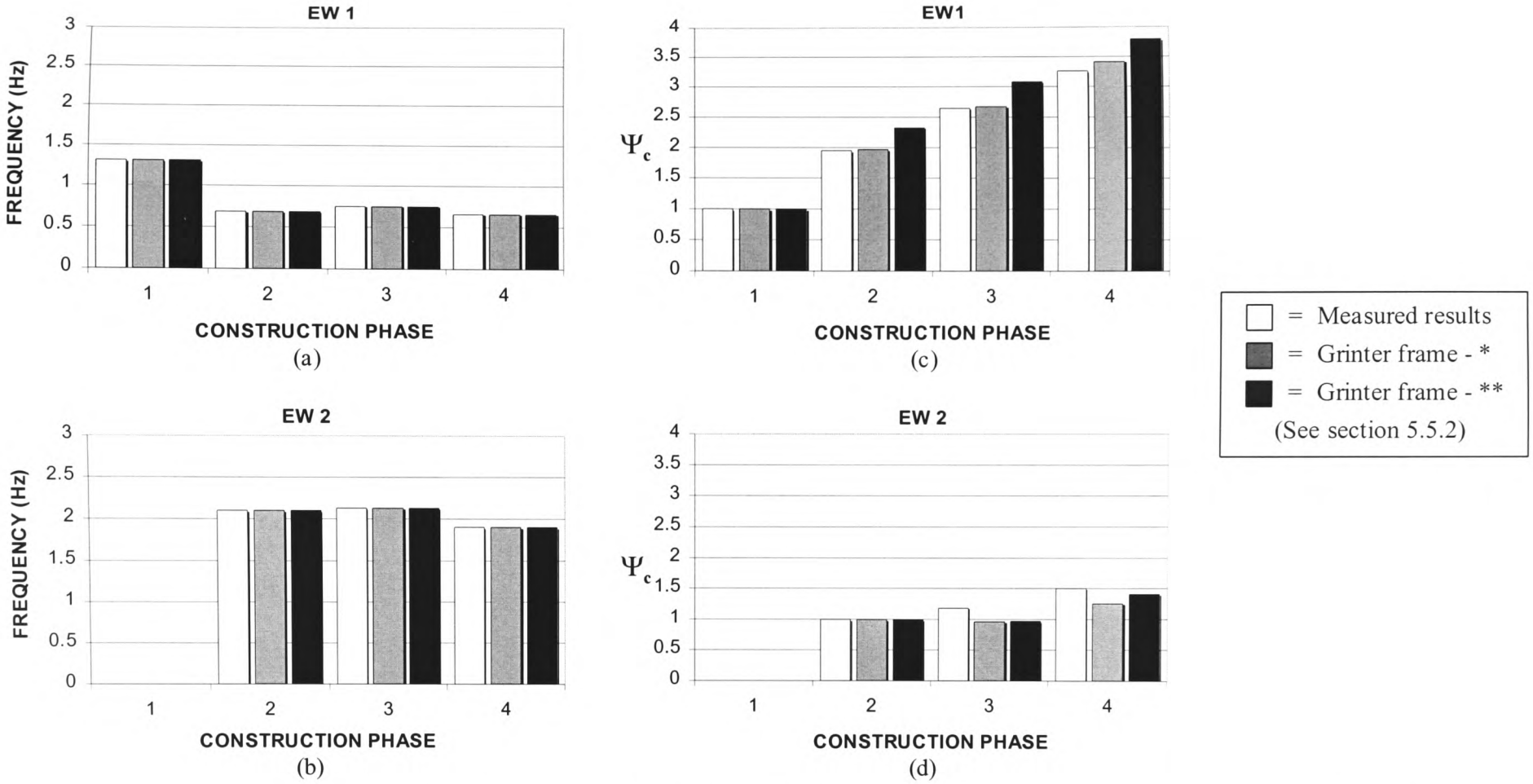

Figure 5.6 – The comparison of natural frequency and whole frame stiffness change from measured and calculated properties using the calibration parameters of Table 5.2: (a)+(c) EW 1, (b)+(d) EW 2

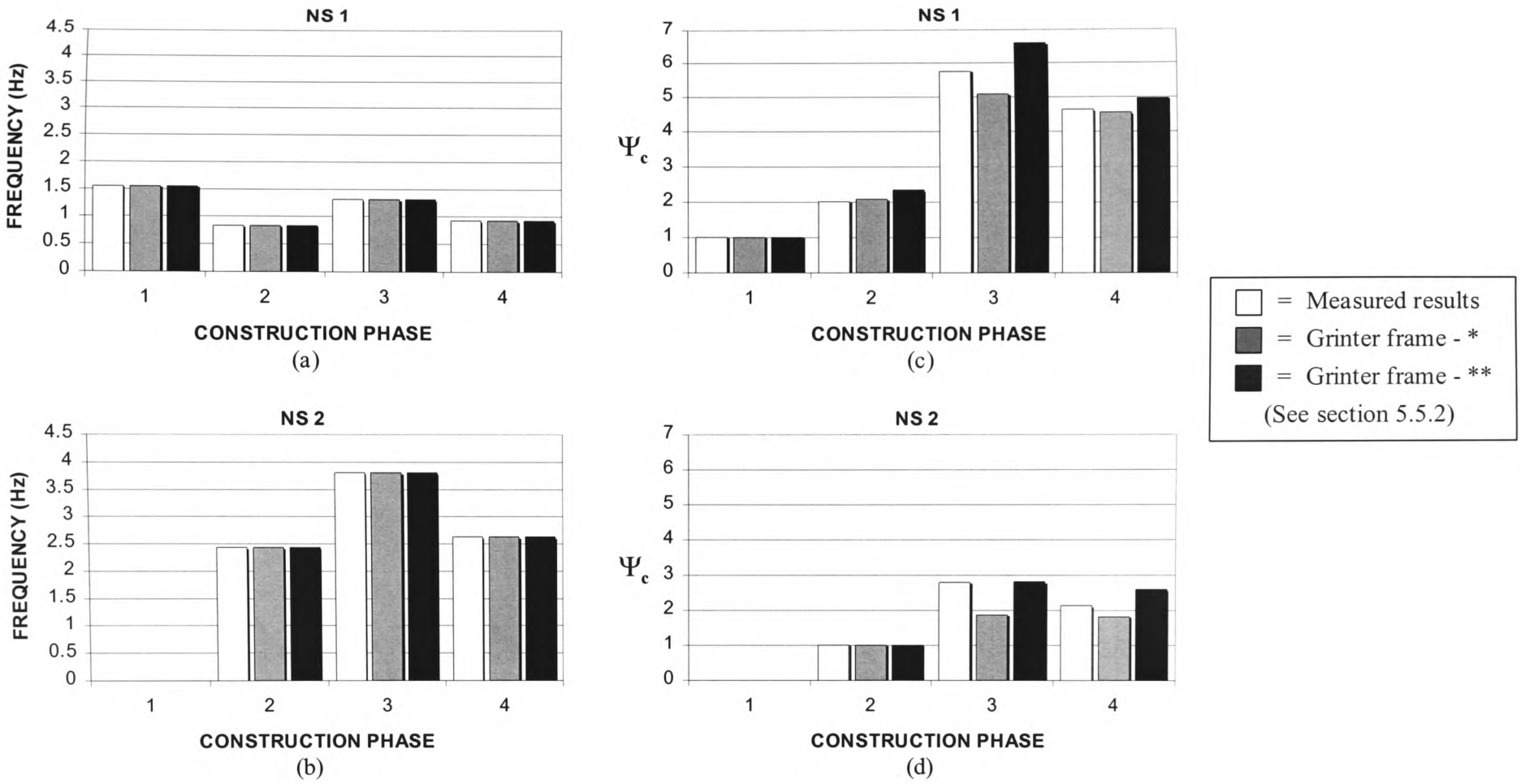

Figure 5.7 – The comparison of natural frequency and whole frame stiffness change from measured and calculated properties using the calibration parameters of Table 5.2: (a)+(c) NS 1, (b)+(d) NS 2

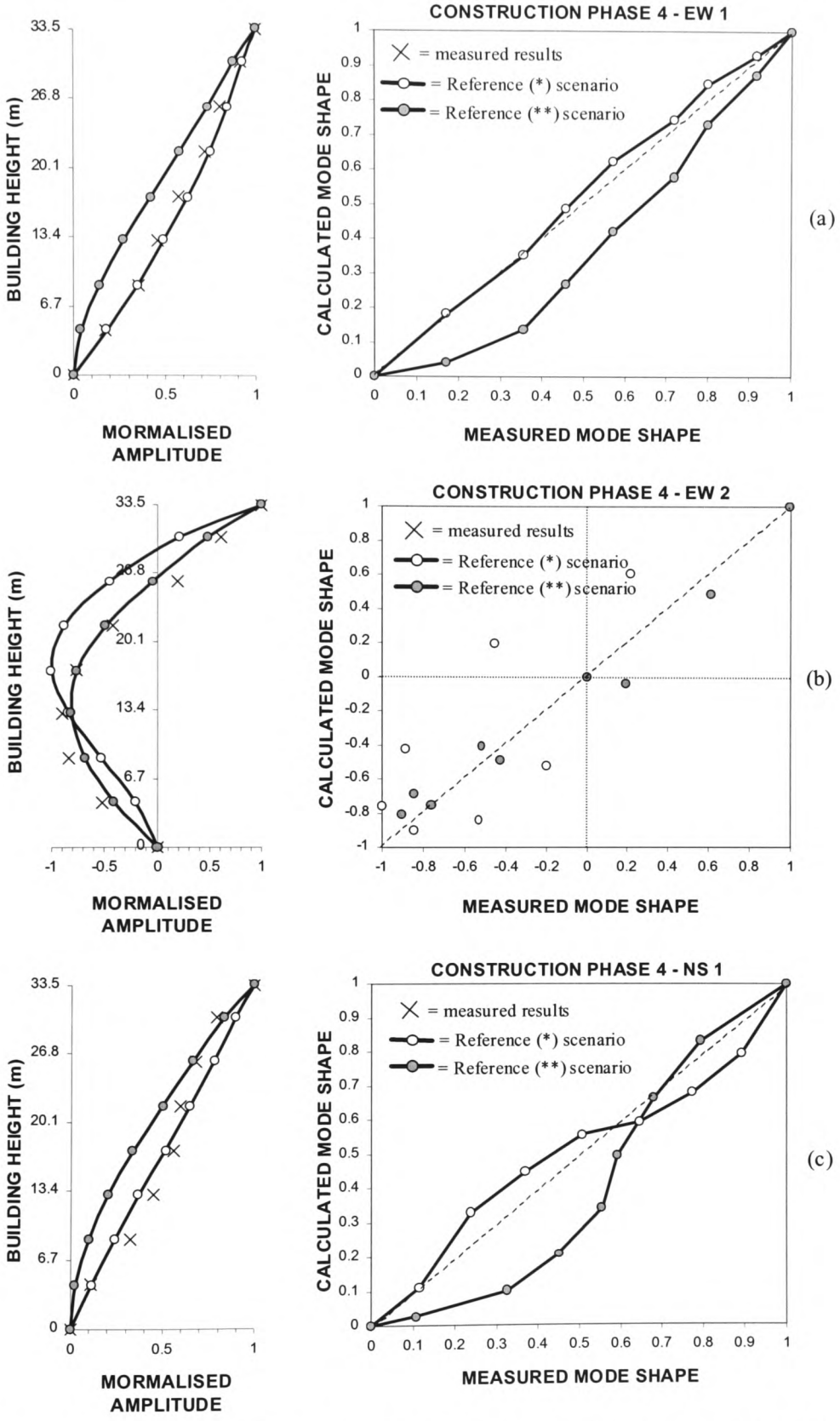

Figure 5.8 – Comparison of measured and calculated mode shapes for construction phase 4: (a) EW 1, (b) EW 2 and (c) NS1.

5.6.1 Calibrated EW and NS properties

The behaviour of the building when vibrating in the EW 1 and NS 1 modes can be captured with reasonable accuracy for all construction phases if the calibration parameters associated with the base node restraint are chosen to reflect minimum values. The beam to column connection at each storey, coincident with these values, indicates a fully fixed condition, which provides a closer comparison of whole-frame stiffness change for all construction phases. The alternative condition that relates to a high rotational restraint at the base, on the other hand, gave a rate of whole-frame stiffness change that overestimated the corresponding measured properties.

Table 5.4 indicates the best choice set of whole frame stiffness properties based on the two result sets considered. Highlighted by the shaded areas of the table, the following main observations can be established.

5.6.1.1 Observations from the EW 1 and NS 1 results

(i) Construction phase 1: To obtain an agreeable comparison with the whole-frame stiffness change from the measured properties, best results are achieved if the beam to column connections of the frame are assumed to be substantially rigid. Coincident with this condition, the base of the building must then be assumed to be flexible, permitting rotation with only marginal restraint.

(ii) Construction phase 2: At phase 2 the added weight of the building appears to contribute to a stiffening at the base as the best results are achieved when the beam to column connections are assumed fixed with an increase in base rotational restraint. Using the results in Table 4.10 of chapter 4 as a basis for comparison, it appears that the restraint at the base of the building has the effect of increasing the whole-frame stiffness. Comparing the un-calibrated results for the pinned base condition for EW 1 (Ψ_c = 1.88, Table 4.10) to the calibrated Ψ_c^* = 1.97 shows an approximate 4% relative increase. Similarly for NS 1 sway, Ψ_c = 1.38 and Ψ_c^* = 2.09, which is a 51% increase. These results demonstrate that the change of stiffness of the frame is greater for the sway behaviour about the stiffer axis of the building.

(iii) Construction phase 3: For convenience, it is reasonable to assume that the nominal increase to the overall building mass did not increase the base restraint any further when the block-work walls were added at phase 3. The additional stiffness must then be due to the structural interaction that may occur between the frame of the building and the wall itself. It is thought that the walls installed on the north and south perimeter regions of each storey increase stiffness in the EW sway direction, while the full height walls on the east and west parts contribute to the NS behaviour. With regard to the EW sway, it was to be expected that the calibration value for α would be low as the walls on the north and south of the building were constructed to 900mm in height. However, the α value corresponding to the NS sway is equally low although the walls were installed to full height on the east and west elevations of the building.

(iv) Construction phase 4: Based on the assumption that the block-work wall influence on frame stiffness remains constant, the calibrated rotational restraint properties give results that suggest a reduction to the base node restraint for the EW 1, while the NS 1 parameter shows an increase to this property. There are a number of reasons that could be discussed in an attempt to justify these changes, but in reality there is simply too little information available to clearly define the properties of the building at construction phase 4.

5.6.1.2 Observations from the EW 2 and NS 2 results

General trends can also be identified for the EW 2 and NS 2, but the behaviour of the frame for both these modes tend to suggest flexible rotational restraints at all joints throughout each construction phase. Without focusing too much on the detail of the joint properties, it is interesting to note that the calibrated results of these modes appear to suggest that the contribution of the block-work walls to overall stiffness of the frame increases at the higher modes. This is consistent with the findings of Chrysostomou (1991) where higher modes were said to induce a condition defined as 'strut reversal' causing an effective increase to the α value. The 'strut reversal' was said to occur during complex deformation patterns of the frame, which was seen to be dependent on the mode of vibration. As the mode of vibration increased, the

deformation of the frame becomes more complex causing the contact between the frame and block-work to increase. This effect is seen to be more pronounced for the NS 2 sway calibrated results.

5.6.2 Mode shape comparison for construction phase 4

The mode shapes associated with the calibrated parameters for construction phase 4 are illustrated by Figure 5.8 and indicate a reasonable compliance with the measured normalised velocity amplitude at this phase. The EW 1 predictions give the best likeness to the measured values, while EW 2 and NS 1 calculations offer what can be best described as an approximation to the measured values.

Unfortunately, these were the only mode shape measurements taken from the building, which is due primarily to the significant amount of effort require to capture such information on a full scale building. However, based on this information it can be seen form Figure 5.8 that the calibrated results, assuming the flexible base scenario, provides the better fit for the EW 1 and NS 1 modes. For the EW 2 mode the best results are achieved when the beam to column connections are assumed completely free. These results also correspond with the assumed best candidate conclusions shown shades on Table 5.4 adding confidence to the calibration methodology formulated.

5.7 Sensitivity of the Calibrated Model and its Application to Damage Detection

The calibration procedure has provided calculated natural frequencies that comply with values taken from vibration response measurements. Placed in the context of the original aim, which was to gain a model capable of accurately capturing the behaviour of the building during construction, this too has also been achieved. Therefore, by interpreting the construction phases as a form of 'reverse damage' a model for the assessment of whole-frame stiffness change has been provided.

However, it is clear that the whole-frame stiffness change is not a realistic perception of the type and extent of damage that would need to be identified to make damage detection from natural frequencies a feasible non-visual method. The stiffness changes considered up to this point have focused on whole-frame influences, while real damage may not affect the entire building.

5.7.1 Sensitivity of the calibrated Grinter frame to localised stiffness change

To assess the sensitivity of the calibrated frame model, a series of analyses were conducted that assumed a complete removal of floor elements, on an individual storey basis, in order to gain an idea of the possible frequency change that may occur. The main assumption considered was that structural damage of the building, after construction phase 4, would have the affect of completely eliminating the contribution of individual floor stiffness to the whole-frame behaviour. Table 5.5 contains the analytical results that were calculated using the modified GRIND program imposing the calibration variables defined for construction phase 4 by Table 5.2. To aid the interpretation of the tabulated results, the floor numbers indicated relate to the storey beam stiffness that was removed, i.e. single storey only.

Table 5.5 – Calculated natural frequency assuming that damage has the effect of causing the removal of individual floor beam stiffness

Floor number	**EW1** f_m **= 0.66 Hz**	**EW2** f_m **= 1.9Hz**	**NS1** f_m **= 0.93 Hz**	**NS2** f_m **= 2.63 Hz**
1	0.664	1.896	0.905	2.577
2	0.663	1.898	0.891	2.595
3	0.642	1.896	0.902	2.625
4	0.646	1.899	0.912	2.616
5	0.662	1.898	0.914	2.577
6	0.649	1.896	0.912	2.519
7	0.652	1.892	0.912	2.490
8	0.649	1.893	0.919	2.483

(All frequencies are quoted in Hz, i.e. cycles per second. f_m is the measured, and thus the calibrated, natural frequency values appropriate to each mode).

5.7.2 Measured natural frequencies obtained from the building after real damage

The reason for choosing to study the eight-storey steel-framed building (SFB) at the BRE Cardington laboratories was mainly due to the actual known damage that was caused to the structure after its construction was complete. As pointed out earlier in chapter 4, the building has been used for various research projects where service load conditions and extreme fire situations have been imposed on the structure. These imposed situations have caused significant damage to the structure providing an ideal opportunity to obtain natural frequency information after their occurrence.

5.7.2.1 Conditions imposed on the building to cause damage

Detailed accounts have been given in numerous publications, such as Grantham (1994) and Martin (1994), regarding the type of test, their results and the aim of such tests conducted on the SFB. These details are not necessarily of importance here, as they discuss primarily the behaviour of the building during service and fire load conditions. However, to give an indication of the tests conducted on the building that correspond to the subsequent natural frequency measurements, a cursory overview follows.

- Damage condition 1: April 1995 – Fire tests were conducted on the completed building to simulate extreme fire on floor 3. The test comprised the localised heating of an individual beam using a furnace. The location of the test was on the south side of the building between grid lines D2 and E2, which is based on the referencing system illustrated in Appendix B. The furnace tests, which generated temperatures in access of 1000°C, caused the beam to buckle and the floors to deflect to a permanent deformed profile measuring approximately 300mm at the beam mid-span.
- Damage condition 2: April / May 1995 – Furnace tests were conducted on the third floor, which covered the beam and column members on grid-lines A2 to C2. The furnace reached temperatures in excess of 1000°C, causing significant damage to the floor beams of the fourth floor. However, the most dramatic effect from this test was the damage that took place to the column on grid line B2. This column was deliberately non-fire protected, which resulted in a

permanent 200mm vertical buckling / shortening at its connection region with beams at the fourth storey. The shortening of the column meant that all floors above this localised buckling also reduced in height by 200mm producing a definite sagging of the floors at each storey around the column at B2.

- Damage condition 3: June / July 1995 – Large fire compartment tests were conducted to simulate the effect of a real fire, where office furniture and other combustible materials were used to induce significant temperatures. The compartment was located on the third floor and covered an area approximating to the region of the floor bounded by grid-lines D1 to D3 and F1 to F3. The temperature in this fire reached in excess of 900°C, which caused significant permanent deformation to the exposed floor beams supporting the fourth floor. The deformed shape of the fourth floor after the fire produced a dish like appearance with mid-span beam deflections being in the range of 200mm to 500mm over the region of the fire.

5.7.2.2 Measured natural frequencies obtained after damage

Within days of the damage conditions identified above, transient response measurements of the building were recorded. Using the procedures identified in chapters 3, the natural frequencies of the building were extracted for comparison with the original measurements gained from the un-damaged structure. Table 5.6 gives the results.

Table 5.6 – Measured natural frequencies from the damaged eight-storey steel-framed building

Damage condition	EW1	EW2	NS1	NS2
1	0.66	1.90	0.93	2.63
2	0.65	1.95	0.94	2.63
3	0.65	1.93	0.93	2.66

(All frequencies are quoted in Hz, i.e. cycles per second).

5.7.3 Discussion on the practicality of detecting damage on a whole frame basis

5.7.3.1 Using the calibrated Grinter substitute frame to detect damage

The calculated frequencies shown by Table 5.5 illustrate that the calibrated frame can provide an indication of the natural frequency change that may occur as a result of changes being made to the stiffness properties of the floor. From studies assuming storey by storey stiffness losses, it is seen that there is a definite change to the calculated frequencies, which would suggest that whole-frame behaviour could provide information for use with damage detection.

However, one must reflect on the practicality of these assumptions, which based on a physical interpretation, would mean a complete removal of an entire floor. Indeed, even in this condition the change of frequency is at most a 6% reduction relative to the value calculated for the original calibrated model (Table 5.5 - NS 2, floor 8), which would suggest that calculations based on smaller floor-stiffness property-adjustments would yield insignificant frequency changes.

5.7.3.2 Using the measured information from whole-frame response measurements

Throughout each of the damage conditions described above the effects on the structure, from a visual perspective, were significant. Buckled beams, deformed floor slabs and shortened columns each describe the type of damage that could be clearly seen. However, the changes in frequency for each of these conditions do not reflect the severity of the damage observed to a magnitude that would cause alarm. For example, after damage condition 2 the frequencies reduced from 0.66Hz to 0.65Hz for EW1 with the NS 1 increasing from 1.9Hz to 1.95Hz. The former of these modes appear, therefore, to be unaffected by the significant damage, while the latter shows an increase in the frequency, which is itself a violation of the assumption that damage effectively reduces structural stiffness, i.e. reducing natural frequency.

It is clear from these measurements that the actual damage produces significantly more complex behavioural changes that are not captured by the whole-frame response characteristics.

5.8 Concluding Discussion

A calibration procedure for use with the Grinter substitute frame analysis has been presented. Accurate natural frequencies and, based on a comparison with limited information, mode shape profiles can be achieved from a back-substitution of measured information.

Adopting the analysis for use as a damage detection method highlights the shortcomings of such whole-frame methods. This 'smearing' approach effectively reduces the likelihood of considering localised structural property variations. This shortcoming does not necessarily indicate that the model will not provide correct natural frequency results. However, interpreting structural changes from measured vibration signals, obtained before and after damage, suggest that the frame response is insensitive to significant structural changes caused by damage.

The information presented in this chapter provides sufficient evidence to suggest that damage detection, on the scale considered in this chapter, is not practical and a more localised approach must be considered. By reducing the number of potential variables, a point may be reached where adjustments to the structural system can be recognised from definite trends in natural frequency changes.

CHAPTER 6

Application of the Calibration Methodology to Quantify Damage in a Composite Floor Slab within a Full-Scale Building

6.1 Introduction

The previous chapter highlighted the shortcomings when using whole-frame response measurements to quantify damage. It was seen that, due to the complexity of the whole-frame characteristics, changes in frequency were difficult to detect even when damage was seen to be significant.

To remove dependence on the whole-frame behaviour, a similar study was undertaken to quantify damage of known location within one of the floors of the steel-framed building. Considering analytical models of the floor, the aim is to use the calibration methodology identified in the previous chapter to examine the structural changes that occur in a concrete floor-slab caused by excessive localised static loads.

6.1.1 The floor structure considered for the study

The floor considered for this study was located at the fifth floor of the eight-storey steel-framed building. This floor was chosen as it offered a unique opportunity to obtain vibration characteristics from a floor in 'pre' and 'post-damaged' conditions. Details of the structural members and overall geometry of the floor are presented in Appendix B, in which general information of the entire building is also contained. This information illustrates 'as-constructed' properties, which is also regarded as being representative of the pre-damage condition of both the whole structure and the floor in question. The construction of the floor is of composite construction, where the steel beams support a concrete deck, the detail of which has been covered in chapter 4.

A visual inspection of the floor was carried out at the time of the 'pre-damage' vibration testing, which was conducted during July 1997, and indicated no structural damage within the vicinity of the floor used for the investigation. No static or fire

loading had been applied to the floor prior to this time providing a region of the slab that was considered 'load-history' free.

6.1.2 Post-damage floor condition

6.1.2.1 The cause of structural damage to the floor

Post-damage dynamic testing was conducted during November 1998, more that one year after the initial vibration information had been measured. During this time a separate research team, not connected with this work, had carried out a series of tests that aimed to study the strength of the concrete deck under extreme static loads. Using a system comprising hydraulic jacks, heavy weight kent-ledge and Macalloy bars, these researchers applied controlled static load to the concrete deck in a four-point loading arrangement. Peel-Cross *et al* (1998) have given a full description of these tests where the main aim was to identify the in-situ performance of the deck for comparison with laboratory tests.

The details of the aforementioned tests and the conclusions of the work are not necessarily of importance here as the tests considered only centre-span deflection of the deck with no record of load distribution or section strain information being given. However, the information that is vital for this study is the subsequent location and visual extent of the damage that was caused.

6.1.2.2 Visual observations of the damage

Peel-Cross *et al* (1998) reported that the applied static load caused a shear failure in the concrete deck, which produced large width cracking in the slab and was said to have occurred directly over the 'on-grid' beams. This damage was observed by the candidate at the time of the 'post-damage' dynamic tests and was seen to have affected three locations on the floor, which are indicated in Figure 6.1. The widths of the cracks along these regions were between 0.5mm and 3mm, which was measured at the surface of the concrete, while the depth in several locations could be measured to approximately 50mm. The steel beams, however, appeared to have been un-affected

by the damage with no evidence of permanent deflection and no observed damage at the region of the beam to column connections. Nevertheless, from these observations it was clear, from a structural point-of-view, that the static load had produced damage on a scale that would be considered unacceptable if such damage was observed in a functioning / occupied building.

6.2 Description and Results of the Dynamic Tests for the Pre and Post-Damaged Floor

6.2.1 Dynamic testing methods

The dynamic testing involved both impact load and steady state forced vibration methods. To obtain the natural frequencies of the floor, for both pre and post-damage conditions, the heel-drop impact load approach was adopted. Using an accelerometer, the response of the floor was recorded over a fixed time length, the duration of which being sufficiently long to allow the ensuing decay of the floor vibration to be captured subsequent to the heel-drop.

To measure the mode shape of the floor corresponding to the fundamental mode of vibration, forced vibration equipment utilising the eccentric mass philosophy described in chapter 3 was used. However, due to unfortunate mechanical problems with this equipment during the pre-damage dynamic testing, mode shapes could not be obtained. Therefore, mode shape information applicable only to the post-damage condition has been included here.

6.2.2 Measured natural frequencies from the floor response signals

6.2.2.1 Pre-damage frequencies

A total of nineteen response signals were recorded, each representing the behaviour of the fifth floor at specific locations throughout its entire area. The locations from which these response signals was retrieved were chosen to coincide with (i) the centre

of the slab bays, and (ii) the centre of grid-line beams along the EW axis of the building. To clarify this definition, the slab 'bays' can be visualised as the areas of the floor bound by the grid-lines consistent with the floor layout shown in Appendix B.

To focus the study on the location of known subsequent damage, only those response signals appropriate to the damage-affects regions of the floor were considered. Figure 6.2 and Table 6.1 presents this information, the referencing of which corresponding to the locations indicated in Figure 6.1. Peak response amplitude, together with the frequency at which it occurs, obtained from the autospectra is quoted in the table where the values relate to the signals that were recorded from the centre-bay positions.

6.2.2.2 Post-damage frequencies

To provide a true indication of any changes that may have occurred to the natural frequencies of the floor as a result of the damage, response signals were recorded at locations consistent with the pre-damage results. The natural frequencies obtained from these signals are shown in Table 6.1, which also indicates the amplitude of the response corresponding to the frequencies being defined.

6.2.2.3 Interpreting the mode order of the floor

The data provided by the autospectra (Figure 6.2) of measured signals does not automatically present evidence that can be used to define the mode of vibration to which the spectral peaks relate. To achieve this, based on the present available information, a comparison of measured and calculated behaviour should be carried out so that the most likely candidate set of predicted frequencies can be nominated as being representative of the values from the response signals. Table 6.1 identifies the vibration mode order associated with the quoted frequencies, which was obtained from comparisons with three FE models of the floor described later in this chapter. To relate the order of the modes to the floor bay areas (Figure 6.1) these predictions comprised both continuous and discontinuous idealisations of the floor bays. To identify the mode order from these models the following was then assumed:

(i) The continuous model (comprising three continuous floor bays) gave natural frequencies that took account of the floor continuity. The mode shapes associated with the calculated frequencies were then used to locate the maximum vibration amplitude, which gave an indication of the position where dominant response of the floor occurs relative to the bay layout. As the aforementioned mode shapes are typically calculated in a normalised form (relative to a maximum amplitude of "1.0"), this interpretation was easily achieved allowing the maximum amplitude point to be recognised, thereby allocating the frequency value to the bay at which this maximum occurred.

(ii) The frequency and assigned mode order gained from (i) above was confirmed with a comparison with the remaining two models (both being discontinuous isolated bays), where good agreement between the two result sets were seen.

6.2.3 Discussion on the results obtained from the autospectra

The autospectra of the measured acceleration response of Table 6.1 and Figure 6.2 appear to show that the natural frequencies of the floor change as a result of the imposed damage. This information was calculated using a Fast Fourier Transform (FFT) routine that allowed the response spectra to be viewed over any desired frequency bandwidth, which enabled the frequencies and their spectral amplitude to be determined. However, the results obtained from the autospectra in this way should be treated with extreme caution as the information produced by the FFT has an accuracy dependent on the amount of response information available from the recorded signal.

Table 6.1 – Pre and Post-damage natural frequencies of the floor from impact response measurements together with relative peak-amplitude readings from FFT

Bay number	**Mode number**	**Information from the response autospectra**			
		Pre-damage		**Post-damage**	
		Frequency f_m (Hz)	**Response (acc^2/Hz)**	**Frequency F_d (Hz)**	**Response (acc^2/Hz)**
Bay 1	1	5.86	7.8	5.86	6.9
	2	7.82	4.2	7.58	3.0
	3	11.98	2.1	11.74	1.4
Bay 2	1	6.84	7.9	6.59	5.6
	2	9.52	4.9	9.28	4.2

(Notes to Table 6.1: 'Response' = peak spectral response amplitude corresponding to the quoted frequency value. f_m = pre-damage frequency, f_d = post-damage frequency).

6.2.3.1 The natural frequency values

The spectra of the FFT is not continuous, but are composed of discrete points, which are separated at intervals relative to the capture rate of the signal and the total time over which the recording was made. Thus, for every signal taken from the floor, each of which was recorded over of 4.096 seconds at a rate of 1kHz, the spectral points are 1000/4096 (i.e. ≈ ¼) Hz apart. Therefore, a value of say 5.86Hz is not resolved to the nearest $1/1000^{th}$ Hz but represents a value of 5.86(± $1/8^{th}$)Hz. Similarly, the frequencies obtained from the floor after damage have the above resolution characteristics, which makes the interpretation of actual frequency change difficult to define precisely. However, consolation must be drawn from the results as the pre and post-damage autospectra gave consistent frequencies at each stage of testing, i.e. pre-damage results are consistent and post-damage results are consistent for the three measurement locations.

Therefore, for the purposes of this study it is assumed that the frequency change was a result of the imposed damage and that the amount by which these frequencies have changed is an indication of the damage extent.

6.2.3.2 Peak spectral response amplitude

The amplitude of the spectral peaks gives some indication of the mode dominance corresponding to the location at which the response was measured. For example, the autospectrum for location 1 (see Figure 6.2) illustrates that the motion of the floor at a frequency of 5.86(± $1/8^{th}$)Hz (pre-damage) dominates the total response, while higher frequency modes participate to a smaller extent. Similarly, but slightly more complicated, location 2 has motion dominated by oscillations at 6.84(± $1/8^{th}$)Hz (pre-damage). This information is useful when defining the vibration modes of the individual floor bays, where dominant amplitudes can usually indicate the fundamental behaviour of the region at which the measurements were taken.

In the context of damage detection, it may also be possible to use this information to reveal the changes that may occur (in a relative sense) to these amplitude peaks that could signify a change in the behaviour between pre-and post-damage response. However, it would be unwise to follow such an assumption with the information presented by the autospectra as the detail regarding the input response is not known. Relative amplitude cannot be assessed accurately as the level of input force from the heel-drop test may be different for each test making a relative comparison difficult to estimate. Therefore, these amplitudes are included only to demonstrate the magnitude of acceleration that can be expected from a single person's heel-drop weighing approximately 79kg.

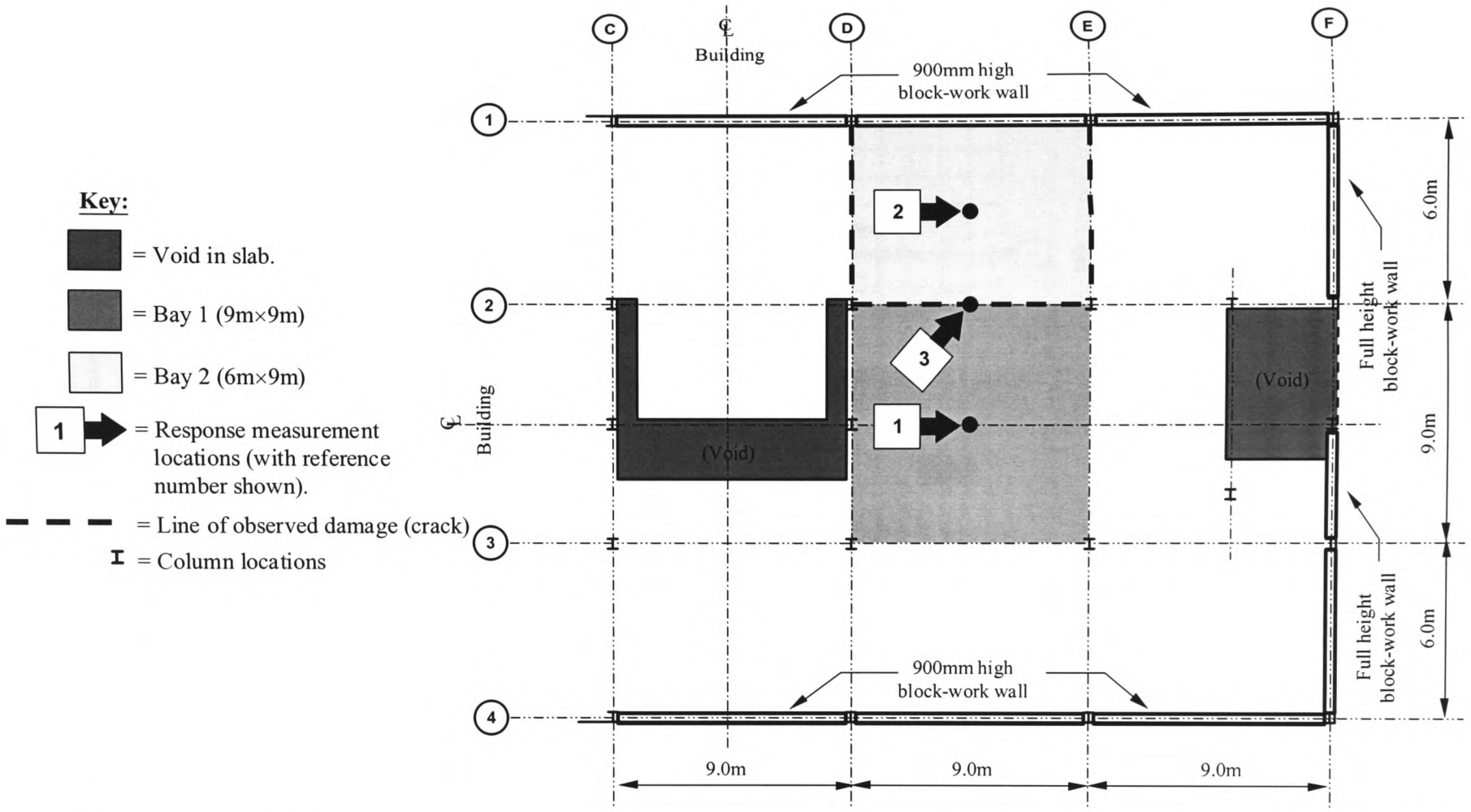

Figure 6.1 – General arrangement of the building at floor 5 showing the bay numbers, response measurement locations and the position of the observed concrete damage (i.e. the cracks in the concrete).

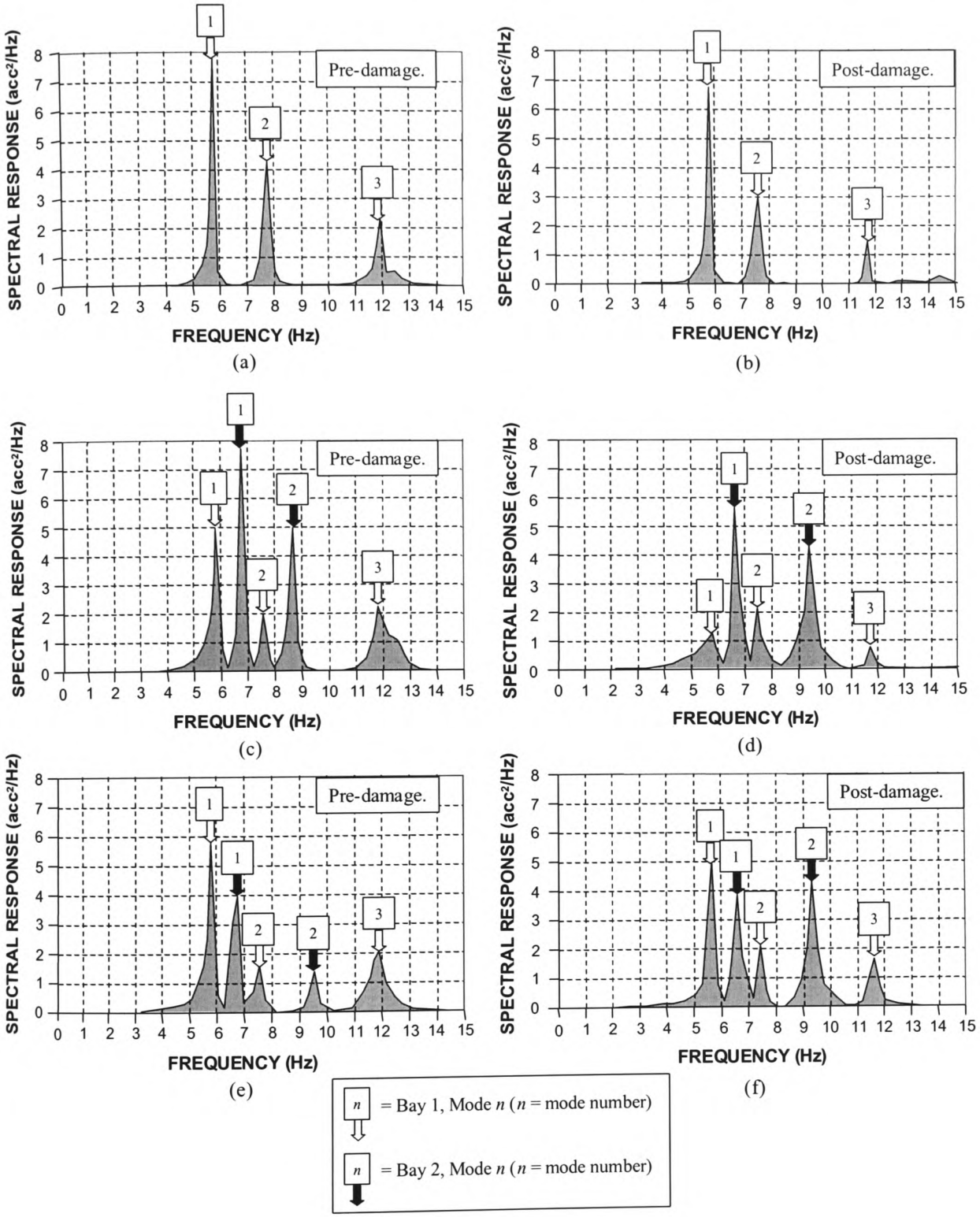

Figure 6.2 – Autospectra information from the damage-affected region of the slab: (a)+(b) location 1, (c)+(d) location 2, and (e)+(f) location 3.

6.2.4 Post-damage mode shape corresponding to the fundamental mode of bay 2

The mode shape associated with the fundamental mode of bay 2 (9m×6m) was measured using two accelerometers and a single forced vibration exciter. Using the method described in chapter 3, where one accelerometer is used as a traveller, and the second as the reference, the amplitude of the floor vibration corresponding to the locations show in Figure 6.3 were measured. The normalised magnitude of the response at these locations was then achieved from a simple ratio of 'traveller' to 'reference' readings providing the values also indicated in Figure 6.3.

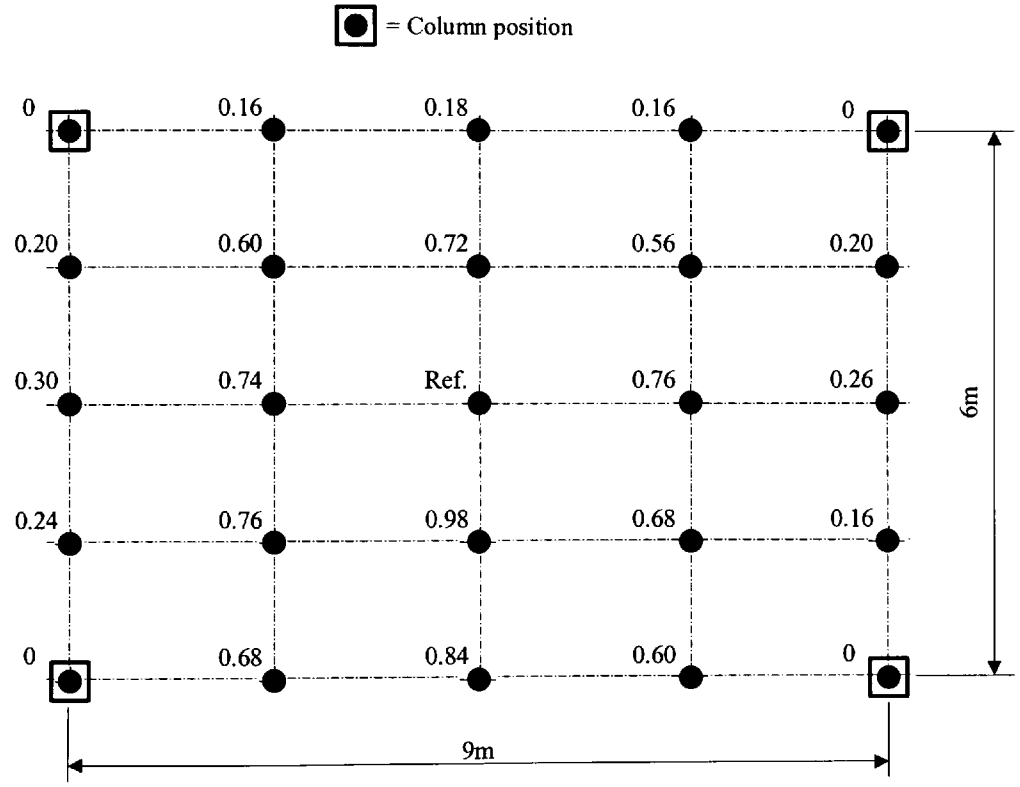

Figure 6.3 – Normalised peak amplitudes at various locations of bay 2 (9m×6m) corresponding to the post-damage fundamental frequency. (Ref. = location of the reference accelerometer and the position of the eccentric-mass exciter used to induce the vibration).

6.3 Predicting the Natural Frequency of the Floor

To examine if the imposed damage can be related to the natural frequency changes, an adequate model of the floor should first be available. This section discusses studies that have been proposed by various authors to accomplish this condition.

6.3.1 Semi-empirical definitions of floor natural frequency

Uchida *et al* (1993) compiled measurements of natural frequency and dynamic deflection for composite steel / concrete floor beams taking into account a variety of floor-span to structural-mass ratios. The aim of the work was to identify a mathematical expression that could be used to predict the deflection of these structures, caused by impact loads such as footfalls and the dropping of weights. This was achieved using a mathematical expression based on a 'Timoshenko' beam element, but it was also shown that measured natural frequencies approximated to a simple expression of the form,

$$f_o \approx \frac{44.96}{L} \tag{6.1}$$

where f_o and L are the fundamental natural frequency in Hz and the floor span length in metres respectively. However, the degree of correlation, between the expression and the measured data, was not discussed with the presented results showing significant scatter about this best-fit equation.

Murray and Allen (1993) considered the calculation of floor slab frequency as a parameter that could be related to static deflection estimates. The expression proposed by these authors was given by,

$$f_o = 0.18\sqrt{\frac{9.81}{\delta_{static}}} \tag{6.2}$$

where δ_{static} is the deflection of the floor caused by its self-weight. This expression has a similar form to that identified by Wyatt (1989), that was given as,

$$f_o = \frac{18}{\sqrt{\delta_{static}}} \tag{6.3}$$

Unfortunately, in both cases no measured frequencies were given to justify the accuracy of these expressions.

6.3.2 'Closed-form' mathematical predictors of floor natural frequencies

6.3.2.1 Calculating natural frequencies neglecting floor continuity

The structural behaviour of continuous floors, subject to static loading, follow strict rules that have now become acceptable methodologies for design. Examples are codes of practice such as BS 5950: Part 4 (1994) for composite structures, and BS 8110: Part 1 (1997) for concrete members where research and practical experience has been combined to offer reliable but simplified mathematical formulations for use in design. However, such 'simplified' rules have also been repeatedly shown to provide unreliable results when considered in the context of vibration analysis. Williams and Waldron (1994), for example, compared the natural frequencies obtained from the response measurements of various building floors to mathematical predictions assuming simple behaviour. One predictor used for the comparison was defined as an 'equivalent beam model' or 'EBM', which was chosen as it matched the assumptions considered for the static analysis of the floors. The expression was given as,

$$f_o = \frac{\pi}{2}\sqrt{\frac{EI}{ml^4}} \tag{6.4}$$

where f_o is the fundamental frequency, E and I are the Young's modulus and bending inertia of the structure respectively, while m and l define its mass and span length assuming simple rotationally free supports. In all cases considered, which included structures such as concrete beam and slab, ribbed floors, flat slabs, waffle slabs, pre-

cast 'T' beams and composite floors, the results of eqn.(6.4) underestimated the actual measured frequencies. The discrepancy ranged between 17% to 54% relative differences, with the authors concluded that the EBM was not appropriate for use with real floor structures. The equivalent-plate approach, which was identified by Timoshenko and Woinowsky-Krieger (1959) as,

$$f_o = \frac{\pi}{2}\sqrt{\left(\frac{D}{m}\right)}\left(\frac{1}{l_x^{\,2}}+\frac{1}{l_y^{\,2}}\right) \tag{6.5}$$

where

$$D = \frac{Eh^3}{12(1-\nu^2)} \tag{6.6}$$

was also found to give inaccurate results when compared to similar measurements. As a results, Williams and Waldron (1994) proposed an amendment to eqn.(6.5) adjusting the mathematical expression to,

$$f_o = \frac{\pi}{4}\sqrt{\left(\frac{E}{3m(1-\nu^2)}\right)}\left(\frac{h_x^{\,3/2}}{l_x^{\,2}}+\frac{h_y^{\,3/2}}{l_y^{\,2}}\right) \tag{6.7}$$

where l_x and l_y are the equivalent-plate plan dimensions, h its thickness, and ν the Poisson's ratio of the floor material. Equation (6.7) was found to provide a better comparison with measured frequencies, but the authors pointed-out that the assumption of a simply supported perimeter, which forms the basis for the formulation of eqns.(6.5) and (6.7), is unrealistic. This is due primarily to the assumption that the perimeter regions of the equivalent-plate imposes a 'zero-displacement' boundary condition, which from a comparison with measured mode shapes from continuous floors, was found to be inaccurate.

6.3.2.2 Calculating natural frequencies of floors with continuity

Feltham (1991) offered a number of proposals to simulate the behaviour of floors taking account of the continuity between adjacent floor regions. Focusing primarily on the analysis of post-tensioned concrete floors, mathematical expressions were

produced for use with flat and waffle slabs, which included provisions for structures with or without stiffening 'on-grid' beams. The expressions given were for two-way spanning structures supported by regularly spaced columns comprising n_x number of bays, each of length l_x, and n_y bays of l_y length. The expressions given were:

(a) with stiffening 'on-grid' beams coincident with column grid-lines:

$$f_x = k_x \frac{\pi}{2}\sqrt{\frac{EI_y}{ml_y^4}} \tag{6.8a}$$

and

$$f_y = k_y \frac{\pi}{2}\sqrt{\frac{EI_x}{ml_x^4}} \tag{6.8b}$$

where,

$$\lambda_x = \frac{n_x l_x}{l_y}\sqrt[4]{\frac{EI_y}{EI_x}} \tag{6.9a}$$

and

$$\lambda_y = \frac{n_y l_y}{l_x}\sqrt[4]{\frac{EI_x}{EI_y}} \tag{6.9b}$$

gives,

$$k_x = 1 + \frac{1}{\lambda_x^2} \tag{6.10a}$$

and

$$k_y = 1 + \frac{1}{\lambda_y^2} \tag{6.10b}$$

The calculated frequencies obtained when using eqns.(6.8) to (6.10) inclusive take account of vibration modes involving multiple bay motion. Therefore, the x and y subscripts denote whole-slab vibration dominated by motion of coupled adjacent bays in the x and y directions respectively. The properties of the slab being defined in the usual manner, with Young's modulus, bending inertia and mass per unit area abbreviated by E, m and I respectively.

(b) without stiffening beams:

$$f'_x = f_x - (f_x - f_b)\left(\frac{\frac{1}{n_x}+\frac{1}{n_y}}{2}\right) \tag{6.11a}$$

and

$$f'_y = f_y - (f_y - f_b)\left(\frac{\frac{1}{n_x}+\frac{1}{n_y}}{2}\right) \tag{6.11b}$$

where

$$f_b = \frac{\frac{\pi}{2}\sqrt{\frac{EI_x}{ml_x^4}}}{\sqrt{\left(1+\frac{EI_x l_y^4}{EI_y l_x^4}\right)}} \tag{6.12}$$

Williams and Waldron (1994) considered the proposals of Feltham (1991) in their studies (identified above), concluding that the expressions gave natural frequencies that were not-only more accurate than the equivalent-plate equation, but also allowed orthotropic floor characteristics to be included in the calculations. However, due to the assumption that the bay dimensions l_x and l_y are equal for all bays, these authors found it difficult to obtain accurate calculations when compared with measurements taken from floors not comprising equally spaced column grids.

6.3.3 Calculating the natural frequencies of floors using finite element analysis

It has been mentioned that natural frequency calculations using mathematical expressions have their limitations, especially with regard to assumed boundary conditions. To overcome these apparent weaknesses, many researchers have turned to analysis using numerical methods, which allow more complex behavioural patterns at the floor perimeter to be considered. Pavic and Waldron (1996) and Plum and Svensson (1993), for example, reported on studies that compared the frequencies from measured response signals to the results calculated using FE analytical methods. The

former of these authors praises this form of analysis, concluding from mode shape and frequency comparisons that a high degree of correlation could be achieved. Indeed, the FE method was shown in chapter 4 to offer approximate results for a whole building frame, making it a universally applicable tool for a range of problems.

6.3.3.1 Material Young's modulus for dynamic analysis

There has been debate for some years as to the correct assignment of material Young's modulus ("*E*") when compiling analytical models of structures for dynamic analysis. Pavic *et al* (1997b) gave a discussion on a number of published reports that offered mathematical expression to the calculation of appropriate "*E*" for concrete when assessing the dynamic behaviour of floors. Focusing on non-composite floors, these authors described a wide variety of proposals for this calculation, each being the result of extensive experimental examinations on laboratory concrete specimens. However, attention was drawn to the significant differences of the "*E*" value that was achieved from the proposed expressions. These differences were seen by the authors to be dependent on the chosen method of testing adopted, which was ultimately reliant on the "... rate of straining during dynamic application of loading". Finally, the authors suggested that, for the analysis of natural frequencies, the Young's modulus of normal weight concrete could be obtained from,

$$E_c = 1.1\left[\frac{9KG}{3K+G}\right] \tag{6.13}$$

where

$$K = 11 + 0.0032\sigma_c{}^2 \tag{6.14}$$

$$G = 9.224 + 0.136\sigma_c + 3.29\times10^{-15}\sigma_c{}^{8.273} \tag{6.15}$$

and σ_c is the uni-axial compressive strength of the concrete from standard laboratory cylinder tests. Applying the E_c value achieved from the above expressions to the analysis of a concrete floor, the authors found that a good correlation with measured frequencies could be gained. This conclusion was the result of comparisons made between the analyses of the floor assuming "*E*" values appropriate to static load-induced strain, and that from the aforementioned expressions where the latter was said to give better estimates. However, it should be noted that the above expression does

not take account of the strain amplitude dependence of the Young's modulus, which was the main criticism of the study prepared by the aforementioned authors.

Other, less complicated suggestions were also given by Murray and Allen (1993) where a simple multiplication of 1.2 to the static load-induced-strain Young's modulus was proposed. However, Wyatt (1989) stated that reliable frequency calculations can be achieved using values of E_c = 38kN/mm2 and E_c = 22kN/mm^2 for normal and light-weight concrete respectively.

6.3.3.2 Modelling the boundary conditions of floors

The added flexibility offered by a FE model, especially with regard to the interpretation of boundary conditions, is probably the most attractive aspect of such an analytical tool. Unlike the mathematical models identified earlier, there are no restrictions governing the arrangement of columns, or the locations of stiffening beams, as these can be chosen and included to suite the configuration of the structure being considered.

However, this added flexibility also has associated uncertainties. There is often question over the correct interpretation that should be used when modelling the connectivity of structural members, and on how these parts affect one-another when combined in the model. Floor continuity and the restraining properties at structural connections are often such examples that need particular attention in this regard. Pavic *et al* (1997) for example, when calculating the natural frequencies of a concrete floor with the FE method, chose to simulate the continuity of the structure by applying a vertical displacement restraint at locations that coincided with perimeter beams. This philosophy assumed that the perimeter beams, which were significantly more stiff than the within-span slab of the floor, effectively produced a 'zero-displacement' boundary. Although this assumption has an acceptable and meaningful basis, the rotational restraint properties of the same boundary were not discussed.

Wyatt (1989), on-the-other-hand, gave a number of recommendations on how to interpret the boundary conditions in such situations stating that "... design provisions

for simple supports will not generally, in practice, act as such in dynamic situations. Large floor areas may thus act as if structurally continuous". Relating such comments to the analysis of floors, comprising steel and concrete parts, and remembering the relevant discussion outlined in chapter 5, it is clear that structural continuity must be born in mind when modelling structures with adjoining members.

6.4 Calculating the Pre and Post-Damage Frequencies of the Building Floor

6.4.1 Calculations based on the semi-empirical and mathematical relationships

Table 6.2 and 6.3 give the calculated fundamental natural frequency of the building floor using the relationships identified in the previous discussion. The tables also identify the section property information, which were used in conjunction with the requirements of each expression. The calculations are based on a 'smeared' interpretation of the actual floor properties. For completeness the results of Tables 6.2 and 6.3 have been presented in a graphical form, which are presented by Figures 6.4 and 6.5 respectively.

Observations:
The results of Figures 6.4 and 6.5 show that all calculated natural frequencies approximate to the measured fundamental values, but the accuracy of the predictions is subjective.

(i) Uchida *et al* (1993): Calculations based on the simple expression by these authors has provided results that are surprisingly close to the measured values. However, a calculated percentage deviation of approximately ±10-15% is not acceptable for use with damage identification. Combined with its overall simplicity, this method will not offer the flexibility required modelling any structural property variations.

(ii) Murray and Allen (1993) and Wyatt (1989): The calculated frequencies obtained using the expressions proposed by these authors depend on estimations of the mid-span displacement of the floor bay. To obtain this estimate, the

recommendations of Wyatt (1989) were incorporated, where the total self-weight deflection of the floor bays was calculated from a summation of the displacement computed for each structural part. The resultant natural frequency value has a more meaningful interpretation, as the displacement and deformation patterns are similar to the assumed deformed profile of the floor during fundamental mode vibration. The calculated frequencies obtained are again close to the measured values, with a small margin of error being achieved for bay 1. However, these methods lack versatility when considered in the context of damage identification, as it is difficult to estimate the effect that adjoining bays will have on the displacement of the floor, especially at the bay perimeter.

(iii) Williams and Waldron (1994): The approach by these authors enables orthotropic properties to be considered. This has been achieved by formulating the expression relative to the structural depth of the floor. However, the method is applicable more appropriately to solid and ribbed concrete slabs, which is not strictly the case with the floor considered here, as steel members are also present. Nevertheless, approximate frequency values have been achieved, which for the 9m×6m bay is surprisingly close.

(iv) Feltham (1991): To make use of the proposals by Feltham (1991) the floor was considered in two ways. (i) Assuming the floor comprised 9m×9m bays, and (ii) assuming 9m×6m bays. These assumptions were necessary, as the proposed expressions have been formulated for application to floors with repeatable bays of similar size. The results achieved relate to the behaviour of the floor assuming vibration about the major or minor stiffness axes, thus giving two frequency values. The column layout and the assigned section properties dictate these axes. With regard to the latter of these points, a 'smeared' approach was adopted where the section properties of the bay about each of its axes were calculated as a whole and then converted to provide a 'per-unit-width' value. The lower of the calculated values should thus signify the fundamental frequency of the floor, which was achieved from the f_y predictions. Therefore, the calculations suggest that the x direction of the slab (EW of building) has a smaller stiffness compared to the y direction (NS of building), which is a true indication of the actual floor property-proportions. In addition, the calculations give close approximations to the measured values with a consistent error for

both bay 1 and bay 2, which is surprising considering that the actual column arrangement was not modelled for these calculations. However, the method was formulated to take account of the continuity of the floor, which in the case of the imposed damage (described earlier) would not allow the possible effects of discontinuity, caused by the damage, to be examined.

Table 6.2 – Calculated fundamental frequencies of the building floor using expressions proposed in literature as referenced – Bay 1: (9m×9m bay)

Reference	**Equation Number**	**Section properties and other parameters**	**Calculated frequency (Hz)**
Uchida *et al* (1993)	6.1	L = 9m	f_o = 4.99 Hz
Murray and Allen (1993)	6.2	δ_{static} = 0.0091m	f_o = 5.91 Hz
Wyatt (1989)	6.3	δ_{static} = 9.1mm	f_o = 5.97 Hz
Williams and Waldron (1994)	6.7	E_c = 22kN/mm^2 ν = 0.3 $\quad$ m = 250 kg/m^2 l_x = 9m $\quad$ l_y = 9m h_x = 75mm $\quad$ h_y = 130mm	f_o = 3.58 Hz
Feltham (1991)	6.8	E_c = 22kN/mm^2 $\quad$ E_s = 205kN/mm^2 l_x = 9m $\quad$ l_y = 9m I_x = 62×10^{-6}m^4/m $\quad$ I_y = 210×10^{-6}m^4/m n_x = 5 $\quad$ n_y = 3 λ_x = 6.78 $\quad$ λ_y = 2.21 k_x = 1.02 $\quad$ k_y = 1.21	f_x = 8.21 Hz f_y = 5.29 Hz
		Measured fundamental frequency =	**f_m = 5.86 Hz**

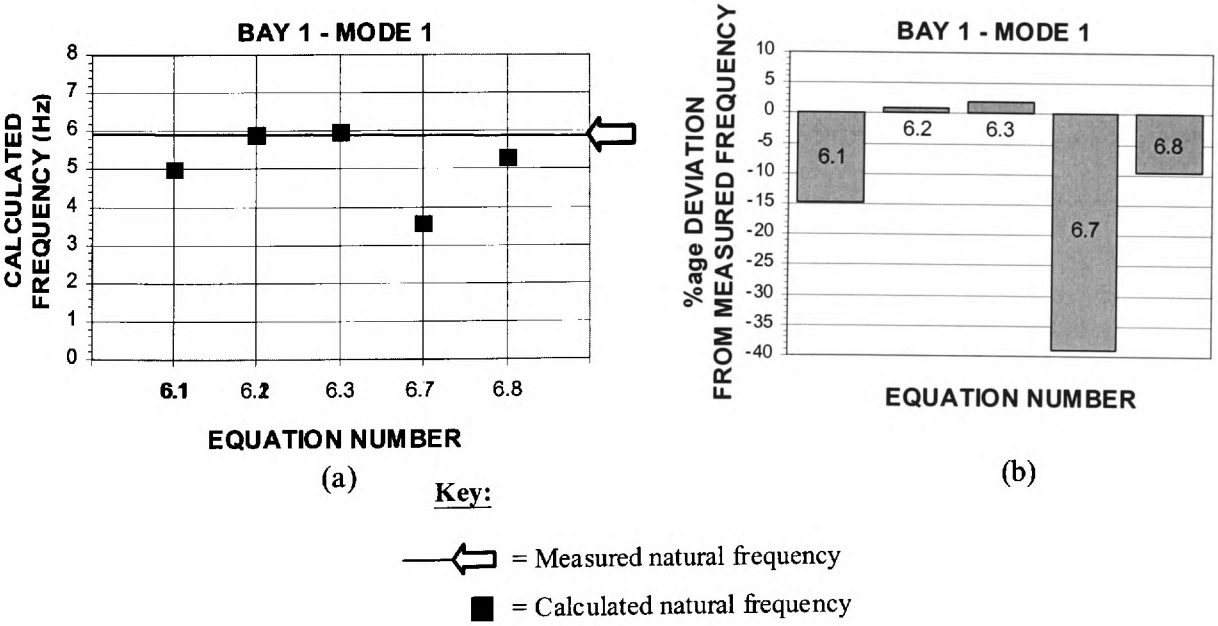

Figure 6.4 – Comparison of measured and calculated fundamental frequency for bay 1 showing (a) the calculated values, and (b) the percentage difference between the measured and calculated values.

Table 6.3 – Calculated fundamental frequencies of the building floor using expressions proposed in literature as referenced– Bay 2: (9m×6m bay)

Reference	**Equation Number**	**Section properties and other parameters**	**Calculated frequency (Hz)**
Uchida *et al* (1993)	6.1	L = 6m	f_o = 7.49 Hz
Murray and Allen (1993)	6.2	δ_{static} = 0.0084m	f_o = 6.15 Hz
Wyatt (1989)	6.3	δ_{static} = 8.4mm	f_o = 6.21 Hz
Williams and Waldron (1994)	6.7	E_c = 22kN/mm^2 ν = 0.3 m = 250 kg/m^2 l_x = 6m l_y = 9m h_x = 75mm h_y = 130mm	f_o = 6.67 Hz
Feltham (1991)	6.8	E_c = 22kN/mm^2 E_s = 205kN/mm^2 l_x = 9m l_y = 6m I_x = 62×10^{-6}m^4/m I_y = 190×10^{-6}m^4/m n_x = 5 n_y = 3 λ_x = 9.92 λ_y = 1.512 k_x = 1.01 k_y = 1.44	f_x = 17.39 Hz f_y = 6.29 Hz
		Measured fundamental frequency =	**f_m = 6.84 Hz**

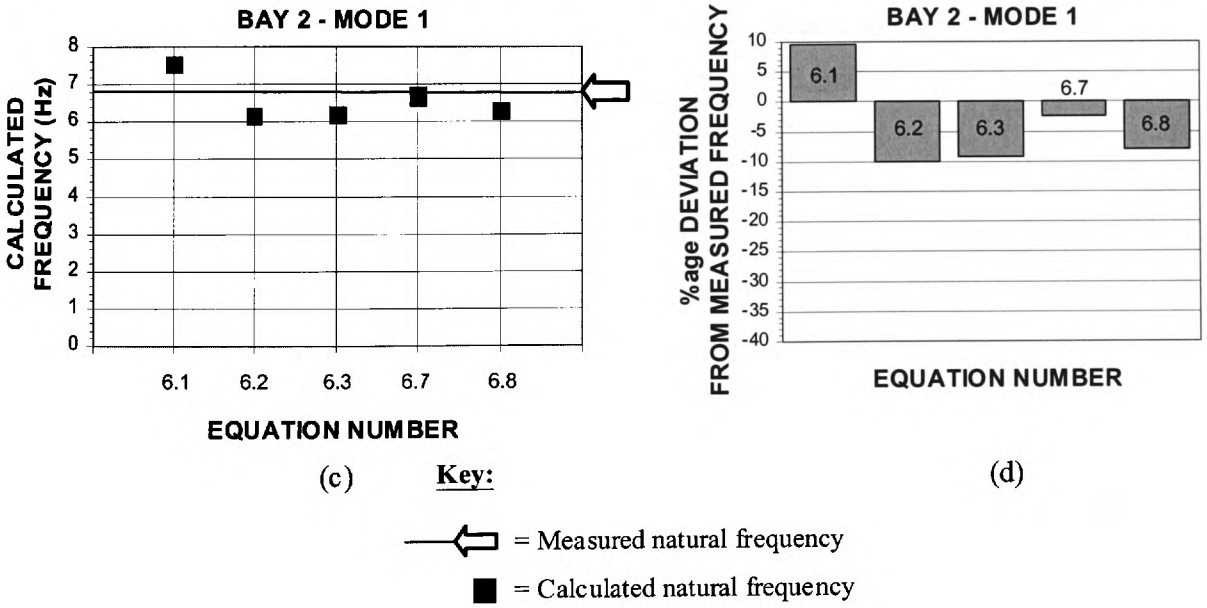

Figure 6.5 – Comparison of measured and calculated fundamental frequency for bay 2 showing (a) the calculated values, and (b) the percentage difference between the measured and calculated values.

6.4.2 Modelling the floor using a FE approach

To take account of floor bay perimeter modelling uncertainties, simplified by the expressions discussed previously, three analytical models were considered using the FE method. Each model comprised the properties of the floor around the region affected by the damage. These analyses were prepared to simulate the properties of the floor in two ways. (i) Assuming localised bay behaviour, and (ii) assuming continuity of the floor over the width of the building using three adjoining bays.

The Oasys GSA computer program was used to compile the FE models where the floor was represented using a 'grillage' method as described by West (1973) and Hambly (1991). This method has been accepted world-wide as an approach for the analysis of bridge decks, but can offer equal reliability to other structural forms such as composite steel / concrete building floors. The analysis is possible due to the similarity between the deck configuration of composite building floors and the arrangement of a bridge deck, where section properties are apportioned to members based on a chosen grid layout. The collective behaviour of the grid, comprising the properties of these members, is therefore assumed to characterise the structure as a whole, which in turn can be modelled using conventional FE analysis.

6.4.3 Description of the FE models – the assigned structural properties

The properties given in this section refer to the structure in a pre-damage condition where all structural elements have properties appropriate to the building in its 'as-constructed' form. In all cases, the Young's modulus for the concrete and steel was assumed to be 22kN/mm^2 and 205kN/mm^2 respectively, which is in accordance with the recommendations by Wyatt (1989).

6.4.3.1 Models 1 and 2 – the localised bays

Models 1 and 2 are representative of the individual floor bays bound by columns that form the 9m×9m (bay 1) and 9m×6m (bay 2) grid respectively. Figure 6.6 illustrates the dimensional aspects of these models, where a member property referencing system

is also included. Table 6.4 presents the properties assigned to the models, which contains information that is common to both bay types.

6.4.3.2 Model 3 – the continuous floor model

The third model combines the properties of 1 and 2 above, simulating their characteristics in the actual floor where continuity between the bays is assumed. The model represents an idealised strip of the floor, which includes the properties of its structural members over the entire width of the building from the north to the south sides. The overall dimensions of the model are 21m×9m and are shown in Figure 6.7 with the member property referencing system corresponding to Table 6.4.

6.4.4 Pre-damage modelling assumptions

6.4.4.1 Grillage element connectivity

(i) Element connectivity throughout the floor area – All nodes of the grillage model simulate the continuous nature of the floor with full fixity being assigned between connecting elements. This assumption ensures that the rotation and displacement of the grillage is distributed throughout the model according to the structural stiffness proportions of the discrete members.

(ii) Composite steel / concrete element connectivity – The connectivity of the grillage elements that represent the composite concrete-slab and steel-beams were assigned full fixity at their connecting nodes. The distribution of rotation at the connecting regions of beams that join perpendicular to one-an-other is thus assumed to be directly proportional to the torsion stiffness of the composite beam. Relative rotational movements that may occur at the beam to beam connections have therefore been neglected, which is consistent with the recommendations of Wyatt (1989) cited earlier. This assumption also takes account of the studies by Nader and Astaneh (1991) and Aoki (1996) where full fixity conditions was found to occur at the joints of steel frames when vibrating at the lower natural frequencies.

(iii) Connectivity at columns – Composite beam elements that connect to the columns are assumed to be rotationally rigid at the connection point. Therefore, to assess the vibration behaviour of the floor it is assumed that the column / beam connection offers significant rotational restraint [again as suggested by Wyatt (1989)].

6.4.4.2 Modelling the continuity at the perimeter of the bays

To simulate continuity in the slab at the perimeter of the bays a 'grounded spring' element was used, which allowed the rotational restraint characteristics imposed by the slab of adjacent bays to be considered. These grounded springs were located at the positions in the models as indicated by Figures 6.6 and 6.7, which allowed the rotational fixity of the slab to be examined ranging from completely free to fully restrained.

6.4.4.3 Other boundary-conditions

To ensure that the models gave results that reflect the behaviour of the floor as closely as possible, a number of additional boundary conditions were introduced. These boundary conditions were considered to be applicable to all models and were also assumed to remain consistent for both pre and post-damage states.

(i) To simulate the significant in-plane stiffness of the floor, all in-plane displacements and rotations were fixed, i.e. by defining 'zero in-plane-displacement' and 'zero in-plane-rotation' at every node of the model [i.e. no membrane direct or shear action after Davies and Fisher (1979)].

(iii) In addition to the rigid out-of-plane rotation assigned at the beam to column connections, it was assumed that each column provided a 'zero-displacement boundary' both in-plane and out-of-plane to the floor.

6.4.5 Post-damage modelling assumptions

The location of the damage offered a unique opportunity to assess the effect of discontinuity at the perimeter of the bays within the floor. To model this behaviour, two approaches were considered, both of which focused on the properties of the concrete slab alone assuming no damage to the steel parts of the structure.

6.4.5.1 Models 1 and 2 – the localised bay models

To model the discontinuity at the location of the observed damage, the properties of the grounded spring elements were studied. Assuming that the damage had the effect of altering the restraining properties provided by adjacent bays, the defects were quantified relative to the change in the magnitude of the restraint relative to pre-damage calibrated characteristics.

6.4.5.2 Model 3 – the continuous floor model

To examine the effect of discontinuity at the damaged perimeter of the continuous floor model, a similar approach as described above was adopted. However, for the damage located at the connection between bays 1 and 2, a 'zero-length spring' element was used, which allowed the continuity of the slab to be considered assuming varying joint restraint stiffness at the connecting nodes. The locations of these elements, appropriate to the location of the observed damage, are illustrated in Figure 6.6.

Table 6.4 – Section properties corresponding to the grillage members indicated by Figures 6.5 and 6.6

Ref. Label	Bending inertia I_x (m^4)	Torsional constant C (m^4)	Element mass (kg/m)	Schematic illustration of member cross-section
B1	1.649×10^{-3}	$^{\otimes}776\times10^{-9}$	170	Longitudinal composite beam. 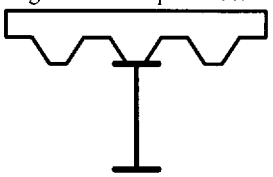
B2	762×10^{-6}	$^{\otimes}236\times10^{-9}$	114	
B3	872×10^{-6}	$^{\otimes}236\times10^{-9}$	84	
B4	278×10^{-6}	$^{\oplus}102\times10^{-6}$	79	Transverse composite beam. 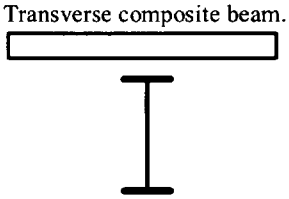
B5	326×10^{-6}	96×10^{-6}	88	
L1	116×10^{-6}	121×10^{-6}	94	Longitudinal slab. 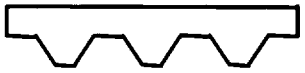
L2	97×10^{-6}	102×10^{-6}	79	
L3	73×10^{-6}	96×10^{-6}	63	
T1	31.6×10^{-6}	121×10^{-6}	94	Transverse slab. 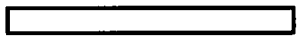
T2	26.4×10^{-6}	102×10^{-6}	79	

(Abbreviations – B = Composite beam, L = Longitudinal slab and T = Transverse slab. These abbreviations also relate to the lettered definitions given in Figures 6.6 and 6.7).

Other notes:

The symbol "⊗" indicates that the quoted torsional constants are based on the properties of the steel beam alone, with the contribution of the slab in this regard being neglected. This interpretation was considered so that the properties assigned to the 'grounded spring' elements would then represent the total rotational restraint of the slab at these regions. Similarly, the symbol "⊕" relates to the torsional constant value of the transverse beam, which will refer to a value corresponding to the steel beam alone for the perimeter beams of models 1 and 2. All other torsional constants were calculated assuming the properties of the slab as recommended by Hambly (1991).

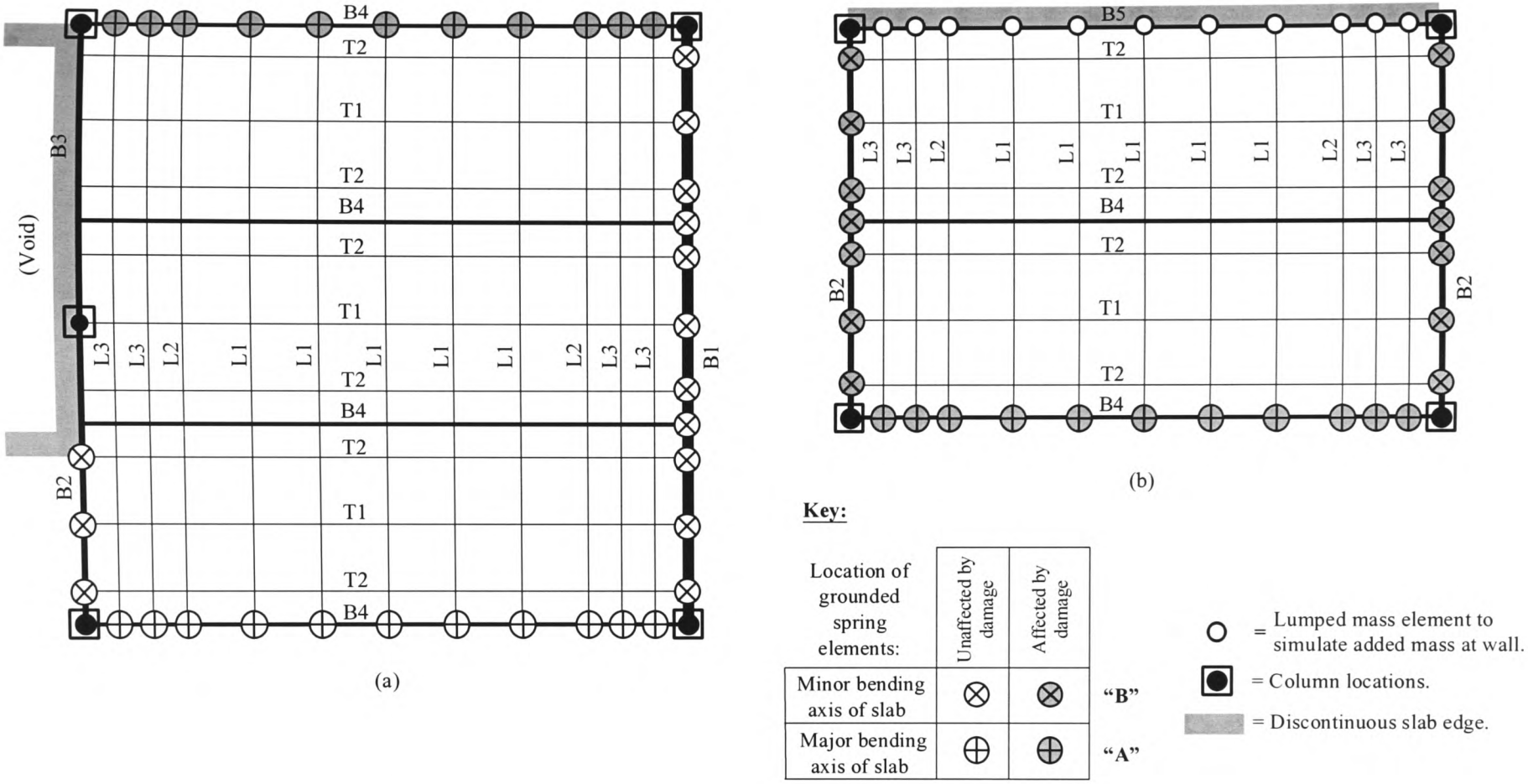

Figure 6.6 – Illustration of grillage models 1 and 2 that represent the idealised properties of the floor at (a) Bay 1, and (b) Bay 2.

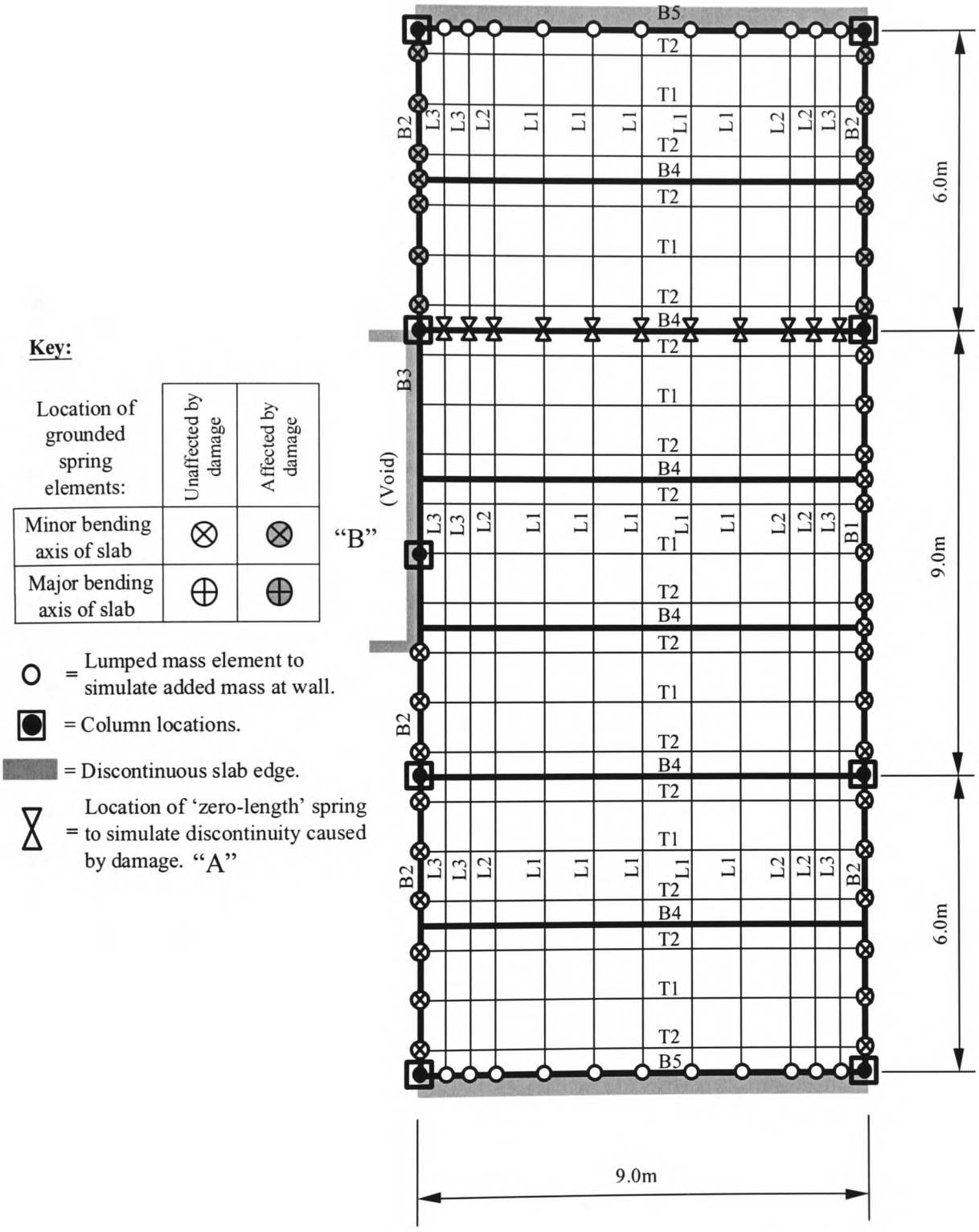

Figure 6.7 – Illustration of the grillage model 3 that represents the idealised properties of the floor with bays 1 and 2 considered in a continuous form

6.5 The Calibration Parameters for the Modelled Floor Areas

6.5.1 The calibration methodology applicable to the floor

The proposals given in chapter 5, in relation to the calibration of natural frequency, has universal applicability to many problems involving structural stiffness properties that may be subject to variation. To calculate the natural frequencies of the modelled floor bays, for a variety of restraint conditions at their perimeter, an identical calibration methodology to that of chapter 5 was considered here.

6.5.2 Rationalising the boundary variables

Within the scope of any analytical problem, where assumptions are made regarding the interpretation of structural behaviour, there is likely to be a degree of variation between assigned-modelled properties and the actual characteristics of the real components. Similarly, components of assumed identical properties might actually possess slightly different characteristics in the structure, even though they comprise comparable attributes.

Fully appreciating these possibilities, a rationalised approach to the calculation of the perimeter restraint variables was considered. The principal assumptions adopted were as follows.

(i) The calculated bending inertia for the composite beams, at the perimeter of the floor bays (i.e. coincident with the grounded spring element locations), was assumed to reflect the vertical restraint of the continuous slab at these points. Thus, the assumption that these zones produce a 'zero-displacement boundary', as discussed by Pavic *et al* (1997), was not imposed.

(ii) The magnitude of the rotational restraint assigned to the 'grounded spring' elements for all models was assumed to be equal for each location on the bay perimeter. This approach was used, as the aim of the study was not to quantify precisely the restraint properties, but to establish their variation from the pre to post-damage conditions. Therefore, the spring elements located along the north to south bay perimeter (relative to the building layout) are assumed to

characterise the contribution of the minor bending-stiffness axis of the adjoining slabs, while the east to west extremities are representative of major axis slab properties.

(iii) A similar assumption is also applicable to the 'zero-length-spring' element that was used to model the damage in the continuous model (model 3), where constant properties were assumed over the length of the region modelled to simulate the discontinuity.

(iv) The section properties calculated for the pre-damage condition (see Table 6.4) were assumed to remain unchanged when assessing the post-damage state. The bending inertia (I_x) of the slab itself was, therefore, assumed not to change as a result of damage. The torsion constant (C) of the affected members was, however, assumed to reduce to a value dependent on the steel beam properties alone for the post-damage state.

(v) Throughout all FE calculations the weight of the floor was incorporated into the element section properties by assigning the mass of the constituent parts relative to the configuration of the grillage [as discussed by West (1973)]. This enabled the natural frequencies to be calculated using a 'consistent mass-matrix' approach, which was selected from the 'dynamic specification module' within the GSA program. Other masses, which are associated with the perimeter block-work wall, were defined using lumped mass elements.

6.5.3 Mathematical relationship of calculated natural frequency for varying restraint conditions

The mathematical relationship that describes the variation of natural frequency for varying joint restraint has been discussed in chapter 5. However, to accommodate a broader band of restraint magnitudes, which was observed from the analyses conducted with all floor models, a modification to eqn.(5.3) of chapter 5 was required. The expression more appropriate to the results obtained from the analysis of the floor was achieved from a definition of β as follows,

$$\beta = \frac{1}{2}\left[\left\{\frac{\tanh\left(\tanh^{-1}(\xi) - \frac{\log_{10}(10^4\rho)\tanh^{-1}(\xi)}{4}\right)}{-\xi}\right\}+1\right] \tag{6.16}$$

where ρ is the restraint magnitude on a scale from "1.0×10^{-6}" to "1" for pinned and fully fixed conditions respectively, and ξ controls the fit of the expression to the FE calculated frequency-variation-profile (FVP). A value of $\xi = 0.99$ was found to give good results. Therefore, β ($0 < \beta < 1$) varies according to the value of ρ, allowing floor natural frequency to be calculated from,

$$f_\beta = f_p + \beta(f_q - f_p) \tag{6.17}$$

where subscripts p and q indicate the frequencies from pinned and fixed perimeter restraints respectively.

6.5.3.1 Frequency-variation-profile obtained from the models with varying perimeter restraint

The FVP's obtained from the models, imposing the perimeter restraint and general modelling conditions outlined earlier, are shown by the graph of Figure 6.8. To clarify the definitions used in this figure, the following abbreviations are introduced, which relate to the floor area shown in Figure 6.9:

f_1 = fully restrained perimeter at "A" with fully restrained perimeter at "B"

f_2 = free perimeter at "A" with fully restrained perimeter at "B"

f_3 = fully restrained perimeter at "A" with free perimeter at "B"

f_4 = free perimeter at "A" with free perimeter at "B"

6.5.3.2 Graphical interpretation of the formulation for the assessment of floor perimeter restraint

It is seen from Figure 6.8 that the frequencies calculated for the various conditions f_1 to f_4 provide profiles that are different for each case, which is unlike the solution seen from the analyses in chapter 5. However, this variation too can be accommodated using a graphical approach. To encompass all possible restraint variables, a more appropriate graph for this case is shown by Figure 6.10. This graph satisfies all possible combinations of restraint and was formulated to embody the characteristics of eqn.(6.17) for the extreme fixity conditions f_1 to f_4. It is also applicable to all vibration modes.

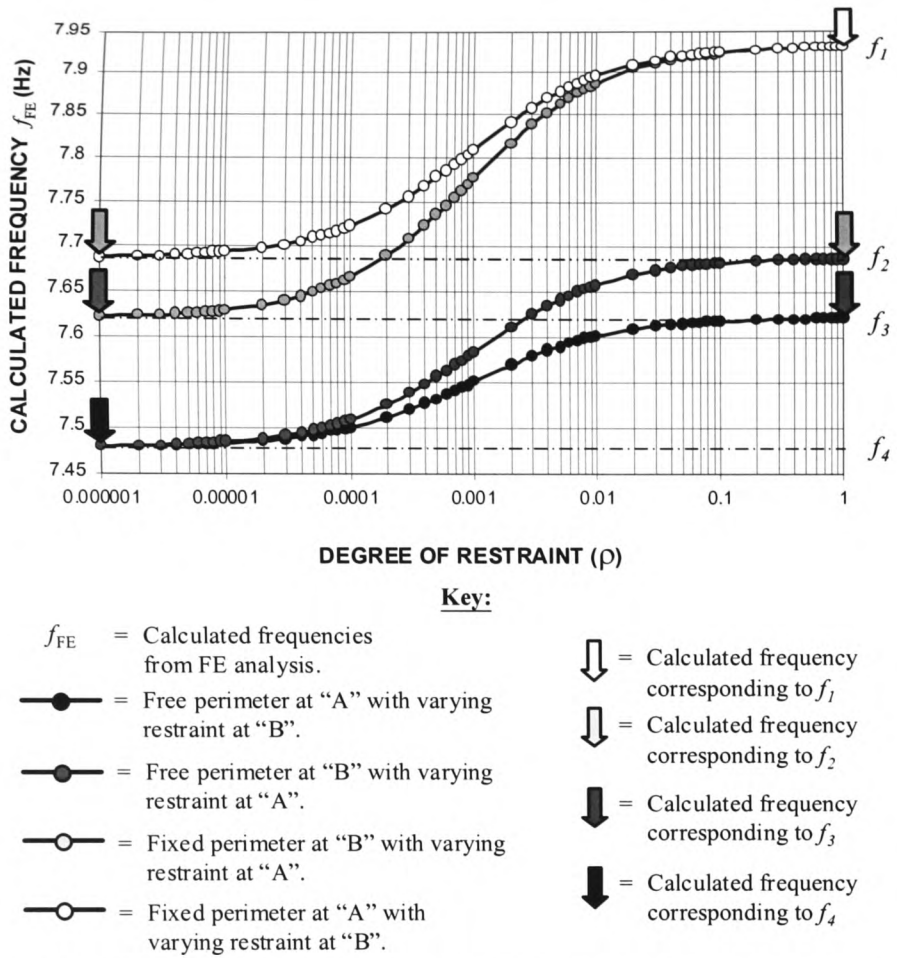

Figure 6.8 – Calculated natural frequencies for a slab with two perimeter "A" and "B" showing the FVP for varying restraint properties (ρ)

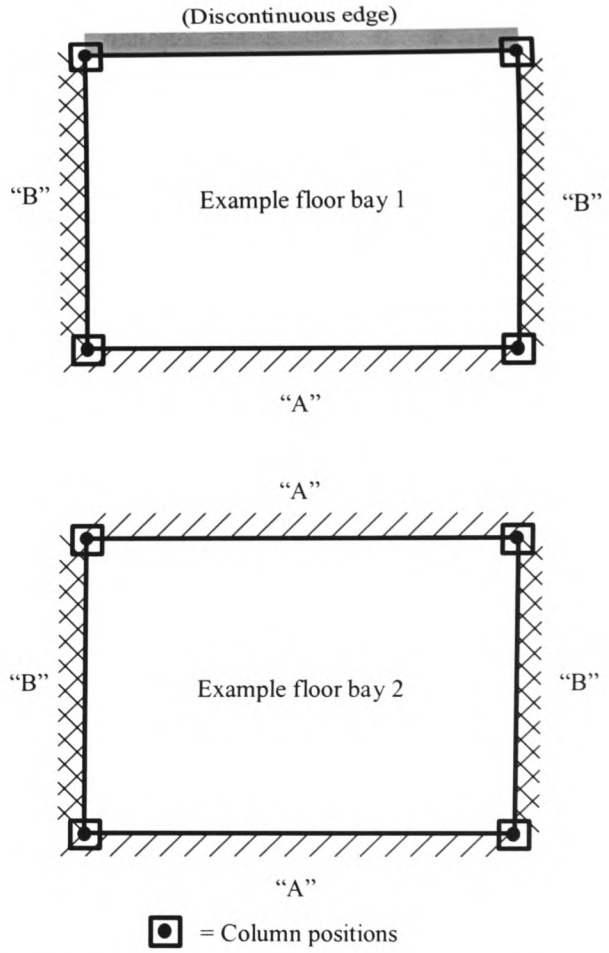

Figure 6.9 – Example floor layouts showing perimeter locations "A" + "B"

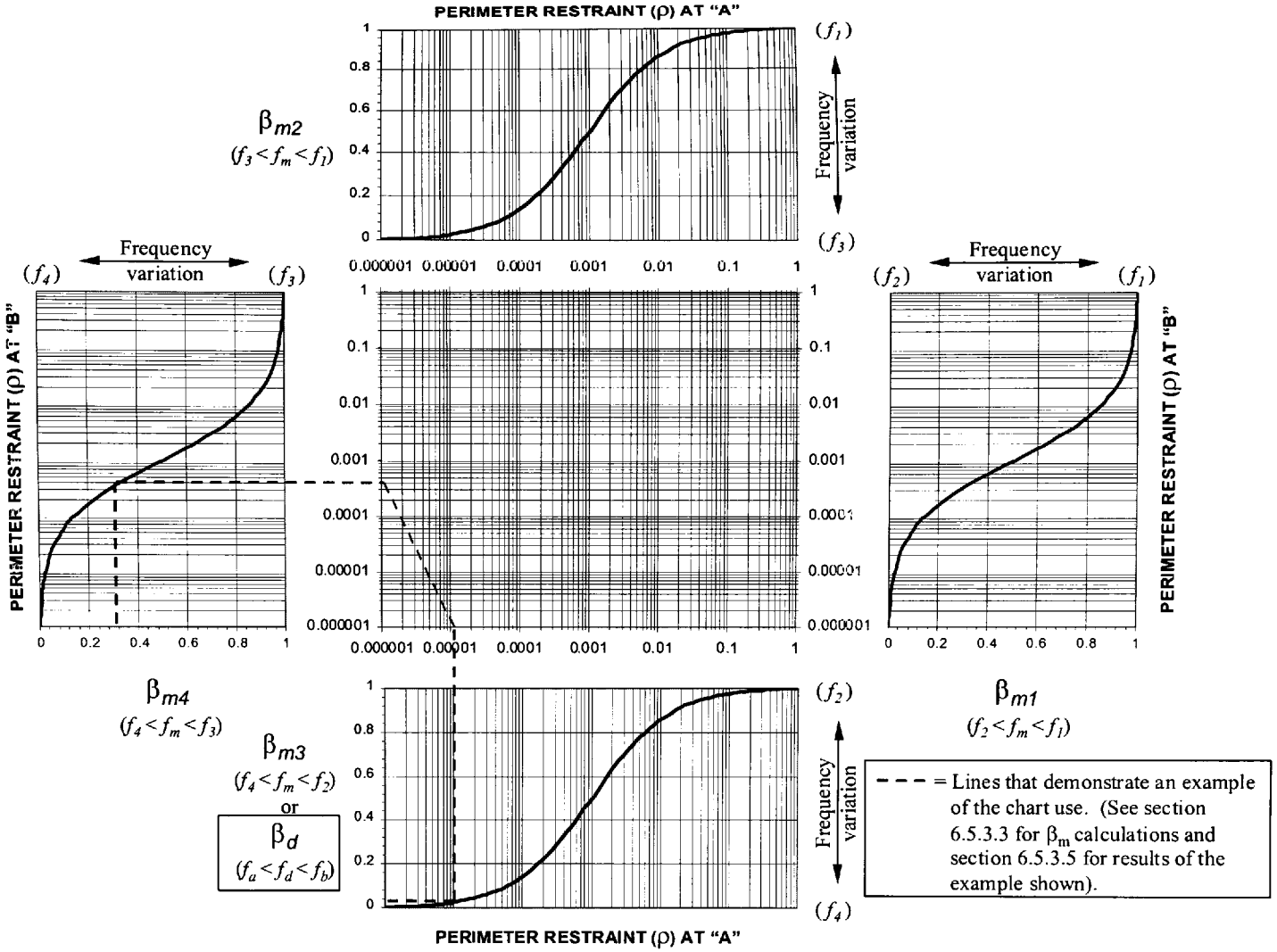

Figure 6.10 –Graphical representation of the restraint variable (β) for a floor bay with perimeter restraint at "A" and "B"

6.5.3.3 Calculating the calibration variables ($\beta_{m\,1,2,3,4}$) corresponding to pre-damage frequencies

To obtain the variable β, which corresponds to the pre-damage natural frequency value, the following expressions should be used in conjunction with the graph of Figure 6.10,

$$\beta_{m1} = \left\{\frac{f_m - f_1}{f_1 - f_2}\right\} + 1, \text{ when } (f_2 < f_m < f_1) \tag{6.18a}$$

$$\beta_{m2} = \left\{\frac{f_m - f_1}{f_1 - f_3}\right\} + 1, \text{ when } (f_3 < f_m < f_1) \tag{6.18b}$$

$$\beta_{m3} = \left\{\frac{f_m - f_2}{f_2 - f_4}\right\} + 1, \text{ when } (f_4 < f_m < f_2) \tag{6.18c}$$

$$\beta_{m4} = \left\{\frac{f_m - f_3}{f_3 - f_4}\right\} + 1, \text{ when } (f_4 < f_m < f_3) \tag{6.18d}$$

where β_m indicates dependence on the measured pre-damage frequencies (f_m) and the subscripts 1 to 4 relate to those included in Figure 6.10. Therefore, to calibrate the perimeter of the floor models, and to define any desired number of combinations, only the frequencies corresponding to f_1, f_2, f_3, f_4 and f_m are required.

6.5.3.4 Calculating the calibration variable (β_d) corresponding to post-damage frequencies

The combination of models 1 to 3 allows a rationalised approach to the calibration of the post-damage frequencies, which is described later. In essence, the calibration is achieved from a single FVP that depends on two extreme fixity conditions. This profile was assigned a calibration variable (β_d), which can be calculated from a combination of measured and calculated frequencies as before using,

$$\beta_d = \left\{\frac{f_m - f_b}{f_b - f_a}\right\} + 1 \tag{6.19}$$

where subscripts a and b indicate extreme restraint conditions of free and fixed respectively. β_d shows dependence on the post-damage frequency. The graph applicable to eqn.(6.19) is given in Figure 6.10.

6.5.3.5 Example use of the proposed graphical method

To demonstrate the use of the graphical method, consider the results obtained from the 9m×9m bay (model 1) for mode 1 as follows:

$$f_1 = 7.80\text{Hz}, f_2 = 7.65\text{Hz}, f_3 = 6.22\text{ Hz and } f_4 = 5.72\text{Hz}.$$

Table 6.1 gave the measured pre-damage natural frequency as f_m = 5.86Hz for this floor bay, which from eqns.(6.18c) and (6.18d) gives,

$$\beta_{m3} = 0.072 \text{ and } \beta_{m4} = 0.282$$

respectively. The perimeter restraint (ρ) combinations relating to these β_m values are obtained by joining a straight line between the ρ values (corresponding to β_m above), from which all possible perimeter restraint combinations are defined. Therefore, to obtain a model that will yield a natural frequency of 5.86Hz, the following are two possible perimeter restraint combinations that could be imposed:

- Possible condition 1 – restraint at "A", $\rho \approx 10\times10^{-6}$, restraint at "B", $\rho = 1\times10^{-6}$
- Possible condition 2 – restraint at "A", $\rho = 1\times10^{-6}$, restraint at "B", $\rho \approx 400\times10^{-6}$

6.5.4 The approach adopted to calibrate the floor models

The calibration methodology presented enables a wide range of possible restraint combinations to be considered. However, a rationalised approach to these conditions is proposed to give the calibration a more focused out-come. The assumptions considered were as follows.

6.5.4.1 Calibrating the models with measured pre-damage frequencies

(i) The perimeter restraint (ρ) at "B" was estimated from model 3, as the continuous nature of the slab for perimeter "A" was embodied in the characteristics of the model itself.

(ii) The ρ value obtained from (i) above was assumed to represent its value applicable to models 1 and 2, allowing the perimeter restraint at "A" to be identified.

6.5.4.2 Calibrating the models with measured post-damage frequencies

The calibrated ρ values from the pre-damage condition, at the locations un-affected by damage, were assumed to remain un-changed while the affected parts of the models were re-calibrated. To determine these adjustments, the natural frequencies of the models were re-evaluated by assuming that the restraint at the affected perimeter only would vary as a consequence of damage. Therefore, using a similar procedure to that considered when assessing the effect of varying restraint at the pre-damage bay perimeter, the FVP corresponding to the varying restraint at the location of the damage alone was examined.

(i) Re-calibrating model 1 – As the damaged part of this model was along one side of the bay, the β_d value was used to signified the change of restraint from a comparison with the initial calibrated results achieved at the pre-damage stage.

(ii) Re-calibrating model 2 – To re-calibrate model 2, which is effected along both the "A" and "B" boundaries, required a similar approach to that considered for the bay at the pre-damage condition. i.e. the parameters of β_{m1} to β_{m4} were re-evaluated relative to the post-damage frequencies. This was necessary as models 1 and 2 represent different floor vibration modes thereby making it difficult to relate the findings of the re-calibration for (i) above to that of model 2 (the perimeter restraint of dissimilar modes has differing affects on the modal behaviour). Therefore, a re-calibration allowed a comparison to be made between pre and post-damage characteristics.

(iii) Re-calibrating model 3 – Model 3 was examined by imposing the restraint at "B" from (i) and (ii) above (appropriate to the mode being considered) so that

the properties of the 'zero-length spring' element could be correlated with the post-damage frequencies using β_d. In this case the properties of the 'zero-length spring' were varied from $\rho = 1\times10^{-6}$ to 1, simulating a rotationally free or fully continuous element connection respectively. This provided a measure of relative change that could further be used to quantify damage.

6.6 Calibration Results for the Pre and Post-Damaged Floor

6.6.1 Results of the calibration using the measured natural frequencies

Table 6.5 presents the calibrated results for the pre-damage floor, while Tables 6.6 and 6.7 contains the findings appropriate to the post-damage frequencies.

6.6.2 Comparison of measured and calibrated mode shape results

The normalised peak amplitude results obtained from the floor at bay 2 were identified earlier in this chapter. This information, which represents the mode shape of the floor bay vibrating at its fundamental frequency, can be compared to the solution gained from analysis to assess the accuracy of the calibration processes adopted.

The mode shape solution resulting from model 2 was used for comparison with the measured results, as this model represents the area of the floor over which the measurements were taken. Figure 6.11 shows these comparisons, which for convenience and clarity have been prepared to illustrate the results at 'sections' of the floor, which is given by Figure 6.12.

Table 6.5 – Calibrated results for the pre-damaged floor

Mode	f_m	f_1	f_2	f_3	f_4	β_{m1}	β_{m2}	β_{m3}	β_{m4}	ρ_m at "A"	ρ_m at "B"
Results applicable to Model 1											
1	5.86	7.801	7.653	6.217	5.728	-	-	0.069	0.27	10×10^{-6}	1×10^{-6}
2	7.82	9.384	9.091	7.796	7.563	-	0.015	0.168	-	4×10^{-6}	90×10^{-6}
3	11.98	14.109	11.616	13.446	11.095	0.146	-	-	0.376	90×10^{-6}	100×10^{-6}
Results applicable to Model 2											
1	6.84	7.263	7.094	6.345	6.173	-	0.539	0.724	-	2000×10^{-6}	400×10^{-6}
2	9.52	10.738	9.633	10.054	9.198	-	-	0.740	0.376	5×10^{-6}	300×10^{-6}
Results applicable to Model 3											
1	5.86	7.543	5.861	-	-	0	-	-	-	-	1×10^{-6}
2	6.84	7.986	6.362	-	-	0.294	-	-	-	-	400×10^{-6}
3	7.82	8.985	7.631	-	-	0.139	-	-	-	-	90×10^{-6}
4	9.52	10.382	9.17	-	-	0.289	-	-	-	-	300×10^{-6}
5	11.98	13.834	11.549	-	-	0.189	-	-	-	-	100×10^{-6}

(Note: ρ_m indicated that the perimeter restraint is relative to the value of f_m).

Table 6.6 – Calibrated results for the post-damaged floor (Model 2 only)

Mode	f_d	f_1	f_2	f_3	f_4	β_{m1}	β_{m2}	β_{m3}	β_{m4}	ρ_d at "A"	ρ_d at "B"
Results applicable to Model 2											
1	6.59	7.263	7.094	6.345	6.173	-	0.267	0.453	-	$500\times10^{-6\nabla}$	$200\times10^{-6\nabla}$
2	9.28	10.738	9.633	10.054	9.198	-	-	0.189	0.096	$1\times10^{-6\nabla}$	$2\times10^{-6\nabla}$

(All frequencies are quoted in Hz, i.e. cycles per second, all other values are dimensionless. The symbol ∇ indicates that the values have been re-evaluated, i.e. represents one possible solution – see notes on the 'approach adopted for calibration'. ρ_d stipulates that the perimeter restraint is relative to the value of f_d).

Table 6.7 – Calibrated results for the post-damaged floor (Models 1 and 3 only)

Mode	f_d	f_a	f_b	β_d	Reference to damage at perimeter only	
					ρ_d at "A"	ρ_d at "B"
Results applicable to Model 1						
1	5.86	No frequency change				
2	7.58	7.548	7.993	0.072	7×10^{-6}	-
3	11.74	11.679	12.298	0.098	10×10^{-6}	-
Results applicable to Model 3						
1	5.86	5.773	5.861	1.0	1.0	-
2	6.59	6.352	6.839	0.488	1000×10^{-6}	-
3	7.58	7.177	7.822	0.625	2000×10^{-6}	-
4	9.28	8.496	9.523	0.763	4000×10^{-6}	-
5	11.74	11.345	11.975	0.627	2000×10^{-6}	-

(All frequencies in Hz, i.e. cycles per second, other values are dimensionless. ρ_d stipulates that the perimeter restraint is relative to the value of f_d).

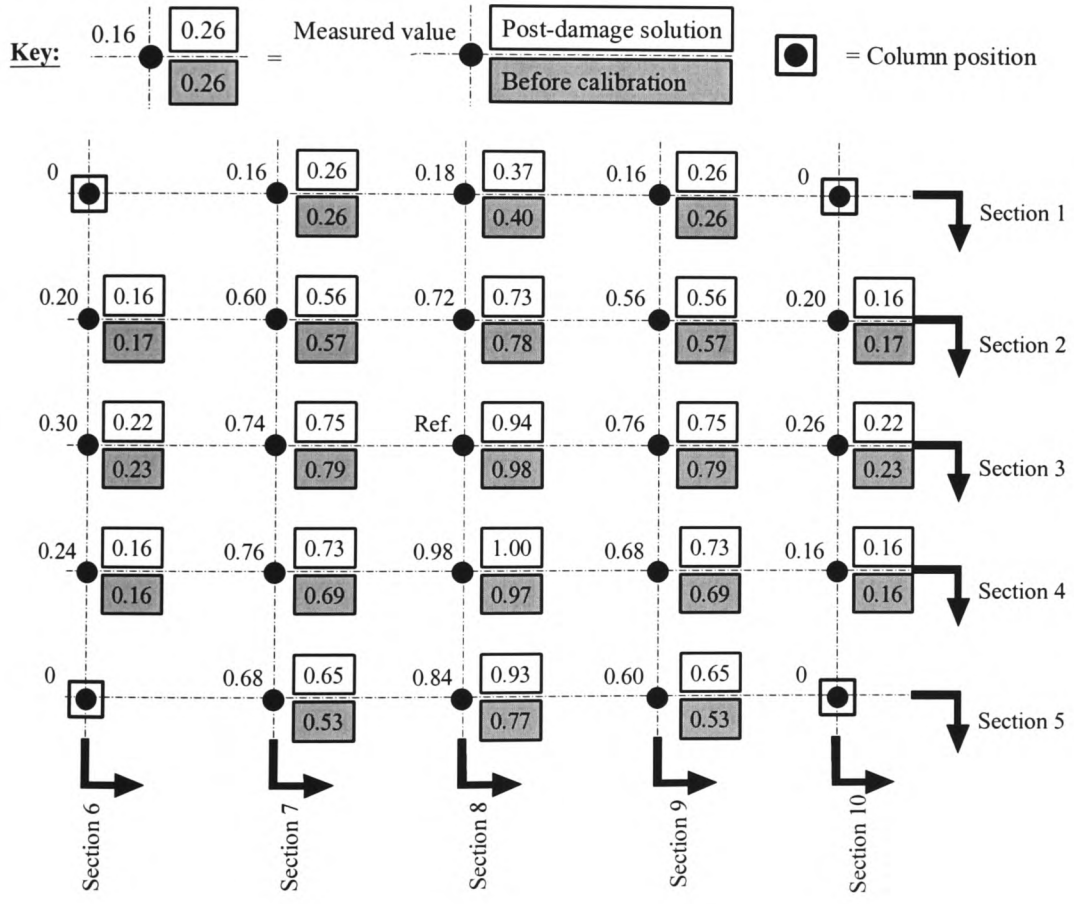

Figure 6.11 – Comparison of measured and calculated mode shape results using the analytical solution gained from model 2. 'Section' referencing system shown refers to the information displayed in Figure 6.12.

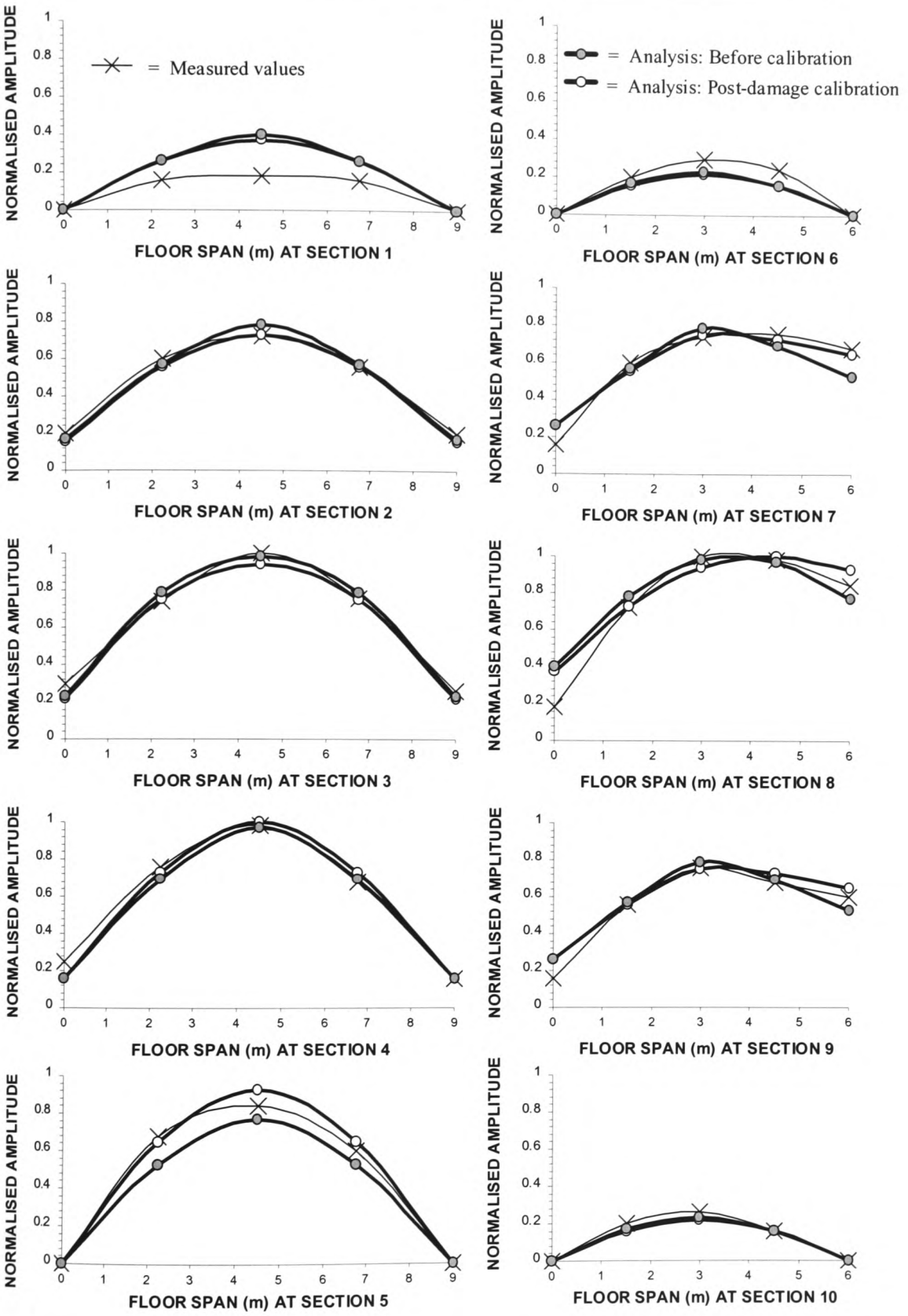

Figure 6.12 – Post-damage measured and calculated mode shape information for bay 2

6.6.3 Using the calibrated results to quantify damage

The aim of the study was not to calculate the actual restraint properties at the floor bay perimeter, but was to quantify the 'change' between result sets based on similar numerical modelling assumptions. The calibrated models, appropriate to the observed damage of the 5th floor of the steel-framed building, are shown in Table 6.8.

6.6.4 Observations and discussion of the calibrated results

Before discussing the results achieved from this process it is worth reflecting on the properties of the FVP itself to recognise its main characteristics and to interpret the values that have been obtained.

6.6.4.1 Using the FVP values of (ρ_m) *and* (ρ_d) *to quantify damage*

The perimeter restraint that forms the basis of the FVP varies from a value of $\rho = 1\times10^{-6}$ to 1.0, where the former value represents a rotational restraint magnitude of 0.0001% of the latter. The FVP represents the transition of fixity between these two extremes, but it should be remembers that a restraint level of 1% (i.e. $\rho = 0.01$) of full fixity attains a natural frequency corresponding to 95% of its value at 100% fixity. This demonstrates that a rapid change of frequency occurs over relatively small restraint levels, making the FVP sensitive to small change for structural parts that are close to being rotationally free.

Another observation seen from the FVP is that a restraint value of 0.1% ($\rho = 0.001$) corresponds to fixity that is neither 'fixed' nor 'pinned', i.e. precisely at the transition point between the two. This represents a division point where restraint levels smaller than this value tend to a pinned condition, while values larger tend more to a fixed condition.

With these features in mind the effect of damage can be gauged by relating the value of ρ, for the pre and post-damage states, to assess the relative fixity change.

Therefore, the 'level' of observed damage calculated from the calibration was as follows:

(i) Results from model 1: The pre and post-damage restraint at the damage-affected perimeter for mode 1 was seen not to change, as there was no change in the measured frequency between the two conditions. Modes 2 and 3, however, suggest that the damage reduce the perimeter restraint at "A" to 17.5% and 11.1% of the pre-damage calibrated level respectively.

(ii) Results from model 2: Similarly, a definite change to the perimeter at "A" and "B" are seen, representing 25% and 50% respectively for mode 1, and 20% and 6.7% respectively for mode 2.

(iii) Results from model 3: Model 3, which represents a more 'realistic' interpretation of the perimeter between bay types 1 and 2, also indicates change between the pre and post-damage calibration. However, it can be seen that the change of restraint (ρ) for this model is more significant. This demonstrates the difference between the localised bay models and that of the continuous form, the former of which being dependent on extreme fixities represented by conditions that range from either fully fixed or fully pinned restraint. Based on the results of model 3, the calibration at the affected region of perimeter "A" suggest that the damage changes the characteristics of the floor from a continuous assumption to one that approximates to the transition point that is neither continuous nor completely pinned. The damage, therefore, appears to induce discontinuity of the floor at concrete slab level with a reduction of restraint that is between 0.1% to 0.4% of the pre-damage calibrated results.

6.6.4.2 Choosing appropriate restraint (ρ) *values*

The results of Table 6.8, and the graph of Figure 6.10, clearly show that there is a wide range of possible restraint combinations (ρ) that will give identical natural frequency values from the calculated β parameters. It seems from the amount of information available relating to the pre and post-damage measurements that there is no clear method to allow an accurate assignment of restraint levels. The approach adopted here has attempted to rationalise this procedure, which enabled quantitative properties of damage to be identified, but again the actual proportions that would be appropriate to

the damage could not be determined precisely. However, in all cases where the post-damage frequency is less than the pre-damage measurement, the restraint combination will "always" indicate a "reduction" at the locations were damage is known to have occurred.

Table 6.8 – Relative perimeter restraint changes obtained from the calibration methodology from measured pre and post-damage natural frequencies.

Mode	f_m	f_d	Perimeter restraint (ρ) at "A"		Perimeter restraint (ρ) at "B"		Relative restraint at "A" after damage (% of ρ_m)	Relative restraint at "B" after damage (% of ρ_m)
			Pre-damage (ρ_m)	Post-damage (ρ_d)	Pre damage (ρ_m)	Post-damage (ρ_d)	$\left(\frac{\rho_d}{\rho_m}\right)\times 100$	$\left(\frac{\rho_d}{\rho_m}\right)\times 100$
Results applicable to Model 1								
1	5.86	5.86	10×10^{-6}	10×10^{-6}	1×10^{-6}	1×10^{-6}	(No change)	
2	7.82	7.58	40×10^{-6}	7×10^{-6}	90×10^{-6}	90×10^{-6}	ρ_d = 17.5% of ρ_m	ρ_d = 100% of ρ_m
3	11.98	11.74	90×10^{-6}	10×10^{-6}	100×10^{-6}	100×10^{-6}	11.1	100
Results applicable to Model 2								
1	6.84	6.59	2000×10^{-6}	$500\times10^{-6\nabla}$	400×10^{-6}	$200\times10^{-6\nabla}$	25.0	50.0
2	9.52	9.28	5×10^{-6}	$1\times10^{-6\nabla}$	300×10^{-6}	$2\times10^{-6\nabla}$	20.0	6.7
Results applicable to Model 3								
1	5.86	5.86	$1.0^{\lozenge}$	$1.0^{\lozenge\nabla}$	1×10^{-6}	$1\times10^{-6\nabla}$	100	100
2	6.84	6.59	$1.0^{\lozenge}$	$1000\times10^{-6\lozenge\nabla}$	400×10^{-6}	$200\times10^{-6\nabla}$	0.1	50.0
3	7.82	7.58	$1.0^{\lozenge}$	$2000\times10^{-6\lozenge\nabla}$	90×10^{-6}	$90\times10^{-6\nabla}$	0.2	100
4	9.52	9.28	$1.0^{\lozenge}$	$4000\times10^{-6\lozenge\nabla}$	300×10^{-6}	$2\times10^{-6\nabla}$	0.4	6.7
5	11.98	11.74	$1.0^{\lozenge}$	$2000\times10^{-6\lozenge\nabla}$	100×10^{-6}	$100\times10^{-6\nabla}$	0.2	100

(The symbol ∇ indicates that the values represent one possible solution. ◊ stipulates that the perimeter restraint is relative to the value assigned to the 'zero-length spring' element, thereby defining a value dependent of a scale between 'continuous' and 'pinned' at the connection between bays – see notes on 'approach adopted for calibration').

6.6.4.3 Observations from mode shape comparison

The calculated mode shapes in Figure 6.12 are (i) the results gained prior to calibration (i.e. before calibration to the pre-damage frequencies) and, (ii) those achieved after calibration of the post-damage frequencies. The solution that would represent the pre-damage calibrations is not indicated, as the mode shape profiles were similar to the post-damage calibrated results.

It is interesting to note that the calculated mode shape, corresponding to the 'before calibration' results, has provided normalised vibration amplitudes that approximate to the measured results. However, from an observational perspective it appears that the calibrated results, with the restraint values imposed from Table 6.8, achieve a better correlation to the measured values. To determine a more accurate estimate as to which of the two solutions correlate to a higher degree with the measured values, calculations using the Modal Assurance Criteria (MAC) were carried out. Therefore, using the definition given by Ewins and Lieven (1988) the following is obtained,

$$\left|MAC(\{\phi\}_c,\{\phi\}_m)\right| = \frac{\left|\{\phi\}_c{}^T\{\phi\}_m\right|^2}{(\{\phi\}_c{}^T\{\phi\}_c)(\{\phi\}_m{}^T\{\phi\}_m)} \tag{6.20}$$

where $\{\phi\}_c$ and $\{\phi\}_m$ are vectors containing the calculated and measured normalised mode shapes respectively. MAC values of 0.982 and 0.987 were calculated, which represent the before and after calibration values respectively. These values are not significantly different, demonstrating that the non-calibrated model 2 captures the mode shape characteristics of the bay to a reasonable degree of accuracy, with the calibrated results merely providing a means of 'fine-tuning' the solution. Alternatively, this could be viewed as confirmatory evidence that mode shapes are not sensitive to damage, which was the conclusion of the work by Chen *et al* (1995) from tests on steel beam members.

6.7 Concluding Discussion

The main out-comes of the study described in this chapter are:

(i) Modelling the floor assuming localised bay behaviour for dynamic analysis appears to provide mode shape and natural frequency results that closely match those obtained from measurements taken from a localised area of the floor. The calibration methodology proposed will enable initial results to be further adjusted to obtain a closer match.

(ii) The continuous model also gave frequencies that agreed with the measurements, which allowed a more detailed interpretation of the floor vibration mode order. Thus, in general terms, this type of model can be especially useful when a measured autospectrum, containing many spectral peaks, needs deciphering.

(iii) From the result of the calibration it appears that the amount of restraint at the perimeter of each bay increases coincident with vibration mode order. Based on the information presented in this chapter, however, definite trends are not clear and as such it would be unwise to extrapolate extensively from the quoted restraint magnitudes.

(iv) Damage located at the perimeter regions of the bays has a definite influence on the perimeter restraint, which is clearer from the results of model 3. To obtain calculated frequencies that matched the measured post-damage frequencies, the restraint properties at the damage required significant reduction.

(v) The formulated FVP has allowed the effect of damage to be quantified using frequency as a basis for defining the changes to the perimeter restraint of the floor.

(vi) To quantify the damage, the calibration methodology outlined allows rotational restraint changes to be compared (in a relative sense) using natural frequencies obtained from the floor before and after damage.

(vii) The proposed method is sensitive to small changes in frequency, which is a consequence of the detail inherent in the formulated FVP. This degree of sensitivity appears to be an essential part of the damage assessment procedure, especially where small changes in natural frequency are observed.

However, the following points should not be ignored:

(viii) Although three damage sites were observed on the surface of the floor considered here, a rationalisation of the restraint properties was introduced, which made it possible to treat similar boundary regions with similar properties – even after damage. This is a significant simplification of damage as the actual properties of the concrete slab, at the damaged regions, are likely to be highly variable.

(ix) The FVP is sensitive to small changes in frequency. However, there is an inherent problem in the practical use of such precision that must be placed in the context of the actual measuring techniques adopted. For example, if frequency is to be used as the indicator of damage, it is important that the limitations of the measurements are understood. Reflecting on the assumptions considered being indicative of damage in the floor, a frequency change corresponding to the resolution of the FFT was presumed to be sufficient to indicate damage. This is clearly an unrealistic assumption, especially as other possible contributors to frequency change, such as temperature or climate influences, have not been taken into account.

To accommodate (viii) and (ix), and to establish definitively if frequency change could be interpreted as a damage indicator, further refinement of the structure is required to allow detailed information to be examined. To establish if frequency and other dynamic characteristics, such as damping and mode shape, are sensitive to the affects of imposed static loads a localised study of specific parts of the structure will be necessary. Therefore, to continue with studies that have focused on the properties of the concrete slab, further investigations will be carried out into possible relationships between change of dynamic characteristics and the affect of static load using localised segments of the floor.

CHAPTER 7

Experimental Results of Static and Dynamic Tests to Identify Damage in Composite Floor-Slab Panels

7.1 Introduction

This chapter contains the static and dynamic test results from eighteen steel / concrete composite floor-slab panels, which comprised of an equal number of two distinctly different sectional profiles. These section were made using segments of a steel-profile floor decking material, called 'ComFlor 70', which is a commercial product often abbreviated to "CF70". This system forms the main material used for the construction of the steel-frame building floors.

The load carrying performance of this floor system is discussed in chapter 8. For strength, it essentially relies on the composite interaction that develops between the steel and concrete parts, which comprise the tensile and compressive elements respectively. The data given in this chapter represents the detailed laboratory results of static and dynamic tests performed on simply supported panels made from the CF70 system. All tests were undertaken within the structural testing facilities at the University of Glamorgan.

7.1.1 Aim of the static load tests

The principle aim of the static load investigation will be to evaluate the structural performance of the panels through a range of load intensities. The data collected from the laboratory tests consist of within-span displacement measurements, and concrete strain-distribution profile across the depth of the panels, each being recorded at consistent static load intervals. This data, which represents the performance of the panels, are used to establish relationships between the level of applied bending moment and the curvature of the panels. The above relationship is commonly termed the Moment-Curvature (M-C) relationship and is a convenient method to interpret the performance of structural elements subject to a range of static loads.

7.1.2 Aim of the dynamic tests

The aim of the dynamic tests will be to produce definitive information and evidence to establish if it is possible to relate dynamic characteristics to the structural changes that occur in composite panels when subjected to static load. The dynamic characteristics considered in the study will include natural frequency, damping, mode shape, and steady-state excitation response, enabling each to be appraised to establish which is most sensitive to the detection of damage in composite floor panels.

7.2 Properties of the Panels and the Static Load Test Set-up

7.2.1 The geometry of standard CF70 units

The width of a standard unit is 900mm, which can be visualised as comprising of either three 'peak' parts or three 'trough' parts as shown in Figure 7.1. The purpose of the profiled appearance is to increase the rigidity of the decking, which enables the weight of in-situ concrete to be carried by the steel deck during the construction of the floor, without the need for additional supporting elements.

7.2.2 The properties of the panels considered for the laboratory tests

To explore the difference between the 'peak' and 'trough' segments, the experimental programme was arranged such that these parts could be treated as separate elements. These elements shall be termed panel types S1 and S2, which are definitions describing the structural members formed from individual 'trough' and 'peak' regions of the decking respectively. The width and length of each panel was 0.3m and 2.66m respectively, which is similar to the specimens considered by Peel-Cross *et al* (1998) for laboratory studies carried out to examine the ultimate capacity of the CF70 floor system. However, the aforementioned authors considered the 'peak' part only, with no mention of the 'trough' region the floor. Therefore, by treating the floor as a system comprising a series of either S1 or S2 parts, a more comprehensive study is possible that will highlight behavioural differences between the two assumed idealisations.

To produce the localised deck segments, strips of steel were cut from the 900mm standard-width units. This cutting was carried out by the British Steel Welsh Technology Centre (BSWTC) to ensure that each panel type comprised identical steel deck properties. Precision cutting techniques were adopted by BSWTC producing clean uniform edges to the steel, which gave nine 'trough' and nine 'peak' segments with identical size and properties for each type.

The composite panels were made using a single mould, which was fabricated from plywood to predetermined dimensions by the University of Glamorgan laboratory technicians. The inner dimensions of the finished mould were 0.3m wide by 0.13m deep having an overall length of 2.66m providing an enclosed rectangular form in which to place the pre-prepared steel segments. The composite panels were, therefore, made on an individual basis by placing single steel segments in the base of the mould to be covered by normal weight concrete (to an overall depth of 0.13m). However, early trials of this casting technique highlighted that an amount of concrete grout loss was observed, which leaked at the interface of the steel segment and the side regions of the timber mould during compaction of the concrete. To prevent this loss of grout, which was thought may have an influence on the hydrated properties of the concrete, a strip of plastic film measuring 20mm in width was placed at the steel edge / timber mount interface to seal any possible gaps. The inclusion of this seal produces the desired affect.

To ensure that the panels did not form a deformed profile during the casting stage, all concrete casting was conducted at laboratory floor level with the underside of the timber form being continuously supported over its entire length. Therefore, after a standing period of 24 hours, at which time the concrete was considered to have hydrated sufficiently (to allow the mould to be re-moved), the panel was de-moulded and allowed to cure on the laboratory floor for a minimum period of 28 days before structural testing. The cross-sectional dimensions of the completed S1 and S2 panel types are shown in Figure 7.1, which corresponds to the calculated structural properties defined in Table 7.1.

Table 7.1 – Exact section properties of the laboratory panels calculated assuming the section geometry of Figure 7.1. (Note that both S1 and S2 have identical exact section properties).

Overall panel depth	**Overall panel width**	**Weight of panels**	**Equivalent area of section**	**Depth to the neutral axis (gross properties)**	**Moment of inertia (gross properties) I**
0.13m	0.3m	79 kg/m	$0.033m^2$	58.2mm	39.7×10^{-6} m^4

(All properties listed are based on an equivalent concrete area assuming a material Young's modulus for steel of 210 kN/mm^2, which is stated in the literature produced by the deck manufacturer. The material properties of concrete are discussed in a later section).

7.2.3 The static load arrangement adopted for the laboratory panels

To be consistent with the static load tests conducted on composite panels by other authors (see chapter 8) a simply supported span arrangement was adopted throughout all laboratory procedures. The distance between these simple supports was consistent at 2.41m. Two especially fabricated steel-frames were used as the supports, with each incorporating a 50mm diameter steel cylinder over which the panels could be placed. Therefore, when in position for testing, the overhang of the panel beyond the supports was 0.125m at each end.

The loading arrangement was also consistent with the published reports of other authors, producing a four-point-bending situation, which results from the application of two point loads (plus the supports), each placed symmetrically about the centre of the panel span. Using a 1.5m-length loading-beam, these point loads were applied through two smooth cylindrical steel bars that were welded to one flange at precisely 1.25m apart (measured between the centre-line of the bars). By incorporating the loading beam, a single hydraulic load cell could be used to apply incremental load, which is shown schematically in Figure 7.2. This figure also demonstrates the bending moment distribution induced by the point loads, clearly indicating the region of the span affected by a constant bending moment.

7.3 Description of Laboratory Tests and Procedures

7.3.1 Determining the properties of the concrete used to make the panels

As part of the laboratory tests, the properties of the concrete used to make the composite panels were tested in accordance with the appropriate British Standard procedures. The principle documents consulted for this purpose have been BS 1881: Parts 102 (1983), 108 (1983), 110 (1983), 111 (1983) and 116 (1983).

To ensure that a comprehensive assessment of the concrete properties could be achieved, a total of six standard-sized 100mm cubes and two standard-sized 300mm height cylinders were cast with each panel. Of these concrete samples, half were cured in water at a constant temperature of 20°C for 28 days, while the remaining samples were cured in the same environment as the panels. Properties of the latter samples were obtained on the same day as the composite panel static loading and as such their age at the time of testing varied between 28 and 92 days.

7.3.2 Procedure adopted for the static loading of the panels

The procedures adopted for the static loading of the panels were categorised into two groupings. The first group, which comprised the testing of five 'S1' and five 'S2' panels, concentrated on the assessment of structural behaviour at successive incremental load magnitudes up to the failure capacity of the panel. The remaining eight panels, comprising of four 'S1' and four 'S2' panels, were also loaded incrementally, but a modified procedure was followed so that a variety of vibration tests could be incorporated between each load stage. Treating these groupings as phase I and phase II respectively. The test procedure was planned as discussed in sections 7.3.2.1 and 7.3.2.2.

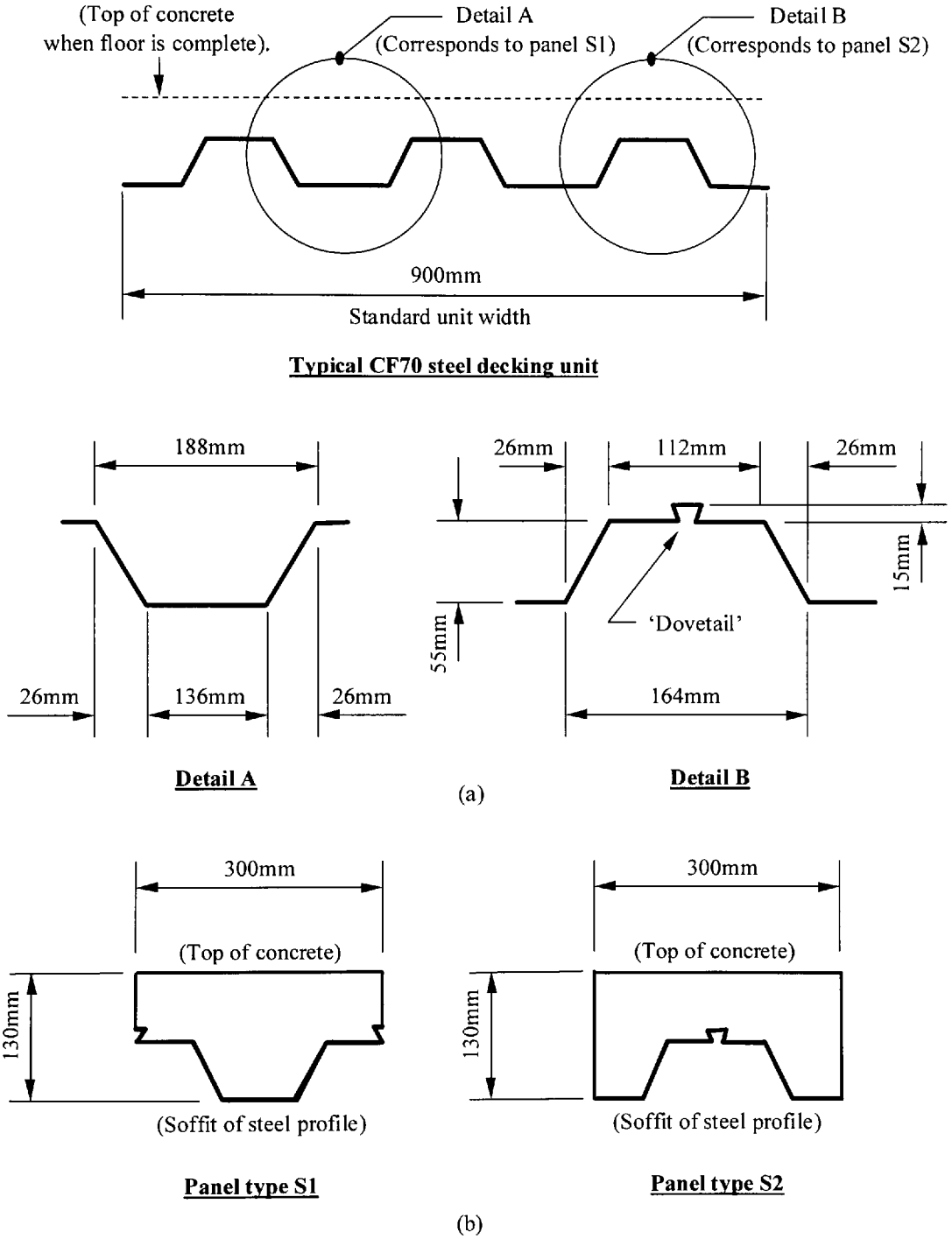

Figure 7.1 – Detail of (a) a typical single CF70 steel deck unit, and (b) a cross-section through the laboratory test panels

7.3.2.1 Load sequencing adopted for the phase I tests

Panels tested during phase I were loaded up to their failure capacity in increments of 0.5kN total applied load (i.e. 0.25kN at each point load). The applied static load was removed only when the panel under test had failed (i.e. no hysteretic quasi-static loading). Data was then collected at the aforementioned load increments, each interval being held for a sufficient time to allow strain and displacement readings to be taken.

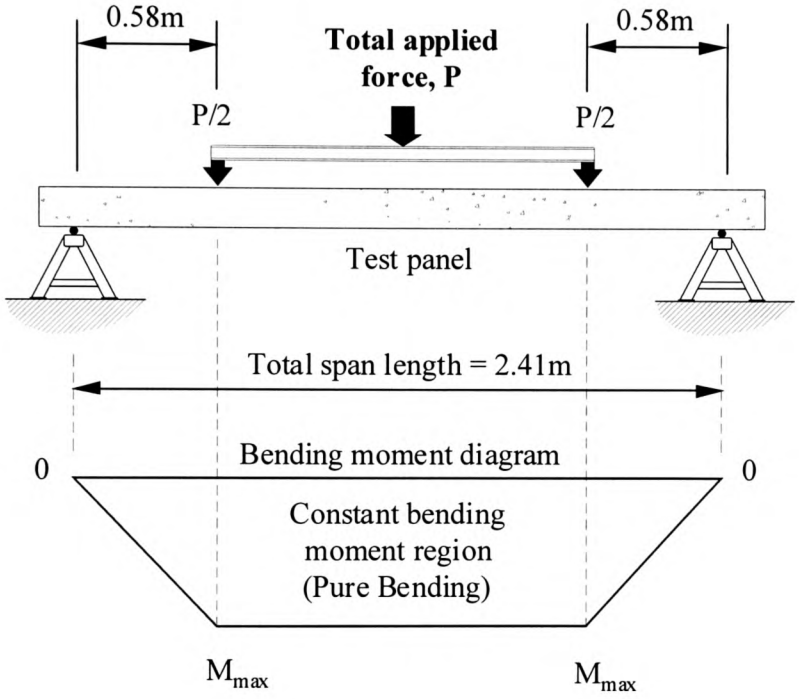

Figure 7.2 – Arrangement adopted for static loading of the panels. (M_{max} represents the level of the maximum applied bending moment).

7.3.2.2 Load sequencing adopted for the phase II tests

Loading of the panels during phase II was carried out in similar incremental stages as above, but each interval was applied at 1 kN total applied load increments (i.e. 0.5 kN at each point load). This increment was based on two initial trial procedures conducted to identify the failure load and dominant failure mechanism of each panel type. From these tests a failure load of approximately 12kN total applied load (average) was obtained, with sudden in-plane shear failure at the steel-concrete interface defining failure of both panel types. The 1kN load increment represented

approximately an 8% increment of the failure load, which allowed static and dynamic data to be correlated in detail throughout the full capacity range of the panels. Therefore, the interval corresponding to the 12 kN load stage could be used as a benchmark for the panels, with normalisation of all other load increments being defined relative to "1".

The following points describe the principal load sequence considered for the phase II static load tests:

(i) Before applying static load, the section strain and panel displacement readings were noted (the location of which are identified later).

(ii) Assemble the loading beam and apply the load interval (1 kN for the first increment).

(iii) With the load applied, record the strain and displacement data.

(iv) Remove the load (and loading beam) and record the strain and displacement data, ensuring that the displacement gauges are not moved until all measurements are noted.

(v) Remove all displacement gauges and conduct the dynamic tests to obtain a record of the panel condition.

(vi) Repeat (i) through (v), but increase the loading interval in (ii) by 1 kN.

The aim of the phase II static load was thus to induce structural changes that are relative to the magnitude of the applied static load only, with no 'damage' being caused by the actions of the dynamic load. If the latter was found to occur, as a result of stage (v), the severity of the added 'damage' could be evaluated from the difference in strains noted from stage (iv) and (vi), the result being incorporated into the findings of the tests.

7.3.3 Methods adopted to record data during the static load tests

7.3.3.1 Recording detailed panel section strains

Strain data was recorded at six transverse levels within the constant bending moment region of the span, three on each side edge of the panels. To record the strain data, a 'Demec extensometer' gauge instrument was used, which can measure strain to the nearest $\varepsilon = 9.8\times10^{-6}$ mm/mm, which represents the amount of movement between two

fixed points. The fixed points were created with steel studs, which could be permanently fixed to the surface of the structure to ensure a consistent data set was obtained. The positions chosen for these studs for the S1 and S2 panels are shown in Figure 7.3(a). A comprehensive data set comprising 36 strain readings for each load increment was achieved.

7.3.3.2 Recording the panel displacement

The in-span displacement of the panels was monitored at three positions using calibrated displacement dial gauges. The accuracy of the gauges allowed the panel displacement to be measured to the nearest 0.01mm. These gauges were placed at the locations illustrated by Figure 7.3(b).

7.3.4 Methods used to induce and measure the vibration response of the panels

The dynamic tests were carried out as part of the phase II tests. These tests were integrated into the static load sequencing as outlined earlier, and were categorised under two main headings, (i) impact force-induced vibration, and (ii) steady-state force-induced vibration. In all cases applicable to (i) and (ii), where decay-of-vibration signals were required, a data capture rate of 1000Hz over an 8.192 second period was adopted (i.e. each digital signal stored on the computer comprised of 8192 data points). The equipment and instrumentation applicable to test categories (i) and (ii) above have been described in chapter 3, which were used to collect dynamic response information from the panels after each static load interval for the following purposes.

7.3.4.1 Impact force-induced vibration

The response signals recorded from the impact tests represent the behaviour of the panels during a condition of free vibration. For this reason, the level of energy imparted to the panels during the action of the impact force was not required, as the ensuing vibration decay is of primary interest. The information acquired from these response signals, therefore, concentrated on the natural frequency and the level of damping inherent in the panels. To determine these properties from the

measurements, a Fast Fourier Transform (FFT) algorithm and the correlation of measured and calculated visco-elastic characteristics were considered, the latter of which being used to determine both the frequency and damping properties.

7.3.4.2 Steady-state-force-induced vibration

The eccentric mass excitation equipment and computer program set-up as outlined in chapter 3 was used to produce and record the steady-state-force-induced vibration response signals. The information collected with this set-up was incorporated into the laboratory investigation for the following purposes.

(i) Response data was collected from the panels using the excitation equipment to initiate the vibration. The signals retrieved from the panels using this method aimed to produce a similar decay response as obtained from vibration initiated by impact. However, the philosophy of the steady-state approach was to ensure that the initial vibration corresponded to the fundamental natural frequency of the panels, from which ensuing decay would comprise characteristics associated with a single frequency of motion only. To obtain the decay signals in this way, the approach adopted was to simply remove the excitation force by switching off the equipment drive motor (see chapter 3), after which the panel vibration was allowed to dissipate. The natural frequency and level of damping was then established from the FFT and correlation with calculated response characteristics as previous.

(ii) To determine the dynamic characteristics of the panel relative to a range of steady-state force frequencies, the Frequency Response Functions (FRFs) corresponding to each static load interval were assembled. These FRFs were determined using the 'frequency sweep' test described in chapter 3, which allowed the response amplitude of the panels to be established at any desired forcing frequency (over a predetermined range). To calculate the natural frequency and damping of the panels from these measurements, a correlation with a calculated FRF, based on assumed behavioural characteristics, was then carried out.

(iii) The steady-state forcing device was also used to determine the mode shape corresponding to the fundamental natural frequency of the panels. This was

achieved using two vibration transducers, each recording the response of the panel at separate locations within the span during excitation at the natural frequency. To define the mode shape from these response signals, one transducer was maintained at a constant location (the 'reference' signal) while the second was moved according to pre-determined locations (the 'traveller' signal). The mode shape was then calculated by relating the peak response from the 'traveller' to the peak reading from the 'reference' signal.

A schematic illustration of the laboratory set-up used for both the impact and steady-state forcing tests is shown by Figures 7.4(a) to (c), each of which indicates the position and number of transducers used to record the vibration response data.

7.3.5 Description of the approach considered for the processing of the measured static and dynamic data identified above

A large volume of data was recorded from the laboratory tests. To rationalise the information presented by this data, a statistically accurate series of consolidated or 'smeared' relationships were incorporated to reflect the characteristics of the original measured results. This was achieved with a least-squares regression of the measurements, which was validated using a correlation approach to assess the accuracy of the regression lines. These analytical considerations were incorporated in their standard form as described by Weltner *et al* (1986), which are outlined briefly under the following headings.

7.3.5.1 Least-squares regression analysis

A series of linear least-squares regression lines were used to achieve the required best approximate relationships from the measured data. The regression lines were established using a mathematical form given by,

$$y = ax + b \tag{7.1}$$

where the y and x correspond to the data from the laboratory tests, for example strain or displacement, against the applied load respectively, while the coefficients a and b are calculated from,

$$a = \frac{\sum_{i=1}^{n} x_i y_i - n\bar{x}\bar{y}}{\sum_{i=1}^{n} x_i^2 - n\bar{x}^2} \tag{7.2}$$

$$b = \bar{y} + a\bar{x} \tag{7.3}$$

The variables $\bar{x}$ and $\bar{y}$ of eqns.(7.2) and (7.3) are the arithmetic mean values associated with the x and y data, which represents the 'centriod' of the test data as a whole. Therefore, n is the number of panels used to compile the data, which for the laboratory test are designated relative to the number of specimens forming each type.

7.3.5.2 Validating the regression lines using a correlation approach

To validate the accuracy of the regression lines, their correlation with the measured data was calculated. In mathematical terms, the correlation was quantified using,

$$R^2 = \frac{\left(\sum_{i=1}^{n} x_i y_i - n\bar{x}\bar{y}\right)^2}{\left(\sum_{i=1}^{n} x_i^2 - n\bar{x}.^2\right)\left(\sum_{i=1}^{n} y_i^2 - n\bar{y}.^2\right)} \tag{7.4}$$

where R^2 is the 'correlation' value specific to the data set being examined.

7.3.5.3 Applying the regression approach to the measured data

To achieve the regression lines the data was first compiled according to type (i.e. strain, displacement or dynamic measurement). This allowed those measurements that

did not conform to the overall data trends to be discarded, which was achieved from a visual inspection of the accumulated data presented in a graphical form.

With the data judged to be in error removed from the compiled results, a series of regression lines defined using a bi-linear form (i.e. two linear relationships in series) was fitted to the remaining data. To achieve best results, the intersection of the bi-linear lines (i.e. the point at which the two linear lines intersect) was varied until the correlation between the regression lines and the measurements was maximised. An appropriate simulation of the measured data was then assigned using the calculated coefficients (of a and b above) associated with the maximised correlation.

7.3.6 Collecting vibration data at varying response amplitudes

The impact tests were carried out by imparting a simple blow to the mid-span region of the panels [Figure 7.4(a)]. By its very nature, such a test makes it difficult to control the amount of energy that is transferred to the panel during the impact, which in turn does not provide a facility for controlling the response amplitude of the ensuing vibration. However, vibrating the panels using the steady state-forcing approach will provide this control, where the amplitude of excitation can be varied by adding (or subtracting) the amount of weight that is incorporated onto the arms of the eccentric mass device. A mathematical justification of this has been shown in chapter 3, which for the purposes of these tests allowed the amplitude dependence of natural frequency and damping to be identified.

To allow the above-mentioned dependencies to be evaluated over a reasonably wide range of amplitudes, a number of decisions needed to be carefully considered. The main consideration, however, was to ensure that the levels of applied force imparted to the panel was varied enough to produce definite changes in the response amplitude, but be small enough not to induce 'damage' when vibrated at their natural frequency. The latter was evaluated using the strain data as described earlier, while the former was satisfied using three excitation force-levels produced by different combinations of steel bolts used in conjunction with the vibration device. The weight of each bolt was 2 grams, which were attached to the arms of the excitation device to give the following:

(i) Excitation force-level 1 – Total eccentric mass = 12.6grams (including arms)
Peak force at a frequency of 1 Hz = 0.019 N.

(ii) Excitation force-level 2 – Total eccentric mass = 8.6grams (including arms)
Peak force at a frequency of 1 Hz = 0.013 N.

(iii) Excitation force-level 3 – Total eccentric mass = 4.6 grams (arms only)
Peak force at a frequency of 1 Hz = 0.007 N.

7.3.7 Choosing to study the fundamental vibration mode behaviour only

All tests focused on the fundamental vibration mode of the panels. The reasons for choosing to concentrate the study on this mode alone are as follows.

(i) The laboratory study aimed to establish data that could be used to promote the potential advantages of using vibration data as a means of assessing the presence of damage in a structure. Therefore, to make the method an attractive and convenient non-destructive, non-invasive technique, the study focused on the fundamental mode to ensure that low forcing and light impact load levels need only be applied to the panels.

(ii) To excite the vibration modes of the panels beyond their fundamental frequency would require high excitation frequencies producing large excitation forces, which may itself cause damage to the panels.

(iii) To induce single mode vibration of the panels in modes other than the fundamental would require more than one excitation device.

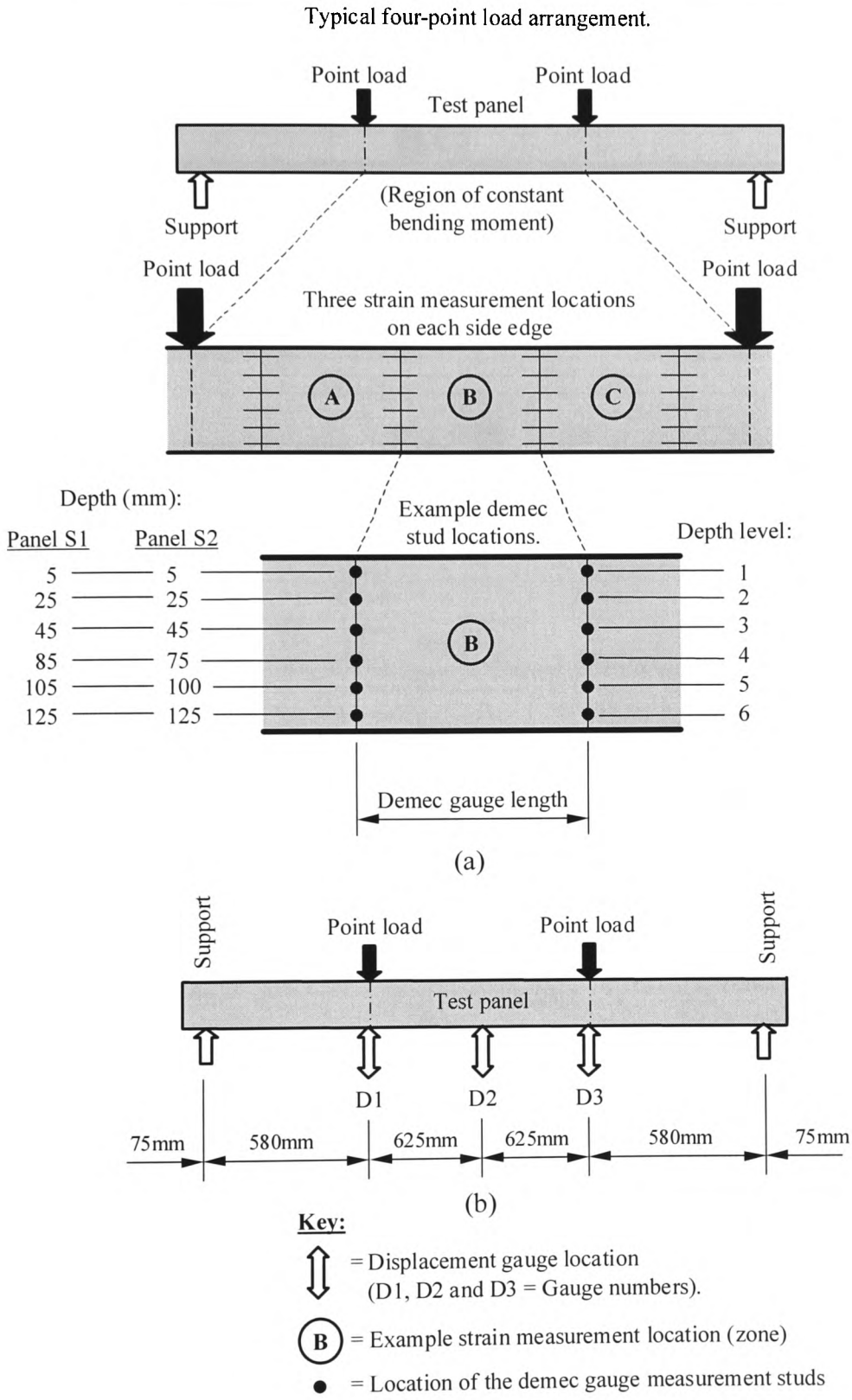

Figure 7.3 – Schematic illustration of (a) the strain measurement locations (on each side) with 'demec extensometer' gauge stud positions shown, and (b) the displacement dial gauge locations.

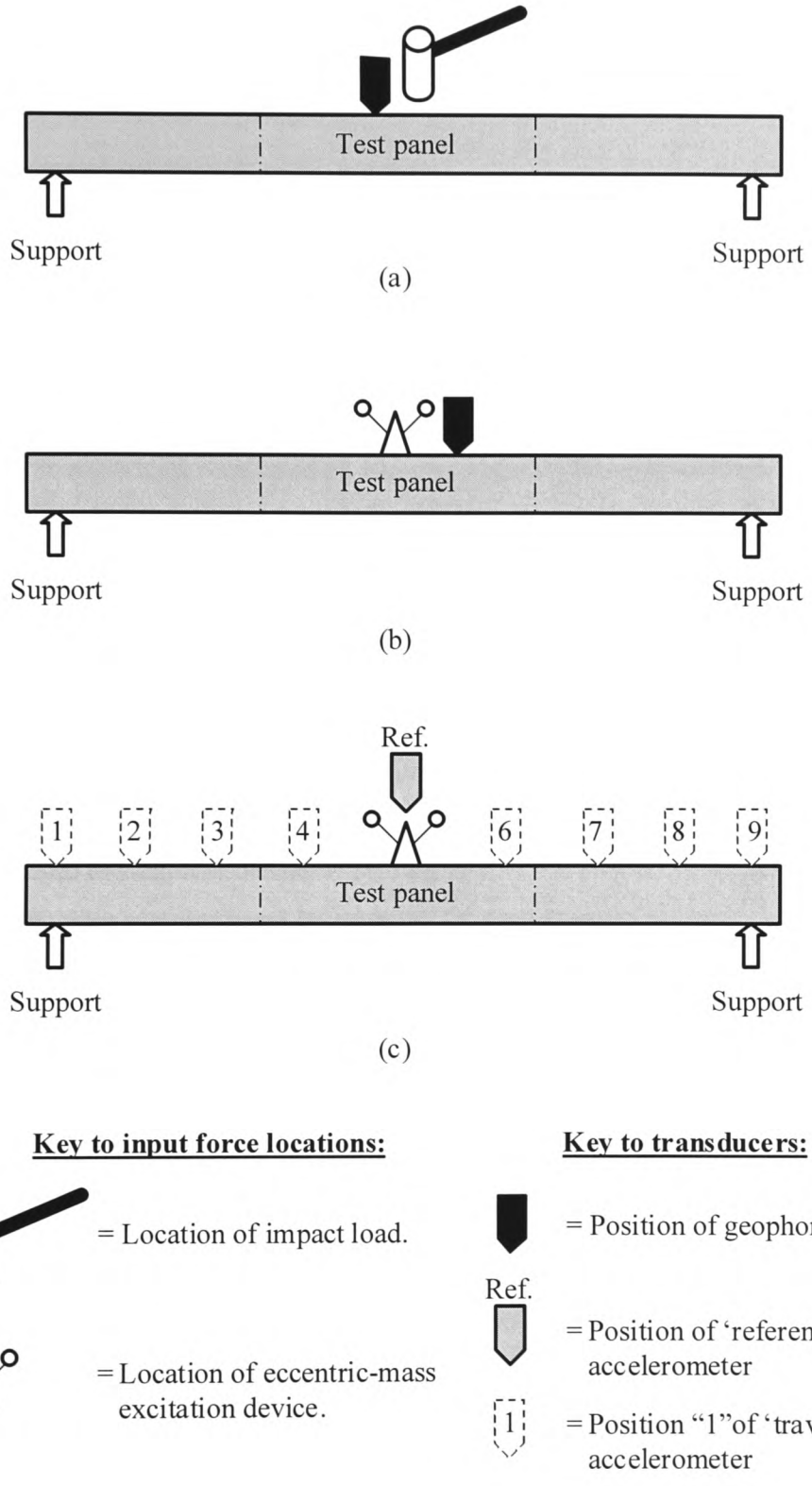

Figure 7.4 – Schematic diagram of (a) the impact-force vibrations test, (b) the frequency sweep tests, and (c) mode shape measurement positions.

7.4 Processed Data from Laboratory Static Load Test Results

7.4.1 Properties of the concrete and the laboratory results from standard tests

7.4.1.1 Compressive strength of the concrete

The concrete used to make the composite beams comprised of normal weight aggregates having a maximum particle size of 20mm. The constituents of the concrete, in terms of its water, cement, aggregate and sand proportions, were in accordance with the standard design mix defined as C35 in BS 5328: Part 2 (1997). Laboratory strength tests conducted on cured samples of this material were carried out in accordance with the requirements of BS 1881: Parts 114 and 116 (1983). The results of the individual tests are included in Appendix C, which were used to calculate the following statistical properties:

(i) Results from samples cured in air (age varies between 28 and 92 days):
Arithmetic mean of all compressive strength tests, $f_{cu(air)} = 50.2$ N/mm^2
(Standard deviation of $f_{cu(air)}$, is 4.1 N/mm^2)
Arithmetic mean of the determined concrete density from all tests = 2456 kg/m^3
(Standard deviation of density = 21.6 kg/m^3)

(ii) Results from samples cured in water (all 28 day values):
Arithmetic mean of all compressive strength tests, $f_{cu(28\ day)} = 57.5$ N/mm^2
(Standard deviation of $f_{cu(28\ day)}$, is 3.5 N/mm^2)
Arithmetic mean of the determined concrete density from all tests = 2485 kg/m^3
(Standard deviation of density = 26.6 kg/m^3)

7.4.1.2 The Young's modulus of the concrete

The elastic modulus of the concrete (E_c) was calculated in accordance with the requirements of BS 1881: Part 121 (1983), from cylinders prepared in accordance with BS 1881: Part 110 (1983). The results of these tests are given in Appendix C, from which the arithmetic mean value was calculated to be E_c = 37.4 kN/mm^2 with a standard deviation of 1.7 kN/mm^2.

7.4.2 Processed section strain data from the static load tests conducted on the panels

7.4.2.1 The calculated strain variation from accumulated data

A total of approximately 6,000 strain readings were recorded from the laboratory tests. To obtain the strain variation corresponding to each of the section depth levels (see Figure 7.3) the regression analysis, described earlier, was followed. Figures 7.5(a) to (f) illustrate the results, which correspond to panel type S1, while Figures 7.6(a) to (f) show the relationships achieved from the S2 panel data.

It should be noted that the measurements used to calculate these bi-linear best-fit lines comprised data from all eighteen laboratory test panels. This was possible due to the fact that the strain data of the phase II tests showed no changes as a result of the dynamic load procedures. Figures 7.7(a) and (b) therefore illustrate collectively the determined average strain for the S1 and S2 panels respectively.

7.4.2.2 The calculated strain distribution obtained from the regression lines

The strain variation calculated from the measured data was finally used to determine two important characteristics concerning the panel behaviour. (i) The position of the neutral axis, and (ii) the curvature of the panel span over the region affected by the constant bending moment. The latter of these attributes is considered later, where a number of methods are explored, but the former can be determined from strain distribution profiles formed using the aforementioned bi-linear relationships.

Figures 7.8 and 7.9 illustrate these profiles for panel types S1 and S2 respectively, from which it is seen that the neutral axis location can be defined as the point were the strain value is found to be zero. It is noted from these figures that a linear regression approach was again adopted to locate the neutral axis, which followed similar procedures to those described earlier. The approach, therefore, assumes that the panel sections remained plane during the application of static load, which complies with the hypothesis that plane sections remain plane during pure bending [Gere and

Timoshenko (1991)]. Figure 7.10 shows the calculated neutral axis depths obtained in this manner.

7.4.3 Processed displacement data from the static load tests

In total, approximately 1,000 displacement measurements were recorded during the panel loading stages. To obtain a representative relationship of displacement, corresponding to the various load intensities, the regression line approach described earlier was considered. Figures 7.11 and 7.12 present the results for panel type S1 and S2 respectively.

7.4.4 Tabulated results of the regression analysis

Tables 7.2 and 7.3 contain the results of the previously described regression analyses to demonstrate the correlation achieved from the strain and displacement data.

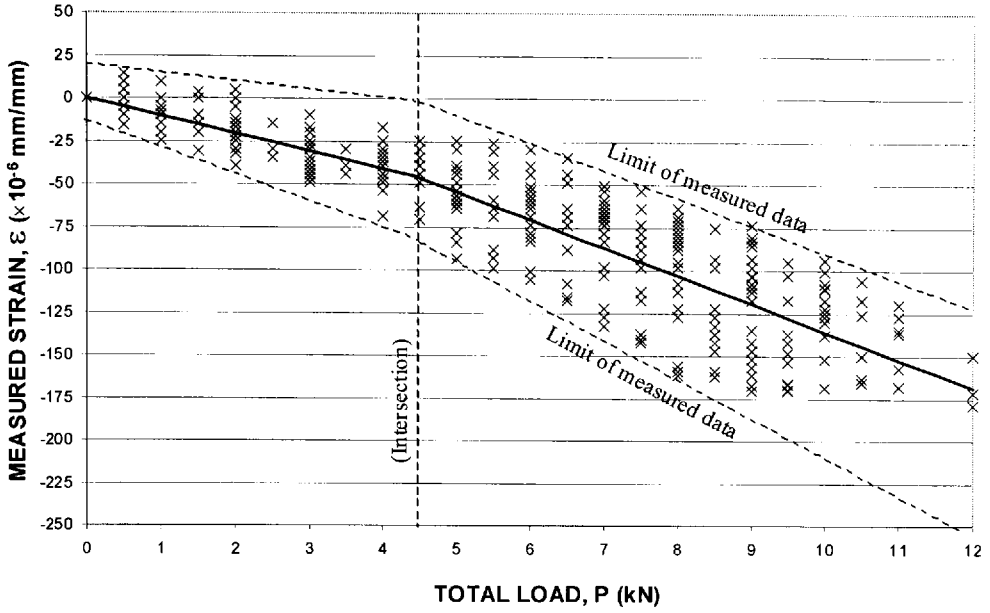

(a)

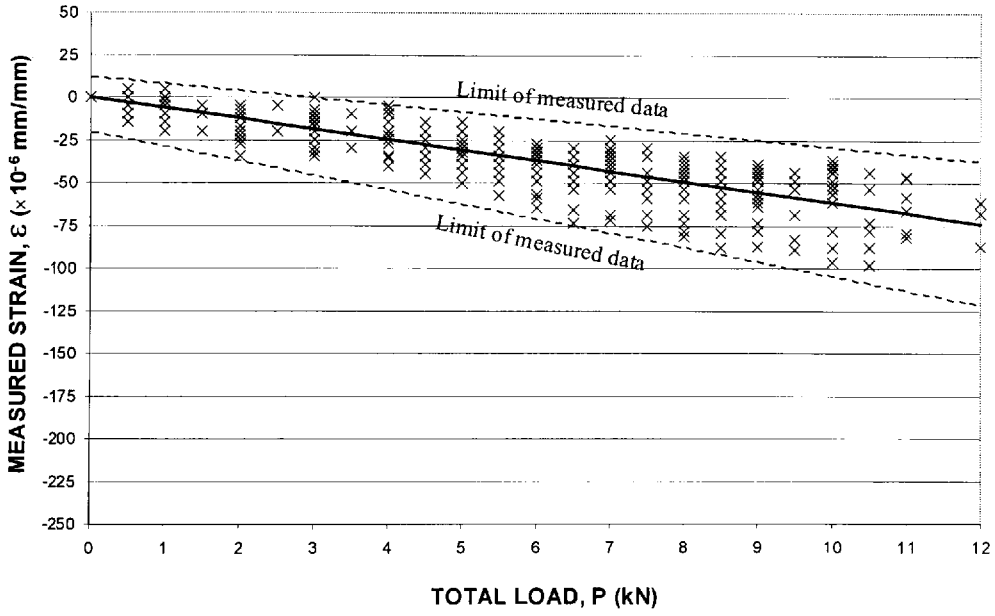

(b)

Key:

× = Measured data (all values - excluding the discarded values - see main text)

——— = Regression line (best-fit linear lines combined in 'series' as appropriate to give best results).

(Intersection) = The intersection point of the regression lines that comprise more than one series of relationships

Limit of measured data = The extent of the measured data included in the regression analysis

Figure 7.5 – Section strain measurements together with the calculated regression lines for panel type S1 at depth levels (a) 1, and (b) 2 [see Figure 7.3(a)]

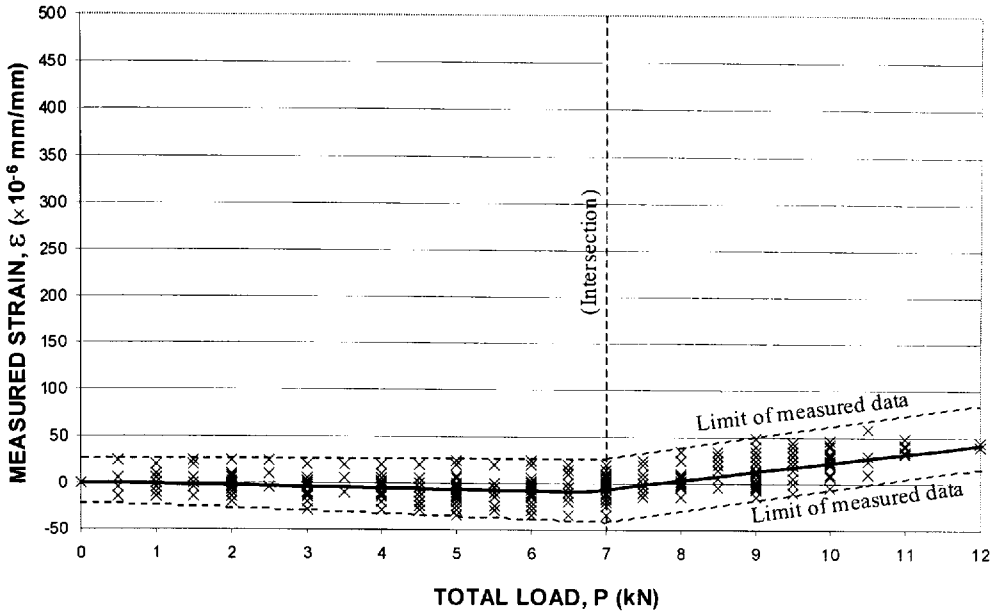

(c)

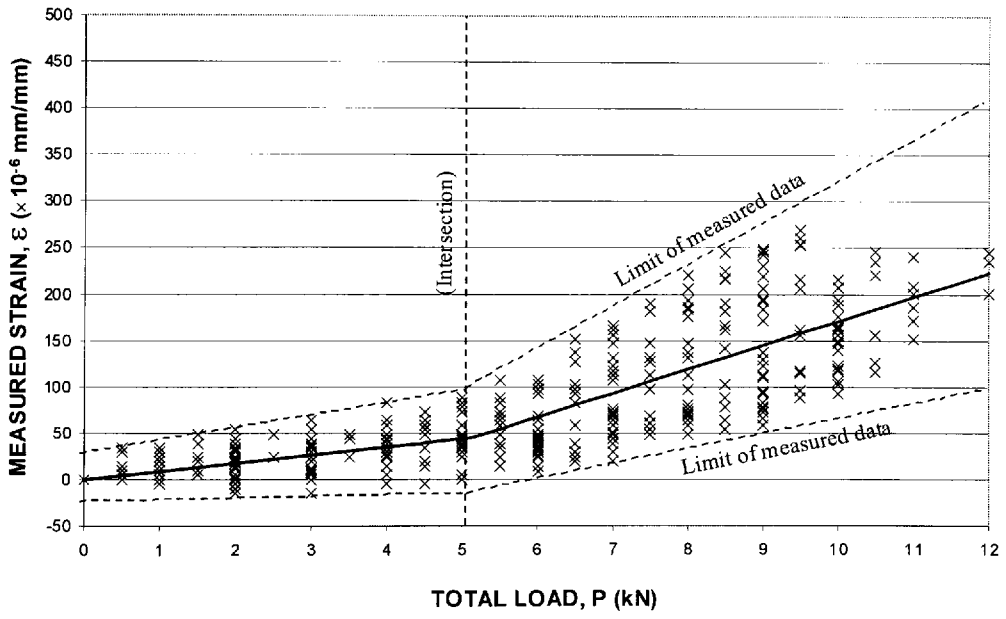

(d)

Key:

× = Measured data (all values - excluding the discarded values - see main text)

—— = Regression line (best-fit linear lines combined in 'series' as appropriate to give best results).

(Intersection) = The intersection point of the regression lines that comprise more than one series of relationships

Limit of measured data = The extent of the measured data included in the regression analysis

Figure 7.5 – Section strain measurements together with the calculated regression lines for panel type S1 at depth level (c) 3, and (d) 4 [see Figure 7.3(a)]

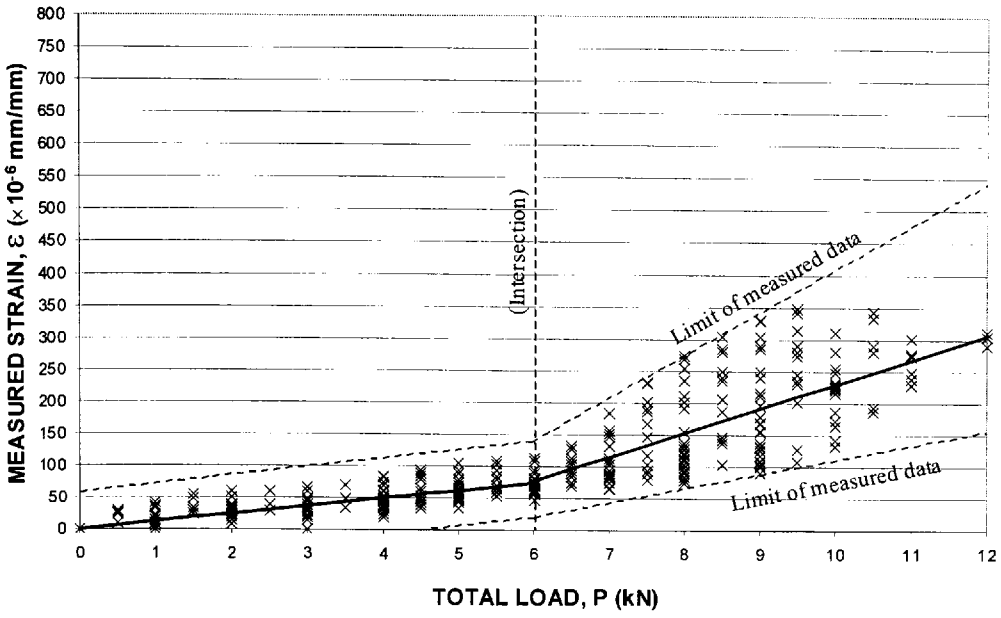

(e)

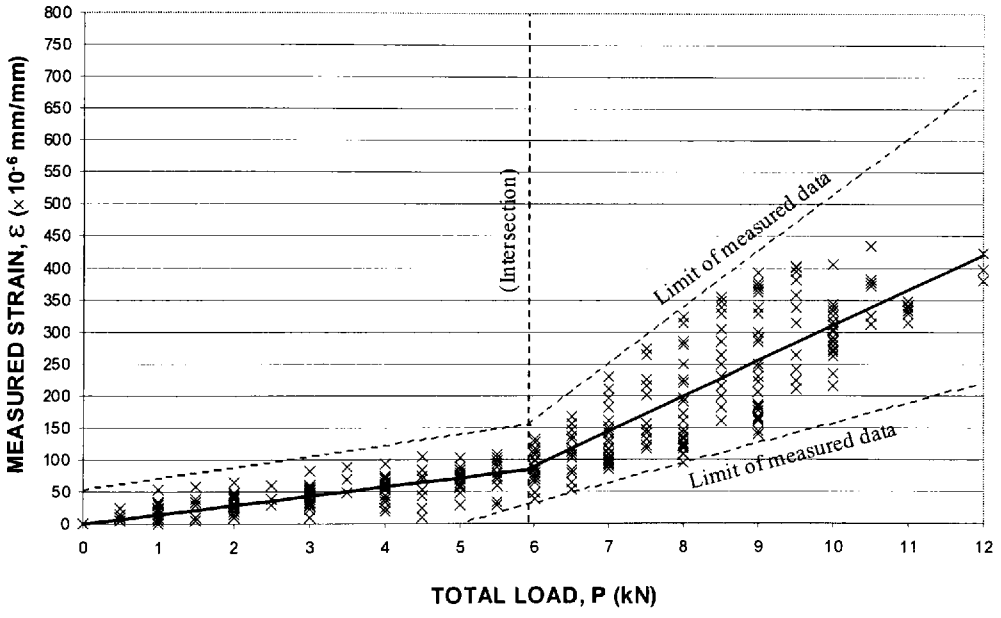

(f)

Key:

× = Measured data (all values - excluding the discarded values - see main text)

——— = Regression line (best-fit linear lines combined in 'series' as appropriate to give best results).

(Intersection) = The intersection point of the regression lines that comprise more than one series of relationships

Limit of measured data = The extent of the measured data included in the regression analysis

Figure 7.5 – Section strain measurements together with the calculated regression lines for panel type S1 at depth level (e) 5, and (f) 6 [see Figure 7.3(a)]

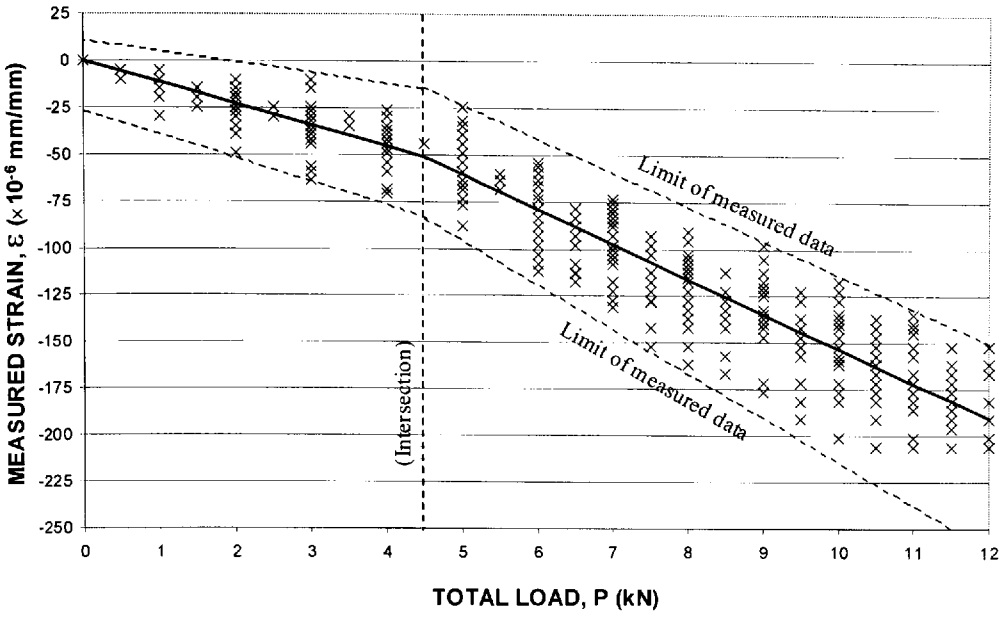

(a)

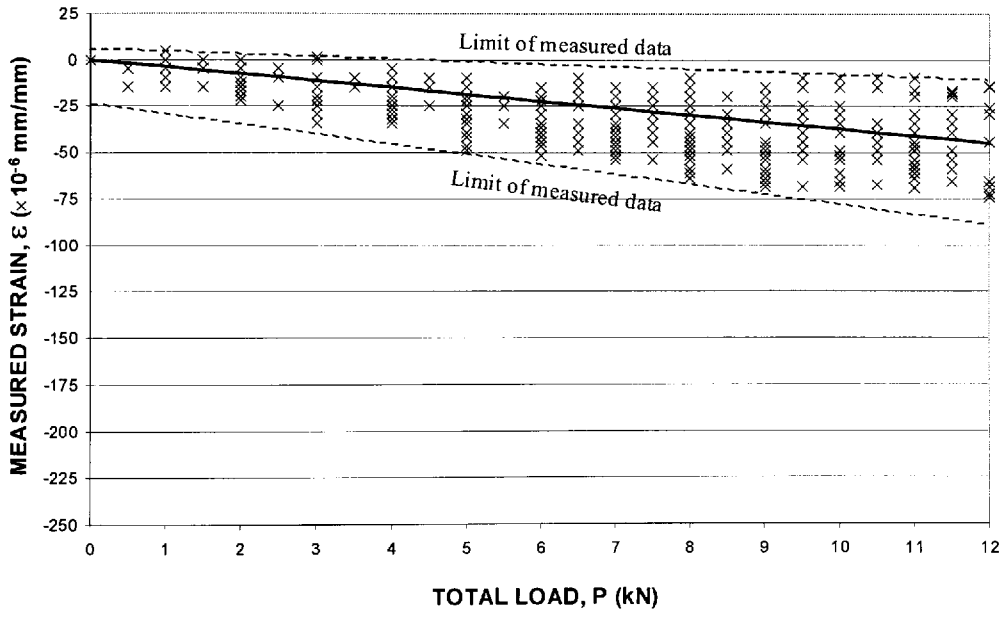

(b)

Key:

× = Measured data (all values - excluding the discarded values - see main text)

——— = Regression line (best-fit linear lines combined in 'series' as appropriate to give best results).

(Intersection) = The intersection point of the regression lines that comprise more than one series of relationships

Limit of measured data = The extent of the measured data included in the regression analysis

Figure 7.6 – Section strain measurements together with the calculated regression lines for panel type S2 at depth level (a) 1, and (b) 2 [see Figure 7.3(a)]

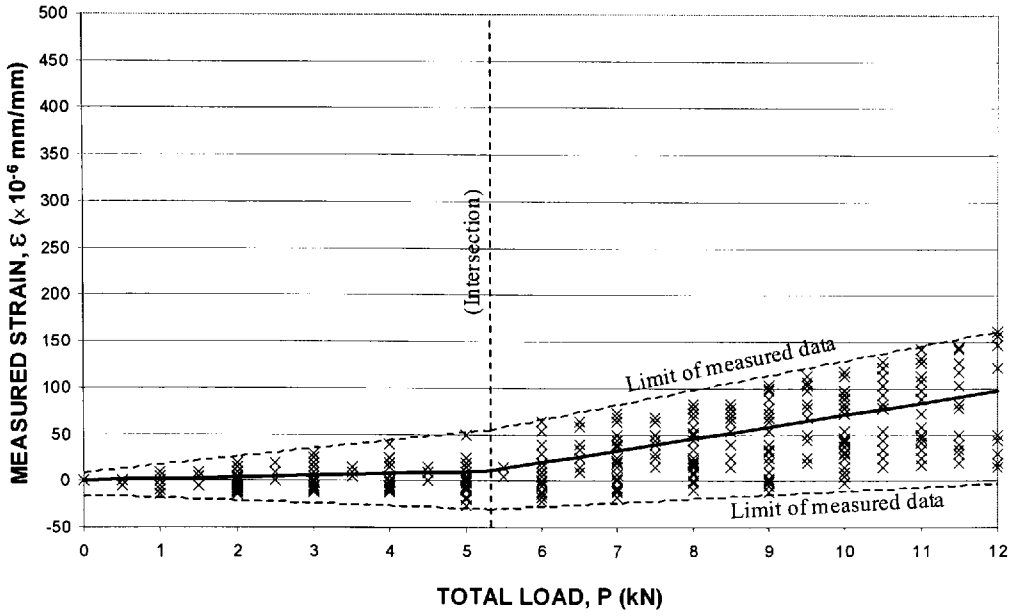

(c)

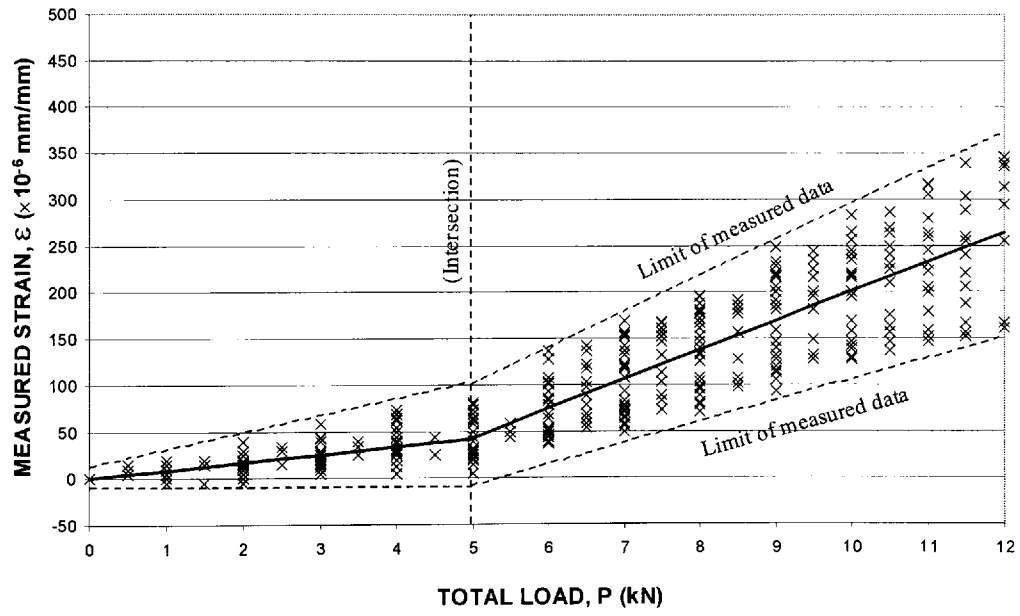

(d)

Key:

× = Measured data (all values - excluding the discarded values - see main text)

——— = Regression line (best-fit linear lines combined in 'series' as appropriate to give best results).

(Intersection) = The intersection point of the regression lines that comprise more than one series of relationships

Limit of measured data = The extent of the measured data included in the regression analysis

Figure 7.6 – Section strain measurements together with the calculated regression lines for panel type S2 at depth level (c) 3, and (d) 4 [see Figure 7.3(a)]

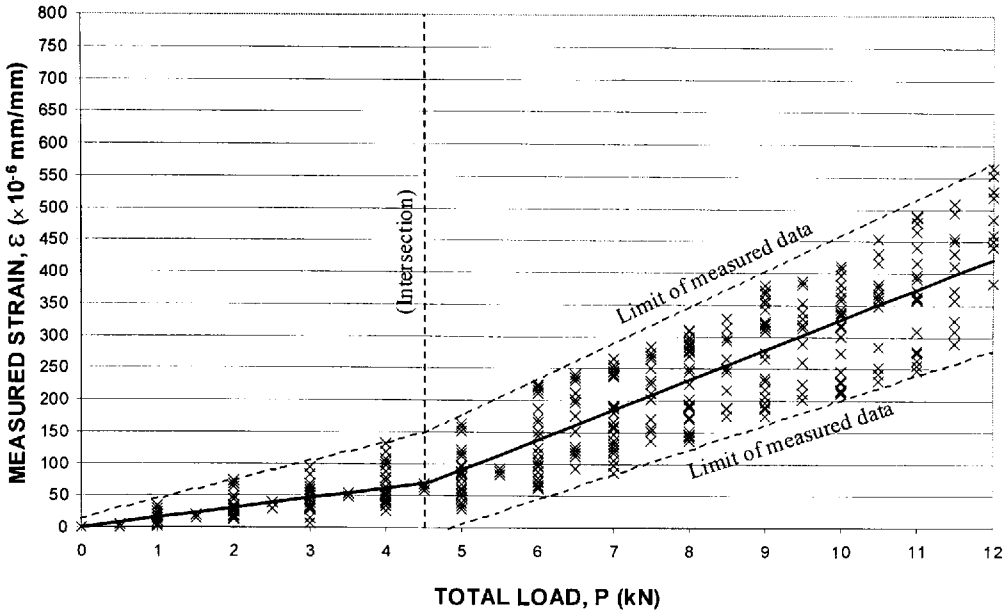

(e)

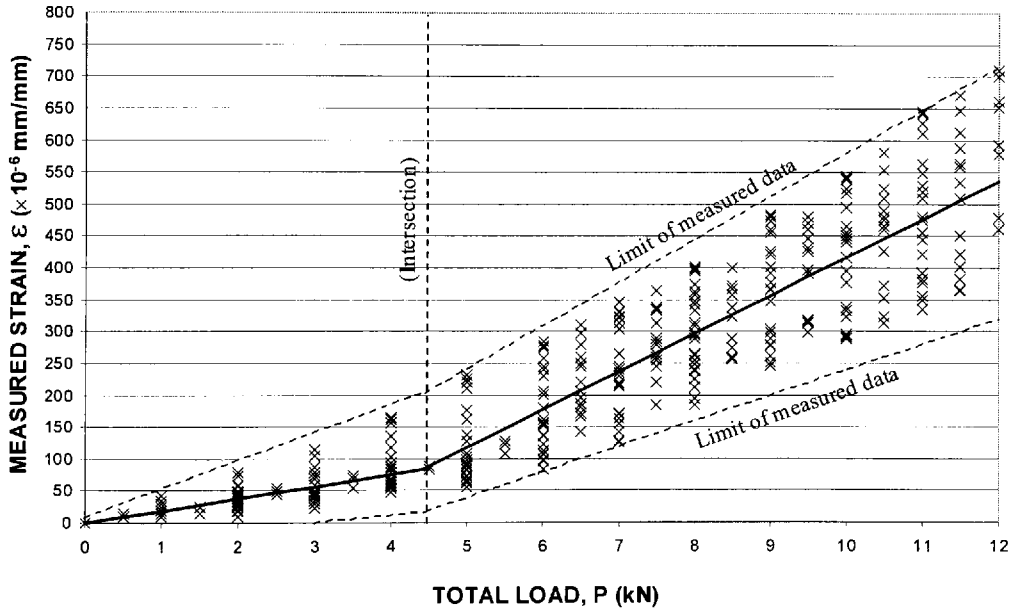

(f)

Key:

× = Measured data (all values - excluding the discarded values - see main text)

—— = Regression line (best-fit linear lines combined in 'series' as appropriate to give best results).

(Intersection) = The intersection point of the regression lines that comprise more than one series of relationships

Limit of measured data = The extent of the measured data included in the regression analysis

Figure 7.6 – Section strain measurements together with the calculated regression lines for panel type S2 at depth level (e) 5, and (f) 6 [see Figure 7.3(a)]

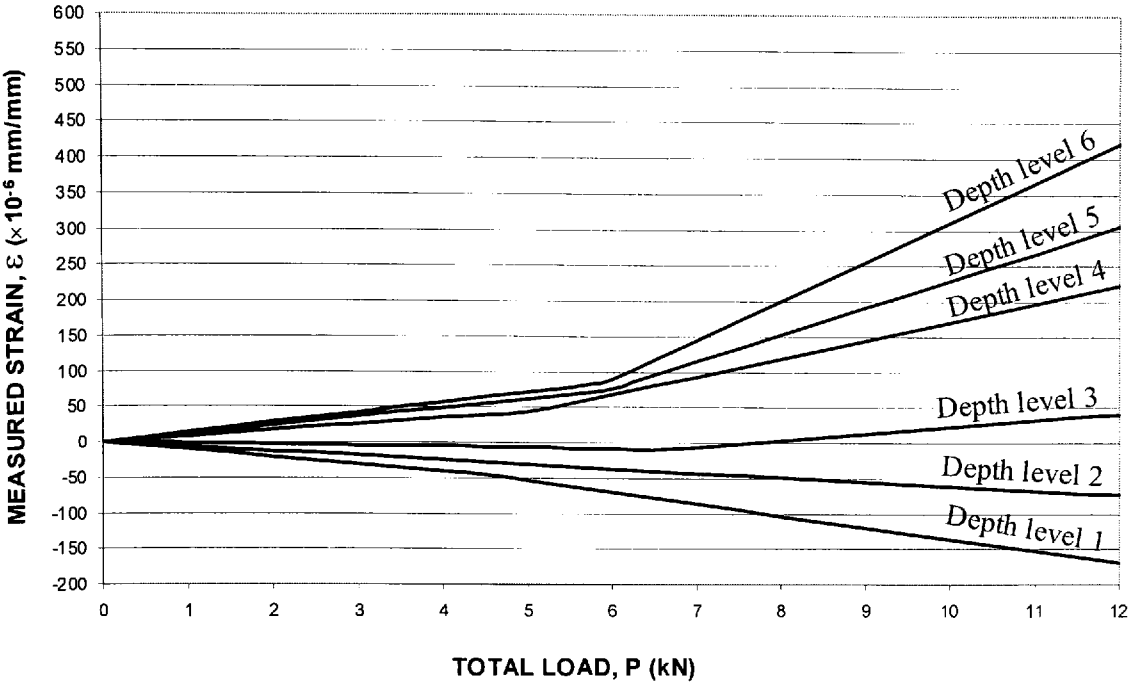

(a)

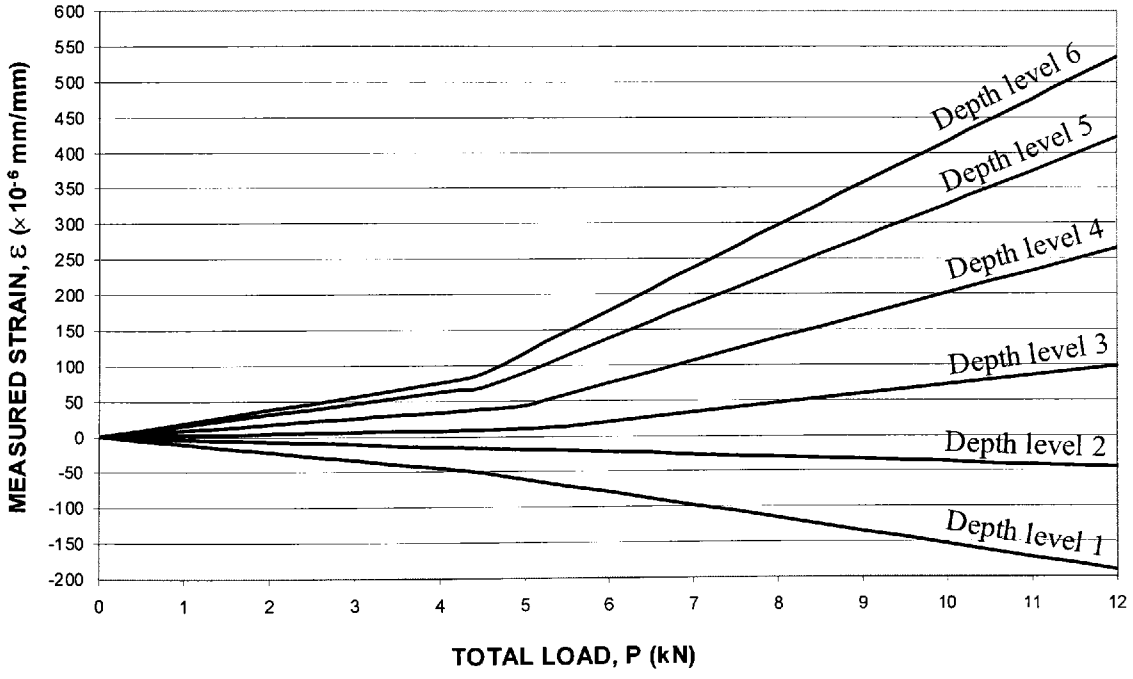

(b)

Figure 7.7 – Collective illustration of the processed strain data (bi-linear regression lines) for (a) panel type S1 [from Figures 7.5(a) to (f)], and (b) panel type S2 [from Figures 7.5(a) to (f)]. The 'Depth level' definitions relate to the positions across the depth of the panel sections as indicated by Figure 7.3.

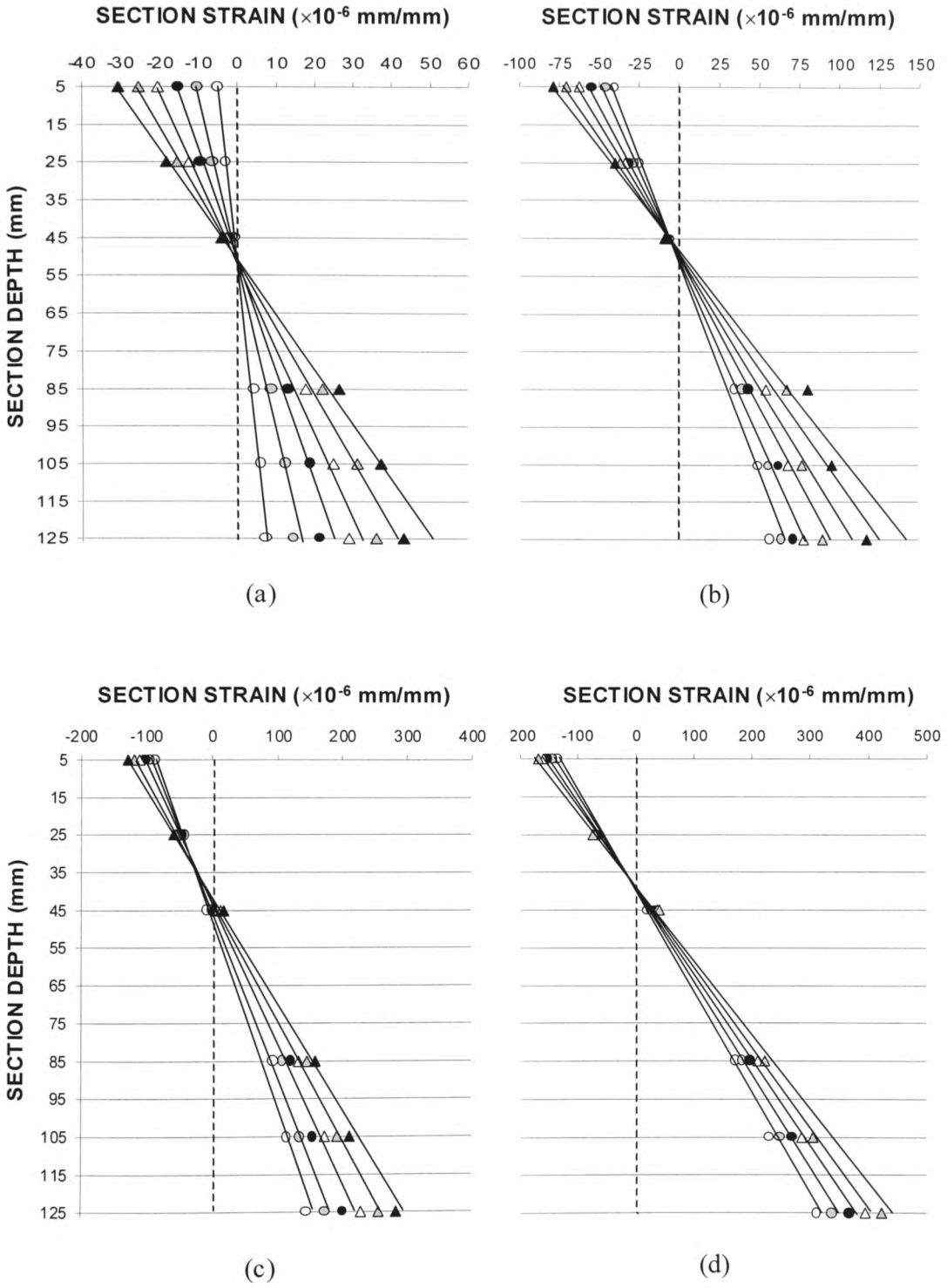

Figure 7.8 – Illustration of section strain calculated from the relationships presented in Figures 7.5(a) to (f) (i.e. Panel type S1). The above diagrams show regression lines used to identify the neutral axis locations of the panel for the load intervals (a) 0.5kN to 3.0kN, (b) 3.5kN to 6kN, (c) 6.5 to 9kN, and (d) 9.5kN to 12kN, (all in steps of 0.5kN total applied load).

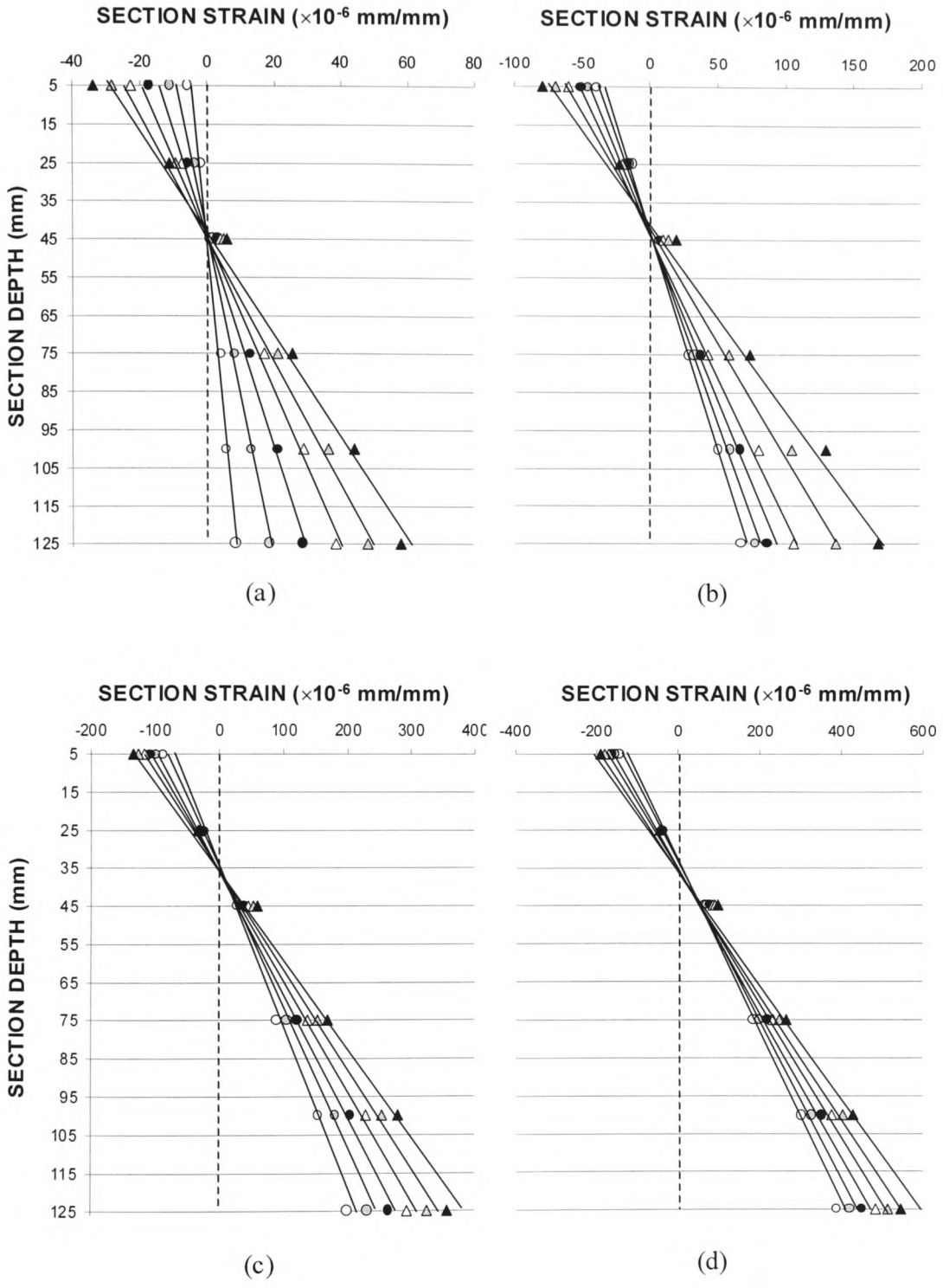

Figure 7.9 – Illustration of section strain calculated from the relationships presented in Figures 7.6(a) to (f) (i.e. Panel type S2). The above diagrams show regression lines used to identify the neutral axis locations of the panel for the load intervals (a) 0.5kN to 3.0kN, (b) 3.5kN to 6kN, (c) 6.5 to 9kN, and (d) 9.5kN to 12kN, (all in steps of 0.5kN total applied load).

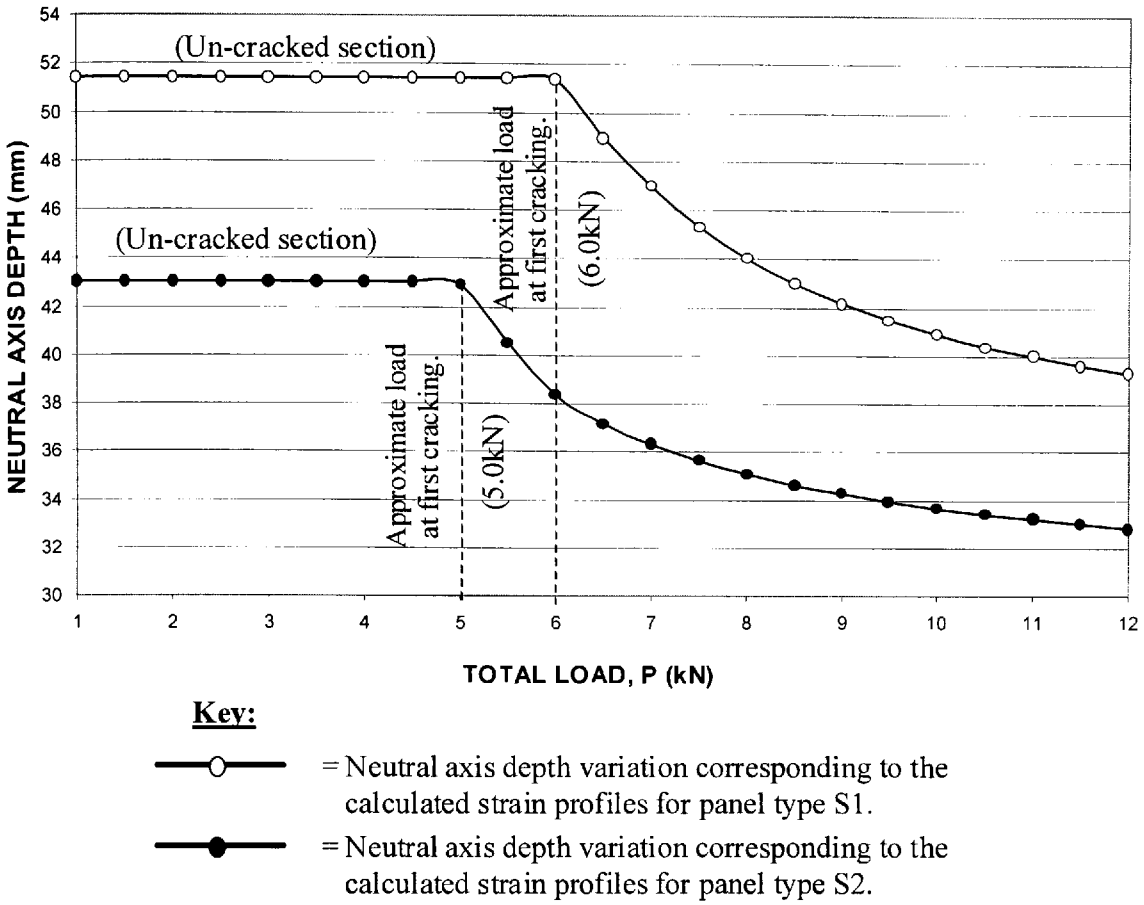

Key:

= Neutral axis depth variation corresponding to the calculated strain profiles for panel type S1.

= Neutral axis depth variation corresponding to the calculated strain profiles for panel type S2.

Figure 7.10 – Neutral axis depth (relative to the top surface of the panels) determined from the regression analysis shown in Figures 7.8 and 7.9 for panel type S1 and S2 respectively.

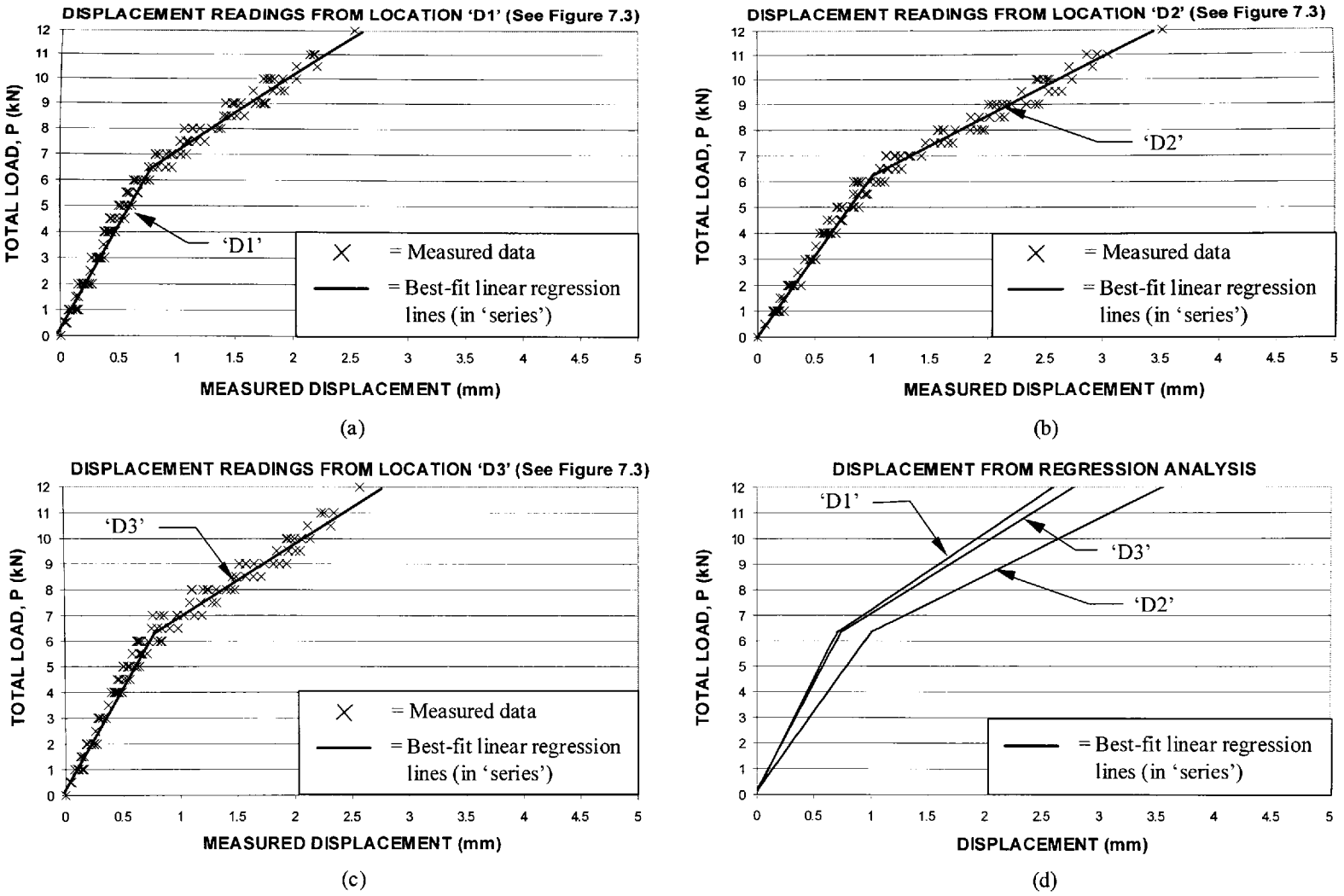

Figure 7.11 – Measured displacement corresponding to panel type S1 at the positions defined in Figure 7.3 as (a) location 'D1', (b) location 'D2', and (c) location 'D3'. The best-fit linear regression lines are also shown, which are displayed in (d).

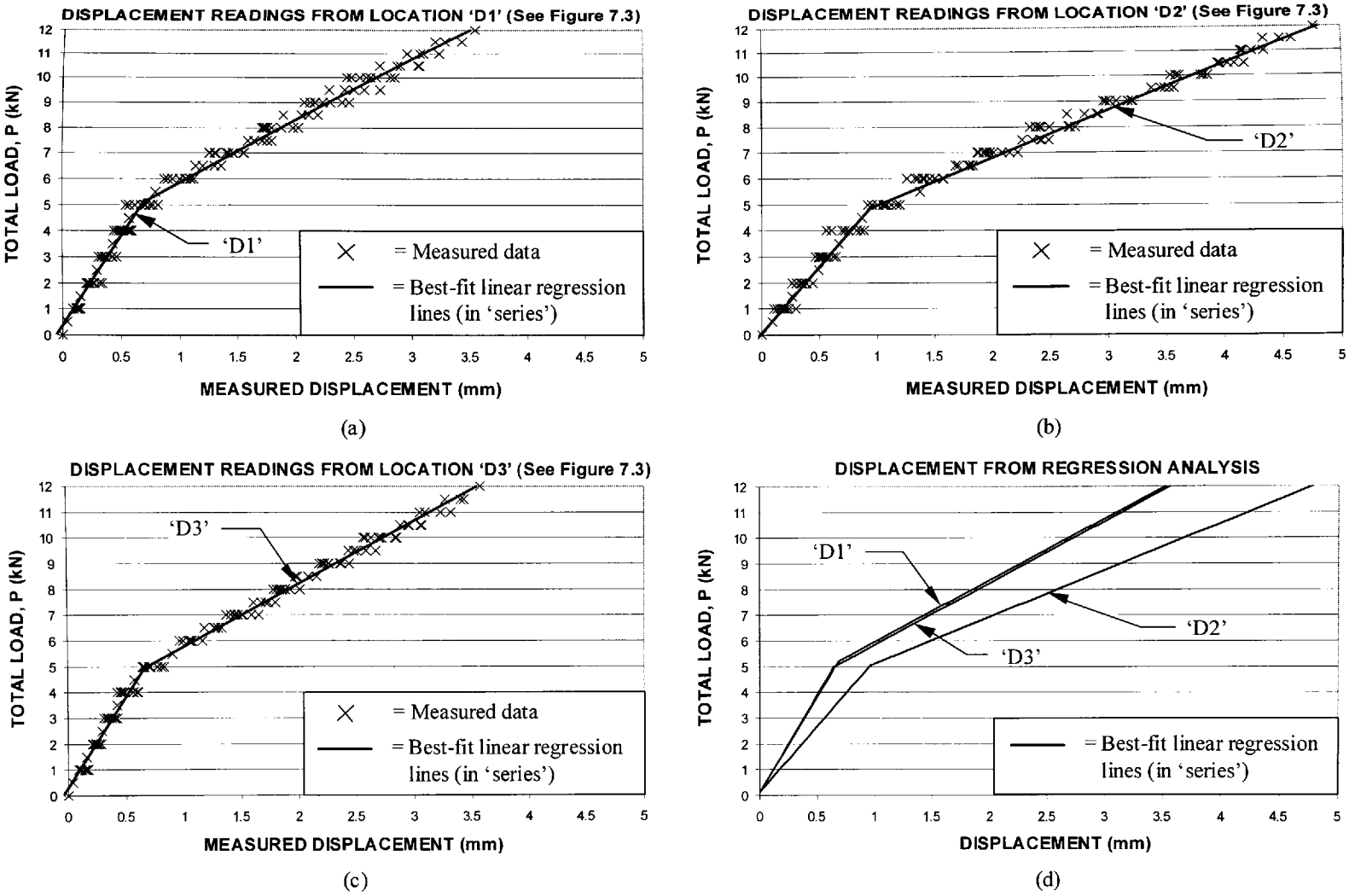

Figure 7.12 – Measured displacement corresponding to panel type S2 at the positions defined in Figure 7.3 as (a) location 'D1', (b) location 'D2', and (c) location 'D3'. The best-fit linear regression lines are also shown, which are displayed in (d).

Table 7.2 – Calculated coefficients determined from the regression analysis of measured strain data for panel type S1 and S2

Depth level	Panel type S1 – (Figures 7.5 to 7.7)						Panel type S2 – (Figures 7.8 to 7.10)					
	Pre-intersection point			Post-intersection point			Pre-intersection point			Post-intersection point		
	R^2	a ($\times 10^{-6}$)	b ($\times 10^{-6}$)	R^2	a ($\times 10^{-6}$)	b ($\times 10^{-6}$)	R^2	a ($\times 10^{-6}$)	b ($\times 10^{-6}$)	R^2	a ($\times 10^{-6}$)	b ($\times 10^{-6}$)
1	0.996	-10.54	0.074	0.966	-15.87	25.70	0.982	-11.28	-1.10	0.985	-18.67	32.55
2	0.978	-6.273	-0.112	(Single regression line)			0.910	-3.59	-0.86	(Single linear regression line)		
3	0.935	1.40	1.51	0.966	9.61	-72.41	0.919	1.97	-1.39	0.901	11.45	-49.25
4	0.865	8.79	6.07	0.940	25.33	-79.51	0.952	8.46	1.37	0.947	30.01	-103.46
5	0.922	12.06	7.78	0.943	38.52	-148.43	0.989	15.26	-1.81	0.959	49.37	-165.99
6	0.948	14.26	1.918	0.951	54.35	-223.49	0.964	19.71	-1.07	0.984	62.46	-205.7

Table 7.3 – Calculated coefficients determined from the regression analysis of measured displacement data for panel type S1 and S2

Location	Panel type S1 – (Figures 7.14)						Panel type S2 – (Figures 7.15)					
	Pre-intersection point			Post-intersection point			Pre-intersection point			Post-intersection point		
	R^2	a	b	R^2	a	b	R^2	a	b	R^2	a	b
D1	0.976	8.82	0.12	0.943	3.01	4.21	0.958	7.39	0.14	0.979	2.40	3.596
D2	0.973	6.17	0.15	0.950	2.23	4.12	0.949	5.11	0.13	0.987	I.82	3.29
D3	0.966	8.32	0.19	0.935	2.78	4.30	0.962	7.58	0.11	0.989	2.41	3.43

(Note: the coefficients a and b relate to the values calculated from the implementation of eqns.(7.2) and (7.3) respectively, while R^2 was obtained from the expression given by eqn.(7.4). The headings 'pre' and 'post-intersection point' relate to the relationships that correspond to the measured data for load intervals 'less than' and 'greater than' the intersection of the bi-linear lines respectively. The intersection point is illustrated on the appropriate figures defined in the table above).

7.5 The Moment – Curvature Relationships

7.5.1 Calculating the moment-curvature relationship

The calculated neutral axis positions and the strain variation relationships obtained from the previous analyses are used here to formulate the Moment–Curvature (M-C) properties of the two panel types. The main advantage of compiling the M-C relationships is that the flexural rigidity, (or 'stiffness' – here termed *EI*) of the panels can be obtained directly from the ratio of the applied bending moment (M) to the amount of curvature (C or 'χ') induced by static loading. To extend the available database, and allow incorporation of all available strain and displacement information, the M-C relationships were formulated using two methods.

7.5.1.1 Method 1 – Moment-curvature from the measured strain information

Gere and Timoshenko (1991) defined the relationship between applied bending moment (M) and the EI as,

$$\frac{M}{EI} = \frac{1}{R} = \frac{\varepsilon}{y} = \chi \tag{7.5}$$

where R is the radius of curvature of the panel over the constant moment region, χ the curvature, and ε is the strain value at a distance y from the neutral axis. To calculate the M-C relationship with eqn.(7.5) the calculated strain variation corresponding to depth level 1 [Figures 7.5(a) and 7.6(a)] was considered. The distance from this level to the position of the calculated neutral axis (x) was thereby determined by subtracting 5mm from the values indicated by Figure 7.10.

7.5.1.2 Method 2 – Moment-curvature from the measured displacement information

The theorem of intersecting chords offers an additional method for the calculation of the M-C relationship, allowing displacement information to be used to crosscheck the results gained from method 1 above. The basis of the theorem applies mainly to the calculation of the curvature (χ), which has been outlined by Delpak (1999) and found

to correspond with the M-C properties determined using strain data from simply supported reinforced concrete beams. The basis of the method relies essentially on the radial arc that forms over the constant bending moment region of the panel during four-point loading. Schematically, this can be visualised as shown by Figure 7.13, where it is seen that the radius of curvature (R) can be assumed to be dependent on the displacement that occurs to the panels between locations 'D1' and 'D3', which have been identified in Figure 7.3. Using the intersecting chord analogy, Delpak (1999) recommended that the radius of curvature (R) – obtained from strain measurements – could be compared directly to a quantity that was given by,

$$\left[D2-\left(\frac{D1+D3}{2}\right)\right]\left\{2R-\left[D2-\left(\frac{D1+D3}{2}\right)\right]\right\}=\left(\frac{L_{cm}}{2}\right)^2 \qquad (7.6)$$

where L_{cm} is the length of the panel between 'D1' and 'D3' (see Figure 7.3). Therefore, the displacement variation calculated from the measured data (Figures 7.11 and 7.12) can be incorporated directly into eqn.(7.6) to calculate R. Finally, the curvature of the panel over the affected region is defined by R^{-1}.

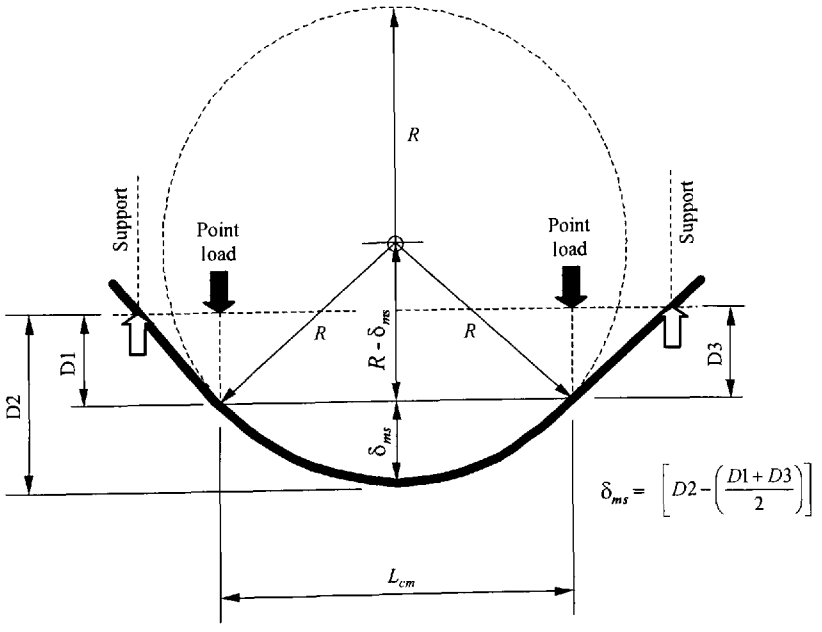

Figure 7.13 – Schematic illustration of a panel during four-point loading showing the assumed static displacement geometry of the member for the calculation of the radius of curvature (R) over the region of the span subjected to constant bending moment.

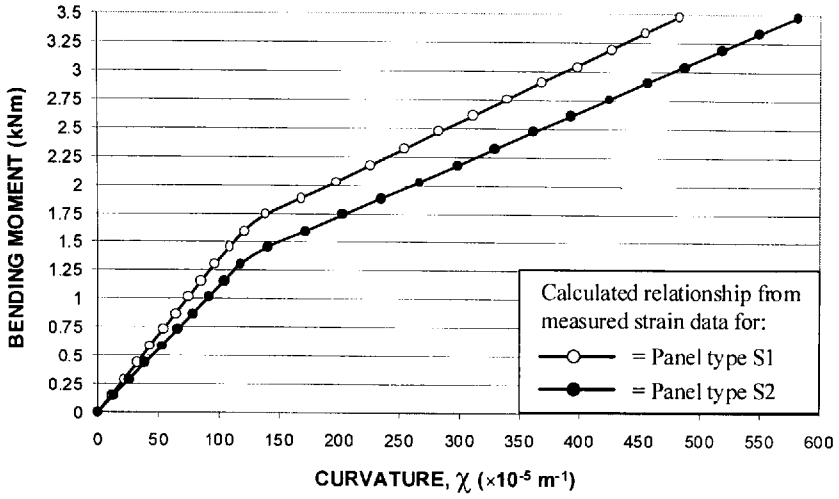

(a)

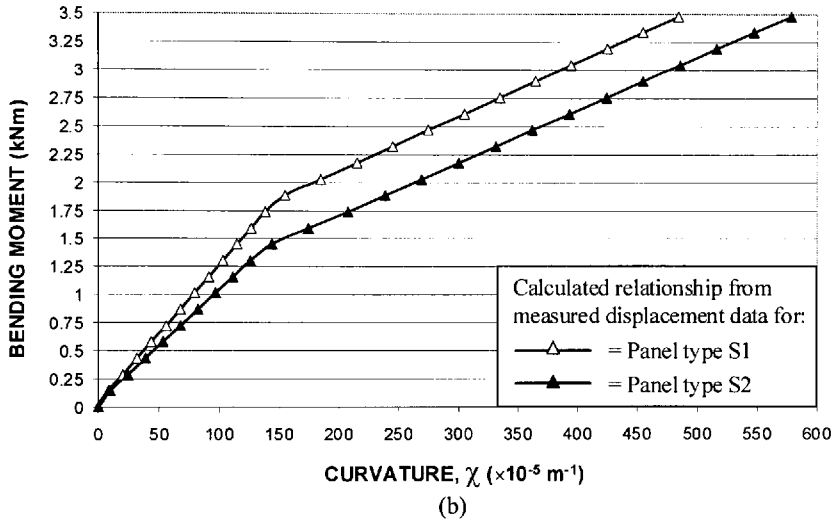

(b)

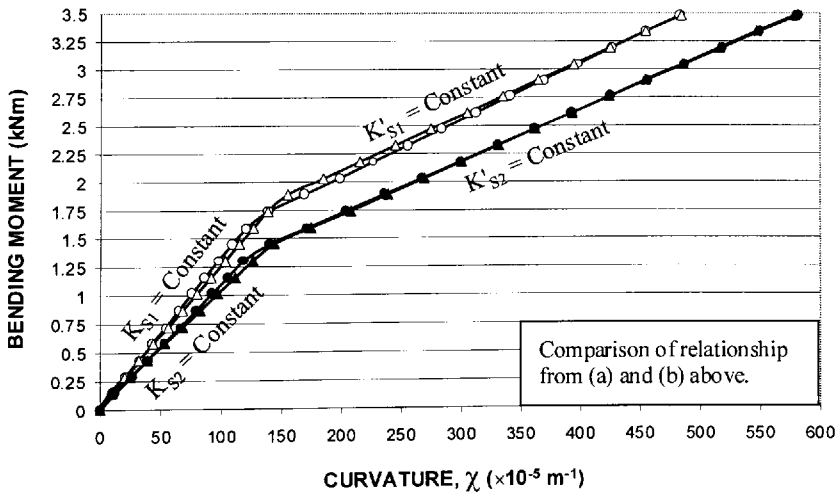

(c)

Figure 7.14 – Moment-curvature relationships from (a) the calculated strain relationships, and (b) calculated displacement variation. (c) compares (a) and (b) above. (K and K' are used above to indicate the two stiffness regimes determined from the measured data for S1 and S2).

7.5.2 The calculated structural stiffness of the panels corresponding to incremental static load

The M-C relationships calculated using the methods described above are presented by Figure 7.14(a) to (c). The latter of these figures illustrates a comparison of the results from these methods for both panel types, where it is seen that a high degree of correlation was achieved. Reflecting on the accuracy exhibited by this comparison, it is evident that all previously formulated relationships have provided a reliable representation of the panel behaviour. In addition, it can be seen from the aforementioned figures that two distinct stiffness regimes are evident, which exists in both panel types. Therefore, having now established the M-C relationships for both panel types, the stiffness (*EI*) can be calculated using eqn.(7.5). The results of the calculations are presented graphically by Figure 7.15, which make use of the information given by Figure 7.14(a).

It should be noted from the data presented by Figure 7.15 that the stiffness of the panels appear to gradually reduce after a certain level of applied bending moment. However, if the panels were assumed to behave in a bi-linear form (as assumed in Figures 7.11 and 7.12 for example) then the stiffness variation obtained would be as indicated by the 'dashed' lines shown in Figure 7.15. It can therefore be deduced that the data of the M-C relationships:

(i) demonstrate a linear behaviour up to applied bending moment levels of 1.74 kNm and 1.45 kNm for S1 and S2 respectively, while

(ii) the stiffness thereafter approximates to a linear form, but actually depicts a gradual 'reduction' in stiffness.

These regimes are indicated in the aforementioned figures and have been defined symbolically by the definition K and K' respectively. The latter of these symbolic terms (expressed by (ii) above), therefore, actually have an asymptotic form, which is relative to the properties of the panel assuming a 'perfect' bi-linear behaviour.

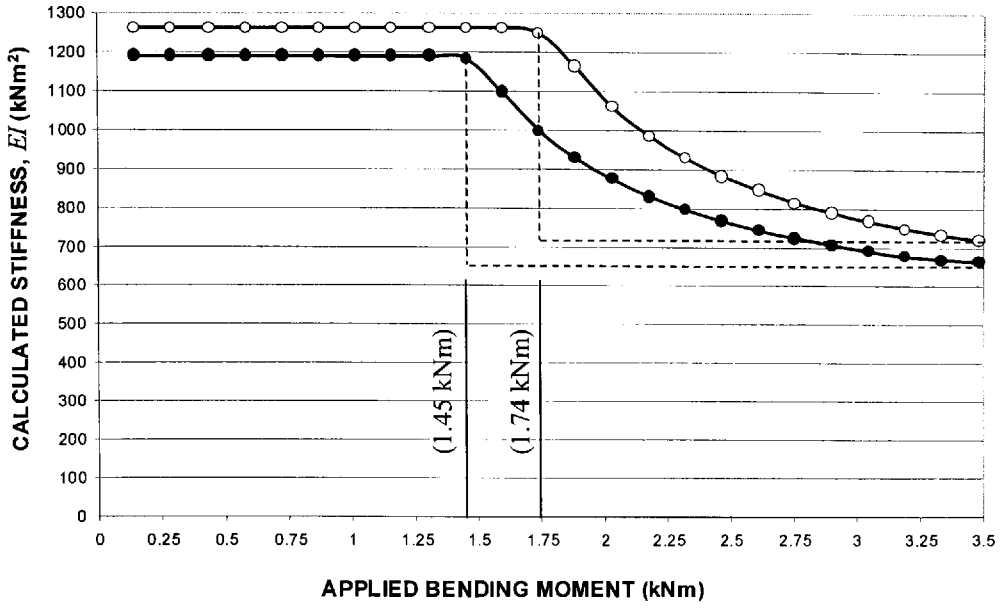

Key:

Calculated stiffness variation corresponding to:

—○— = Panel type S1

—●— = Panel type S2

--------- = Lines to illustrate the stiffness variation of the panels if the bi-linear relationships were strictly interpreted as assumed for the load / displacement behaviour of Figures 7.11 and 7.12 (See section 7.5.2).

Figure 7.15 – The calculated stiffness (*EI*) corresponding to the applied bending moment of each static load interval. Calculations based on the M-C relationship of Figure 7.14(a).

7.6 Processed Data from the Dynamic Tests

The data collected from the dynamic tests relate to the phase II panels identified previously. However, due to the consistency observed throughout the strain and displacement measurements used to compile the M-C relationships, the results of the dynamic tests are considered to be representative of all S1 and S2 panels.

7.6.1 The information presented

A large volume of dynamic response information was captured from the dynamic tests, from which a number of characteristics relating to the changing condition of the

panels through static load intervals were observed. Within the scheme of the test procedure outlined earlier, the number of response signals collected was as follows:

- Impact induced vibration = 3 signals for each load interval.
- Steady state force induced vibration = 3 tests per load interval (1 test for each of the excitation force-levels described earlier).
- Frequency sweep test = 3 tests per load interval (1 test for each of the excitation force-levels).

Using the information collected from these signals, the following is presented in this chapter:

(i) Natural frequencies calculated using a FFT of the measured impact and decay-of-vibration response signals.

(ii) Natural frequency and damping determined from a correlation of measured impact and decay-of-vibration signals with the calculated response assuming viscous characteristics (i.e. a visco-elastic model).

(iii) Natural frequency and damping determined from a correlation of measured and calculated FRFs, the latter being with the visco-elastic model.

(iv) Amplitude dependency of the panel natural frequency and damping.

(v) Non-linear frequency-dependent behaviour of the panels at high static load levels.

To consolidate (i) to (v) above, the main findings are presented in graphical form, while the associated data has been included in Appendix C. In addition, to avoid duplication, trends observed from the data that showed consistency within panel groupings have been displayed using typical results.

7.6.2 Normalisation of the response amplitudes

All impact, decay-of-vibration and steady-state frequency sweep response signals were recorded using a velocity transducer, sometimes called a 'geophone' (see chapter 3 for geophone specification). To rationalise the manner, in which the response information is presented, all measured signals have been normalised relative to a constant velocity value. Therefore, the response magnitude used for the normalisation was taken to be the largest velocity amplitude recorded from the frequency sweep tests. All other

response signals were then divided by this value producing data that was normalised relative to a peak value of "1".

This approach was chosen to demonstrate the consistency observed throughout the recorded signals, and to allow a convenient illustration of the amplitude dependency that was found in the panel frequency and damping results. It also ensured that the quality of the recorded responses could be assessed for consistency, with each normalised signal being an indication of vibration behaviour without necessarily being concerned with their response magnitudes. However, it is recognised that vibration amplitudes that are beyond the maximum value used may exhibit behavioural trends that are different to those observed and identified in this work. Therefore, the results presented in this chapter correspond to vibration amplitudes of less than (or equal to) 0.01 m/s (or approximately 0.04mm) at the centre span location. This amplitude level was calculated from the integration of the aforementioned velocity response signal (i.e. the maximum), which was achieved using a numerical algorithm prepared by BRE as part of the computer software suite used in other parts of this study.

7.6.3 The natural frequency and damping values determined from the impact and decay-of-vibration response signals.

7.6.3.1 Natural frequencies from a FFT of the measured response signals

The measured impact response and decay-of-vibration signals were used in conjunction with the FFT approach to determine the natural frequencies of the panels after each loading interval. The resolution of the autospectra achieved was 0.122 Hz, allowing the natural frequency of the panels to be defined to within ±0.061 Hz. Figure 7.16 shows samples of the measured response signals obtained from the panels, which are representative of impact and decay signals recorded from panel type S1. The figure also displays the peak amplitude of the response signals over a 50Hz bandwidth, which was calculated from the autospectra determined with the FFT algorithm. The single peak that is seen signifies the dominant response amplitude, from which the natural frequency of the panel was determined. Examining the spectral response over larger bandwidths also indicated the single peak as shown, which was seen to be a characteristic of all autospectra results. Based on this evidence, it is reasonable to

assume that the signals represent dynamic characteristics of the panels that relate to the lowest mode of vibration only, i.e. the fundamental mode having its maximum vibration amplitude at the mid-span of the panel.

However, a number of signals were found to be inconsistent with this clear, single mode dominance, displaying instead a spectral density with many amplitude peaks. These 'noisy' signals corresponded mainly to panel type S2 at load intervals close to failure of the panels. These signals were considered to be of insufficient quality for inclusion in the study, as it was difficult to identify the spectral peaks associated with the natural frequency of the panel, and were therefore removed from the data set.

7.6.3.2 Natural frequency and damping from the correlation of measured and calculated decay-of-vibration response

To take advantage of the single mode behaviour identified above, the natural frequency and damping was determined by correlating measured and calculated response values. The procedure adopted to achieve the correlation made use of the software obtained from BRE, which yielded the required data from a comparison of measured and calculated free-vibration response. To ensure that a consistent set of results was achieved, the correlation was performed over a fixed 2 seconds region (2000 data points) of the measured signals. In addition, the amplitude of vibration chosen to represent the start point for correlation was chosen to be similar of all signals, thereby ensuring that the determined dynamic characteristics were relative to a constant amplitude value.

7.6.3.3 Compiled natural frequency and damping values

The natural frequency and damping percentage determined with the methods identified above have been compiled and shown in Figures 7.17 and 7.18 respectively. The results are presented in two ways, (i) relative to the values as calculated, and (ii) in a normalised form, which provides an indication of frequency and damping change with each successive interval of the static load tests.

7.6.4 Natural frequency and damping from the correlation of measured and calculated frequency response functions

A sample of the 'frequency sweep' test data, together with an indication of the accuracy to which the calculated visco-elastic model represents the measurements, is given by Figure 7.19. The figure demonstrates the general trend that was observed throughout the entire 'frequency sweep' tests, which clearly reveals the behavioural changes of the panel through each interval of the static loading.

The natural frequency and damping percentage calculated from all panels is shown in Figures 7.20 to 7.23, which are displayed relative to the three excitation-force-levels used to obtain the results (see section 7.3.6). These figures have been prepared using the previously mentioned normalised scale, and illustrate the changes that occurred to the panels with increased static load.

7.6.5 Amplitude dependency of natural frequency and damping

The decision to study three excitation force-levels was made to allow the natural frequency and damping of the panels to be evaluated over a fixed amplitude range. Figures 7.20 to 7.23 clearly show that these properties are dependent on the magnitude of the vibration amplitude. In general terms, the information appears to indicate that the excitation force-level influences the rate-of-change of the natural frequency and damping.

To explore these findings in greater detail, further analysis was carried out to establish if a similar amplitude dependent behaviour was embodied in a single vibration event, for which the impact and decay-of-vibration signals were re-considered. To ensure that these results were consistent and relative to those described previously, the refined analysis concentrated on the same regions of the aforementioned response signals (i.e. relative to the maximum normalised amplitudes described earlier). However, instead of treating a total time period of 2 seconds, the frequency and damping was determined corresponding to a time segment of 0.2 seconds (200 data points in each segment). The result is a set of ten frequency and damping values that relate to smaller regions of the signals. Therefore, if the dynamic behaviour of the panels was

dependent on the amplitude of vibration, then the individual frequency and damping values within the response of each individual signal were expected to indicate a change.

Figures 7.24 to 7.27 show the results of the refined analysis, which illustrate that the natural frequency and damping values become progressively more amplitude dependent as the static load intervals increase. To facilitate a convenient interpretation of the results, the frequency and damping have been given as ratios of values calculated from the regression lines of Figures 7.17 and 7.18, corresponding to the 'zero' loading point, (i.e. before the application of any load). Therefore, a frequency or damping ratio of "1" indicate the respective values for the panels in a pristine condition, deviations from which are indicative of the changes that occur as a result of the applied bending moment.

Figures 7.28 and 7.29 emphasis these changes with a series of 'surfaces' that display collectively the results of Figures 7.24 and 7.25 and Figures 7.26 and 7.27 respectively. These 'surface plot diagrams' have been compiled using the regression lines illustrated on the aforementioned figures, symbolising the trends observed throughout all the measured response signals.

7.6.6 Frequency-dependent behaviour observed in the measured frequency sweep data

In addition to the amplitude dependency found to exist in the natural frequency and damping results, the data from frequency sweep tests also indicate that the frequency response of the panels change as the static load level increases. Figures 7.30(a) to (c) display samples of the measured FRFs to demonstrate generally the findings. The main observations of the aforementioned figures are:

(i) The FRFs show a near perfect correlation to the visco-elastic model for all three excitation force-levels when the panel condition was pristine.

(ii) As the static load intervals increase, the measured FRFs appears to deviate away from the calculated visco-elastic relationship. However, as Figure 7.30(b) and (c) illustrate, the amount of deviation appears to depend on the excitation force-level considered.

7.6.7 Mode shape profiles determined from measured response signals

A sample of the fundamental mode shape is shown in Figure 7.31, which was taken from a typical S1 panel. However, to yield information that can be used as a measure of possible mode shape change, which could be present in the data recorded after each successive load interval, an alternative method of data presentation has been adopted.

The Modal Assurance Criteria (MAC) has already been identified as a means of assessing the degree of correlation between two mode-shape data sets. Similarly, in the context of damage evaluation, the MAC is a valid method of quantifying the difference that may exist between mode shapes taken from a pre and post-damage structure. To maximise the information available from the recorded data, but eliminating the need to scrutinise the mode shape profiles on an individual basis, the MAC values have been calculated relative to the mode shape of the panel determined from the data at 'zero' load. Therefore, a MAC value of "1" describes a mode shape matching that from the panel in a pristine condition, while values that are less than this represent change. The larger the deviation, the greater the difference between the mode shapes, which in turn could be indicative of changes occurring to the panels as a result of the applied bending moment. Figure 7.32 illustrates the calculated MAC values for all the phase II tested panels.

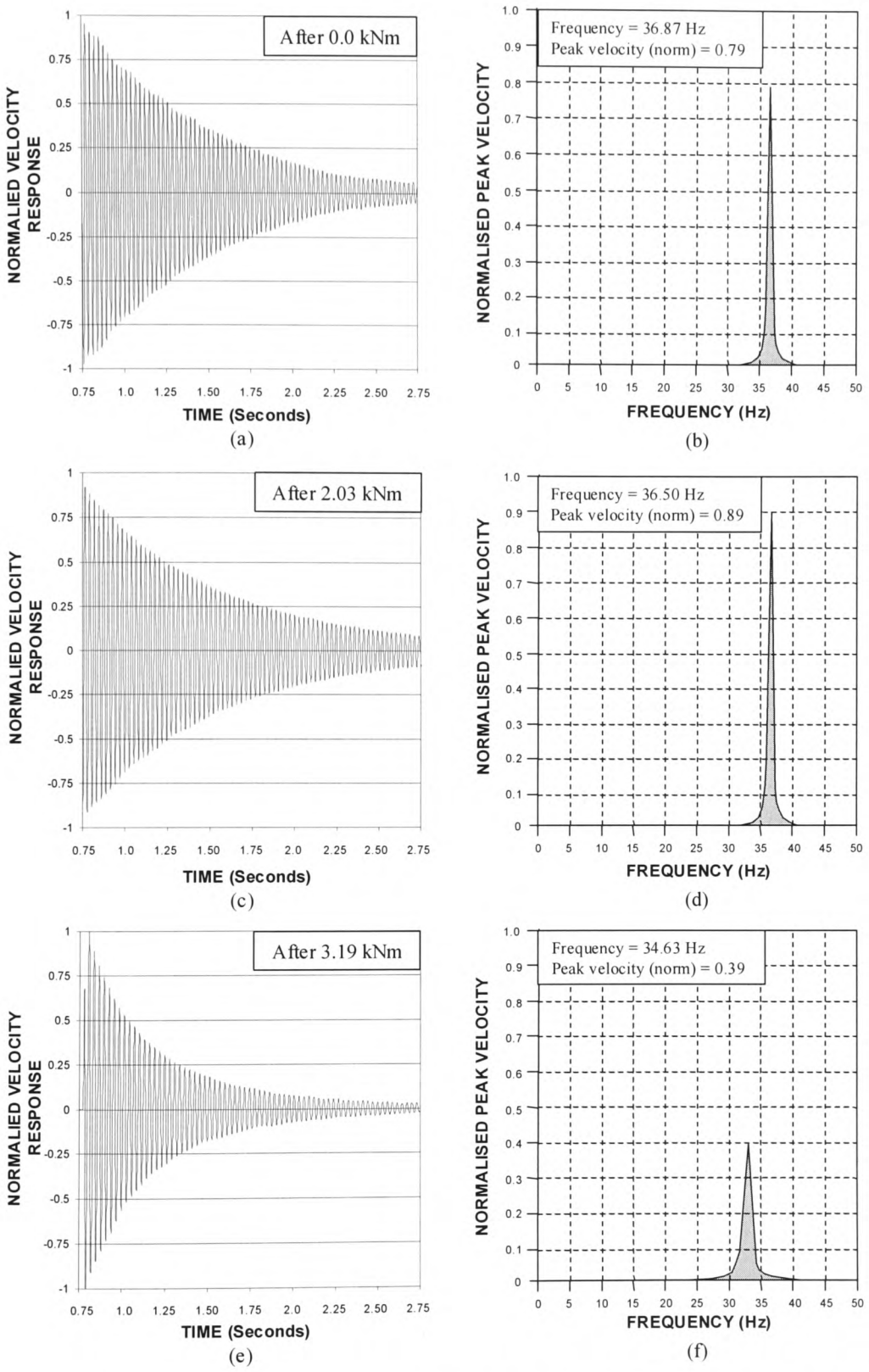

Figure 7.16 – Sample response signals showing the recorded time dependent data together with the associated frequency content obtained after an applied bending moment of (a)+(b) zero, (c)+(d) 2.03 kNm, and (e)+(f) 3.19 kNm

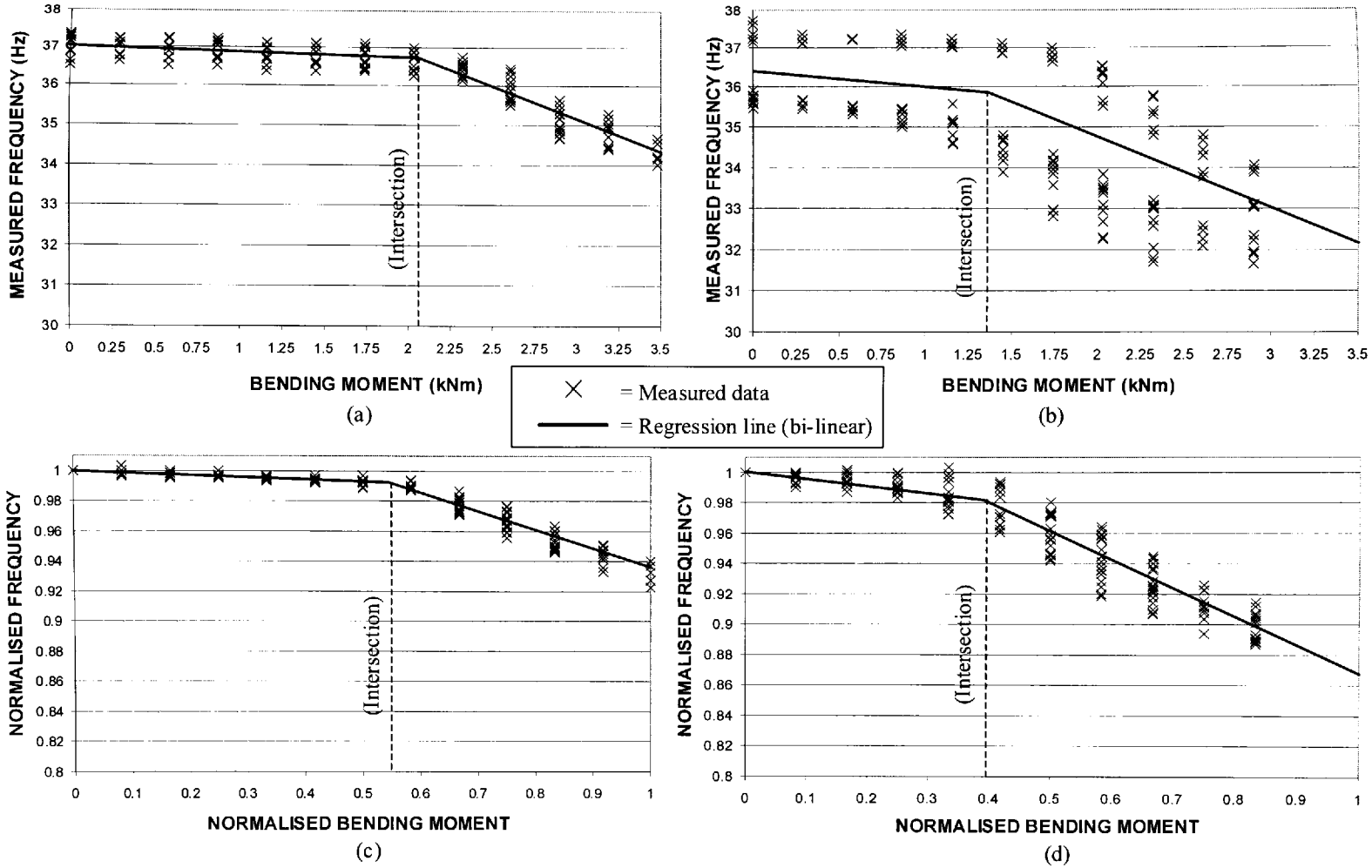

Figure 7.17 – Natural frequency obtained from the impact and the decay-of-vibration signals for (a)+(c) panel type S1, and (b)+(d) panel type S2. The bi-linear regression lines show the approximate trend of the presented data, the intersection of the lines being identified.

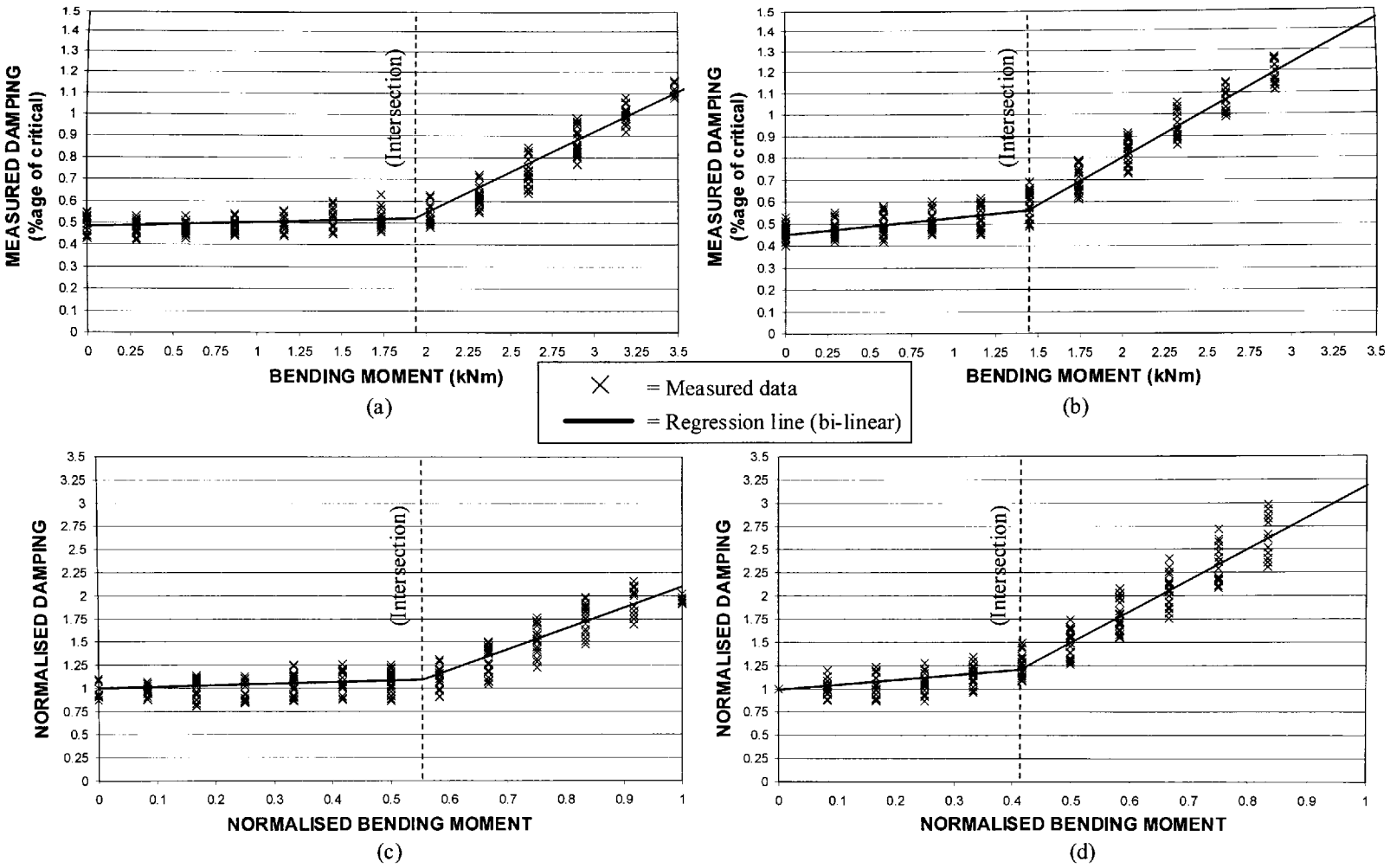

Figure 7.18 – Damping obtained from the impact and decay-of-vibration signals for (a)+(c) panel type S1, and (b)+(d) panel type S2. The bi-linear regression lines show the approximate trend of the presented data, the intersection of the lines being identified.

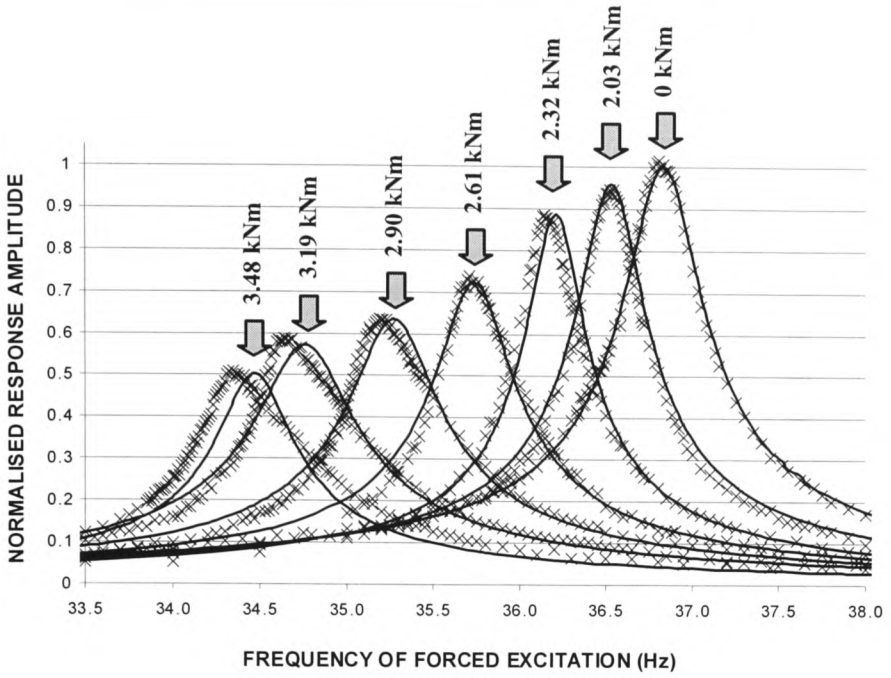

(a)

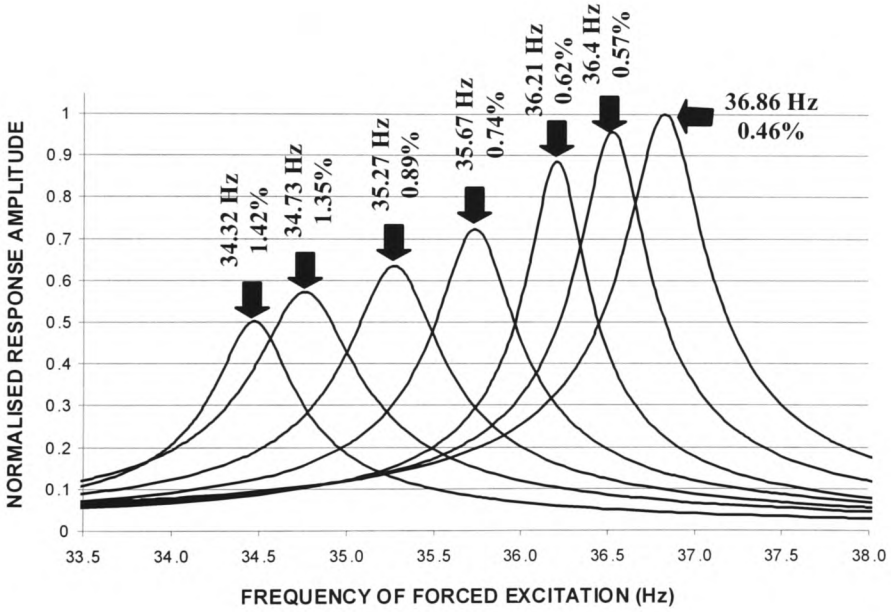

(b)

Key:

× = Measured data

= 'Best-fit' visco-elastic relationship.

= Bending moment applied to the panel before the response readings were take

= Calculated natural frequency (Hz) and percentage of critical damping (%) determined from the correlation.

Figure 7.19 – Sample 'frequency sweep' data showing the change observed to the measured FRF at each static load interval (type S1 shown). Data corresponding to applied bending moment levels of between 0.29kNm and 1.74kNm have been removed for clarity.

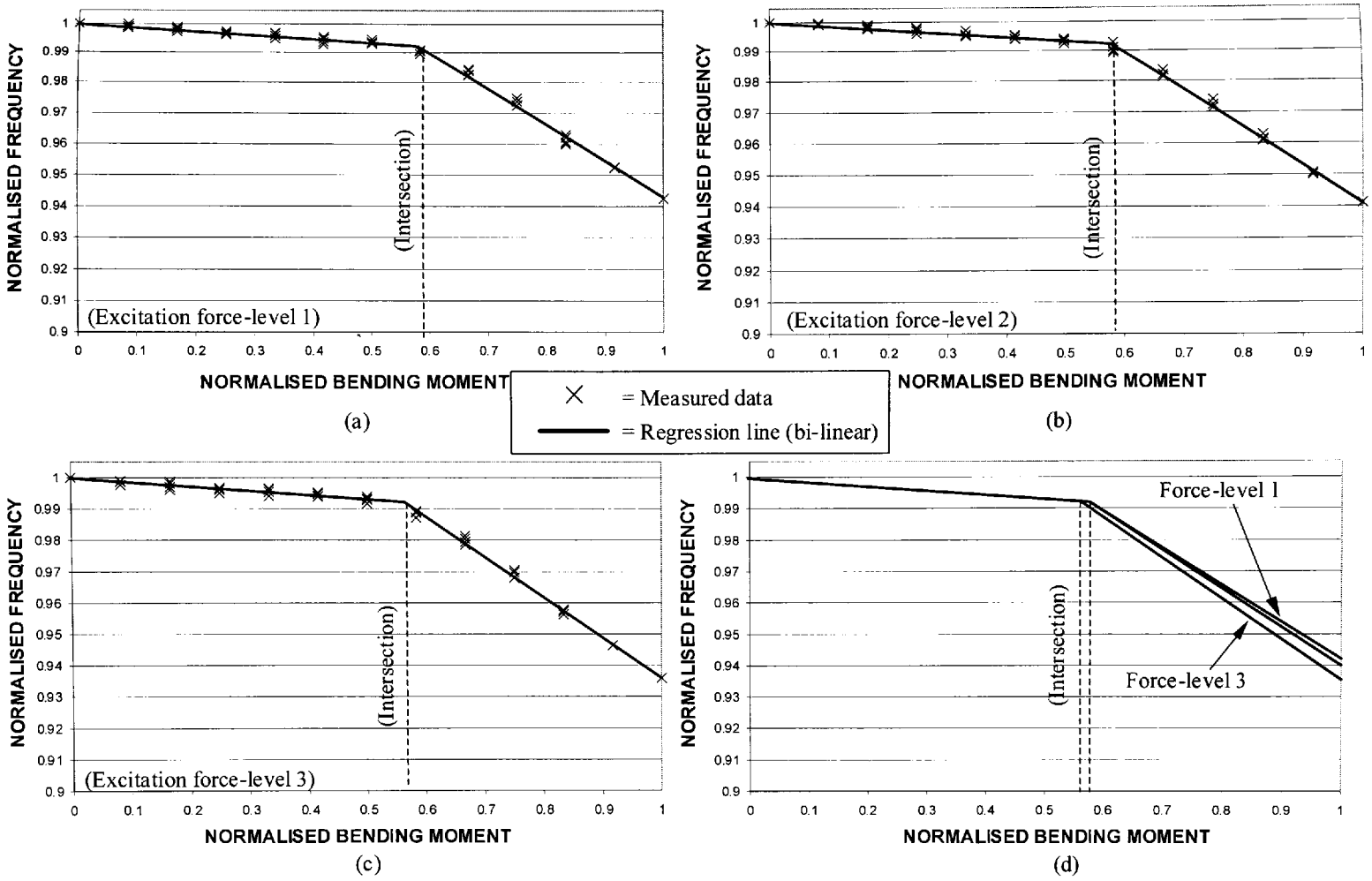

Figure 7.20 – Natural frequency obtained from the frequency sweep tests for panel type S1 showing the results in a normalised form with data recorded using excitation force-level (a) 1, (b) 2, (c) 3, while (d) gives a comparison of the various force-levels.

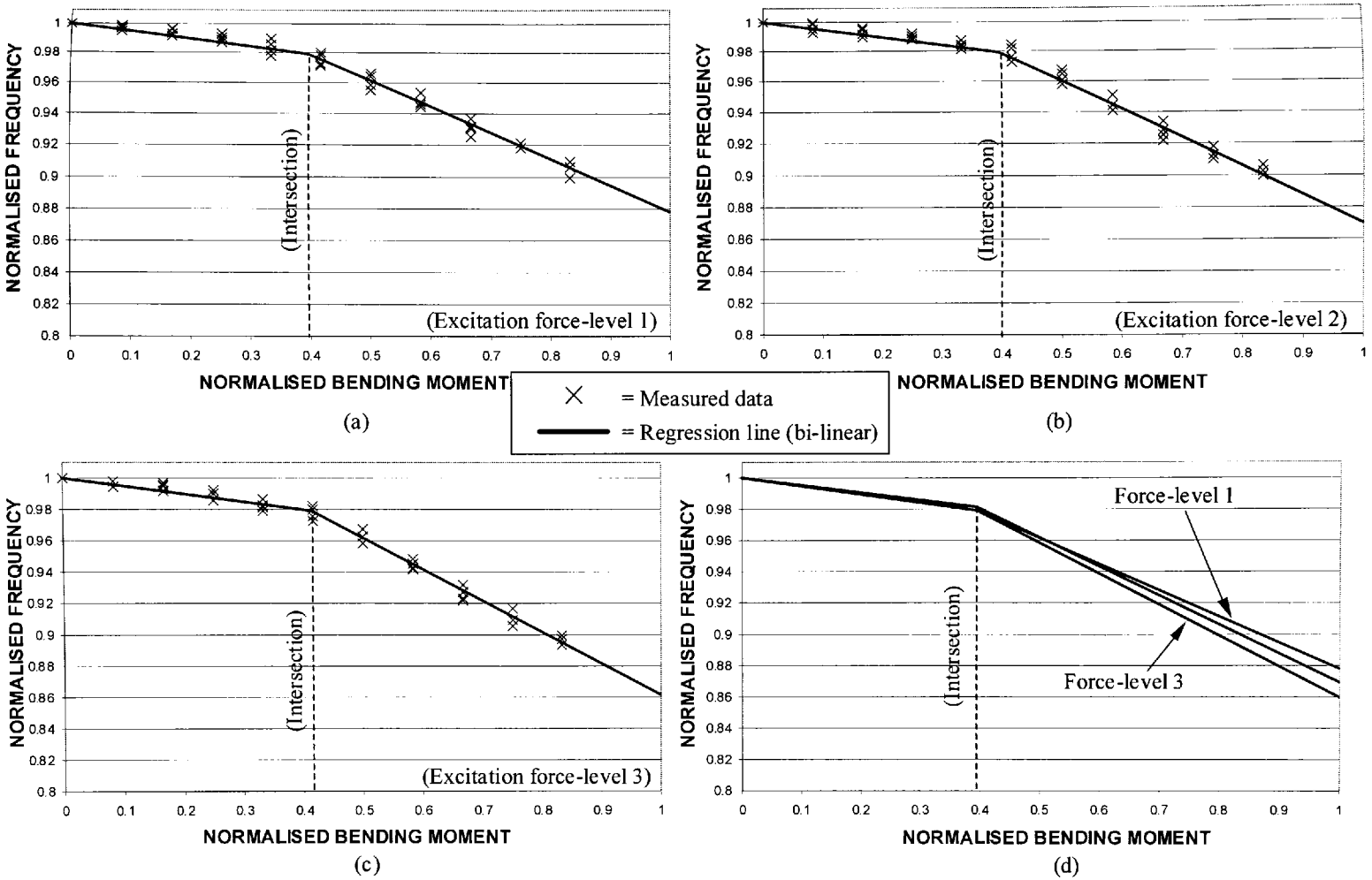

Figure 7.21 – Natural frequency obtained from the frequency sweep tests for panel type S2 showing the results in a normalised form with data recorded using excitation force-level (a) 1, (b) 2, (c) 3, while (d) gives a comparison of the various force-levels.

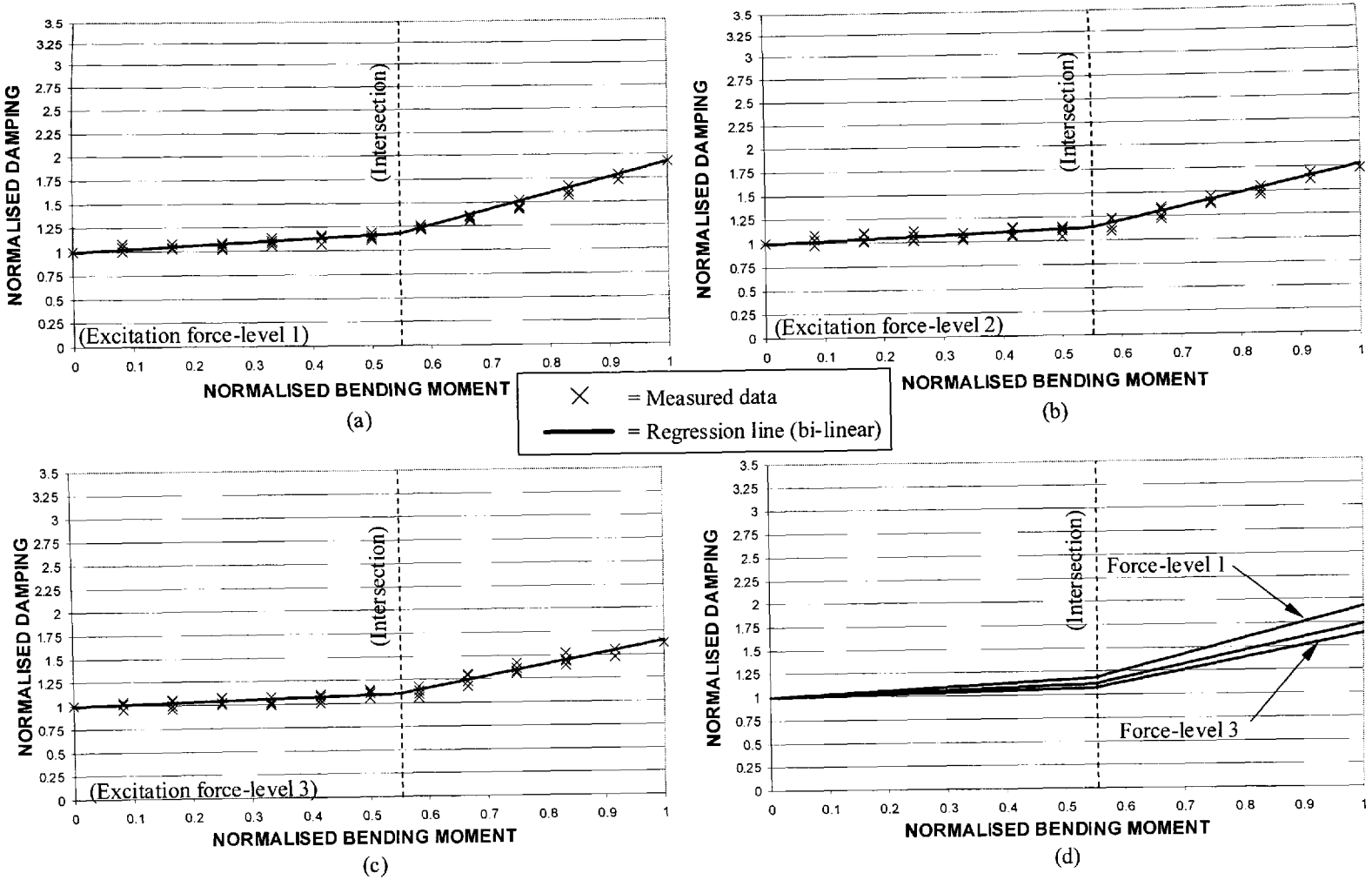

Figure 7.22 – Damping obtained from the frequency sweep tests for panel type S1 showing the results in a normalised form with data recorded using excitation force-level (a) 1, (b) 2, (c) 3, while (d) gives a comparison of the various force-levels.

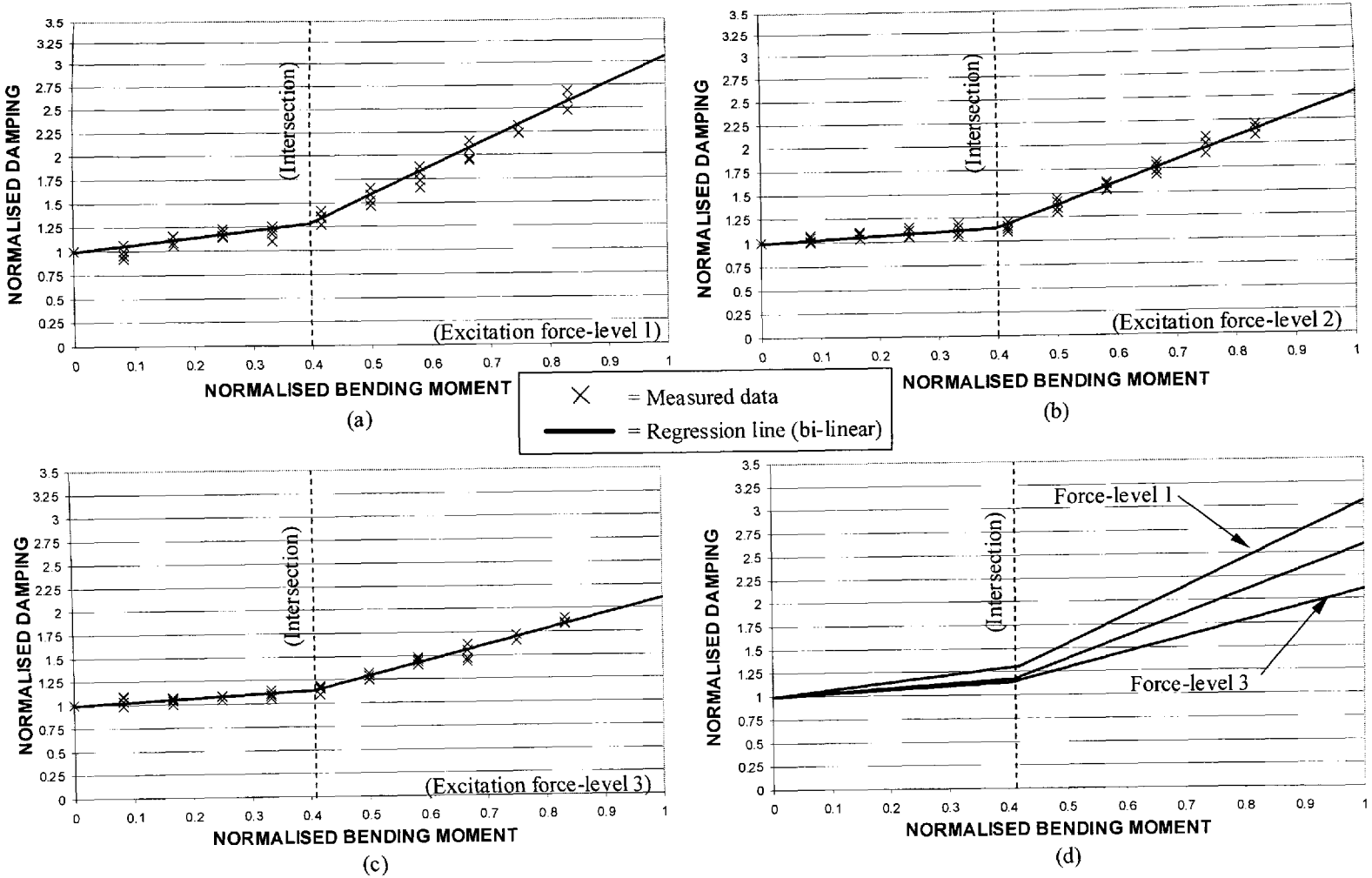

Figure 7.23 – Damping obtained from the frequency sweep tests for panel type S2 showing the results in a normalised form with data recorded using excitation force-level (a) 1, (b) 2, (c) 3, while (d) gives a comparison of the various force-levels.

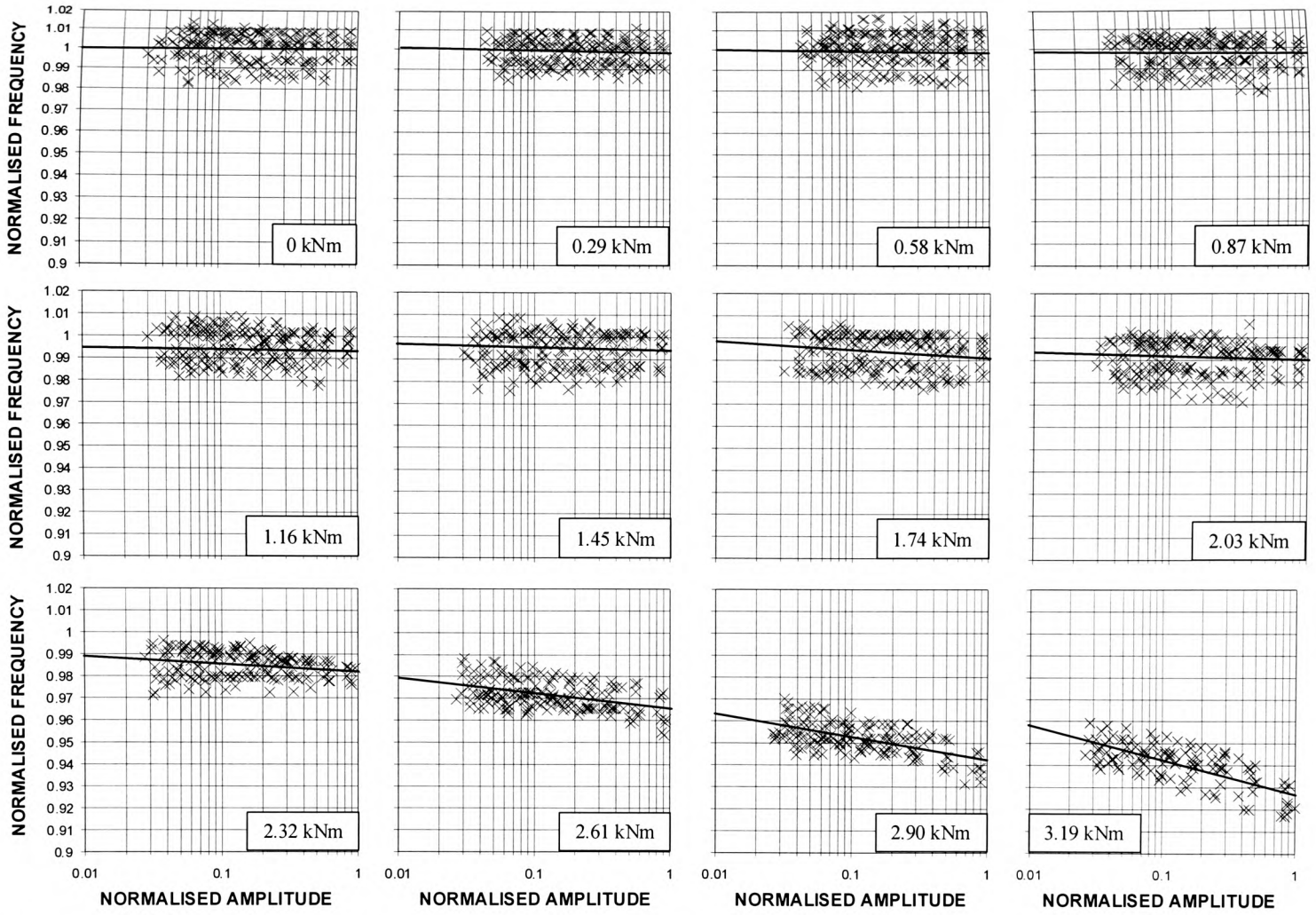

Figure 7.24 – Amplitude dependence of normalised frequency shown for panel type S1. The bending moment values shown represent the level applied to the panel before the response signals were taken. The solid lines indicate the principal trends.

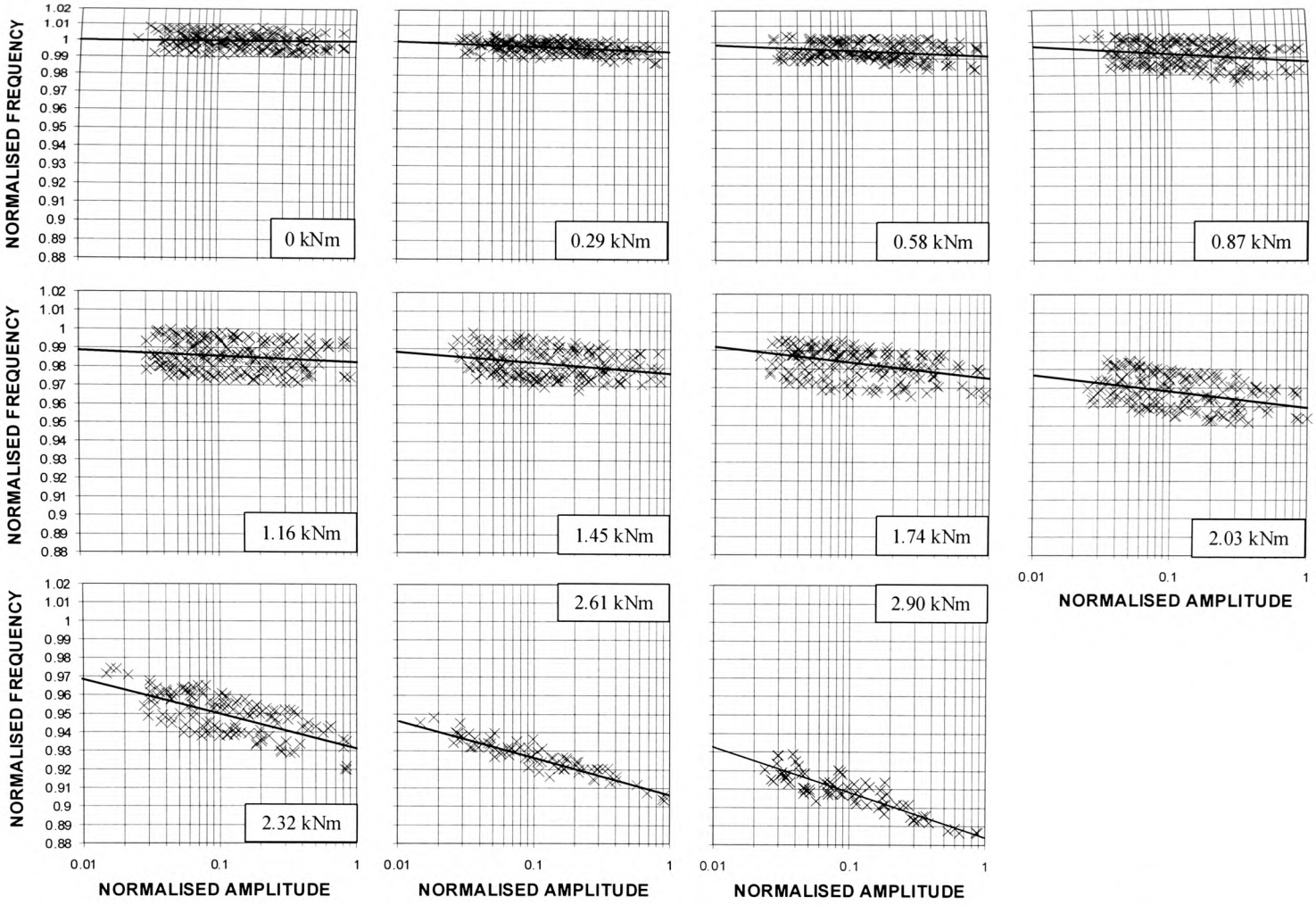

Figure 7.25 – Amplitude dependence of normalised frequency shown for panel type S2. The bending moment values shown represent the level applied to the panel before the response signals were taken. The solid lines indicate the principal trends.

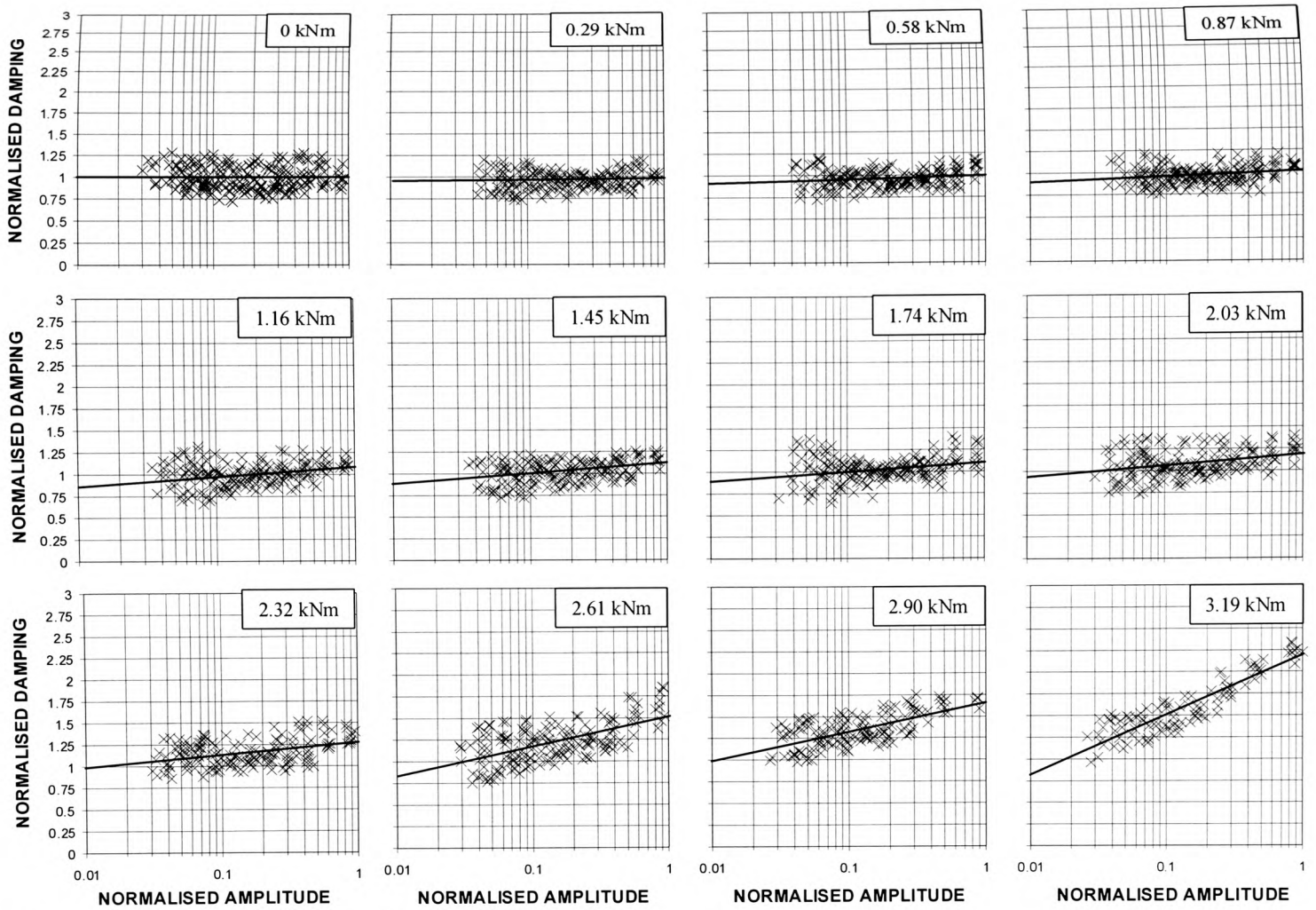

Figure 7.26 – Amplitude dependence of normalised damping shown for panel type S1. The bending moment values shown represent the level applied to the panel before the response signals were taken. The solid lines indicate the principal trends.

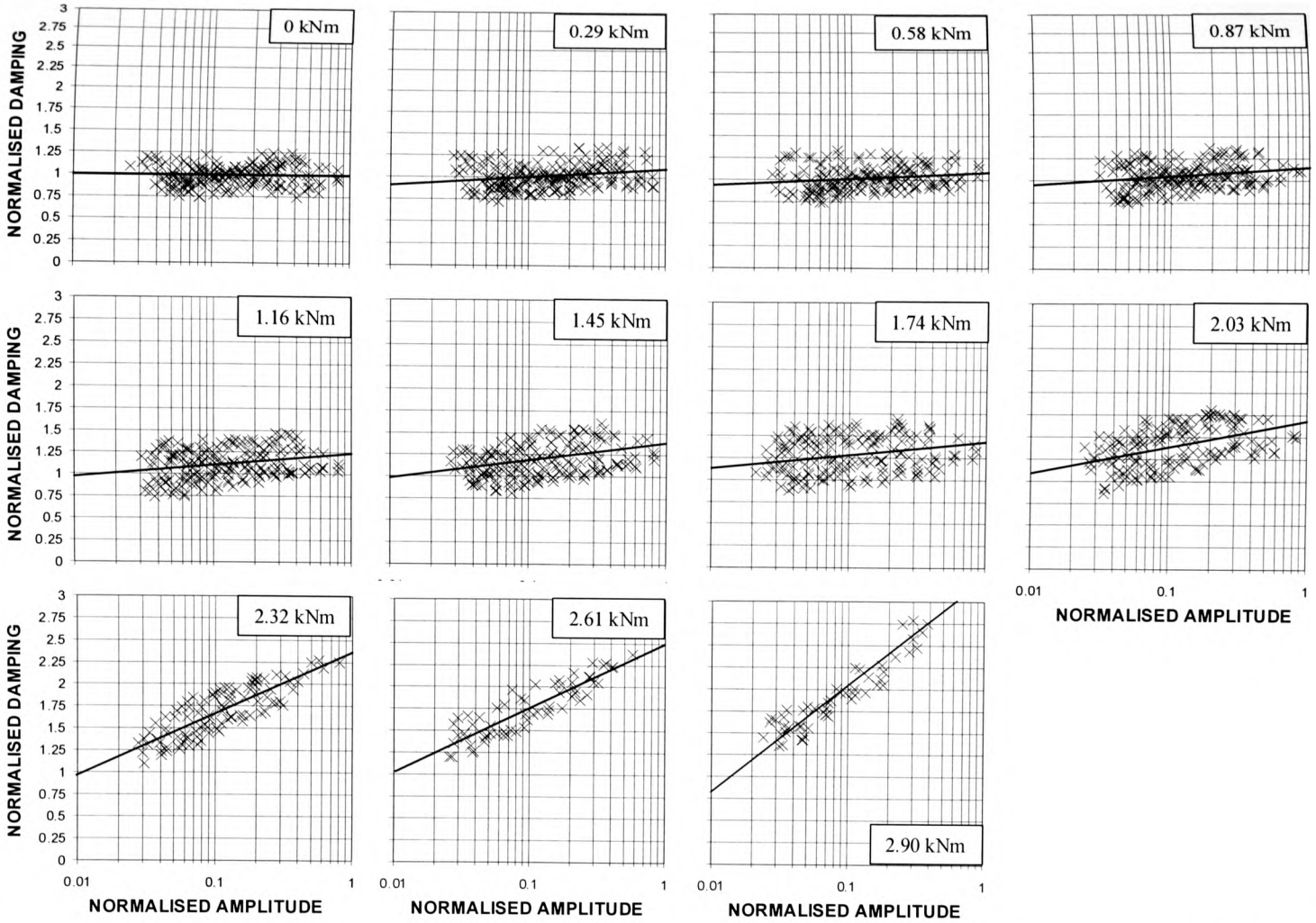

Figure 7.27 – Amplitude dependence of normalised damping shown for panel type S2. The bending moment values shown represent the level applied to the panel before the response signals were taken. The solid lines indicate the principal trends.

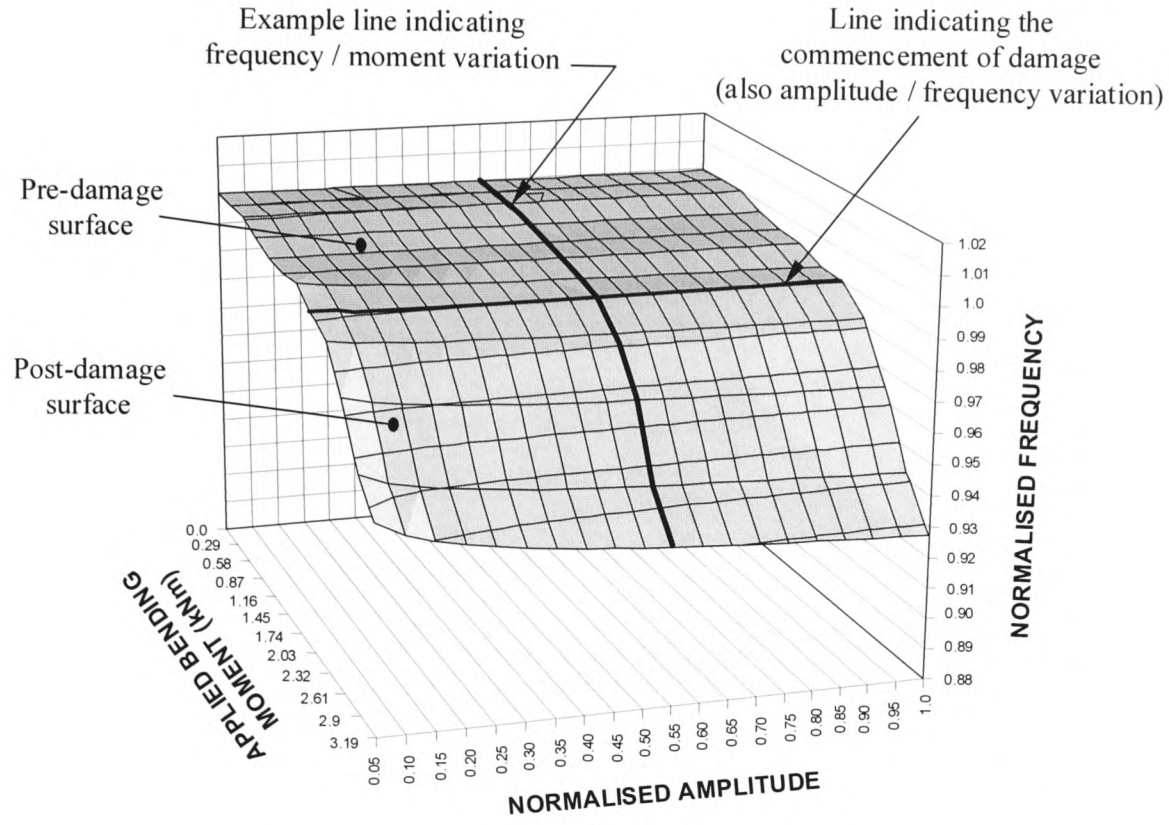

(a)

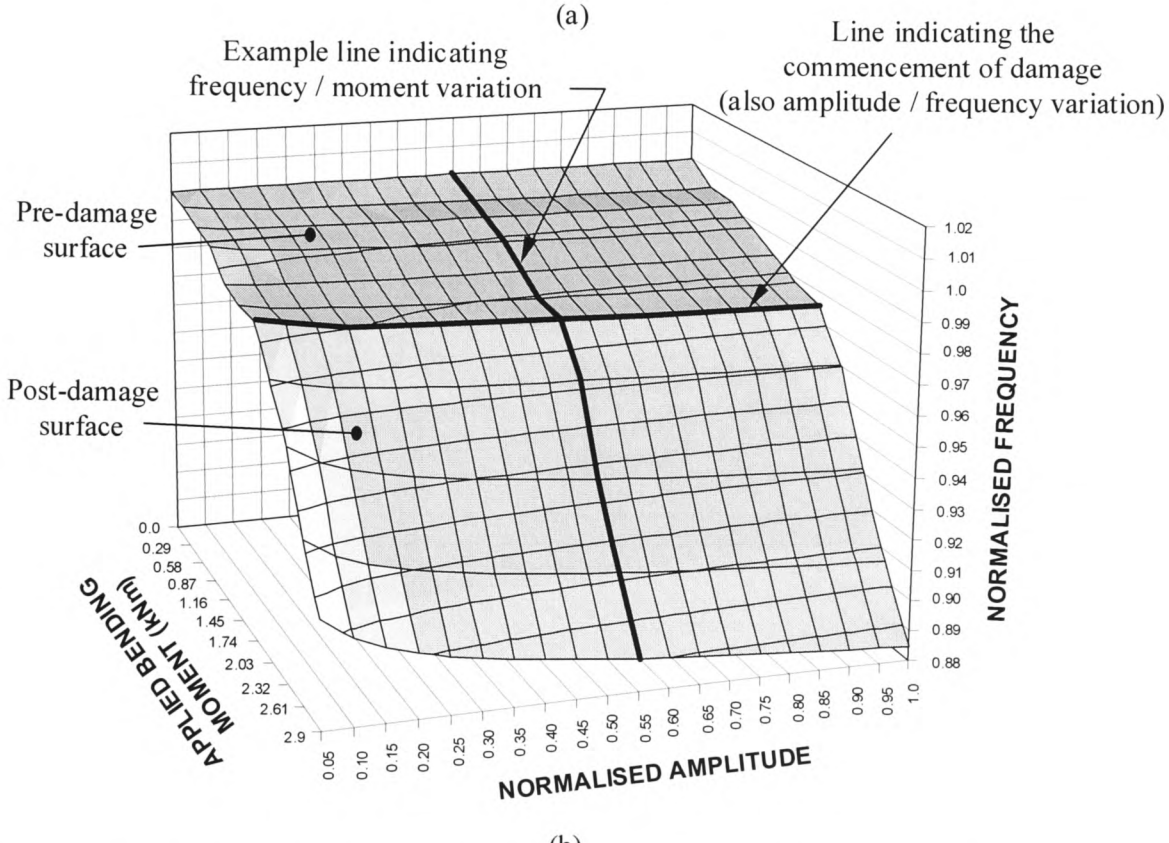

(b)

Figure 7.28 – Surface plot diagram showing the natural frequency variation observed from the measured response signals for panel type (a) S1, and (b) S2.

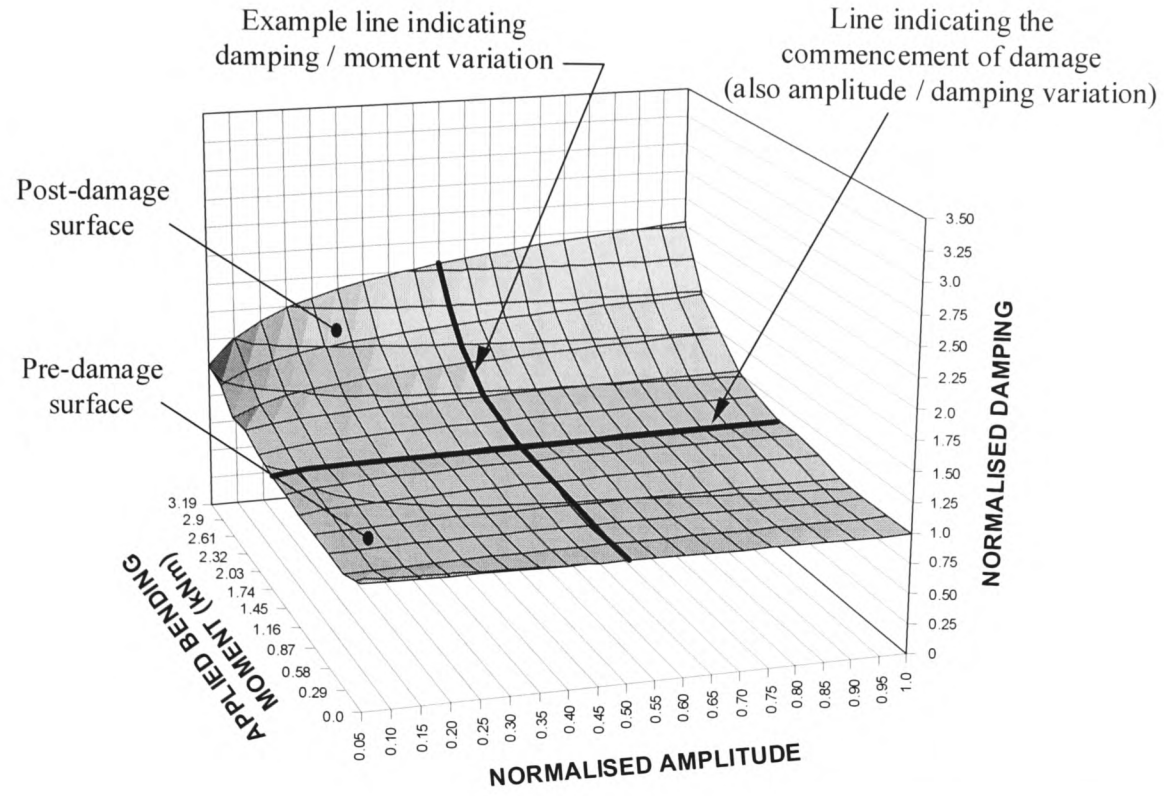

(a)

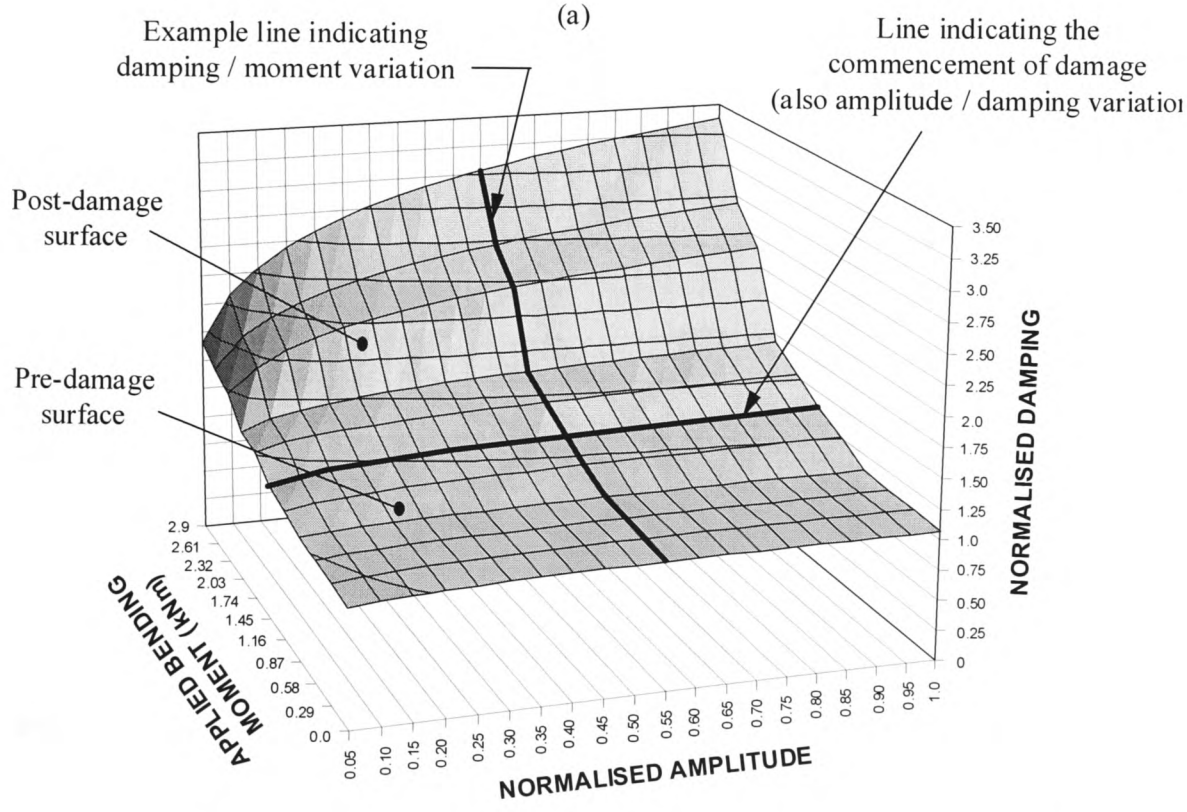

(b)

Figure 7.29 – Surface plot diagram showing the damping variation observed from the measured response signals for panel type (a) S1, and (b) S2.

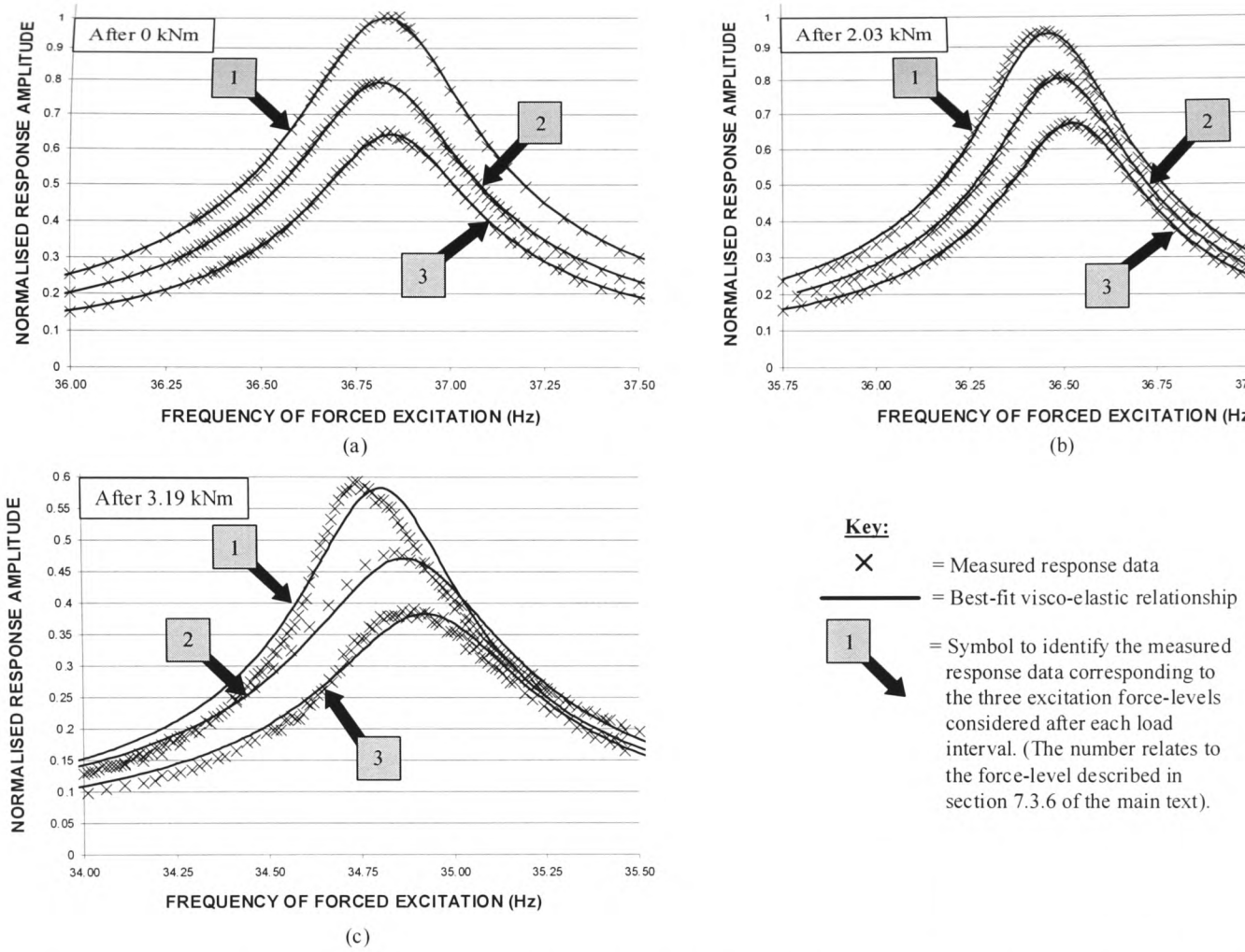

Figure 7.30 – Illustration of the frequency dependence of the FRFs observed from the frequency sweep data that was recorded after (a) 0 kNm, (b) 2.03 kNm, and (c) 3.19 kNm of applied bending moment. (Panel type S1 shown).

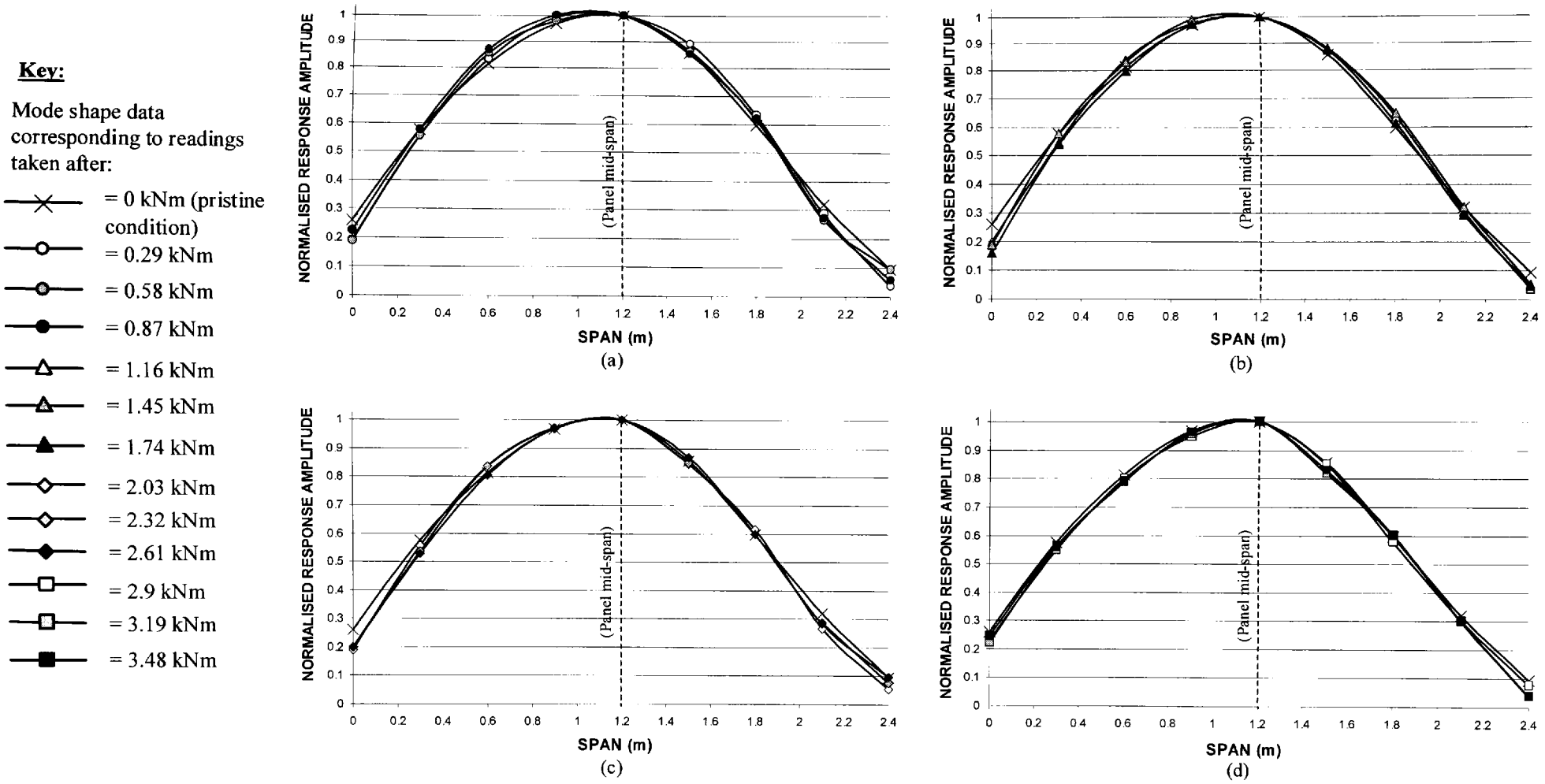

Figure 7.31 – Sample mode shape profiles (panel type S1 shown) corresponding to measurements taken after (a) 0.29 kNm to 0.87 kNm, (b) 1.16 kNm to 1.74 kNm, (c) 2.03 kNm to 2.61 kNm, and (d) 2.9 kNm to 3.48 kNm applied bending moment.

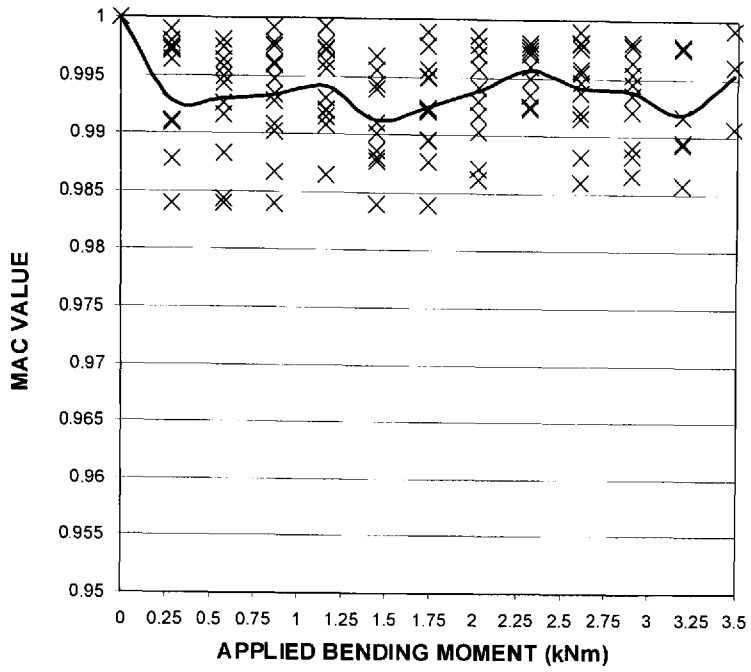

(a)

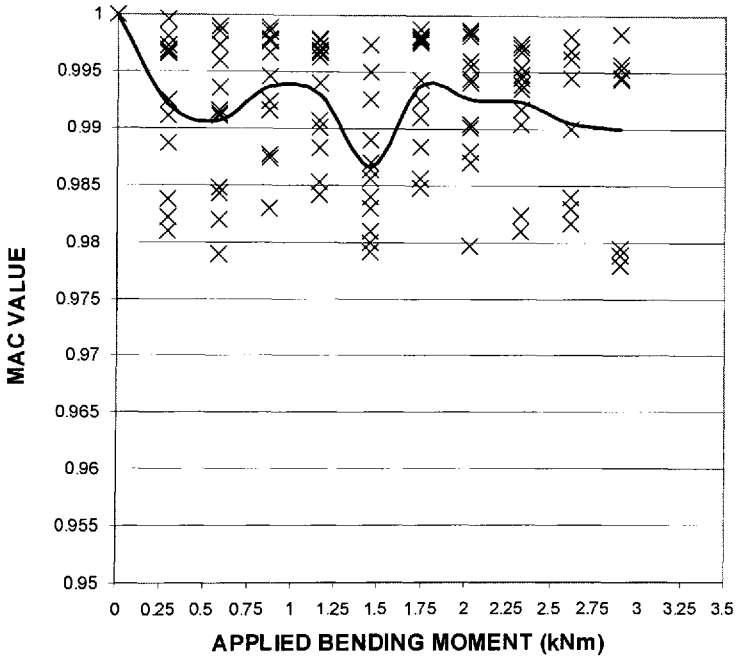

(b)

Key:

× = MAC values calculated using the mode shape data obtained after each loading interval.

— = Line connecting the arithmetic mean of the MAC values at each load interval.

Figure 7.32 – Modal Assurance Criteria (MAC) values calculated using the mode shape data established from the measured data recorded after each loading interval for panel types (a) S1, and (b) S2.

7.7.2 Possible cause of the observed stiffness reduction portrayed by the moment-curvature relationships

The behaviour typified by the M-C relationships is characteristic of that observed from similar static load tests conducted on reinforced concrete members by Yang (1996). This study found that cracking of the concrete in the tensile regions of reinforced members could be identified from changes observed in the M-C relationship – even at low tensile strain levels. It is feasible that the data collected from the composite panels demonstrate a comparable behaviour, with concrete cracking being the cause of the stiffness changes seen (Figure 7.14). Assuming that the changes are due to concrete cracking alone, it is possible that the stiffness reduction, or 'degradation' (Figure 7.15), is due wholly to the gradual cracking of the concrete in the tensile region of the panels, the severity of which increases with subsequent load intervals. Therefore, for convenience and clarity in future discussions of this chapter, the loading range corresponding to constant stiffness will be referred to as "pre-cracking", while subsequent stages shall be termed "post-cracking". The dividing point of these behavioural trends thus being defined as the 'first-cracking' point.

However, it is appreciated that the 'post-cracking' behaviour may be influenced by other mechanisms, such as loss of bond between the steel and concrete parts of the panels, and as such will require additional clarification (dealt with in chapter 8).

7.7.3 Interpreting the observed stiffness change as a form of structural damage

The processed M-C relationships offer an ideal basis from which to examine the sensitivity of the measured frequency and damping changes for use as damage identification variables. Treating the post-cracking behaviour as being indicative of progressive damage provides a quantitative measure against which dynamic properties can be related. However, this does not suggest that the cracking of concrete, which occurs normally to a certain extent in reinforced members, is itself damage, but it merely allows the results that have been obtained from dynamic tests to be qualified relative to an established set of physical parameters.

7.7.4 Quantitative comparison of damage extent against the observed natural frequency and damping changes

Figures 7.17(c)+(d) and 7.18(c)+(d) can be regarded as trends that portray the general rate-of-change of the dynamic properties through staged loading, as they were calculated with no regard to their possible amplitude dependence. This information could thus be treated as symptomatic of overall changes occurring to the panels during progressive damage. Figures 7.33 and 7.34 show these natural frequency and damping trends relative to the stiffness (*EI*) calculated from the M-C relationships (Figure 7.15). To enable the dynamic property changes to be assessed quantitatively, the stiffness values have been normalised, thereby defining the un-damage panels with the index "1". The main features observed from these figures are discussed below.

Natural frequency changes:

(i) Between 100% (pristine condition) and 75% stiffness, the natural frequency of the panels reduced to 99% and 97% of the undamaged values for S1 and S2 respectively.

(ii) As degradation of the panels continues beyond the 75% stiffness point, there is a definite increase in the rate-of-change of the natural frequency value. The regression lines included on the aforementioned figures clarify the observed trend, where the frequency at the threshold of panel failure reduces to approximately 93% and 90% of the un-damaged value for S1 and S2 respectively.

Damping-value changes:

(i) Between 100% and 75% stiffness, the panel damping increases by approximately 20% and 35% for S1 and S2 respectively.

(ii) Thereafter, the rate of damping change increases with the values close to failure being approximately 110% (S1) and 170% (S2) higher than those determined for the panels in a pristine condition.

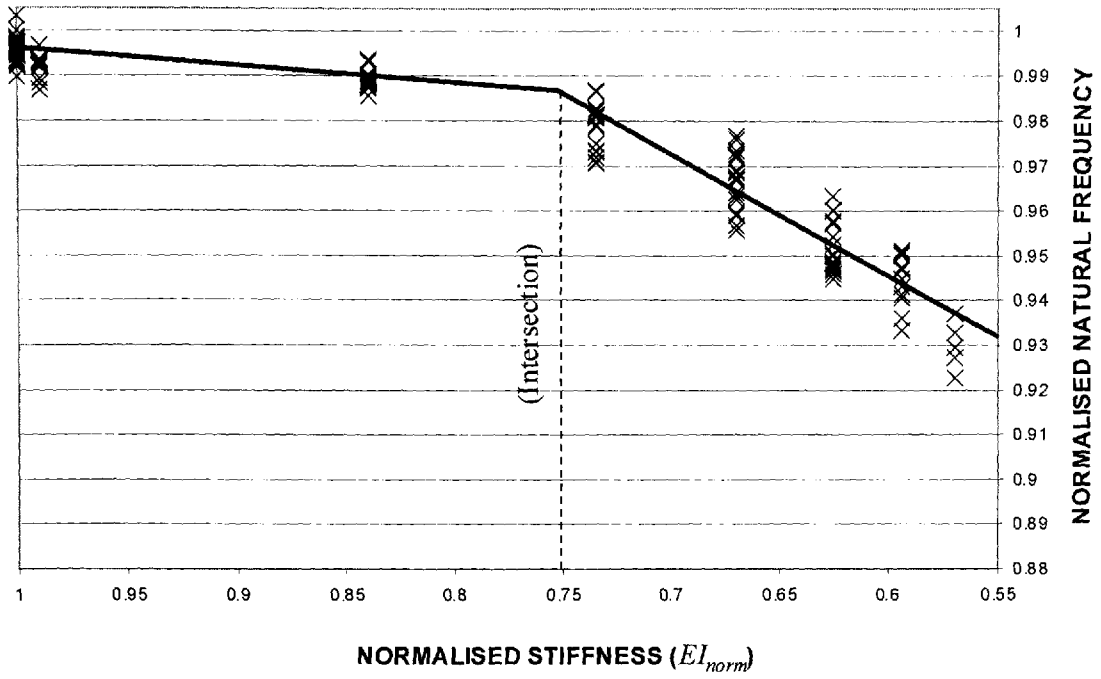

(a)

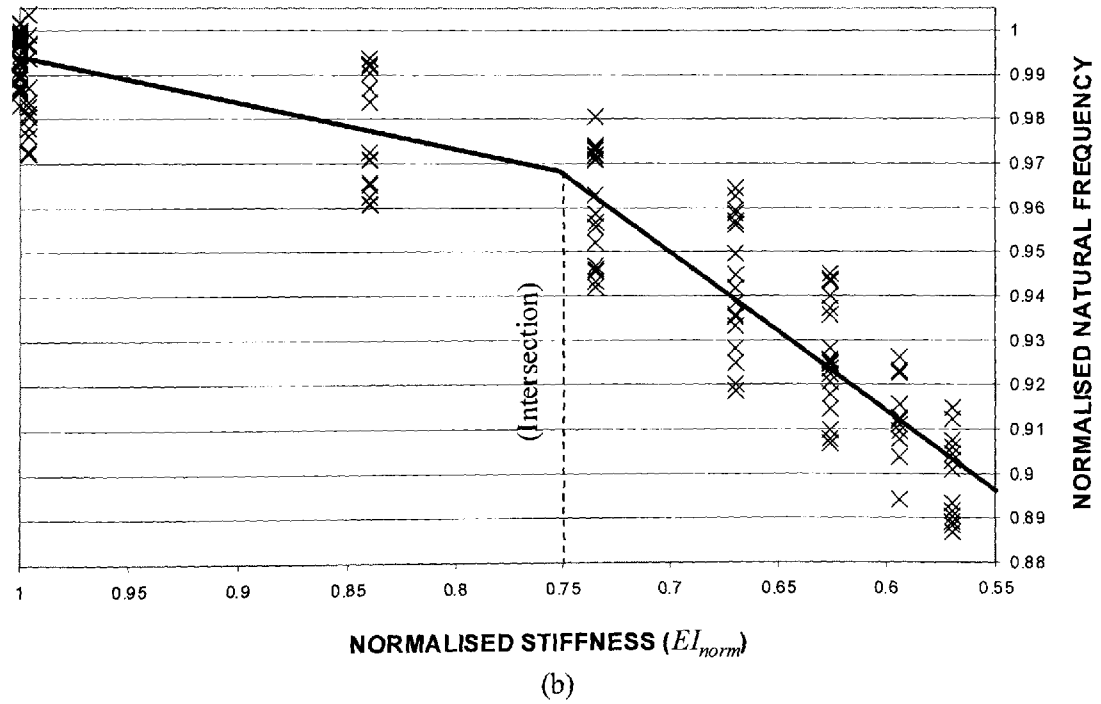

(b)

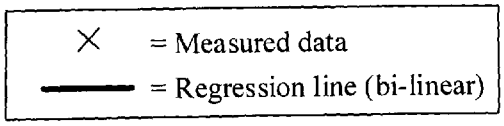

Figure 7.33 – Comparison between the natural frequency obtained from measurements and the calculated stiffness from the M-C relationships using a normalised scale for panel type (a) S1, and (b) S2.

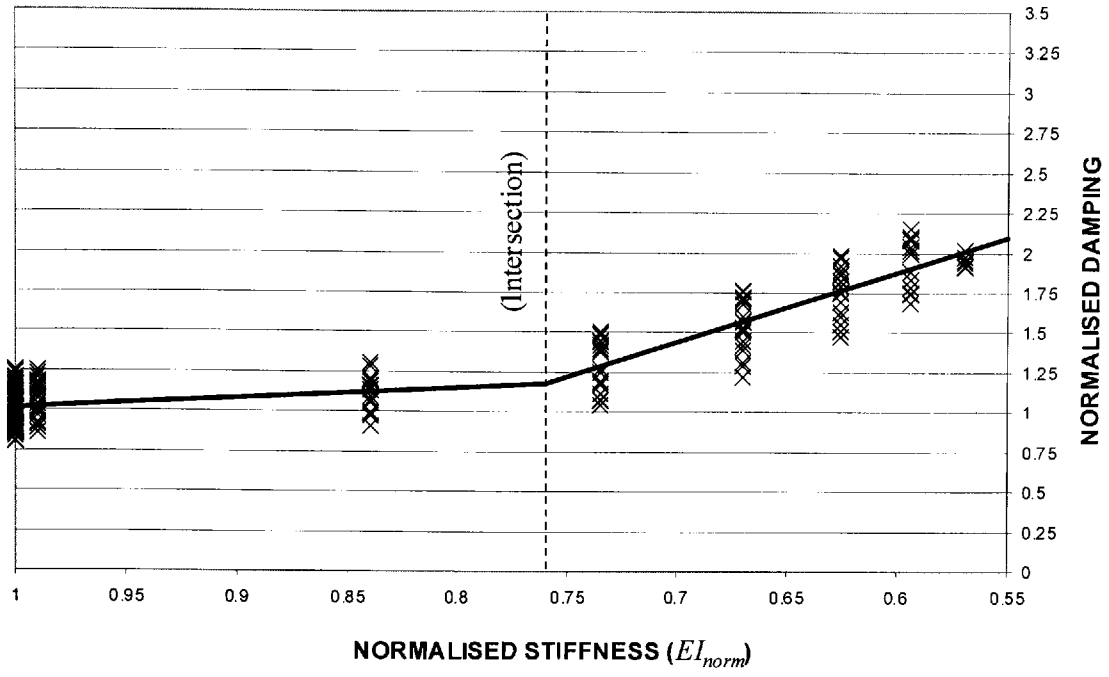

(a)

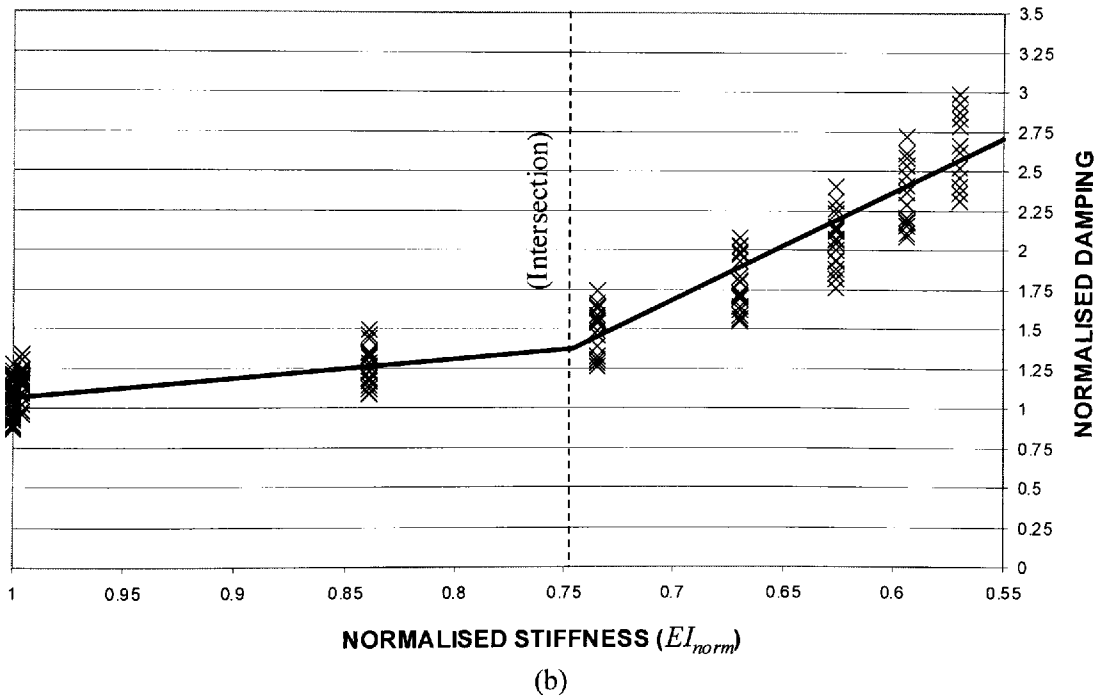

(b)

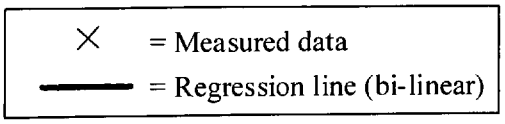

Figure 7.34 – Comparison between the damping obtained from measurements and the calculated stiffness from the M-C relationships using a normalised scale for panel type (a) S1, and (b) S2.

7.8 Concluding Remarks

7.8.1 Using natural frequency to detect damage in the panels

For the purposes of the study, the structural changes were introduced in a controlled manner using static load allowing strain and displacement data to be recorded. This data can be interpreted as a benchmark of the panel behaviour, with which the dynamic properties could be compared.

Comparing the M-C relationships (Figure 7.14) with the natural frequency results (Figure 7.17) it is found that the point at which 'first-cracking' of the panels occurred coincided with an increased rate-of-change of frequency drop for both panel types. Therefore, the degradation that occurred as a result of the applied loading sequence was also reflected in the frequency measurements. However, a somewhat different picture was revealed when the frequency measurements were plotted against the calculated stiffness variation (Figure 7.33). This latter figure shows that the majority of the changes that occurred to the frequency appear to coincide approximately with the 75% stiffness point, with only a relatively small change occurring between 100% and 75% stiffness. These trends were observed for both the S1 and S2 members, which appears to highlight a degree of commonality in the dynamic properties of the panels through the progressive damage process.

7.8.2 Using damping changes to detect damage in panels

Throughout this chapter, damping has been determined assuming that the vibration response of the panels could be modelled using visco-elastic characteristics. This assumption provided a means of 'extracting' the damping using a percentage quantity relative to a critical value (critical being 100%). This method was used as a basis on which the change in damping due to damage was assessed. The trends observed in the data were similar to the results obtained from the frequency change studies. However, the amount of change that occurred to the damping values was greater, suggesting that this dynamic property could offer a more sensitive parameter for damage identification purposes.

7.8.3 Amplitude dependence of natural frequency and damping

Generally, it was found that the values of natural frequency and damping decreased and increased respectively as the amplitude of vibration was increased. In addition, the amplitude dependence of both natural frequency and damping appears to be influenced by the presence of damage. As damage progresses, the amplitude dependence is effected more intensively. Figures 7.24 to 7.27 illustrate the amount by which these dependencies change where viable relationships have been identified. It appears from the results displayed that the natural frequency and damping (determined from vibration only events) change relative to amplitude on a logarithmic scale. Using 'best-fit' regression lines (shown on the aforementioned figures) to highlight these trends, allowed a series of 'surface plot' diagrams to be identified (Figures 7.28 and 7.29). As a result of the information presented by these diagrams, three important points should be noted:

(i) Damping has a significant amplitude dependency, especially at later stages of damage.

(ii) Although the natural frequency shows amplitude dependency, its variation in comparison to (ii) is small.

(iii) Amplitude dependency can have a significant influence on the interpretation of damage extent. Clearly, if the results of Figures 7.33 and 7.34 were used as a 'benchmark' of typical panel degradation versus dynamic property change, then neglecting the affects of the amplitude dependency could give a false indication of the amount of damage present.

7.8.4 Using mode shape measurements to detect damage

The mode shape information and the calculated MAC values reveal no definite trends to which the observed structural changes can be related (Figures 7.31 and 7.32).

7.8.5 Non-linear frequency-dependent behaviour of the damaged panels

The behaviour of the panels reflected in the measured FRF data demonstrate the added complexity that occurred to the vibration behaviour at later stages of damage (Figure 7.30). As damage progresses, it is clear that the measured properties deviate from the

perfect visco-elastic model, suggesting that non-linear behavioural trends occur. This non-linearity was also found to increase, as further damage was imposed.

However, from a structural perspective, it is not clear how the non-linearity was caused as the FRF, based on visco-elastic assumptions, can only provide a 'best-fit' to the measurements allowing 'equivalent' properties to be identified.

7.8.6 Aspects that need clarification

The results presented in this chapter have revealed a number of interesting trends; the most prominent of which being that natural frequency and damping both signify the onset of damage. However, there are a number of issues that should be clarified. These are:

(i) The stiffness changes exhibited by the M-C relationship have been interpreted as being induced by cracking of the concrete, which would be a reasonable conclusion to make if the panels had been made from conventional reinforced concrete (RC) [as found by Yang (1996)]. Since the panels were made using profiled-steel deck units, there may have been different 'degradation' mechanism to those of RC members. Therefore, to investigate the most likely cause of the observed structural changes, a study should be conducted to:
   (a) identify the cause of the panel degradation from published literature, and
   (b) compile M-C relationships using numerical models of material behaviour to confirm the applicability of (a) to the panels by comparing measured and calculated results.

(ii) Unlike the method adopted to quantify the amplitude dependency of the vibration, the visco-elastic FRF model could not be used to clarify the frequency-dependent response of the damaged panels. Therefore, to establish the amount of non-linearity that occurs, and to examine if it could also help toward the identification of damage, further analytical examination of these characteristics will be required.

Item (i) and (ii) above are considered in chapters 8 and 9 respectively.

CHAPTER 8

Calculating the Behaviour of Composite Floor-Slab Panels Subjected to Incremental Static Load

8.1 Introduction

This chapter presents a numerical model that simulates accurately the moment-curvature relationships of the composite floor-slab panels tested in the laboratory (discussed in chapter 7). The core of this chapter comprises two main sections that discuss aspects of previously published studies prepared by various authors, which are incorporated into the numerical model assumptions. Therefore, these sections can be broadly categorised as:

(i) A review of published literature that has focused on studies conducted to determine the characteristics of composite member behaviour when subjected to statically applied loading.

(ii) The formulation of various computational models that aim to predict the loaded behaviour of these composite members, from which one model is calibrated against measurements taken from the laboratory tests.

8.2 Predicting the Ultimate Strength of Composite Floor-Slab Panels

The ultimate strength and the failure characteristics of composite floors have been studied over the past four decades. During that time, a number of researchers have reported on numerical and experimental studies that aim to clarify the behaviour of these members when loaded statically. The main contributors to these studies are identified in the following sections together with their analytical contributions and interpretations of the static load carrying performance of this form of structural member.

8.2.1 Initial Development

During the early development of the composite floor system, which utilised a steel sheet manufactured with a pre-determined profile, it was normal practice to assume that the steel element offered no strength enhancement to the final floor product. Conventional reinforced concrete (RC) theory was used to justify strength provisions, and the floor was normally constructed incorporating steel bars in the bottom region of the concrete. In the 1960's, Bryl (1967) studied and reported on a new realisation that the steel profile and hardened concrete interacted to provide a truly composite member eliminating the need for the reinforcing bars. It was thought that, through the development of bond between the concrete and steel, no additional mechanical means of material connectivity would be required to produce the desired composite action. However, it was recognised early in the development of the composite analogy that the load carrying attributes of the combined concrete and steel element would be significantly different to those assuming RC principles. From a series of experimental studies conducted in the UK, America, Germany, Holland and France using simply supported lengths of composite members subjected to symmetrical four-point loading (i.e. two symmetrically placed point loads plus the two support reactions), Bryl (1967) compiled a description of the failure mode idealised to a two-phase process:

(i) the break-down of bond at the steel and concrete interface thought to initiate when cracking of the concrete commenced, quickly followed by;
(ii) a rapid loss of interaction at the steel and concrete interface (i.e. slip) resulting in strength and stiffness loss, which leads to a sudden and dramatic failure as a result of excessive slip between the steel and concrete.

This form of structural failure has now become recognised as the most dominant for composite floor-slab members tested in this way, the combination of (i) and (ii) being typically referred to as an 'in-plane shear bond failure' or sometimes as 'slip failure'. To account for this behaviour in design, a 'factor of safety' approach was initially assumed to be sufficient. This was applied to capacity predictions made using conventional RC theory where Bryl (1967) suggested values ranging between 3.15 and 4.6. These factors were found to depend on the surface texture of the steel part, which was thought to have an influence on the ultimate capacity of the member.

After these relatively basic initial conclusions, the 'American Steel and Iron Institute' (ASII) provided funding to Iowa State University (ISU), USA to carry out experimental studies aimed at further understanding the failure characteristics of composite floors. The main purpose was clearly to maximise the potential of the system and to make it a commercially viable alternative to other forms of floor construction. Reporting generally on these studies, Schuster (1976) discussed methods that could be adopted to improve the bond strength and thus the in-plane shear resistance between the steel and concrete. Examples of such methods being the application of special surface coatings applied to the steel sheet, which effectively adjusted its surface texture increasing the total bond between the two elements. The conclusions confirmed the work of Bryl (1967), adding that not only ultimate capacity, but also the overall structural behaviour through loading was dependent on the efficiency of the interface to transfer in-plane stresses. Schuster (1976) also made note of the possible disadvantage of the composite system, where the steel part of the structure conceals the formation of initial concrete cracking, thereby making it difficult to recognise the on-set of the rapid post-cracking degradation. Realising that visual means of assessing the potential failure of composite floors was effectively useless; the urgency for accurate predictive methods, based on calculations, was addressed.

8.2.2 Predicting the in-plane shear resistance of composite floor-slab panels

8.2.2.1 Linear regression method

No longer reliant on an arbitrary factor of safety approach to failure predictions, Porter and Ekberg (1972, 1976, 1980) and Porter *et al* (1976) reported on a combined experimental / semi-empirical study aimed at identifying an equation to predict the in-plane shear resistance of the composite system. Three equations were considered, all of which depended on data collected from experimental investigations conducted on composite elements tested by four-point loading. Adopting a linear regression approach, the equations were formulated to quantify the total resistance obtained when the samples were loaded to failure.

$$\frac{V_u s}{bd} = \frac{md}{L'}\sqrt{f_c'} + k\rho \tag{8.1}$$

$$\frac{V_u s}{bd} = \frac{m\rho d}{L'} + k\sqrt{f_c'} \tag{8.2}$$

$$\frac{V_u s}{bd} = m\left\{\frac{f_c'\rho d}{L'}\right\}^{1/3} + k \tag{8.3}$$

These equations are noticeably a simple variation on a similar theme where the basic form can be written as $V_u / bd = \{mx + k\}$ (i.e. a linear regression approach), with V_u being the total in-plane shear strength at the failure load. An additional parameter s, normally taken as unity, was also included, which allowed for variation to the properties at the steel / concrete interface. The governing parameters of each equation are also similar, where L', , b, d and f_c' are shear span, percentage area of steel relative to concrete, composite floor sample width, depth from top of concrete to centroid of steel and compressive strength of concrete respectively. The quantities of m and k, which are taken as constants, were calculated from the regression analysis using the experimental data and was defined respectively as the slope and zero intercept of a linear "V_u / bd" against "x" plot.

To estimate values of m and k with a reasonable degree of accuracy, the authors point out that a minimum of eight floor samples should be tested for each type of steel profile, i.e. eight samples for each ratio of . Based on a minimum of two profile types, the authors concluded that eqn.(8.2) provided the most accurate basis on which to assess the total in-plane shear resistance. From the analysis, it was found that this equation portrayed the least percentage error, relative to the regression analysis, for all samples considered. In addition, the authors suggest that the resistance obtained from the regression approach be reduce by 20% to account for the non-ductile nature of the member.

From reports of Porter, Schuster and Ekberg at ISU, (identified earlier) a document was compiled and published by the American Society of Civil Engineers (ASCE 1984). This specification document contains design advice for engineers with specific experimental requirements for manufacturers of the steel profile, and is based on the work of the aforementioned authors.

8.2.2.2 Multi-linear regression method

Following the publication of the ASCE (1984) document, research continued to advance towards a better understanding of the mechanisms responsible for the in-plane shear failure. Seleim and Schuster (1985) returned to the problem by offering a slightly different calculation concept to the original proposals outlined in the ASCE (1984) document. The in-plane shear failure was described as a three component problem involving:

(a) Chemical bond – the bond produced between the cement paste of the hydrated concrete and the steel surface;
(b) Mechanical bond – the resistance offered by the surface impressions, commonly termed the embossments, as slip failure is activated, and;
(c) Frictional bonds – the intransigent nature of the steel and concrete interface, normally associated with the surface roughness of materials in contact.

However, the authors assumed that the components of (b) and (c) were difficult to separate and were therefore combined to provide a single effect, maintaining the characteristics of in-plane shear resistance reported by earlier authors. The realisation that the chemical bond could also influence the strength of the composite member infused an additional complication needing further study. It was also pointed out that the in-plane shear resistance would only be activated after the chemical bond had been completely overcome, which was noticed as being coincident with cracking of the concrete. It was therefore stressed that failure of composite members could often result after the loss of chemical bond alone, i.e. in situations were the chemical bond strength was greater than the combined influence of the mechanical and frictional bonds. A factor causing further complication was suggested as being due to vertical separation, which takes place between the steel and concrete parts during failure. No attempt was made to include this effect in the analysis, but it was stated that vertical separation could be avoided by incorporating re-entrant shapes into the profile of the steel sheet.

Continuing with the symmetrical four-point load arrangement, and simple supported members, the expressions proposed by Seleim and Schuster (1985) for the calculation of the chemical and mechanical / frictional bonds were:

$$V_{ch} = \frac{(k_1 t + k_2)bd}{L'} \tag{8.4}$$

$$V_{sh} = (k_3 t + k_4)bd \tag{8.5}$$

where V_{ch} is the peak chemical bond resistance force, and V_{sh} is the combined mechanical and frictional bonds at failure. b and d are as defined for eqn.(8.3), and k_1, k_2, k_3 and k_4 are unknown coefficients obtained from measured data. In terms of total resistance at failure (V_u), eqns.(8.4) and (8.5) combine to give,

$$V_u = V_{ch} + V_{sh} = \left(\frac{k_1 t}{L'} + \frac{k_2}{L'} + k_3 t + k_4\right)bd \tag{8.6}$$

Again, in order to obtain a reasonable degree of accuracy, a minimum number of eight experimental samples were recommended. Unfortunately, typical k values were not reported, but it was concluded that eqn.(8.6) could achieve a similar degree of accuracy as eqn.(8.2), which was based on an examination of the percentage error of the equation results relative to the measured data. Other conclusions to emerge from their research were the discovery that the total resistance, V_u, did not change when (a) a different percentage area of steel was used without increasing member depth, and (b) the compressive strength of the concrete changed.

8.2.3 Dominant in-plane shear transfer mechanism

As the knowledge of the in-plane shear failure mechanism matured, research attention focused on the incorporation of web embossments indented into the web of the steel profile as a method of enhancing the in-plane shear resistance. It was recognised, from the work of Luttrell (1987) and Easterling and Young (1992) for example, that changing the orientation of the embossments had an influence on the strength and performance of the composite member through static load. Jolly and Zubair (1987) carried out extensive experimental investigations, which compared the failure capacity

of members with similar load and span configurations for different embossment types. Five embossment types were considered, each being characterised in terms of their basic shape, i.e. diamond, cross, vertical, split vertical and staggered circle. All specimens performed similarly up to a load that initiated cracking of the concrete (i.e. loss of the chemical bond). Thereafter, each profile type performed differently, with the better capacity at failure being achieved from members containing a vertical embossment configuration. Wright *et al* (1987) also made this observation where the moment capacity was found to vary depending on the number and spacing of the embossments along the length of the span. Using a steel profile with no embossment detail, i.e. plain surface where the chemical bond is the only in-plane shear transfer device, the relative differences in load capacity were determined, the results of which are shown in Table 8.1.

Table 8.1 – Relative load capacity at failure for composite members with different embossment arrangement, Jolly and Zubair (1987).

Type	Plain	Cross	Diamond	Split Vertical	Staggered Circle	Vertical
Relative Capacity at Failure	1.0	1.25	1.34	2.05	2.6	2.7
Number of Specimens	6	2	3	4	1	4

(Relative capacity values are quoted using an average value for each type given by Jolly and Zubair (1987). All embossments located on the web of the steel profile).

8.2.4 Moment capacity predictions for composite floor-slab panels

Following on from the concept of regression, Luttrell (1986, 1987) put forward a slightly different method of calculation for use in structural design, which returned to the 'factor of safety' approach,

$$M_t = kM_f \tag{8.7}$$

where M_f is the bending moment capacity of a fully composite member assuming conventional RC theory, M_t is the bending moment capacity at failure of the composite floor. k is a relaxation factor, which takes account of the reduced failure load due to in-plane shear mechanisms.

of members with similar load and span configurations for different embossment types. Five embossment types were considered, each being characterised in terms of their basic shape, i.e. diamond, cross, vertical, split vertical and staggered circle. All specimens performed similarly up to a load that initiated cracking of the concrete (i.e. loss of the chemical bond). Thereafter, each profile type performed differently, with the better capacity at failure being achieved from members containing a vertical embossment configuration. Wright *et al* (1987) also made this observation where the moment capacity was found to vary depending on the number and spacing of the embossments along the length of the span. Using a steel profile with no embossment detail, i.e. plain surface where the chemical bond is the only in-plane shear transfer device, the relative differences in load capacity were determined, the results of which are shown in Table 8.1.

Table 8.1 – Relative load capacity at failure for composite members with different embossment arrangement, Jolly and Zubair (1987).

Type	Plain	Cross	Diamond	Split Vertical	Staggered Circle	Vertical
Relative Capacity at Failure	1.0	1.25	1.34	2.05	2.6	2.7
Number of Specimens	6	2	3	4	1	4

(Relative capacity values are quoted using an average value for each type given by Jolly and Zubair (1987). All embossments located on the web of the steel profile).

8.2.4 Moment capacity predictions for composite floor-slab panels

Following on from the concept of regression, Luttrell (1986, 1987) put forward a slightly different method of calculation for use in structural design, which returned to the 'factor of safety' approach,

$$M_t = kM_f \tag{8.7}$$

where M_f is the bending moment capacity of a fully composite member assuming conventional RC theory, M_t is the bending moment capacity at failure of the composite floor. k is a relaxation factor, which takes account of the reduced failure load due to in-plane shear mechanisms.

Interestingly, Luttrell (1986, 1987) described in detail the mechanisms of failure identified by Seleim and Schuster (1985), but chose a solution that could be applied directly to the more conventional moment capacity equation for ease of use in structural design. However, the solution relied on results from experimental work, where appropriate k values could be calculated using:

$$k = \frac{k_3}{(k_1 + k_2)} \tag{8.8}$$

where:

$$k_1 = \frac{1}{D_d} + \frac{t}{p_h D_d} \text{ when } p_s p_h < 0.6 \tag{8.9}$$

$$k_1 = (t - 0.03)\left(1700 p_h^{\,2}\sqrt{\frac{p_s}{D_d}} - 32\right) + 2.4 - \sqrt{p_s p_h} \text{ when } p_s p_h > 0.6 \tag{8.10}$$

$$k_2 = \frac{100 t^{1.5}}{D\sqrt{p_h}} \text{ when } p_s p_h < 0.6 \tag{8.11}$$

$$k_2 = \frac{(D - 27.5t)\sqrt{p_s}\, D_d^{\,2}}{1316\,(0.01 + 0.85\, p_h)} \text{ when } p_s p_h > 0.6 \tag{8.12}$$

$$k_3 = 0.87 + 0.01\left(\frac{B}{B_c}\right)\left(69 - 2.2\frac{B}{B_c}\right) \text{ for all values of } p_s p_h \tag{8.13}$$

The variables for use with eqns.(8.8) to (8.13) were given as:

B = the width of the floor panel, usually taken the width of a standard steel panel;

B_c = individual profile or 'flute' width;

D = total slab depth;

D_d = overall depth of the steel profile;

p_h = embossment projection dimension;

p_s = embossment intensity factor calculated from, p_s = 12(n/m)

n = length of embossment projection;

m = spacing of the embossments.

To examine the performance of the proposed method, the author compiled experimental data collected at West Virginia University, USA, which was conducted over a period of eighteen years. Segregating the data by profile type, i.e. steel profiles with horizontally and vertically aligned embossments defined as types one and two

respectively, it was found that type two allowed a greater moment-capacity to be generated. All test data were collected from simply supported elements assuming the symmetrical four-point load arrangement recommended by ASCE (1984). Again, typical values for the k_1 to k_3 coefficients were not given, but graphical evidence showing good agreement between calculated and observed moment capacity was presented using sample data.

Alternative method of capacity prediction were presented by Stark and Brekelmans (1990), but these methods simply offered a variation to the 'factor of safety' approach assuming RC principles.

8.2.5 Displacement characteristics of composite floor-slab panels

A common method of investigating the load carrying performance of any structural member is to examine its displacement behaviour during the application of static load. For composite elements that incorporate concrete as one of its dominant materials, this assessment of load behaviour can accentuate the changing characteristics of the member normally associated with concrete cracking and other major stiffness losses. For composite floor members the definition of this relationship can be especially important owing to the low displacement magnitudes normally found near to the failure load. Klaiber and Porter (1981) reported on a study centring on this particular aspect and found generally that the in-plane shear failure of simply supported samples occurred at approximately 50% of the ultimate failure capacity. Concluding from comparisons made between measured and calculated displacement relationships, the authors provided advice on suitable section properties for use when predicting the displacement beyond the point of initial cracking. This culminated with an expression that was recommended for use with displacement calculations, given as,

$$I_e = \left(\frac{M_{cr}}{M_a}\right)^3 I_g + \left[1 - \left(\frac{M_{cr}}{M_a}\right)^3\right] I_{cr} \qquad (8.14)$$

where:

I_e = Effective bending inertia for displacement calculations;

I_g = Gross or uncracked bending inertia of the section;

I_{cr} = Bending inertia of the section assuming the concrete to be cracked up to the neutral axis of the section;

M_{cr} = The maximum bending moment across the member span at the point of concrete cracking;

M_a = The maximum bending moment across the member span at the load stage being considered.

Although this elaborate computation was offered to calculate displacement, the authors suggest that an average bending inertia based on the values of I_g and I_{cr} would also predict the measured results with reasonable accuracy.

8.2.6 Ultimate load capacity of continuous composite floor-slab panels

Simple experimental methods can be used to understand the failure mechanisms of composite members. However, the importance of treating the in-use composite floor as a continuous member was outlined by Roeder (1981) where large two-way spanning floor bays were studies. Metal shear studs, connecting the steel profile to the edge support members, were installed in an attempt to simulate as much as possible the in-use characteristics of the floor. To evaluate the failure criteria, this study concentrated on the mid-span displacement of the floor during the applications of a centrally imposed single static point load. From the experimentation it was found that a 50% increase of moment capacity could be achieved relative to the proportions normally gained from testing based on the ASCE (1984) recommendations. In addition, it was noted that the conventional in-plane slip failure did not occur, but evidence of a punching shear failure was observed. The failure was again non-ductile with small displacement measurements being recorded immediately before complete collapse and no visual signs of structural distress.

Contemplating an out-of-plane shear failure mechanism, but avoiding the elaboration of continuous member testing, Patrick (1989) and Patrick and Bridge (1992) put forward a compromise, which maintained a single span experimental set-up. It was realised that a continuous test arrangement offered a more realistic idea of static load performance. The philosophy was to fabricate the test members such that the in-plane shear failure could not occur. This was achieved by extending the test sample beyond

the simple support locations providing a larger in-plane shear transfer surface. This approach increased the moment capacity of the member enabling out-of-plane shear failure to be observed. Extending the sample length by 1.0m beyond the supports, experiments demonstrated that the out-of-plane shear failure was similar in appearance to that found in conventional RC beams containing no shear reinforcement. In simplistic terms, this failure can be characterised by the development of significant diagonal cracking beneath the location of applied point loads, which also induces yielding of the tension reinforcement. Therefore, even in situations where in-plane failure does not dominate, the authors found that the full moment capacity, based on RC principles, could not be achieved. It was further added that the mode of failure remained non-ductile in nature, as diagonal tension cracking was seen to propagate rapidly on the elevation of the members, which commenced at the support points [similar to that observed in RC members by Yang (1996)].

8.2.7 Incorporating experimental results into numerical models

In an attempt to bring together the in-plane shear mechanisms studied by the previous authors, Daniels and Crisinel (1993a, 1993b) formulated a numerical model that simulated the composite member behaviour at incremental loads. An earlier report by Kubic and Daniels (1979) also considered numerical calculations, but the assumption that the in-plane shear resistance at the interface of steel and concrete could be ignored was criticised by Daniels and Crisinel (1993a & b) as being too simplistic to offer any reasonable reflection of the real behaviour. The main basis of the more complex model by Daniels and Crisinel (1993a, 1993b) took account of chemical, frictional and mechanical bond stresses, all of which were simplified to a single shear stress relationship. The stress magnitude was calculated from localised push-off tests that related the amount of slip that occurred between the steel and concrete to the total amount of force applied.

To calibrate the formulated numerical models, comparisons were made with experimental data taken from tests designed to appraise an array of in-plane shear transfer devices. Divided into six groups, the variations considered were as identified in Table 8.2. As part of this investigation, valuable information relating to the behaviour of loaded continuous members was also obtained. Extending the study even

further, the provision of additional anchorage, in the form of mechanical fasteners between the steel and concrete, and hogging reinforcement at supports was also included.

Adopting the grouping terminology used in Table 8.2, the experimental study revealed that group F members performed best in terms of both ductility and moment capacity at failure. Ductility was gauged relative to the mid-span displacement of the members at a load that induced cracking of the concrete in the tension zones. This load was also noted as the point at which the chemical bond was completely overcome.

Table 8.2 –Member groupings used for experimental investigation by Daniels and Crisinel (1993b)

Group	**Span type**	**Web embossments orientation**	**End anchorage provisions**	**Additional reinforcement**
A	Single span	None	None	None
B	Single span	Vertical	None	None
C	Single span	Vertical	Edge anchorage at span ends	None
D	Three span	Vertical	None	None
E	Three span	Vertical	Anchorage at supports	None
F	Three span	Vertical	Anchorage at supports	Nominal mesh over supports

To appraise the performance of the member groupings, the authors introduced criteria that could be used to signify two critical stages of the member behaviour. These limits were determined from the experimental data and were designated as the 'serviceability deflection limit state', and the 'ultimate deflection limit state'. For universal application to all groupings, these limits were quoted as *L/250* and *L/50* for serviceability and ultimate conditions respectively. A service limit was defined as the point when cracking of the concrete was observed, while the ultimate limit was used as a cut-off point at which failure was thought to be imminent. The salient results of the experimental phase are summarised in Table 8.3.

Table 8.3 – Experimental results by Daniels and Crisinel (1993b)

Grouping	M/M_u at First Cracking	M/M_u at *L/250*	M/M_u at *L/50*	Failure Mode
A	0.24	-	-	Brittle
B	0.24	0.43	0.65	In-plane shear
C	0.24	0.43	0.83	In-plane shear
D	0.24	0.43	-	In-plane shear
E	0.24	0.55	0.90	In-plane shear
F	0.26	0.70	1.0	In-plane shear

(M relates to the maximum mid span bending moment for each grouping, while M_u is the moment at failure for grouping type F. Values quoted were interpreted from graphical output presented in the aforementioned publication).

Interestingly, the experimental result show that the moment at which first cracking occurred was similar for all members. This suggests that the chemical bond mechanism does not depend on the addition or type of incorporated shear transfer device. It is also noted that the ultimate capacities of the composite members increase significantly when a continuous system is adopted. This is not surprising as the results contained in Table 8.3 for the continuous members were collected using four-point loading applied over a single span. The increased moment capacity can therefore be attributed to an increase in the contact area at the steel / concrete interface over the unloaded parts of the continuous span, which ultimately contribute to the total in-plane shear resistance of the member. Nevertheless, the importance of broadening the study to continuous forms of construction had been identified.

After calibration, prepared from the comparisons between the measured and calculated results, the findings of the study were:

(i) The chemical bond is completely overcome at the point when cracking of the concrete occurs.

(ii) The frictional and mechanical bond combine to produce a single resisting force that commences at an initial value when cracking of the concrete initiates, increasing to a peak value just before failure, which drops to zero when failure occurs.

(iii) The in-plane shear stress calculated between the steel and concrete from (ii) above could be simplified to a mechanism that is distributed evenly along the width and shear span of the loaded member, i.e. a smeared model approach. The calculated value for grouping type 'B', which replicates the panel arrangement discussed in chapter 7, was given as ranging from 1.5 N/mm^2 to 2 N/mm^2. However, these authors neglected the contribution of concrete in the tensile region of the section, casting question over the quoted values.

8.3 Calculating the Load Carrying Performance of Composite Floor-Slab Panels Subjected to Incremental Loading

The previous discussions highlighted that the failure mode of composite floor-slabs is likely to be non-ductile or brittle in nature, even under a continuous support regime. Unlike conventional reinforced concrete elements, this brittle failure is due mainly to the rapid breakdown of bond between the steel and concrete. It is also seen that the main focus of the studies was to establish the capacity of the composite members at failure.

The aforementioned publications do not generally provide detailed proposals that can be used to determine the behaviour of the members through incremental stages of applied load, which is required here to compare with the results of chapter 7. To obtain an adequate numerical model of the static load behaviour of the panels a more detailed approach was needed.

The remaining part of this chapter examines the numerical models that were compiled to predict the moment-curvature relationship of the composite panels. The analytical models were compiled using mathematical stress-strain relationships that have been published by various authors and were prepared to identify a single model capable of accurately predicting the moment-curvature behaviour.

Before discussing the mathematical models, it is worth briefly identifying the main characteristics that are considered. In simple terms, the measured moment-curvature results showed that the flexural rigidity of the panels displayed a two-phase behaviour,

i.e. an initial linear phase, reflecting constant stiffness, followed by degradation or loss of stiffness. The cause of the degradation is of main concern for this study and the mechanisms that are responsible for the loss of section stiffness are examined using the analytical models. Therefore, the main characteristic that must be incorporated into the models is the ability to replicate the degradation of the panel. This degradation is likely to be the results of two material failure mechanisms, which complies with the discussion of published literature outlined earlier. These are:

(1) Cracking of Concrete: It is often assumed that concrete offers no tensile strength to the overall capacity of a reinforced concrete structure after cracking has taken place. However, research conducted by authors (cited later) has shown that the tensile strength of concrete can contribute significantly to the stiffness of a structure, even after the concrete has cracked. Taking account of these findings, for analytical investigations in general, the predicted stiffness of a structure is found to be larger than that assuming no concrete tensile strength. In addition, the characteristics of the post-cracking degradation are influenced by the distribution of tensile stresses throughout the section. It is therefore not unreasonable to speculate that the main source of the stiffness loss, seen from the measured behaviour of the composite panels, can be attributed to cracking of the concrete.

(2) Loss of bond: The composite action that exists between the steel and concrete of the panels are dependent on the bond strength at their interface. Three components contribute to the bond strength, which were identified in the review of literature above as chemical bond, friction bond and mechanical bond. Each of these components has different strength characteristics with the chemical bond offering the least resistance to tensile or shear stresses. It was also identified in the review of literature that the chemical bond is overcome when cracking of the concrete takes place. The mechanical and friction bond, however, are dependent on the surface conditions at the steel / concrete interface, which are mobilised after cracking occurs. These mechanisms may contribute to the stiffness of the panels, but are difficult to defined individually as part of the analytical predictions. Therefore, treating the friction and mechanical bond strength as a combined mechanism, its contribution to the overall post-cracking stiffness of the panels was considered.

8.3.1 Constitutive material relationships for concrete in tension

The material stress-strain relationships used for the analytical models of this chapter were taken from published work by various authors. A brief description of these relationships is given below.

8.3.1.1 Linear stress-strain relationship

Concrete is often treated as a linear-elastic material in both compression and tension at low strain levels. This is the approach recommended by British codes of practice for design and analysis of concrete structures (BS 8110: Part 2). In this document it is also suggested that for analysis it can be assumed that concrete maintains a tensile strength of 1 N/mm^2 after cracking, which is a simplified means of taking account of the effect of tension stiffening. This provision is recommended to ensure that calculations of flexural rigidity include the contribution of the cracked concrete in the tensile zones. Immediately after cracking, the tensile strength of concrete at the position of steel reinforcement is assumed to be constant. Using conventional notation, the stress before cracking is taken as:

$$f_{ct} = \varepsilon_{ct} E_c \text{ , when } f_{ct} < 1 \text{ N/mm}^2 \tag{8.15}$$

where f_{ct}, ε_{ct}, and E_c are the concrete tensile stress, concrete tensile strain and the material Young's modulus respectively. Thereafter, the concrete stress will have a constant magnitude of 1 N/mm^2 at the level of embedded steel, the distribution of which reducing linearly throughout the section to zero at the neutral axis. However, this relationship is too simplistic for the calculation of tension stiffening in composite floor-slab panels, as the post-cracking behaviour of the concrete may also depend on the resistance between the steel and concrete interface.

8.3.1.2 Vebo and Ghali (1977)

A tri-linear idealisation was proposed by Vebo and Ghali (1977), and replicates the tensile stress-strain behaviour as a piecewise series of linear relationships. This model assumes that the degradation of structural stiffness during cracking is the result of changes to the elastic modulus of the concrete. Figure 8.1(a) illustrates the proposed relationship, demonstrating the discrete form of the stress-strain behaviour.

In mathematical form, the relationship of Figure 8.1(a) can be defined as follows:

$$f_{ct} = 0.75\ \varepsilon_{ct} E_c, \text{ for } \varepsilon_{ct} \quad \left\{\frac{1.2 f_{cr}}{E_c}\right\} \tag{8.16}$$

$$f_{ct} = 0.9 f_{cr} - \varepsilon_{ct} E_c/5, \text{ for } \left\{\frac{1.2 f_{cr}}{E_c}\right\} < \varepsilon_{ct} < \left\{\frac{3.45 f_{cr}}{E_c}\right\} \tag{8.17}$$

$$f_{ct} = 0.45 f_{cr} - \varepsilon_{ct} E_c/20, \text{ for } \varepsilon_{ct} > \left\{\frac{3.45 f_{cr}}{E_c}\right\} \tag{8.18}$$

where f_{cr} is the concrete tensile stress at which cracking of the concrete commences.

8.3.1.3 Belarbi and Hsu (1994)

A method proposed by Belarbi and Hsu (1994) also considered a piecewise solution to the tensile behaviour. However, instead of modelling degradation as a process dictated by changes to the material Young's modulus, the post cracking behaviour was defined as a function of the crack strain directly. Figure 8.1(b) illustrates the stress-strain relationship, which is represented mathematically by the following.

$$f_{ct} = \varepsilon_{ct} E_{ct}, \text{ when } \varepsilon_{ct} < \varepsilon_{cr} \tag{8.19}$$

and

$$f_{ct} = f_{cr}\left(\frac{\varepsilon_{cr}}{\varepsilon_{ct}}\right)^{0.4}, \text{ when } \varepsilon_{ct} \geq \varepsilon_{cr} \tag{8.20}$$

where ε_{cr} is the concrete tensile strain at which the concrete is assumed to crack.

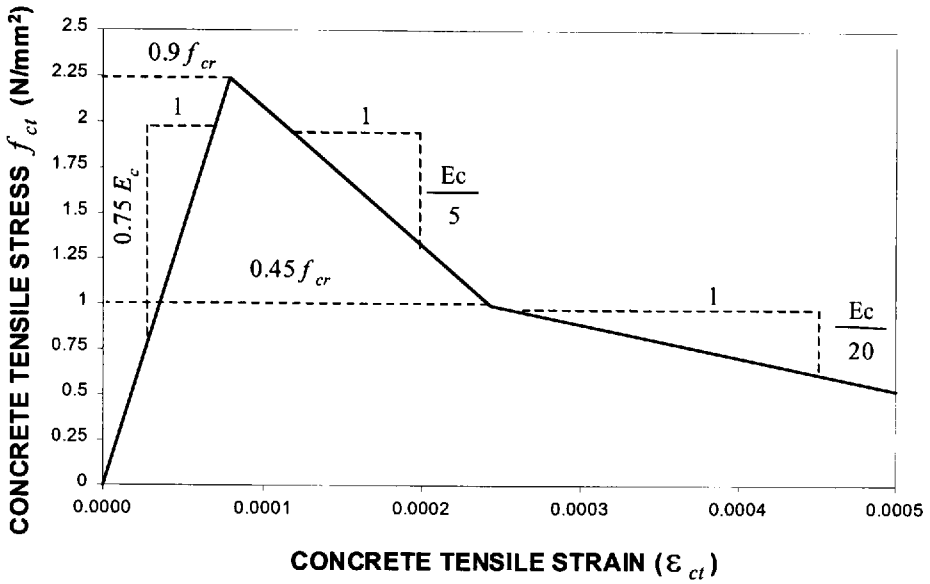

(a)

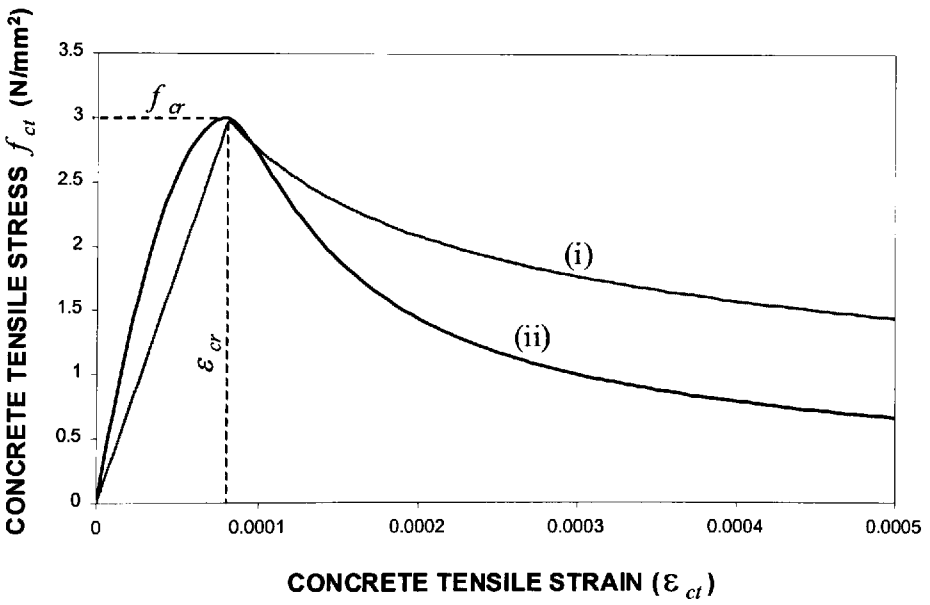

(b)

Figure 8.1 – Example stress-strain relationships for concrete in tension showing (a) proposals by Vego and Ghali (1977), and (b) relationships by (i) Berarbi and Hsu (1994) and (ii) Marzouk and Chen (1993)

8.3.1.4 Marzouk and Chen (1993)

Marzouk and Chen (1993) produced a relationship that captured in detail the fundamental behaviour of the concrete in tension using two convenient mathematical expressions. These authors suggest that their solution replicates what was defined as a four phases degradation process identified as (i) an initial linear proportion, (ii) a pre-crack non-linear phase, followed by (iii) post-crack non-linear degradation, eventually tailing off to (iv) zero stress at large strain. Figure 8.1(b) shows the resultant stress-strain relationships, which is characterised mathematically using,

$$f_{ct} = f_{cr}\left\{2\frac{\varepsilon_{ct}}{\varepsilon_{cr}} - \left(\frac{\varepsilon_{ct}}{\varepsilon_{cr}}\right)^2\right\} \text{ when, } \frac{\varepsilon_{ct}}{\varepsilon_{cr}} < 1 \tag{8.21}$$

$$f_{ct} = \left\{\frac{f_{cr}\dfrac{\varepsilon_{ct}}{\varepsilon_{cr}}}{1.3863\left(\dfrac{\varepsilon_{ct}}{\varepsilon_{cr}} - 1\right)^{1.6655} + \dfrac{\varepsilon_{ct}}{\varepsilon_{cr}}}\right\} \text{ when, } \frac{\varepsilon_{ct}}{\varepsilon_{cr}} \geq 1 \tag{8.22}$$

Apart from the methods identified above, other authors have also proposed mathematical approaches to calculate tension-stiffening effects. However, these other methods rely more on principles of fracture mechanics, which is outside the scope of study considered here. Feenstra and Borst (1995) and Karihaloo (1995) are examples of published work based on these methods.

8.3.2 Constitutive material relationships for concrete in compression

8.3.2.1 Ghoneim and MacGregor (1994)

The compressive stress-strain relationships suggested by Ghoneim and MacGregor (1994), and also discussed by El-Metwally (1994), takes account of strain softening, which is assumed to commence when the maximum compressive strength of the material is reached. The method used to calculate this relationship is convenient in that it relies on a single expression to predict both pre and post-peak strength characteristics, and was defined as,

$$f_c = 2f_c' \left\{ \frac{\left(\frac{\varepsilon_c}{\varepsilon_0}\right)}{1+\left(\frac{\varepsilon_c}{\varepsilon_0}\right)^2} \right\} \tag{8.23}$$

where f_c is the compressive stress of the concrete, which depends on (i) peak compressive stress, (ii) peak compressive strain, and (iii) the strain of the concrete during loading, defined by f_c', ε_o and ε_c respectively. Figure 8.2 shows the stress-strain diagram obtained using this relationship.

8.3.2.2 Hsu and Zhang (1996) [and Pang and Hsu (1996)]

An expression proposed by Hsu and Zhang (1996) and Pang and Hsu (1996) was developed to consider bi-axial compressive stresses. To incorporate this expression into the analysis of a section subjected to uni-axial stress, the influence of the orthogonal out-of-plane strain can be treated as zero. Two expressions define the stress-strain relationship, which simulate pre and post-peak stress compressive behaviour. Shown in a graphical form by Figure 8.2, the equations used to predict the behaviour of the concrete in compression were given by,

$$f_c = \xi f_c' \left[2\left(\frac{\varepsilon_c}{\xi\varepsilon_0}\right) - \left(\frac{\varepsilon_c}{\xi\varepsilon_0}\right)^2 \right], \text{ when } \left(\frac{\varepsilon_c}{\xi\varepsilon_0}\right) \le 1 \tag{8.24}$$

and,

$$f_c = \xi f_c' \left[1 - \left\{ \frac{\left(\frac{\varepsilon_c}{\xi\varepsilon_0}\right) - 1}{\left(\frac{2}{\xi}\right) - 1} \right\}^2 \right], \text{ when } 1 < \left(\frac{\varepsilon_c}{\xi\varepsilon_0}\right) \le 1.5 \tag{8.25}$$

where,

$$\xi = \frac{0.9}{\sqrt{1 + 400\,\varepsilon_r}} = 0.9 \text{ if } \varepsilon_r = 0 \tag{8.26}$$

and ε_r is the orthogonal strain (i.e. out-of-plane to the principal compressive section strain).

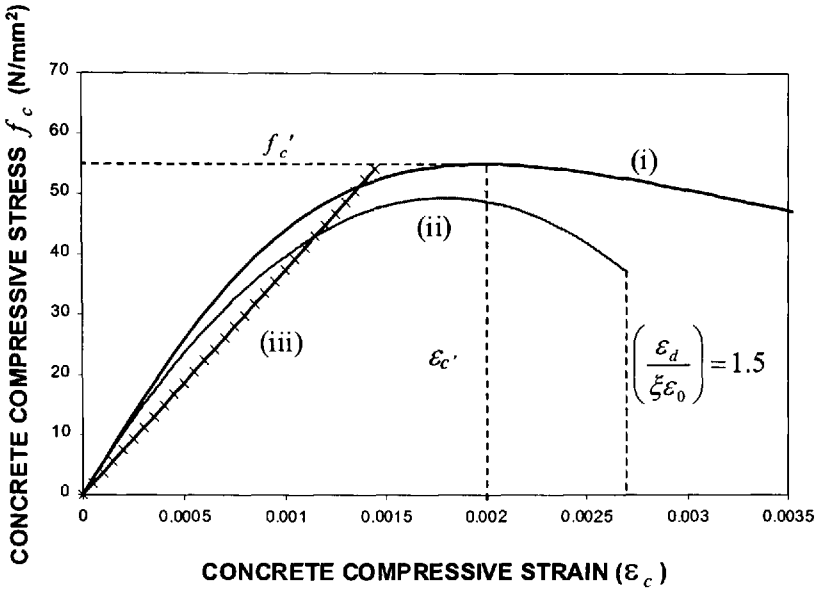

Figure 8.2 – Example stress-strain relationships for concrete in compression showing proposals by (i) Hsu and Zhang (1996), and (ii) Ghoneim and MacGregor (1994) with (iii) showing a linear stess-strain relationship.

8.4 Parametric Study using the Stress-Strain Relationships

The parametric study was compiled to examine the moment-curvature relationship of the panels using analytical models comprising various combinations of stress-strain expressions as identified above, which are defined in Table 8.4. The aim of the study was to identify a single analytical model that could closely fit the measured moment-curvature results (see chapter 7).

8.4.1 The parametric study constants

The dimensional aspects of the two panel types were taken as being consistent with the geometry as given in chapter 7. The Young's modulus and compressive strength of the concrete were also assumed to remain constant being taken as 37.4 kN/mm^2 and 55 N/mm^2 respectively, which corresponds with the laboratory results of chapter 7.

Table 8.4 – Material stress-strain relationships used for the parametric study (Defined using author names)

Model Number	Concrete in Tension (Author names)	Concrete in Compression (Author names)	Steel in Tension (Assumed behaviour)
1	Vebo and Ghali	(Linear)	(Elastic-perfectly-plastic)
2	Vebo and Ghali	Hsu and Zhang	(Elastic-perfectly-plastic)
3	Vebo and Ghali	Ghoneim and MacGregor	(Elastic-perfectly-plastic)
4	Belarbi and Hsu	(Linear)	(Elastic-perfectly-plastic)
5	Belarbi and Hsu	Hsu and Zhang	(Elastic-perfectly-plastic)
6	Belarbi and Hsu	Ghoneim and MacGregor	(Elastic-perfectly-plastic)
7	Marzouk and Chen	(Linear)	(Elastic-perfectly-plastic)
8	Marzouk and Chen	Hsu and Zhang	(Elastic-perfectly-plastic)
9	Marzouk and Chen	Ghoneim and MacGregor	(Elastic-perfectly-plastic)

Other items of information that were not available from the laboratory results, but were necessary for use with the analytical expressions, were taken from the recommendations given by Belarbi and Hsu (1994). These recommendations were:

- The compressive strain at which strain softening takes place, $\varepsilon = 2000\times10^{-6}$ mm/mm,
- The maximum compressive strain of the concrete is, $\varepsilon = 3500\times10^{-6}$ mm/mm.
- The cylinder compressive strength of concrete can be taken as 80% of its characteristic strength from standard 100mm laboratory cubes.

8.4.2 The parametric study variable

Belarbi and Hsu (1994) noted from experimental studies that cracking of simply supported RC members was seen to occur consistently at a concrete tensile strain of between $\varepsilon = 50\times10^{-6}$ to 60×10^{-6} mm/mm. These values were obtained from tests conducted on normally reinforced concrete members, where steel bars positioned in the lower part of the section (i.e. the tension face) were said to promote the tensile

resistance of the concrete beyond its strength determined from un-reinforced concrete samples.

The concrete tensile strength of the composite panels (chapter 7) is not known, however, and a more general approach that encompasses a range of possible limiting tensile strain values was required. The variable thus considered for the parametric study was the influence of various ε_{cr} values (i.e. the tensile strain at which cracking commences). Therefore, the range of values chosen for this study were $\varepsilon_{cr} = 30\times10^{-6}$ to 80×10^{-6}, which includes the strain levels defined by the aforementioned authors.

8.4.3 Calculating the moment-curvature relationships

The moment-curvature relationship was calculated using nine similar computer programs prepared using FORTRAN 77 code. A flow chart showing the basic computational path of these programs is shown in Figure 8.3, the main steps of which follow the philosophy as set out by Scott (1983):

(i) Initially, the program seeks to calculate the neutral axis of the panel for a given strain value assigned to the top surface of the section. To calculate the neutral axis depth, the program starts by assuming its position a short distance away from the top surface of the section, which is maintained over the full width of the panel.

(ii) Based on this 'first guess' the program calculates the tensile and compressive stress distribution throughout the panel allowing the total section forces to be computed.

(iii) If the forces calculated in (ii) do not balance, the program increases the neutral axis location and recalculates the stresses.

(iv) The correct neutral axis location is found when equilibrium of the forces is achieved. To ensure a solution of reasonable accuracy, the force equilibrium and the neutral axis depth were calculated to the nearest 0.5N and 0.001mm respectively.

(v) Having identified the neutral axis position, the curvature is calculated in the usual way from a ratio of the top strain magnitude to the neutral axis depth.

(vi) Finally, the moment capacity of the panel is obtained by multiplying the panel forces by their distance away from the neutral axis location found in (iv).

A sample of the moment-curvature relationships calculated using procedure (i) to (vi) above is given by Figure 8.4, which includes the measured results for comparison.

8.4.4 The parametric study results

8.4.4.1 Pre-cracking stiffness

The pre-crack stiffness represents the flexural rigidity of the panels when the maximum tensile strain of the concrete is less than the value at which cracking is assumed to commence. To be consistent with the data of chapter 7, this condition will be regarded as being representative of the panel in an undamaged form. Table 8.5 gives the pre-cracking stiffness (EI) of the panels calculated from the models, which has been arranged to illustrate the relative differences of predicted values obtained for each combination. The table shows:

(A) The influence of various compressive stress-strain relationships on the predictions made with similar tensile stress-strain expressions.
(B) The influence of various tensile stress-strain expression with similar compressive stress-strain relationships.

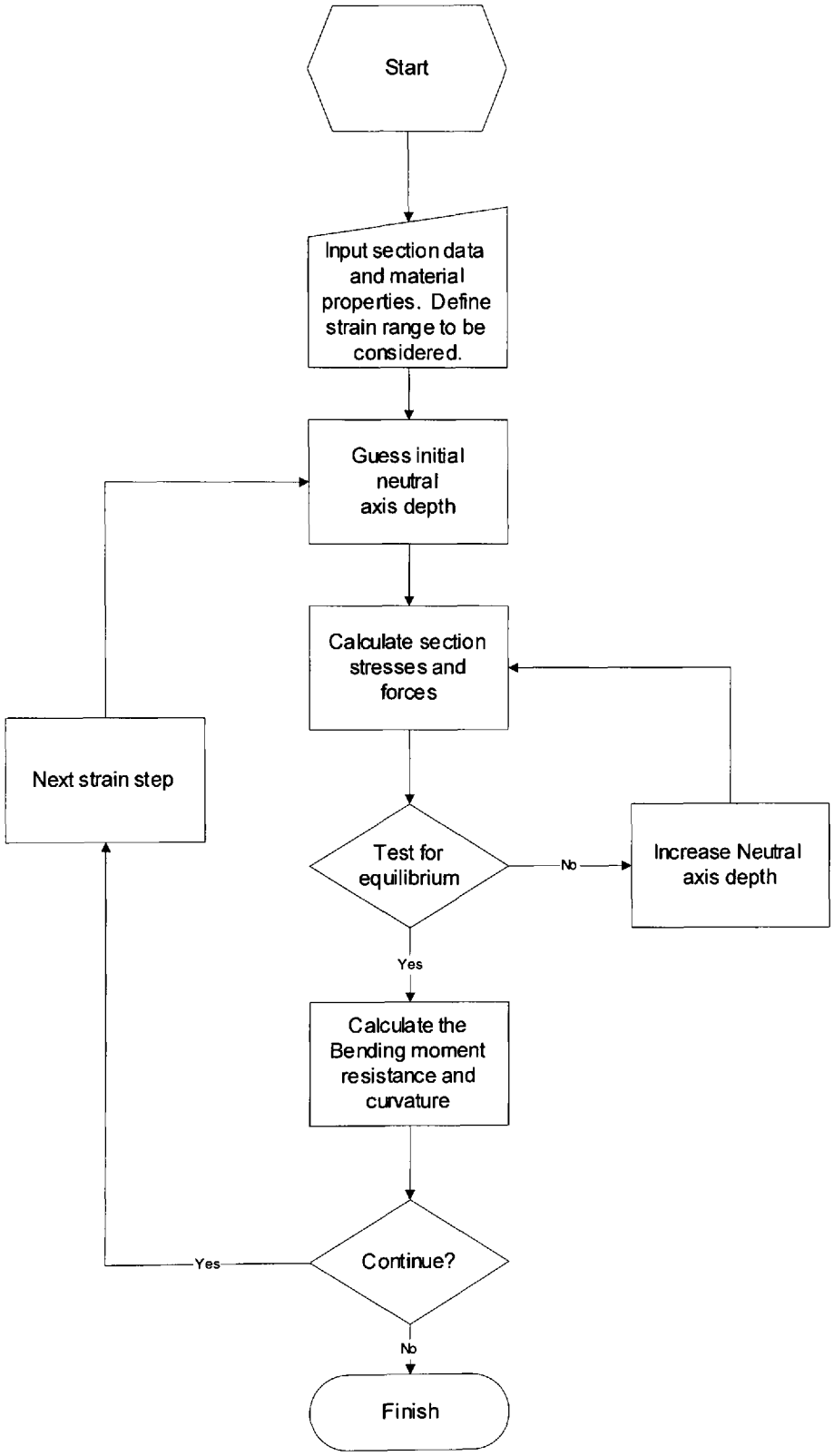

Figure 8.3 – Computer program flow chart used to calculate the moment-curvature relationships from the nine analytical models.

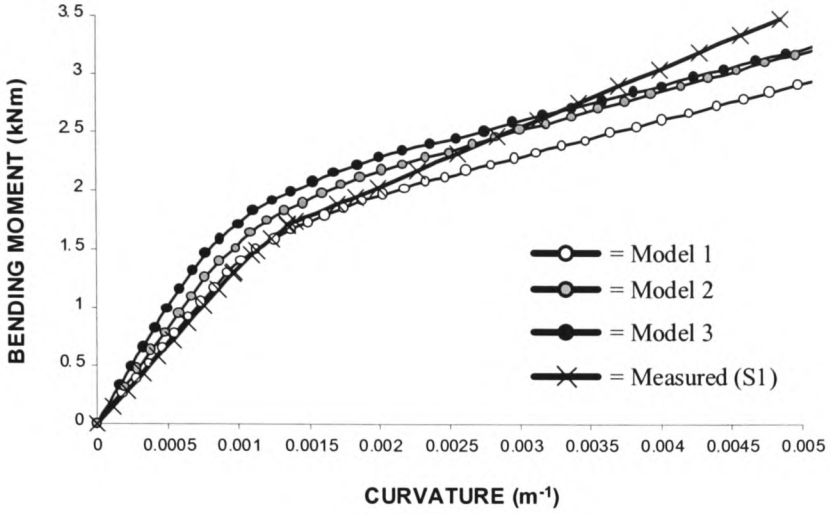

(a)

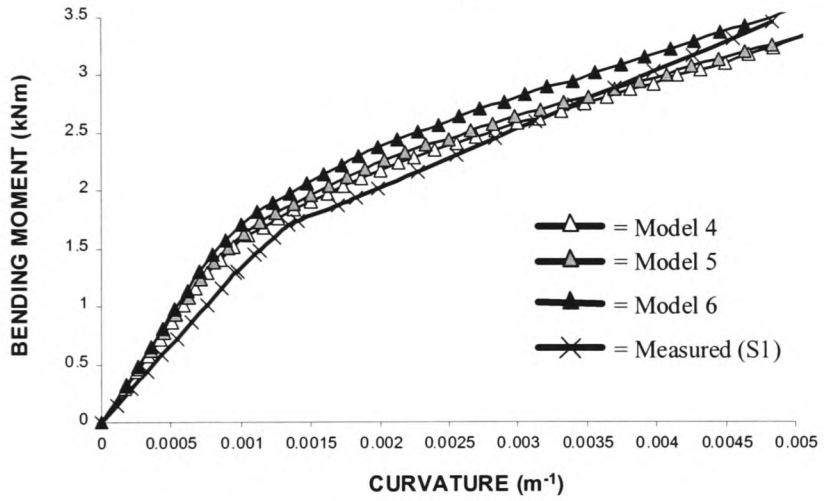

(b)

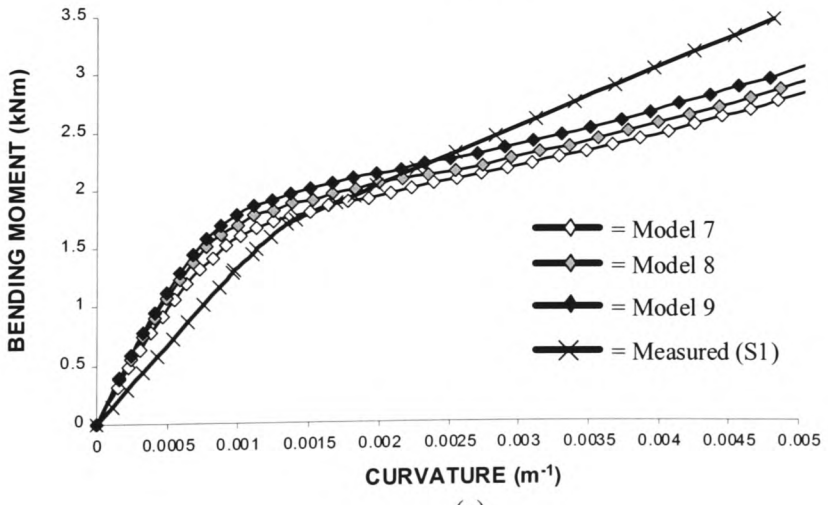

(c)

Figure 8.4 – Calculated moment-curvature relationships from (a) models 1 to 3, (b) models 4 to 6, and (c) models 7 to 9, (all with $\varepsilon_{cr} = 50\times10^{-6}$)

Table 8.5 – Pre-cracking stiffness and associated relative values for (A) and (B) described above.

(A)				(B)			
Model number		**Calculated EI (kNm^2)**	**Relative stiffness**	**Model number**		**Calculated EI (kNm^2)**	**Relative stiffness**
1	Group 1	1408	1.0	1	Group 4	1408	1.0
2		1532	1.088	4		1571	1.116
3		2003	1.423	7		1975	1.403
4	Group 2	1571	1.0	2	Group 5	1532	1.0
5		1709	1.088	5		1709	1.116
6		2236	1.423	8		2149	1.403
7	Group 3	1975	1.0	3	Group 6	2003	1.0
8		2149	1.088	6		2236	1.116
9		2810	1.423	9		2810	1.403

(Model numbers are shown depending on (A) similar tensile stress-strain relationships and (B) similar compressive stress-strain relationships).

Notes and observations from Table 8.5:

(i) The groupings marked 1 to 6 have been included to show the similar tensile or compressive concrete stress-strain relationships. For example,

- Group 1 represents models with tensile stress-strain relationships based on Vebo and Ghali (1977) combined with various compressive stress-strain relationships.
- Group 6 represents models with compressive stress-strain relationships based on Ghoneim and Gregor (1994) combined with various tensile relationships.

(ii) There are consistent relative changes in the calculated pre-cracking stiffness for model groupings 1 to 3 and 4 to 6.

8.4.4.2 Bending moment at first cracking

The bending moment at first cracking reflects the capacity of the panel when the tensile strain reaches the assigned peak value at the extreme fibres of the section. At this strain, unrecoverable 'damage' is assumed to occur within the panel, which can also be observed from calculations as being coincident with the point where there is a distinctive change in the moment-curvature relationship (see Figure 8.4).

The calculated bending moment at first cracking determined with models 1 to 9 is shown in Table 8.6 which, to clarify its change relative to the assigned cracking strain, has also been presented in Figure 8.5.

Table 8.6 – Calculated bending moment at first cracking from models 1 to 9

Cracking strain	1	2	3	4	5	6	7	8	9
	Calculated bending moment at first cracking (kNm)								
30×10^{-6}	0.55	0.92	1.13	0.83	1.03	1.18	0.66	0.89	1.10
40×10^{-6}	0.85	1.11	1.31	1.05	1.22	1.36	0.88	1.07	1.27
50×10^{-6}	1.08	1.31	1.51	1.24	1.38	1.49	1.06	1.23	1.41
60×10^{-6}	1.31	1.46	1.63	1.41	1.51	1.63	1.22	1.36	1.54
70×10^{-6}	1.53	1.61	1.77	1.56	1.67	1.76	1.38	1.49	1.63
80×10^{-6}	1.64	1.76	1.88	1.73	1.81	1.86	1.53	1.62	1.72

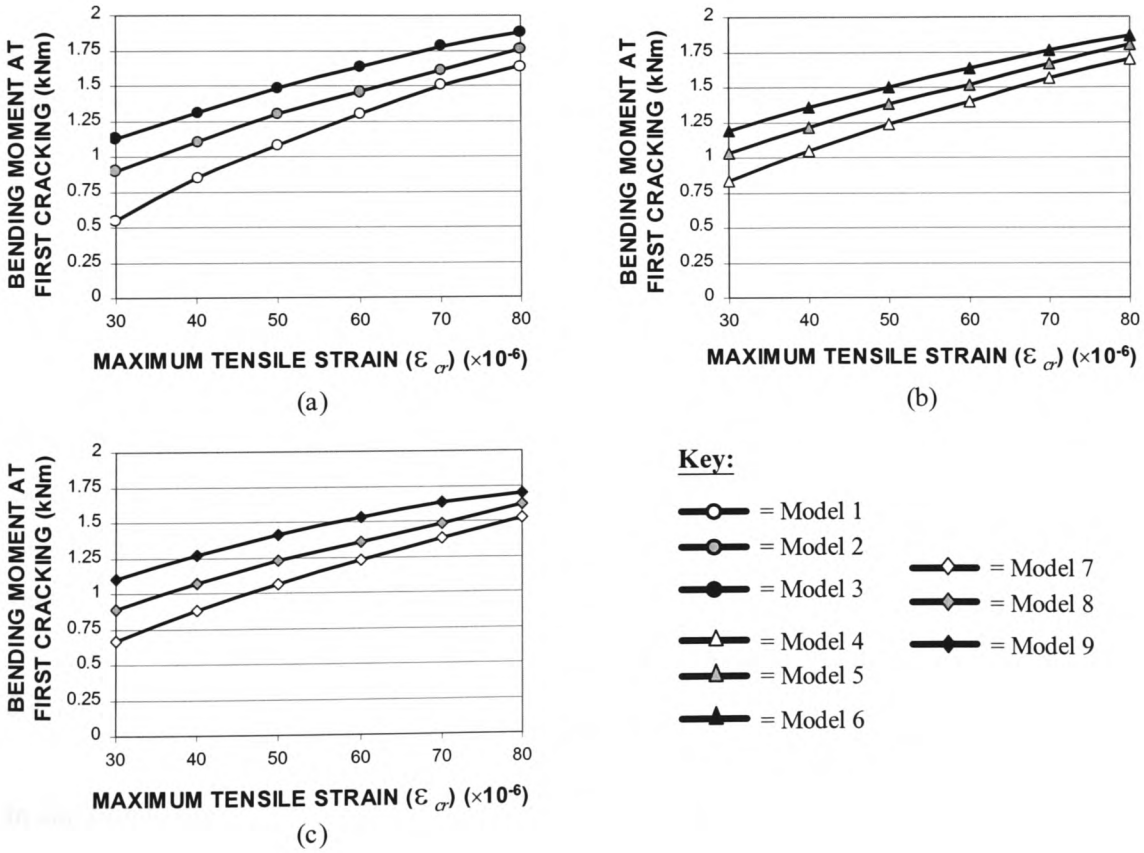

Figure 8.5 – Calculated bending moment at first cracking determined using (a) models 1 to 3, (b) models 4 to 6, and (c) models 7 to 9.

8.4.4.3 Post-cracking degradation

The post-cracking degradation characterises the rate at which the stiffness of the section reduces as a result of concrete cracking. This degradation can be gauged using the prepared analytical models by calculating the rate at which determined values of EI change after the cracking strain (ε_{cr}) is reached. Defining the normalised post-cracking bending moment (Π_{norm}), and the corresponding curvature value (χ_{norm}), the relative stiffness reduction can be determined using,

$$\Im = \frac{\Pi_{norm}}{\chi_{norm}} \tag{8.27}$$

The results calculated from eqn.(8.27) indicate the rate-of-change of EI after cracking, which returns a value of unity when Π_{norm} and χ_{norm} correspond to the cracking point. Therefore, from the equation the post-cracking stiffness ($EI_{post\text{-}crack}$) can be calculated relative to the stiffness of the panel at cracking (EI_{crack}) using,

$$EI_{post-crack} = \Im EI_{crack} \tag{8.28}$$

The variation of $\Im$ with Π_{norm}, calculated using the analytical models identified in Table 8.4, is shown in Figure 8.6, which also includes the same calculations obtained using the measured moment-curvature results. The characteristics seen from measured data were similar for both the S1 and S2 sections. However, it is also seen that the analytical models overestimate the rate of panel degradation compared to the measured values.

8.4.4.4 Calculated section stresses

In addition to the aforementioned quantities, the models can also be used to predict the section stresses. Although only useful as an indication of the 'ideal' stress distribution, a sample of the output for models 3, 6 and 9 is given by Figure 8.7. These models represent calculations that are based on the three concrete stress-strain relationships in tension.

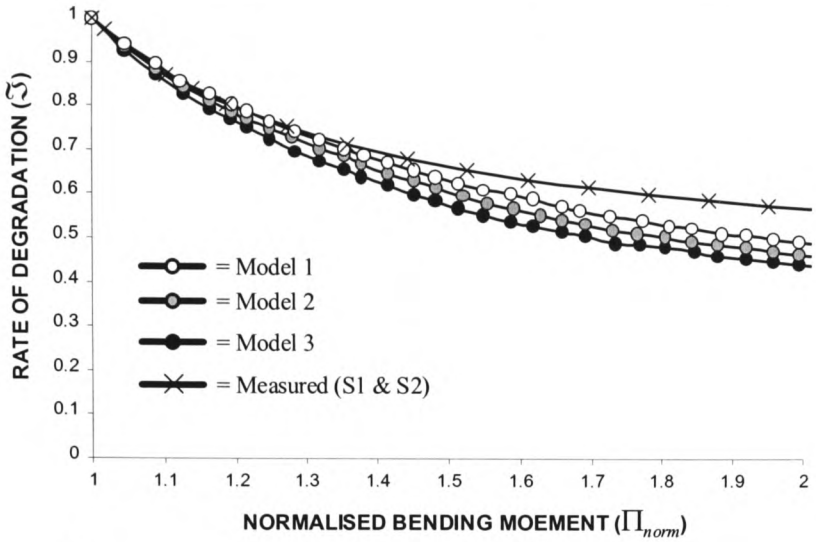

(a)

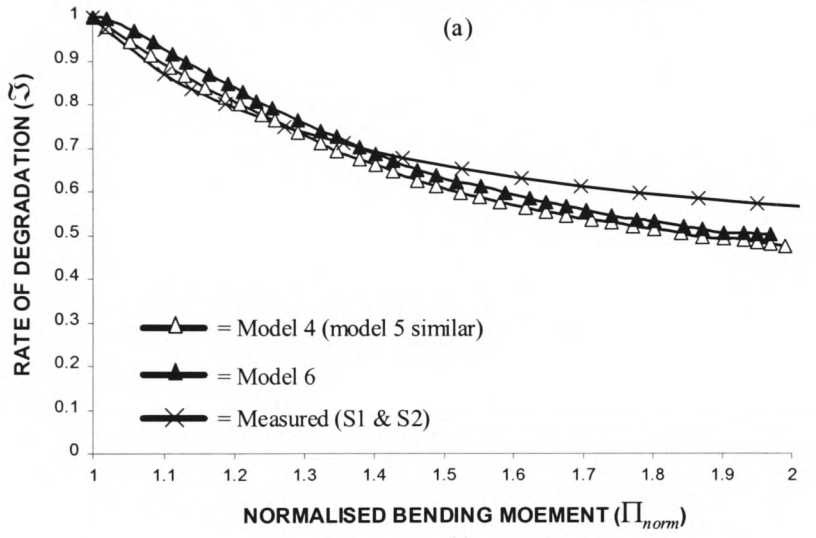

(b)

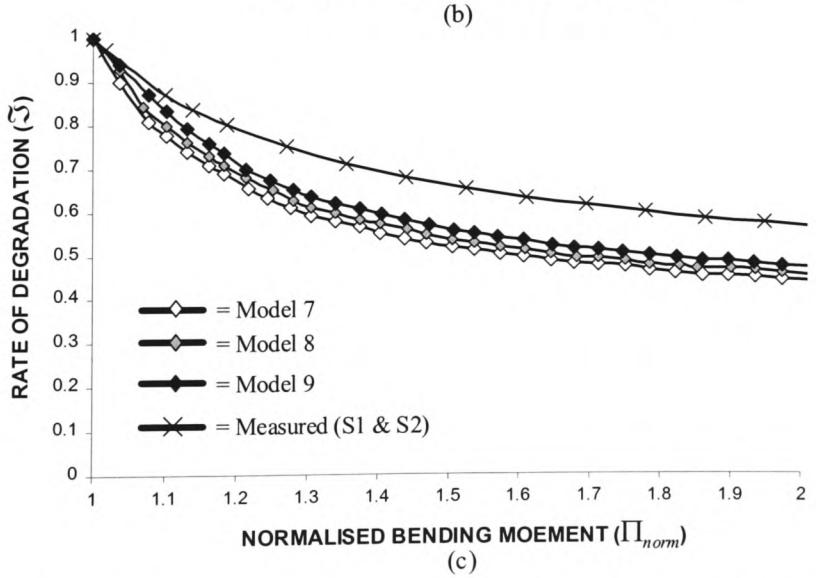

(c)

Figure 8.6 – Rate-of-change of post-cracking stiffness calculated from analytical models (a) 1 to 3, (b) 4 to 6, and (c) 7 to 9. (Measured values shown for comparison).

8.4.5 Choosing the most accurate predictive model for the present work

The parametric study has provided an insight into the performance of the surveyed analytical models. The results demonstrate the variety of behavioural predictions that can be achieved, even though the models prepared are based on similar section geometry and material strength values.

8.4.5.1 Similarities between the model predictions

The models all appear to provide moment-curvature relationships that correspond to the behavioural trends seen from the measured data. The results form a two phase relationship that comprise an initial linear part, corresponding to a pre-damage condition, followed by a segment that illustrates degradation of the section, or 'damaged' behaviour.

8.4.5.2 Differences between the model predictions

Although the characteristics of the models are similar, the calculated values of pre-crack stiffness, post-crack degradation and the moment at first cracking are different. Within these differences, however, it does appear that similar trends are embodied in models that comprise identical tensile stress-strain relationships. This is evident from the calculated normalised degradation values, which are shown in Figure 8.6.

8.4.5.3 The chosen model for calibration with the measured results

Any one of the prepared models has the potential to be calibrated against the measured moment-curvature results. However, to rationalise the process, only model 1 was calibrated as it gave results that were closest to the measured values for the post-crack degradation.

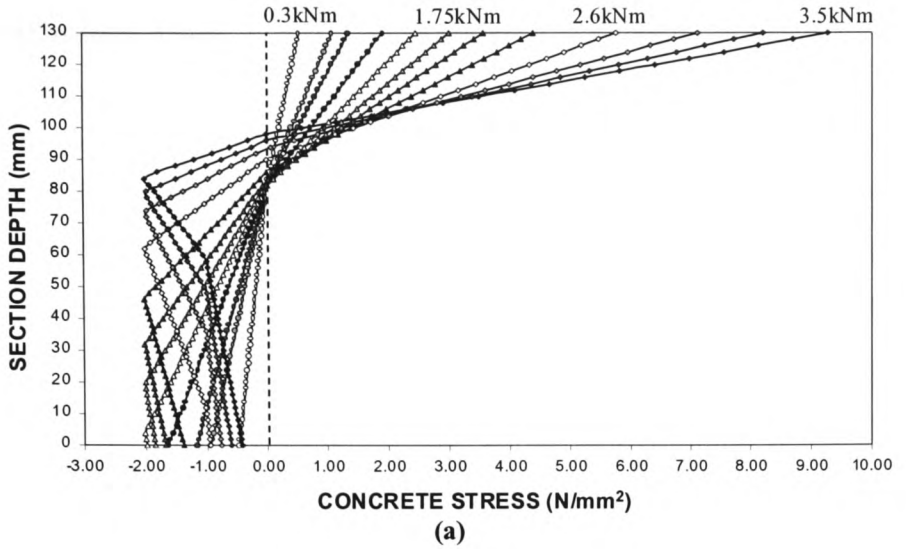

(a)

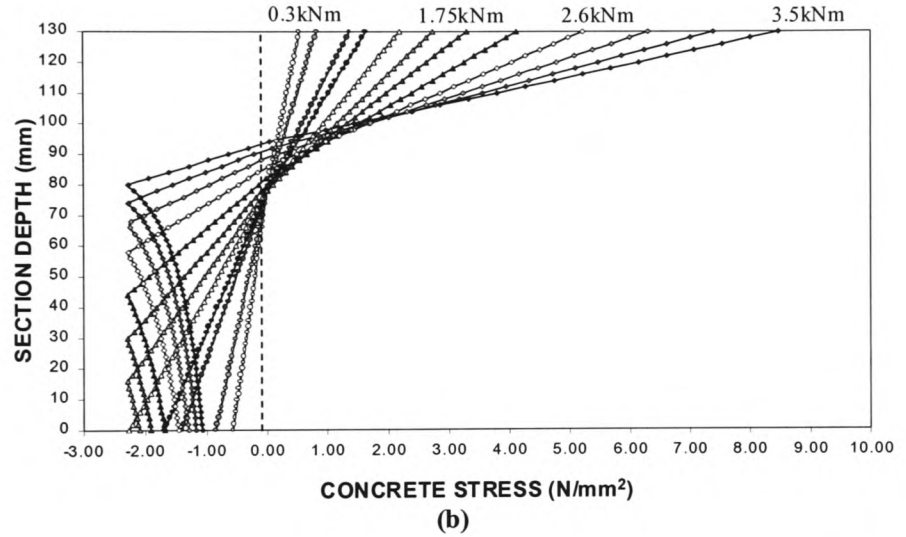

(b)

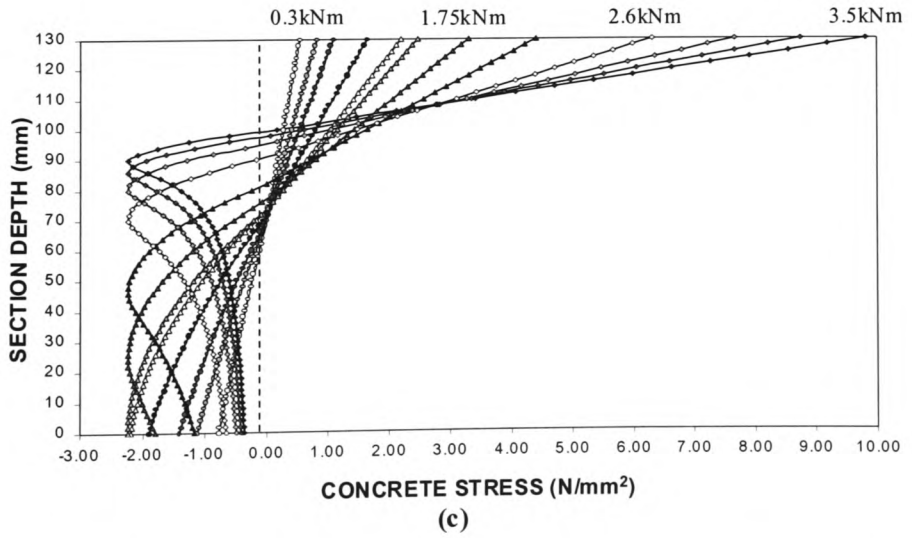

(c)

Figure 8.7 – Distribution of concrete stress calculated for the concrete panels using (a) model 3, (b) model 7, and (c) model 9, (all assuming $\varepsilon_{cr} = 50\times10^{-6}$)

8.5 Calibrating Model 1

The calibration considered two features:

1) the addition of a friction bond mechanism assumed to act at the interface of the concrete and the steel-profile;
2) the possibility that the dimensions of the laboratory panels were actually less than the precise sizes noted in chapter 7.

The first of these considerations was incorporated to account for the over-estimated stiffness loss produced by calculations as seen from Figure 8.6. Therefore, it is assumed that the friction bond that acts at the steel / concrete interface is responsible for enhancing the tensile resistance of the concrete at that location. The second feature was mainly considered to account for possible inaccuracies in the section geometry, which may have an influence on the calculated behaviour.

8.5.1 The bond stress mechanism

The bond mechanism was calculated as a function of the strain at the steel / concrete interface, and was defined relative to an assumed initial stress value ($\tau_{initial}$), which represents a smeared idealisation of total bond at the interface (N/mm^2). This value was assumed to mobilise when cracking of the panels commenced. Taking account of the recommendation of Daniels and Crisinel (1993b), where the bond was assumed to be effective over the shear span only, the bond force at the concrete / steel interface was calculated using,

$$F_{bond} = L_{shear}\tau_{bond} \text{ with units of N/mm} \qquad (8.29)$$

where L_{shear} is shear span and τ_{bond} is the post-cracking bond stress assumed to be proportional to $\tau_{initial}$.

8.5.1.1 Trial functions used to calculate τ_{bond}

To obtain an appropriate relationship that would suit the measured moment-curvature results, a number of functions were considered to calculate τ_{bond}, two of which are shown in Table 8.7. These were found to provide calculated moment-curvature relationships that compared well to the measured results and are based on similar principles to the assumptions considered by Poh and Attard (1993). These expressions are therefore based on the assumption that the bond stress increases from an initial value at cracking to a peak value at failure, the latter being found from comparisons made between calculated and measured characteristics.

Table 8.7 – Example trial functions used to predict the variation of bond stress at the steel / concrete interface of the composite panels

Function	Graphical presentation of function	Equation number
$\tau_{bond} = \left\{\frac{\varepsilon_{ct}}{\varepsilon_{cr}}\right\}^{n} \tau_{initial}$	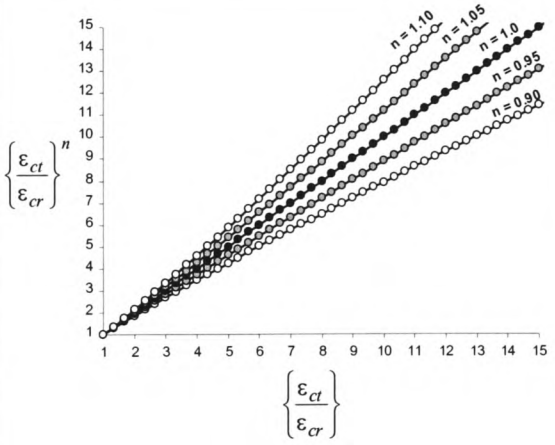	(8.30)
$\tau_{bond} = \left\{\frac{\varepsilon_{ct} - \varepsilon_{cr}}{\varepsilon_{cr}}\right\}^{n} \tau_{initial}$	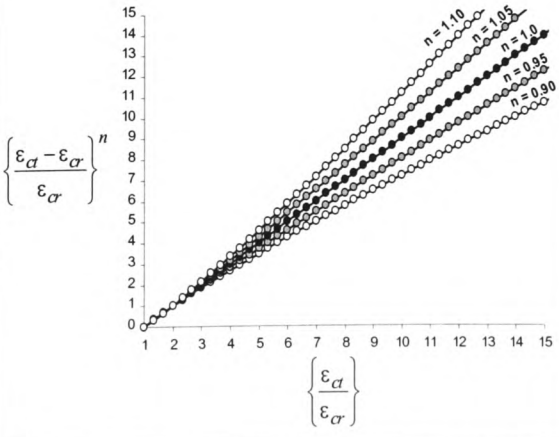	(8.31)

(In all cases, $\varepsilon_{ct} \geq \varepsilon_{cr}$, i.e. the bond stress is mobilised at the cracking strain).

Essentially, both expressions provide similar characteristics, but the difference between eqn.(8.30) and eqn.(8.31) is that the latter assumes zero bond stress at cracking, while the former assumes a non-zero bond stress at cracking. The former was found to give the best predictions.

8.5.1.2 Introducing a "section-efficiency factor"

The discussions so far assumed that the geometry of the S1 and S2 panels were precisely as indicated in chapter 7, i.e. the panel sections were '100% efficient' with no imperfections. However, there is an additional consideration that could influence the efficiency of the section, which should be incorporated to enable 'fine-tuning' of the calculated behaviour.

Panels S1 and S2 (chapter 7) clearly represent two different regions of a typical composite floor-slab having different section geometry, but the cross-sectional area and calculated bending inertia of each are identical. Therefore, to allow possible geometric imperfections to be included, an additional calibration variable was introduced. This variable was assumed only to influence the width of the section, thereby adjusting the properties to reflect results in terms of an 'effective-section'.

This approach also has practical implications, which are evident when placed in context to the method adopted to make the composite panels. Reflecting on the laboratory preparation stages described in chapter 7, it was noted that a length of plastic film was used to seal the mould at the locations were the steel profile made contact with the timber form-work. This film, measuring approximately 20mm wide, prevented the development of bond between the steel and concrete at its location, and it is with this regard that the 'effective-section' philosophy refers. Therefore, using a "section-efficiency factors" scale between "0" and "1", where the latter represents 100% section efficient, values less than "1" are deemed to indicate a reduction to the section width commencing from its outer edges. For example, all laboratory panel were 300mm wide, which if subject to a "section-efficiency factor" of 0.9 would mean a panel of width 270mm, i.e. for analysis 15mm would be ignored on each of the panel section edges.

8.5.2 The influence of the calibration parameters on the moment-curvature relationship

8.5.2.1 The bond stress mechanism

The inclusion of the bond stress mechanism has the affect of increasing the available tensile forces in the section, which in-turn promotes bending moment capacity resulting in an enhanced post-cracking stiffness. To demonstrate this influence, Figure 8.8(a) and (b) has been included, which is based on calculations that incorporate eqn.(8.30) with various value of the exponent '*n*' (see Table 8.7).

8.5.2.2 Introducing the "section-efficiency factor"

The influence of the "section-efficiency factor" on the predicted moment-curvature behaviour differs between the S1 and S2 sections. To illustrate this difference Table 8.8, and also Figure 8.9, has been prepared, which contains the pre-crack stiffness values calculated using model 1 for varying section widths.

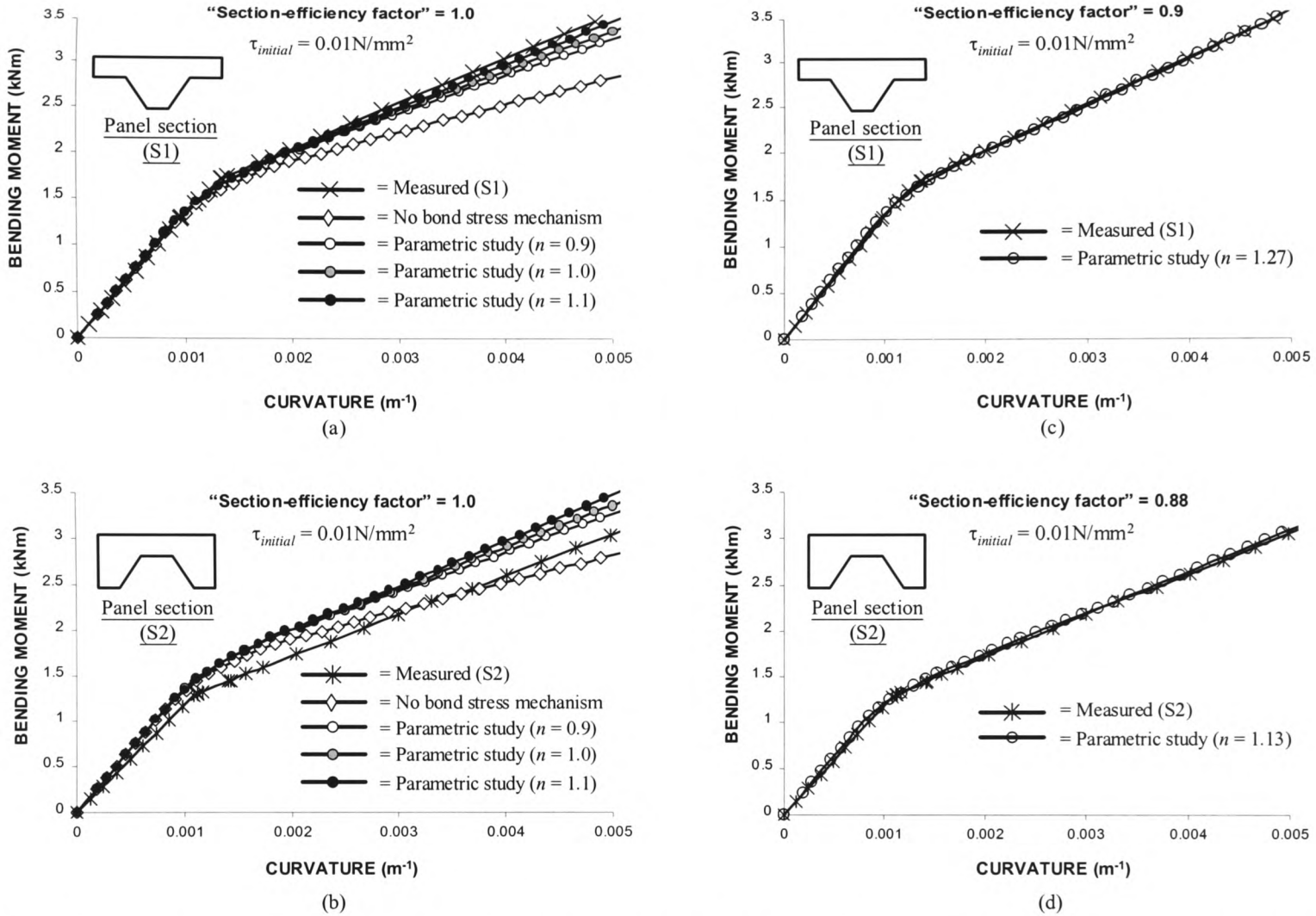

Figure 8.8 – Comparison of measured and calculated moment-curvature relationships, showing parametric study examples and calibrated results for (a)+(c) panel S1, and (b)+(d) panel S2

Table 8.8 – Calculated pre-crack stiffness for the panels subject to various "section-efficiency factors" – Model 1 used for calculations

"Section-efficiency factor"	**Pre-crack stiffness Panel S1 (kNm^2)**	**Pre-crack stiffness Panel S2 (kNm^2)**
0.80	1172	964
0.82	1214	1030
0.84	1252	1085
0.86	1285	1135
0.88	1314	1182
0.90	1340	1228
0.92	1360	1271
0.94	1378	1312
0.96	1394	1353
0.98	1405	1385
1.0	1408	1408

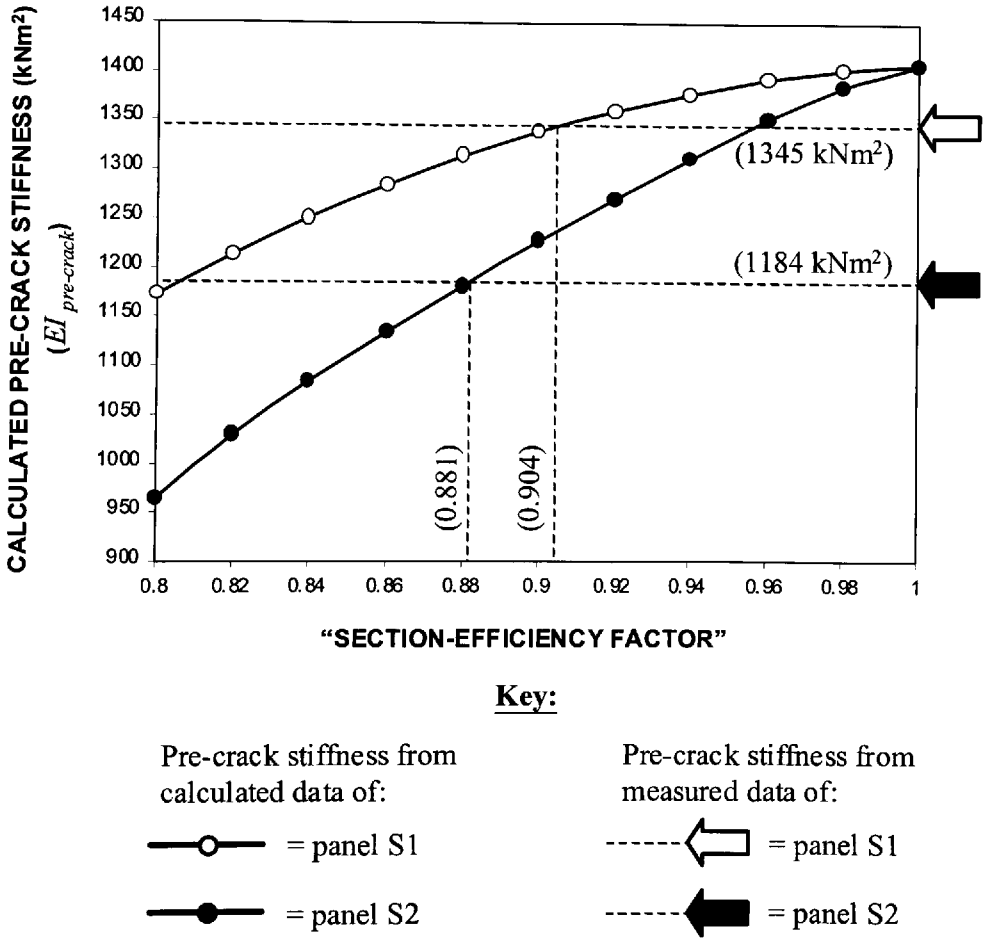

Figure 8.9 – Calculated pre-crack stiffness ($EI_{pre\text{-}crack}$) determined for various "section-efficiency factors" (measured values also indicated).

8.5.3 The calibrated moment-curvature predictions

The calibrated moment-curvature predictions are shown in Figure 8.8(c) and (d). The properties used to produce these calibrated results were as follows:

8.5.3.1 Panel S1

- Concrete cracking strain, $\varepsilon_{cr} = 60 \times 10^{-6}$ mm/mm
- Initial smeared friction bond stress, $\tau_{initial} = 0.01 N/mm^2$
- Bond stress at a calculated bending moment of resistance of 3.48kNm = $6.3 N/mm^2$ (i.e. at the average failure load of the panel – see chapter 7).
- Effective section width = 90%
- The exponent in *n* of eqn.(8.30) (see Table 8.7) = 1.27

8.5.3.1 Panel S2

- Concrete cracking strain, $\varepsilon_{cr} = 60 \times 10^{-6}$ mm/mm
- Initial smeared friction bond stress, $\tau_{initial} = 0.01 N/mm^2$
- Bond stress at a calculated bending moment of resistance of 3.48kNm = $7.2 N/mm^2$ (i.e. at the average failure load of the panel – see chapter 7).
- Effective section width = 88%
- The exponent in *n* of eqn.(8.30) (see Table 8.7) = 1.13

8.5.4 The neutral axis depth variation determined from the calibrated S1 and S2 panel models

The variation of the neutral axis depth determined from the measured data has been presented in chapter 7. This variation also gives some insight into the behaviour of the panels throughout the various loading intervals, which signifies that changes to the section occur at stages thought to depict concrete cracking. To further demonstrate the accuracy of the calibrated model, and to justify the assumption that cracking of the concrete is the main cause of the neutral axis depth change, Figure 8.10 shows the measured values obtained from panels S1 and S2 compared with the calculated results. The figure clearly demonstrates the applicability of the assumptions incorporated into

the model, which has provides predictions that match those determined from laboratory data.

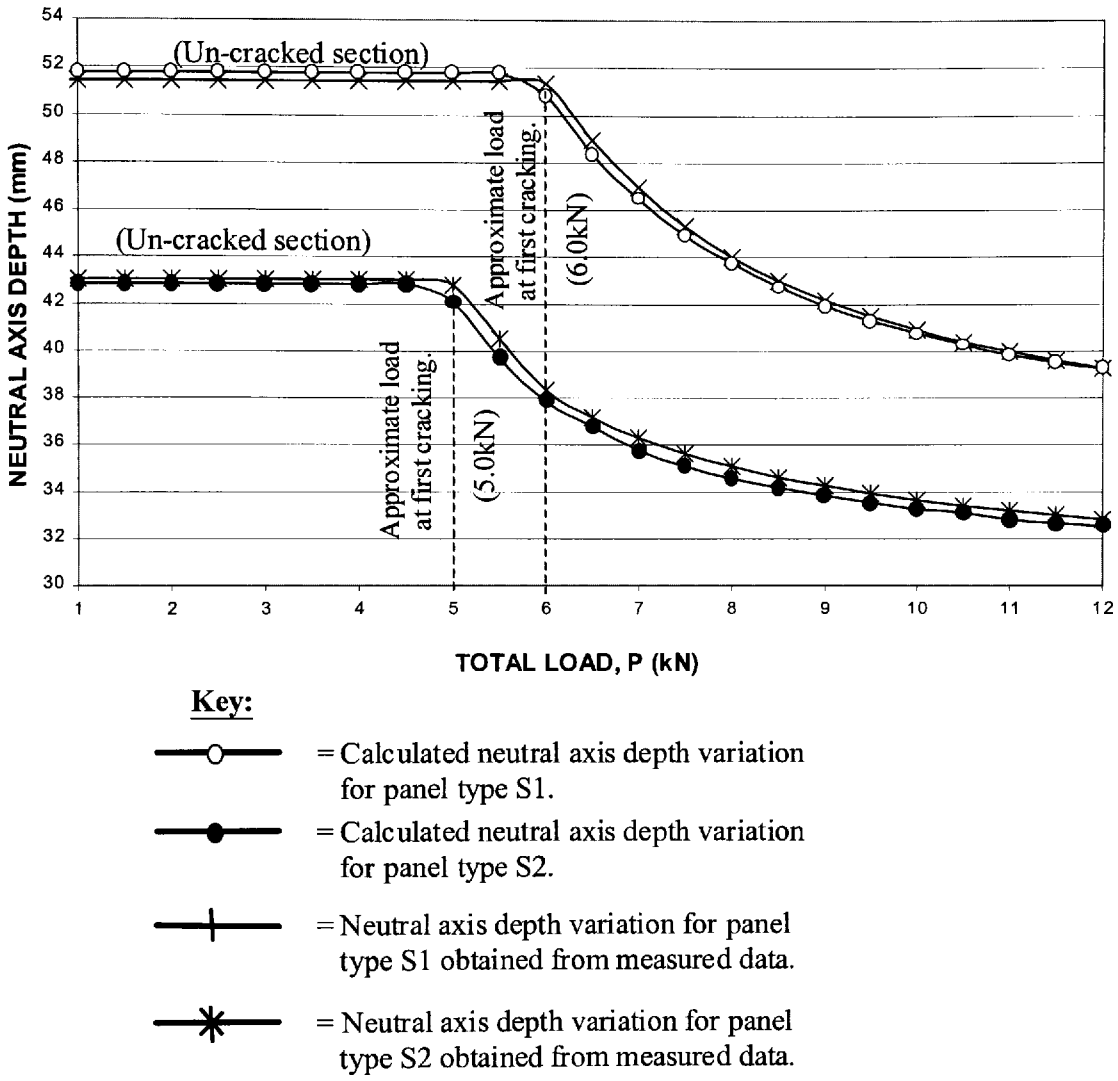

Figure 8.10 – Comparison of the neutral axis depth variation obtained from the calibrated numerical model and from measured experimental data.

8.6 Concluding Discussion

8.6.1 Observations from the study presented in this chapter

The study has shown that analytical models prepared by combining different mathematical relationships of stress against strain can provide a range of moment-curvature relationships. It is noted that these relationships represent the behaviour of the S1 and S2 panels seen from laboratory data, reflecting the structural characteristics of the members when subjected to static load. The degradation or 'damage' that was calculated using the calibrated model is therefore indicative of the damage imposed by the application of static load only, with no structural changes to the panels being imposed as a result of the dynamic load tests. The salient points to note from the findings presented in this chapter are:

(i) The moment-curvature behaviour of the panels can be calculated using existing mathematical stress-strain relationships for concrete in compression and tension.

(ii) The pre-cracking stiffness of the panels can be calculated using a linear compressive stress-strain relationship for concrete, with no account of strain softening being required. When incorporated into analytical models, the measured Young's modulus value obtained from standard laboratory tests was found to give accurate moment-curvature predictions.

(iii) To accurately predict the post-cracking behaviour of the panels, an additional section stress component was required. This component was attributed to friction / bond stresses that could develop at the interface of the steel and concrete and was assumed to be effective over the shear span of the member only. A smeared bond stress relationship has therefore been proposed, which calculates bond forces as a function of the strain at the concrete / steel interface and an initial value assumed to be mobilised when cracking of the section occurs. Assigning a smeared stress of $0.01N/mm^2$ to this initial value gave predicted moment-curvature relationships for the S1 and S2 panels that matched the post-crack results obtained from measurements.

(iv) To 'fine-tune' the moment-curvature predictions an "section-efficiency factor" was introduced. This factor was found to influence the calculated stiffness values of panel S2 to a greater extent than the S1 sections. Assigning section-

efficiency factors of 0.90 and 0.88 to panels S1 and S2 respectively produced calculated moment-curvature results that matched those from measurements.

(v) The calculated bending moment at first cracking for both panels was found to match the measured results assuming a cracking strain value of $\varepsilon = 60\times10^{-6}$ mm/mm. This value was used in combination with the aforementioned calibration variables and was appropriate for use with both the S1 and S2 panels.

8.6.2 Concluding remarks

The inclusion of an additional stress mechanism, which aims to simulate the behaviour of the concrete / steel profile interaction, appears to be a sufficiently accurate model to compensate for the discrepancies observed from calculations assuming concrete cracking characteristics alone. It is clear that, based on the information available from the measured data, this assumption cannot be directly validated. To produce such a validation, which may be possible if the relative movement between the concrete / steel profile of the panels during load was known, a comparison of measured and calculated results would need to be carried out. However, it is the opinion of the candidate that the model, assumed to replicate the friction / bond stress mechanism, is sufficient here to support two main findings. These are:

(i) Before the section property changes commence, i.e. during the pre-damaged condition, the section remained intact with no cracking of the concrete and no in-plane degradation of the concrete / steel parts occurring.

(ii) The degradation or post-damaged behaviour of the panels during load, initially assumed to be affected by cracking of the concrete alone, is actually influenced by two processes, i.e. concrete cracking and in-plane shear failure at the concrete / steel profile interface.

With these findings, a clear definition of the panel behaviour has emerged, which allows the results obtained from the dynamic tests to be assigned to the static load data with the knowledge that a clear distinction between pre and post-damage conditions was achieved in the laboratory.

CHAPTER 9

Modelling the Characteristics of Measured Frequency Response Functions obtained from Damaged Composite Panels

9.1 Introduction

It has been shown in chapter 7 that the Frequency Response Functions (FRFs), measured from the composite panels at various stage of 'damage', appear to exhibit modified characteristics that differ from the behaviour represented by the linear visco-elastic model. The extent of the modification, which was found from comparisons between measured and calculated FRFs, appear to show a dependency on the extent of damage and the amplitude of vibration to which the panels were subjected. To examine how the FRF characteristics change with damage, and to provide an additional parameter on which damage identification can be based, this chapter focuses on a method of mathematically modelling the frequency response behaviour of the damaged panels. Using the formulation, which is based on the 'visco-elastic' model (identified in Appendix A), three scalar quantities are presented that are used to quantify damage from the available laboratory data.

This chapter is presented in three main sections, which are:

(i) A discussion of the findings from chapter 7 and 8 placed in the context of information drawn from literature, which have published methods of numerical modelling, and suggestions of how modified visco-elastic vibration can be interpreted.

(ii) A presentation of the formulated mathematical expression that has been prepared by the candidate to model the FRF measurements collected from laboratory tests on the panels.

(iii) The use of the formulation in (ii) as a method to relate the extent of damage to the parameters determined from the mathematical expression.

9.2 The Non-linear Vibration Behaviour of Structures – A Reflection on Published Work and its Applicability to the Current Research

9.2.1 Introductory comments

The terminology "non-linear" is often used in publications that aim to provide guidance on method that can be used to model the modified vibration behaviour of structures, which differs from the formulations that can be solved using conventional linear mathematics. There has been debate for many years concerning the most probable causes that could be responsible for the non-linear vibration behaviour often observed in damaged structural members. The majority of this attention has been placed on whether the phenomena is caused by stiffness or damping non-linearity under certain conditions of vibration, both of which have emerged equally as seemingly plausible approaches.

This section has been prepared to highlight a number of these studies, but the aim is not to identify all published work that has been produced on the subject. Therefore, the focus is to discuss a chosen few reports that demonstrate hypotheses relevant to the present work, which will help clarify the possible cause(s) of the modified behaviour found from the laboratory measurements.

9.2.2 Non-linear stiffness and its affect on vibration behaviour

The FRFs presented in chapter 7, with particular reference to those measured during the post-damage stages of the laboratory tests, show behavioural trends that are typical of the mathematical expression proposed by Duffing's equation [see Jordan and Smith (1987)]. Duffing's equation has long been recognised as an approach that can be used for the analysis of non-linear vibrating systems, and is usually written in a form given by,

$$\ddot{x} + c\dot{x} + kx \pm \mu x^3 = F\cos\omega_f t \qquad (9.1)$$

where k, c are F are stiffness, damping and applied force respectively. ω_f is the frequency of excitation, while x is displacement. The "dot" notion represents differentiation with respect to time. The equation can be seen to be a variation on a linear differential equation, but with the addition of the μx^3 term makes the expression non-linear with respect to displacement (i.e. a stiffness related term), with μ being a constant. Solving eqn.(9.1) for the steady state in x, and examining the response amplitude for varying ω_f, gives a FRF with characteristics that represent either a 'softening' or 'hardening' spring. This terminology [presented in texts such as that by Thompson and Stewart (1986)] describes the behaviour that is portrayed by the aforementioned equation, which characterises the vibration of a mass / spring system where the latter either 'softens' or 'hardens' as the frequency of excitation is increased. The differences between these two spring types can be distinguished from the FRFs calculated for each, the features of which are often referred to as indicating either a 'positive' or 'negative skew' dependent on whether μ is positive or negative respectively. To clarify this point, a 'negative skew', for example, was observed from the damaged panel FRFs of chapter 7, which can be characterised as a function that 'leans' towards lower excitation frequencies.

These characteristics were examined by Ellis (1993) where 'frequency sweep' tests [discussed in chapter 3] on tall buildings at a range of amplitudes gave FRF measurements that closely resembled those obtained from eqn.(9.1). In this case, the behaviour of the building showed a 'negative skew', while studies on glass panels using similar testing methods gave 'positive skew' characteristics. For both these structures, it was also seen that the severity of the skew became exaggerated as the amplitude of vibration was increased.

The report prepared by Ellis (1993) appears to point clearly to an appropriate solution that will satisfy the behaviour observed from the panels in the present work. But, as pointed out in the above citation, eqn.(9.1) does not fully explain all facets of the observed behaviour seen from the test measurements. The results of chapter 7 have shown that the natural frequencies of the composite panels exhibit amplitude dependency, which would also have some affect on their frequency response. However, the study also demonstrates that the damping was seen to vary more

significantly with amplitude compared to frequency variation, which should be taken into account when formulating an appropriate FRF model. It is possible, therefore, that the modified behaviour observed in the panel FRFs (chapter 7) comprise the influence of both frequency and damping, the latter being regarded as the more dominant.

9.2.3 Published evidence to support the assumption that damping has a greater influence than stiffness on the modified vibration behaviour

Penzien (1964) conducted tests on reinforced and pre-stressed concrete beams to examine their damping characteristics when made from a variety of concrete constituent compositions. This author studied the nature of measured FRF change when the members were subjected to static pre-loads. The study highlighted a number of interesting outcomes, some of which were similar to the findings presented in this thesis. One of the items discussed by the above author, which is applicable to the candidate's research, is that the changes observed from measured FRFs were thought to be linked to damping fluctuations that occurred as a result of cracking of the pre-loaded beams. Although the study did not consider the variation of the damping to the extent examined in the present work, it was concluded that its influence should not be ignored when predicting the dynamic response of cracked concrete members.

Jeary (1995) discussed this aspect of damping versus damage in a report that focused on a typhoon damaged full-scale building. The study discussed the influence of concrete cracking on the changing characteristics of damping and considered the differences between damaged and undamaged concrete on a macro-scale. Within the discussion of the report, the author stated that '...it is the damping characteristics that tell-tale signs appear which allow the onset of damage (in concrete) to be highlighted well in advance of a dangerous situation'. These comments were placed in the context of damping and its amplitude dependency using what was termed a 'plateau model' [also described by Fang *et al* (1997)]. The model comprised three levels, which were called low, medium and high vibration amplitude effects. Using this plateau approach the author described how damping non-linearity, and its change with amplitude, could be linked to damage (cracking) and its extent. A description offered to explain why

the damping was more strongly linked to vibration non-linearity was also given, where is was noted that:

(i) The low amplitude characteristics of damping are largely unchanged by the occurrence of damage.

(ii) The point at which damping begins to become influenced by the presence of damage is relative to the amplitude of vibration to which the structure is subjected.

(iii) As damage severity increases, the amplitude at which damping begins to vary (or become 'non-linear' with respect to amplitude) becomes smaller as the 'work' required by a defect to induce additional energy dissipation is reduced.

These points appear to give an accurate reflection of the behaviour noted from the panel investigations, which will help to rationalise the approach that will be used to model the measured behaviour.

The reports cited above give evidence to support the relationship between cracking (particularly in concrete members) and damping induced non-linearity. Comparing the comments identified above to the findings of chapters 7 and 8, it follows that the cause of the adjusted FRF characteristics, seen from the panels, could be strongly linked to the occurrence of a modified damping behaviour. This reflects the proposals by Jeary (1995), where it is reasonable to assume that the above-mentioned modification is caused primarily by the dissipation of energy at the location of cracks, which is exaggerated by (i) the presence of more cracks (i.e. progressive damage), and (ii) increased vibration amplitude levels. To place this in the context of the panel tests, the mechanisms that occur during pre and post-damage conditions are relative to a two-phase process, i.e. (i) a visco-elastic phase, and (ii) a combined visco-elastic plus some additional characteristic that dissipated energy in a slightly modified way.

9.2.4 Discussion of the possible damping mechanism exhibited by the composite panels

Given the evidence that is available (chapters 7 and 8) it is not unreasonable to assume that before cracking of the concrete occurred (pre-damage), no inter-surface friction could take place within the main body of the panel sections. In this condition the FRF of the panels can be modelled successfully, and with a high degree of correlation, assuming a visco-elastic model. When cracking of the concrete commences (post-damage), however, irregular surfaces are generated within the section that provide an additional mechanism for the dissipation of energy during vibration. Under these circumstances, the energy of the vibration would dissipate as heat, which would be generated by the combined actions of friction at a macro and microscopic crack surfaces level. This action could also provide a basis to explain the amplitude dependent nature of the damping, where larger excitation conditions would generate larger friction at the crack surfaces producing greater energy dissipation.

To predict vibration response with a model that assumes energy dissipation as a result of friction only, a 'coulomb friction' damping model would be appropriate [the formulation of which has been presented in text such as that by Thomson (1993) and Beards (1996)]. However, one major difference between the vibration response predicted with the coulomb assumption, and the results that were repeatedly found from the post-damaged panels, is that this mathematical model does not exhibit an exponential type decay-of-vibration. This form of decay was found to be dominant in all the response signals obtained from the laboratory, and as such should be maintained when choosing an appropriate mathematical solution.

9.2.5 Recent published reports on the prediction of non-linear vibration

Makris and Constantinou (1991) considered the analysis of vibration using a coulomb friction / viscous model that could exhibit a stick / slip behaviour. The approach proposed by these authors was to treat the problem in two parts involving the combined analysis of a visco-elastic and a stick / slip / stick model. When solved, the results from these models were added together to form the steady-state behaviour,

which was achieved using a method similar to the convolution integration as outlined in Clough and Penzien (1993). With this method, Makris and Constantinou above explained that the stick / slip / stick behaviour could be varied depending on the number of '...stops per vibration cycle...' required. The result was a model that replicated the behaviour of a single-degree-of-freedom (sdof) oscillatory having an unsymmetrical 'step like' waveform to represent the steady-state response. It was also shown that the FRF portrayed 'positive skew' characteristics that varied depending on the amplitude level being analysed.

Whiteman and Ferri (1996) devised a formulation that could be used to predict the FRF of a sdof oscillator, which incorporated a displacement-dependent dry friction damper. The friction model assumed a stick / slip / stick type behaviour, but unlike the authors cited previously, this study aimed to simulate a more fluent steady state vibration displacement that avoided the 'step like' waveform, the latter of which was referred to as a 'discontinuous' model. To obtain the solution to the formulated partial differential equation of motion, which included the friction damper as a displacement dependent term, the authors used a '...Runge-Kutta time integration technique...'. The FRF calculated using this approach gave a 'skew' type profile, which could be adjusted depending on the level of amplitude dependence assigned to the friction model (termed a 'ramp coefficient' by the authors).

Iwan and Huang (1996) presented a detailed investigation into the analysis of 'softening-spring and hardening-spring Duffing models' using a 'Monte Carlo' technique as part of the non-linear differential equation of motion solution procedure. The study shows that at large amplitudes of vibration the calculated response of these models can become chaotic in nature with rapid displacement growth occurring, which the authors felt would not provide a meaningful application to structural problems. However, the authors used the formulated sdof expression to predict the response of a spring-mass system to earthquake type load, which gave displacement results assuming non-linear stiffness and an additional parameter to account for non-linear damping. Focusing on the peak amplitude results, the study showed that the models that incorporated these non-linear terms predicted higher displacement values than those assuming linear parameters. Therefore, the model was proposed as a method for

the inelastic analysis of sdof systems. Bruneau and Wang (1996) also carried out similar studies where the formulated expressions considered non-linear damping as a function of a '...bi-linear hysteretic yield model'.

Crespo and Ruotolo (1996) formulated an expression to obtain the FRF of sdof and higher order (two dof) cantilevers containing cracks. The non-linear model was formulated to consider non-propagating cracks, while non-linear stiffness, which was the main focus of the study, was based on the assumption that the cracks open and close during oscillation [an approach also considered by Eccles *et al* (1999)]. By varying the depth of the cracks, which was modelled as a two-phase stiffness problem (i.e. open crack phase and closed crack phase), the authors demonstrated its influence on the calculated FRF. The function was thus shown to change depending on the level of cracking assumed, which mainly indicated a reduction in the natural frequency. However, no skew characteristics were noted in the presented FRFs.

9.3 Background to the Trial Solution Process

Before dealing with the approach that was found to provide a good match to the measured post-damage FRFs, it is worth reflecting on a number of the trials that were considered prior to the study that gave an appropriate solution. By illustrating the process undertaken to reach the final solution, a discussion of non-appropriate mathematical forms can also be presented.

9.3.1 Closed form solutions to the differential equation of motion – Formulation 1

9.3.1.1 Establishing a modified differential equation of motion

The initial trials aimed to replicate the observed measured FRF behaviour by focusing on a formulation that made adjustments to linear Second-Order Differential Equations (SODE), which aimed to introduce additional velocity dependent terms in an attempt to account for a modified damping behaviour. Remembering that a linear visco-elastic

system can be represented by the differential equation of motion written as [Meirovitch (1986)],

$$\ddot{x}+2\zeta\omega_n\dot{x}+\omega_n{}^2x=\frac{F_o}{m}\sin(\omega_f t) \tag{9.2}$$

where ζ, ω_n and ω_f are the damping ratio, natural frequency and forcing frequency respectively, while x, m and F_o are displacement, system mass and applied dynamic force. Consider eqn.(9.2) with an adjustment in the form,

$$\ddot{x}+2\zeta\omega_n g(x)\dot{x}+\omega_n{}^2x=\frac{F_o}{m}\sin(\omega_f t) \tag{9.3}$$

where $g(x)$ is a function that adjusts the velocity component of the linear SODE. To determine the form of $g(x)$, the aforementioned expression can be re-arranged to give,

$$g(x)=\frac{\frac{F_o}{m}\sin(\omega_f t)-\ddot{x}-\omega_n{}^2x}{2\zeta\omega_n\dot{x}} \tag{9.4}$$

To achieve the steady-state solution to eqn.(9.3), it should be assumed that the response of the system can be expressed using a sinusoidal form given by,

$$x=X\sin(\omega_f t+\varphi) \tag{9.5}$$

where X is the peak steady-state amplitude of the vibrating system when excited at a frequency of ω_f, and

$$\varphi=\tan^{-1}\left(\frac{2\zeta\omega_n\omega_f}{\omega_n{}^2-\omega_f{}^2}\right) \tag{9.6}$$

is the phase between the F_o and x, $g(x)$ can be re-written as,

$$g(x)=\frac{\frac{F_o}{Xm}\left[x\cos\varphi-\sqrt{X^2-x^2}\sin\varphi\right]+(\omega_f{}^2-\omega_n{}^2)x}{2\zeta\omega_n\omega_f\sqrt{X^2-x^2}} \tag{9.7}$$

In eqn.(9.7) $g(x)$ has been reduced to a form that is dependent only on the displacement of the system, which provides the basis for the desired formulation (i.e. amplitude dependent damping). To rationalise this expression, eqn.(9.7) can also be written as,

$$g(x)=\frac{x\left[\frac{F_o}{Xm}\cos\varphi+\omega_f{}^2-\omega_n{}^2\right]}{2\zeta\omega_n\omega_f\sqrt{X^2-x^2}}-\left[\frac{\frac{F_o}{Xm}\sin\varphi}{2\zeta\omega_n\omega_f}\right] \tag{9.8}$$

where
$$\left[\frac{\frac{F_o}{Xm}\sin\varphi}{2\zeta\omega_n\omega_f}\right]=+1 \text{ when } \omega_n>\omega_f \tag{9.9a}$$

and
$$\left[\frac{\frac{F_o}{Xm}\sin\varphi}{2\zeta\omega_n\omega_f}\right]=-1 \text{ when } \omega_n<\omega_f \tag{9.9b}$$

which appears to point to a solution that will produce a displacement response having different characteristics at excitation frequencies below the natural frequency compared to those when the forcing frequency is higher than ω_n. Taking eqns.(9.9a) and (9.9b) into account, eqn.(9.8) can have the form,

$$g(x)=\frac{x\left[\frac{F_o}{Xm}\cos\varphi+\omega_f{}^2-\omega_n{}^2\right]}{2\zeta\omega_n\omega_f\sqrt{X^2-x^2}}\pm 1 \tag{9.10}$$

Substituting eqn.(9.10) into eqn.(9.3) then gives,

$$\ddot{x}+2\zeta\omega_n\left\{\frac{x\left[\frac{F_o}{Xm}\cos\varphi+\omega_f{}^2-\omega_n{}^2\right]}{2\zeta\omega_n\omega_f\sqrt{X^2-x^2}}\pm 1\right\}\dot{x}+\omega_n{}^2x=\frac{F_o}{m}\sin(\omega_f t) \qquad (9.11)$$

To obtain the steady-state solution to eqn.(9.11), a power series expression was used, which assumed that the total displacement x could be calculated using,

$$x=x_1+\eta x_2+\eta^2x_3+\ldots+\eta^{n-1}x_n \quad \text{(where } n \text{ = integer values)} \qquad (9.12)$$

Considering the aforementioned expansion of x when n = 2, (i.e. a first-order expansion), substituting eqn.(9.12) into eqn.(9.11), and collecting like η terms gives,

$$\ddot{x}_1+2\zeta\omega_n\dot{x}_1+\omega_n{}^2x_1=\frac{F_o}{m}\sin(\omega_f t) \qquad (9.13a)$$

$$\ddot{x}_2\pm 2\zeta\omega_n\dot{x}_2+\omega_n{}^2x_2=-2\zeta\omega_n\frac{\left[\frac{F_o}{Xm}\cos\varphi+\omega_f{}^2-\omega_n{}^2\right]\sqrt{X^2-(x_1{}^2+2\eta x_1x_2)}\left\{x_1\ \dot{x}_1\right\}}{2\zeta\omega_n\omega_f\{X^2-(x_1{}^2+2\eta x_1x_2)\}} \qquad (9.13b)$$

where eqn.(9.13a) is the linear SODE as presented by eqn.(9.2). The solution to eqn.(9.11) incorporating eqn.(9.12) is therefore seen to be a combination of the linear SODE, which is modified by an equation of motion having the form of eqn.(9.13b). In order to simplify the solution process, it will be assumed that,

$$X=X_{\max}=\frac{F_o}{m}\left[\frac{1}{\sqrt{(2\zeta\omega_n{}^2)^2}}\right] \qquad (9.14)$$

where $X_{\max}$ is the peak steady-state amplitude of the linear SODE when ω_f is equal to ω_n. If the required adjustment to the linear FRF is small, η will also be of a modest magnitude, which allows eqn.(9.13b) to be written as,

$$\ddot{x}_2 \pm 2\zeta\omega_n \dot{x}_2 + {\omega_n}^2 x_2 = -2\zeta\omega_n \frac{\left[\frac{F_o}{X_{\max} m}\cos\varphi + {\omega_f}^2 - {\omega_n}^2\right]\sqrt{{X_{\max}}^2 - {x_1}^2}\left\{x_1 \dot{x}_1\right\}}{2\zeta\omega_n\omega_f\{{X_{\max}}^2 - {x_1}^2\}}$$

(9.15)

It is assumed that the steady-state response of eqn.(9.11) has a sinusoidal form, an appropriate displacement trial solution of eqn.(9.12) can be achieved by setting,

$$x_1 = A\sin(\omega_f t) + B\cos(\omega_f t) \tag{9.16a}$$

$$x_2 = C\sin(2\omega_f t) + D\cos(2\omega_f t) \tag{9.16b}$$

which can be substituted into eqns.(9.13a) and (9.15) respectively to yield,

$$A = \frac{F_o}{m}\frac{({\omega_n}^2 - {\omega_f}^2)}{({\omega_n}^2 - {\omega_f}^2)^2 + (2\zeta\omega_n\omega_f)^2} \tag{9.17a}$$

$$B = -\frac{F_o}{m}\frac{2\zeta\omega_n\omega_f}{({\omega_n}^2 - {\omega_f}^2)^2 + (2\zeta\omega_n\omega_f)^2} \tag{9.17b}$$

$$C = \left\{\frac{(B^2 - A^2)}{2}\right\}\kappa - \left\{\left(\frac{4\zeta\omega_n\omega_f AB}{({\omega_n}^2 - 4{\omega_f}^2)}\right)\left(\frac{({\omega_n}^2 - 4{\omega_f}^2)}{({\omega_n}^2 - 4{\omega_f}^2)^2 + (4\zeta\omega_n\omega_f)^2}\right)\kappa\right\}$$

(9.17c)

$$D = \frac{-(AB)\kappa - 4\zeta\omega_n\omega_f C}{({\omega_n}^2 - 4{\omega_f}^2)} \tag{9.17d}$$

where
$$\kappa = 2\zeta\omega_n \frac{\left[\frac{F_o}{X_{\max} m}\cos\varphi + \omega_f{}^2 - \omega_n{}^2\right]\sqrt{X_{\max}{}^2 - x_1{}^2}}{2\zeta\omega_n\omega_f\{X_{\max}{}^2 - x_1{}^2\}} \tag{9.18}$$

and eqns.(9.17c) and (9.17d) are subject to the following conditions:

(a) if $\omega_n > \omega_f$, eqns.(9.17c) and (9.17d) remain unchanged, while

(b) if $\omega_n < \omega_f$, eqns.(9.17c) and (9.17d) become

$$C = \left\{\frac{(B^2 - A^2)}{2}\right\}\kappa + \left\{\left(\frac{4\zeta\omega_n\omega_f AB}{(\omega_n{}^2 - 4\omega_f{}^2)}\right)\left(\frac{(\omega_n{}^2 - 4\omega_f{}^2)}{(\omega_n{}^2 - 4\omega_f{}^2)^2 + (4\zeta\omega_n\omega_f)^2}\right)\kappa\right\} \tag{9.19a}$$

$$D = \frac{-(AB)\kappa + 4\zeta\omega_n\omega_f C}{(\omega_n{}^2 - 4\omega_f{}^2)} \tag{9.19b}$$

Thus, eqns.(9.17a to d) to (9.19a and b) can be used in conjunction with eqns.(9.12) and (9.16a and b) to calculate the displacement response. Finally, to calculate the FRF for varying values of η, it is possible to determine the modified peak amplitude produced by the aforementioned formulation by assigning the time t in eqns.(9.16a) and (9.16b) with,

$$t = \left\{\frac{\frac{\pi}{2} + \varphi}{\omega_f}\right\} \tag{9.20}$$

which is consistent with the peak value that would be obtained from the linear SODE as assigned to eqn.(9.5). Figure 9.1 presents the FRF obtained using the mathematical expressions formulated above, which illustrates the amount of change that occurs to the linear solution as η is increased.

9.3.1.2 Discussion on the formulated closed form solution

The initial trial outlined above was based on the assumption that the adjusted FRF could be obtained using a function that would contain components of displacement (x) relative to the peak amplitude X. A simplification was introduced, which assigned the maximum peak steady-state amplitude (X_{max}) with a value that would be obtained from a linear SODE when excited at the natural frequency. This simplification allowed a convenient solution to the adjusted equation of motion, which was found to comprise two parts, (i) a linear visco-elastic part, plus (ii) a modified equation containing the components of the function $g(x)$.

Figure 9.1 illustrates the characteristics of the modified FRF, which also indicates the visco-elastic solution for comparison. The main points to note from this comparison are:

(i) The modified FRF gives a profile that approximates to the visco-elastic solution, but has the affect of 'sharpening' the resonance peak.

(ii) The solution portrays no 'skew' characteristics, as the modified profile remains 'symmetrical' relative to the visco-elastic FRF.

(iii) As η increases, the modified FRF characteristics remain approximately consistent with regard to (i) and (ii) above. The arrows in Figure 9.1 illustrate the main adjustment that is caused as a result of increasing η.

Clearly, the modified FRF obtained from the above formulations does not match the measurements taken from the damaged composite panels presented in chapter 7. The reasons that could be given for the lack of 'skew' mentioned in (ii) above are not entirely clear, as the expected outcome due to eqns.(9.9a) and (9.9b) appear to indicate that the displacement response when (i) $\omega_n > \omega_f$, and (ii) $\omega_n < \omega_f$ would have different characteristics.

It is possible that the approach considered above might eventually lead to an appropriate solution that would match the FRFs obtained from the damaged panels if higher components of 'n' in eqn.(9.12) were introduced. However, the presence of other components in $g(x)$, such as m, F_o and φ, may have an influence on the formulation that is not applicable to the characteristics required for a 'skewed' FRF

solution. To continue the analysis, which aims to achieve the latter, a number of trials were considered that were similar in approach to that outlined above, but chose to limit the number of components in $g(x)$ to those thought to be most appropriate. To represent the system behaviour, subsequent analyses focused on making adjustments to the linear SODE as before.

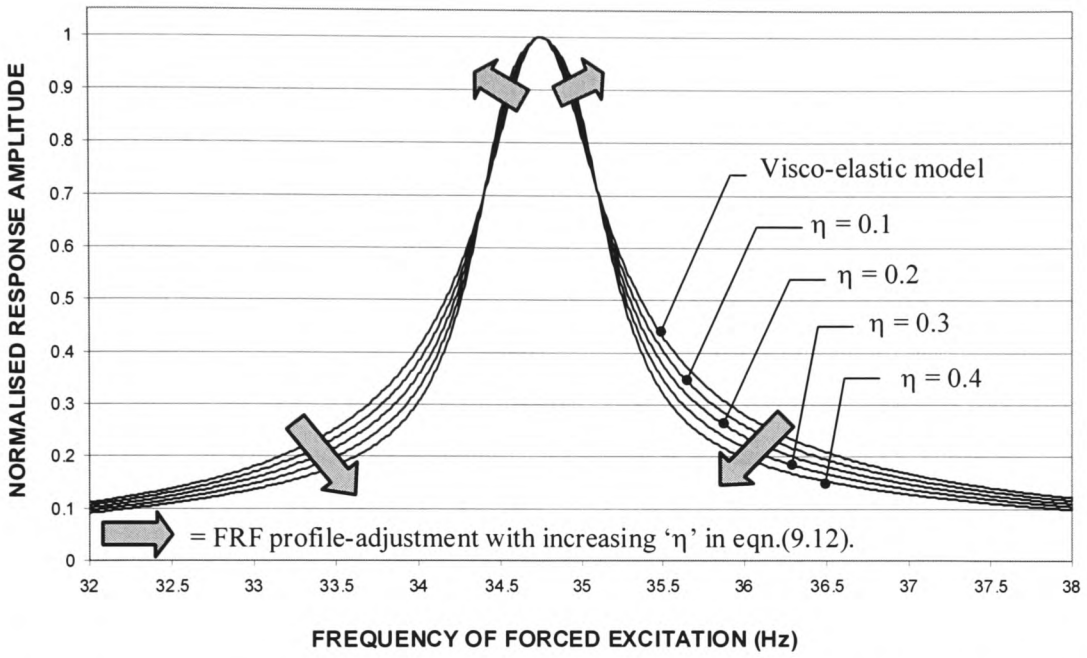

Figure 9.1 – Illustration of the adjusted FRF obtained from the modified differential equation of motion given by eqn.(9.11) above. The profiles indicated in this figure were calculated using $n = 2$ in eqn.(9.12).

9.3.2 Method based on 'perturbation' of the linear visco-elastic model – Formulation 2

9.3.2.1 Using a first-order perturbation

Consider the following,

$$\ddot{x} + 2\zeta\omega_n\left(1 + \varepsilon\frac{x}{X_{\max}}\frac{\omega_f}{\omega_n}\right)\dot{x} + \omega_n{}^2 x = \frac{F_o}{m}\sin(\omega_f t) \qquad (9.21)$$

where the $g(x)$ has been replaced with a function containing components of the system parameters, restricted to displacement and excitation frequency terms. In eqn.(9.21) ε represents a first-order perturbation, which enables small changes to be introduced into the expression. It is also noted that the adjustment has focused on the velocity dependent terms only, which again aims to simulate a modified damping behaviour. In essence, $\left(1+\varepsilon\frac{x}{X_{\max}}\frac{\omega_f}{\omega_n}\right)$ comprises of two dimensionless components, which aim to alter the behaviour of the damping:

(i) relative to the ratio between the displacement of the system (x) and the peak steady-state amplitude ($X_{\max}$) at the natural frequency [again, assuming the latter to be the linear solution], and

(ii) using a quantity that is dependent on the ratio between the forcing and natural frequency.

The most important aspect relates to (i) above, where the damping has been modified to have vibration amplitude dependence. To obtain a solution to eqn.(9.21), it can be assumed that the displacement has the form,

$$x(t) = x_u(t) \text{ when } \varepsilon = 0 \tag{9.22a}$$

$$x(t) = x_u(t) + \varepsilon x_p(t) \text{ when } \varepsilon \quad 0 \tag{9.22b}$$

where $x_u(t)$ and $x_p(t)$ are the 'un-perturbed' and 'perturbed' displacement solutions respectively. Considering the case when ε 0, eqn.(9.22b), and its derivatives with respect to time, can be substituted into eqn.(9.21) to give,

$$\ddot{x}_u + 2\zeta\omega_n \dot{x}_u + \omega_n{}^2 x_u = \frac{F_o}{m}\sin(\omega_f t) \tag{9.23a}$$

$$\ddot{x}_p + 2\zeta\omega_n \dot{x}_p + \omega_n{}^2 x_p = 2\zeta\omega_n\left(\frac{x}{X_{\max}}\frac{\omega_f}{\omega_n}\right)\dot{x}_u\, x_u \tag{9.23b}$$

(neglecting second-order ε terms). It is assumed that the steady-state solution to eqns.(9.23a) and (9.23b) can be expressed using an oscillatory form as before,

$$x_u = A\sin(\omega_f t) + B\cos(\omega_f t) \tag{9.24a}$$

$$x_p = C\sin(2\omega_f t) + D\cos(2\omega_f t) \tag{9.24b}$$

where the components of A, B, C and D can be determined. Substituting eqns.(9.24a) and (9.24b) into eqns.(9.23a) and (9.23b), these components can be defined as,

$$A = \frac{F_o}{m}\frac{(\omega_n{}^2 - \omega_f{}^2)}{[(\omega_n{}^2 - \omega_f{}^2)^2 + (2\zeta\omega_n\omega_f)^2]} \tag{9.25a}$$

$$B = -2\frac{F_o}{m}\frac{\zeta\omega_n\omega_f}{[(\omega_n{}^2 - \omega_f{}^2)^2 + (2\zeta\omega_n\omega_f)^2]} \tag{9.25b}$$

$$C = \frac{\zeta\omega_n\omega_f\left(\frac{x}{X_{\max}}\frac{\omega_f}{\omega_n}\right)\left(A^2 - B^2\right)\left(\omega_n{}^2 - 4\omega_f{}^2\right) + 8\zeta^2\omega_n{}^2\omega_f{}^2\left(\frac{x}{X_{\max}}\frac{\omega_f}{\omega_n}\right)(AB)}{[(\omega_n{}^2 - 4\omega_f{}^2)^2 + (4\zeta\omega_n\omega_f)^2]}$$

(9.25c)

$$D = \frac{2\zeta\omega_n\omega_f\left(\frac{x}{X_{\max}}\frac{\omega_f}{\omega_n}\right)(AB) - 4\zeta\omega_n\omega_f C}{(\omega_n{}^2 - 4\omega_f{}^2)} \tag{9.25d}$$

which is used to calculate the steady-state displacement as defined by eqn.(9.22b). To calculate the FRF, the peak amplitudes corresponding to a range of ω_f values can again be achieved by setting time t as given by eqn.(9.20).

The FRF calculated using eqn.(9.22b) is shown in Figure 9.2(a). The figure illustrates the modified profile of the FRF corresponding to various values assigned to ε, but it should be noted that the magnitude of the latter required to induce change is actually quite large. At the outset is appears that the assumption of the required 'perturbation'

(i.e. the amount of system damping change) being small has been violated, which suggests that higher orders of ε may by required.

9.3.2.2 Using a second-order perturbation

To assess the influence of higher ε components, the solution to eqn.(9.21) was also sought based on a second-order perturbation, which has the form,

$$x(t) = x_u(t) + \varepsilon x_{p1}(t) + \varepsilon^2 x_{p2}(t) \tag{9.26}$$

Substituting eqn.(9.26), and its derivatives, into eqn.(9.21) and collecting ε terms of similar order (neglecting those with third-order components) gives,

$$\ddot{x}_u + 2\zeta\omega_n \dot{x}_u + \omega_n{}^2 x_u = \frac{F_o}{m}\sin(\omega_f t) \tag{9.27a}$$

$$\ddot{x}_{p1} + 2\zeta\omega_n \dot{x}_{p1} + \omega_n{}^2 x_{p1} = 2\zeta\omega_n \left(\frac{x}{X_{\max}}\frac{\omega_f}{\omega_n}\right)\dot{x}_u\, x_u \tag{9.27b}$$

$$\ddot{x}_{p2} + 2\zeta\omega_n \dot{x}_{p2} + \omega_n{}^2 x_{p2} = 2\zeta\omega_n \left(\frac{x}{X_{\max}}\frac{\omega_f}{\omega_n}\right)\left(\dot{x}_{p1}\, x_u + x_{p1}\, \dot{x}_u\right) \tag{9.27c}$$

It is noted that eqns.(9.27a) and (9.27b) are similar to eqns.(9.23a) and (9.23b), and as such allow eqns.(9.24a) and (9.24b) to be assigned the components of A, B, C and D as given by eqns.(9.25a) to (9.25d). To determine the contribution of the second-order perturbation term, a trial solution of the form,

$$x_{p2} = E\sin(3\omega_f t) + F\cos(3\omega_f t) + G\sin(\omega_f t) + H\cos(\omega_f t) \tag{9.28}$$

was required, which after substitution into eqn.(9.27c) gave,

$$E = \frac{3\zeta\omega_n\omega_f\left(\frac{x}{X_{\max}}\frac{\omega_f}{\omega_n}\right)(AC-BD)\left(\omega_n{}^2-9\omega_f{}^2\right)+18\zeta^2\omega_n{}^2\omega_f{}^2\left(\frac{x}{X_{\max}}\frac{\omega_f}{\omega_n}\right)(AD+BC)}{(\omega_n{}^2-9\omega_f{}^2)^2+(6\zeta\omega_n\omega_f)^2}$$

(9.29a)

$$F = \frac{3\zeta\omega_n\omega_f\left(\frac{x}{X_{\max}}\frac{\omega_f}{\omega_n}\right)(AD-BC)-6\zeta\omega_n\omega_f E}{(\omega_n{}^2-9\omega_f{}^2)} \qquad (9.29b)$$

$$G = \frac{-\zeta\omega_n\omega_f\left(\frac{x}{X_{\max}}\frac{\omega_f}{\omega_n}\right)(AC-BD)\left(\omega_n{}^2-\omega_f{}^2\right)+2\zeta^2\omega_n{}^2\omega_f{}^2\left(\frac{x}{X_{\max}}\frac{\omega_f}{\omega_n}\right)(BC-AD)}{(\omega_n{}^2-\omega_f{}^2)^2+(2\zeta\omega_n\omega_f)^2}$$

(9.29c)

$$H = \frac{\zeta\omega_n\omega_f\left(\frac{x}{X_{\max}}\frac{\omega_f}{\omega_n}\right)(BC-AD)-2\zeta\omega_n\omega_f G}{(\omega_n{}^2-\omega_f{}^2)} \qquad (9.29d)$$

Adopting a similar procedure to that assumed for the first-order perturbation [i.e. calculating the displacement when time t is equal to eqn.(9.20)] the FRF is achieved. Figure 9.2(b) illustrates the influence of various ε magnitudes, where it can be seen that in order to produce a modified FRF, value of ε remains relatively large.

9.3.2.3 Discussion on the perturbation approach

It can be seen from the FRFs presented in Figure 9.2(a) that the amount of perturbation (ε) required to produce an appreciable change to the linear visco-elastic solution was larger, while higher orders of ε [Figure 9.2(b)] required a reduced amount of adjustment. In both cases considered, it is clear that the approach is not appropriate, as the assumption that the amount of change to the linear SODE will be small has not

been fulfilled. Reflecting on the two cases considered, it is possible that the magnitude of ε might reduce if further components of $\varepsilon^n x_{pn}(t)$ (where n = integer greater than 2) in eqn.(9.26) are considered. Incorporating additional components in this way could then lead to a solution that would give the desired magnitude for ε. However, there are two main problems associated with such a progression, (i) eqn.(9.26) with the addition of further terms becomes excessively complicated, due to the need to further extend the steady-state displacement trial solution, and (ii) it appears that the calculated FRF profile does not match that observed from the measurements taken from the damaged panels. The former of these points is a problem that could be solved with further manipulation of the system equations, but the practicality of developing a method that appear not to provide the required solution must be taken into account.

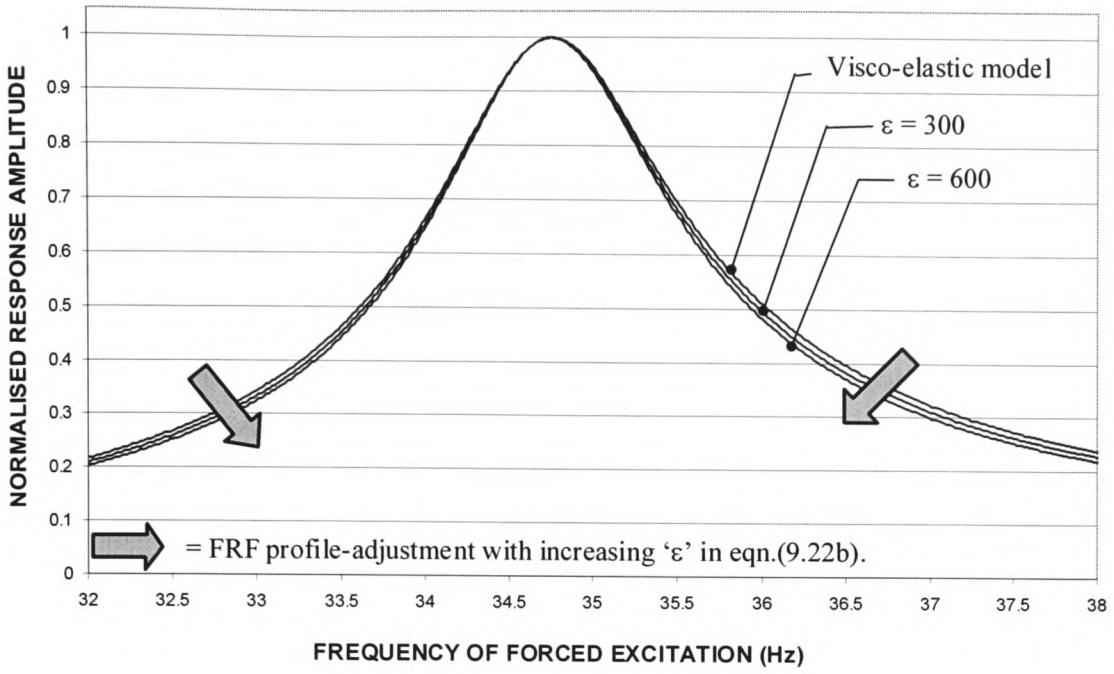

(a)

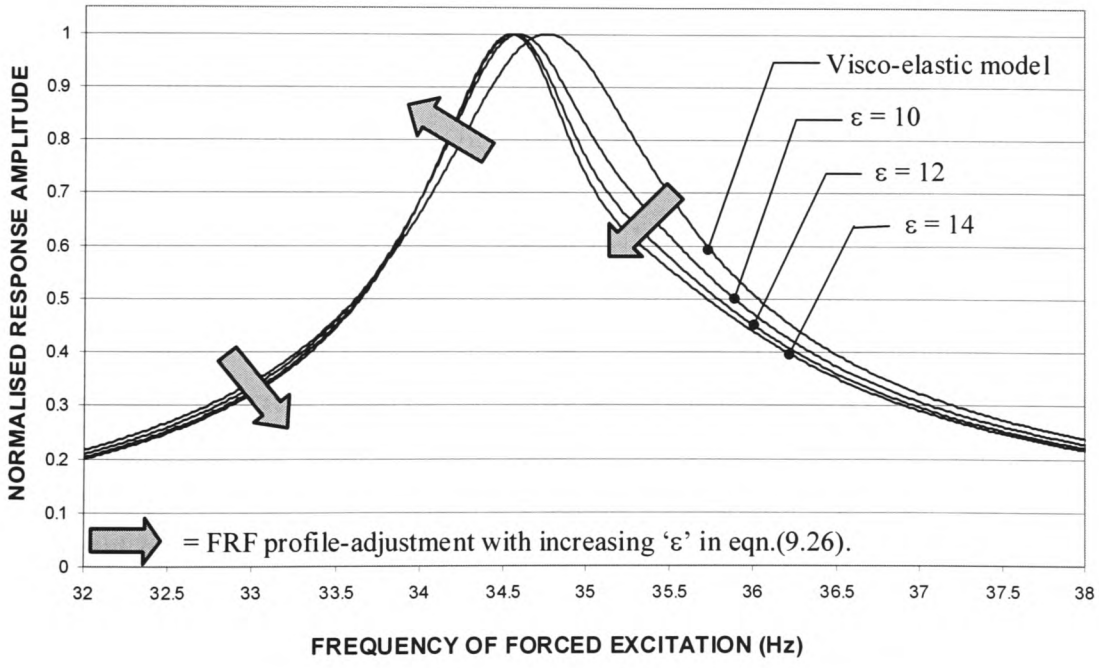

(b)

Figure 9.2 – Illustration of the adjusted FRF obtained from the modified differential equation of motion given by eqn.(9.21) above. The profiles indicated in this figure were calculated using (a) eqn.(9.22b) and (b) eqn.(9.26).

9.3.3 Method assuming a combined 'visco-elastic and coulomb-friction' damper – Formulation 3

9.3.3.1 Using an 'equivalent viscous' coulomb-friction damper

The methods considered above have focused on the possibility that the modified FRF can be produced with adjustments made to the velocity dependent components of the linear SODE. These have been shown to provide in-appropriate solutions, and appear not to offer a convenient way forward.

As an alternative, the condition of a combined 'visco-elastic and coulomb-friction' damper was considered. This assumption relates directly to the discussion presented in section 9.2.4, where it was stated that the behaviour of the panel damping after damage might be composed of a viscously dominated response modified by the presence of a friction energy dissipater.

Consider the following equation of motion,

$$\ddot{x}+\left[2\zeta\omega_n+\left\{\frac{4F_d}{\pi\omega_f Xm}\right\}\right]\dot{x}+\omega_n{}^2x=\frac{F_o}{m}\sin(\omega_f t) \tag{9.30}$$

In eqn.(9.30), the term $\left[2\zeta\omega_n+\left\{\frac{4F_d}{\pi\omega_f Xm}\right\}\right]$ is the combined damping model, which makes use of the formulated 'equivalent viscous' coulomb-friction energy dissipater as presented by Thomson (1996) where F_d is the friction force. To calculate the peak steady-state amplitude of the equation of motion presented above, it is again convenient to assume that the displacement response can be determined using eqn.(9.5). Substituting eqn.(9.5), and its derivatives, into eqn.(9.30) and collecting like sine terms gives,

$$\omega_f{}^2 X \sin(\omega_f t - \varphi + \pi) + 2\zeta\omega_n\omega_f X \sin(\omega_f t - \varphi + \frac{\pi}{2}) \ldots$$

$$\ldots + \frac{4F_d}{\pi m}\sin(\omega_f t - \varphi + \frac{\pi}{2}) + \omega_n{}^2 X \sin(\omega_f t - \varphi) = \frac{F_o}{m}\sin(\omega_f t) \qquad (9.31)$$

Instead of solving for x, it is noted from eqn.(9.31) that X can be obtained directly from a representation of its 'vector relationship', which is shown graphically by Figure 9.3. Using this graphical approach, which takes account of all components contained in the differential equation of motion above, it can be seen that equilibrium of the system is satisfied only if,

$$\left[\frac{F_o}{m}\right]^2 = \left[\left\{(\omega_n{}^2 - \omega_f{}^2)X\right\}^2 + \left\{2\zeta\omega_n\omega_f X + \frac{4F_d}{\pi m}\right\}^2\right] \qquad (9.32)$$

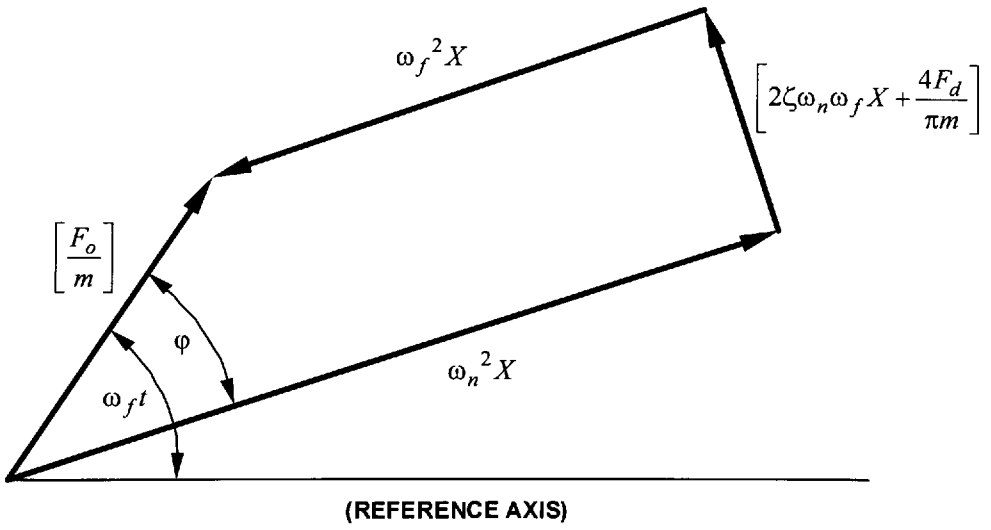

Figure 9.3 – Vector relationship for steady-state forced vibration with a combined visco-elastic plus an equivalent viscous coulomb-friction damper.

Expanding eqn.(9.32), and collecting terms relative to powers of X, gives,

$$\left(\omega_n{}^4 + \omega_f{}^4 - 2\omega_n{}^2\omega_f{}^2 + 4\zeta^2\omega_n{}^2\omega_f{}^2\right)X^2 + \left(\frac{16F_d\zeta\omega_n\omega_f}{\pi m}\right)X \ldots$$

$$\ldots + \left(\frac{16F_d{}^2}{\pi^2 m^2} - \frac{F_o{}^2}{m^2}\right) = 0 \tag{9.33}$$

which can be seen to be a quadratic equation with a solution of the form,

$$X = \frac{-e \pm \sqrt{e^2 - 4df}}{2d} \tag{9.34}$$

where $$d = \left(\omega_n{}^4 + \omega_f{}^4 - 2\omega_n{}^2\omega_f{}^2 + 4\zeta^2\omega_n{}^2\omega_f{}^2\right) \tag{9.35a}$$

$$e = \left(\frac{16F_d\zeta\omega_n\omega_f}{\pi m}\right) \tag{9.35b}$$

and $$f = \left(\frac{16F_d{}^2}{\pi^2 m^2} - \frac{F_o{}^2}{m^2}\right) \tag{9.35c}$$

The adjusted phase (φ) can also be found, which is determined using,

$$\tan\varphi = \frac{2\zeta\omega_n\omega_f X + \dfrac{4F_d}{\pi m}}{(\omega_n{}^2 - \omega_f{}^2)X} \tag{9.36}$$

The solution to eqn.(9.34) for varying ωf is presented by Figure 9.4, which illustrates the adjusted FRF relative to the visco-elastic behaviour caused when different values of F_d are considered. The values of F_d that were used to compile the above-mentioned figure are shown in relative terms, i.e. $F_d \times 1$, to $F_d \times 4$.

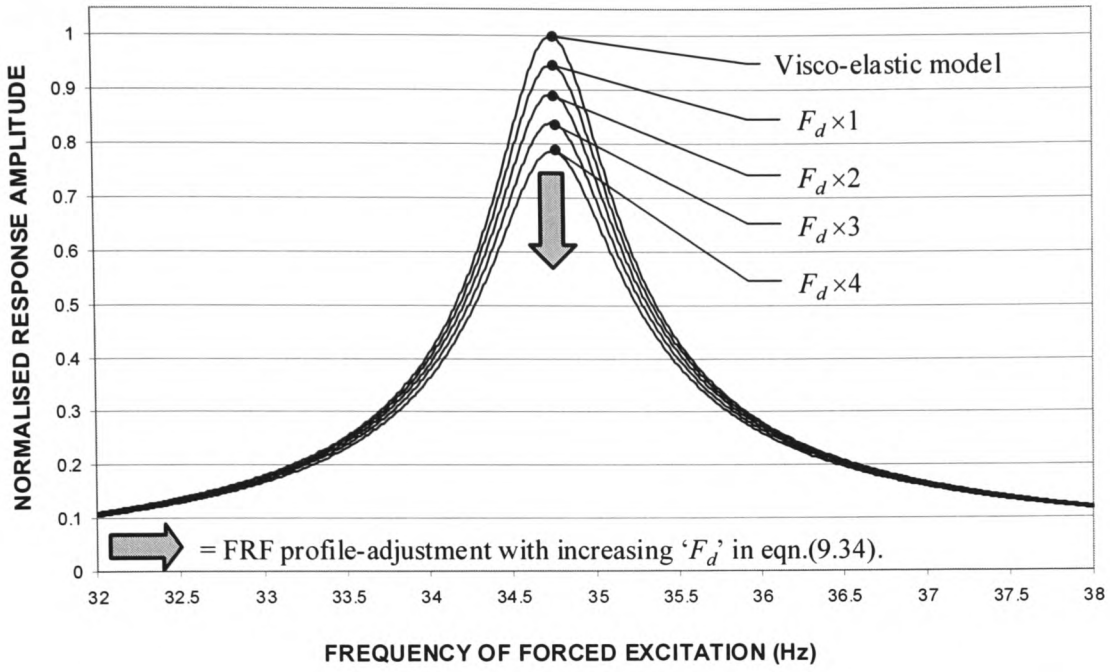

Figure 9.4 – Illustration of the adjusted FRF obtained from the combined visco-elastic and equivalent viscous coulomb-friction damper given by eqn.(9.30) above.

9.3.3.2 Discussion on the combined damper approach

The combined viscous and coulomb-friction damper included above has shown that the peak steady-state amplitude solution obtained for eqn.(9.30) provides modified FRF characteristics, but unfortunately, the solution does not provide a 'skew' type profile. The reasons that could be given for the lack of FRF 'skew' from this approach could be attributed mainly to the formulation adopted. It can be seen from eqn.(9.32) that the influence of the added damper, on the 'force vector relationship' of Figure 9.3, serves only to increase the damping force by an amount that remains constant with no dependency on the peak steady-state amplitude. With regard to the affect of adding such a constant, there will clearly be no induced variation to the viscous damper through the frequency range of the FRF, as the added equivalent model merely increases the former by an amount dependent only on F_d. As a result, no fluctuation of damping is introduced, making the modified FRF appear simply to reflect

characteristics that could be achieved if an increased value of viscous damping were considered.

9.4 Formulating a Mathematical Expression to Fit a Modified FRF Characteristic of the Damaged Composite Panels

The salient aims of this method are to:

(i) Produce a mathematical expression that can be used to match the FRF of post-damaged composite panels observed from measurements by incorporating additional terms into the formulation of the existing visco-elastic FRF model.

(ii) Using (i), determine the extent to which the FRF characteristics are affected by the presence of damage.

(iii) Establish if the results of (ii) can provide a basis for use as an additional damage identification parameter.

9.4.1 The trial mathematical expressions

The mathematical expressions considered in this section were formulated in an attempt to reflect the main characteristic of the FRFs obtained from the measurements that are presented in chapter 7. It was seen from the latter that the visco-elastic properties dominated the response of the panels at all stages of imposed damage, and as such the expressions considered from herein were prepared to maintain this observation. The formulations themselves make use of the linear visco-elastic FRF model, which has the form,

$$\frac{X}{F_o} = \frac{1}{k}\left(\frac{1}{\sqrt{\left[1-\left(\frac{\omega_f}{\omega_n}\right)^2\right]^2 + \left[2\zeta\left(\frac{\omega_f}{\omega_n}\right)\right]^2}} \right) \tag{9.37}$$

and is equivalent to eqn.(9.14). To obtain a response function that resembles that observed from measurements, an adjustment to eqn.(9.37) was considered in the form of,

$$\frac{X}{F_o} = \frac{1}{k}\left(\frac{1}{\sqrt{\left[1-\left(\frac{\omega_f}{\omega_n}\right)^2\right]^2 + \left[2\zeta\left(\frac{\omega_f}{\omega_n}\right)-\gamma\right]^2}} \right) \tag{9.38}$$

where γ is a function that modifies the damping characteristics. It should be noted at this stage that the modification does not aspire to simulate the behaviour that could be attributed to an appropriate damping model, but aims simply to find a solution that will provide a 'skewed' FRF profile.

Without presenting all the γ functions considered, only the composition that was found to provide the required characteristics of the measured FRFs will be presented. However, for completeness, Table 9.1 has been included to illustrate a number of the trials that have been considered, but were found not to be appropriate.

9.4.2 The function that successfully produce the required modified FRF

After numerous trail functions in γ, the solution that was found to modify the FRF corresponding to the measurements obtained from the damaged panels was achieved when,

$$\gamma = \frac{\left\{\frac{\omega_f}{\omega_n}\right\}\left\{a\left[1-\left(\frac{\omega_f}{\omega_n}\right)\right]\right\}}{\left\{1+b\left(\frac{\omega_f}{\omega_n}\right)^{2n}\right\}} \tag{9.39}$$

Equation (9.39) is dimensionless, while 'a', 'b' and 'n' are constants that can be adjusted to suit the required FRF profile, which enables its characteristics to be modelled at each level of imposed damage.

9.4.3 The influence of parameter adjustment on the proposed formulation

To demonstrate the affect that different values of 'a', 'b' and 'n' in eqn.(9.39) have on the profile of the adjusted visco-elastic expression, Figures 9.5(a) to (c) have been prepared. The main points to note from these figures are described in the following discussions.

9.4.3.1 Influence of the constant 'b'

The influence of 'b' on the profile of the adjusted FRF is illustrated by Figure 9.5(a). To make the influence easier to identify, a number of arrows have been included on the figure as before, which show the direction of the change in 'deformation' as 'b' reduces, which occurs relative to the linear visco-elastic function. The example portrayed by this figure assumes that the values of 'a' and 'n' remain constant. The actual values that have been assigned to these constants are not important for the illustrated demonstration. But to emphasis the sensitivity of the adjusted FRF, the figure shows three functions, one that reflects the profile obtained from the visco-elastic model, while the remaining lines showing the change that is created when 'b' has relative values of '1' and '10'.

9.4.3.2 Influence of the constant 'a'

Figure 9.5(b) show the variation that occurs to the adjusted profile when 'b' and 'n' remain constant, while 'a' is varied. The arrows have again been included to show the profile changes created, which in this case depict the adjustment that results when 'a' is increased. A total of five FRF profiles are illustrated with one being the visco-elastic response as before. The remaining four functions were the result of changes made to 'a', which represent relative values on a scale of '1' to '4'.

9.4.3.3 Influence of the constant 'n'

Figure 9.5(c) shows the FRF of the adjusted response with '*a*' and '*b*' maintained at constant values, while '*n*' varies with relative values from '1' to '4'. The visco-elastic model is again included for comparison, while the four functions that represent the aforementioned variation influence the change in the profile as indicated by the arrows, which illustrate increasing '*n*' values.

9.4.3.4 Characteristics of the adjusted FRF

The influence of the constants '*a*', '*b*' and '*n*' change the profile of the FRF in the following way:

(i) Changes to '*a*' and '*b*' deviate the peak of the FRF to simulate the shifting of the resonance frequency relative to the visco-elastic model.

(ii) Adjustments made to '*n*' produces a rotation (or 'skew') of the resonance peak allowing this feature to be replicated, as seen from the measurements taken from the damaged panels (chapter 7).

9.4.4 Applying the adjusted FRF to measurements taken from the damaged composite panels

The FRFs presented in chapter 7 indicate that the frequency response behaviour of the un-damaged composite panels could be modelled accurately assuming the visco-elastic model in its standard form. No further analysis of the panels corresponding to this condition was therefore carried out. The post-damaged results, however, did show that the measurements deviate from the visco-elastic model, the extent of which was seen to change. The latter aspect, i.e. the amount of deviation, is of main concern here where the proposed expression allows the change to be quantified.

Table 9.1 – Sample trial functions for γ found not to produce the required FRF modifications

Trial function	Graphical display of modified FRF
$\gamma = a\left[1 - \frac{\omega_f}{\omega_n}\right]$	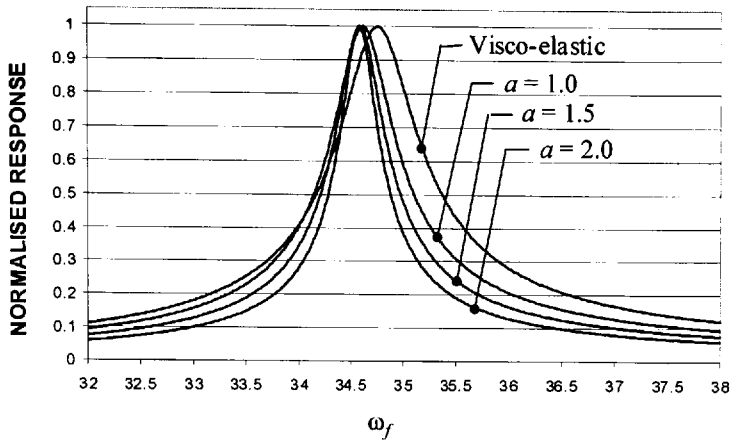
$\gamma = a\left[1 - b\frac{\omega_f}{\omega_n}\right]$	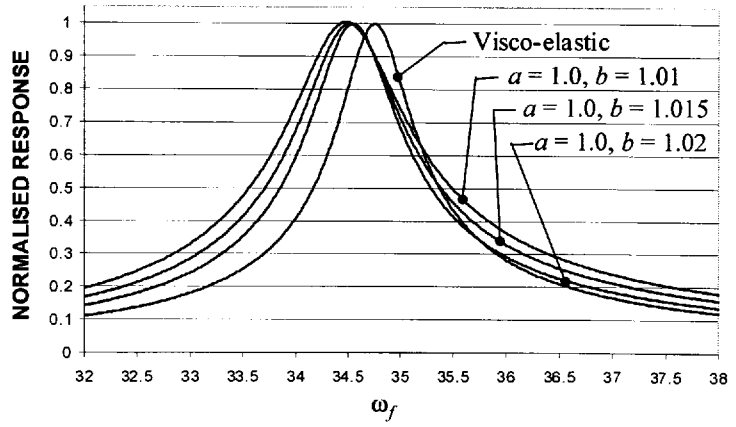
$\gamma = a\left[1 - \frac{\omega_f}{\omega_n}\right]e^{-n}$	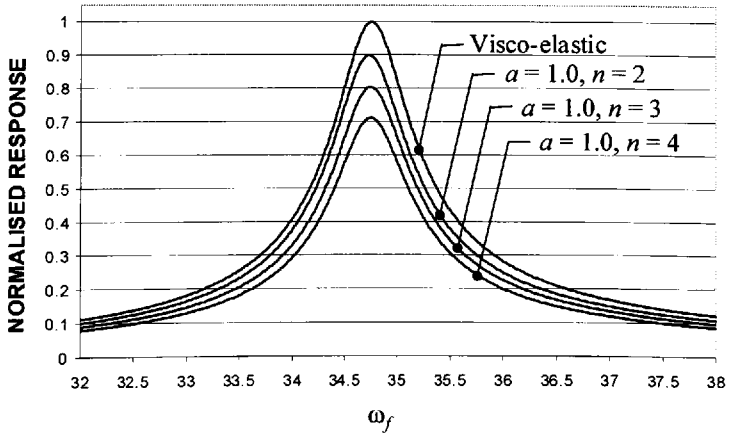

(where a, b, and n are constants).

9.4.4.1 Applying the function to the results recorded from a full panel test at a constant excitation-force-level

Figures 9.6(a) and (b) show a comparison of eqn.(9.38), incorporating eqn.(9.39), and the results obtained from the measured post-damaged panel FRFs. The example shown is typical of all panels, but the amount of adjustment required to make the expressing fit the measurements varied.

9.4.4.2 The influence of the 'a', 'b' and 'n' constants at various excitation force-levels

To illustrate the value change of the constants '*a*' and '*n*', Figures 9.7(a) to (c) have been included. It is seen from the figure that the above constants show change with amplitude of vibration, which is an expected outcome. However, it should be noted that the dominant change is due to the values assigned to the constant '*n*', which is the parameter responsible for the skew of the response peak as identified earlier. In all cases, the value of '*b*' was kept constant.

9.4.5 Possible influence of the adjusted FRF on the characteristics of the damping

The discussion above has identified that the proposed adjustment gives an appropriate model to match measured FRFs. However, it is not clear how damping is affected by the imposed modification.

To obtain a measure of the damping modification, and to establish its fluctuation throughout the range of frequencies that make up the FRF, a number of steps can be taken. It is clear from eqns.(9.38) and (9.39) that both ζ and γ are regulated in a manner that is mainly dependent on the ratio of $\frac{\omega_f}{\omega_n}$. Using this knowledge, and assuming that the influence of γ can be related directly to a modification of ζ, it is possible to examine the effect of the former on the latter by defining,

$$\left[2\zeta\left(\frac{\omega_f}{\omega_n}\right)-\gamma\right]=\left[2\zeta_{\text{mod}}\left(\frac{\omega_f}{\omega_n}\right)\right] \tag{9.40}$$

thereby making,

$$\zeta_{\text{mod}}=\zeta-\frac{1}{2}\left(\frac{\omega_n}{\omega_f}\right)\gamma \tag{9.41}$$

where ζ_{mod} is the modified damping ratio. Figure 9.10 shows eqn.(9.41) corresponding to a range of forcing frequencies ω_f, and illustrates the characteristics of the modified damping relative to the various n parameters used in eqn.(9.39).

9.5 Result of Applying the Proposed Expression to all Damaged Panels

9.5.1 The procedure adopted to fit the adjusted FRF to the measured data

(i) To produce a fit of eqn.(9.38), incorporating eqn.(9.39), to the measure FRF, the approach adopted was to first introduce changes to the constant 'a' using the results of the best-fit visco-elastic correlation of chapter 7 as a basis for the adjustment. Assigning different values to 'a' had the effect of moving the position of the response peak relative to the profile gained from the linear visco-elastic calculations along the frequency axis, which resembled that of a natural frequency shift. Thus, starting at an appropriate value, followed by successive trials at a regular increasing interval, the value of 'a' that provided the best fit was noted when the peak of the calculated response function [eqn.(9.38)] was in line with that observed from the measured data.

(ii) Secondly, having found an appropriate value of 'a', the constant 'n' was similarly varied until the skew of the profile matched the measurements.

(iii) In all cases, no variation of 'b' was required, which remained at a constant value of 1.5 throughout the calculated / measurement fitting procedure.

(iv) Finally, with all constants established for one FRF, subsequent profiles that represented the measurements after additional applied load increments were found by making modifications to the values determined from the previous curve fit. With this approach the effect of changing 'a' and 'n' could be assessed on a relative basis, where the influence of added 'damage' was identified from the amount of adjustment that was needed after each interval.

9.5.2 Main points to note from the results

The measured FRFs that were obtained from the panels during the pre-damage stages of the laboratory tests were found to reflect closely the profile of the response function calculated with the linear visco-elastic model, with no evidence of profile skew being observed. As a result, it was decided to concentrate the study on the post-damage stages of the tests only, the results of which have been compiled and presented by Figures 9.8 and 9.9.

The values that have been assigned to the constants 'a' and 'n' have a magnitude that was dictated by the parameters of natural frequency and the damping ratio. Values of 'a' and 'n' would therefore probably yield different quantities if applied to structures with contrasting natural frequency and damping values to those found from the panel measurements. To facilitate a clearer interpretation, the changes to 'a' and 'n' have been normalised and included in the aforementioned figures.

Results from modifications required to the constant 'a':

(i) The change of the constant 'a', with progressive damage, was found to provided inconclusive results. Although the general trend of 'a' for panel type S1 appears to indicate a gradual increase (relative change of 1.0 at 'first-damage' to $\approx$1.15 at impending failure), the individual values are scattered. This is also reflected in the results from panel type S2, where the trend is even less distinguishable.

(ii) For both S1 and S2 panels, the results given in Figure 9.8 are those obtained using data from all three excitation-force-levels. It is clear from the results that 'a' appears not to show any trend that could be related to the various force-levels considered in this study.

(iii) It is the candidate's opinion that the lack of a visible repeatable trend in 'a', could be attributed to a factor involving the amount of measured data that was collected during the laboratory tests. Throughout the studies carried out and presented in this chapter, the commencing point of the correlation of measured and adjusted FRFs was based in the information determined in chapter 7. i.e. the values of natural frequency and damping adopted for the adjusted expression were as calculated assuming the linear visco-elastic model. The FRFs that are obtained using the visco-elastic model [eqn.(9.37)] depend on the amount of measured data and on the frequency range over which the correlation is considered. Therefore, the natural frequency and damping that is obtained from one data set, comprising a certain number of response amplitude data points, will yield different dynamic characteristics to one with a dissimilar data composition (under similar test conditions) due to the correlation procedures. Since the value assigned to 'a' merely modifies the position of the response peak [see Figure 9.5(b)], variations in the accuracy of the initial correlation will be reflected in the adjusted expression of eqn.(9.38).

Modifications required to the constant 'n':

(i) Unlike the findings identified above, the variation of 'n' found from the study showed a definite trend. In addition, its change with amplitude of vibration was also distinguishable.

(ii) The results indicate that the 'skew' of the measured FRFs changes after each interval of progressive damage, and that the amount of change in 'n' is 'near linear', as demonstrated by the regression lines included in Figure 9.9.

(iii) A presentation of the results using a normalised scale also indicates an additional interesting feature, which appears to suggest that the variation of 'n' throughout damage for the three excitation-force-levels is approximately similar.

(iv) The amount that 'n' varies, as indicated by the normalised scale, for panel types S1 and S2 were calculated to be 2.0 and 2.5 respectively. Each division within this range therefore reflecting the progressive increase in the amount of modified damping that occurred to the frequency response of the panels.

9.6 Concluding Discussion

The aim of this chapter was to present a mathematical expression that could be fitted to the measured FRFs obtained from the laboratory tests. Initial trials that focused on modifications made to a linear differential equation of motion produced in-appropriate solutions. As a consequence, further studies concentrated on an approach that introduced adjustments to the visco-elastic FRF expression directly. Using the adjusted expression, a formulation has emerged that was seen to match the profile of the FRFs measured from the damaged composite panels, which provides an additional indication of progressive defects.

Throughout the latter part of the study, it has been assumed that any adjustment to the FRF of the viscous model should focus on modifications introduced to its damping. However, it is stressed by the candidate that the adjusted expression [eqn.(9.38)] was not formulated to replicate the behaviour of the panels in a manner that could be used to calculate transient or steady state response properties (i.e. time varying response). But, it has been shown that it is possible to identify modified damping throughout the frequency range of the FRF, which generally shows that:

(i) when $(\omega_f < \omega_n)$, $\zeta_{mod} < \zeta$

(ii) when $(\omega_f > \omega_n)$, $\zeta_{mod} > \zeta$.

Although the 'skew' of the FRF appears to occur when the panels became damaged, the candidate accepts that other structures [such as those considered by Ellis (1993)] may show frequency dependent FRF modifications at large amplitudes, even when damage is not present. Clearly, taking the latter into account, there appears to be a relationship between amplitude of vibration and frequency dependent modifications, the detail of which is not precise. Nevertheless, by considering a modified FRF, the study presented in this chapter suggests that damping may have a much larger influence on the response characteristics of damaged structures as opposed to stiffness related changes.

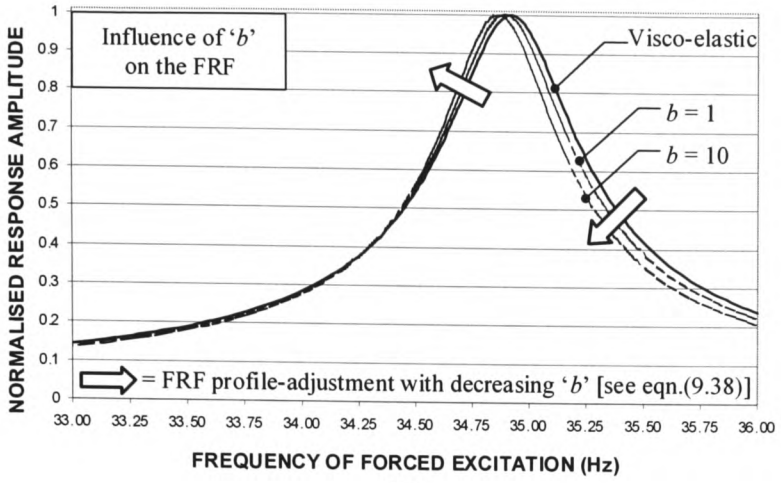

(a)

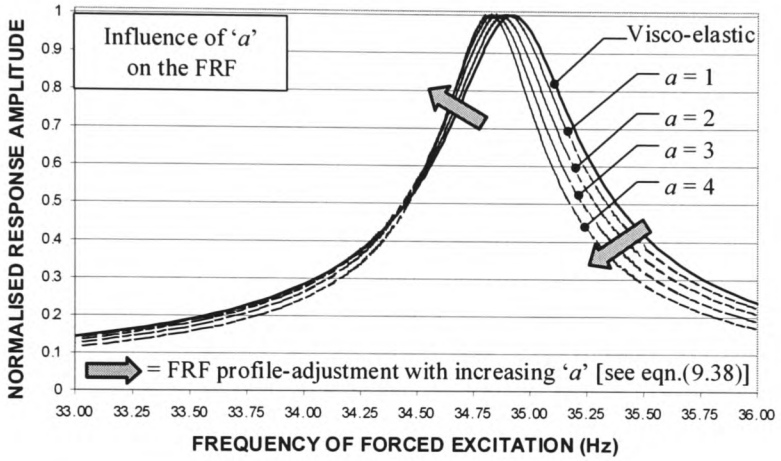

(b)

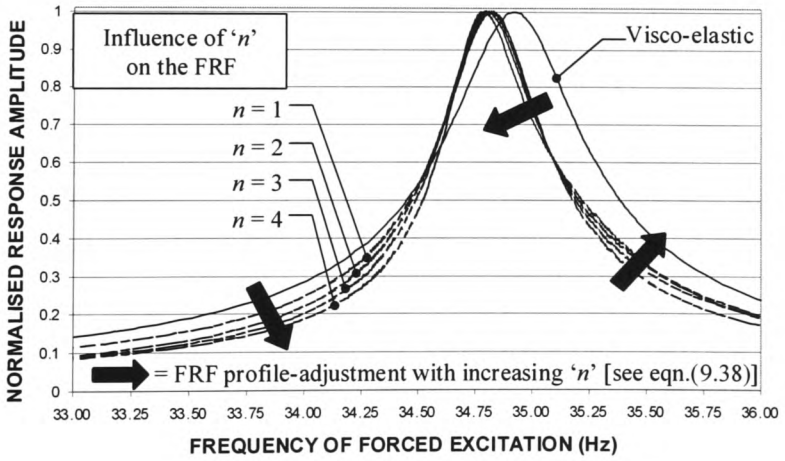

(c)

Figure 9.5 – Illustration of the adjusted FRF of eqn.(9.38) showing the influence of the constants (a) '*b*', (b), '*a*', and (c) '*n*'. Arrows indicate the segment of the response profile adjusted by the changes made to the constants as noted.

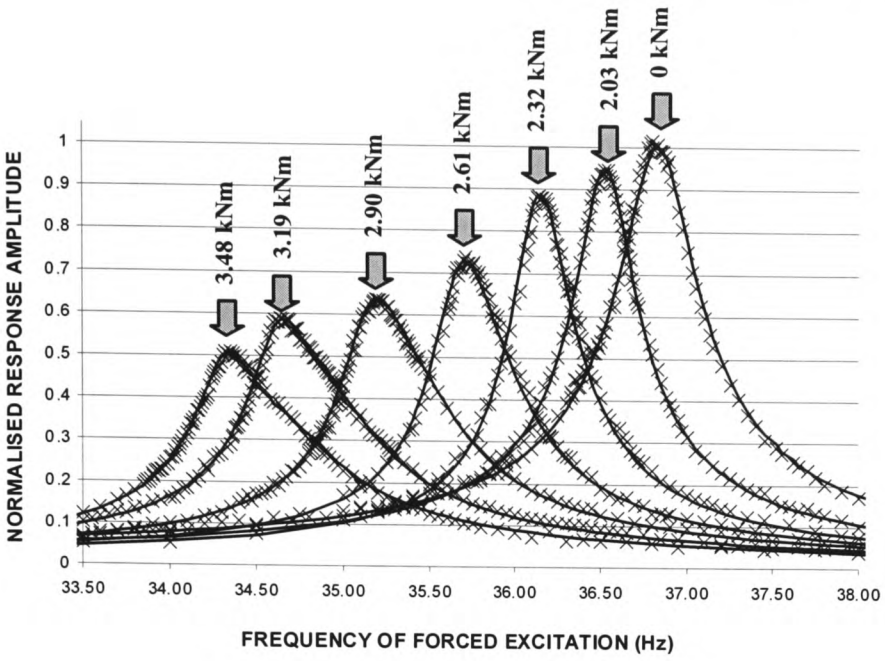

(a)

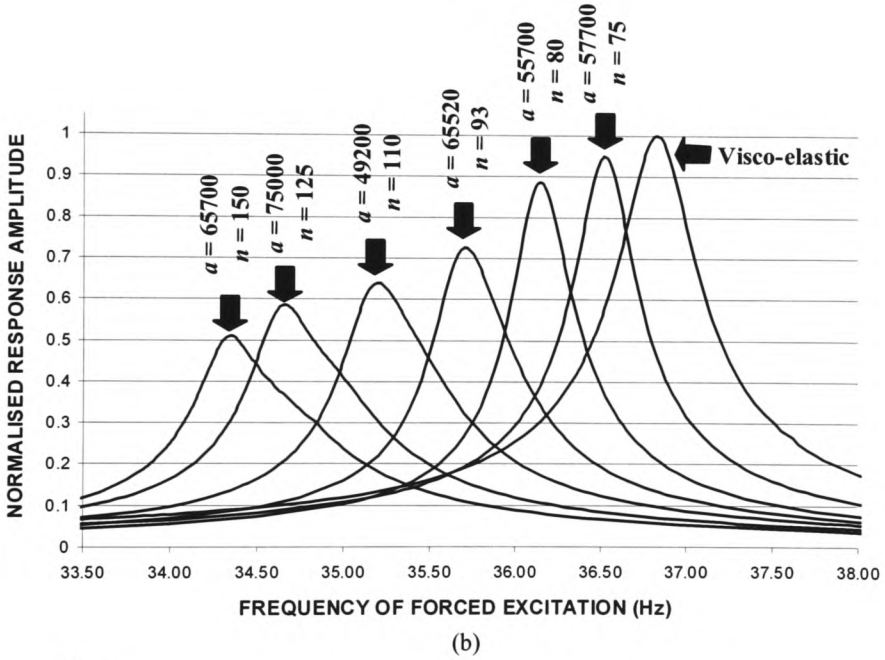

(b)

Key:

× = Measured data

— = Best-fit relationship using eqn.(9.38) - Unless otherwise stated

⇩ = Bending moment applied to the panel before the response readings were taken.

▼ = Constant '*a*' and '*n*' required to obtain a good fit. All cases, '*b*' = 1.5

Figure 9.6 – Sample 'frequency sweep' data showing the changes observed to the measured FRF (natural frequency and damping as Figure 7.19 – chapter 7). (a) Measured results against the adjusted FRF of eqn.(9.38), (b) illustrates the profile of the FRFs with measured data removed.

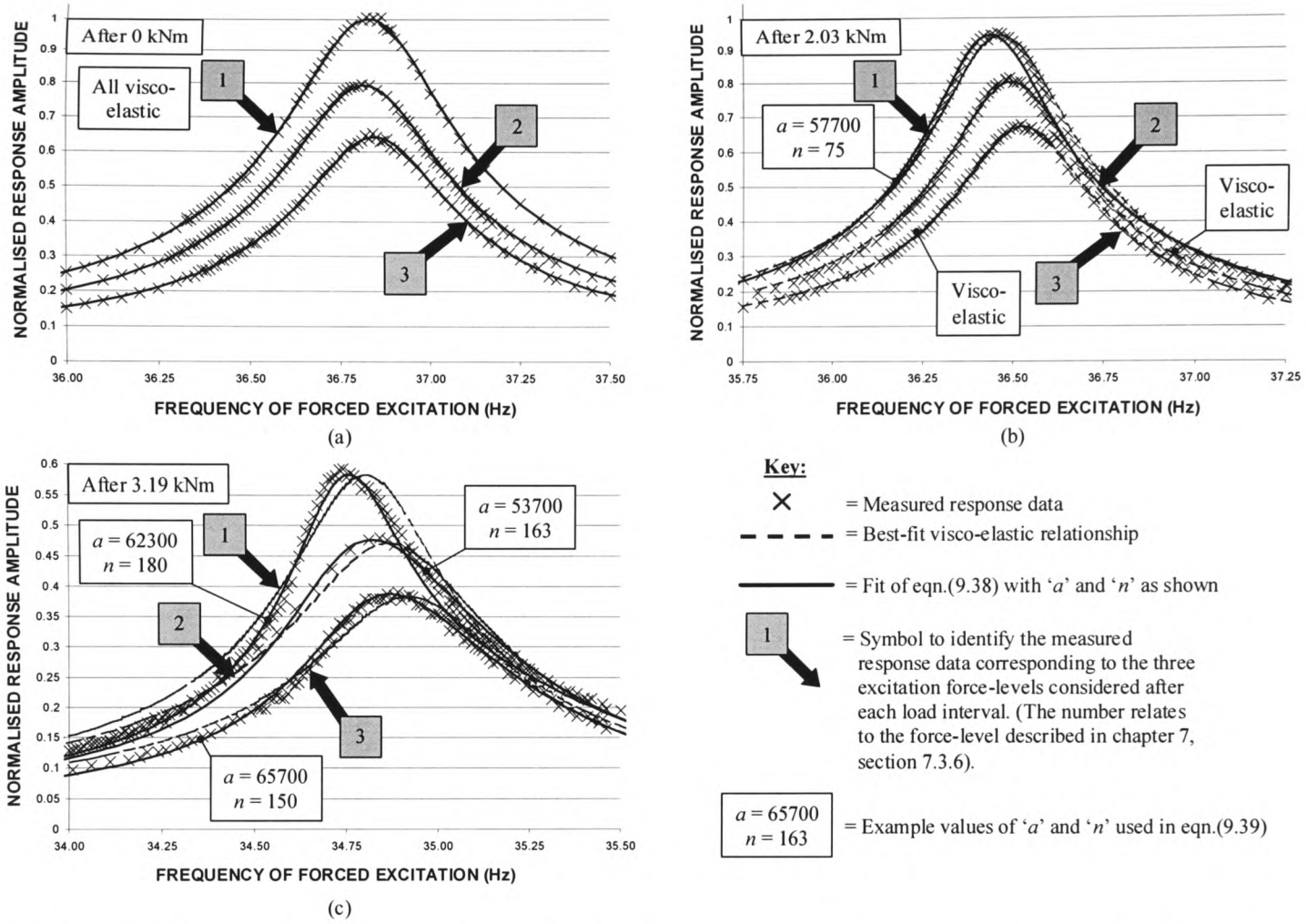

Figure 9.7 – Illustration of the frequency dependence of the FRFs observed from the frequency sweep data recorded after (a) 0 kNm, (b) 2.03 kNm, and (c) 3.19 kNm of applied bending moment. (Panel type S1 shown). Adjusted FRF of eqn.(9.38) also included.

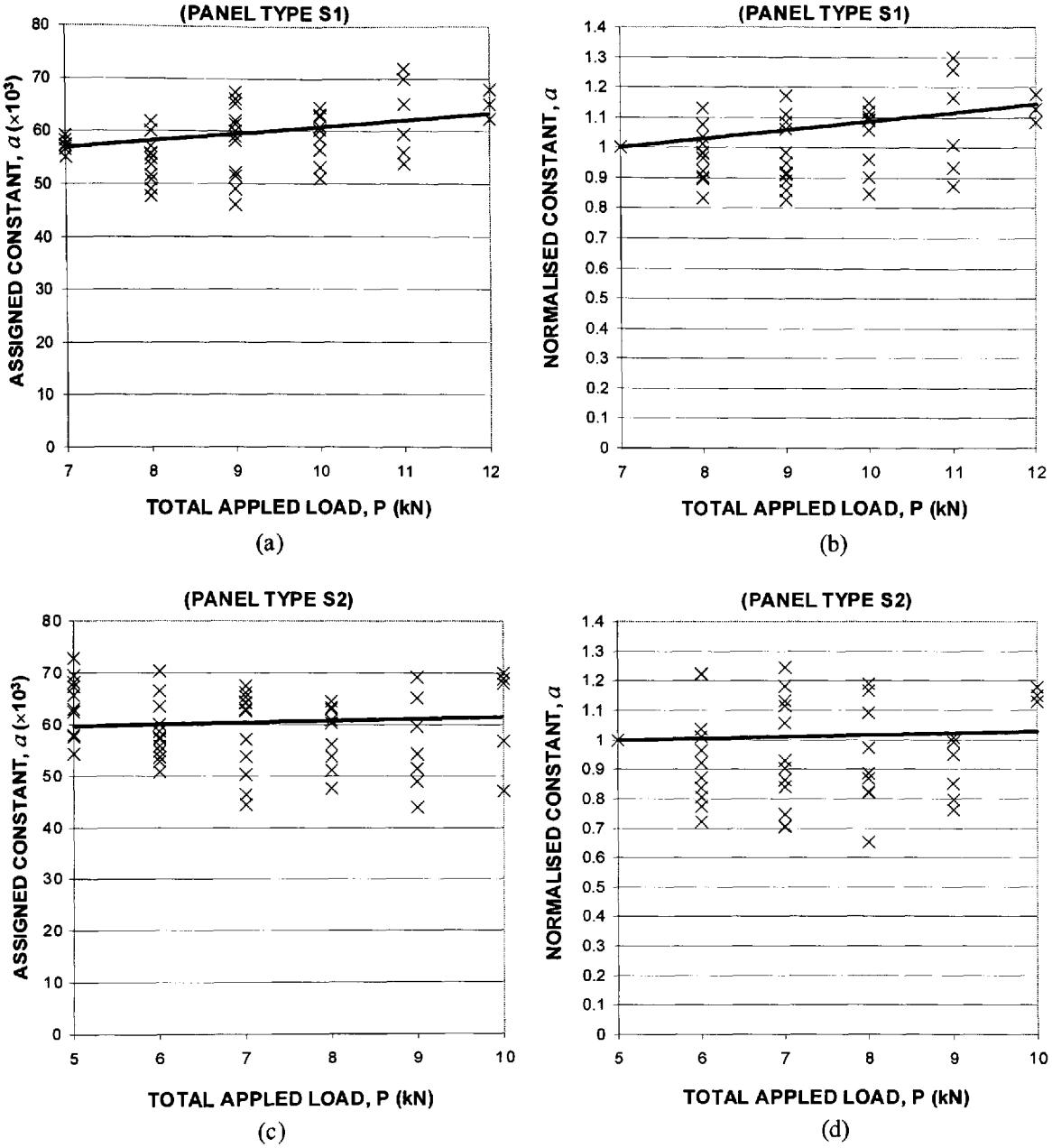

Figure 9.8 – Compiled results obtained from a fit of the adjusted FRF expression [eqn.(9.38)] to the measured data of the post-damaged panel sections. The figure presents the actual values of 'a' required, which have been normalised to show the change corresponding to progressive damage. (a)+(b) Panel type S1, (c)+(d) Panel type S2.

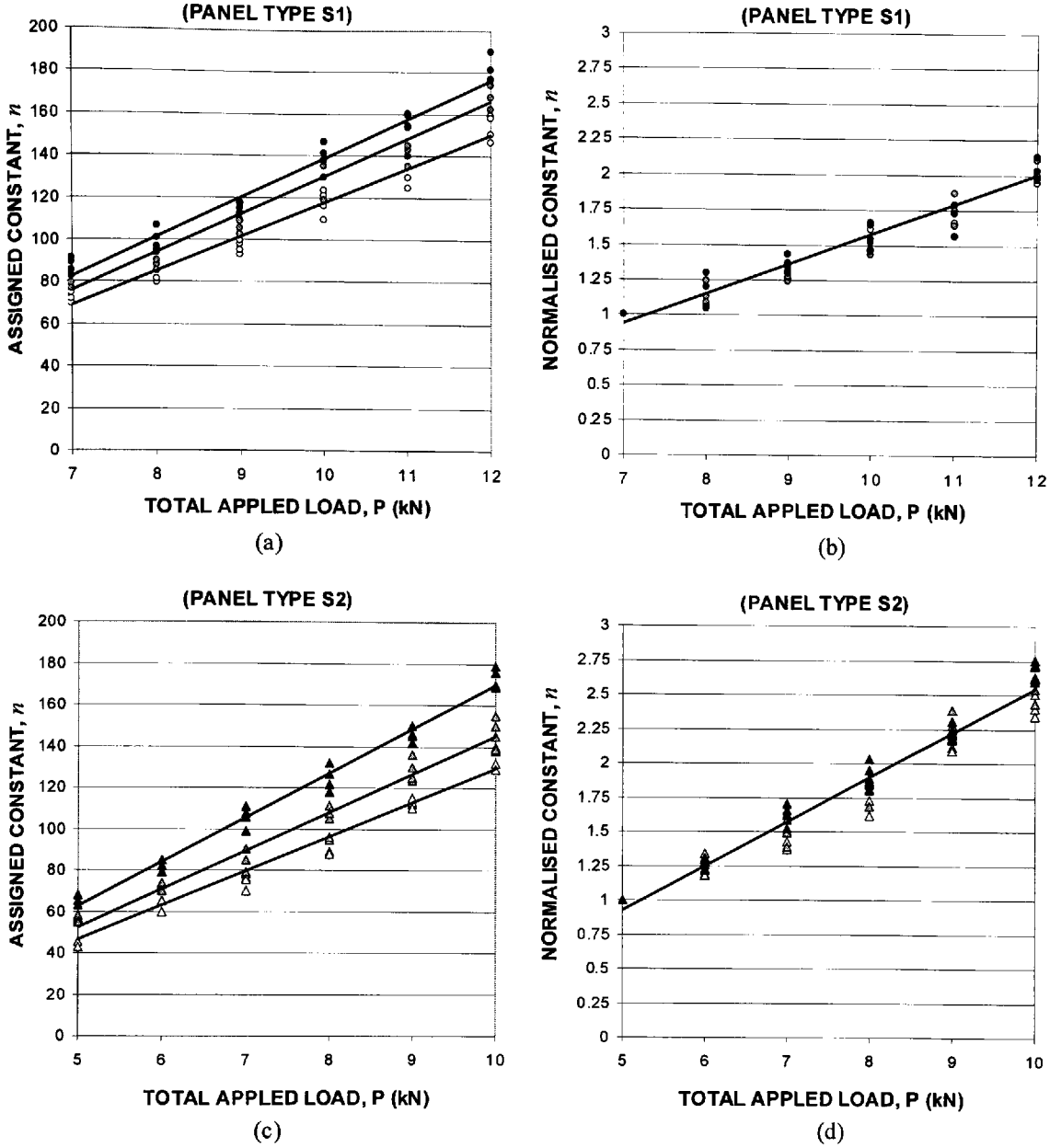

Figure 9.9 – Compiled results obtained from a fit of the adjusted FRF expression [eqn.(9.38)] to the measured data of the post-damaged panels. The figure presents the actual values of 'n' required, which have been normalised to show the change corresponding to progressive damage. (a)+(b) Panel type S1, (c)+(d) Panel type S2.

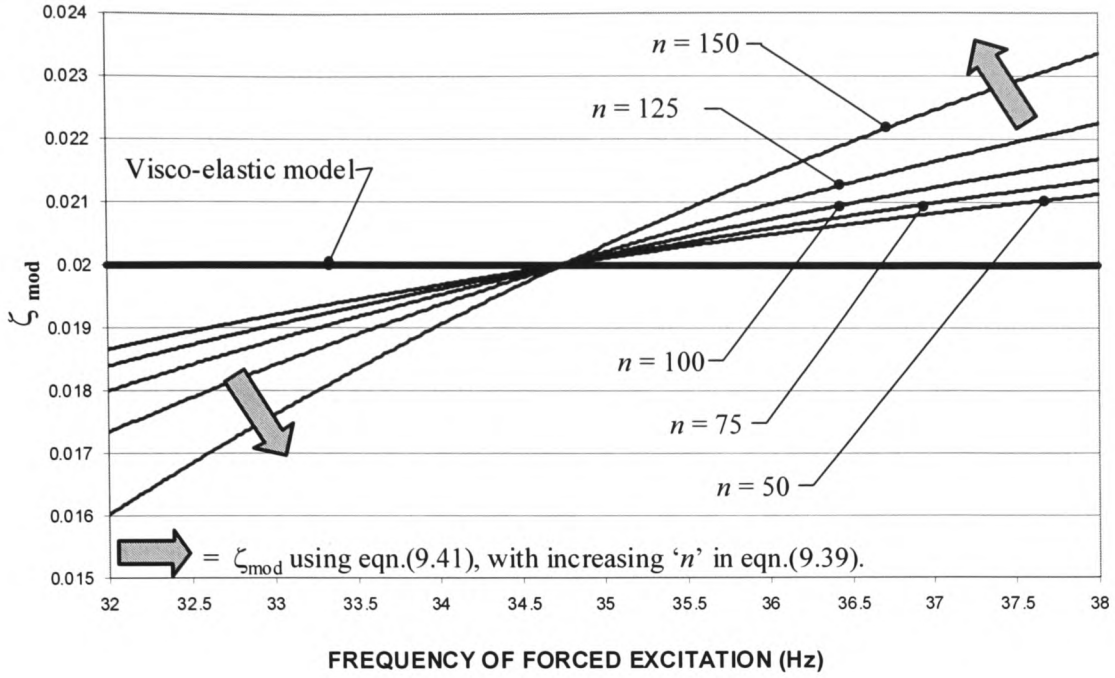

Figure 9.10 – Illustration of the modified damping properties, ζmod, using eqn.(9.41), with increasing values of 'n' in eqn.(9.39).

CHAPTER 10

Conclusions and Recommendations

10.1 Foreword to the Conclusions

A number of studies have been presented in this thesis that involve identifying dynamic characteristics as determined from actual vibration response measurements. It is shown that these can be used to assess damage in structures of varying complexity in conjunction with mathematical or numerical models. To provide a comprehensive investigation, the study has focused on the whole-frame performance and localised behaviour of a full-scale test building where damage severity was known to exist to varying extents. Three scales of damage have been studied, which were:

(i) Large scale damage, which would render the structure unacceptable for use (i.e. fire induced damage where large portions of the structure were affected),

(ii) Medium scale damage, which could be attributed to localised cracking of concrete floors (i.e. damage induced by excessive load at certain points within the structure causing damage to the regions around the locations of the applied load), and

(iii) Small scale damage, which could be interpreted as the cracking of discrete elements that make up the fabric of the building (i.e. damage within localised elements as if isolated and removed from the structure).

Chapter 4 presented a study that used vibration response data collected from an un-damaged eight-storey steel-framed building in order to establish the accuracy of analytical models, which were prepared to predict its natural frequencies. A number of natural frequencies were determined from response measurements that represented the motion of the building as a whole (i.e. whole-frame behaviour). The outcome of the study showed that the two numerical models, prepared to reflect the structural properties of the building 'as-built', did not produce calculations that matched those seen from measurements.

To overcome the observed discrepancies, chapter 5 presented a study that aimed to calibrate one of the numerical model by introducing aspects of structural behaviour

that were felt to account for the differences in measured and calculated frequencies reported in chapter 4. The study showed that assumptions relating to structural properties of members at their connections (joint-fixity) and non-structural parts, such as in-fill-walls, significantly influenced the calculated natural frequency results. A calibration methodology was proposed, which allowed the properties of the aforementioned structural parts to be identified using a rational graphical method, from which a calibrated model was achieved (this utilised the frequency measurements taken from the undamaged building). Mode shape measurements were also used during this process as a means of identifying appropriate modifications to the numerical model in order to produce an accurate calibrated set of natural frequencies.

The aim of the above studies was to establish if it would be possible to relate calculated natural frequencies, from a calibrated model of the undamaged structure, to similar measurements taken after damage. However, data obtained subsequent to large-scale damage, showed that the natural frequencies of the building did not change by an amount that would be regarded definitive (as opposed to marginal daily variations owing to ambient temperature, etc.).

In chapter 6 a study was presented that examined in more detail localised characteristic behaviour of the steel-framed building by focusing on natural frequency measurements taken from one of its floor slabs. This study made use of the calibration methodology proposed in chapter 5, which enabled measurements taken from the slab before and after damage to be calibrated against numerical models. From this comparison, it was found that perceptible changes in the frequencies, which were observed in the measurements, could be related to stiffness modifications at the boundaries of the floor areas affected by the damage. As a result, the extent of the defects at the locations of the known damage could be quantified allowing its influence on the continuity of the slab to be defined.

The contents of chapters 7 then discussed the methodology of treating individual representative parts (panels) of the floor slab, which was considered in chapter 6. Following a thorough laboratory schedule of static and dynamic testing, this study showed how strain and deflection data could be used to determine the mechanical

performance of the panels through stages of static load, which was related to information collected from the dynamic tests. Considerable effort was dedicated to this task, where natural frequency, damping and mode shapes were obtained corresponding to the appropriate stages of static loading. The study also considered the properties of these dynamic characteristics relative to the amplitude of vibration, in order to examine if the former would influence the latter.

Chapter 8 presented a detailed study into the static load resistance of the panels, which was conducted to establish the mechanisms that were responsible for the degradation, as gleaned from the test results of chapter 7. The study showed that the degradation of the panels was likely to be due to the development of concrete cracking that occurred at certain levels of applied bending moment. It also identified that the development and demise of friction bond within the section was an important factor.

Chapter 9 entailed a number of mathematical model, which could be used to extract additional parameters relating to the damage from frequency response functions obtained from the composite panels of chapter 7.

10.2 The Conclusions

The main conclusions drawn from the present work are:

(i) This work has demonstrated that there is a considerable amount of knowledge to be gained regarding the true behaviour of engineering structure from comparisons made between measured and calculated natural frequencies and mode shapes. In this study, it was found that numerical models, prepared to reflect the 'as-built' structure of a building and one of its floors, did not yield solutions that accurately reflected measurements. The calibration methodology that has been proposed could therefore be used as a means of establishing the de facto properties of certain parts of the structure. Prepared in a graphical form, this method can be used for any structure where the influence of varying fixity / stiffness at (for example) jointed parts can be established using a scalar quantity. To achieve the calibration, only the extreme fixity conditions need be analysed,

which saves a significant amount of analytical effort especially when the structure being considered comprised a large number of jointed parts.

(ii) It is clear that the effectiveness of damage identification from changes in natural frequency increases as the complexity of the structure being considered reduces. As a result of the studies presented in this thesis, damage detection within structures that have a comparable scale and complexity to the eight-storey steel-framed building are clearly impractical. The number of potential variables (from a structural standpoint) within the structure is simply far too extensive to designate accurate reasons for the observed frequency changes. In addition, whole-frame response appears not to be significantly affected by the presence of damage, even when the defects are extremely severe. Therefore, it is the candidate's opinion that damage identification on a large scale using only whole-frame (or whole-structure – if a different structural form is being considered) response measurements will yield very little useful information, and as such should be avoided.

(iii) Studies conducted to consider damage identification on a scale comparable to a building floor slab appears to indicate that a localised approach could be more practical. However, within the study presented in this thesis, it was assumed that changes in measured frequencies that were equal to the resolution of the autospectra, obtained from a fast Fourier transform, was a reasonable indication of damage, which itself is a bold presumption. But, the damage that had occurred to the floor was actually quite severe, which would have been noticed from a visual inspection with limited effort (i.e. by removing floor tiles for example) without the need for a single vibration test.

(iv) Although (iii) has identified a negative aspect of applying damage detection to floor slabs, it should be recognised that vibration data used in this way could provide a means of identifying potential damage sites where visual inspection would require significant effort or would yield little or no result. The natural frequencies of an area of floor can be established very quickly, which allows a large number of such sites to be assessed in a small amount of time. It is here that the strength of the method is more prominent, where detailed investigations can be carried out on those locations that are found to indicate frequency changes over time.

(v) By far the most promising use of dynamic characteristics for damage identification is found when applied to structures at element level. The studies performed on panels made to replicate parts of the floor slab, clearly show that natural frequencies and damping are influenced by the presence of damage. It is also apparent that these properties change to reflect the amount of damage imposed, and was found to occur repeatedly for many similar panels. A numerical model was established to define the degradation of the panels caused by static load. It was found from this study that damping and natural frequency measurements were sufficiently sensitive to detect cracking of the concrete. However, an interesting outcome is the finding that damping appears to be a better indicator of damage compared to the natural frequency, where larger changes to the magnitude of the former compared to the latter were found to occur after the defects had been introduced.

(vi) Having stated that damping and frequency indicate damage at element level, the importance of the amplitude dependence of these properties should be noted. The tests conducted in the laboratory have indicated that vibration measurements used to interpret damage should recognise the range of results that can be obtained if dissimilar response amplitudes are considered.

(vii) Interestingly, it was seen from the study that both natural frequency and damping characteristics changed with amplitude relative to a mathematically predictable scale. In the case of the composite panels, it was shown that the aforementioned characteristics had an amplitude dependency, which was relative to a logarithmic scale. With this knowledge, it may be possible to overcome (vi) above even if dynamic characteristics relative to similar amplitudes are not available. Thus, by obtaining data at a small number of amplitudes, additional data can be established from the projection of their general trend (i.e. using the logarithmic relationship). However, it should be noted that the previously mentioned logarithmic relationship was defined from data that represented vibration response over a fixed amplitude range, results beyond which may indicate a modified trend.

(viii) Mode shapes established from the response measurements gave very little insight into the changes that were occurring to the structural properties of the panels as a result of damage. This finding appears to suggest that the relative

amplitude of the points considered defining the mode shapes were not influenced by the distributed damage that occurred within the span of the members. Using a correlation exercise (the MAC value), to gauge the difference between mode shapes measured throughout damage relative to the panel in a pristine condition, no evidence of neither repeatable nor noticeable trends were found. However, the importance of the mode shape data for other uses, such as those involved in the calibration of measured and calculated dynamic characteristics, should not be dismissed.

(ix) A mathematical model has been proposed that can accurately match the profile of measured Frequency Response Functions (FRF) allowing additional parameters relative to the changing state of the dynamic characteristics of the panels to be defined. In the case of the model formulated in this thesis, it was found that the non-linear nature of the FRF, which was seen to produce a skew of the profile relative to that determined from a visco-elastic model, became exaggerated as progressive damage was induced. The parameters extracted from the application of this model were found to give an indication of the amount of change of the FRF skew characteristics, again using a scalar quantity. However, the candidate should like to point out that this model has not been prepared as a possible idealisation of the panel behaviour under transient or steady-state time varying dynamic response. But, the method does offer an additional means of assessing the changes that occur to the vibration characteristics of the panels as the latter become progressively damaged.

10.3 The Recommendations for Future Work

The research approach adopted for the studies presented, has followed that which can be termed as a 'top-down' procedure. As such, the application of the damage identification methodology was carried out at a relatively complex form of structural representation prior to considering a more 'simply defined' set of elements. On reflection of the conclusions, it is the candidate's opinion that a 'bottom-up' procedure should be followed for any future work in this area of research, where the findings from tests on smaller members are extended to larger structures. The extension at each

structural level could then be conducted at a more refined stage of complexity, which could be used to build-up a library of damage indicators at each step to identify those dynamic characteristics that remain sensitive to the onset of degradation. It is the candidate's opinion that the damping properties of a structure will provide sufficient sensitivity, and as such should be incorporated in any future damage identification studies.

Taking the above points into account, the candidate recommends that the work of this thesis could be extended to incorporate some or all of the following suggestions:

(i) The information collected from the laboratory work conducted on the composite panels could be used to extend the study by considering a larger representative segment of the building floor slab in order to repeat the static load / dynamic test procedure. Focusing on the changes that occur to the frequency, damping and FRFs, establish if these dynamic characteristics have similar trends to those presented in this thesis. Then, by building up a library of the behavioural trends due to damage, identify if the results can be projected to more complex structural parts.

(ii) The numerical model of chapter 8 that was used to identify the probable cause for the degradation, based on strain and displacement data, indicate that concrete cracking and interface friction have characteristics that contribute to the manner in which degradation of the panels occur. Information established from this study supported the assumption that cracking was responsible for the degradation. This has provided a basis on which the natural frequency and damping changes (from chapter 7) could be related to the structural stiffness reduction of the panels. However, the study has not identified the influence of temperature changes on the dynamic properties of the panels, which in hindsight should have been established. Therefore, the candidate recommends that further tests could be carried out to identify the dynamic characteristics of the panels when subjected to a range of ambient temperatures – as well as temperature gradient throughout the panels. The candidate does not propose to link this study to structural changes due to temperature variations.

(iii) The natural frequency and damping of the panels have been identified as being dependent on amplitude relative to a logarithmic scale. With this knowledge, it

should be possible to formulate a mathematical (or numerical) model that could match the time varying decay-of-vibration response of the panels at stages of damage. This approach may then provide a basis for a refined visco-elastic model, which could be used to calculate the vibration response of cracked concrete members. It is suggested that the visco-elastic model has been shown to be an accurate representation of the response of un-cracked members, with a piecewise solution being appropriate for cracked sections.

REFERENCES

Adams, R. D., Walton, D., Flitcroft, J. E. and Short, D. (1975). "Vibration testing as a non-destructive test tool for composite materials". Proceedings of the American Society of Testing and Materials, Journal of Composite Reliability, STP 580, pp. 159 – 175.

Agbabian, M. S., Masri, S. F., Miller, R. K. and Caughey, T. K. (1991). "System identification approach to detection of structural changes". Proceedings of the American Society of Civil Engineers, Journal of Structural Engineering, Volume 117, No. 2, pp. 370 – 390.

Ahmadian, H., Mottershead, J. E. and Friswell, M. I. (1996). "Damage detection from substructure modes". Proceedings of the 21st International Seminar on Modal Analysis, Noise and Vibration Engineering, Leuven, Belgium, pp. 983 – 991.

Alampalli, S., Fu, G. and Dillon, E. W. (1997). "Signal versus noise in damage detection by experimental modal analysis". Proceedings of the American Society of Civil Engineers, Journal of Structural Engineering, Volume 123, No. 2, pp. 237 – 245.

Allemang, R. J. and Brown, D. L. (1983). "Correlation coefficients for modal vector analysis". Proceedings of the 1st International Modal Analysis Conference, Kissimmee, pp. 110 – 116.

American Society of Civil Engineers, ASCE (1984). "Standard specification for the design and construction of composite slabs and commentary on specifications for the design and construction of composite slabs". Published by the American Society of Civil Engineers.

Anderson, T. J. and Nayfeh, A. H. (1996) "Natural frequencies and mode shapes of laminated composite plates: experiments and FEA". Journal of Vibration and Control, Volume 2, Part 4, pp.381 – 414.

Aoki, S. (1996) "Dynamic characteristics of welded structures". Journal of Nuclear Engineering and Design, Volume 160, pp. 379 – 385.

Beards, C. F. (1993). "Structural vibration analysis and damping". Published by Arnold, an imprint of John, Wiley and Sons Inc., 1996.

Belarbi, A. and Hsu, T. T. C. (1994). "Constitutive laws of concrete in tension and reinforcing bars stiffened by concrete". American Concrete Institute Structural Journal, Volume 91, No. 4, pp. 465 – 474.

Bendat, J. S. and Piersol, A. G. (1980) "Engineering applications of correlation and spectral analysis". Published by John Wiley and Son, 1980.

Brandon, J. A. and Mathias, M. H. (1995). "Complex oscillatory behaviour in a cracked beam under sinusoidal exciatation". Journal of Sound and Vibration, Volume 186, Number 2, pp. 350 – 354.

Bravery, P. N. R. (1993) "Cardington Large Building Test Facility – Construction details for the first building". A summary report prepared by the Building Research Establishment (BRE) on the eight-storey steel-framed building – Available from BRE.

Bruneau, M. and Wang, N. (1996). "Some aspects of energy methods for the inelastic seismic response of ductil SDOF structures". Engineering Structures, Volume 18, Number 1, pp. 1 – 12.

Bryl, S. (1967). "The composite effect of profiled steel plate and concrete in deck slabs". Paper presented at the 23rd International Congress of Steel Information Centres, Volume No. 10, pp. 448 – 454.

BS 4: Part 1: 1993. "Specification for hot rolled sections". British Standards Institution. (ISBN 0-580-21637-3).

BS 1881: Parts 102, 108, 110, 111, 114, 116, 121. Parts of the Code of Practice for concrete testing. British Standards Institution.

BS 5328: Part 2: 1997. "Methods for specifying concrete mixes". British Standards Institution. (ISBN 0-580-26723-7).

BS 5950: Part 1: 1990. "Code of practice for design in simple and continuous construction: Hot-rolled steel sections". British Standards Institution. (ISBN 0-580-18566-4)

BS 8110: Part 1: 1997. "Structural use of concrete – Code of practice for design and construction". British Standards Institution. (ISBN 0-580-26208-1)

Cao, H., Ellis, B. R. and Littler, J. D. (1995) "The use of the maximum entropy method for the spectral analysis of wind-induced data recorded on buildings". Proceedings of the 9th International Conference of Wind Engineering, New Delhi, India, pp. 1293 – 1304.

Cao, H., Ellis, B. R. and Littler, J. D. (1997) "The use of the maximum entropy method for the spectral analysis of wind-induced data recorded on buildings". Journal of Wind and Industrial Aerodynamics, Volume 72, pp. 81 – 93.

Cases, J. R. and Aparicio, A. (1994). "Structural damage identification from dynamic test data". Proceedings of the American Society of Civil Engineers, Journal of Structural Engineering, Volume 120, No. 8, pp. 2437 – 2449.

Caverson, R. G., Waldron, P. and Williams, M. (1994) "Review of vibration guidelines for suspended concrete slabs". Canadian Journal of Civil Engineering, Volume 21, pp. 931 – 938.

Cawley, P. and Adams, R. D. (1979). "The location of defects in structures from measurements of natural frequencies". Journal of Strain Analysis, Volume 4, Part 2, pp. 49 – 57.

Clough, R. W. and Penzien, J. (1993). "Dynamics of structures". (International Second Edition), Published by McGraw Hill Inc., 1993.

Cole, H. A. (1968) "On the line analysis of random vibrations". Proceedings of the Americal Society of Mechanical Engineers' 9th Structural Dynamics Materials Conference, Palm Springs, California, 1968.

Cooley, J. W. and Tukey, J. W. (1969) "An algorithm for the machine calculation of complex Fourier series". Papers on Digital Processing, MIT Press, (Reprint of an original paper published in Mathematics of Computation, Volume 19, 1965, pp. 297 – 301).

Chajes, M. J., Romstad, K. M. and McCallen, D. B. (1993) "Analysis of multiple-bay frames using continuum model". The American Society of Civil Engineers, Journal of Structural Engineering, Volume 119, No. 2, February 1991, pp. 522 – 545.

Chajes, M. J., Zhang, L. and Kirby, J. T. (1996) "Dynamic analysis of tall building using reduced-order continuum models". The American Society of Civil Engineers, Journal of Structural Engineering, Volume 122, No. 11, November 1996, pp. 1284 – 1291.

Chen, H. L., Spyrakos, C. C. and Venkatesh, G. (1995). "Evaluating structural deterioration by dynamic response". Proceedings of the American Society of Civil Engineers, Journal of Structural Enginering, Volume 121, Number 8, August 1995, pp. 1197 – 1204.

Chondros, T. G. and Dimarogonas, A. D. (1998). "A continuous cracked beam vibration theory". Journal of Sound and Vibration, Volume 215, No. 1, pp. 17 – 34.

Chrysostomou, C. Z. (1991) "Effects of degrading in-fill walls on the non-linear seismic response of two-dimensional steel frames". A Thesis submitted to Cornell University in fulfilment of the requirement for PhD, January 1991.

Crema, L. B., Castellani, A. and Coppotelli, G. (1995). "Generalization of non-destructive damage evaluation using modal parameters". Proceedings of the 13th International Modal Analysis Conference, Nashville, Tennessee, pp. 428 – 433.

Crespo, P. and Ruotolo, R. (1996). "Non-linear modelling of a cracked beam". Proceedings of the 14th International Modal Analysis Conference, Dearborn Michigan, Volume 1, pp. 1017 – 1022.

Daniels, B. J. and Crisinel, M. (1993a). "Composite slab behaviour and strength analysis. Part I : Calculation procedure". Proceedings of the American Society of Civil Engineers, Journal of Structural Engineering, Volume 119, No. 1, pp. 16 – 35.

Daniels, B. J. and Crisinel, M. (1993b). "Composite slab behaviour and strength analysis. Part 2 : Comparisons with test results and parametric analysis". Proceedings of the American Society of Civil Engineers, Journal of Structural Engineering, Volume 119, No. 1, pp.36 – 50.

Das, P. C., Owen, J. S., Eccles, B. J., Woodings, M. A. and Choo, B. S. (1997). "Role of dynamic testing in assessment of bridges". Transport Research Report Record Number 1594, Part 2, pp. 115 – 124.

Davies, J. M. and Fisher, J. (1979) "The diaphragm action of composite slabs". Proceedings of the Institution of Civil Engineers, Volume 67, Part 2, pp. 891 – 906.

Delpak, R. (1999). Private communications, Internal report, University of Glamorgan.

Dimarogonas, A. (1996). "Vibration for engineers". (Second Edition), Published by Prentice Hall International Publishers Inc., 1996.

Earthquake Engineering Research Institute. (2000). "Lessons learned over time: Learning from earthquakes". Published by the Earthquake Engineering Research Institute, Volume III, ISBN 0-943198-97-6.

Easterling, W. S. and Young, C. S. (1992). "Strength of composite slabs". Proceedings of the American Society of Civil Engineers, Journal of Structural Engineering, Volume 118, No. 9, pp. 2370 – 2389.

Eccles, B. J., Owen, J. S., Choo, B. S. and Woodings, M.A. (1999) "Non-linear vibration of cracked reinforced concrete beams". Proceedings of the EURODYN '99 Conference, Rotterdam, Structural Dynamics, pp. 357 – 364.

Eccles, B. J., Owen, J. S., Woodings, M. A. and Choo, B. S. (1997). "A proposed new approach to full life quantitative bridge assessment". Proceedings of the 7th International Conference on Structural Faults and Repair, Edinburgh, pp. 479 – 486.

Ellis, B. R. (1980). "An assessment of the accuracy of predicting the fundamental natural frequency of buildings and the implications concerning dynamic analysis of structures". Proceedings of the Institution of Civil Engineers, Part 2, Volume 69, September 1980.

Ellis, B. R. (1986) "The significance of dynamic soil-structure interaction in tall buildings". Proceedings of the Institution of Civil Engineers, Ground Engineering Group, Volume 81, Part 2, Paper No. 9001, June 1986, pp. 221 – 242.

Ellis, B. R. (1993). "On the non-linear characteristics of structural elements at high amplitudes of vibration". Proceedings of the EURODYN'93 Conference, Rotterdam 1993, pp. 879 – 887.

Ellis, B. R. (1994) "Dynamic testing". Proceedings of the 1st Cardington Conference, BRE, Cardington, UK, Section 2, paper 1.

Ellis, B. R. (1995) "The combined use of remote laser measurements and simple modal analysis". The International Symposium Non-Destructive Testing in Civil Engineering (NDT-CE), 26th – 28th September 1995, pp. 319 – 326.

Ellis, B. R. (1996) "Full-scale measurements of the dynamic characteristics of buildings in the UK". Journal of Wind Engineering and Industrial Aerodynamics, Volume 59, Parts 2 – 3, pp. 365 – 382.

Ellis, B. R. (1998). "Non-destructive dynamic testing of stone pinnacles on the Palace of Westminster". Proceedings of the Institution of Civil Engineers, Structures and Buildings, Volume 128, August 1998, pp. 300 – 307.

Ellis, B. R. and Ji, T. (1996) "Dynamic testing and numerical modelling of the Cardington Steel Framed Building from construction to completion". Journal of the Institution of Structural Engineers, Volume 74, No. 11, June 1996, pp. 186 – 192.

Ellis, B. R. and Ji, T. (1997) "Human-structure interaction in vertical vibrations". Proceedings of the Institution of Civil Engineers, Structures and Buildings, Volume 122, February 1997, pp. 1 – 9.

Ellis, B. R., Kerridge, B. and Osborne, K. (1993) "Vibration characteristics of shallow floor structures". Colloquium on Structural Serviceability of Buildings, Goteborg, June 1993, pp. 303 – 307.

Ellis, B. R. and Littler, J. D. (1988) "Dynamic response of nine similar tower blocks". Journal of Wind Engineering and Industrial Aerodynamics, Volume 28, Parts, 1 – 3, pp. 339 – 349.

El-Metwally, E. (1994). "Method of segmental length for instability analysis of reinforced concrete beam-columns". American Concrete Institute Structural Journal, Volume 91, No. 6, pp. 666 – 677.

Ewins, D. J. (1984). "Modal Testing: Theory and Practice". Mechanical Engineering Research Studies, Engineering Dynamics Series, Published by John Wiley & Son Inc.

Fang, J. Q., Li, Q. S., Jeary, A. P. and Wong, C. K. (1997). "Field measurements of damping in tall buildings". A publication from the Department of Building and Construction, City University of Hong Kong, presented on the World Wide Web (www).

Farrar, C. R. and Cone, K. M. (1995). "Vibration testing of the I-40 bridge before and after the introduction of damage". Proceedings of the 13th International Modal Analysis Conference, Nashville, Tennessee, pp. 203 – 209.

Feenstra, P. H. and Borst, R. (1995). "Constitutive model for reinforced concrete". Proceedings of the American Society of Civil Engineers, Journal of Engineering Mechanics, Volume 121, No. 5, pp. 587 – 595.

Feltham, I. (1991) "Post-tensioned concrete floor-design handbook: Appendix G". Published by the Concrete Society, Technical Report Number 43.

Friswell, M. I. and Penny, J. E. T. (1992). "The use of vibration data and model updating to detect damage". Proceedings of the Structural Integrity Assessment Conference, Manchester, pp. 225 – 235.

Friswell, M. I., Penny, J. E. T. and Garvey, S. D. (1996). "A combined generic and eigensensitivity algorithm for the location of damage in structures". Proceedings of the International Conference on Identification in Engineering Systems, Swansea, pp. 357 – 367.

Friswell, M. I., Penny, J. E. T. and Garvey, S. D. (1997). "Parameter subset selection in damage detection". Inverse Problems in Engineering, Volume 5, No. 3, pp. 189 – 215.

Friswell, M. I., Penny, J. E. T. and Lindfield, G. (1995). "The location of damage from vibration data using generic algorithms", Proceedings of the 13th International Modal Analysis Conference, Nashville, Tennessee, pp. 1640 – 1646.

Friswell, M. I., Penny, J. E. T. and Wilson, D. A. L. (1994). "Using vibration data and statistical measures to locate damage in structures". The International Journal of Analytical and Experimental Modal Analysis, Volume 9, No. 4, pp. 239 – 254.

Garstka, B., Krätzig, W. B. and Strangenberg, F. (1993). "Damage assessment in cyclically loaded reinforced concrete members". Proceedings of the Structural Dynamics EURODYN'93 Conference, Balkema, Totterdam, pp. 121 – 127.

Gere, J. M. and Timoshenko, S. P. (1991). "Mechanics of materials". Published by Chapman and Hall, (ISBN 0-412-36880-3).

Ghali, A, and Neville, A. M. (1989). "Structural analysis: A unified classical and matrix approach". Third Edition, Published by Chapman and Hall.

Ghoneim, M. G. and MacGregor, J. G. (1994). "Prediction of the ultimate strength of reinforced plates under combined inplane and lateral loads". American Concrete Institute Structural Journal, Volume 91, No. 6, pp. 688 – 696.

Grantham, R. (1994) "Service loading studies": 'on the Steel-framed building at Cardington'. Proceedings of the 1st Cardington Conference, Cardington, 16 – 17 November 1994, Section 2, Paper 4.

Griffiths, D. V. and Smith, I. M. (1991). "Numerical methods for engineers". Published by Blackwell Scientific Publishers, 1991.

Gudmundson, P. (1982). "Eigenfrequency changes of structures due to cracks, notches or other geometrical changes". Journal of the Mechanics and Physics of Solids, Volume 30, Part 5, pp. 339 – 353.

Hambly, E. C. (1991). "Bridge deck behaviour". Published by E & FN Spon, (ISBN 0-419-17260-2).

Hampe, E. and Schwarz, J. (1994) "Seismische einwirkungen auf bauwerke unterschiedlichen risikopotentials; Europäische regelwerke".

Hearn, G. and Testa, R. B. (1991). "Modal analysis for damage detection in structures". Proceedings of the American Society of Civil Engineers, Journal of Structural Engineering, Volume 117, No. 10, pp. 3042 – 3063.

Hefei, X. D. and Luz, E. (1986) "Experimentelle bestimmung der eigenfrequenzen und eigenscgwingungsformen am mpa-hochhaus der Universität Stuttgart" Fachkolloquium Experimentelle Mechanik, Ingenieurwissenschaftliches Zentrum, October 1986, pp. 149 – 156.

Howson, W. P. (1979) "A compact method for computing the eigenvalues and eigenvectors of plane frames". Proceedings of the First International Conference and Exhibition on Structural Software, September 1979, Southampton, (20 pages).

Howson, W. P. (1985) "A teaching, analysis and design program for the complete eigensolution of plane frames using microcomputers". Proceedings of the International Conference on Education, Practice and Promotion of Computational Methods in Engineerings using Small Computers (EPMESC), University of Wales, Cardiff, August 1985, (16 pages).

Howson, W. P. and Williams, F. W. (1985) "A unified approach to the static, buckling and vibration analysis and design of structures with collinear nodes using microcomputers". Proceedings of the Second International Conference on Civil and Structural Engineering Computing, Printed by Civil-Comp Press, (8 pages).

Hsu, T. T. C. and Zhang, L. (1996) "Tension stiffening in reinforced concrete membrane elements". American Concrete Institute Structural Journal, Volume 93, No. 1, pp. 108 – 115.

Hu, J. and Liang, R. Y. (1993). "An intergrated approach to detection of cracks using vibration characteristics". Journal of the Franklin Institute, Volume 330, Part 5, pp. 841 – 853.

Ismail, F., Ibrahim, A. and Martin, H. R. (1990). "Identification of fatigue cracks from vibration testing". Journal of Sound and Vibration, Volume 140, Number 2, pp. 305 – 317.

Iwan, W. D. and Huang, C. T. (1996). "On the dynamic response of non-linear systems with parametric uncertainties". International Journal of Non-Linear Mechanics, Volume 31, Number 5, pp. 631 – 645.

Jauregui, D. V. and Farrar, C. R. (1996). "Damage identification algorithms applied to numerical modal data from a bridge". Proceedings of the 14th International Modal Analysis Conference, Dearborn, Michigan, pp. 119 – 125.

Jeary, A. P. (1992) "Establishing non-linear damping characteristics of structures from non-stationary response time-histories". Journal of the Institution of Structural Engineers, Volume 70, No. 4, February 1992, pp. 61 – 66.

Jeary, A. P. (1995). "Integrity monitoring of structures". Proceedings of the 9th International Conference on Wind Engineering, New Delhi, India, Volume 4, pp. 2189 – 2200.

Jeary, A. P. and Ellis, B. R. (1981) "Vibration tests of structures at various amplitudes". Proceedings of the American Society of Civil Engineers' Conference on Dynamics of Structures, Atlanta, Georgia, pp. 281 – 294.

Jeary, A. P. and Ellis, B. R. (1983) "On the predicting the response of tall buildings to wind excitation". Journal of Wind Engineering and Industrial Aerodynamics, Volume 13, Parts 1 – 3, pp. 173 – 182.

Jolly, C. K. and Zubair, A. K. M. (1987). "The efficiency of shear-bond interlock between steel sheeting and concrete". Proceedings of the International Conference on Steel and Aluminium Structures, Cardiff, U.K, Volume 2, pp. 127 – 136.

Jordan, D. W. and Smith, P. (1987). "Non-linear ordinary differential equations". Oxford Applied Mathematics and Computing Science Series, Published by Clarendon Press, (Second edition).

Karihaloo, B. L. (1995). "Fracture mechanics and structural concrete". Published by Longman Scientific Technical, Concrete Design and Construction Series (ISBN 0-582-21582-X).

Kliber, F. W. and Porter, M. L. (1981). "Uniform loading for steel-deck reinforced slabs". Proceedings of the American Society of Civil Engineers, Journal of the Structures Division, Volume 107, ST11, pp. 2097 – 2111.

Krawczuk, M. (1992). "A cracked Timoshenko beam finite element". Proceedings of the 17th International Seminar on Modal Analysis – Katholieke University, Leuven, pp. 67 – 81.

Kubic, C. R. and Daniels, J. H. (1979). "Two-way flexure of steel-deck-reinforced slabs". Proceeding of the American Society of Civil Engineers, Journal of the Structural Division, Volume 105, ST6, pp. 1039 – 1053.

Leung, Y. T. and Cheung, Y. K. (1980) "A new frame super-element in static and dynamic analysis". Proceedings of the 7th Australian Conference on Mechanics, Structures and Materials, 1980, pp. 19 – 24.

Leung, Y. T. and Cheung, Y. K. (1981) "Dynamic analysis of frames by a two-level finite element method". Journal of Sound and Vibration, Volume 74, pp. 1 – 9.

Lieven, N. A. J. and Ewins, D. J. (1988). "Spatial correlation of mode shapes, the Co-ordinate Modal Assurance Criterion (COMAC)". Proceedings of the 6th Intertational Analysis Conference, Society of Experimental Mechanics, Bethal, pp. 690 – 695.

Littler, J. D. (1988) "Forced vibration tests on Sheffield arts tower". Proceedings of the SECED Civil Engineering Conference, Bristol, pp. 61 – 79.

Littler, J. D. and Ellis, B. R. (1990) "Interim findings from full-scale measurements at Hume Point". Journal of Wind Engineering and Industrial Aerodynamics, Volume 36, Parts 1 – 3, pp. 1181 – 1190.

Littler, J. D. and Ellis, B. R. (1992) "Full-scale measurements to determine the response of Hume Point to wind loading". Journal of Wind Engineering and Industrial Aerodynamics, Volume 42, Parts 1 – 3, pp. 1085 – 1096.

Liu, P. (1995). "Identification and damage detection of trusses using modal data". Proceedings of the American Society of Civil Engineers, Journal of Structural Engineering, Volume 121, No. 4, pp. 599 – 607.

Luttrell, L. D. (1986). "Method for predicting strength in composite slabs". Proceedings of the Eighth International Speciality Conference on Cold-Formed Steel Structures, St. Louis, Missouri, USA, pp. 419 – 431.

Luttrell, L. D. (1987). "Flexural strength of composite slabs". Proceedings of the International Conference on Steel and Aluminium Structures, Volume 2, pp. 106 – 116.

Luz, E. (1989) "Seismic loading on highrise buildings with coupled lateral and torsional modes". Proceedings of the ERCAD Conference, Berlin, 1989 (13 pages).

Luz, E. (1991) "Ermittlung der erdebenbeanspruchung von hochhäusern mittels einfacher machanischer modele". Kolloquium erdbebeningenieurwesen, 1991, pp. 205 – 219.

Luz, E. (1992) "Experimetal modal analysis using ambient vibration". The International Journal of Analytical and Experimental Modal Analysis, Volume 7, No. 1, January 1992, pp. 29 – 39.

Luz, E. and Haide, M. (1990) "Examples of seismic loading on different highrise buildings with coupled lateral and torsional modes". Proceedings of the ninth European Conference on Earthquake Engineering, Moscow, Volume 7A, 1990, pp. 151 – 160.

Luz, E. and Gurr, S. (1981) "Computation of vibrations of buildings in order to study the earthquake resistance". Ingenieur Archiv, Volume 51, 1981, pp. 75 – 88.

Maguire, J. R. and Severn, R. T. (1987) "Assessing the dynamic properties of prototype structures by hammer testing". Proceedings of the Institution of Civil Engineers, Volume 83, Part 2, pp. 769 – 784.

Makris, N. and Constantinou, M. C. (1991). "Analysis of motion resisted by friction: Constant coulomb and linear / coulomb friction". Mechanics of Structures and Machines, Volume 19, Part 4, pp. 477 – 500.

Mannan, M. A. and Richardson, M. H. (1990). "Detection and location of structural cracks using FRF measurements". Proceedings of the 8th International Modal Analysis Conference, Florida USA, Volume 1, pp. 652 – 657.

Martin, D. M. (1994) "The behaviour of a multi-storey steel-framed building subjected to natural fires". Proceedings of the 1st Cardington Conference, Cardington, 16 – 17 November 1994, Section 3, Paper 1.

Mayers, R. L. (1995). "An experimental algorithm for detecting damage applied to the I-40 bridge over the Rio Grande". Proceedings of the 13th International Modal Analysis Conference, Nashville, Tennessee USA, February 1995, pp. 219 – 225.

Marzouk, H. M. and Chen, Z. (1993). "Finite element analysis of high-strength concrete slabs". American Concrete Institute Structures Journal, Volume 90, No. 5, pp. 505 – 513.

Mazurek, D. F. and DeWolf, J. T. (1990) "Experimental study of bridge monitoring techniques". Proceedings of the American Society of Civil Engineers, Journal of Structural Engineering, Volume 16, No. 9, September 1990, pp. 2532 – 2549.

McConnell, K. G. (1996). "Vibration Testing: Theory and Practice". Published by John Wiley & Son Inc.

Mehrabi, A. and Corley, W. G. (2000) "Cable-supported bridges and structures: health and safety monitoring and problem solving". The Journal of the Institution of Structural Engineers, Volume 78, Number 9, May 2000, pp. 17 – 20.

Meinhold, W., Ebert, M. and Bucher, C. (1996). "A contribution to detecting structural damage by dynamic testing". Proceedings of the Structural Dynamics EURODYN'96 Conference, Balkema, Totterdam, pp. 997 – 1004.

Meirovitch, L. (1986). "Elements of Vibration Analysis". Mechanical Engineering Series, Published by McGraw-Hill International Editors.

Meneghetti, M. and Maggiore, A. (1995). "Local modal sensitivity". Proceedings of the 13th International Modal Analysis Conference, Nashville, Tennessee, pp. 192 – 193.

Messina, A., Jones, I. A. and Williams, E. J. (1996). "Damage detection and localisation using natural frequency changes". Proceedings of the International Conference on Identification in Engineering Systems, pp. 67 – 76.

Murray, T. M. and Allen, D. E (1993) "Floor vibration: A new design approach". Proceedings of the International Colloquium of Structural Serviceability of Buildings, Goteborg, June 1993, pp. 119 – 124.

Nader, M. N. and Astaneh, A. (1991) "Dynamic behaviour of flexible, semi-rigid and rigid steel frames". Journal of Construction Steel Research, Volume 18, pp. 179 – 192.

Nader, M. N. and Astaneh, A. (1996) "Shaking table tests of rigid, semi-rigid and flexible steel frames". Proceedings of the American Society of Civil Engineers, Journal of Structural Engineering, Volume 122, No. 6, June 1996, pp. 589 – 596.

Newland, D. E. (1993). "Introduction to random vibrations, spectral and wavelet analysis". (Third Edition), Published by Longman Singapore Publishers Ltd, 1993.

Oller, S., Oñate, E., Miquel, J. and Botello, S. (1996). "A plastic damage constitutive model for composite materials". International Journal of Solids and Structures, Volume 13, No. 17, pp. 2501 – 2518.

Osborne, K. P. and Ellis, B. R. (1990) "Vibration design and testing of a long-span lightweight floor". Journal of the Institution of Structural Engineers, Volume 68, No. 10, May 1990, pp. 181 – 186.

Owen, J. S., Eccles, B. J., Woodings, M. A. and Choo, B. S. (1996). "Dynamic testing of reinforced concrete beams". Proceedings of the 2nd DTA / NAFEMS International Conference on Structural Dynamic Modelling, pp. 119 – 128.

Pandey, A. K., Biswas, M. and Samman, M. M. (1991). "Damage detection from changes in curvature mode shapes". Journal of Sound and Vibration, Volume 145, No. 2, pp. 321 – 332.

Pang, D. and Hsu, T. T. C. (1996). "Fixed angle softened truss model for reinforced concrete". American Concrete Institute Structural Journal, Volume 93, No. 2, pp. 197 – 207.

Patrick, M. (1989) "Design of continuous composite slabs – The issue of ductility". The Australian Institute of Steel Construction, Volume 23, Part 3, pp.2 – 10.

Patrick, M. and Bridge, R. Q. (1992). "Design of composite slabs for vertical shear". Proceedings of the International Conference on Steel Structures, Trout Lodge, Missouri, pp. 304 – 321.

Pavic, A. (1997). "Progress report No. 3". An internal report of the University of Sheffield, Centre for Cement and Concrete, on DoE Partners in Technology Research Project, November 1997.

Pavic, A., Crouch, R. S. and Waldron, P. (1997) "The interactive process of linking the experimental modal testing and FE modelling of a full-scale concrete structure". A case study prepared by the Centre for Cement and Concrete, University of Sheffield, (Internal report).

Pavic, A., Reynolds, P. and Waldron, P. (1997b) "Modal testing of a full-scale concrete floor: Test specifics and QA procedures". Proceedings of the 3rd International Conference on Modern Practice in Stress and Vibration Analysis, University College Dublin, Ireland, 3rd – 5th September 1997.

Pavic, A. and Waldron, P. (1996) "Parameter estimation and FE model correlation using modal testing of an experimental full-scale high strength concrete floor".

Proceedings of the International Conference in Identification in Engineering Systems, Swansea, March 1996, (10 pages).

Pavic, A., Waldron, P. and Reynolds, P. (1996) "Vibration of post-tensioned concrete floors". Internal progress report of the University of Sheffield, Report No. CI 39/3/393(cc0952), September 1996.

Pavic, A., Williams, M. S. and Waldron, P. (1994) "Dynamic FE model for post-tensioned concrete floors calibrated against field test results". Dynamic Testing Agency's International Conference, Engineering Integrity Assessment, East Kilbride, Glasgow, 11th – 12th May 1994.

Peel-Cross, J., Gilbert, S., Rankin, B. and Long, A. (1998) "Arching action in composite metal deck concrete slabs". Proceedings of the 3rd Cardington Conference, Whole building research: the laterst developments, Section 2, Paper 1, (7 pages).

Peng, X. and Fang, L. (1997). "Thermomechanically consistent continuum damage model for concrete materials". Proceedings of the American Society of Civil Engineers, Journal of Engineering Mechanics, Volume 123, No. 1, pp. 60 – 69.

Penny, J. E. T., Wilson, D. A. L. and Friswell, M. I. (1993). "Damage location in structures using vibration data". Proceedings of the 11th International Modal Analysis Conference, Kissimmee, Florida, pp. 861 – 867.

Penzien, P. (1964). "Damping characteristics of pre-stressed concrete". Journal of the American Concrete Institute, Volume 61, Part 9, pp. 1125 – 1148.

Plum, C. M. and Svensson, E. (1993) "Dynamic response of a composite slab in an office building". Proceedings of the International Colloquium of Structural Serviceability of Buildings, Goteborg, June 1993, pp. 309 – 314.

Plumier , A. and Schleich, J. B. (1993) "Seismic resistance of steel and composite frame structures". Journal of Construction Steel Research, Volume 27, pp. 159 – 176.

Poh, K. W. and Attard, M. M. (1993). "Calculating the load-deflection behaviour of simply-supported composite slabs with interface slip". Engineering Structures, Volume 15, No. 5, pp. 359 – 367.

Porter, M. L. and Ekberg, C. E. (1972). "Summary of full-scale laboratory tests of concrete slabs reinforced with cold-formed steel decking". Proceedings of the Ninth International Congress of the Association of Bridge and Structural Engineering, pp. 173 – 183.

Porter, M. L. and Ekberg, C. E. (1976). "Recommendations for steel deck floor slabs". Proceedings of the American Society of Civil Engineers, Journal of the Structural Division, Volume 102, ST11, pp. 2121 – 2136.

Porter, M. L. and Ekberg, C. E. (1980) "Coating effects of cold-formed steel deck slabs". Proceedings of the 5th International Conference on Cold-Formed Steel Structures, St. Louis, pp. 369 – 386.

Porter, M. L., Ekberg, C. E., Greimann, L. F. and Elleby, H. A. (1976). "Shear-bond analysis of steel-deck-reinforced slabs". Proceedings of the American Society of Civil Engineers, Journal of the Structural Division, Volume 102, ST12, pp. 2255 – 2268.

Press, W. H., Teukolsky, S. A., Vetterling, W. T. and Flannery, B. P. (1992). "Numerical recipes in Fortran 77". (Second Edition), Published by Cambridge University Press, 1992.

Qingbin, L., Chuhan, Z. and Guanglun, W. (1996). "Dynamic damage constitutive model of concrete in uni-axial tension". Engineering fracture mechanics, Volume 53, No. 3, pp. 449 – 455.

Reynolds, P., Pavic, A. and Waldron, P. (1998) "Modal testing of a 150-tonne concrete slab incorporating a false floor system". Proceedings of the 16th International Modal Analysis Conference (IMAC), California, USA, February 1998.

Roberts, E. H. and Wood, R. H. (1981a) "A simplified method for evaluating the natural frequencies and corresponding modal shapes of multi-storey frames". The Journal of the Institution of Structural Engineers, Volume 59B, No. 1, March 1981, pp. 1 – 9.

Roberts, E. H. and Wood, R. H. (1981b) "Correspondence on: A simplified method for evaluating the natural frequencies and corresponding modal shapes of multi-storey frames". The Journal of the Institution of Structural Engineers, Volume 59B, No. 4, December 1981, pp. 64 – 65.

Roeder, C. W. (1981). "Point loads on composite deck-reinforced slabs". Proceedings of the American Society of Civil Engineers, Journal of the Structural Division, Volume 107, ST12, pp. 2421 – 2428.

Ruotolo, R., Surace, C., Crespo, P. and Storer, D. (1996). "Harmonic analysis of the vibration of a cantilever beam with a closing crack". Computers and Structures, Volume 61, Number 6, pp. 1057 – 1074.

Sadeghi, K., Lamirault, J. and Sieffert, J. G. (1993). "Damage indicator improvement applied on RC structures subjected to cyclic loading". Proceedings of the Structural Dynamics EURODYN'93 Conference, Balkema, Totterdam, pp. 129 – 137.

Salane, H. J. and Baldwin, J. W. (1990). "Identification of modal properties of bridges". Proceedings of the American Society of Civil Engineers, Journal of Structural Engineering, Volume 116, No. 7, pp. 2008 – 2021.

Salane, H. J., Baldwin, L. W. and Duffield, R. C. (1987). "Dynamics approach for monitoring bridge deterioration". Transport Research Record Number 832, pp. 21 – 28.

Salawu, O. S. (1997). "Assessment of bridges: use of dynamic testing". Canadian Journal of Civil Engineering, 1997, Volume 24, Part 2, pp.218 – 228.

Salawu, O. S. (1997b). "Detection of structural damage through changes in frequency: a review". Engineering Structures, Volume 19, Part 9, pp. 718 – 723.

Samman, M. M. and Biswas, M. (1994a). "Vibration testing for non-destructive evaluation of bridges. I: Theory". Proceedings of the American Society of Civil Engineers, Journal of Structural Engineering, Volume 120, No. 1, pp. 269 – 289.

Samman, M. M. and Biswas, M. (1994b). "Vibration testing for non-destructive evaluation of bridges. II: Results". Proceedings of the American Society of Civil Engineers, Journal of Structural Engineering, Volume 120, No. 1, pp. 290 – 306.

Sanders, D. R., Stubbs, N. and Kim, Y. I. (1989). "Global non-destructive detection in composite structures". Proceedings of the 7th International Modal Analysis Conference, pp. 1501 – 1507.

Seliem, S. S. and Schuster, R. M. (1985). "Shear-bond resistance of composite deck-slabs". Canadian Journal of Civil Engineering, Volume 12, No. 2, pp. 316 – 324.

Schuster, R. M. (1976), "Composite steel-deck concrete floor systems". Proceedings of the American Society of Civil Engineers, Journal of the Structural Division, Volume 102, ST5, pp. 889 – 917.

Scott, R. H. (1983) "The short-term moment-curvature relationship for reinforced concrete beams". Proceedings of the Institution of Civil Engineers, Volume 75, Part 2, pp.725 – 734.

Shi, Z. Y., Law, S. S. and Zhang, L. M. (1998). "Structural damage localisation from modal strain energy change". Journal of Sound and Vibration, Volume 218, No. 5, pp. 825 – 844.

Smith, S. B. (1963) "In-filled frames". A Thesis submitted for PhD to the University of Bristol, 1963.

Snæbjörnsson, J. T., Hjorth-Hansen, E. and Sigbjörnsson, R. (1996) "Variability of natural frequency and damping ratio of a concrete building: Case study in system identification". Proceedings of the Structural Dynamics – EURODYN'96 Conference, Rotterdam, pp. 949 – 959.

Stark, J. W. B. and Brekelmans, J. W. P. M. (1990). "Plastic design of continuous composite slabs". Journal of Construction Steel Research, Volume 15, Nos. 1 & 2, pp. 23 – 47.

Stubbs, N., Kim, J. and Farrar, C. R. (1995). "Field verification of a non-destructive damage localisation and severity estimation algorithm". Proceedings of the 13th International Modal Analysis Conference, Nashville, Tennessee, pp. 210 – 217.

Takabatake, H. (1996) "A simplified analysis of doubly symmetric tube structures by the finite difference method". The Structural Design of Tall Buildings, Volume 5, pp. 111 – 128.

Thomson, W. T. (1993). "Theory of vibration with applications". (Fourth Edition), Published by Prentice Hall International Publishers, 1993.

Thomspon, J. M. T. and Stewart, H. B. (1986). "Non-linear dynamics and chaos". Published by John Wiley and Sons, (First edition).

Timoshenko, S. P. and Woinowsky-Krieger, S. (1959). "Theory of plates and shells". Published by McGraw-Hill International Editions, (ISBN 0-07-085820-9).

Tongue, B. H. (1996). "Principles of Vibration". Published by Oxford University Press Inc., 1996.

Uchida, N., Tsukagoshi, H., Aoyagi, T. and Takanashi, K. (1993). "Measurement of floor vibration". Colloquium on Structural Serviceability of Buildings, Goteborg, June 1993, pp. 133 – 140.

Vebo, A. and Ghali, A. (1977). "Moment-curvature relationship of reinforced concrete slabs". Proceedings of the American Society of Civil Engineers, Journal of the Structural Division, Volume 103, ST3, pp. 515 – 531.

Waldron, P. Pavic, A. and Reynolds, P. (1996). "Vibration of post-tensioned concrete floors". Progress report No. 1 – An internal report of the University of Sheffield, Centre for Cement and Concrete, September 1996.

Weltner, K., Grosjean, J., Schuster, P. and Weber, W. J. (1986). "Mathematics for engineers and scientists". Published by Stanley Thornes Publishers, (ISBN 0-85950-120-5).

West, R. (1973). "Recommendations on the use of grillage analysis for slab and pseudo-slab bridge decks". Cement and Concrete Association and the Construction Industry Research and Information Association, 1973.

Whiteman, W. E. and Ferri, A. A. (1996). "Displacement-dependent dry friction damping of a beam-like structure". Journal of Sound and Vibration, Volume 193, Number 3, pp. 313 – 329.

Williams, F. W., Bond, M. D. and Fergusson, L. (1983) "Accuracy of natural frequencies given by substitute sway frames with cladding". Proceedings of the Institution of Civil Engineers, Part 2, No. 75, March 1983, pp. 129 – 135.

Williams, M. S. and Waldron, P. (1994) "Evaluation of methods for predicting occupancy-induced vibration in concrete floors". Journal of the Institution of Structural Engineers, Volume 72, No. 20, October 1994, pp. 324 – 340.

Williams, C. and Tsang, W. F. (1988) "Determination of structural parameters from full-scale vibration tests". Proceedings of the SECED Civil Engineering Conference, Bristol, 1988, pp. 33 – 59.

Wise, C. M., Bridges, H. W., Walsh, S. R., Smith, C. J., Cross, P. T. and Bailey, P. A. (1996). "The new Commerzbank headquarters, Frankfurt, Germany". The Journal of the Institution of Structural Engineers, Volume 74, No. 7, April 1996, pp. 111 – 122.

Wolff, T. and Richardson, M. (1989). "Fault detection in structures from changes in their modal parameters". Proceedings of the 7th International Conference of the Modal Analysis Society, pp. 87 – 94.

Wood, M. G., Bailey, M., Friswell, M. I., Penny, J. E. T. and Purkiss, J. A. (1991). "Damage location in reinforced concrete beams using vibration responses". Proceedings of the 9th International Modal Analysis Conference, Florence Italy, April 1991, pp. 139 – 144.

Wood, R. H. (1974a) "Effective length of columns in multi-storey buildings – Part 1". The Journal of the Institution of Structural Engineers, Volume 52, No. 7, July 1974, pp. 235 – 244.

Wood, R. H. (1974b) "Effective length of columns in multi-storey buildings – Part 2". The Journal of the Institution of Structural Engineers, Volume 52, No. 8, July 1974, pp. 295 – 302.

Wood, R. H. (1974c) "Effective length of columns in multi-storey buildings – Part 3". The Journal of the Institution of Structural Engineers, Volume 52, No. 9, July 1974, pp. 341 – 346.

Wood, R. H. and Roberts, E. H. (1975) "A graphical method of predicting sidesway in the design of multi-storey buildings". Proceedings of the Institution of Civil Engineers, Part 2, No. 59, June 1975, pp. 353 – 372.

Wright, H. D., Evans, H. R. and Harding, P. W. (1987). "The use of profiled steel sheeting in floor construction". Journal of Construction Steel Research, Volume 7, No. 4, pp. 279 – 295.

Wyatt, T. A. (1989) "Design guide on the vibration of floors". Published by the Steel Construction Institute, 1989.

Yang, C. Y. (1996) "Behaviour of concrete sections reinforced with tension only steel". MSc Thesis presented in partial fulfilment of the requirements for Master of Science, submitted to the University of Glamorgan, 1996.

Zhang, Y. H., Friswell, M. I. and Mottershead, J. E. (1994). "A comparison of methods to locate damage in structures". Proceedings of the 19th International Seminar on Modal Analysis, Tools for Noise and Vibration Analysis, Leuven, Belgium, pp. 683 – 695.

Zienkiewicz, O. C. (1977). "The finite element method". Third Edition, Published by McGraw-Hill, London.

Zimmerman, D. C. and Kaouk, M. (1992). "Structural damage detection using a subspace rotation algorithm". Proceedings of the 33rd AIAA Structures, Structural dynamics and Material Conference, pp. 2341 – 2350.

Zimmerman, D. C., Kaouk, M. and Simmermacher, T. (1995a). "On the role of engineering insight and judgement structural damage detection". Proceedings of the 13th International Modal Analysis Conference, Nashville, Tennessee, pp. 414 – 420.

Zimmerman, D. C., Simmermacher, T. and Kaouk, M. (1995b). "Structural damage detection using frequency response functions". Proceedings of the 13th International Modal Analysis Conference, Nashville, Tennessee, pp. 178 – 184.

APPENDIX A

Theoretical Aspects of Modal Analysis and the Rationale of Modal Testing

A.1 Vibration Response Signals – Theoretical Considerations

A.1.1 Sinusoidal excitation of single-degree-of-freedom systems

It is unlikely that a structure can be realistically modelled as a 'perfect' single-degree-of-freedom (sdof) system. However, the characteristics of this model are extremely useful and are regularly used to represent other systems that comprise many more degrees-of-freedom. The relevance of the sdof system, and its use with higher order systems, is considered later in this appendix, but for now it is worth identifying some of the basic characteristics that control the behaviour of simple linear sdof structures.

A.1.1.1 Steady state undamped response

The classical idealisation of a sdof undamped system is given by Figure A.1(a), where a mass (m) is supported by a spring of stiffness (k) and displacement is permitted in one direction only. The equation of motion describing the behaviour of this system is written in conventional form as,

$$m\ddot{x}(t)+kx(t)=f(t) \text{ or } \ddot{x}(t)+\omega_n{}^2x(t)=\frac{1}{m}f(t) \text{ if } \omega_n{}^2=\frac{k}{m} \qquad \text{(A.1)}$$

and ω_n is the natural or resonance frequency of the system. The expression reflects the combined forces induced by the system when in motion and stipulates that the combined kinetic $\left(m\ddot{x}\right)$ and potential energy (kx) must be in equilibrium with the energy of the function, $f(t)$. Assuming that the forcing function is sinusoidal in nature,

i.e.

$$f(t) = F_o \sin(\omega_f t) \tag{A.2}$$

where F_o and ω_f are the force magnitude and frequency of excitation respectively, from which a steady state solution for displacement, $x(t)$, is obtained as,

$$x(t) = \frac{F_o}{m}\left(\frac{1}{\omega_n{}^2 - \omega_f{}^2}\right)\sin(\omega_f t) \tag{A.3}$$

Although extremely simple, eqn.(A.3) is very useful in that a basic understanding of the condition of resonance can be achieved. Focussing on the positive peak amplitude values of this displacement response signal, i.e. when $\omega_f t = \frac{n\pi}{2}$ where n = 1, 5, 9, 13, 17,..., etc, and defining the produce of the equation in terms of a normalised quantity, a response model known as the Frequency Response Function (FRF) is defined.

$$\frac{X}{F_o} = \frac{1}{m}\left(\frac{1}{\omega_n{}^2 - \omega_f{}^2}\right) \tag{A.4}$$

From eqn.(A.3) it can be deduced that,

$$\frac{X}{F_o} \to \infty \text{ as } \omega_f \to \omega_n,\ \frac{X}{F_o} \to \frac{1}{k} \text{ as } \omega_f \to 0, \text{ and } \frac{X}{F_o} \to 0 \text{ as } \omega_f \to \infty \tag{A.5}$$

where X is the peak amplitude of motion and ω_n is the natural oscillatory frequency of the system. Therefore, the condition of resonance occurs as the applied forcing frequency reaches that of the natural frequency of the system.

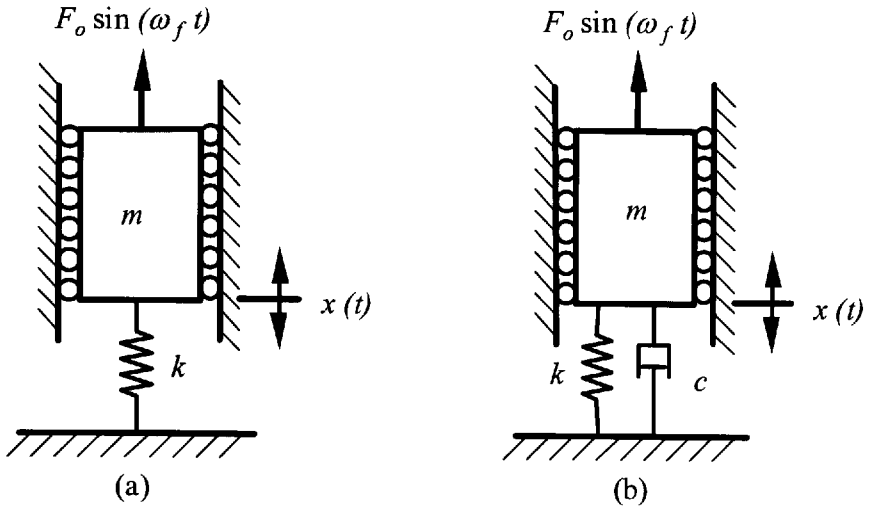

Figure A.1 – Single-degree-of-freedom systems comprising: (a) spring stiffness (k) and mass (m); and (b) spring stiffness (k), mass (m) and damping (c).

A.1.1.2 Steady state damped response

In reality, the condition of 'near-infinte' amplitude is very unlikely to occur and when dealing with civil engineering type structures is not possible due to mechanisms that contribute to the dispersal of the applied force energy. Examples of such mechanisms could be the friction at a bolted connection or the fretting of two surfaces in contact. Whatever the mechanism, it is usual to assume the overall contribution can be regarded as one, which is modelled as an energy dissipation mechanism or 'damping'.

Taking damping into account, the spring-mass sdof system earlier described is modified to comprise three components, i.e. the spring (k), the mass (m) and the damper (c), and is shown diagrammatically in Figure A.1(b). The equation of motion of eqn.(A.1) now becomes,

$$m\ddot{x}(t) + c\dot{x}(t) + kx(t) = f(t) \text{ or, } \ddot{x}(t) + 2\zeta\omega_n \dot{x}(t) + \omega_n{}^2 x(t) = f(t) \qquad \text{(A.6)}$$

where $\zeta = \dfrac{c}{c_c}$ is a damping ratio expressing the magnitude of the damper, c, relative to a critical value, $c_c = 2m\omega_n$. This critical value is important as it represents a

condition that would prevent the occurrence of oscillatory motion of the free vibrating system. Damping expressed in this way is defined as visco-elastic, which characterises energy dissipation as a quantity that is relative to the velocity of the system when in motion.

Assuming the forcing function of eqn.(A.2) and describing the system response with,

$$x(t) = X\sin\left(\omega_f t - \varphi\right) \tag{A.7}$$

where φ is a phase angle between the force $[f(t)]$ and the displacement $[x(t)]$, the FRF for the damped sdof system can be defined as,

$$\frac{X}{F_o} = \frac{1}{k}\left(\frac{1}{\sqrt{\left[1-\left(\frac{\omega_f}{\omega_n}\right)^2\right]^2 + \left[2\zeta\left(\frac{\omega_f}{\omega_n}\right)\right]^2}}\right) \tag{A.8}$$

Three characteristics can again be defined from this relationship,

$$\frac{X}{F_o} \to \frac{1}{2\zeta k} \text{ as } \omega_f \to \omega_n,\ \frac{X}{F_o} \to \frac{1}{k} \text{ as } \omega_f \to 0, \text{ and } \frac{X}{F_o} \to 0 \text{ as } \omega_f \to \infty \tag{A.9}$$

Equation (A.8) is a useful expression as it allows the response of the system to be gauged relative to the amount of damping present. Also, it is seen from eqn.(A.9) that the amplitude of motion at the resonance frequency no longer has an infinite value but is controlled by the presence of the damping terms.

A.1.2 Transient response of a damped Single-degree-of-freedom system

The steady state response of a damped sdof system is only part of the overall solution to the equation of motion given by eqn.(A.6), and will generally only occur when the

system is excited in a manner that comprises a single sinusoidal component. This will only truly occur when the transient stage of the vibration has diminished, which for a sdof system subject to continuous sinusoidal loading will largely depend on the initial condition of the response at the start of the vibration event. Treating the transient response in isolation, however, will help to define additional important characteristics of a viscously damped sdof system.

A.1.2.1 Viscously damped decay of vibration

The equation of motion for the free vibration of a viscously damped sdof system can be expressed as,

$$\ddot{x}(t) + 2\zeta\omega_n \dot{x}(t) + \omega_n{}^2 x(t) = 0 \tag{A.10}$$

Equation (A.10) has a number of solutions, which depend on the magnitude of the damping ratio, ζ. However, in the majority of cases, where civil engineering structures are concerned, it is highly likely that the amount of damping present in the system will be low relative to the critical value of c_c. For this condition it is convenient to assume that the displacement will be oscillatory and that is can be described using,

$$x(t) = e^{s(t)} \tag{A.11}$$

where s is obtained by substituting eqn.(A.11) into the differential equation of (A.10), and solving for the roots of the characteristics equation. The results is a general solution in complex form, which can be written as,

$$x(t) = e^{-\zeta\omega_n(t)}\left(A\sin\sqrt{1-\zeta^2}\omega_n(t) + B\cos\sqrt{1-\zeta^2}\omega_n(t) \right) \tag{A.12}$$

where A and B are arbitrary constants determined from initial conditions. With initial conditions $x(0)$ and $\dot{x}(0)$, eqn.(A.12) becomes,

$$x(t) = e^{-\zeta\omega_n(t)}\left(\frac{\dot{x}(0)+\zeta\omega_n x(0)}{\sqrt{1-\zeta^2}\omega_n}\sin\sqrt{1-\zeta^2}\omega_n(t) + x(0)\cos\sqrt{1-\zeta^2}\omega_n(t)\right) \quad \text{(A.13)}$$

Two important characteristics can be drawn from this expression. The first is that the oscillation frequency of the system depends on the level of the damping ratio, ζ, which can be termed the 'frequency of damped oscillation'. Secondly, the response of the system subjected to the initial conditions at time $t = 0$ will 'decay' exponentially to zero, which is controlled by the decay function $e^{-\zeta\omega_n(t)}$ (the decay-of-vibration).

A.1.3 The response of systems with more than one degree-of-freedom (the rationale of modal testing)

The assumption of a single-degree-of-freedom is a simplistic condition unlikely to be encountered in real civil type structures. Nevertheless, this system is actually a useful and meaningful representation of real structural behaviour and will later be used to demonstrate methods often adopted for the extraction of modal information such as natural frequency and damping. Before exploring these methods, it is first necessary to demonstrate how the characteristics identified earlier can be used to examine the behaviour of more complicated multi-degree-of-freedom (mdof) structures.

A.1.3.1 Orthogonality of system equations – the basis for modal analysis

When dealing with structures that are more complicated that a simple sdof system, it is usual to consider the behaviour as a series of linear discrete degrees-of-freedom (dofs) that collectively reflect the fundamental characteristics of the overall system. A popular means of achieving this, which has itself received considerable attention in both its application and performance development, is the use of the Finite Element (FE) method. Indeed, as seen from the review of literature discussed in chapters 4, 5 and 6, the FE method plays an important role for the detection of damage in structural systems where the natural frequencies and mode shapes can be calculated using,

$$([K]+[\omega^2][M])[\Phi]=0 \tag{A.14}$$

In this equation, $[K]$ is a matrix of system stiffness and $[M]$ a matrix of system mass, while $[\omega^2]$ and $[\Phi]$ are matrices containing the eigen-values and eigen-vectors respectively of the system.

For symmetrical matrices $[K]$ and $[M]$, which for engineering problem is most often the case, the solution to eqn.(A.14) can be achieved using well documented methods [Griffiths and Smith (1991), Press *et al* (1992) are examples]. To examine the response of these systems to forced vibration, a useful relationship exists that allows the combined system equation of (A.14) to be de-coupled so that individual vibration modes can be examined in isolation. This relationship is probably the most important in modal analysis and is a condition best known as the 'orthogonality of the natural modes'.

Consider the vibration of a spring-mass system using the conventional matrix notation,

$$[K][\ddot{\Lambda}]+[M][\Lambda]=0 \tag{A.15}$$

where $[K]$ and $[M]$ are matrices containing properties of spring stiffness and mass respectively corresponding to the number of system dofs. $[\ddot{\Lambda}]=\{\ddot{x}_1,\ddot{x}_2,...,\ddot{x}_n\}^T$ and $[\Lambda]=\{x_1,x_2,...,x_n\}^T$ are vectors that represent the acceleration and displacement respectively and are again consistent with the system dofs. Expressed in terms of the eigen-value problem, eqn.(A.15) becomes

$$[K][\Phi]=[\omega_n{}^2][K][\Phi] \tag{A.16}$$

where $[\omega_n{}^2]$ is now a diagonal matrix whose elements correspond to the natural frequencies of each of the n dofs (the eigen-values) and $[\Phi]$ is a matrix of system

eigen-vectors given by $[\Phi]=[\{\phi\}_1 \vdots \{\phi\}_2 \vdots,...,\vdots \{\phi\}_n]$, the mode shapes. Writing eqn.(A.16) in terms of two individual modes, say 1 and 2

$$[K]\{\phi\}_1 = \omega_1{}^2[M]\{\phi\}_1 \tag{A.17a}$$

$$[K]\{\phi\}_2 = \omega_2{}^2[M]\{\phi\}_2 \tag{A.17b}$$

and pre-multiplying both sides of eqn.(A.17) by $\{\phi\}_2{}^T$, and eqn.(A.17b) by $\{\phi\}_1{}^T$ gives,

$$\{\phi\}_2{}^T[K]\{\phi\}_1 = \omega_1{}^2\{\phi\}_2{}^T[M]\{\phi\}_1 \tag{A.18a}$$

$$\{\phi\}_1{}^T[K]\{\phi\}_2 = \omega_2{}^2\{\phi\}_1{}^T[M]\{\phi\}_2 \tag{A.18b}$$

To make the next step easier, eqn.(A.18b) is transposed to give,

$$\{\phi\}_2{}^T[K]\{\phi\}_1 = \omega_2{}^2\{\phi\}_2{}^T[M]\{\phi\}_1 \tag{A.18c}$$

and eqn.(A.18a) is subtracted from (A.18c) giving,

$$\left(\omega_2{}^2 - \omega_1{}^2\right)\{\phi\}_2{}^T[M]\{\phi\}_1 = 0 \tag{A.19}$$

This expression is useful as it suggests that for values of $\omega_1{}^2 \neq \omega_2{}^2$,

$$\{\phi\}_2{}^T[M]\{\phi\}_1 = 0 \tag{A.20}$$

which defines the eigen-vectors of mode 1 and 2 as being orthogonal with respect to the mass matrix [*M*].

In addition, if the eigen-vectors of the individual modes are normalised relative to the mass matrix to give,

$$\{\tilde{\phi}\}_1^T [M] \{\tilde{\phi}\}_1 = 1 \tag{A.21a}$$

$$\{\tilde{\phi}\}_2^T [M] \{\tilde{\phi}\}_2 = 1 \tag{A.21b}$$

where the tilde indicates that the eigen-vectors are now mass normalised, eqn.(A.16) can now be re-written as,

$$[\tilde{\Phi}]^T [K][\tilde{\Phi}] = [\omega_n{}^2][\tilde{\Phi}]^T [M][\tilde{\Phi}] \tag{A.22}$$

where $[\tilde{\Phi}]$ is the modal matrix comprised of the mass normalised modal vectors. And due to the relationships of eqn.(A.20a) or (A.20b), (A.22) gives,

$$[\tilde{\Phi}]^T [K][\tilde{\Phi}] = \omega_m{}^2 \tag{A.23}$$

Introducing a linear transformation vector, $\{q\}=\{q_1, q_2, ..., q_n\}^T$, such that,

$$[\Lambda] = [\tilde{\Phi}]\{q\} \text{ and } [\ddot{\Lambda}] = [\tilde{\Phi}]\{\ddot{q}\} \tag{A.24}$$

are the displacement and acceleration respectively of the mdof system. Pre-multiplying eqn.(A.16) by $[\Phi]^T$, and defining the expression in relation to mass normalised terms, then gives

$$[\tilde{\Phi}]^T [K][\tilde{\Phi}]\{\ddot{q}\} + [\tilde{\Phi}]^T [M][\tilde{\Phi}]\{q\} = 0 \tag{A.25}$$

Due to the relationships of eqns.(A.20), (A.21) and (A.23), a system of de-coupled equations is formed and given by,

$$\begin{aligned}
&\ddot{q}_1+\omega_1{}^2 q_1 = 0 \\
&\ddot{q}_2+\omega_2{}^2 q_2 = 0 \quad (n = \text{number of dofs}) \\
&\vdots \\
&\ddot{q}_n+\omega_n{}^2 q_n = 0
\end{aligned} \tag{A.26}$$

Similarly, for a viscously damped structure subjected to a vector of forcing functions, the de-coupled equations of motion are written,

$$\begin{aligned}
&\ddot{q}_1+2\zeta_1\omega_1\dot{q}_1+\omega_1{}^2 q_1 = \{\tilde{\phi}\}_1{}^T f(t) \\
&\ddot{q}_2+2\zeta_2\omega_2\dot{q}_2+\omega_2{}^2 q_2 = \{\tilde{\phi}\}_2{}^T f(t) \quad (n = \text{number of dofs}) \\
&\vdots \\
&\ddot{q}_n+2\zeta_n\omega_n\dot{q}_n+\omega_n{}^2 q_n = \{\tilde{\phi}\}_n{}^T f(t)
\end{aligned} \tag{A.27}$$

where ζ_i, and ω_i are the damping and natural frequency values appropriate to the individual natural modes, $\{\tilde{\phi}\}_i$ is the mass normalised eigen-vector that represents the i^{th} mode shape, and $i = 1, 2, \ldots, n$. Therefore, the total response at the i^{th} dof to the forcing function $f(t)$ can be calculated from a linear superposition of individual sdof system equations.

The significance of these equations is that the original mdof system has been reduced to a series of sdof systems. Therefore, if the solution to eqn.(A.16) is known (i.e. the natural frequencies and associated mass normalised mode shapes) the response of the structure to any arbitrary loading can be calculated.

A.1.3.2 Multi-degree-of-freedom frequency response function

Equation (A.27) has a useful application in that the displacement of a mdof system can be regarded as a simple summation of the sdof responses, which can be expressed as,

$$\{X_i\} = \{\tilde{\phi}_i\}_1 \{X_i\}_1 + \{\tilde{\phi}_i\}_2 \{X_i\}_2 + ,...,+ \{\tilde{\phi}_i\}_n \{X_i\}_n \qquad \text{(A.28)}$$

where i = 1, 2, ..., n, $\{X_i\}$ is the total peak amplitude of the i^{th} dof, $\{\tilde{\phi}_i\}_n$ is the i^{th} element of the n^{th} mass normalised eigen-vectors, and $\{X_i\}_n$ is the response of the i^{th} dof of mode n. Therefore, for a system subjected to a steady-state sinusoidal forcing function where the response of each dof is assumed to be of the form given by eqn.(A.7), the combined FRF at the j^{th} dof can be calculated from,

$$\frac{X_j}{F} = \sum_{i=1}^{n} \frac{\{\tilde{\phi}_j\}_i \{X_j\}_i}{\{\tilde{\phi}\}_i^T f(t)} = \sum_{i=1}^{n} \frac{\{\tilde{\phi}_j\}_i}{k_i} \left(\frac{1}{\sqrt{\left[1 - \left(\frac{\omega_f}{\omega_i}\right)^2\right]^2 + \left[2\zeta_i \left(\frac{\omega_f}{\omega_i}\right)\right]^2}} \right) \qquad \text{(A.29)}$$

where i = 1, 2, ..., n modes, and k_i can be described as the *modal stiffness* of mode i.

A.2 Determining of Natural Frequency and Damping

Theoretical aspects of vibration and modal analysis presented in section A.1 above identify the characteristics of visco-elastic systems, and how mdof systems with separated modes can be regarded as a superposition of individual sdof systems.

This section discusses how the candidate made use of these principles to determine quantities of damping and natural frequency from measured response records taken from the structures studied for this thesis (i.e. expanding on the information given in chapter 3).

A.2.1 Damping and natural frequency from decay-of-vibration records

Throughout all vibration studies included in this thesis, no attempt was made to measure the input forces used to induce transient excitation of the tested structures. This does not present a problem for the determination of the modal properties, provided that a number of issues are taken into account.

For the most part, the natural frequency and damping of the fundamental mode was of primary interest. Therefore, before analysing the vibration data the first priority was to ensure that the captured signal reflected a single vibration mode, which corresponded to the desired natural frequency of the structure. This was checked using a Fast Fourier Transform (FFT). The FFT allowed the frequency spectrum (autospectrum) of the signal to be determined. If the autospectrum indicated a single dominant response peak, the captured data could be analysed assuming that it represented a single mode of vibration. Only then could the decay-of-vibration response signal be used to obtain damping and natural frequency values representing single mode behaviour.

A.2.1.1 Damping from logarithmic decrement

A convenient means of assessing the damping of a structure is to quantify the rate of decay of the free oscillatory vibration. In general, the faster the rate of decay, the larger the damping. This can be achieved using the logarithmic decrement, δ, which is obtained from the natural logarithm of the ratio of any two successive amplitudes. Therefore, assuming that the vibration is viscous in nature, the logarithmic decrement is calculated using,

$$\delta = \ln \frac{x_i}{x_{i+1}} = \frac{2\pi\zeta}{\sqrt{1-\zeta^2}} \tag{A.30}$$

where x_i and x_{i+1} are two successive peak amplitudes of the captured time dependant decay signal. Solving for the damping ratio, ζ, eqn.(A.30) becomes,

$$\zeta = \frac{\delta}{\sqrt{4\pi^2 + \delta^2}} \tag{A.31}$$

where δ is the logarithmic decrement. The derivation of eqn.(A.31) is not new, and for a full explanation the reader is directed to text by Thomson (1993), Clough and Penzien (1993) or Tongue (1996).

A.2.1.2 Damping from curve fitting

A more accurate means of identifying damping, which at the same time clarifies the characteristics of the decay, is the use of algorithms that fit theoretical equations of vibration decay to the data of captured signals. The advantage of this approach is that a comparison can be made between measured data and theoretical predictions allowing the accuracy of the assumed damping model to be assessed.

Where defined in this thesis, eqn.(A.31) was used to extract the damping from decay of vibration signals. An additional advantage of using this approach is that a crosscheck on the system natural frequency can be achieved, as the equation depends not only on the damping factor, ζ, but also in ω_n.

A.2.2 Damping and natural frequency from the FRF

An alternative to methods that use time dependant data is to consider the system response in the frequency domain. The method employed for the studies in this thesis made use of the relationship of eqn.(A.29), which represents the FRF for a system with well separated modes of vibration. However, to obtain the damping and natural frequency of the fundamental mode, it is sufficient to use the equation with $n = 1$, which assumes that the frequency response comprises vibration components of a single mode only.

A.3 The Basis of the Fast Fourier Transform (FFT)

It is well established that any periodic function of period, T, can be represented as a series of sinusoidal components in the form of a Fourier series. In general terms the Fourier series of a time varying signal has the form,

$$x(t) = a_o + 2\left\{\sum_{m=1}^{\infty} a_m \cos\frac{2\pi m}{T}t + \sum_{m=1}^{\infty} b_m \sin\frac{2\pi m}{T}t\right\} \tag{A.32}$$

where

$$a_o = \frac{1}{T}\int_o^T x(t)dt \tag{A.33}$$

$$a_m = \frac{1}{T}\int_o^T x(t)\cos\frac{2\pi m}{T}tdt \tag{A.34}$$

$$b_m = \frac{1}{T}\int_o^T x(t)\sin\frac{2\pi m}{T}tdt \tag{A.35}$$

are the Fourier coefficients of the signal. An alternative way of presenting these coefficients is to use complex notation, such that eqns.(A.33) to (A.35) can be replaced by,

$$\underset{m\geq o}{A_m} = a_m - ib_m = \frac{1}{T}\int_o^T x(t)e^{-i\left(\frac{2\pi m}{T}t\right)}dt \tag{A.36}$$

which represents the Fourier coefficients of the continuous response signal $x(t)$. Applying this expression to a discrete signal where the response information for $x(t)$ is defined by a finite data sequence, say $\{x_r\}$, where r = 0, 1, 2, ..., $N-1$, and N is the number of Fourier terms comprising the signal, eqn.(A.36) becomes,

$$A_m = \frac{1}{N}\sum_{r=o}^{N-1}\{x_r\}e^{-i\left(\frac{2\pi m}{N}r\right)}, \text{ where } m = 0, 1, 2, \ldots, N-1 \qquad \text{(A.37)}$$

Equation (A.37) is described as a discrete Fourier transform (DFT). However, to calculate all A_m coefficients requires a significant number of calculations, i.e. N multiplications of $\{x_r\}e^{-i\left(\frac{2\pi m}{N}r\right)}$ for N values of A_m. For the full sequence A_m, this would require N^2 multiplications. This is unacceptable for a large sequence, not only from a computational standpoint, but also due to the round-off errors that would occur as a result of numerical truncation (if compiled by single precision computers).

To solve this problem, Cooley and Tukey (1969) proposed a method based on the DFT, which became known as the fast Fourier transform (FFT) method, and is the approach used throughout this thesis.

A.3.1 FFT using the Cooley and Tukey (1969) method

The method by Cooley and Tukey (1969) is based on a concept now known as partitioning, where the original finite sequence $\{x_r\}$, where r = 0, 1, 2, ..., $N-1$, is divided into shorter sequences $\{y_r\}$ and $\{z_r\}$ given by,

$$\{y_r\} = \{x_{2r}\} \text{ and } \{z_r\} = \{x_{2r+1}\} \text{ where r} = 0, 1, 2, \ldots, \left(\frac{N}{2}-1\right) \qquad \text{(A.38)}$$

The DFT of these shorter series now become,

$$Y_m = \frac{1}{(N/2)}\sum_{r=o}^{N/2-1}\{y_r\}e^{-i\left(\frac{2\pi m}{N/2}r\right)} \text{ where } m = 0, 1, 2, \ldots, \left(\frac{N}{2}-1\right) \qquad \text{(A.39a)}$$

$$Z_m = \frac{1}{(N/2)}\sum_{r=o}^{N/2-1}\{z_r\}e^{-i\left(\frac{2\pi m}{N/2}r\right)} \text{ where } m = 0, 1, 2, \ldots, \left(\frac{N}{2}-1\right) \qquad \text{(A.39b)}$$

allowing the original DFT of eqn.(A.37) to be obtained from,

$$A_m = \frac{1}{(N)}\left\{ \sum_{r=o}^{N/2-1} \{y_r\} e^{-i\left(\frac{2\pi m}{N/2} r\right)} + e^{-i\left(\frac{2\pi m}{N/2}\right)} \sum_{r=o}^{N/2-1} \{z_r\} e^{-i\left(\frac{2\pi m}{N/2} r\right)} \right\} \qquad \text{(A.40}$$

or

$$A_m = \frac{1}{2}\left\{ Y_m + e^{-i\left(\frac{2\pi m}{N}\right)} Z_m \right\} \qquad \text{(A.41)}$$

Therefore, the DFT of the original sequence $\{x_r\}$ can be obtained from the DFT's of the two sub-sequences $\{y_r\}$ and $\{z_r\}$. In addition, if the length of the original sequence is equal to,

$$N = 2^n \qquad \text{(A.42)}$$

where n is an integer value, then the new sequences can be reduced into further sub-sequences, and so on, until each contains a single term. However, eqn.(A.41) will only take care of half the required A_m values for m = 0, 1, 2, ..., $\left(\frac{N}{2}-1\right)$ as given by eqn.(A.39a & b). Therefore, to ensure that all A_m terms are obtained the full solution becomes,

$$A_m = \frac{1}{2}\left\{ Y_m + e^{-i\left(\frac{2\pi m}{N}\right)} Z_m \right\}$$

$$A_{m+\frac{N}{2}} = \frac{1}{2}\left\{ Y_m + e^{-i\left(\frac{2\pi m}{N}\right)} Z_m \right\} \qquad \text{(A.43)}$$

and is the basis of the FFT analysis, often termed the computational butterfly technique.

APPENDIX B

The Eight-Storey Steel-Framed Building at the Large Building Test Facility, Cardington, UK – 'As-Built' Structural Details

General Notes:

The information presented in this Appendix relates to the general arrangement of the structural members for the eight-storey steel-framed building. Other information that should be considered is as follows:

(i) Vertical cross bracing was installed in the building, which extends the full height of the structure. The locations of these braced zones are coincident with the grid-line referencing system (shown on the diagrams) and comprise of 250mm wide by 15mm thick flat steel plates, which are positioned diagonally between floor. Connectivity at the ends of the bracing members is via bolted steel cleat joints, which are located at the intersection of the beams and columns at each floor over the affected region. The locations where these bracing members have been installed are listed below, and have been given relative to the grid-line system shown on the diagrams:

- along grid-lines A, C, D and F – from grid line 2a to 3.
- along grid-line 3 – from grid lines A to A1 and E1 to F
- along grid-line 2a – from grid-lines C to C1 and C1 to D

(ii) Masonry walls have also been installed at various parts of the structure. These walls are 140mm thick and have been constructed to full storey height in some locations, and 900mm in others. Again using the grid-line referencing system, the positions of these walls are:

- along grid-lines A and F – full storey height at all stories (except the 8^{th})
- along grid-lines a and 4 – 900mm high from the finished floor level at all storey levels.

(iii) Each floor of the building has been constructed using a composite system incorporating steel profile decking produced by PMF Ltd. The trade name of the decking is ComFlor 70, where the finished composite floor spans parallel to

grid-lines A to F. (Shaded area on the diagrams indicate voided zones within the slab).

Key for use with structural steel layout:

Member reference	**Member type**
A	305×165×40 UB Grade 50
B	356×171×51 UB Grade 50
C	254×146×31 UB Grade 50
D	168.3×10 CHS Grade 43
E	610×229×101 UB Grade 50
F	686×254×170 Grade 50
G	305×305×137 UC Grade 50
H	254×254×89 UC Grade 50
J	305×305×198 UC Grade 50

All members have the shapes and dimensions as set out in BS 4 : Part 1: 1993, while Grades 50 and 43 refer to steel with minimum yield strengths of 350N/mm^2 and 275N/mm^2 respectively.

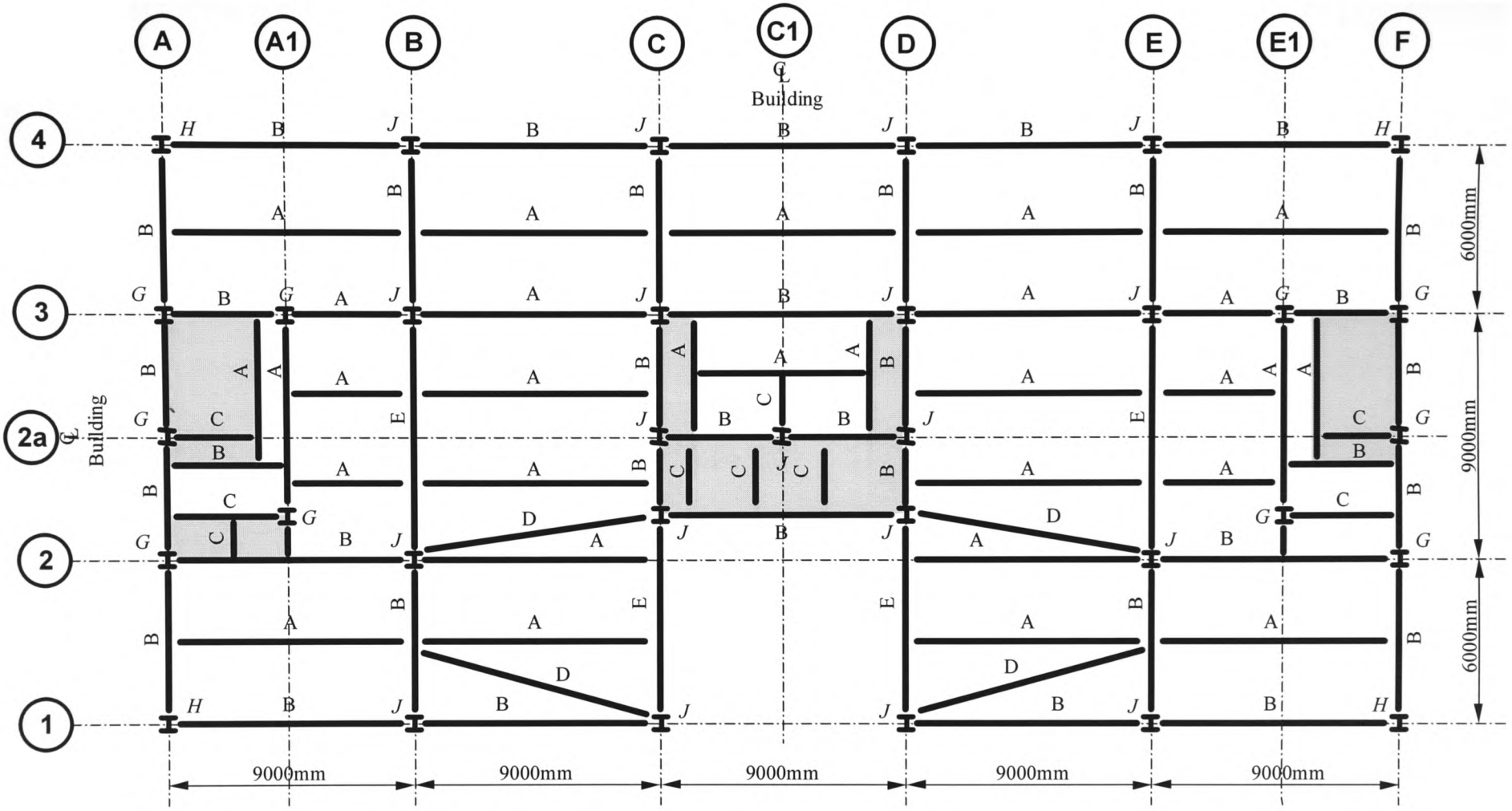

Figure B.1 – Plan on 1st floor showing the general layout of the main structural elements

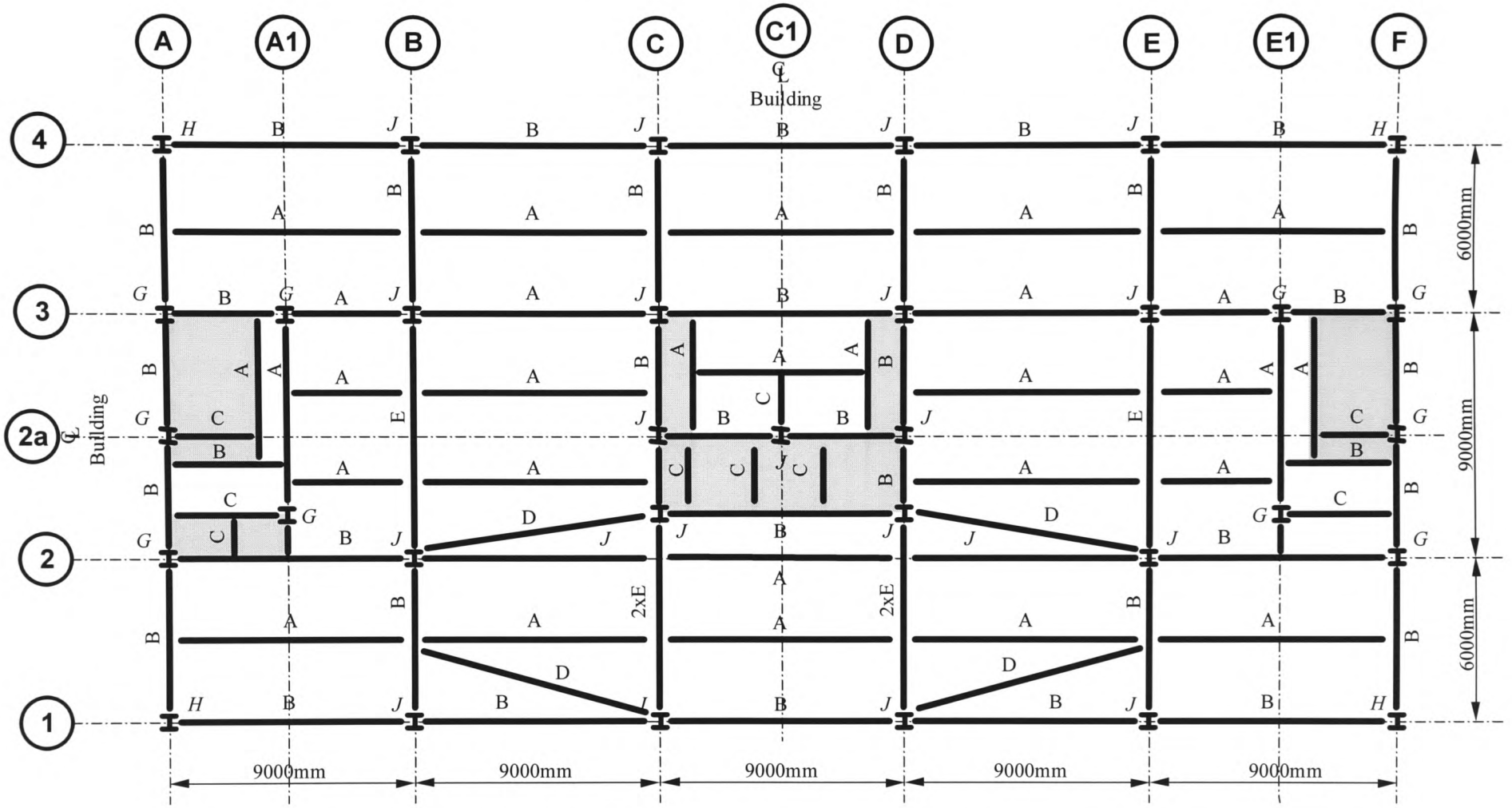

Figure B.2 – Plan on 2nd floor showing the general layout of the main structural elements

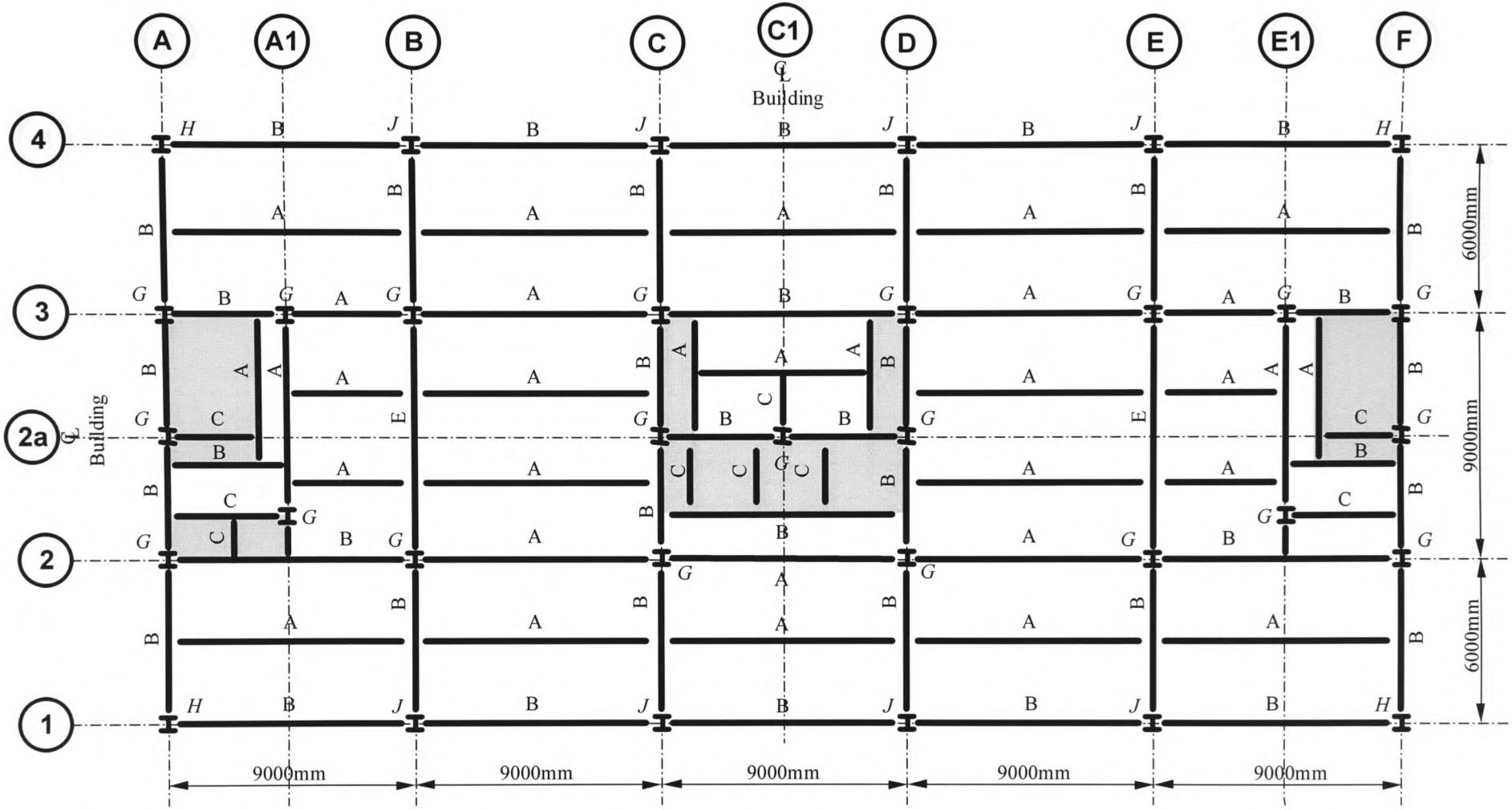

Figure B.3 – Plan on the 3rd and 4th floors (similar) showing the general layout of the main structural elements

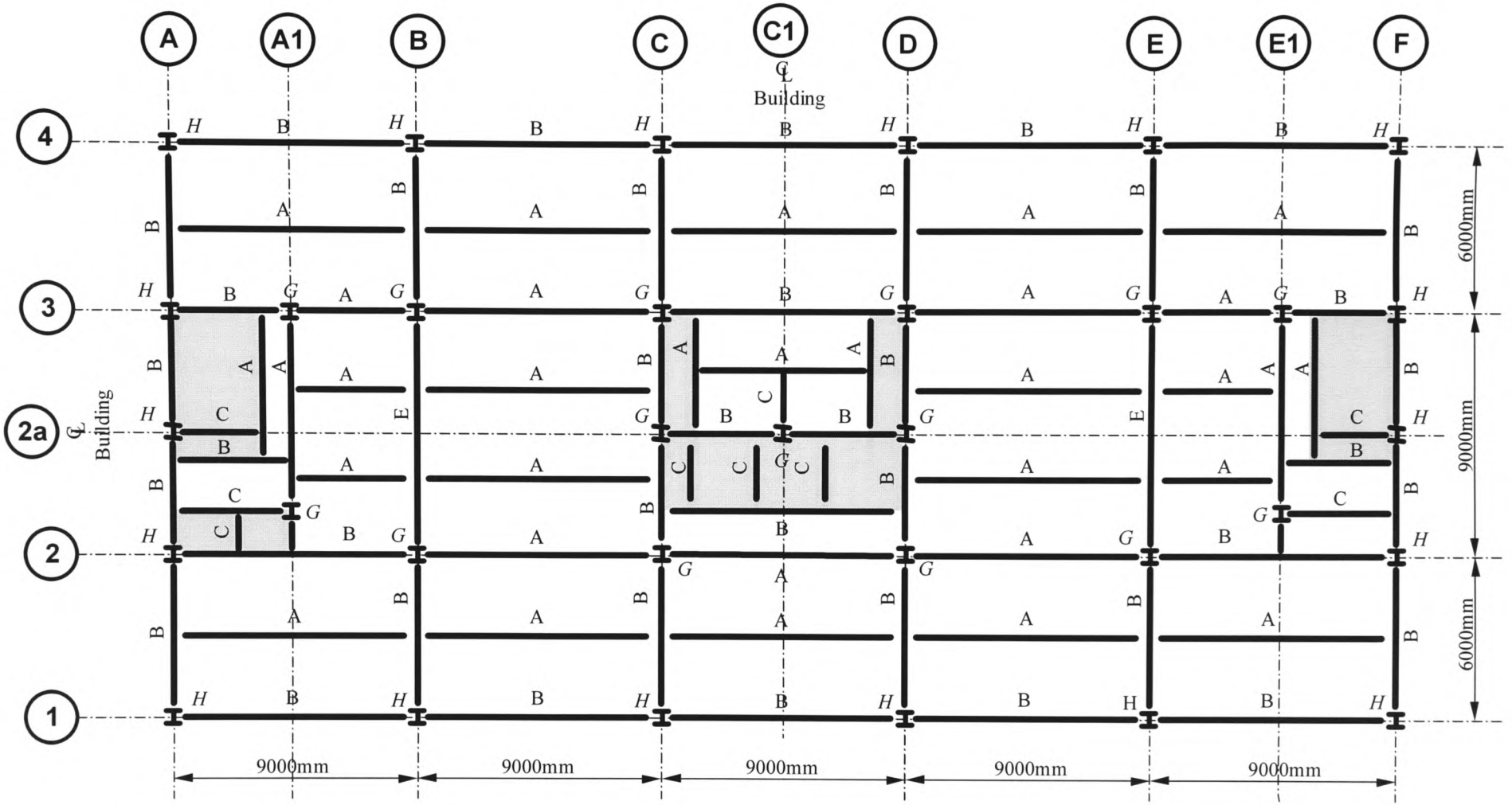

Figure B.4 – Plan on the 5th floor showing the general layout of the main structural elements

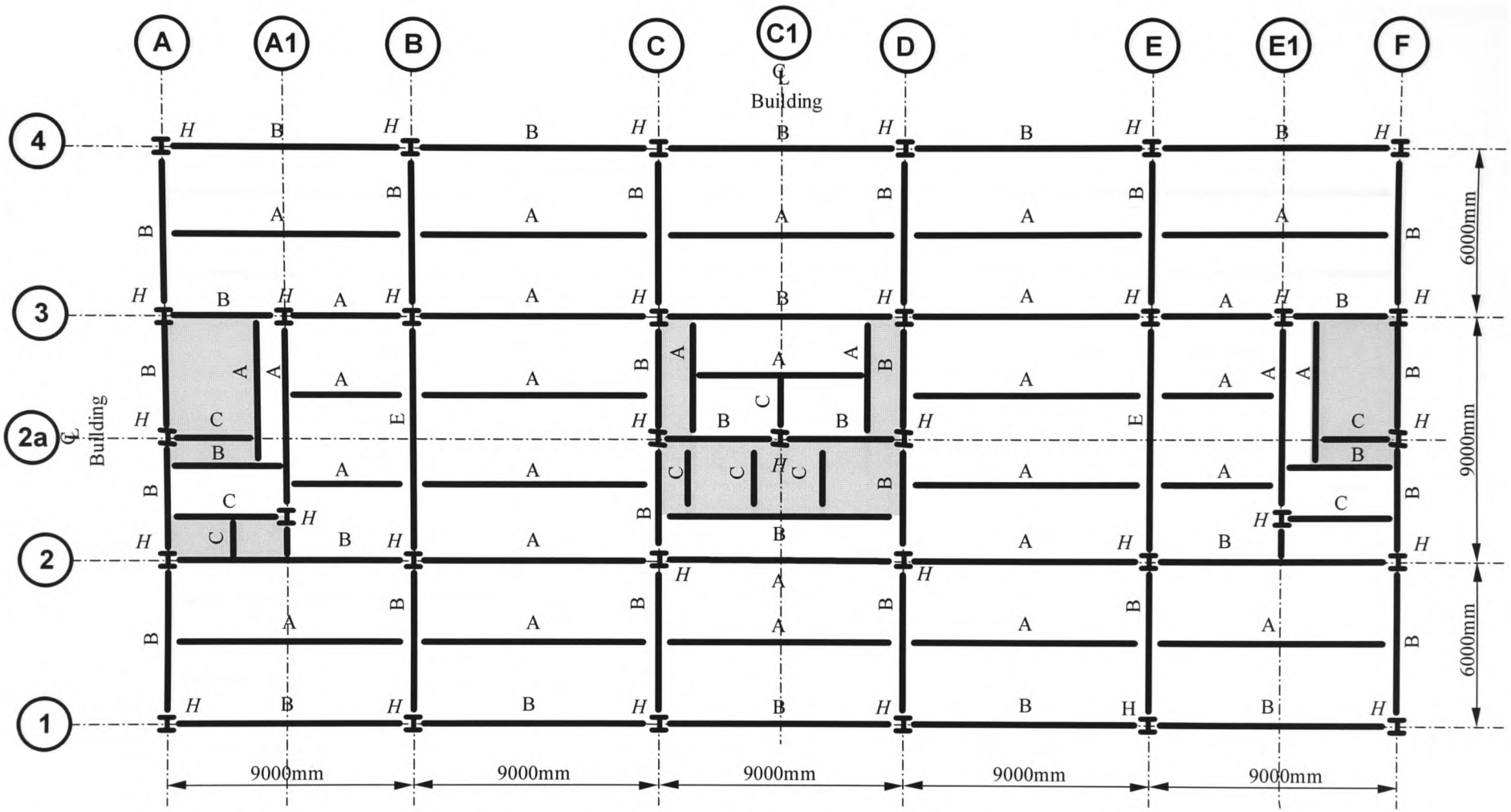

Figure B.5 – Plan on the 6th and 7th floors (similar) showing the general layout of the main structural elements

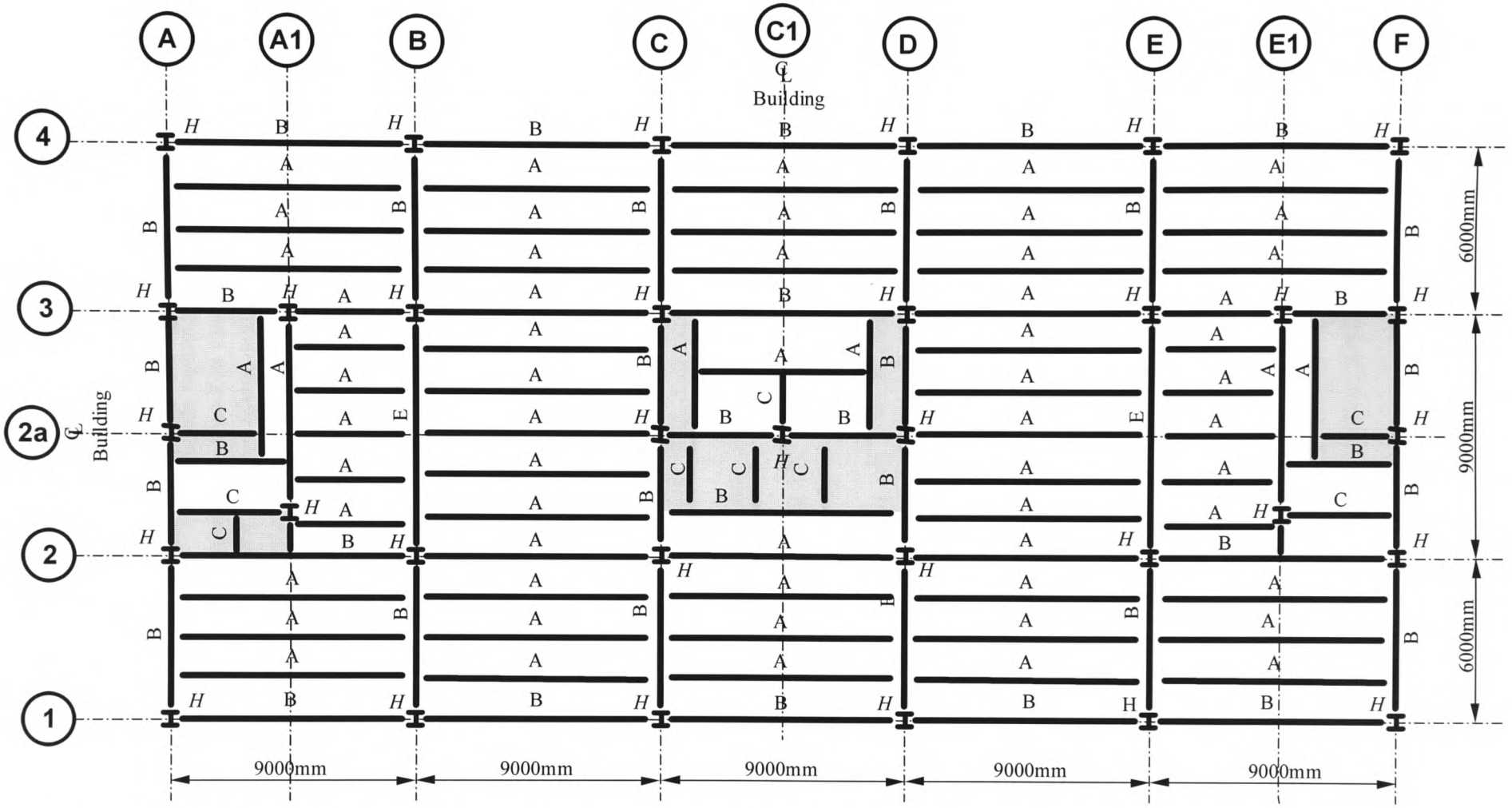

Figure B.6 – Plan on the 8th floor showing the general layout of the main structural elements

APPENDIX C

Laboratory Readings Obtained from the Composite Steel / Concrete Panels

Content:

Measured strain data recorded from the composite panels tested in the laboratory.

Table C.1 – Panel S1 – Number 1: Strain data

Total Load kN	Depth level 1 - Zone			Depth level 2 - Zone			Depth level 3 - Zone			Depth level 4 - Zone			Depth level 5 - Zone			Depth level 6 - Zone		
	A	B	C	A	B	C	A	B	C	A	B	C	A	B	C	A	B	C
	Strain × 10^{-6}			Strain × 10^{-6}			Strain × 10^{-6}			Strain × 10^{-6}			Strain × 10^{-6}			Strain × 10^{-6}		
0	0	0	0	0	0	0	0	0	0	0	0	0	0	0	0	0	0	0
1	-9.8	-7.35	-7.35	4.9	-2.45	-4.9	4.9	0	0	34.3	24.5	29.4	22.05	34.3	22.05	19.6	31.85	22.05
2	-22.05	-22.05	-19.6	-4.9	-4.9	-12.25	0	4.9	-2.45	19.6	24.5	29.4	29.4	26.95	22.05	31.85	29.4	29.4
3	-26.95	-34.3	-39.2	-19.6	-17.15	-12.25	-2.45	-2.45	2.45	34.3	24.5	24.5	29.4	34.3	46.55	51.45	53.9	46.55
4	-53.9	-53.9	-44.1	-34.3	-26.95	-40.4	-4.9	-9.8	-12.25	24.5	24.5	29.4	53.9	34.3	36.75	61.25	53.9	58.8
5	-49	-44.1	-49	-24.5	-26.95	-14.7	-2.45	7.35	-2.45	44.1	41.65	49	63.7	56.35	68.6	83.3	73.5	83.3
6	-73.5	-80.85	-73.5	-56.35	-44.1	4.9	-19.6	-12.25	-14.7	49	46.55	53.9	56.35	63.7	63.7	85.75	85.75	83.3
7	-68.6	-73.5	-71.05	-44.1	-41.65	-36.75	-7.35	0	-12.25	68.6	44.1	58.8	85.75	80.85	83.3	107.8	110.25	110.25
8	-88.2	-68.6	-80.85	-44.1	-49	-34.3	-2.45	0	2.45	80.85	71.05	68.6	127.4	98	110.25	142.1	134.75	142.1
9	-103.9	-102.9	-112.7	-56.35	-61.25	-58.8	-2.45	-7.35	4.9	93.1	75.95	122.5	137.15	124.95	178.85	166.6	164.15	230.3
10	-127.4	-117.6	-111.05	-56.35	-53.85	-51.45	29.4	24.5	31.85	166.6	120.05	147	222.95	186.2	222.95	303.8	235.15	286.65
11	-168.1	-134.75	-136.7	-81.9	-66.3	-79.5	34.3	39.2	34.3	186.2	151.9	240.1	237.65	247.45	301.35	338.1	313.6	340.55
12	-171.5	-150	-178.85	-61.25	-68.1	-87.3	44.1	39.2	44.1	235.2	200.9	245	303.8	289.1	311.15	423.85	397	379.75

Table C.2 – Panel S1 – Number 2: Strain data

Total Load kN	Depth level 1 - Zone			Depth level 2 - Zone			Depth level 3 - Zone			Depth level 4 - Zone			Depth level 5 - Zone			Depth level 6 - Zone		
	A	B	C	A	B	C	A	B	C	A	B	C	A	B	C	A	B	C
	Strain × 10^{-6}			Strain × 10^{-6}			Strain × 10^{-6}			Strain × 10^{-6}			Strain × 10^{-6}			Strain × 10^{-6}		
0	0.0	0.0	0.0	0.0	0.0	0.0	0.0	0.0	0.0	0.0	0.0	0.0	0.0	0.0	0.0	0.0	0.0	0.0
1	-9.8	-19.6	0.0	-19.6	-9.8	-4.9	4.9	-4.9	0.0	24.5	19.6	4.9	19.6	14.7	34.3	34.3	24.5	24.5
2	-29.4	-31.9	-29.4	-27.0	-22.1	-17.2	-19.6	2.5	-7.4	-9.8	0.0	2.5	22.1	7.4	24.5	29.4	27.0	29.4
3	-17.2	-19.6	-17.2	-7.4	-12.3	-9.8	4.9	0.0	2.5	39.2	24.5	36.8	44.1	29.4	39.2	56.4	49.0	46.6
4	-36.8	-36.8	-24.5	-14.7	-22.1	-7.4	-2.5	2.5	0.0	49.0	29.4	24.5	61.3	49.0	36.8	71.1	56.4	61.3
5	-58.8	-39.2	-49.0	-76.1	-29.4	-29.4	-12.3	-7.4	-17.2	34.3	44.1	29.4	63.7	44.1	46.6	71.1	56.4	63.7
6	-61.3	-51.5	-44.1	-31.9	-36.8	-29.4	-7.4	0.0	2.5	53.9	49.0	27.0	73.5	73.5	71.1	100.5	78.4	83.3
7	-71.1	-58.8	-61.3	-36.8	-39.2	-36.8	4.9	2.5	-2.5	76.0	44.1	71.1	80.9	66.2	85.8	107.8	90.7	107.8
8	-95.3	-78.4	-71.1	-46.6	-44.1	-36.8	7.4	2.5	2.5	98.0	63.7	73.5	154.4	73.5	83.3	191.1	117.6	122.5
9	-134.8	-107.8	-110.3	-58.8	-49.0	-46.6	14.7	4.9	2.5	129.9	83.3	112.7	169.1	110.3	154.4	249.9	161.7	205.8
10	-127.4	-110.3	-100.5	-53.9	-36.8	-41.7	46.6	41.7	27.0	188.7	149.5	161.7	227.9	232.0	215.6	316.1	269.5	272.0

Table C.3 – Panel S1 – Number 3: Strain data

Total Load kN	Depth level 1 - Zone			Depth level 2 - Zone			Depth level 3 - Zone			Depth level 4 - Zone			Depth level 5 - Zone			Depth level 6 - Zone		
	A	B	C	A	B	C	A	B	C	A	B	C	A	B	C	A	B	C
	Strain × 10^{-6}			Strain × 10^{-6}			Strain × 10^{-6}			Strain × 10^{-6}			Strain × 10^{-6}			Strain × 10^{-6}		
0	0.0	0.0	0.0	0.0	0.0	0.0	0.0	0.0	0.0	0.0	0.0	0.0	0.0	0.0	0.0	0.0	0.0	0.0
1	-9.8	-14.7	-9.8	0.0	-4.9	-9.8	0.0	0.0	0.0	9.8	9.8	4.9	4.9	19.6	4.9	19.6	4.9	19.6
2	-14.7	-19.6	-14.7	-7.4	-7.4	-12.3	-2.5	9.8	7.4	24.5	17.2	12.3	34.3	31.9	34.3	39.2	49.0	39.2
3	-49.0	-29.4	-46.6	-29.4	-29.4	-24.5	-9.8	-9.8	-12.3	19.6	12.3	7.4	22.1	27.0	22.1	31.9	27.0	22.1
4	-31.9	-31.9	-31.9	-19.6	-19.6	-19.6	2.5	2.5	0.0	29.4	29.4	27.0	46.6	44.1	51.5	61.3	56.4	63.7
5	-44.1	-41.7	-49.0	-31.9	-19.6	-24.5	-4.9	-7.4	0.0	39.2	36.8	46.6	58.8	49.0	61.3	76.0	68.6	73.5
6	-63.7	-56.4	-58.8	-34.3	-31.9	-36.8	-12.3	-4.9	-7.4	44.1	31.9	41.7	46.6	61.3	58.8	73.5	68.6	85.8
7	-63.7	-61.3	-66.3	-36.8	-24.5	-31.9	4.9	0.0	7.4	51.5	51.5	63.7	83.3	66.2	88.2	100.5	95.6	107.8
8	-85.8	-76.0	-88.2	-44.1	-36.8	-41.7	0.0	0.0	2.5	73.5	76.0	68.6	98.0	78.4	120.1	125.0	95.6	132.3
9	-93.1	-80.9	-98.0	-41.7	-39.2	-41.7	12.3	9.8	2.5	110.3	73.5	95.6	132.3	90.7	156.8	186.2	139.7	183.8
10	-129.9	-107.8	-129.9	-49.0	-39.2	-44.1	39.2	22.1	27.0	193.6	122.5	156.8	279.3	164.2	220.5	325.9	279.0	301.4
11	-127.4	-120.1	-157.2	-58.4	-47.0	-46.4	49.0	31.9	41.7	200.9	171.5	208.3	276.9	227.9	274.4	333.2	328.0	347.9

Table C.4 – Panel S1 – Number 4: Strain data

Total Load kN	Depth level 1 - Zone			Depth level 2 - Zone			Depth level 3 - Zone			Depth level 4 - Zone			Depth level 5 - Zone			Depth level 6 - Zone		
	A	B	C	A	B	C	A	B	C	A	B	C	A	B	C	A	B	C
	Strain × 10^{-6}			Strain × 10^{-6}			Strain × 10^{-6}			Strain × 10^{-6}			Strain × 10^{-6}			Strain × 10^{-6}		
0	0.0	0.0	0.0	0.0	0.0	0.0	0.0	0.0	0.0	0.0	0.0	0.0	0.0	0.0	0.0	0.0	0.0	0.0
1	-24.5	-9.8	-14.7	-9.8	-14.7	0.0	4.9	9.8	0.0	9.8	14.7	14.7	14.7	9.8	19.6	19.6	14.7	24.5
2	-19.6	-12.3	-17.2	-4.9	-7.4	-17.2	2.5	7.4	7.4	19.6	22.1	31.9	36.8	24.5	27.0	46.6	31.9	41.7
3	-27.0	-36.8	-41.7	-14.7	-17.2	-31.9	-4.9	-2.5	0.0	24.5	34.3	29.4	34.3	31.9	39.2	51.5	49.0	41.7
4	-46.6	-39.2	-44.1	-22.1	-24.5	-22.1	0.0	-2.5	-12.3	34.3	34.3	41.7	51.5	49.0	53.9	63.7	53.9	56.4
5	-61.3	-56.4	-53.9	-39.2	-34.3	-27.0	-12.3	-9.8	-14.7	34.3	24.5	34.3	51.5	44.1	49.0	71.1	56.4	71.1
6	-51.5	-53.9	-51.5	0.0	-27.0	-29.4	0.0	2.5	-2.5	63.7	36.8	39.3	78.4	71.2	80.9	98.0	85.8	98.0
7	-83.3	-61.3	-50.6	-44.1	-44.1	-53.9	-17.2	-12.3	-17.2	49.0	44.1	39.2	66.2	66.2	85.8	93.1	85.8	102.9
8	-71.1	-73.5	-76.0	-44.1	-41.7	-39.2	-2.5	-2.5	-2.5	73.5	7.4	80.9	93.1	83.3	90.7	117.6	110.3	120.1
9	-83.3	-85.8	-83.3	-44.1	-53.9	-44.1	-4.9	0.0	0.0	83.3	66.2	78.4	117.6	100.5	129.9	244.0	145.0	161.7
10	-107.8	-122.5	-125.0	-61.3	-53.9	-56.4	7.4	19.6	19.6	102.9	164.2	139.7	171.5	247.5	225.4	310.0	291.6	284.2

Table C.5 – Panel S1 – Number 5: Strain data

Total Load kN	Depth level 1 - Zone			Depth level 2 - Zone			Depth level 3 - Zone			Depth level 4 - Zone			Depth level 5 - Zone			Depth level 6 - Zone		
	A	B	C	A	B	C	A	B	C	A	B	C	A	B	C	A	B	C
	Strain × 10^{-6}			Strain × 10^{-6}			Strain × 10^{-6}			Strain × 10^{-6}			Strain × 10^{-6}			Strain × 10^{-6}		
0	0.0	0.0	0.0	0.0	0.0	0.0	0.0	0.0	0.0	0.0	0.0	0.0	0.0	0.0	0.0	0.0	0.0	0.0
0.5	4.9	0.0	-4.9	14.7	4.9	-4.9	-4.9	-24.5	24.5	14.7	34.3	29.4	9.8	24.5	24.5	24.5	4.9	14.7
1	-19.6	-9.8	-14.7	0.0	4.9	-14.7	9.8	-9.8	29.4	14.7	14.7	34.3	14.7	34.3	34.3	53.0	24.5	29.4
1.5	-19.6	-14.7	-19.6	-4.9	-4.9	-9.8	4.9	-4.9	24.5	19.6	24.5	24.5	24.5	34.3	49.0	58.0	34.3	39.2
2	-24.5	-14.7	-29.4	-4.9	-9.8	-19.6	9.8	-19.6	24.5	24.5	34.3	44.1	24.5	34.3	58.8	63.7	39.2	44.1
2.5	-34.3	-14.7	-29.4	-4.9	-4.9	-19.6	9.8	-4.9	24.5	24.5	24.5	49.0	29.4	39.2	58.8	60.0	39.2	29.4
3	-39.2	-24.5	-34.3	0.0	-14.7	-34.3	4.9	-4.9	19.6	44.1	19.6	53.9	34.3	44.1	58.8	82.0	53.9	53.9
3.5	-44.1	-29.4	-39.2	-9.8	-19.6	-29.4	4.9	-9.8	19.6	49.0	24.5	44.1	34.3	49.0	68.6	88.2	49.0	68.6
4	-49.0	-34.3	-44.1	-14.7	-19.6	-34.3	4.9	-9.8	19.6	39.2	24.5	49.0	44.1	53.9	73.5	93.0	63.7	73.5
4.5	-49.0	-34.3	-49.0	-19.6	-19.6	-34.3	4.9	-14.7	19.6	53.9	49.0	58.8	53.9	53.9	88.2	105.0	68.6	83.3
5	-63.7	-39.2	-58.8	-19.6	-24.5	-29.4	4.9	-9.8	24.5	44.1	34.3	44.1	58.8	58.8	93.1	103.0	68.6	88.2
5.5	-63.7	-44.1	-63.7	-29.4	-29.4	-39.2	0.0	-14.7	19.6	58.8	39.2	58.8	58.8	68.6	102.9	108.0	73.5	98.0
6	-73.5	-53.9	-68.6	-29.4	-29.4	-39.2	4.9	-19.6	19.6	49.0	29.4	68.6	68.6	63.7	107.8	132.3	78.4	107.8
6.5	-73.5	-49.0	-73.5	-34.3	-29.4	-44.1	0.0	-9.8	19.6	58.8	39.2	83.3	83.3	88.2	102.9	147.0	83.3	107.8
7	-83.3	-58.8	-73.5	-34.3	-29.4	-44.1	-4.9	-9.8	19.6	73.5	68.6	122.5	88.2	88.2	107.8	147.0	117.6	132.3
7.5	-73.5	-53.9	-78.4	-34.3	-29.4	-44.1	9.8	-4.9	24.5	68.6	49.0	98.0	88.2	102.9	117.6	147.0	117.6	142.1
8	-88.2	-63.7	-63.7	-39.2	-39.2	-44.1	4.9	-14.7	24.5	68.6	49.0	112.7	98.0	102.9	137.2	161.7	132.3	147.0
8.5	-93.1	-75.3	-93.1	-44.1	-34.3	-53.9	14.7	-4.9	24.5	88.2	53.9	102.9	102.9	102.9	137.2	181.3	200.0	161.7
9	-98.0	-73.5	-112.7	-39.2	-44.1	-44.1	9.8	-14.7	24.5	83.3	58.8	137.2	102.9	107.8	166.6	181.3	222.0	181.3
9.5	-102.9	-95.0	-117.6	-49.0	-44.1	-49.0	4.9	-9.8	44.1	89.0	115.0	161.7	107.8	127.4	245.0	210.7	242.0	264.6
10	-107.8	-94.0	-127.4	-49.0	-44.1	-44.1	9.8	-4.9	68.6	93.1	106.0	215.6	132.3	142.1	279.3	215.6	262.0	343.0
10.5	-117.6	-106.0	-125.9	-73.5	-53.9	-44.1	9.8	-14.7	58.8	116.0	126.0	235.2	187.0	193.0	333.2	325.0	313.0	372.4

Table C.6 – Panel S1 – Number 6: Strain data

Total Load kN	Depth level 1 - Zone			Depth level 2 - Zone			Depth level 3 - Zone			Depth level 4 - Zone			Depth level 5 - Zone			Depth level 6 - Zone		
	A	B	C	A	B	C	A	B	C	A	B	C	A	B	C	A	B	C
	Strain × 10^{-6}			Strain × 10^{-6}			Strain × 10^{-6}			Strain × 10^{-6}			Strain × 10^{-6}			Strain × 10^{-6}		
0	0.0	0.0	0.0	0.0	0.0	0.0	0.0	0.0	0.0	0.0	0.0	0.0	0.0	0.0	0.0	0.0	0.0	0.0
0.5	14.7	9.8	-4.9	0.0	-14.7	0.0	4.9	-4.9	-4.9	4.9	0.0	9.8	26.0	9.8	29.4	9.8	9.8	9.8
1	9.8	9.8	-4.9	0.0	-4.9	0.0	19.6	-14.7	-14.7	29.4	24.5	4.9	42.0	19.6	37.0	14.7	19.6	19.6
1.5	0.0	3.6	-19.6	9.8	-9.8	-9.8	19.6	-14.7	0.0	9.8	39.2	39.2	55.0	24.5	55.0	29.4	34.3	29.4
2	4.9	0.0	-19.6	4.9	-9.8	-9.8	9.8	-14.7	0.0	24.5	53.9	34.3	50.0	39.2	63.0	24.5	39.2	44.1
3	-9.8	-9.8	-29.4	-14.7	-14.7	-9.8	19.6	-14.7	-4.9	24.5	34.3	53.9	66.0	49.0	0.0	34.3	58.8	53.9
4	-29.4	-16.9	-44.1	-14.7	-9.8	-24.5	9.8	-29.4	-14.7	44.1	58.8	58.8	83.3	58.8	82.0	34.3	68.6	63.7
4.5	-29.4	-24.5	-44.1	-14.7	-29.4	-19.6	19.6	-14.7	-4.9	63.7	73.5	49.0	93.1	58.8	108.0	53.9	68.6	68.6
5	-29.4	-24.5	-49.0	-19.6	-24.5	-19.6	19.6	-19.6	-19.6	73.5	83.3	78.4	88.2	73.5	105.0	49.0	88.2	78.4
5.5	-39.2	-25.9	-58.8	-39.2	-24.5	-19.6	19.6	-24.5	-39.2	88.2	73.5	88.2	107.8	78.4	119.0	58.8	88.2	102.9
6	-44.1	-39.2	-63.7	-34.3	-39.2	-29.4	24.5	-24.5	-34.3	102.9	63.7	93.1	112.7	107.8	132.0	63.7	117.6	98.0
6.5	-49.0	-44.1	-63.7	-39.2	-49.0	-44.1	14.7	-14.7	-34.3	137.2	98.0	137.2	102.9	112.7	148.0	78.4	137.2	117.6
7	-63.7	-53.9	-78.4	-44.1	-49.0	-44.1	14.7	-19.6	-34.3	156.8	117.6	132.3	112.7	132.3	184.0	98.0	161.7	151.9
7.5	-73.5	-63.7	-98.0	-49.0	-49.0	-49.0	19.6	-14.7	-14.7	191.1	132.3	147.0	147.0	166.6	232.0	147.0	200.9	215.6
8	-88.2	-83.3	-107.8	-53.9	-44.1	-49.0	24.5	-14.7	0.0	220.5	147.0	176.4	191.1	200.9	269.0	196.0	225.4	279.3
8.5	-98.0	-98.0	-122.5	-53.9	-39.2	-49.0	29.4	-4.9	19.6	245.0	161.7	191.1	235.2	240.1	309.0	249.9	303.8	328.3
9	-117.6	-107.8	-151.9	-63.7	-53.9	-44.1	39.2	4.9	14.7	246.0	184.0	195.0	249.9	284.2	328.0	298.9	328.3	372.4
9.5	-137.2	-117.6	-142.1	-68.6	-53.9	-49.0	39.2	0.0	14.7	260.0	205.8	215.6	279.3	289.1	348.0	338.1	357.7	401.8

Table C.7 – Panel S1 – Number 7: Strain data

Total Load kN	Depth level 1 - Zone			Depth level 2 - Zone			Depth level 3 - Zone			Depth level 4 - Zone			Depth level 5 - Zone			Depth level 6 - Zone		
	A	B	C	A	B	C	A	B	C	A	B	C	A	B	C	A	B	C
	Strain × 10^{-6}			Strain × 10^{-6}			Strain × 10^{-6}			Strain × 10^{-6}			Strain × 10^{-6}			Strain × 10^{-6}		
0	0.0	0.0	0.0	0.0	0.0	0.0	0.0	0.0	0.0	0.0	0.0	0.0	0.0	0.0	0.0	0.0	0.0	0.0
0.5	4.9	-9.8	-15.7	0.0	-9.8	9.8	-4.9	-14.7	-4.9	-24.5	-34.3	29.4	24.5	24.5	-14.7	-14.7	-29.4	-14.7
1	-4.9	-33.1	-19.6	-14.7	-24.5	9.8	-9.8	-34.3	-4.9	29.4	9.8	19.6	4.9	4.9	4.9	-14.7	-14.7	9.8
1.5	-9.8	-45.0	-30.7	-19.6	-29.4	-19.6	0.0	-34.3	4.9	49.0	24.5	4.9	34.3	24.5	29.4	4.9	-24.5	9.8
2	-19.6	-48.8	-39.2	-19.6	-34.3	-24.5	4.9	-44.1	-4.9	39.2	34.3	-14.7	34.3	34.3	29.4	14.7	-24.5	24.5
3	-19.6	-59.6	-44.1	-29.4	-49.0	-9.8	4.9	-29.4	4.9	63.7	53.9	4.9	49.0	44.1	44.1	29.4	-19.6	9.8
4	-44.1	-75.0	-68.6	-4.9	-58.8	-9.8	-4.9	-19.6	0.0	83.3	63.7	44.1	68.6	58.8	83.3	44.1	19.6	24.5
4.5	-39.2	-71.7	-70.5	-14.7	-63.7	-34.3	-14.7	-19.6	0.0	117.6	73.5	34.3	83.3	63.7	78.4	44.1	9.8	24.5
5	-49.0	-83.7	-93.1	-29.4	-63.7	-39.2	-14.7	-29.4	0.0	127.4	88.2	24.5	78.4	44.1	88.2	58.8	29.4	29.4
5.5	-30.7	-92.8	-98.8	-29.4	-49.0	-44.1	-29.4	-14.7	-4.9	156.8	107.8	24.5	102.9	63.7	93.1	68.6	73.5	29.4
6	-29.4	-100.6	-105.4	-34.3	-39.2	-49.0	-44.1	-19.6	-9.8	181.3	107.8	9.0	107.8	58.8	93.1	78.4	88.2	39.0
6.5	-34.3	-115.7	-117.6	-39.2	-44.1	-34.3	-39.2	-4.9	0.0	151.9	93.1	20.0	132.3	73.5	93.1	107.8	107.8	64.0
7	-53.9	-122.3	-127.4	-44.1	-53.9	-53.9	-53.9	0.0	4.9	172.0	147.0	29.4	156.8	93.1	102.9	127.4	151.9	116.0
7.5	-83.3	-140.4	-142.1	-49.0	-58.8	-53.9	-58.8	4.9	0.0	194.0	181.3	54.0	186.2	117.6	117.6	132.3	156.8	156.0
8	-98.0	-156.0	-161.7	-73.5	-68.6	-78.4	-68.6	24.5	-4.9	217.0	184.0	73.5	200.9	132.3	191.1	220.5	249.9	107.8
8.5	-142.1	-162.0	-132.3	-58.8	-63.7	-88.2	-58.8	29.4	19.6	230.0	182.0	78.4	240.1	186.2	205.8	264.6	284.2	216.0
9	-156.8	-170.5	-147.0	-63.7	-63.7	-78.4	-34.3	49.0	14.7	248.0	243.0	58.8	289.1	240.1	215.6	338.1	367.5	176.4
9.5	-166.9	-166.3	-170.0	-68.6	-68.6	-53.9	-34.3	73.5	24.5	254.0	269.0	96.0	313.6	274.4	235.2	382.2	401.0	224.0

Table C.8 – Panel S1 – Number 8: Strain data

Total Load kN	Depth level 1 - Zone			Depth level 2 - Zone			Depth level 3 - Zone			Depth level 4 - Zone			Depth level 5 - Zone			Depth level 6 - Zone		
	A	B	C	A	B	C	A	B	C	A	B	C	A	B	C	A	B	C
	Strain × 10^{-6}			Strain × 10^{-6}			Strain × 10^{-6}			Strain × 10^{-6}			Strain × 10^{-6}			Strain × 10^{-6}		
0	0.0	0.0	0.0	0.0	0.0	0.0	0.0	0.0	0.0	0.0	0.0	0.0	0.0	0.0	0.0	0.0	0.0	0.0
1	-9.8	9.8	-19.6	0.0	-14.7	4.9	0.0	0.0	-14.7	19.6	-4.9	24.5	0.0	19.6	-14.7	0.0	0.0	9.8
2	-19.6	0.0	-19.6	-9.8	-9.8	-4.9	-4.9	9.8	-19.6	44.1	-24.5	14.7	24.5	19.6	-4.9	9.8	24.5	19.6
3	-34.3	-19.6	-39.2	-24.5	-24.5	-14.7	0.0	0.0	-14.7	53.9	-14.7	9.8	19.6	39.2	14.7	34.3	39.2	34.3
4	-44.1	-24.5	-44.1	-24.5	-34.3	-24.5	0.0	0.0	-4.9	63.7	-4.9	29.4	34.3	39.2	19.6	53.9	53.9	68.6
4.5	-49.0	-39.2	-49.0	-24.5	-34.3	-19.6	0.0	4.9	-29.4	53.9	-4.9	49.0	39.2	58.8	39.2	53.9	53.9	73.5
5	-58.8	-44.1	-63.7	-34.3	-39.2	-29.4	-4.9	0.0	-34.3	83.3	0.0	49.0	53.9	63.7	53.9	73.5	73.5	83.3
5.5	-63.7	-44.1	-63.7	-39.2	-34.3	-29.4	-4.9	0.0	-9.8	83.3	14.7	63.7	58.8	68.6	83.3	34.3	88.2	98.0
6	-58.8	-53.9	-73.5	-39.2	-44.1	-34.3	-4.9	4.9	0.0	102.9	14.7	93.1	58.8	88.2	88.2	48.0	107.8	127.4
6.5	-68.6	-68.6	-88.2	-44.1	-53.9	-39.2	0.0	9.8	0.0	127.4	29.4	102.9	83.3	107.8	127.4	53.9	132.3	156.8
7	-98.0	-102.9	-102.9	-53.9	-68.6	-53.9	9.8	4.9	-4.9	166.6	73.5	161.7	156.8	147.0	170.0	210.7	181.3	230.3
7.5	-112.7	-117.6	-112.7	-53.9	-68.6	-53.9	19.6	19.6	9.8	191.1	98.0	191.1	191.1	200.9	230.3	264.6	225.4	274.4
8	-122.5	-122.5	-127.4	-53.9	-68.6	-58.8	24.5	34.3	9.8	205.8	137.2	194.0	210.7	235.2	254.0	284.2	284.2	313.6
8.5	-127.4	-147.0	-137.2	-53.9	-68.6	-58.8	24.5	34.3	24.5	225.4	166.6	217.0	249.9	279.3	284.2	328.3	338.1	347.9
9	-161.7	-151.9	-151.9	-58.8	-73.5	-63.7	34.3	29.4	14.7	230.0	193.0	206.0	284.2	303.8	303.8	377.3	362.6	372.4

Table C.9 – Panel S1 – Number 9: Strain data

Total Load kN	Depth level 1 - Zone			Depth level 2 - Zone			Depth level 3 - Zone			Depth level 4 - Zone			Depth level 5 - Zone			Depth level 6 - Zone		
	A	B	C	A	B	C	A	B	C	A	B	C	A	B	C	A	B	C
	Strain × 10^{-6}			Strain × 10^{-6}			Strain × 10^{-6}			Strain × 10^{-6}			Strain × 10^{-6}			Strain × 10^{-6}		
0	0.0	0.0	0.0	0.0	0.0	0.0	0.0	0.0	0.0	0.0	0.0	0.0	0.0	0.0	0.0	0.0	0.0	0.0
1	-9.8	-14.7	-14.7	-19.6	-4.9	-9.8	-4.9	-4.9	-4.9	0.0	0.0	-24.5	9.8	9.8	4.9	19.6	-4.9	4.9
2	-29.4	-19.6	-4.9	-28.9	-9.8	-19.6	-9.8	0.0	-4.9	-4.9	4.9	-9.8	14.7	19.6	19.6	29.4	19.6	29.4
3	-34.3	-29.4	-19.6	-34.3	-14.7	-19.6	-19.6	-4.9	-9.8	0.0	4.9	-24.5	34.3	19.6	14.7	34.3	29.4	29.4
4	-49.0	-39.2	-34.3	-35.5	-19.6	-24.5	-9.8	0.0	-4.9	14.7	44.1	4.9	44.1	29.4	24.5	63.7	39.2	53.9
4.5	-63.3	-44.1	-39.2	-44.6	-29.4	-39.2	-24.5	-9.8	-9.8	14.7	19.6	34.3	44.1	34.3	49.0	68.6	53.9	68.6
5	-78.4	-58.8	-58.8	-50.0	-34.3	-44.1	-24.5	-9.8	-9.8	24.5	4.9	58.8	34.3	49.0	58.8	78.4	68.6	78.4
5.5	-88.2	-68.6	-63.7	-57.2	-44.1	-49.0	-29.4	-14.7	-4.9	49.0	34.3	68.6	63.7	53.9	68.6	93.1	78.4	93.1
6	-83.3	-78.4	-73.5	-64.5	-44.1	-58.8	-29.4	-19.6	-19.6	34.3	24.5	98.0	78.4	63.7	88.2	112.7	83.3	107.8
6.5	-107.8	-68.6	-73.5	-73.5	-29.4	-65.7	-19.6	-14.7	-9.8	83.3	24.5	127.4	93.1	68.6	73.5	166.6	102.9	112.7
7	-132.3	-83.3	-78.4	-71.7	-34.3	-53.9	-24.5	-9.8	-9.8	107.8	19.6	112.7	151.9	63.7	73.5	196.0	127.4	142.1
7.5	-137.2	-93.1	-88.2	-75.3	-44.1	-58.8	-14.7	-9.8	-4.9	112.7	61.0	127.4	147.0	78.4	93.1	225.4	122.5	147.0
8	-159.0	-112.7	-112.7	-81.3	-49.0	-58.8	4.9	0.0	4.9	186.2	58.8	132.3	274.0	117.6	112.7	324.0	171.5	191.1
8.5	-159.0	-127.4	-132.3	-79.5	-58.8	-68.6	4.9	4.9	4.9	215.6	63.7	142.1	304.0	142.1	147.0	354.0	215.6	230.3
9	-167.5	-142.1	-142.1	-87.3	-63.7	-73.5	19.6	19.6	19.6	220.0	112.7	171.5	330.0	210.7	196.0	393.0	284.2	289.1
9.5	-170.5	-153.6	-148.2	-89.2	-68.6	-83.3	19.6	34.3	29.4	253.0	117.6	156.8	341.0	230.3	200.9	394.0	313.6	313.6
10	-151.8	-138.0	-168.7	-96.4	-78.4	-88.2	19.6	24.5	24.5	207.0	117.6	176.4	310.0	254.8	220.5	406.0	338.1	333.2
10.5	-165.7	-163.3	-150.0	-98.2	-78.4	-88.2	24.5	29.4	29.4	246.0	156.8	220.5	343.0	289.1	279.3	435.0	382.2	377.3

Table C.10 – Panel S2 – Number 1: Strain data

Total Load kN	Depth level 1 - Zone			Depth level 2 - Zone			Depth level 3 - Zone			Depth level 4 - Zone			Depth level 5 - Zone			Depth level 6 - Zone		
	A	B	C	A	B	C	A	B	C	A	B	C	A	B	C	A	B	C
	Strain × 10^{-6}			Strain × 10^{-6}			Strain × 10^{-6}			Strain × 10^{-6}			Strain × 10^{-6}			Strain × 10^{-6}		
0	0.0	0.0	0.0	0.0	0.0	0.0	0.0	0.0	0.0	0.0	0.0	0.0	0.0	0.0	0.0	0.0	0.0	0.0
1	-9.8	-4.9	-14.7	-9.8	-4.9	-9.8	-4.9	4.9	-9.8	14.7	19.6	9.8	9.8	-10.0	14.7	19.6	19.6	24.5
2	-27.0	-24.5	-22.1	-19.6	-22.1	-12.3	-14.7	-7.4	-9.8	17.2	14.7	9.8	14.7	14.7	17.2	19.6	29.4	27.0
3	-36.8	-31.9	-31.9	-19.6	-19.6	-22.1	-9.8	-9.8	-12.3	17.2	19.6	24.5	34.3	39.2	31.9	41.7	49.0	46.6
4	-39.2	-41.7	-44.1	-31.9	-22.1	-24.5	-9.8	-4.9	-7.4	31.9	29.4	29.4	39.2	44.1	51.5	53.9	63.7	66.2
5	-73.5	-44.1	-63.7	-49.0	-22.1	-39.2	-17.2	-7.4	-4.9	27.0	24.5	31.9	46.6	117.6	53.9	61.3	98.0	80.9
6	-59.7	-66.2	-71.1	-41.7	-36.8	-39.2	-22.1	-12.3	-14.7	36.8	44.1	46.6	61.3	78.4	73.5	83.3	112.7	98.0
7	-73.5	-76.0	-78.4	-51.5	-46.6	-41.7	-12.3	-17.2	-12.3	49.0	58.8	56.4	85.8	117.6	98.0	155.0	142.1	125.0
8	-110.3	-105.4	-122.5	-58.8	-58.8	-51.5	7.4	0.0	19.6	139.7	95.0	196.0	193.6	294.0	286.7	237.7	343.0	362.6
9	-117.6	-125.0	-139.7	-63.7	-68.6	-61.3	2.5	0.0	19.6	159.3	132.0	218.1	218.1	367.5	318.5	276.9	426.3	401.8
10	-147.0	-139.7	-156.8	-53.9	-61.3	-51.5	31.9	44.1	46.6	245.0	283.0	283.0	335.7	457.0	412.0	416.5	540.0	543.9
11	-156.8	-151.9	-176.4	-58.8	-63.7	-61.1	49.0	46.6	58.8	259.7	317.0	305.0	362.6	480.0	488.0	443.5	610.0	644.4
12	-161.7	-166.6	-191.1	-68.6	-74.0	-72.5	44.1	49.0	14.7	254.8	346.0	336.0	383.0	553.0	563.5	478.0	701.0	700.7

Table C.11 – Panel S2 – Number 2: Strain data

Total Load kN	Depth level 1 - Zone			Depth level 2 - Zone			Depth level 3 - Zone			Depth level 4 - Zone			Depth level 5 - Zone			Depth level 6 - Zone		
	A	B	C	A	B	C	A	B	C	A	B	C	A	B	C	A	B	C
	Strain × 10^{-6}			Strain × 10^{-6}			Strain × 10^{-6}			Strain × 10^{-6}			Strain × 10^{-6}			Strain × 10^{-6}		
0	0.0	0.0	0.0	0.0	0.0	0.0	0.0	0.0	0.0	0.0	0.0	0.0	0.0	0.0	0.0	0.0	0.0	0.0
1	-4.9	-4.9	-14.7	0.0	0.0	-9.8	-9.8	0.0	-14.7	9.8	19.6	14.7	14.7	14.7	19.6	24.5	29.4	24.5
2	-22.1	-24.5	-17.2	-9.8	-9.8	-9.8	-2.5	-12.3	-9.8	14.7	14.7	12.3	19.6	17.2	12.3	24.5	24.5	31.9
3	-31.9	-27.0	-27.0	-19.6	-19.6	-14.7	-4.9	-4.9	-2.5	12.3	17.2	22.1	31.9	34.3	29.4	39.2	44.1	46.6
4	-41.7	-36.8	-46.6	-24.5	-22.1	-27.0	-9.8	-2.5	-2.5	24.5	24.5	24.5	34.3	34.3	41.7	53.9	56.4	61.3
5	-44.1	-31.9	-34.3	-31.9	-29.4	-19.6	-17.2	-2.5	-4.9	31.9	22.1	29.4	53.9	51.5	51.5	63.7	63.7	66.2
6	-78.4	-53.9	-56.4	-39.2	-29.4	-22.1	4.9	-4.9	-2.5	85.8	51.5	46.6	125.0	71.1	95.6	154.4	95.6	134.8
7	-100.5	-85.8	-78.4	-44.1	-39.2	-41.7	0.0	0.0	7.4	120.1	93.1	76.0	166.6	122.5	159.3	218.1	169.1	213.2
8	-112.7	-90.7	-95.6	-49.0	-41.7	-41.7	22.1	14.7	9.8	134.8	125.0	102.9	188.7	174.0	200.9	247.5	225.4	262.2
9	-120.1	-105.4	-112.7	-51.5	-49.0	-44.1	19.6	9.8	31.9	181.3	127.4	139.7	230.3	176.4	274.4	298.9	289.1	347.9
10	-147.0	-117.6	-122.5	-53.9	-53.9	-49.0	36.8	9.8	41.7	218.1	142.1	169.1	301.4	210.7	316.1	377.3	289.0	394.5
11	-144.6	-134.8	-139.7	-53.9	-56.4	-46.6	41.7	17.2	58.8	223.0	223.0	200.9	308.7	256.0	360.2	392.0	334.0	455.7

Table C.12 – Panel S2 – Number 3: Strain data

Total Load kN	Depth level 1 - Zone			Depth level 2 - Zone			Depth level 3 - Zone			Depth level 4 - Zone			Depth level 5 - Zone			Depth level 6 - Zone		
	A	B	C	A	B	C	A	B	C	A	B	C	A	B	C	A	B	C
	Strain × 10^{-6}			Strain × 10^{-6}			Strain × 10^{-6}			Strain × 10^{-6}			Strain × 10^{-6}			Strain × 10^{-6}		
0	0.0	0.0	0.0	0.0	0.0	0.0	0.0	0.0	0.0	0.0	0.0	0.0	0.0	0.0	0.0	0.0	0.0	0.0
1	-19.6	-9.8	-9.8	-14.7	-9.8	-4.9	4.9	-4.9	-9.8	9.8	9.8	9.8	14.7	4.9	24.5	24.5	9.8	34.3
2	-39.2	-22.1	-27.0	-22.1	-12.3	-17.2	2.5	-4.9	-9.8	24.5	19.6	24.5	49.0	29.4	31.9	56.4	17.2	41.7
3	-58.8	-44.1	-41.7	-34.3	-29.4	-34.3	-7.4	-9.8	-12.3	44.1	9.8	24.5	63.7	34.3	31.9	85.8	23.0	58.8
4	-58.8	-53.9	-53.9	-24.5	-19.6	-29.4	-2.5	0.0	0.0	68.6	36.8	53.9	107.8	41.7	73.5	134.8	47.0	85.8
5	-24.5	-58.8	-39.2	-9.8	-29.4	-34.3	-9.8	2.5	9.8	61.3	19.6	78.4	85.8	46.6	95.6	73.5	89.0	107.8
6	-107.8	-93.1	-98.0	-51.5	-46.6	-39.2	14.7	-17.2	-12.3	137.2	44.1	100.5	210.7	66.2	144.6	257.3	19.6	178.9
7	-107.8	-80.9	-98.0	-29.4	-36.8	-49.0	36.8	2.5	0.0	156.0	66.2	132.3	254.8	105.4	188.7	321.0	29.4	240.1
8	-127.4	-105.4	-115.2	-41.7	-51.5	-63.7	51.5	-2.5	17.2	195.0	80.9	178.9	310.0	144.0	249.9	394.5	29.4	296.5
9	-137.2	-132.3	-147.0	-46.6	-58.8	-66.2	73.5	-4.9	24.5	248.0	115.0	220.5	380.0	196.0	308.7	482.7	24.5	365.1

Table C.13 – Panel S2 – Number 4: Strain data

Total Load kN	Depth level 1 - Zone			Depth level 2 - Zone			Depth level 3 - Zone			Depth level 4 - Zone			Depth level 5 - Zone			Depth level 6 - Zone		
	A	B	C	A	B	C	A	B	C	A	B	C	A	B	C	A	B	C
	Strain × 10^{-6}			Strain × 10^{-6}			Strain × 10^{-6}			Strain × 10^{-6}			Strain × 10^{-6}			Strain × 10^{-6}		
0	0.0	0.0	0.0	0.0	0.0	0.0	0.0	0.0	0.0	0.0	0.0	0.0	0.0	0.0	0.0	0.0	0.0	0.0
1	-14.7	-14.7	-19.6	-14.7	0.0	-9.8	-4.9	4.9	-4.9	9.8	19.6	14.7	14.7	14.7	14.7	24.5	29.4	19.6
2	-27.0	-17.2	-27.0	-9.8	-9.8	-17.2	0.0	2.5	-12.3	14.7	19.6	24.5	31.9	31.9	27.0	46.6	44.1	36.8
3	-36.8	-27.0	-29.4	-19.6	-14.7	-19.6	0.0	-2.5	-2.5	24.5	27.0	19.6	34.3	44.1	27.0	39.2	49.0	46.6
4	-41.7	-44.1	-49.0	-34.3	-19.6	-24.5	-9.8	-2.5	-12.3	24.5	39.2	27.0	49.0	58.8	41.7	61.3	93.1	61.3
5	-58.8	-66.2	-66.2	-34.3	-41.7	-46.6	-19.6	-27.0	-4.9	4.9	31.9	14.7	39.2	61.3	34.3	55.0	63.7	71.1
6	-73.5	-83.3	-78.4	-46.6	-36.8	-39.2	-14.7	9.8	0.0	39.2	107.8	49.0	71.1	151.9	73.5	105.4	230.3	98.0
7	-93.1	-105.4	-88.2	-53.9	-39.2	-51.5	-7.4	22.1	-9.8	71.1	169.1	58.8	117.6	237.7	106.0	142.1	330.0	127.4
8	-115.2	-112.7	-112.7	-61.3	-46.6	-53.9	-9.8	22.1	-9.8	71.1	188.7	71.1	137.0	276.9	147.0	195.0	374.0	184.0
9	-132.3	-134.8	-137.2	-68.6	-53.9	-68.6	-12.3	31.9	-2.5	105.0	232.8	93.1	190.0	321.0	190.0	247.0	480.0	252.0
10	-134.8	-151.9	-159.3	-68.6	-49.0	-68.6	-2.5	46.6	4.9	158.0	265.0	129.9	231.0	396.9	215.0	324.0	524.0	292.0

Table C.14 – Panel S2 – Number 5: Strain data

Total Load kN	Depth level 1 - Zone			Depth level 2 - Zone			Depth level 3 - Zone			Depth level 4 - Zone			Depth level 5 - Zone			Depth level 6 - Zone		
	A	B	C	A	B	C	A	B	C	A	B	C	A	B	C	A	B	C
	Strain × 10^{-6}			Strain × 10^{-6}			Strain × 10^{-6}			Strain × 10^{-6}			Strain × 10^{-6}			Strain × 10^{-6}		
0	0.0	0.0	0.0	0.0	0.0	0.0	0.0	0.0	0.0	0.0	0.0	0.0	0.0	0.0	0.0	0.0	0.0	0.0
0.5	-9.8	-4.9	-4.9	-14.7	-4.9	-4.9	-4.9	-4.9	0.0	14.7	9.8	4.9	0.0	4.9	4.9	9.8	9.8	14.7
1	-9.8	-9.8	-19.6	-14.7	-9.8	-4.9	0.0	0.0	4.9	0.0	9.8	9.8	14.7	9.8	9.8	29.4	14.7	19.6
1.5	-19.6	-24.5	-14.7	-14.7	-4.9	0.0	-4.9	4.9	9.8	-4.9	19.6	14.7	14.7	19.6	19.6	24.5	14.7	24.5
2	-19.6	-14.7	-14.7	-19.6	0.0	0.0	-4.9	9.8	9.8	4.9	24.5	24.5	24.5	19.6	29.4	34.3	44.1	29.4
2.5	-29.4	-24.5	-24.5	-24.5	-9.8	-4.9	0.0	19.6	9.8	14.7	34.3	29.4	29.4	39.2	39.2	49.0	53.9	44.1
3	-24.5	-29.4	-29.4	-14.7	-9.8	0.0	9.8	19.6	14.7	14.7	39.2	29.4	49.0	49.0	44.1	58.8	68.6	44.1
3.5	-29.4	-34.3	-34.3	-14.7	-9.8	-9.8	4.9	14.7	9.8	24.5	39.2	34.3	53.9	53.9	49.0	73.5	68.6	53.9
4	-29.4	-34.3	-44.1	-29.4	-4.9	-4.9	4.9	19.6	14.7	19.6	44.1	39.2	49.0	63.7	53.9	83.3	78.4	68.6
4.5	-44.1	-44.1	-44.1	-24.5	-14.7	-9.8	0.0	14.7	9.8	24.5	44.1	44.1	58.8	63.7	68.6	83.3	88.2	88.2
5	-44.1	-49.0	-53.9	-39.2	-14.7	-19.6	4.9	19.6	14.7	24.5	44.1	49.0	68.6	83.3	78.4	93.1	102.9	102.9
5.5	-68.6	-63.7	-60.0	-34.3	-24.5	-19.6	4.9	14.7	14.7	44.1	49.0	58.8	88.2	83.3	93.1	122.5	107.8	127.4
6	-73.5	-63.7	-73.5	-39.2	-24.5	-19.6	9.8	14.7	29.4	53.9	49.0	78.4	98.0	98.0	117.6	137.2	122.5	161.7
6.5	-93.1	-88.2	-83.3	-44.1	-24.5	-19.6	9.8	34.3	34.3	58.8	102.9	102.9	122.5	176.4	151.9	166.6	220.5	205.8
7	-98.0	-98.0	-93.1	-44.1	-29.4	-19.6	19.6	39.2	49.0	63.7	107.8	122.5	132.3	191.1	181.3	171.5	245.0	245.0
7.5	-112.7	-112.7	-102.9	-44.1	-29.4	-14.7	24.5	49.0	63.7	83.3	132.3	156.8	156.8	225.4	230.3	220.5	289.1	313.6
8	-127.4	-117.6	-117.6	-49.0	-29.4	-9.8	34.3	58.8	83.3	98.0	147.0	176.4	171.5	245.0	269.5	240.1	308.7	347.9
8.5	-132.3	-122.5	-122.5	-49.0	-34.3	-19.6	39.2	63.7	83.3	98.0	156.8	186.2	186.2	264.6	294.0	259.7	338.1	372.4
9	-98.0	-137.2	-132.3	-53.9	-34.3	-14.7	39.2	73.5	102.9	112.7	186.2	220.5	205.8	308.7	323.4	279.3	392.0	421.4
9.5	-151.9	-147.0	-142.1	-53.9	-39.2	-9.8	49.0	83.3	112.7	132.3	200.9	235.2	225.4	338.1	338.1	298.9	431.2	445.9
10	-156.8	-147.0	-156.8	-49.0	-34.3	-14.7	53.9	98.0	117.6	147.0	220.5	235.2	245.0	362.6	338.1	333.2	465.5	450.8
10.5	-147.0	-156.8	-166.6	-44.1	-34.3	-9.8	53.9	93.1	112.7	164.0	225.4	240.1	230.3	362.6	347.9	313.6	465.5	460.6
11	-142.1	-156.8	-171.5	-49.0	-39.2	-19.6	49.0	88.2	112.7	159.0	230.3	245.0	247.0	357.7	362.6	350.0	480.2	475.3
11.5	-151.9	-171.5	-181.3	-53.9	-49.0	-19.6	39.2	83.3	127.4	167.0	220.5	254.8	326.0	372.4	357.7	364.0	450.8	509.6

Table C.15 – Panel S2 – Number 6: Strain data

Total Load kN	Depth level 1 - Zone			Depth level 2 - Zone			Depth level 3 - Zone			Depth level 4 - Zone			Depth level 5 - Zone			Depth level 6 - Zone		
	A	B	C	A	B	C	A	B	C	A	B	C	A	B	C	A	B	C
	Strain × 10^{-6}			Strain × 10^{-6}			Strain × 10^{-6}			Strain × 10^{-6}			Strain × 10^{-6}			Strain × 10^{-6}		
0	0.0	0.0	0.0	0.0	0.0	0.0	0.0	0.0	0.0	0.0	0.0	0.0	0.0	0.0	0.0	0.0	0.0	0.0
1	-19.6	-14.7	-14.7	-4.9	-4.9	-4.9	0.0	-4.9	0.0	4.9	4.9	4.9	1.0	14.7	9.8	9.8	19.6	9.8
2	-34.3	-24.5	-29.4	-14.7	-4.9	-39.2	-4.9	0.0	0.0	0.0	4.9	4.9	-5.0	24.5	19.6	34.3	24.5	24.5
3	-44.1	-39.2	-44.1	-19.6	-14.7	-24.5	-4.9	-4.9	-9.8	4.9	4.9	4.9	6.0	29.4	14.7	68.6	39.2	29.4
4	-58.8	-49.0	-44.1	-24.5	-14.7	-29.4	-9.8	0.0	-4.9	4.9	19.6	13.0	26.0	39.2	39.2	68.6	117.6	53.9
5	-68.6	-58.8	-58.8	-29.4	-19.6	-34.3	-4.9	4.9	-4.9	39.2	29.4	19.6	29.0	58.8	53.9	98.0	137.2	83.3
6	-93.1	-78.4	-83.3	-29.4	-24.5	-29.4	19.6	14.7	4.9	68.6	63.7	68.6	88.2	107.8	63.7	151.9	200.9	107.8
6.5	-107.8	-88.2	-93.1	-34.3	-14.7	-44.1	24.5	24.5	9.8	98.0	78.4	63.7	117.6	122.5	93.1	181.3	220.5	171.5
7	-122.5	-102.9	-107.8	-34.3	-24.5	-44.1	39.2	19.6	24.5	117.6	83.3	78.4	147.0	137.2	156.8	230.3	235.2	230.3
7.5	-127.4	-102.9	-117.6	-29.4	-24.5	-44.1	49.0	29.4	39.2	132.3	88.2	112.7	171.5	151.9	200.9	264.6	254.8	284.2
8	-142.1	-117.6	-127.4	-39.2	-29.4	-44.1	49.0	24.5	49.0	151.9	107.8	132.3	191.1	151.9	225.4	289.1	254.8	308.7
8.5	-156.8	-122.5	-132.3	-44.1	-29.4	-44.1	53.9	39.2	53.9	156.8	107.8	127.4	215.6	188.0	249.9	323.4	289.1	338.1
9	-171.5	-137.2	-137.2	-44.1	-34.3	-44.1	63.7	34.3	53.9	181.3	112.7	147.0	235.2	186.2	274.4	347.9	303.8	377.3
9.5	-171.5	-147.0	-156.8	-44.1	-39.2	-49.0	68.6	44.1	68.6	196.0	127.4	181.3	259.7	200.9	313.6	396.9	318.5	431.2
10	-181.3	-151.9	-161.7	-49.0	-39.2	-53.9	73.5	44.1	78.4	200.9	142.1	196.0	274.4	215.6	333.2	416.5	338.1	455.7
10.5	-191.1	-161.7	-171.5	-49.0	-39.2	-53.9	78.4	44.1	83.3	210.7	147.0	210.7	284.2	252.0	357.7	426.3	372.4	490.0
11	-186.2	-166.6	-181.3	-53.9	-44.1	-53.9	73.5	49.0	98.0	205.8	147.0	230.3	274.4	278.0	392.0	421.4	377.3	529.2
11.5	-191.1	-171.5	-181.3	-53.9	-49.0	-58.8	78.4	49.0	102.9	205.8	156.8	240.1	290.0	290.0	411.6	421.4	382.2	563.5

Table C.16 – Panel S2 – Number 7: Strain data

Total Load kN	Depth level 1 - Zone			Depth level 2 - Zone			Depth level 3 - Zone			Depth level 4 - Zone			Depth level 5 - Zone			Depth level 6 - Zone		
	A	B	C	A	B	C	A	B	C	A	B	C	A	B	C	A	B	C
	Strain × 10^{-6}			Strain × 10^{-6}			Strain × 10^{-6}			Strain × 10^{-6}			Strain × 10^{-6}			Strain × 10^{-6}		
0	0.0	0.0	0.0	0.0	0.0	0.0	0.0	0.0	0.0	0.0	0.0	0.0	0.0	0.0	0.0	0.0	0.0	0.0
1	-19.6	-9.8	-9.8	0.0	4.9	-14.7	0.0	9.8	0.0	4.9	9.8	4.9	19.6	19.6	19.6	24.5	19.6	14.7
2	-49.0	-24.5	-19.6	-9.8	-4.9	-14.7	4.9	9.8	4.9	9.8	0.0	19.6	29.4	19.6	44.1	39.2	9.8	24.5
3	-56.0	-14.7	-34.3	-19.6	1.5	-19.6	4.9	14.7	4.9	9.8	14.7	39.2	53.9	39.2	68.6	73.5	39.2	34.3
4	-71.0	-34.3	-49.0	-34.3	-4.9	-19.6	-9.8	24.5	14.7	19.6	29.4	49.0	78.4	58.8	98.0	93.1	88.2	58.8
5	-77.0	-39.2	-68.6	-39.2	-19.6	-29.4	0.0	24.5	9.8	39.2	49.0	68.6	122.5	88.2	112.7	176.4	127.4	107.8
6	-112.0	-73.5	-83.3	-44.1	-14.7	-34.3	4.9	63.7	29.4	44.1	83.3	102.9	171.5	102.9	166.6	205.8	205.8	156.8
6.5	-113.0	-88.2	-98.0	-49.0	-14.7	-39.2	9.8	58.8	39.2	53.9	117.6	122.5	210.7	127.4	200.9	245.0	196.0	186.2
7	-131.0	-102.9	-102.9	-49.0	-19.6	-39.2	14.7	68.6	49.0	63.7	137.2	142.1	240.1	186.2	245.0	264.6	235.2	215.6
7.5	-151.9	-128.0	-98.0	-53.9	-24.5	-39.2	14.7	68.6	68.6	73.5	151.9	166.6	269.5	210.7	274.4	279.3	245.0	259.7
8	-127.4	-161.7	-107.8	-58.8	-19.6	-34.3	19.6	78.4	73.5	88.2	161.7	181.3	298.9	225.4	298.9	313.6	264.6	294.0
8.5	-137.2	-166.6	-112.7	-58.8	-19.6	-34.3	24.5	83.3	78.4	98.0	176.4	191.1	328.3	245.0	313.6	367.5	274.4	338.1
9	-147.0	-171.5	-122.5	-63.7	-14.7	-44.1	24.5	88.2	98.0	112.7	200.9	215.6	357.7	264.6	343.0	392.0	303.8	367.5
9.5	-156.8	-181.3	-137.2	-68.6	-14.7	-39.2	19.6	98.0	102.9	127.4	215.6	225.4	382.2	289.1	352.8	426.3	313.6	431.2
10	-176.4	-181.3	-142.1	-65.3	-9.8	-34.3	14.7	112.7	112.7	127.4	240.1	240.1	406.7	318.5	372.4	445.9	333.2	441.0
10.5	-181.3	-191.1	-151.9	-67.1	-14.7	-34.3	14.7	122.5	122.5	137.2	249.9	264.6	431.2	347.9	377.3	475.3	352.8	480.2
11	-186.2	-200.9	-166.6	-69.1	-16.2	-49.0	24.5	132.3	127.4	147.0	264.6	279.3	465.5	372.4	396.9	509.6	382.2	519.4
11.5	-205.8	-196.0	-166.6	-65.8	-18.2	-34.3	19.6	142.1	117.6	156.8	289.1	303.8	494.9	411.6	431.2	534.1	401.8	558.6
12	-200.9	-200.9	-181.3	-65.6	-14.0	-44.1	19.6	161.7	156.8	161.7	313.6	313.6	529.2	450.8	441.0	578.2	460.6	592.9

Table C.17 – Panel S2 – Number 8: Strain data

Total Load kN	Depth level 1 - Zone			Depth level 2 - Zone			Depth level 3 - Zone			Depth level 4 - Zone			Depth level 5 - Zone			Depth level 6 - Zone		
	A	B	C	A	B	C	A	B	C	A	B	C	A	B	C	A	B	C
	Strain × 10^{-6}			Strain × 10^{-6}			Strain × 10^{-6}			Strain × 10^{-6}			Strain × 10^{-6}			Strain × 10^{-6}		
0	0.0	0.0	0.0	0.0	0.0	0.0	0.0	0.0	0.0	0.0	0.0	0.0	0.0	0.0	0.0	0.0	0.0	0.0
1	-14.7	-9.8	-29.4	0.0	0.0	0.0	4.9	4.9	0.0	19.6	9.8	19.6	29.4	14.7	34.3	43.0	19.6	19.6
2	-29.4	-19.6	-49.0	-9.8	0.0	-9.8	19.6	0.0	14.7	39.2	19.6	39.2	73.5	34.3	68.6	78.0	58.8	73.5
3	-39.2	-39.2	-63.7	-2.5	0.0	-9.8	29.4	14.7	24.5	43.0	29.4	58.8	95.0	49.0	83.0	114.0	58.8	105.0
4	-53.9	-44.1	-68.6	-4.9	-14.7	-4.9	39.2	4.9	44.1	62.0	39.2	73.0	131.0	73.5	118.0	165.0	58.8	156.8
5	-73.5	-63.7	-88.2	-14.7	-14.7	-9.8	49.0	9.8	53.9	81.0	44.1	73.0	157.0	98.0	163.0	225.0	88.2	210.7
6	-88.2	-83.3	-107.8	-14.7	-14.7	-14.7	53.9	19.6	53.9	127.4	53.9	127.4	215.6	107.8	215.6	277.0	107.8	245.0
6.5	-93.1	-83.3	-112.7	-9.8	-19.6	-14.7	63.7	14.7	58.8	142.1	68.6	137.2	240.1	112.7	230.3	310.0	142.0	249.9
7	-102.9	-93.1	-117.6	-19.6	-14.7	-14.7	63.7	24.5	73.5	151.9	73.5	156.8	240.1	127.4	249.9	332.0	164.0	303.8
7.5	-117.6	-98.0	-122.5	-19.6	-19.6	-14.7	68.6	14.7	68.6	156.8	73.5	161.7	269.5	137.2	264.6	334.0	185.0	313.6
8	-122.5	-107.8	-132.3	-29.4	-39.2	-24.5	68.6	24.5	73.5	171.5	78.4	171.5	279.3	142.1	284.2	401.8	212.0	333.2
8.5	-127.4	-122.5	-142.1	-29.4	-39.2	-29.4	68.6	14.7	73.5	181.3	102.0	181.3	294.0	175.0	298.9	400.0	256.0	357.7
9	-137.2	-122.5	-147.0	-29.4	-44.1	-29.4	78.4	24.5	78.4	191.1	120.0	191.1	313.6	189.0	313.6	455.7	262.0	377.3
9.5	-147.0	-127.4	-156.8	-29.4	-44.1	-29.4	78.4	24.5	83.3	200.9	132.0	196.0	318.5	212.0	328.3	460.6	317.0	392.0
10	-156.8	-137.2	-171.5	-39.2	-49.0	-29.4	83.3	24.5	93.1	215.6	139.0	215.6	343.0	227.0	357.7	494.9	296.0	402.2
10.5	-161.7	-142.1	-176.4	-34.3	-49.0	-34.3	93.1	24.5	102.9	230.3	176.0	230.1	367.5	243.0	364.2	509.6	324.0	440.9
11	-171.5	-156.8	-186.2	-34.3	-53.9	-29.4	98.0	24.5	107.8	245.0	179.0	256.3	396.9	263.0	385.7	548.8	356.0	469.3
11.5	-176.4	-161.7	-191.1	-34.3	-53.9	-29.4	102.9	29.4	117.6	259.7	188.0	260.7	411.6	309.0	395.3	588.0	366.0	510.8

Table C.18 – Panel S2 – Number 9: Strain data

Total Load kN	Depth level 1 - Zone			Depth level 2 - Zone			Depth level 3 - Zone			Depth level 4 - Zone			Depth level 5 - Zone			Depth level 6 - Zone		
	A	B	C	A	B	C	A	B	C	A	B	C	A	B	C	A	B	C
	Strain × 10^{-6}			Strain × 10^{-6}			Strain × 10^{-6}			Strain × 10^{-6}			Strain × 10^{-6}			Strain × 10^{-6}		
0	0.0	0.0	0.0	0.0	0.0	0.0	0.0	0.0	0.0	0.0	0.0	0.0	0.0	0.0	0.0	0.0	0.0	0.0
1	-19.6	-4.9	-14.7	0.0	4.9	-14.7	-14.7	9.8	4.9	4.9	-4.9	14.7	19.6	24.5	19.6	14.7	24.5	19.6
2	-19.6	-9.8	-9.8	-9.8	-4.9	0.0	-14.7	14.7	9.8	4.9	-4.9	29.4	63.7	29.4	44.1	29.4	44.1	49.0
3	-29.4	-9.8	-29.4	-14.7	-14.7	-19.6	-4.9	19.6	0.0	29.4	19.6	24.5	58.8	49.0	53.9	78.4	68.6	58.8
4	-44.1	-26.2	-44.1	-9.8	-9.8	-19.6	0.0	19.6	4.9	63.7	44.1	44.1	102.9	63.7	88.2	161.7	93.1	102.9
5	-14.7	-34.3	-73.5	-19.6	-9.8	-24.5	14.7	68.6	14.7	63.7	58.8	58.8	157.0	151.0	122.5	232.0	220.5	161.7
6	-102.9	-73.5	-98.0	-19.6	-14.7	-24.5	-4.9	83.3	39.2	93.1	127.4	108.0	224.0	220.5	186.2	274.0	284.2	240.1
6.5	-117.6	-78.4	-107.8	-9.8	-14.7	-39.2	24.5	88.2	34.3	88.2	137.2	137.0	240.1	235.2	196.0	297.0	280.0	259.7
7	-127.4	-83.3	-122.5	-14.8	-14.7	-29.4	24.5	93.1	44.1	93.1	132.3	153.0	264.6	240.1	240.1	346.0	323.4	313.6
7.5	-142.1	-93.1	-122.5	-19.6	-19.6	-34.3	24.5	74.4	44.1	102.9	147.0	168.0	284.2	264.6	249.9	364.0	338.1	333.2
8	-151.9	-102.9	-137.2	-14.7	-24.5	-29.4	19.6	83.5	44.1	107.8	166.6	195.0	308.7	289.1	289.1	399.0	362.6	357.7
9	-176.4	-122.5	-142.1	-19.6	-14.7	-24.5	24.5	100.0	68.6	127.4	205.8	228.0	372.4	352.8	308.7	473.0	460.6	426.3
9.5	-191.1	-122.5	-156.8	-24.5	-24.5	-34.3	24.5	106.4	68.6	149.0	225.4	244.0	387.1	387.1	338.1	480.0	470.4	460.6
10	-200.9	-127.4	-161.7	-24.5	-14.7	-29.4	29.4	113.7	88.2	142.1	245.0	256.0	411.6	382.2	362.6	518.0	539.0	494.9
10.5	-205.8	-137.2	-166.6	-34.3	-9.8	-34.3	34.3	129.3	78.4	156.8	269.5	286.0	416.0	453.0	382.2	554.0	581.0	524.3
11	-205.8	-142.1	-176.4	-34.3	-9.8	-34.3	34.3	142.1	98.0	151.9	279.3	316.0	441.0	490.0	416.5	641.0	627.2	563.5
11.5	-196.0	-151.9	-186.2	-19.6	-16.8	-39.2	34.3	144.8	117.6	151.9	289.1	339.0	455.7	509.6	450.8	671.0	646.8	612.5
12	-205.8	-151.9	-191.1	-26.0	-14.7	-29.4	29.4	146.6	122.5	167.0	294.0	339.0	460.6	519.4	485.1	710.5	661.5	651.7

Measured displacement data recorded from the composite panels tested in the laboratory.

Table C.19 – Panel S1 – Numbers 1 and 2: Displacement data

Panel S1 – Number 1				**Panel S1 – Number 2**			
Total load (kN)	**Displacement (mm) at:**			**Total load (kN)**	**Displacement (mm) at:**		
	D1	**D2**	**D3**		**D1**	**D2**	**D3**
0	0	0	0	0	0	0	0
1	0.14	0.17	0.15	1	0.15	0.19	0.14
2	0.25	0.31	0.25	2	0.25	0.31	0.22
3	0.35	0.45	0.35	3	0.34	0.45	0.32
4	0.43	0.59	0.45	4	0.43	0.58	0.43
5	0.55	0.73	0.56	5	0.52	0.7	0.5
6	0.65	0.88	0.66	6	0.63	0.84	0.63
7	0.77	1.07	0.79	7	0.74	0.98	0.71
8	0.89	1.22	0.92	8	0.88	1.16	0.86
9	1.23	1.69	1.23	9	1.15	1.57	1.14
10	1.61	2.19	1.6	10	1.78	2.35	1.62
11	1.97	2.61	1.87	-	-	-	-
12	2.26	3.11	2.22	-	-	-	-

Table C.20 – Panel S1 – Numbers 3 and 4: Displacement data

Panel S1 – Number 3				**Panel S1 – Number 4**			
Total load (kN)	**Displacement (mm) at:**			**Total load (kN)**	**Displacement (mm) at:**		
	D1	**D2**	**D3**		**D1**	**D2**	**D3**
0	0	0	0	0	0	0	0
1	0.13	0.18	0.14	1	0.15	0.19	0.15
2	0.23	0.32	0.25	2	0.23	0.32	0.24
3	0.33	0.47	0.32	3	0.34	0.47	0.35
4	0.41	0.58	0.43	4	0.42	0.57	0.42
5	0.52	0.7	0.54	5	0.55	0.73	0.55
6	0.63	0.84	0.63	6	0.67	0.86	0.64
7	0.7	0.99	0.76	7	0.75	1.02	0.76
8	0.92	1.23	0.94	8	0.88	1.18	0.85
9	1.09	1.48	1.05	9	1.05	1.41	1.06
10	1.61	2.19	1.59	10	1.57	2.03	1.528
11	1.91	2.62	1.92	-	-	-	-

Table C.21 – Panel S1 – Numbers 5 and 6: Displacement data

Panel S1 – Number 5				Panel S1 – Number 6			
Total load (kN)	Displacement (mm) at:			Total load (kN)	Displacement (mm) at:		
	D1	D2	D3		D1	D2	D3
0	0	0	0	0	0	0	0
0.5	0.05	0.06	0.04	0.5	0.04	0.06	0.04
1	0.1	0.13	0.1	1	0.08	0.13	0.08
1.5	0.15	0.2	0.14	1.5	0.13	0.2	0.13
2	0.21	0.26	0.19	2	0.18	0.27	0.18
2.5	0.26	0.32	0.23	3	0.27	0.41	0.28
3	0.31	0.41	0.29	4	0.38	0.57	0.4
3.5	0.37	0.46	0.35	4.5	0.43	0.65	0.47
4	0.42	0.54	0.4	5	0.5	0.74	0.54
4.5	0.47	0.61	0.45	5.5	0.58	0.87	0.64
5	0.58	0.69	0.51	6	0.65	0.98	0.72
5.5	0.6	0.76	0.56	6.5	0.74	1.13	0.83
6	0.63	0.84	0.62	7	0.85	1.31	0.97
6.5	0.69	0.92	0.67	7.5	1.08	2.36	1.28
7	0.76	1	0.74	8	1.3	3.43	1.65
7.5	0.83	1.1	0.81	8.5	1.55	4.47	1.91
8	0.89	1.19	0.88	9	1.68	4.66	2.05
8.5	0.97	1.3	0.96	9.5	1.99	6.04	2.28
9	1.05	1.43	1.06	-	-	-	-
9.5	1.17	1.62	1.24	-	-	-	-
10	1.5	2.33	1.78	-	-	-	-
10.5	1.63	2.55	1.93	-	-	-	
11	1.78	2.83	2.16	-	-	-	-

Table C.22 – Panel S1 – Numbers 7 and 8: Displacement data

Panel S1 – Number 7				Panel S1 – Number 8			
Total load (kN)	Displacement (mm) at:			Total load (kN)	Displacement (mm) at:		
	D1	D2	D3		D1	D2	D3
0	0	0	0	0	0	0	0
0.5	0.04	0.06	0.05	1	0.07	0.14	0.08
1	0.1	0.14	0.11	2	0.15	0.28	0.18
1.5	0.15	0.22	0.16	3	0.27	0.45	0.3
2	0.2	0.29	0.22	4	0.39	0.64	0.44
3	0.32	0.45	0.35	4.5	0.44	0.73	0.51
4	0.44	0.63	0.49	5	0.5	0.84	0.6
4.5	0.51	0.72	0.56	5.5	0.57	0.96	0.69
5	0.58	0.83	0.64	6	0.7	1.14	0.83
5.5	0.66	0.94	0.71	6.5	0.91	1.48	1.05
6	0.74	1.06	0.8	7	1.24	2.02	1.4
6.5	0.84	1.19	0.9	7.5	1.46	2.36	1.69
7	0.97	1.38	1.03	8	1.65	2.66	1.94
7.5	1.1	1.58	1.18	8.5	1.81	2.93	2.11
8	1.3	1.91	1.4	9	2.03	3.28	2.46
8.5	1.54	2.29	1.69	-	-	-	-
9	1.75	2.59	1.89	-	-	-	-
9.5	2.15	3.04	2.14	-	-	-	-

Table C.23 – Panel S1 – Numbers 9 and Panel S2 – Number 1: Displacement data

Panel S1 – Number 9				**Panel S2 – Number 1**			
Total load (kN)	**Displacement (mm) at:**			**Total load (kN)**	**Displacement (mm) at:**		
	D1	**D2**	**D3**		**D1**	**D2**	**D3**
0	0	0	0	0	0	0	0
1	0.15	0.23	0.16	1	0.14	0.21	0.15
2	0.27	0.38	0.27	2	0.23	0.33	0.24
3	0.38	0.55	0.39	3	0.34	0.49	0.35
4	0.51	0.73	0.52	4	0.46	0.6	0.45
4.5	0.58	0.85	0.6	5	0.57	0.77	0.58
5	0.64	0.94	0.67	6	0.67	0.91	0.68
5.5	0.72	1.05	0.75	7	0.8	1.11	0.77
6	0.8	1.16	0.84	8	1.24	1.69	1.23
6.5	0.96	1.35	0.97	9	1.72	2.23	1.72
7	1.09	1.57	1.12	10	2.11	2.93	2.1
7.5	1.24	1.78	1.28	11	2.8	3.59	2.8
8	1.51	2.23	1.59	-	-	-	-
8.5	1.7	2.51	1.79	-	-	-	-
9	1.92	2.83	2.03	-	-	-	-
9.5	2.07	3.04	2.19	-	-	-	-
10	2.22	3.28	2.39	-	-	-	-
10.5	2.43	3.57	2.61	-	-	-	-

Table C.24 – Panel S2 – Numbers 2 and 3: Displacement data

Panel S2 – Number 2				**Panel S2 – Number 3**			
Total load (kN)	**Displacement (mm) at:**			**Total load (kN)**	**Displacement (mm) at:**		
	D1	**D2**	**D3**		**D1**	**D2**	**D3**
0	0	0	0	0	0	0	0
1	0.13	0.19	0.14	I	0.15	0.23	0.16
2	0.21	0.3	0.22	2	0.27	0.38	0.28
3	0.31	0.42	0.33	3	0.42	0.55	0.42
4	0.43	0.56	0.42	4	0.59	0.75	0.56
5	0.54	0.7	0.55	5	0.75	1	0.77
6	0.65	0.9	0.69	6	1.09	1.41	1.05
7	0.94	1.31	0.99	7	1.26	1.72	1.3
8	1.27	1.74	1.29	8	1.63	2.15	1.59
9	1.53	2.1	1.52	9	3.06	3.21	2.36
10	1.85	2.45	1.79	-	-	-	-
11	3.07	4.43	3.05	-	-	-	-

Table C.25 – Panel S2 – Numbers 4 and 5: Displacement data

Panel S2 – Number 4				Panel S2 – Number 5			
Total load (kN)	Displacement (mm) at:			Total load (kN)	Displacement (mm) at:		
	D1	D2	D3		D1	D2	D3
0	0	0	0	0	0	0	0
1	0.15	0.21	0.15	0.5	0.04	0.09	0.04
2	0.26	0.35	0.28	1	0.09	0.15	0.09
3	0.37	0.51	0.38	1.5	0.15	0.35	0.16
4	0.5	0.7	0.48	2	0.15	0.44	0.22
5	0.7	0.95	0.71	2.5	0.29	0.53	0.29
6	1	1.39	1.04	3	0.36	0.62	0.35
7	1.31	1.81	1.35	3.5	0.43	0.72	0.42
8	1.54	2.14	1.59	4	0.52	0.82	0.49
9	1.91	2.57	1.92	4.5	0.6	0.95	0.57
10	2.27	3.06	2.27	5	0.71	1.08	0.66
-	-	-	-	5.5	0.81	1.23	0.76
-	-	-	-	6	0.92	1.35	0.86
-	-	-	-	6.5	1.14	1.57	1.06
-	-	-	-	7	1.42	1.91	1.28
-	-	-	-	7.5	1.79	2.41	1.67
-	-	-	-	8	2.02	2.66	1.83
-	-	-	-	8.5	2.19	2.9	1.99
-	-	-	-	9	2.4	3.2	2.2
-	-	-	-	9.5	2.68	3.58	2.5
-	-	-	-	10	2.92	3.84	2.69
-	-	-	-	10.5	3.59	5.76	3.79
-	-	-	-	11	4.18	6.16	4.05
-	-	-	-	11.5	4.8	6.65	4.4

Table C.26 – Panel S2 – Numbers 6 and 7: Displacement data

Panel S2 – Number 6				Panel S2 – Number 7			
Total load (kN)	Displacement (mm) at:			Total load (kN)	Displacement (mm) at:		
	D1	D2	D3		D1	D2	D3
0	0	0	0	0	0	0	0
1	0.09	0.1	0.09	1	0.09	0.13	0.1
2	0.2	0.26	0.21	2	0.22	0.15	0.25
3	0.33	0.44	0.31	3	0.36	0.53	0.4
4	0.47	0.62	0.46	4	0.56	0.82	0.6
5	0.67	0.92	0.64	5	0.77	1.12	0.83
6	1.05	1.45	0.99	6	1.06	1.57	1.15
6.5	1.2	1.68	1.15	6.5	1.3	1.95	1.4
7	1.4	1.97	1.34	7	1.55	2.3	1.65
7.5	1.59	2.25	1.53	7.5	1.75	2.57	1.83
8	1.79	2.49	1.69	8	1.92	2.81	2.01
8.5	2.05	2.79	1.9	8.5	2.11	3.08	2.22
9	2.23	3.06	2.08	9	2.3	3.36	2.44
9.5	2.42	3.33	2.27	9.5	2.5	3.68	2.67
10	2.64	3.61	2.48	10	2.69	3.93	2.87
10.5	2.9	3.94	2.69	10.5	2.87	4.19	3.07
-	-	-	-	11	3.07	4.46	3.28
-	-	-	-	11.5	3.28	4.78	3.51
-	-	-	-	12	3.47	5.05	3.71

Table C.27 – Panel S2 – Numbers 8 and 9: Displacement data

Panel S2 – Number 8				Panel S2 – Number 9			
Total load (kN)	Displacement (mm) at:			Total load (kN)	Displacement (mm) at:		
	D1	D2	D3		D1	D2	D3
0	0	0	0	0	0	0	0
1	0.21	0.29	0.2	1	0.2	0.25	0.17
2	0.43	0.59	0.43	2	0.34	0.43	0.3
3	0.66	0.91	0.67	3	0.5	0.64	0.45
4	0.9	1.24	0.9	4	0.77	1	0.71
5	1.12	1.56	1.13	5	1.18	1.59	1.06
6	1.33	1.86	1.36	6	1.6	2.15	1.44
6.5	1.45	2.03	1.48	6.5	1.78	2.38	1.6
7	1.56	2.18	1.59	7	1.99	2.71	1.87
7.5	1.68	2.34	1.71	7.5	2.13	2.92	2.03
8	1.79	2.49	1.81	8	2.3	3.16	2.2
8.5	1.89	2.64	1.93	9	2.77	3.81	2.37
9	2	2.79	2.05	9.5	2.97	4.09	2.88
9.5	2.12	2.96	2.17	10	3.21	4.41	3.12
10	2.24	3.16	2.3	10.5	3.49	4.76	3.37
10.5	2.41	3.36	2.47	-	-	-	-
11	2.62	3.63	2.69	-	-	-	-
11.5	2.78	3.85	2.84	-	-	-	-

Natural frequency data determined using an FFT of measured impact-response signals obtained from the panels tested in the laboratory. Frequencies quoted to the nearest one decimal place.

Table C.28 – Panel S1 – Numbers 1 and 2: Natural frequency data (from FFT)

Panel S1 – Number 1				Panel S1 – Number 2			
Total load (kN)	Natural frequency (Hz)			Total load (kN)	Natural frequency (Hz)		
	Set 1	Set 2	Set 3		Set 1	Set 2	Set 3
0	36.9	36.8	36.9	0	37.3	37.3	37.3
1	36.8	36.8	36.8	1	37.2	37.2	37.2
2	36.7	36.7	36.7	2	37.2	37.2	37.2
3	36.7	36.7	36.7	3	37.2	37.2	37.2
4	36.7	36.7	36.7	4	37.1	37.1	37.1
5	36.6	36.6	36.6	5	37.1	37.1	37.1
6	36.4	36.5	36.6	6	37.0	37.0	37.0
7	36.4	36.4	36.4	7	36.9	36.9	36.9
8	36.2	36.2	36.2	8	36.6	36.5	36.5
9	35.7	35.7	35.7	9	35.6	35.6	35.5
10	35.0	34.9	34.9	10	34.8	34.7	34.7
11	34.4	34.5	34.4	-	-	-	-
12	34.0	34.2	34.2	-	-	-	-

Table C.29 – Panel S1 – Numbers 3 and 4: Natural frequency data (from FFT)

Panel S1 – Number 3				Panel S1 – Number 4			
Total load (kN)	Natural frequency (Hz)			Total load (kN)	Natural frequency (Hz)		
	Set 1	Set 2	Set 3		Set 1	Set 2	Set 3
0	37.2	37.2	37.1	0	37.1	37.1	37.1
1	37.0	37.1	37.0	1	37.1	37.1	37.1
2	37.0	37.0	37.0	2	37.0	37.0	37.0
3	37.1	37.0	37.0	3	37.0	37.0	37.0
4	37.0	37.0	37.0	4	36.9	36.9	36.9
5	36.9	36.9	36.9	5	36.9	36.9	36.9
6	36.9	36.9	36.9	6	36.8	36.8	36.8
7	36.8	36.7	36.8	7	36.8	36.8	36.8
8	36.5	36.5	36.5	8	36.6	36.6	36.6
9	36.4	36.1	36.1	9	36.3	36.3	36.3
10	35.3	35.2	35.3	10	35.3	-	-
11	34.7	34.7	35.0	-	-	-	-

Table C.30 – Panel S2 – Numbers 1 and 2: Natural frequency data (from FFT)

Panel S2 – Number 1				Panel S2 – Number 1			
Total load (kN)	Natural frequency (Hz)			Total load (kN)	Natural frequency (Hz)		
	Set 1	Set 2	Set 3		Set 1	Set 2	Set 3
0	37.2	37.1	37.1	0	35.5	35.6	35.6
1	37.1	37.1	37.1	1	35.5	35.5	35.5
2	37.2	37.2	37.2	2	35.4	35.3	35.3
3	37.1	37.1	37.0	3	35.1	35.0	35.1
4	37.1	37.0	37.0	4	35.6	34.6	34.6
5	36.9	36.9	36.9	5	34.8	33.9	34.2
6	36.7	36.7	36.7	6	33.0	33.0	32.8
7	36.1	36.5	36.5	7	32.3	32.7	32.3
8	35.4	35.3	35.3	8	31.8	32.0	31.7
9	33.9	33.8	34.4	-	-	-	-
10	33.0	33.1	33.1	-	-	-	-

Table C.31 – Panel S2 – Numbers 3 and 4: Natural frequency data (from FFT)

Panel S2 – Number 3				Panel S2 – Number 4			
Total load (kN)	Natural frequency (Hz)			Total load (kN)	Natural frequency (Hz)		
	Set 1	Set 2	Set 3		Set 1	Set 2	Set 3
0	35.9	35.8	35.7	0	35.9	35.8	35.8
1	35.6	35.7	35.7	1	35.6	35.8	35.8
2	35.6	35.5	35.5	2	35.5	35.5	35.5
3	35.5	35.4	35.3	3	35.5	35.5	35.4
4	35.1	35.1	35.1	4	35.2	35.2	35.2
5	34.7	34.7	34.7	5	34.8	34.8	34.8
6	34.0	33.9	34.2	6	34.1	33.9	34.3
7	33.5	33.5	33.4	7	33.6	33.6	33.6
8	33.1	33.0	33.0	8	33.2	33.2	33.2
9	32.1	32.3	32.3	9	32.4	32.8	32.5
10	31.9	31.9	31.7	10	32.1	32.2	31.9

Natural frequency data determined using an FFT of measured decay-of-vibration signals obtained from the panels tested in the laboratory. Frequencies quoted to the nearest one decimal place.

Table C.32 – Panel S1 – Numbers 1 and 2: Natural frequency data (from FFT)

Panel S1 – Number 1				**Panel S1 – Number 2**			
Total load (kN)	**Natural frequency (Hz)**			**Total load (kN)**	**Natural frequency (Hz)**		
	Set 1	**Set 2**	**Set 3**		**Set 1**	**Set 2**	**Set 3**
0	36.9	36.9	36.9	0	37.2	37.2	37.4
1	36.7	36.7	36.7	1	37.2	37.2	37.2
2	36.9	36.9	36.9	2	37.2	37.2	37.2
3	36.7	36.7	36.7	3	37.2	37.2	37.2
4	36.7	36.7	36.7	4	37.1	37.1	37.1
5	36.6	36.6	36.6	5	37.1	37.1	37.1
6	36.6	36.6	36.6	6	37.0	37.0	37.1
7	36.5	36.5	36.5	7	37.0	37.0	37.0
8	36.3	36.4	36.4	8	36.7	36.7	36.7
9	35.9	35.9	35.9	9	35.9	36.0	36.0
10	35.4	35.4	35.4	10	35.3	35.2	35.3
11	35.0	34.9	35.0	-	-	-	-
12	34.6	34.6	34.7	-	-	-	-

Table C.33 – Panel S1 – Numbers 3 and 4: Natural frequency data (from FFT)

Panel S1 – Number 3				**Panel S1 – Number 4**			
Total load (kN)	**Natural frequency (Hz)**			**Total load (kN)**	**Natural frequency (Hz)**		
	Set 1	**Set 2**	**Set 3**		**Set 1**	**Set 2**	**Set 3**
0	37.1	37.1	37.1	0	36.6	36.5	36.6
1	37.1	37.1	37.1	1	36.6	36.6	36.6
2	37.0	37.0	37.0	2	36.5	36.5	36.5
3	37.1	37.1	37.1	3	36.5	36.5	36.5
4	37.0	37.0	37.0	4	36.4	36.4	36.5
5	36.9	36.9	37.0	5	36.4	36.4	36.4
6	37.0	37.0	37.0	6	36.4	36.4	36.4
7	36.9	36.9	36.9	7	36.3	36.3	36.4
8	36.6	36.6	36.6	8	36.1	36.3	36.3
9	36.3	36.3	36.4	9	35.9	35.9	35.9
10	35.5	35.6	35.6	10	35.3	35.3	35.3
11	35.2	35.3	35.3	-	-	-	-

Table C.34 – Panel S2 – Numbers 1 and 2: Natural frequency data (from FFT)

Panel S2 – Number 1				Panel S2 – Number 2			
Total load (kN)	Natural frequency (Hz)			Total load (kN)	Natural frequency (Hz)		
	Set 1	Set 2	Set 3		Set 1	Set 2	Set 3
0	37.2	37.4	37.2	0	37.6	37.7	37.7
1	37.2	37.2	37.2	1	37.4	37.4	37.4
2	37.2	37.2	37.2	2	37.2	37.2	37.2
3	37.2	37.2	37.2	3	37.4	37.4	37.4
4	37.1	37.1	37.1	4	37.0	37.0	37.2
5	37.0	37.0	37.0	5	37.1	37.1	37.1
6	36.9	37.0	37.0	6	36.6	36.6	36.6
7	36.3	36.3	36.4	7	35.5	35.5	35.6
8	35.7	35.8	35.8	8	34.8	34.8	34.9
9	34.7	34.8	34.8	9	34.3	34.4	34.4
10	34.0	33.9	34.1	10	34.1	34.1	34.1

Table C.35 – Panel S2 – Numbers 3 and 4: Natural frequency data (from FFT)

Panel S2 – Number 3				Panel S2 – Number 4			
Total load (kN)	Natural frequency (Hz)			Total load (kN)	Natural frequency (Hz)		
	Set 1	Set 2	Set 3		Set 1	Set 2	Set 3
0	35.6	35.6	35.6	0	35.8	35.8	35.8
1	35.5	35.5	35.5	1	35.6	35.6	35.6
2	35.4	35.4	35.5	2	35.5	35.5	35.5
3	35.2	35.2	35.2	3	35.4	35.4	35.4
4	34.8	34.8	34.8	4	35.2	35.2	35.2
5	34.3	34.4	34.4	5	34.8	34.8	34.8
6	33.6	34.3	33.6	6	34.2	34.1	34.1
7	33.8	33.0	33.1	7	33.6	33.6	33.6
8	32.6	32.6	32.7	8	33.2	33.1	33.2
-	-	-	-	9	32.6	32.5	32.6
-	-	-	-	10	32.2	32.2	32.4

Damping data determined using the BRE suite of computer programs (see chapter 3) from measured impact response signals obtained from the panel laboratory test. This data was obtained from the signals over a fixed time length and relative to consistent maximum amplitude.

Table C.36 – Panel S1 – Numbers 1 to 4 – Damping from decay-of-vibration signals

Total Load kN	Panel S1 – Number 1			Panel S1 – Number 2			Panel S1 – Number 3			Panel S1 – Number 4		
	Damping %age critical			Damping %age critical			Damping %age critical			Damping %age critical		
	Set 1	Set 2	Set 3	Set 1	Set 2	Set 3	Set 1	Set 2	Set 3	Set 1	Set 2	Set 3
0	0.55	0.51	0.49	0.43	0.44	0.43	0.44	0.44	0.43	0.43	0.43	0.46
1	0.53	0.53	0.50	0.46	0.47	0.46	0.46	0.43	0.45	0.42	0.42	0.42
2	0.48	0.49	0.46	0.46	0.45	0.45	0.48	0.50	0.48	0.43	0.44	0.43
3	0.48	0.50	0.48	0.45	0.45	0.44	0.47	0.47	0.46	0.44	0.44	0.45
4	0.50	0.49	0.49	0.48	0.45	0.44	0.50	0.55	0.53	0.45	0.47	0.45
5	0.49	0.49	0.48	0.48	0.46	0.48	0.53	0.52	0.54	0.48	0.46	0.45
6	0.53	0.51	0.49	0.47	0.49	0.50	0.50	0.51	0.46	0.49	0.48	0.48
7	0.50	0.51	0.48	0.52	0.50	0.50	0.51	0.53	0.49	0.48	0.51	0.49
8	0.59	0.56	0.57	0.64	0.55	0.60	0.56	0.67	0.66	0.55	0.60	0.61
9	0.64	0.65	0.68	0.76	0.74	0.71	0.71	0.72	0.74	0.68	0.66	0.72
10	0.77	0.83	0.86	0.85	0.82	0.77	0.82	0.77	0.85	0.81	0.82	0.80
11	1.01	0.98	0.96	-	-	-	0.95	0.92	1.00	-	-	-
12	1.09	1.08	1.11	-	-	-	-	-	-	-	-	-

Table C.37 – Panel S2 – Numbers 1 to 4 – Damping from decay-of-vibration signals

Total Load kN	Panel S2 – Number 1			Panel S2 – Number 2			Panel S2 – Number 3			Panel S2 – Number 4		
	Damping %age critical			Damping %age critical			Damping %age critical			Damping %age critical		
	Set 1	Set 2	Set 3	Set 1	Set 2	Set 3	Set 1	Set 2	Set 3	Set 1	Set 2	Set 3
0	0.43	0.44	0.48	0.47	0.46	0.45	0.49	0.48	0.44	0.51	0.53	0.44
1	0.45	0.44	0.42	0.53	0.55	0.54	0.46	0.49	0.50	0.45	0.47	0.42
2	0.45	0.45	0.43	0.58	0.54	0.54	0.46	0.47	0.49	0.45	0.46	0.46
3	0.46	0.45	0.47	0.51	0.50	0.50	0.54	0.49	0.53	0.48	0.46	0.46
4	0.46	0.48	0.47	0.56	0.56	0.52	0.59	0.60	0.59	0.49	0.52	0.52
5	0.49	0.52	0.52	0.60	0.53	0.55	0.66	0.64	0.64	0.57	0.58	0.58
6	0.68	0.73	0.72	0.61	0.64	0.63	0.65	0.74	0.68	0.65	0.67	0.67
7	0.90	0.85	0.88	0.77	0.73	0.76	0.84	0.81	0.76	0.74	0.83	0.79
8	1.01	0.88	0.99	0.91	0.92	0.96	0.89	0.89	0.90	0.88	0.93	0.93
9	1.15	1.09	1.10	1.01	1.00	1.07	-	-	-	1.01	1.03	1.06
10	1.26	1.18	1.26	1.15	1.18	1.13	-	-	-	1.14	1.16	1.17

Damping data determined using the BRE suite of computer programs (see chapter 3) from measured decay-of-vibration signals obtained from the panel laboratory test. This data was obtained from the signals over a fixed time length and relative to consistent maximum amplitude.

Table C.38 – Panel S1 – Numbers 1 to 3 – Damping from decay-of-vibration signals

Total Load kN	Panel S1 – Number 1			Panel S1 – Number 2			Panel S1 – Number 3		
	Damping %age critical			Damping %age critical			Damping %age critical		
	Set 1	Set 2	Set 3	Set 1	Set 2	Set 3	Set 1	Set 2	Set 3
0	0.53	0.55	0.54	0.53	0.52	0.52	0.48	0.48	0.48
1	0.52	0.52	0.52	0.50	0.51	0.49	0.48	0.48	0.49
2	0.48	0.47	0.48	0.49	0.49	0.50	0.51	0.53	0.53
3	0.50	0.50	0.51	0.49	0.49	0.49	0.53	0.53	0.54
4	0.53	0.53	0.53	0.52	0.52	0.52	0.56	0.56	0.56
5	0.60	0.59	0.60	0.53	0.52	0.52	0.56	0.56	0.57
6	0.53	0.52	0.58	0.54	0.54	0.52	0.63	0.57	0.58
7	0.57	0.57	0.58	0.57	0.55	0.57	0.62	0.63	0.63
8	0.62	0.61	0.63	0.59	0.61	0.62	0.71	0.72	0.71
9	0.74	0.83	0.72	0.83	0.82	0.79	0.68	0.85	0.72
10	0.89	0.91	0.96	0.97	0.95	0.98	0.86	0.92	0.84
11	1.03	1.02	1.08	1.08	1.06	1.05	1.00	0.99	1.01
12	1.16	1.12	1.15	-	-	-	-	-	-

Table C.39 – Panel S2 – Numbers 1 to 3 – Damping from decay-of-vibration signals

Total Load kN	Panel S2 – Number 1			Panel S2 – Number 2			Panel S2 – Number 3		
	Damping %age critical			Damping %age critical			Damping %age critical		
	Set 1	Set 2	Set 3	Set 1	Set 2	Set 3	Set 1	Set 2	Set 3
0	0.42	0.42	0.42	0.53	0.48	0.50	0.50	0.46	0.40
1	0.42	0.42	0.43	0.53	0.49	0.54	0.49	0.48	0.48
2	0.42	0.43	0.43	0.53	0.57	0.56	0.50	0.48	0.48
3	0.45	0.45	0.49	0.57	0.58	0.60	0.46	0.47	0.51
4	0.45	0.46	0.48	0.62	0.59	0.58	0.51	0.54	0.52
5	0.49	0.49	0.50	0.65	0.69	0.63	0.66	0.62	0.65
6	0.61	0.73	0.73	0.79	0.78	0.78	0.78	0.75	0.66
7	0.92	0.90	0.89	0.90	0.88	0.90	0.81	0.83	0.86
8	1.06	1.02	1.01	1.02	1.02	1.04	0.88	0.89	0.86
9	1.12	1.14	1.14	-	-	-	1.09	1.01	0.99
10	1.25	1.23	1.27	-	-	-	1.20	1.13	1.11

Natural frequency data determined using the BRE suite of computer programs (see chapter 3) from measured Frequency Response Functions (FRF) obtained from the panel laboratory test.

Table C.40 – Panel S1 – Numbers 1 and 2: Natural frequency data (from FRF)

Panel S1 – Number 1				Panel S1 – Number 2			
Total load (kN)	Natural frequency (Hz)			Total load (kN)	Natural frequency (Hz)		
	Force level 1	Force level 2	Force level 3		Force level 1	Force level 2	Force level 3
0	36.83	36.82	36.80	0	37.28	37.25	37.23
1	36.74	36.79	36.74	1	37.23	37.22	37.23
2	36.78	36.73	36.76	2	37.14	37.22	37.16
3	36.65	36.67	36.66	3	37.16	37.14	37.09
4	36.70	36.65	36.65	4	37.11	37.09	37.04
5	36.61	36.60	36.61	5	37.10	37.08	36.96
6	36.52	36.54	36.56	6	37.03	37.02	37.00
7	36.43	36.45	36.47	7	36.80	36.85	36.84
8	36.14	36.14	36.16	8	36.51	36.58	36.65
9	35.74	35.86	35.84	9	36.09	36.18	36.20
10	35.27	35.39	35.44	10	35.65	35.86	35.76
11	34.85	35.00	35.04	-	-	-	-
12	34.47	34.65	34.68	-	-	-	-

Table C.41 – Panel S1 – Numbers 3 and 4: Natural frequency data (from FRF)

Panel S1 – Number 3				Panel S1 – Number 4			
Total load (kN)	Natural frequency (Hz)			Total load (kN)	Natural frequency (Hz)		
	Force level 1	Force level 2	Force level 3		Force level 1	Force level 2	Force level 3
0	37.12	37.11	37.07	0	36.56	36.50	36.55
1	37.07	37.08	37.04	1	36.52	36.49	36.49
2	37.00	37.03	36.97	2	36.48	36.45	36.47
3	36.98	37.04	36.98	3	36.43	36.41	36.43
4	36.98	36.93	36.96	4	36.35	36.39	36.43
5	36.93	36.89	36.84	5	36.34	36.32	36.38
6	36.90	36.86	36.87	6	36.30	36.29	36.30
7	36.72	36.78	36.72	7	36.14	36.24	36.21
8	36.40	36.50	36.42	8	35.78	35.84	35.96
9	36.02	36.08	36.10	9	35.45	35.45	35.63
10	35.53	35.66	35.67	10	35.00	35.07	35.08
11	35.12	35.25	34.84	-	-	-	-

Table C.42 – Panel S2 – Numbers 1 and 2: Natural frequency data (from FRF)

Panel S2 – Number 1				Panel S2 – Number 2			
Total load (kN)	Natural frequency (Hz)			Total load (kN)	Natural frequency (Hz)		
	Force level 1	Force level 2	Force level 3		Force level 1	Force level 2	Force level 3
0	37.03	37.08	37.11	0	37.51	37.49	37.48
1	36.95	37.07	37.07	1	37.30	37.21	37.28
2	36.92	36.93	36.98	2	37.20	37.10	37.15
3	36.73	36.78	36.85	3	37.14	37.14	37.12
4	36.53	36.61	36.72	4	36.81	36.91	36.95
5	36.37	36.50	36.37	5	36.76	36.81	36.67
6	35.82	35.78	35.79	6	36.11	36.27	36.21
7	35.12	35.26	35.39	7	35.36	35.41	35.46
8	34.51	34.63	34.77	8	34.58	34.81	34.93
9	33.94	34.04	34.20	9	34.11	34.22	34.42
10	33.22	33.60	33.76	10	33.74	33.73	33.97

Table C.43 – Panel S2 – Numbers 3 and 4: Natural frequency data (from FRF)

Panel S2 – Number 3				Panel S2 – Number 4			
Total load (kN)	Natural frequency (Hz)			Total load (kN)	Natural frequency (Hz)		
	Force level 1	Force level 2	Force level 3		Force level 1	Force level 2	Force level 3
0	35.48	35.41	35.54	0	35.68	35.76	35.75
1	35.41	35.36	35.44	1	35.60	35.59	35.62
2	35.33	35.22	35.40	2	35.50	35.46	35.50
3	34.98	35.01	35.07	3	35.32	35.33	35.35
4	34.74	34.75	34.75	4	35.06	35.15	35.08
5	34.51	34.44	34.52	5	34.81	34.90	34.77
6	34.00	33.92	33.95	6	34.35	34.36	34.27
7	33.42	33.32	33.56	7	33.73	33.77	33.87
8	32.75	32.64	32.88	8	33.08	33.09	33.26
-	-	-	-	9	32.30	32.55	32.83
-	-	-	-	10	31.87	32.27	32.15

Damping data determined using the BRE suite of computer programs (see chapter 3) from measured Frequency Response Functions (FRF) obtained from the panel laboratory test.

Table C.44 – Panel S1 – Numbers 1 to 4 – Damping from FRF's

Total Load kN	Panel S1 – Number 1			Panel S1 – Number 2			Panel S1 – Number 3			Panel S1 – Number 4		
	Damping %age critical			Damping %age critical			Damping %age critical			Damping %age critical		
	Set 1	Set 2	Set 3	Set 1	Set 2	Set 3	Set 1	Set 2	Set 3	Set 1	Set 2	Set 3
0	0.58	0.58	0.50	0.42	0.45	0.44	0.45	0.43	0.42	0.47	0.47	0.45
1	0.60	0.63	0.54	0.40	0.47	0.46	0.46	0.45	0.44	0.45	0.46	0.45
2	0.61	0.64	0.54	0.42	0.46	0.46	0.47	0.47	0.43	0.45	0.47	0.47
3	0.59	0.59	0.52	0.45	0.48	0.47	0.48	0.48	0.43	0.47	0.48	0.49
4	0.58	0.59	0.53	0.42	0.46	0.50	0.46	0.47	0.46	0.51	0.49	0.50
5	0.58	0.61	0.54	0.46	0.52	0.50	0.49	0.49	0.49	0.49	0.51	0.52
6	0.61	0.66	0.58	0.48	0.50	0.50	0.51	0.45	0.47	0.52	0.54	0.53
7	0.61	0.66	0.62	0.46	0.55	0.54	0.51	0.47	0.51	0.55	0.58	0.57
8	0.68	0.71	0.66	0.54	0.60	0.59	0.55	0.54	0.57	0.61	0.62	0.59
9	0.76	0.81	0.73	0.60	0.65	0.63	0.60	0.59	0.64	0.64	0.65	0.65
10	0.81	0.87	0.78	0.64	0.70	0.71	0.64	0.63	0.70	0.68	0.71	0.71
11	0.86	0.93	0.87	-	-	-	0.70	0.73	0.75	-	-	-
12	0.94	1.00	0.96	-	-	-	-	-	-	-	-	-

Table C.45 – Panel S2 – Numbers 1 to 4 – Damping from FRF's

Total Load kN	Panel S2 – Number 1			Panel S2 – Number 2			Panel S2 – Number 3			Panel S2 – Number 4		
	Damping %age critical			Damping %age critical			Damping %age critical			Damping %age critical		
	Set 1	Set 2	Set 3	Set 1	Set 2	Set 3	Set 1	Set 2	Set 3	Set 1	Set 2	Set 3
0	0.35	0.40	0.40	0.74	0.67	0.55	0.80	0.68	0.67	0.44	0.47	0.52
1	0.38	0.42	0.37	0.87	0.86	0.70	0.71	0.81	0.64	0.50	0.47	0.52
2	0.35	0.37	0.36	0.77	0.75	0.77	0.63	0.65	0.64	0.49	0.45	0.55
3	0.38	0.42	0.41	0.80	0.82	0.74	0.68	0.72	0.67	0.48	0.50	0.53
4	0.40	0.40	0.44	0.84	0.96	0.82	0.78	0.69	0.68	0.51	0.51	0.48
5	0.48	0.44	0.45	0.67	0.71	0.65	0.82	0.77	0.69	0.57	0.57	0.57
6	0.50	0.41	0.45	0.60	0.68	0.60	0.80	0.86	0.79	0.77	0.70	0.68
7	0.59	0.48	0.42	0.65	0.67	0.63	0.98	0.98	0.92	0.79	0.74	0.71
8	0.62	0.68	0.67	0.77	0.74	0.78	0.88	0.92	0.75	0.66	0.74	0.74
9	0.62	0.74	0.72	0.82	0.86	0.78	-	-	-	0.79	0.71	0.67
10	0.71	0.72	0.75	0.75	0.72	0.79	-	-	-	0.85	0.91	0.93

Mode shape data determined using measured steady-state vibration response signals obtained from the panel laboratory test.

Table C.46 – Panel S1 – Numbers 1 – Normalised mode shape data

Span position (m)	After 0 kN			1 kN			2 kN			3 kN		
	Set 1	Set 2	Set 3	Set 1	Set 2	Set 3	Set 1	Set 2	Set 3	Set 1	Set 2	Set 3
0	0.21	0.13	0.26	0.19	0.17	0.19	0.18	0.20	0.19	0.20	0.19	0.22
0.3	0.55	0.56	0.57	0.54	0.62	0.56	0.53	0.56	0.55	0.54	0.53	0.57
0.6	0.79	0.84	0.81	0.78	0.82	0.83	0.88	0.86	0.85	0.79	0.83	0.87
0.9	1.01	0.98	0.97	0.98	0.98	0.99	0.98	0.98	0.98	0.98	1.01	1.00
1.2	1.00	1.00	1.00	1.00	1.00	1.00	1.00	1.00	1.00	1.00	1.00	1.00
1.5	0.86	0.90	0.86	0.85	0.89	0.89	0.84	0.98	0.87	0.82	0.91	0.85
1.8	0.61	0.63	0.60	0.63	0.63	0.63	0.62	0.63	0.62	0.56	0.63	0.62
2.1	0.29	0.29	0.32	0.32	0.29	0.29	0.28	0.27	0.27	0.30	0.33	0.27
2.4	0.08	0.06	0.10	0.05	0.12	0.04	0.05	0.09	0.09	0.05	0.05	0.06
Span position (m)	**4 kN**			**5 kN**			**6 kN**			**7 kN**		
	Set 1	Set 2	Set 3	Set 1	Set 2	Set 3	Set 1	Set 2	Set 3	Set 1	Set 2	Set 3
0	0.18	0.17	0.20	0.19	0.19	0.19	0.12	0.18	0.16	0.20	0.18	0.19
0.3	0.57	0.55	0.54	0.53	0.55	0.58	0.50	0.53	0.54	0.54	0.55	0.56
0.6	0.82	0.82	0.84	0.83	0.83	0.83	0.90	0.82	0.80	0.81	0.81	0.84
0.9	0.94	0.95	0.97	0.92	0.96	0.99	0.99	0.95	0.97	0.94	0.97	0.97
1.2	1.00	1.00	1.00	1.00	1.00	1.00	1.00	1.00	1.00	1.00	1.00	1.00
1.5	0.85	0.85	0.88	0.93	0.85	0.88	0.82	0.84	0.87	0.84	0.85	0.85
1.8	0.64	0.62	0.63	0.67	0.60	0.65	0.61	0.59	0.61	0.62	0.60	0.62
2.1	0.29	0.24	0.30	0.31	0.31	0.32	0.26	0.27	0.29	0.29	0.30	0.27
2.4	0.14	0.15	0.04	0.05	0.10	0.05	0.05	0.05	0.05	0.05	0.09	0.05
Span position (m)	**8 kN**			**9 kN**			**10 kN**			**11 kN**		
	Set 1	Set 2	Set 3	Set 1	Set 2	Set 3	Set 1	Set 2	Set 3	Set 1	Set 2	Set 3
0	0.18	0.17	0.20	0.18	0.21	0.20	0.17	0.17	0.23	0.18	0.19	0.22
0.3	0.55	0.59	0.54	0.52	0.52	0.53	0.44	0.49	0.55	0.50	0.51	0.56
0.6	0.81	0.79	0.84	0.76	0.87	0.81	0.77	0.78	0.80	0.77	0.78	0.79
0.9	0.94	0.96	0.97	0.91	0.91	0.97	0.87	0.89	0.95	0.91	0.91	0.96
1.2	1.00	1.00	1.00	1.00	1.00	1.00	1.00	1.00	1.00	1.00	1.00	1.00
1.5	0.83	0.83	0.85	0.86	0.81	0.87	0.78	0.79	0.85	0.84	0.82	0.82
1.8	0.65	0.60	0.64	0.59	0.57	0.60	0.57	0.55	0.58	0.60	0.60	0.60
2.1	0.31	0.28	0.29	0.29	0.28	0.28	0.28	0.27	0.30	0.30	0.31	0.30
2.4	0.04	0.05	0.08	0.06	0.05	0.10	0.05	0.06	0.08	0.04	0.03	0.04

Table C.47 – Panel S1 – Numbers 2 – Normalised mode shape data

Span position (m)	After 0 kN			1 kN			2 kN			3 kN		
	Set 1	Set 2	Set 3	Set 1	Set 2	Set 3	Set 1	Set 2	Set 3	Set 1	Set 2	Set 3
0	0.23	0.21	0.19	0.20	0.19	0.18	0.18	0.18	0.21	0.20	0.18	0.21
0.3	0.52	0.51	0.54	0.50	0.51	0.51	0.51	0.54	0.65	0.49	0.54	0.53
0.6	0.77	0.70	0.70	0.77	1.27	0.75	0.75	0.77	0.92	0.80	0.80	0.81
0.9	0.93	0.85	0.85	0.97	0.93	0.92	0.91	1.04	1.06	0.96	0.86	0.86
1.2	1.00	1.00	1.00	1.00	1.00	1.00	1.00	1.00	1.00	1.00	1.00	1.00
1.5	0.89	0.79	0.76	0.84	0.80	0.80	0.82	0.82	0.82	0.90	0.87	0.86
1.8	0.59	0.58	0.59	0.56	0.58	0.60	0.61	0.60	0.59	0.64	0.64	0.62
2.1	0.27	0.28	0.29	0.27	0.27	0.28	0.29	0.31	0.31	0.28	0.29	0.31
2.4	0.08	0.06	0.02	0.04	0.04	0.03	0.06	0.06	0.06	0.02	0.06	0.02
Span position (m)	**4 kN**			**5 kN**			**6 kN**			**7 kN**		
	Set 1	Set 2	Set 3	Set 1	Set 2	Set 3	Set 1	Set 2	Set 3	Set 1	Set 2	Set 3
0	0.18	0.18	0.16	0.19	0.19	0.21	0.24	0.20	0.21	0.22	0.21	0.21
0.3	0.54	0.53	0.54	0.55	0.50	0.55	0.57	0.53	0.53	0.54	0.60	0.61
0.6	0.80	0.80	0.77	0.78	0.74	0.81	0.82	0.80	0.81	0.80	0.80	0.87
0.9	0.97	0.97	0.94	0.91	0.88	0.97	0.94	1.01	1.23	0.98	0.99	0.97
1.2	1.00	1.00	1.00	1.00	1.00	1.00	1.00	1.00	1.00	1.00	1.00	1.00
1.5	0.89	0.90	0.85	0.86	0.80	0.74	0.89	0.85	0.88	0.87	0.88	0.88
1.8	0.65	0.66	0.64	0.56	0.56	0.56	0.68	0.73	0.63	0.58	0.63	0.60
2.1	0.31	0.34	0.29	0.26	0.23	0.31	0.28	0.99	0.31	0.26	0.30	0.28
2.4	0.06	0.06	0.06	0.09	0.08	0.06	0.05	0.04	0.05	0.02	0.03	0.05
Span position (m)	**8 kN**			**9 kN**			**10 kN**					
	Set 1	Set 2	Set 3	Set 1	Set 2	Set 3	Set 1	Set 2	Set 3			
0	0.27	0.20	0.25	0.20	0.20	0.19	0.21	0.22	0.20			
0.3	0.59	0.57	0.57	0.61	0.58	0.54	0.52	0.53	0.51			
0.6	0.80	0.79	0.79	0.85	0.80	0.81	0.84	0.80	0.26			
0.9	0.93	0.95	0.96	0.98	1.10	1.03	0.96	0.97	0.30			
1.2	1.00	1.00	1.00	1.00	1.00	1.00	1.00	1.00	1.00			
1.5	0.89	0.86	0.90	0.86	0.88	0.89	0.86	0.86	0.84			
1.8	0.61	0.64	0.63	0.60	0.61	0.61	0.62	0.61	0.60			
2.1	0.30	0.30	0.29	0.28	0.29	0.37	0.26	0.27	0.33			
2.4	0.04	0.03	0.02	0.03	0.06	0.03	0.03	0.07	0.16			

Table C.48 – Panel S1 – Numbers 3 – Normalised mode shape data

Span position (m)	After 0 kN			1 kN			2 kN			3 kN		
	Set 1	Set 2	Set 3	Set 1	Set 2	Set 3	Set 1	Set 2	Set 3	Set 1	Set 2	Set 3
0	0.22	0.21	0.22	0.23	0.23	0.20	0.23	0.23	0.20	0.20	0.21	0.22
0.3	0.53	0.55	0.50	0.58	0.50	0.51	0.50	0.49	0.49	0.55	0.52	0.52
0.6	0.76	0.76	0.82	0.77	0.78	0.80	0.75	0.80	0.74	0.77	0.78	0.81
0.9	0.90	0.94	0.94	0.96	0.91	0.91	0.91	0.96	0.90	0.91	0.93	0.94
1.2	1.00	1.00	1.00	1.00	1.00	1.00	1.00	1.00	1.00	1.00	1.00	1.00
1.5	0.86	0.87	0.89	0.89	0.86	0.89	0.86	0.83	0.89	0.82	0.84	0.84
1.8	0.62	0.62	0.57	0.58	0.69	0.64	0.62	0.64	0.61	0.60	0.62	0.60
2.1	0.31	0.27	0.30	0.30	0.31	0.34	0.32	0.30	0.31	0.29	0.27	0.26
2.4	0.06	0.03	0.10	0.04	0.04	0.06	0.09	0.04	0.03	0.07	0.12	0.06
Span position (m)	4 kN			5 kN			6 kN			7 kN		
	Set 1	Set 2	Set 3	Set 1	Set 2	Set 3	Set 1	Set 2	Set 3	Set 1	Set 2	Set 3
0	0.22	0.21	0.17	0.21	0.20	0.21	0.19	0.19	0.20	0.20	0.18	0.20
0.3	0.48	0.55	0.54	0.54	0.53	0.51	0.55	0.50	0.50	0.51	0.50	0.54
0.6	0.77	0.75	0.78	0.77	0.78	0.79	0.77	0.75	0.76	0.76	0.77	0.79
0.9	0.89	0.92	0.93	0.90	0.90	0.96	0.94	0.93	0.94	0.93	0.94	0.98
1.2	1.00	1.00	1.00	1.00	1.00	1.00	1.00	1.00	1.00	1.00	1.00	1.00
1.5	0.81	0.82	0.84	0.83	0.82	0.85	0.84	0.87	0.84	0.86	0.86	0.88
1.8	0.60	0.60	0.59	0.59	0.60	0.63	0.63	0.64	0.63	0.64	0.62	0.61
2.1	0.27	0.29	0.29	0.28	0.27	0.31	0.30	0.29	0.32	0.32	0.30	0.30
2.4	0.02	0.02	0.05	0.07	0.03	0.03	0.02	0.02	0.04	0.04	0.07	0.04
Span position (m)	8 kN			9 kN			10 kN			11 kN		
	Set 1	Set 2	Set 3	Set 1	Set 2	Set 3	Set 1	Set 2	Set 3	Set 1	Set 2	Set 3
0	0.19	0.19	0.19	0.19	0.19	0.18	0.19	0.18	0.19	0.19	0.19	0.23
0.3	0.51	0.47	0.50	0.56	0.54	0.54	0.56	0.50	0.50	0.61	0.49	0.53
0.6	0.75	0.77	0.76	0.78	0.81	0.82	0.80	0.80	0.83	0.78	0.76	0.79
0.9	0.93	0.94	0.92	0.96	0.95	0.94	0.97	0.96	0.95	0.96	0.96	0.97
1.2	1.00	1.00	1.00	1.00	1.00	1.00	1.00	1.00	1.00	1.00	1.00	1.00
1.5	0.85	0.86	0.86	0.90	0.89	0.85	0.88	0.85	0.87	0.88	0.85	0.87
1.8	0.62	0.64	0.63	0.66	0.64	0.63	0.64	0.64	0.65	0.66	0.63	0.61
2.1	0.28	0.31	0.31	0.33	0.27	0.30	0.30	0.29	0.27	0.29	0.28	0.30
2.4	0.04	0.03	0.04	0.03	0.05	0.01	0.04	0.05	0.03	0.04	0.02	0.04

Table C.49 – Panel S1 – Numbers 4 – Normalised mode shape data

Span position (m)	After 0 kN			1 kN			2 kN			3 kN		
	Set 1	Set 2	Set 3	Set 1	Set 2	Set 3	Set 1	Set 2	Set 3	Set 1	Set 2	Set 3
0	0.21	0.20	0.23	0.21	0.21	0.19	0.20	0.23	0.22	0.20	0.19	0.21
0.3	0.55	0.56	0.55	0.56	0.52	0.57	0.54	0.57	0.53	0.52	0.58	0.56
0.6	0.80	0.79	0.77	0.78	0.78	0.79	0.81	0.80	0.77	0.80	0.82	0.76
0.9	0.95	0.91	0.91	0.98	0.93	0.92	0.95	0.93	0.97	0.98	0.97	0.93
1.2	1.00	1.00	1.00	1.00	1.00	1.00	1.00	1.00	1.00	1.00	1.00	1.00
1.5	0.82	0.91	0.90	0.85	0.85	0.81	0.89	0.87	0.85	0.86	0.87	0.87
1.8	0.67	0.67	0.67	0.61	0.60	0.57	0.69	0.61	0.64	0.57	0.58	0.60
2.1	0.31	0.29	0.33	0.29	0.27	0.35	0.35	0.32	0.29	0.30	0.26	0.32
2.4	0.07	0.08	0.08	0.04	0.08	0.08	0.03	0.01	0.03	0.08	0.08	0.06
Span position (m)	**4 kN**			**5 kN**			**6 kN**			**7 kN**		
	Set 1	Set 2	Set 3	Set 1	Set 2	Set 3	Set 1	Set 2	Set 3	Set 1	Set 2	Set 3
0	0.21	0.23	0.26	0.13	0.20	0.19	0.21	0.22	0.21	0.27	0.19	0.21
0.3	0.53	0.62	0.53	0.54	0.58	0.53	0.52	0.63	0.53	0.57	0.57	0.59
0.6	0.80	0.81	0.84	0.82	0.83	0.82	0.81	0.79	0.78	0.78	0.81	0.82
0.9	0.96	0.92	0.98	0.95	0.96	0.94	0.97	0.99	0.93	0.98	1.00	0.98
1.2	1.00	1.00	1.00	1.00	1.00	1.00	1.00	1.00	1.00	1.00	1.00	1.00
1.5	0.83	0.85	0.81	0.80	0.84	0.85	0.82	0.88	0.85	0.82	0.87	0.88
1.8	0.60	0.61	0.61	0.60	0.60	0.61	0.71	0.63	0.58	0.63	0.66	0.61
2.1	0.27	0.27	0.36	0.31	0.34	0.33	0.34	0.29	0.30	0.33	0.34	0.36
2.4	0.04	0.07	0.06	0.04	0.02	0.08	0.02	0.09	0.05	0.05	0.02	0.07
Span position (m)	**8 kN**			**9 kN**			**10 kN**					
	Set 1	Set 2	Set 3	Set 1	Set 2	Set 3	Set 1	Set 2	Set 3			
0	0.23	0.19	0.18	0.21	0.22	0.19	0.21	0.20	0.22			
0.3	0.59	0.57	0.57	0.61	0.57	0.62	0.58	0.54	0.59			
0.6	0.86	0.84	0.85	0.86	0.82	0.80	0.79	0.79	0.84			
0.9	1.00	0.98	0.97	0.98	0.95	0.93	0.97	0.93	0.95			
1.2	1.00	1.00	1.00	1.00	1.00	1.00	1.00	1.00	1.00			
1.5	0.86	0.88	0.90	0.87	0.90	0.86	0.85	0.86	0.88			
1.8	0.69	0.69	0.70	0.64	0.66	0.65	0.62	0.60	0.61			
2.1	0.26	0.34	0.30	0.34	0.34	0.31	0.27	0.26	0.34			
2.4	0.07	0.08	0.03	0.03	0.05	0.04	0.05	0.02	0.02			

Table C.50 – Panel S2 – Numbers 1 – Normalised mode shape data

Span position (m)	After 0 kN			1 kN			2 kN			3 kN		
	Set 1	Set 2	Set 3	Set 1	Set 2	Set 3	Set 1	Set 2	Set 3	Set 1	Set 2	Set 3
0	0.19	0.19	0.19	0.19	0.19	0.19	0.19	0.19	0.20	0.21	0.20	0.20
0.3	0.60	0.61	0.60	0.56	0.57	0.60	0.58	0.62	0.56	0.60	0.58	0.61
0.6	0.85	0.93	0.89	0.85	0.83	0.83	0.88	0.88	0.89	0.83	0.86	0.85
0.9	0.95	1.01	0.98	0.97	0.98	0.94	1.01	1.01	0.97	0.99	0.98	0.96
1.2	1.00	1.00	1.00	1.00	1.00	1.00	1.00	1.00	1.00	1.00	1.00	1.00
1.5	0.92	0.97	0.96	0.96	0.97	0.95	0.94	0.91	0.96	0.96	0.95	0.95
1.8	0.74	0.75	0.74	0.66	0.67	0.66	0.64	0.64	0.71	0.68	0.68	0.68
2.1	0.36	0.36	0.36	0.31	0.33	0.31	0.31	0.31	0.35	0.33	0.33	0.33
2.4	0.07	0.11	0.16	0.07	0.06	0.06	0.10	0.12	0.13	0.10	0.10	0.11
Span position (m)	4 kN			5 kN			6 kN			7 kN		
	Set 1	**Set 2**	**Set 3**	**Set 1**	**Set 2**	**Set 3**	**Set 1**	**Set 2**	**Set 3**	**Set 1**	**Set 2**	**Set 3**
0	0.19	0.20	0.20	0.20	0.21	0.19	0.26	0.24	0.20	0.23	0.22	0.20
0.3	0.58	0.55	0.55	0.64	0.60	0.55	0.63	0.57	0.62	0.56	0.60	0.57
0.6	0.81	0.83	0.83	0.83	0.88	0.83	0.90	0.85	0.87	0.89	0.91	0.85
0.9	0.94	0.95	0.94	0.95	1.01	0.95	0.95	0.97	0.96	0.98	1.01	0.98
1.2	1.00	1.00	1.00	1.00	1.00	1.00	1.00	1.00	1.00	1.00	1.00	1.00
1.5	0.88	0.96	0.92	0.90	0.97	0.93	0.96	0.94	0.90	0.94	0.95	0.95
1.8	0.62	0.68	0.67	0.67	0.69	0.63	0.71	0.66	0.69	0.69	0.72	0.67
2.1	0.31	0.34	0.34	0.33	0.33	0.30	0.35	0.32	0.34	0.34	0.32	0.32
2.4	0.11	0.10	0.09	0.10	0.10	0.11	0.10	0.12	0.12	0.11	0.11	0.10
Span position (m)	8 kN			9 kN			10 kN					
	Set 1	**Set 2**	**Set 3**	**Set 1**	**Set 2**	**Set 3**	**Set 1**	**Set 2**	**Set 3**			
0	0.17	0.19	0.18	0.15	0.15	0.14	0.15	0.15	0.15			
0.3	0.57	0.59	0.54	0.51	0.52	0.51	0.54	0.55	0.54			
0.6	0.86	0.87	0.82	0.80	0.83	0.85	0.86	0.87	0.86			
0.9	0.97	1.00	0.95	0.94	0.98	0.93	0.98	1.02	0.98			
1.2	1.00	1.00	1.00	1.00	1.00	1.00	1.00	1.00	1.00			
1.5	0.88	0.97	0.89	0.88	0.91	0.91	0.94	0.94	0.94			
1.8	0.61	0.66	0.65	0.64	0.66	0.65	0.66	0.69	0.68			
2.1	0.28	0.30	0.30	0.30	0.32	0.31	0.32	0.33	0.31			
2.4	0.14	0.12	0.13	0.08	0.07	0.07	0.08	0.08	0.07			

Table C.51 – Panel S2 – Numbers 2 – Normalised mode shape data

Span position (m)	After 0 kN			1 kN			2 kN			3 kN		
	Set 1	Set 2	Set 3	Set 1	Set 2	Set 3	Set 1	Set 2	Set 3	Set 1	Set 2	Set 3
0	0.28	0.38	0.34	0.33	0.35	0.26	0.32	0.34	0.33	0.33	0.32	0.33
0.3	0.63	0.61	0.61	0.60	0.67	0.57	0.64	0.62	0.60	0.63	0.65	0.62
0.6	0.90	0.87	0.89	0.88	0.93	0.89	0.89	0.90	0.88	0.92	0.87	0.90
0.9	1.05	1.01	1.04	1.03	0.99	1.03	1.05	1.01	1.05	1.05	1.02	1.01
1.2	1.00	1.00	1.00	1.00	1.00	1.00	1.00	1.00	1.00	1.00	1.00	1.00
1.5	0.95	0.89	0.94	0.87	0.91	0.93	0.94	0.88	0.88	0.91	0.90	0.88
1.8	0.76	0.65	0.71	0.70	0.74	0.71	0.79	0.68	0.70	0.74	0.73	0.70
2.1	0.47	0.47	0.49	0.46	0.48	0.43	0.47	0.45	0.47	0.45	0.49	0.49
2.4	0.08	0.10	0.10	0.12	0.20	0.17	0.10	0.15	0.08	0.08	0.10	0.13
Span position (m)	**4 kN**			**5 kN**			**6 kN**			**7 kN**		
	Set 1	**Set 2**	**Set 3**	**Set 1**	**Set 2**	**Set 3**	**Set 1**	**Set 2**	**Set 3**	**Set 1**	**Set 2**	**Set 3**
0	0.31	0.40	0.33	0.29	0.35	0.35	0.31	0.31	0.30	0.29	0.29	0.29
0.3	0.64	0.66	0.58	0.62	0.63	0.62	0.56	0.55	0.55	0.55	0.55	0.58
0.6	0.91	0.91	0.85	0.92	0.86	0.92	0.84	0.84	0.82	0.85	0.85	0.84
0.9	1.01	1.00	1.01	1.02	0.99	1.03	0.98	0.98	1.05	1.00	1.00	1.01
1.2	1.00	1.00	1.00	1.00	1.00	1.00	1.00	1.00	1.00	1.00	1.00	1.00
1.5	0.92	0.92	0.92	0.93	0.91	0.91	0.91	0.85	0.88	0.88	0.89	0.91
1.8	0.76	0.75	0.69	0.73	0.74	0.73	0.65	0.66	0.64	0.66	0.66	0.65
2.1	0.50	0.52	0.50	0.44	0.45	0.43	0.40	0.47	0.38	0.39	0.39	0.38
2.4	0.06	0.07	0.07	0.04	0.06	0.06	0.05	0.05	0.04	0.03	0.03	0.03
Span position (m)	**8 kN**			**9 kN**			**10 kN**					
	Set 1	**Set 2**	**Set 3**	**Set 1**	**Set 2**	**Set 3**	**Set 1**	**Set 2**	**Set 3**			
0	0.28	0.29	0.29	0.25	0.28	0.27	0.23	0.28	0.29			
0.3	0.58	0.59	0.60	0.55	0.56	0.56	0.59	0.60	0.59			
0.6	0.86	0.85	0.92	0.86	0.83	0.82	0.89	0.84	0.89			
0.9	1.02	1.01	1.05	1.01	1.01	0.99	1.02	0.98	1.04			
1.2	1.00	1.00	1.00	1.00	1.00	1.00	1.00	1.00	1.00			
1.5	0.94	0.88	0.93	0.89	0.89	0.89	0.93	0.92	0.92			
1.8	0.71	0.71	0.72	0.66	0.66	0.65	0.72	0.69	0.69			
2.1	0.40	0.41	0.40	0.45	0.37	0.37	0.42	0.39	0.39			
2.4	0.02	0.02	0.03	0.03	0.03	0.03	0.03	0.03	0.03			

Table C.52 – Panel S2 – Numbers 3 – Normalised mode shape data

Span position (m)	After 0 kN			1 kN			2 kN			3 kN		
	Set 1	Set 2	Set 3	Set 1	Set 2	Set 3	Set 1	Set 2	Set 3	Set 1	Set 2	Set 3
0	0.29	0.26	0.27	0.28	0.20	0.30	0.26	0.26	0.25	0.22	0.20	0.20
0.3	0.64	0.59	0.57	0.63	0.62	0.63	0.58	0.59	0.61	0.52	0.58	0.55
0.6	0.90	0.89	0.84	0.93	0.90	0.89	0.92	0.86	0.88	0.88	0.85	0.86
0.9	1.02	1.02	0.96	1.02	1.02	0.97	0.99	1.00	1.00	0.99	0.99	0.95
1.2	1.00	1.00	1.00	1.00	1.00	1.00	1.00	1.00	1.00	1.00	1.00	1.00
1.5	0.84	0.86	0.81	0.89	0.85	0.83	0.82	0.85	0.86	0.81	0.81	0.84
1.8	0.66	0.59	0.59	0.65	0.62	0.56	0.61	0.60	0.62	0.59	0.59	0.57
2.1	0.36	0.32	0.28	0.35	0.34	0.36	0.35	0.33	0.33	0.31	0.31	0.30
2.4	0.07	0.11	0.07	0.06	0.06	0.05	0.09	0.09	0.09	0.07	0.06	0.06
Span position (m)	4 kN			5 kN			6 kN			7 kN		
	Set 1	Set 2	Set 3	Set 1	Set 2	Set 3	Set 1	Set 2	Set 3	Set 1	Set 2	Set 3
0	0.21	0.21	0.21	0.20	0.20	0.20	0.23	0.24	0.26	0.23	0.24	0.24
0.3	0.55	0.56	0.55	0.53	0.53	0.54	0.57	0.58	0.61	0.58	0.61	0.59
0.6	0.89	0.89	0.90	0.91	0.86	0.87	0.91	0.92	0.91	0.92	0.91	0.89
0.9	1.01	1.01	0.97	1.02	1.02	0.98	1.02	0.98	0.95	1.02	1.00	0.97
1.2	1.00	1.00	1.00	1.00	1.00	1.00	1.00	1.00	1.00	1.00	1.00	1.00
1.5	0.86	0.86	0.85	0.83	0.83	0.84	0.80	0.79	0.88	0.83	0.88	0.88
1.8	0.62	0.63	0.63	0.60	0.61	0.61	0.57	0.56	0.64	0.60	0.64	0.59
2.1	0.32	0.33	0.33	0.31	0.32	0.32	0.29	0.29	0.33	0.30	0.33	0.31
2.4	0.14	0.10	0.13	0.09	0.09	0.09	0.06	0.07	0.12	0.07	0.09	0.10

Span position (m)	8 kN		
	Set 1	Set 2	Set 3
0	0.24	0.23	0.24
0.3	0.60	0.60	0.63
0.6	0.89	0.87	0.85
0.9	1.02	1.00	0.96
1.2	1.00	1.00	1.00
1.5	0.84	0.86	0.84
1.8	0.63	0.63	0.65
2.1	0.32	0.30	0.31
2.4	0.11	0.12	0.11

Table C.53 – Panel S2 – Numbers 4 – Normalised mode shape data

Span position (m)	After 0 kN			1 kN			2 kN			3 kN		
	Set 1	Set 2	Set 3	Set 1	Set 2	Set 3	Set 1	Set 2	Set 3	Set 1	Set 2	Set 3
0	0.36	0.38	0.38	0.33	0.34	0.35	0.36	0.34	0.33	0.33	0.37	0.34
0.3	0.63	0.67	0.62	0.64	0.66	0.66	0.63	0.66	0.66	0.66	0.63	0.68
0.6	0.93	0.95	0.92	0.88	0.94	0.95	0.94	0.94	0.96	0.91	0.93	0.93
0.9	0.98	1.02	1.01	0.98	0.98	1.01	1.05	1.00	1.01	0.98	1.03	1.01
1.2	1.00	1.00	1.00	1.00	1.00	1.00	1.00	1.00	1.00	1.00	1.00	1.00
1.5	0.91	0.84	0.88	0.91	0.91	0.94	0.94	0.88	0.89	0.95	0.88	0.92
1.8	0.61	0.63	0.62	0.60	0.63	0.63	0.60	0.62	0.68	0.62	0.65	0.67
2.1	0.38	0.40	0.37	0.37	0.40	0.36	0.36	0.38	0.36	0.38	0.38	0.41
2.4	0.05	0.03	0.03	0.03	0.03	0.03	0.03	0.07	0.03	0.03	0.04	0.03
Span position (m)	4 kN			5 kN			6 kN			7 kN		
	Set 1	Set 2	Set 3	Set 1	Set 2	Set 3	Set 1	Set 2	Set 3	Set 1	Set 2	Set 3
0	0.34	0.36	0.42	0.35	0.35	0.35	0.28	0.28	0.28	0.26	0.27	0.27
0.3	0.61	0.63	0.68	0.66	0.62	0.67	0.56	0.58	0.60	0.55	0.63	0.57
0.6	0.94	0.95	0.93	0.90	0.89	0.97	0.90	0.91	0.89	0.92	0.91	0.90
0.9	1.00	1.01	1.03	1.02	0.98	1.01	1.01	0.97	1.01	0.99	1.01	1.04
1.2	1.00	1.00	1.00	1.00	1.00	1.00	1.00	1.00	1.00	1.00	1.00	1.00
1.5	0.92	0.90	0.93	0.91	0.90	0.93	0.89	0.88	0.87	0.90	0.85	0.89
1.8	0.60	0.61	0.60	0.63	0.63	0.62	0.64	0.59	0.58	0.64	0.59	0.62
2.1	0.39	0.36	0.37	0.41	0.38	0.37	0.34	0.34	0.34	0.31	0.33	0.33
2.4	0.03	0.02	0.03	0.02	0.00	0.02	0.02	0.00	0.02	0.03	0.02	0.02
Span position (m)	8 kN			9 kN			10 kN					
	Set 1	Set 2	Set 3	Set 1	Set 2	Set 3	Set 1	Set 2	Set 3			
0	0.27	0.26	0.29	0.31	0.31	0.31	0.28	0.30	0.31			
0.3	0.58	0.64	0.61	0.67	0.67	0.68	0.61	0.67	0.60			
0.6	0.92	0.90	0.88	0.87	0.88	0.87	0.94	0.92	0.89			
0.9	0.99	0.99	1.03	1.01	1.00	0.98	1.01	1.01	1.02			
1.2	1.00	1.00	1.00	1.00	1.00	1.00	1.00	1.00	1.00			
1.5	0.87	0.86	0.89	0.88	0.89	0.90	0.90	0.88	0.93			
1.8	0.64	0.56		0.63	0.65	0.66	0.66	0.60	0.63			
2.1	0.37	0.31	0.32	0.37	0.38	0.38	0.37	0.37	0.36			
2.4	0.02	0.02	0.02	0.02	0.02	0.02	0.04	0.04	0.06			

Properties of the concrete determined from standard laboratory tests carried out on 100mm cube samples.

Table C.54 – Concrete properties – all 100mm cubes

Panel Number	Age of concrete (moisture cured)	Density (kg/m^3)	Compressive strength (N/mm^2)	Age of concrete (air cured)	Density (kg/m^3)	Compressive strength (N/mm^2)
S1-1	28 day	2469	52.3	50 days	2455	49.8
S1-2	28 day	2456	53.4	61 days	2459	55.8
S1-3	28 day	2468	55.8	61 days	2448	54.8
S1-4	28 day	2461	52.2	65 days	2418	54.8
S1-5	28 day	2472	53.6	53 days	2473	52.1
S1-6	28 day	2501	63.3	52 days	2484	53.9
S1-7	28 day	2509	58.8	86 days	2469	49.1
S1-8	28 day	2507	61.2	92 days	2467	44.0
S1-9	28 day	2468	57.9	32 days	2437	51.1
S2-1	28 day	2509	48.9	63 days	2471	43.6
S2-2	28 day	2491	55.7	72 days	2427	49.7
S2-3	28 day	2490	55.0	70 days	2454	53.7
S2-4	28 day	2475	56.8	78 days	2466	53.6
S2-5	28 day	2493	57.1	51 days	2494	49.6
S2-6	28 day	2457	57.5	40 days	2419	42.8
S2-7	28 day	2511	60.2	32 days	2462	44.8
S2-8	28 day	2493	59.0	38 days	2481	51.2
S2-9	28 day	2514	60.1	35 days	2444	53.4

Properties of the concrete determined from standard laboratory tests carried out on 150mm diameter, 300mm long cylinders.

Table C.55 – Concrete properties – all cylinder tests

Panel Number	Age of concrete (moisture cured)	Strain Range to which E_c value applies	Concrete Young's Modulus (E_c) (kN/mm^2)	Age of concrete (air cured)	Strain Range to which E_c value applies	Concrete Young's Modulus (E_c) (kN/mm^2)
S1-1	28 day	0 – 550μ	30.6	50 days	0 – 500μ	41.8
S1-2	28 day	0 – 500μ	32.8	61 days	0 – 500μ	42.2
S1-3	28 day	0 – 550μ	39.7	61 days	0 – 550μ	43.7
S1-4	28 day	0 – 500μ	35.7	65 days	0 – 500μ	42.8
S1-5	28 day	0 – 500μ	35.6	53 days	0 – 550μ	43.9
S1-6	28 day	0 – 550μ	38.4	52 days	0 – 500μ	41.2
S1-7	28 day	0 – 500μ	39.2	86 days	0 – 600μ	43.2
S1-8	28 day	0 – 600μ	34.8	92 days	0 – 500μ	46.8
S1-9	28 day	0 – 500μ	32.5	32 days	0 – 500μ	39.8
S2-1	28 day	0 – 500μ	29.8	63 days	0 – 600μ	42.5
S2-2	28 day	0 – 500μ	35.2	72 days	0 – 500μ	45.6
S2-3	28 day	0 – 500μ	36.3	70 days	0 – 500μ	44.5
S2-4	28 day	0 – 500μ	41.3	78 days	0 – 500μ	46.2
S2-5	28 day	0 – 500μ	46.3	51 days	0 – 500μ	41.3
S2-6	28 day	0 – 550μ	39.8	40 days	0 – 550μ	39.9
S2-7	28 day	0 – 500μ	37.8	32 days	0 – 500μ	38.9
S2-8	28 day	0 – 500μ	29.2	38 days	0 – 550μ	40.2
S2-9	28 day	0 – 500μ	38.8	35 days	0 – 500μ	41.2

(Note: $\mu = \times 10^{-6}$ mm/mm)

APPENDIX D

List of Published Papers and Other Activities Associated with the Research

Conference Publications:

Delpak, R., Howson, P. and Richards, V. M. (1997) "Comparisons of measured and calculated natural frequencies using a simplified analytical approach". Proceedings of the 5th International Conference on Modern Building Materials, Structures and Techniques, Vilnius, Lithuania, (6 pages).

Ellis, B. R., Moore, D. B., Delpak, R., Richards, V. M. and Luke, S. (1997) "The dynamic characteristics of a multi-storey steel-framed building". Proceedings of the 4th International Kerensky Conference on Structures in the New Millennium, Hong-Kong, 3-5 September 1997, pp.235 – 240.

Journal Publication:

Richards, V. M. (1998) "Identifying the potential failure of composite floor slabs from measured vibration response". Journal of the South Wales Institute of Engineers, Volume 16, December 1998, pp.38 – 53.

Prizes from work in connection with the research:

The David Douglas Award 1998 – For a paper presented to, and later published by, the South Wales Institute of Engineers. Title of paper as above.

Regional Winner of the Institution of Civil Engineers' Graduate Paper Writing Competition 1999 for a paper entitled "The vibration performance of a continuous floor subjected to impact loading".

Miller Prize Winner 1999 – For a paper presented to the Institution of Civil Engineers. Title of Paper: "Non-destructive testing for damage evaluation of structural components using measured dynamic response".

James Forrest Medal 2000 – For a paper presented to the Institution of Civil Engineers. Title of Paper: "The vibration behaviour of continuous floors".